UNIVERSITY OF OKLAHOMA

GRADUATE COLLEGE

REGULATION OF CONFORMATIONAL INTERCONVERSIONS IN SYMMETRIC AND ASYMMETRIC [2]CATENANES

A DISSERTATION

SUBMITTED TO THE GRADUATE FACULTY

in partial fulfillment of the requirements for the

degree of

Doctor of Philosophy

By

DAVID EVERETT MARTYN

Norman, OK

2006

REGULATION OF CONFORMATIONAL INTERCONVERSIONS IN SYMMETRIC AND ASYMMETRIC [2]CATENANES

A DISSERTATION APPROVED FOR THE
DEPARTMENT OF CHEMISTRY AND BIOCHEMISTRY

BY

Ronald L. Halterman, Chair

Daniel T. Glatzhofer

Kenneth M. Nicholas

Edgar A. O'Rear

Wai Tak Yip

ACKNOWLEDGEMENTS

My deepest thanks and respect goes to my mentor Dr. Ronald Halterman for his years of support, encouragement, and understanding. I could not have asked for or chosen a better advisor. Several years ago, he presented me with the opportunity to embark on a new project. It has allowed me to grow as a chemist in ways I had not foreseen and for that, I am in his debt. Special thanks go to Dr. Susan Alguindigue for her guidance, expertise, and work in the NMR facility. I would like to thank all the faculty and staff in the Chemistry and Biochemistry Department who have provided support in a myriad of ways. My fellow graduate students past and present deserve praise for helping push me to be a better chemist.

My wonderful family helped make all this possible. My wife Tami is an amazing woman. Since first we met, she has become my devoted friend, confidant, lover, and mother of our children. I am a better person because of her and I cannot imagine life without her. She is truly a blessing. Our two boys Eric and Isaac have been an inspiration and spending time with them is always enlightening. Eric has shown me that there is no such thing as a stranger and that a tender, caring heart is a powerful asset. Isaac has shown me that force of will can be a powerful thing. No matter what the obstacle, there is always a way to overcome it if you are tenacious. Both of you have shown me the importance of play in learning and how much a person can learn by simply observing. I see a bright future for both of you and I am excited to be part of it. Finally, I would like to thank my parents and grandparents for their support. Wonderful teachers have surrounded me my entire life. I am truly blessed.

TABLE OF CONTENTS

REGULATION OF CONFORMATIONAL INTERCONVERSIONS IN SYMMETRIC AND ASYMMETRIC [2]CATENANES

ABSTRACT

For centuries, humans have been fascinated with machines that convert one form of energy into another form. These devices come in a variety of manifestations, several of which are molecular in size. One feature unites all of these devices; they require selected input of energy to function, and this energy modulates an energy potential. A molecular device driven selectively and entirely by random thermal energy has not been demonstrated and according to sound, and well-established theory, such a device cannot exist. While previous attempts to probe this stricture met with failure, we hoped to succeed where others failed by incorporating a component lacking in previous designs. We hoped to modulate the energy potential using random thermal energy through incorporation of a molecular gate. In our studies, we investigated control of molecular motion as it could pertain to the emerging area of molecular machines and ratchets. We based our studies on the movement in mechanically interlocked molecular rings known as catenanes. These [2]catenanes possessed a dibenzo-34-crown-10 ether interlocked with a ring containing two 4,4'-dipyridiniums connected by aryl tethers. These novel catenanes contain bistable binding sites separated and connected by biasing or non-biasing tethers.

Using non-biasing tethers, consisting of phenyl rings designed to be blocking or non-blocking in nature, we were able to control the pathway for interconversion.

Through the appropriate incorporation of blocking groups on one or both of two phenyl tethers it was possible to block one or both of the two pathways for circumrotation in our bistable catenanes. The free energies of activation required for circumrotation over the open, non-blocking pathways were calculated at 11 to 13 kcal/mol. The isomer ratios for these catenanes were 1 to 1 indicating the two conformations were isoenergetic. Using these symmetric catenanes, we demonstrated the ability to dictate the pathway over which circumrotation occurred in a non-covalently bound system.

Using asymmetric, non-biasing tethers we determined the extent to which the isomer ratios were dependant on the symmetry of the catenanes, and measured the thermodynamic preference displayed between the two conformers. Circumrotation in these catenanes required between 11 and 15 kcal/mol of energy. We found the conformer stabilities were symmetry dependent displaying isomer ratios of between 1.5:1 and 3.5:1. This indicated that one conformation was more stable.

Using asymmetric, biasing tethers we sought to drive circumrotation preferentially in one direction using a gate that would discriminate between the two conformations. Allosteric interaction between the gate and catenated crown ether would either allow or disallow translocation over the gate based on the direction of circumrotation. The free energies of activation for circumrotation were calculated at 11 to 19 kcal/mol. While two gating catenane systems did appear to display the anticipated characteristics, the results were not convincing and could be attributed to other phenomenon.

Through these studies we established the ability to regulate the free energy of activation for circumrotation by increasing or decreasing the steric bulk of the tether

substituents. By making the steric bulk on the tethers large enough we were able to dictate the path over which circumrotation would occur. We showed that introduction of asymmetry perturbed the isoenergetic nature of the binding sites. Two exceptions to this trend were observed and displayed the anticipated characteristics. We established the ability of a gate to exist in both a high and low energy conformations thereby presenting energetically different pathways for circumrotation.

Chapter 1

Molecular Machinations

Section 1.1 Introduction

In this thesis, we are investigating control of molecular motion as it could pertain to the emerging area of molecular machines and ratchets. We based our studies on the movement in mechanically interlocked molecular rings known as catenanes. To put our studies in perspective we must initially discuss the background of molecular machines and ratchets as well as the preparation and study of [2]catenanes. The chapters that follow these background reviews cover our preparation and study of novel catenanes containing bistable binding sites and biasing or non-biasing tethers.

Section 1.2 Molecular Machines, Motors, and Devices

For centuries, humans have been fascinated with machines that convert one form of energy into another form. These macroscopic devices come in a variety of manifestations ranging from something as simple as a solid fuel rocket motor to an intricate internal combustion engine, each of which are composed of individual components working together to achieve a specific function.[1] This concept has been extended to the nano[2] and molecular levels[1,3,4,5,6,7,8,9] with some success. Like their macroscopic antecessors, these molecular machines possess five distinct characteristics: a function, a way of monitoring actions that perform the function, a cyclical nature to

the actions, the duration of time before the device performs its action again, and energy requirements for causing the device to act.[1,9] These answers belong to a set of fundamental questions asked of any machine: what does it do, how does it do what it does, will it do what it did again, how often does it do what it does, and finally the all important question, what does it take to make it do what it does? To put the final question another way, what are the device's energy requirements? In each example, we take a form of potential energy and convert it into some useable form of work, typically with very low efficiency. This has lead to the development of smaller, more efficient motors.[9,10] However, after recognition that this "top-down" approach to engineering miniature motors would eventually reach its practical limits, and tools with which to study molecular motors became increasingly capable, a "bottom-up" approach gained greater attention.[1,11] Chemists, routinely manipulating atoms and molecules, were already utilizing this approach to design, and in a unique position to be able to devise new molecular approaches to manufacturing machines.[1] Thus, two decades ago, chemists began looking toward development of molecular devices and motors.[5] It was and remains a process of consciously designing and synthesizing molecules capable of undergoing some sort of conformational change effecting movement of one molecular architecture relative to another.[7] Of particular interest to the scientific community has been the Brownian ratchet model for such motors[12,13] first described in a thought experiment by Feynman[14] and shown in Figure 1.2.1. In this proposed device, a molecular ratchet and pawl model would select forward movement that *ipso facto* prohibits backward movement and does so solely by random thermal motion of Brownian particles. On the surface, it appears to be feasible. However, upon further

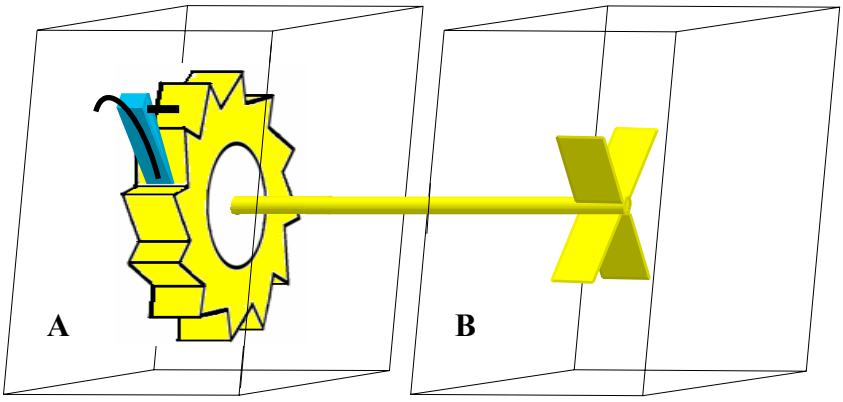

Figure 1.2.1. Feynman's *Gedankenmaschine*, or Thought Machine: A Molecular Ratchet and Pawl. Adapted from ref. 14

analysis, Feynman describes the complications arising in such a system and concludes such a thing to be impossible. This ratchet (yellow) and pawl (blue) are contained in box A at some temperature and are connected to a vane in a second box (B) by an axle at the same temperature. The pawl engages the ratchet and is held in place by a spring (black). Brownian motion in box B would cause the vane to move randomly. Sometimes it would vibrate in a left-handed fashion, and sometimes in a right-handed fashion. In our figure, the pawl and gear would serve to discriminate between oscillations of the vane, preferentially allowing forward, and in this case left-handed motion. However, this would violate Carnot's hypothesis and the second law of thermodynamics.[14] A closer examination of the system reveals the problems. When the pawl moves over a tooth of the gear it must be returned to its energy minimum for the system to work, and this is accomplished via the spring. Without the spring, the pawl would not discriminate between motion in one direction or another and would not be terribly useful as a ratchet. Moving against the force of the spring requires energy. For the pawl to move over the tooth, its energy barrier, the vane must transfer enough

energy to overcome the barrier to rotation. Now let us assume the vane has added enough energy to move the pawl up in box A and allow rotation. There is now enough energy in box A to overcome the barrier to rotation and it cannot dissipate. We remember that the spring, pawl, and gear are all experiencing the same fluctuations and oscillations moving the vane. The energy input causes the contents of box A to oscillate faster and now if the vane moves in the reverse direction, the pawl is just as likely to be up as it is down. Thus, Feynman's hypothetical thermally driven molecular ratchet ends up doing nothing.

A variation on this theme was Smoluchowski's trapdoor (Figure 1.2.2).[15,16,17] In this thought experiment we have a gate held in place by a spring and hinged in such a way that it can only swing to the right. When a highly energetic molecule hits the spring-loaded gate from the left-side it moves allowing the molecule to move to the right side. However, a molecule approaching from the right-side of the gate will not be allowed through. Again, the gate cannot dissipate heat so it begins to oscillate and vibrate from the molecular interactions and soon cannot discriminate between molecules on the right or on the left allowing them to move at random. Our two compartments are isoenergetic and the energy barrier to movement between the

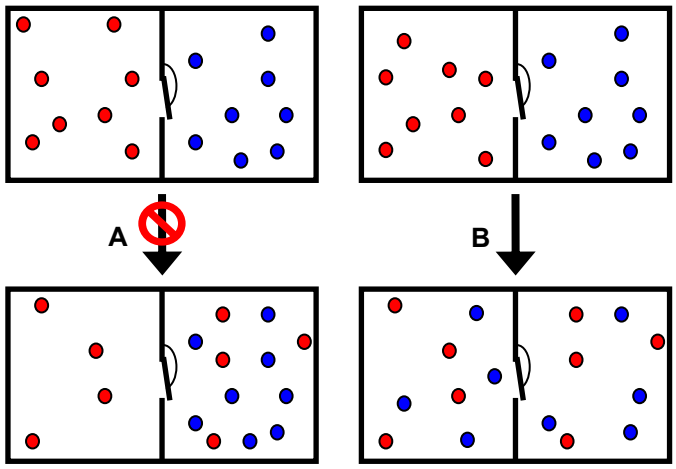

Figure 1.2.2. Smoluchowski's trapdoor.

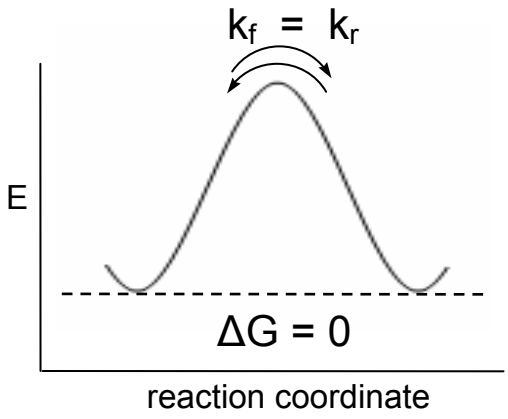

Figure 1.2.3. Principle of microscopic reversibility; for two isoenergetic ground states $k_f = k_r$.

two compartments is equal. This is the principle of microscopic reversibility. For two states of equal energy, the energy barrier for the forward and reverse directions must be equal (Figure 1.2.3). The molecules never stop analyzing the reaction pathways, or possibilities. Put another way it means that given enough time all possible reaction pathways are equally probable and the lowest energy pathway will be followed.

While theory states that a thermally driven ratchet is not possible, many chemically driven examples of molecular ratchets, such as the ATP synthase, exist in the natural world.[18,19] Each utilizes a gradient or external power source to drive movement of the ratchet. For example, the structure of ATP synthase is composed of two distinct parts; there is an F_1 power stroke motor and an F_0 Brownian ratchet, which interact to form adenosine triphosphate (ATP), the energy currency of life, from adenosine diphosphate (ADP) and inorganic phosphate.[19] A shaft, the γ-subunit, ties the power stroke motor to the Brownian ratchet. The potential energy surface of the F_0 ratchet is controlled by a membrane potential, and as ions cross an ion channel in the enzyme, the thermal fluctuations of the ratchet are biased in one direction. As long as the potential is favorable the molecular ratchets keeps ATP synthase from reversing direction. In this manner proteins, such as ATP synthase, utilize random thermal energy and intermolecular attractions to produce mechanical energy from chemical energy.

Stating something is impossible often seems an invitation for others to challenge the validity of such a statement. This invitation is not lost on chemists and has lead some to design molecular systems that probe Feynman's *Gedankenmaschine*. One of the most interesting and controversial additions to the literature on synthetic molecular ratchets came from T. Ross Kelly's laboratory at Boston College.[20,21] Over the course of several publications, Kelly proposed the synthetic basis for a thermally driven molecular ratchet. While molecular motors and ratchets are ubiquitous in nature[19] none are exclusively thermally driven and to suggest such a device, let alone attempt to build one, might be considered scientific heresy as the previously mentioned and well-established theory argues against the possibility of such a device.[22] However, it has been noted that theory does not dictate experimental result, but should rather describe it and predict future results.

Kelly's exploration of Feynman's ratchet was one of the first attempts to synthesize a true thermally driven molecular ratchet.[21] Previous work by Kelly *et al.* had produced a "molecular brake" which utilized a triptycene connected to a 2,2'dipyridyl via a single covalent bond between carbon five of the dipyridyl group and the triptycene bridging carbon as shown in Figure 1.2.4.[23] This brake could be turned on or off by addition or removal of a metal ion, respectively. Addition of Hg^{2+} turned the brake "on" by coordinating the two nitrogens of the dipyridyl forcing a conformational change in the molecule, which resulted in one ring of the dipyridyl being forced between two of the phenyl rings on the triptycene. This imposed an energy barrier to rotation of triptycene in the form of steric interactions. At room temperature little or no rotation was observed using variable temperature NMR. At

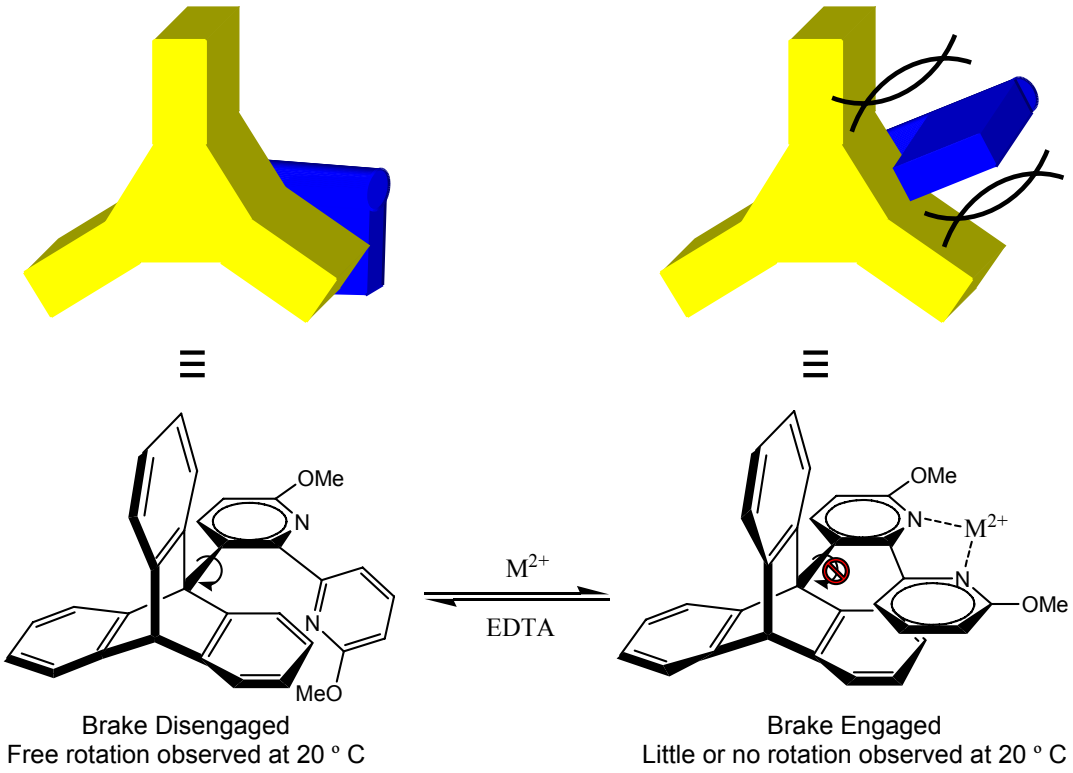

Figure 1.2.4. Kelly's molecular brake.

higher temperatures the brake was observed to slip periodically, and rotate slowly as the molecule gained enough energy to overcome the barrier to rotation. Removal of the coordinating mercury ion with EDTA lowered, or released the energy barrier thus allowing free rotation of the triptycene at room temperature. This research set the stage for Kelly's series of publications exploring molecular ratchets based on a triptycene gear.

Armed with the previous data Kelly developed a novel ratchet system utilizing triptycene and helicene that is analogous to Feynman's molecular ratchet possessing: a gear, a pawl which permits only unidirectional rotation, and a spring which prevents the pawl from disengaging the gear (Figure **1.2.5b**).[20,24] It is essentially Feynman's ratchet

with an axle length of zero, with the gear and vane incorporated into one structure (**1.2.5a**). In the working molecular analogue triptycene serves as the gear and vane, [4]helicene as the pawl, and the sigma bond between the two acting as the spring preventing the helicene from disengaging the triptycene (Figure 1.2.6).

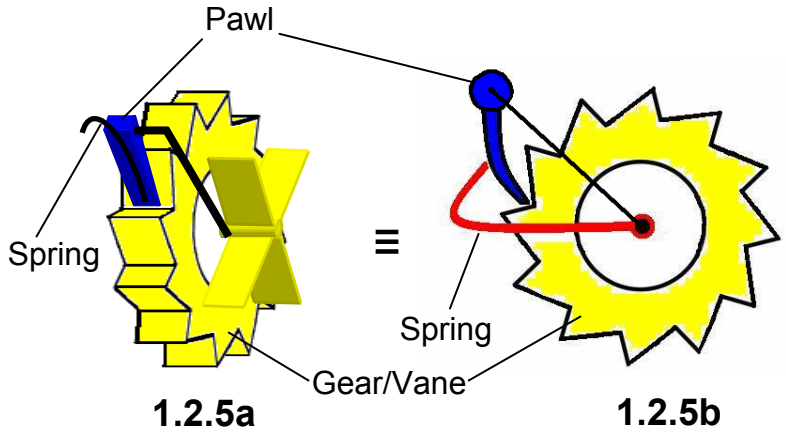

Figure 1.2.5. Kelly's vision of a molecular ratchet.

Of particular interest to Kelly was the calculated energy diagram for rotation, which was asymmetric, indicating the potential for unidirectional rotation, which Kelly hoped to use to explore the possibility of the forward and reverse rates being unequal for two isoenergetic energy minima (Figure 1.2.7). Room temperature proton NMR

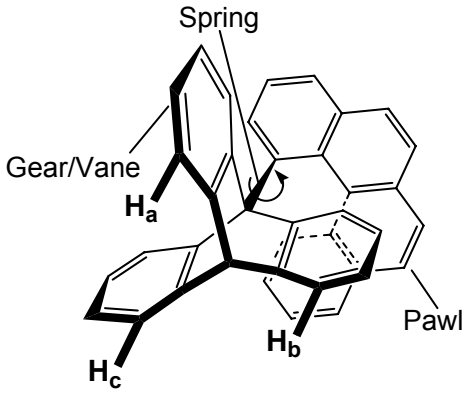

Figure 1.2.6. Kelly's proposed thermally-driven molecular ratchet.

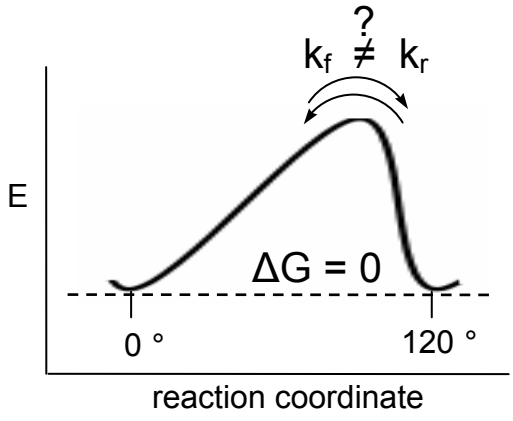

Figure 1.2.7. Asymmetric energy potential calculated for Kelly's molecular ratchet.

experiments revealed the ratchet system was immobile with one distinct ^{1}H NMR signal for each of the three protons indicated in Figure 1.2.6 of the triptycene, however high temperature spectra showed slow rotation. To determine the direction of rotation spin polarization transfer NMR experiments were utilized. Two possible outcomes were possible. The first potentially mind blowing possibility was observing polarization transfer to only one of the two other proton peaks which would indicate unidirectional motion. The second possibility would be equal transfer to both proton peaks indicating bidirectionality of movement, or equal rotation in both directions. The results were clear. The rate in the forward and reverse directions was equal regardless of the asymmetric nature of the potential as shown in Figure 1.2.8. For many the experimental outcome was reassuring, as equal transfer to both of the other protons was observed. The second law and the principle of microscopic reversibility survived the trial.

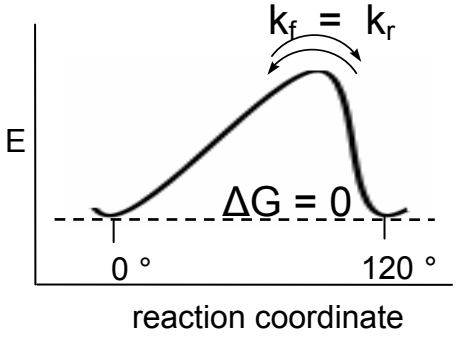

Figure 1.2.8. Kelly's thermally-driven molecular ratchet fails; $k_f = k_r$.

From the ashes of his thermally driven molecular ratchet Kelly developed a chemically driven system.[25] As seen in Figure 1.2.9, a means was devised to introduce an energy barrier, or brick wall as Kelly put it, to reverse rotation. This high-energy barrier serves as a trap preventing rotation back to the low-energy conformation and the now reduced barrier, or energy of activation, to rotation presents an exergonic pathway to the more stable rotational conformation. In effect, the energy potential was modulated by addition of a high-energy chemical species similar to natural processes

such as those found in F_0 browning ratchet of ATP synthase that uses a membrane potential to rectify the thermal balance.

To effect this modulation of potential an amine was added to one ring of the triptycene and a hydroxypropyl tether was added to the end of the helicene (Figure 1.2.9). Through careful separations at low temperatures, each of the rotational conformers could be isolated. In Figure 1.2.9 proton H_A is labeled for reference. Addition of phosgene to **1.2.9a** converted the amine to its corresponding isocyanate **1.2.9b** priming the system for reaction. When the [4]helicene rotates clockwise **1.2.9c** the alcohol approaches and reacts with the isocyanate producing a urethane linkage which traps the ratchet in a high energy conformation **1.2.9d**. Counter clockwise rotation was impossible requiring spontaneous cleavage of a stable covalent bond,

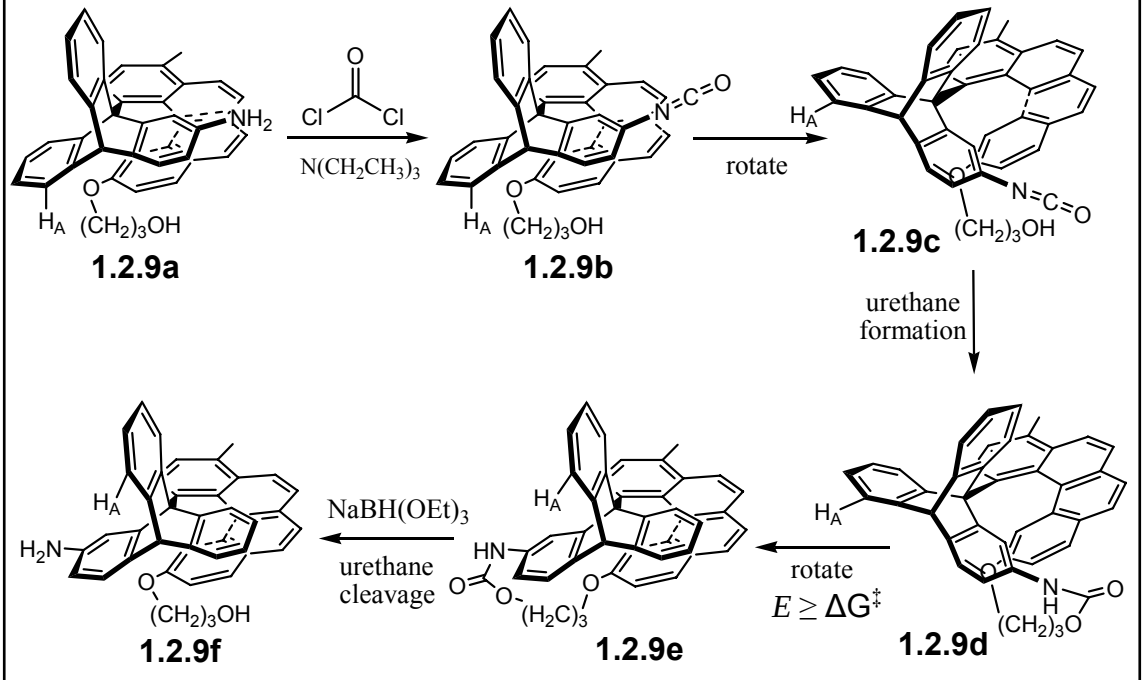

Figure 1.2.9. Kelly's successful molecular ratchet powered by phosgene. Adapted from ref. 25.

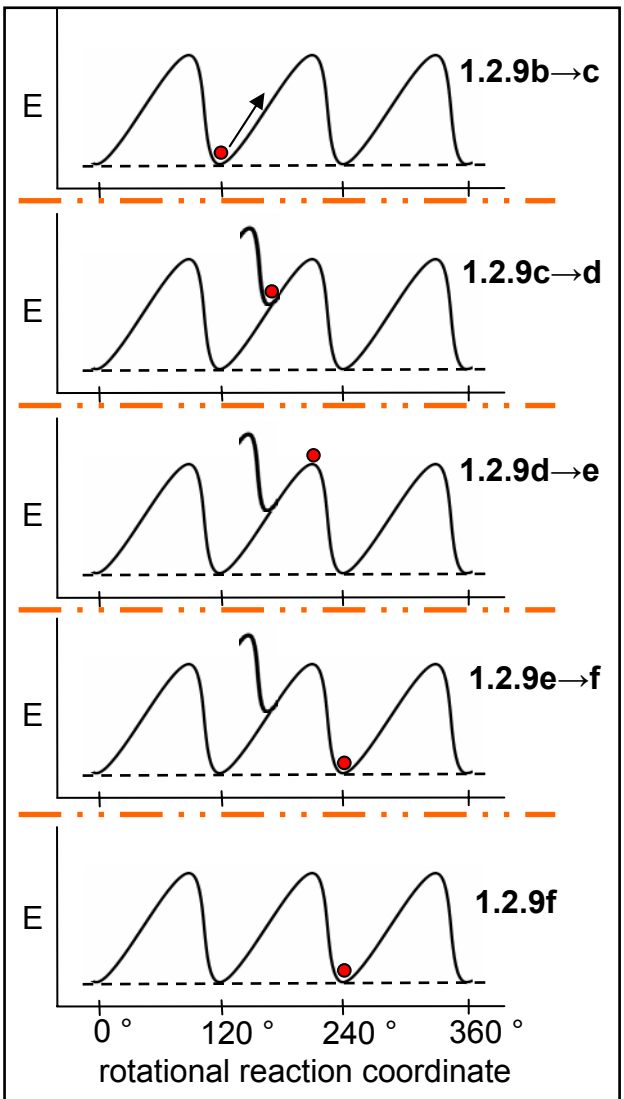

Figure 1.2.10. Introduction of a barrier to reverse reaction makes $k_f < k_r$.

leaving clockwise rotation to the low-energy conformation **1.2.9e** the only pathway available. After rotation to this conformer, the urethane group is chemically cleaved giving the associated rotational conformer **1.2.9f**. Treatment of the new conformational isomer with isocyanate did not produce the reverse rotation.

In Figure 1.2.10, we see the energy coordinate diagrams for the various stages of rotation and reaction. We begin with **1.2.9b→c** where moving in a clockwise direction allows interaction between the reactive groups forming a covalent bond and a barrier to reverse rotation as shown by **1.2.9c→d**. Ambient temperatures drive the clockwise rotation over the lower energy barrier (**1.2.9d→e**) forming the more thermodynamically stable conformation (**1.2.9e→f**). Thus, Kelly *et al*. achieved unidirectional rotation in his triptycene-helicene based system forming **1.2.9f**, but not without significant addition of energy in the form of phosgene and bench work.

Examples of synthetic molecular motors similar to Kelly's working ratchet, which require selective energy input to operate, are numerous in the literature.[26,27] These ratchets and shuttles utilize a variety of energy sources to stimulate conformational change including photochemical, electrochemical (oxidation/reduction), and chemical (coordination, bond forming/break, pH). Some of the more interesting examples utilize photoisomerization to induce energy differences between several electronic states driving unidirectional motion. The first system utilizing photoisomerization to induce unidirectional rotation between electronic states was developed at the same time Kelly was synthesizing his thermally driven molecular ratchet system. Feringa and Harada used repetitive cycles of photo- and thermal isomerization in biphenylanthrylidenes to produce the first synthetic rotor to undergo unidirectional rotation via photochemical isomerization.[27]

The systems consisted of a set of four distinct steps in which the molecule was irradiated to form a high energy conformation, allowed to relax to a lower energy conformation, irradiated again to a new high energy conformation, and finally allowed to relax back to the original conformation (Figure 1.2.11). In the first system developed irradiation of (*P*,*P*)-*trans*-**1.2.11a**, at low temperatures where 280 nm $\geq \lambda <$ 380 nm, causes isomerization of the double bond connecting the two halves of the molecule which inverts the helicity and causes the axial methyl groups to rotate to the higher-energy, less favorable equatorial orientation. This isomerization produces the high-energy strained (*M*,*M*)-*cis*-**1.2.11b** conformation which suffers from steric interactions between the two methyl groups. Upon heating to 20 ° C an irreversible helical inversion occurs and the equatorial methyl groups flips back into the more favorable

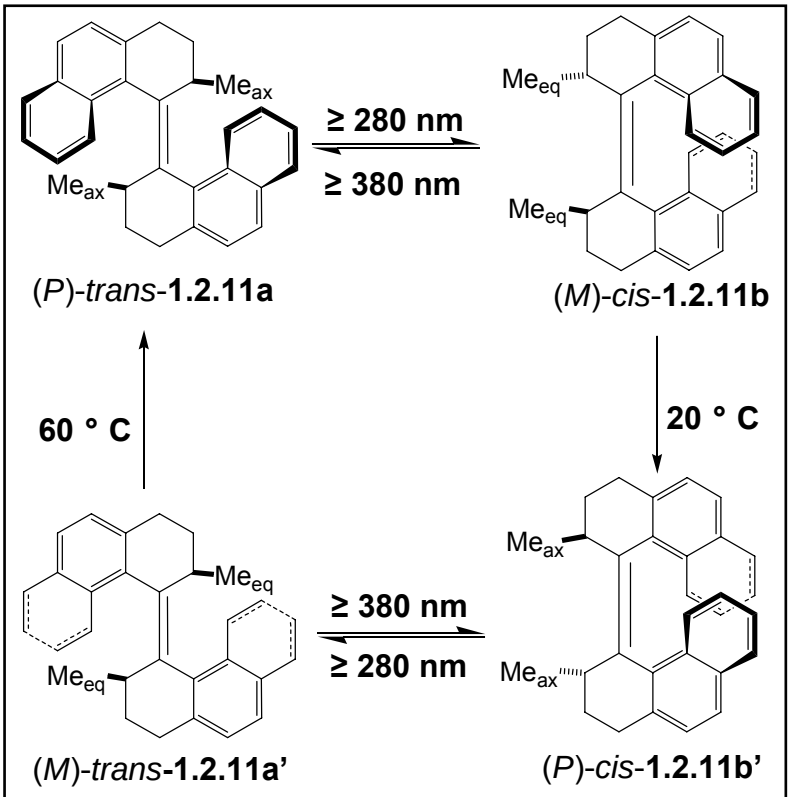

Figure 1.2.11. Feringa's first photochemically driven molecular ratchet. Adapted from ref. 27.

axial position releasing the steric strain on the system and producing the lower-energy cis-conformation (*P,P*)-*cis*-**1.2.11b'**. At this point, the molecule has undergone an internal 180 ° rotation from its starting conformation. Another irradiation/isomerization cycle using the same wavelengths converts the cis-isomer to the trans-isomer (*P,P*)-*trans*-**1.2.11a'** again inverting the helicity and causing the methyl carbons to flip back to a higher-energy equatorial position. Heating to 60 ° C completes the 360 ° rotation by allowing another irreversible helical inversion producing the more stable isomer (*P,P*)-*trans*-**1.2.11a** in which the methyls are in the less sterically demanding axial orientation. The orientation of the methyl group, either low energy axial, or high-energy equatorial, along with an irreversible helical inversion controlled the directionality of the system. This was the first synthetic system in which controlled unidirectional motion of a rotor was observed.[27]

Building on this success asymmetric designs were synthesized that eliminated the inherent difficulties in studying the symmetric biphenylanthrylidene system[27], allowed for tuning of the rotational barriers[28], and aided development of a system capable of being mounted to a surface.[29] The first of the "second-generation" series incorporated 2-methyl-2,3-dihydrothiopyran helicene and a (thio)xanthene bearing various functional groups used for tuning the rate of rotation. As with the symmetric system the asymmetric rotor displayed controllable unidirectional rotation based on a series of photochemical excitations and thermodynamically controlled relaxations as shown in Figure 1.2.12.[28,30] Irradiation of (*M*)-*trans*-**1.2.12a** at 365 nm causes isomerization of the double bond which inverts the helicity and causes rotation to the

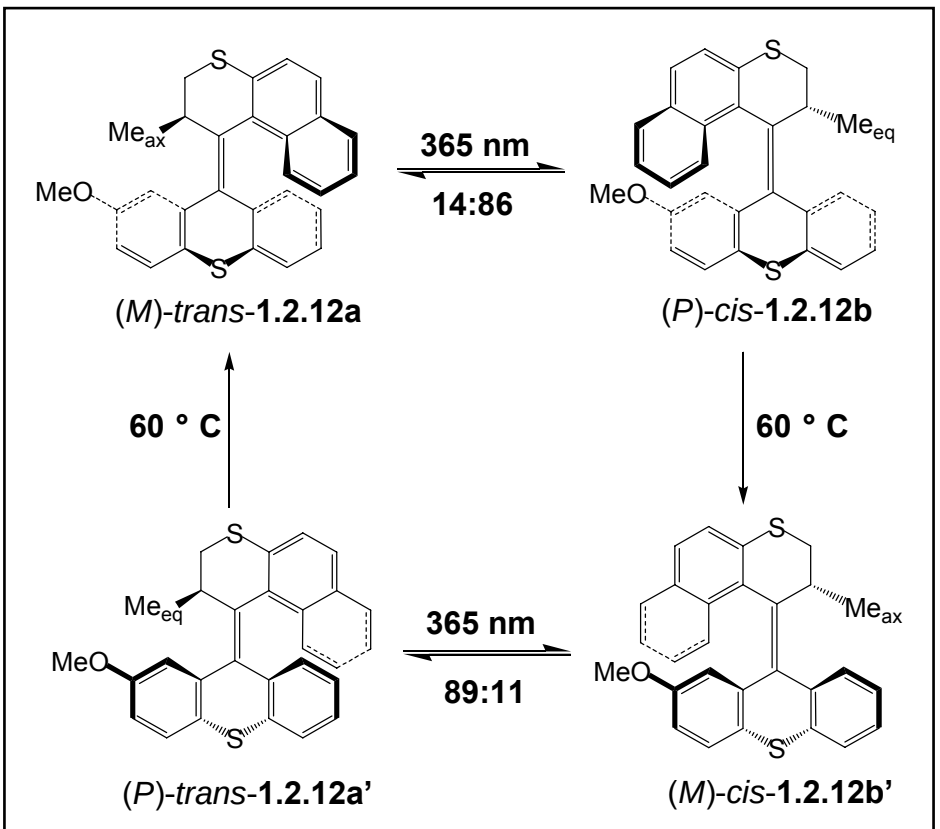

Figure 1.2.12. Feringa's second generation ratchet. Adapted from ref. 28.

higher-energy, less favorable equatorial orientation found in (*P*)-*cis*-**1.2.12b**. Upon heating to 60 ° C an irreversible helical inversion occurs and the equatorial methyl groups flips back into the more favorable axial position releasing the steric strain on the system and producing the lower-energy cis-conformation (*M*)-*cis*-**1.2.12b'**. At this point, the molecule has undergone a 180 ° rotation from its starting conformation. Another irradiation/isomerization cycle using the same wavelength converts the cis-isomer to the trans-isomer (*P*)-*trans*-**1.2.12a'** again inverting the helicity and causing the methyl carbon to flip back to a higher-energy equatorial position. Heating to 60 ° C completes the 360 ° rotation by allowing another irreversible helical inversion producing the more stable isomer (*M*)-*trans*-**1.2.12a** in which the methyl resides in the less sterically demanding axial orientation.

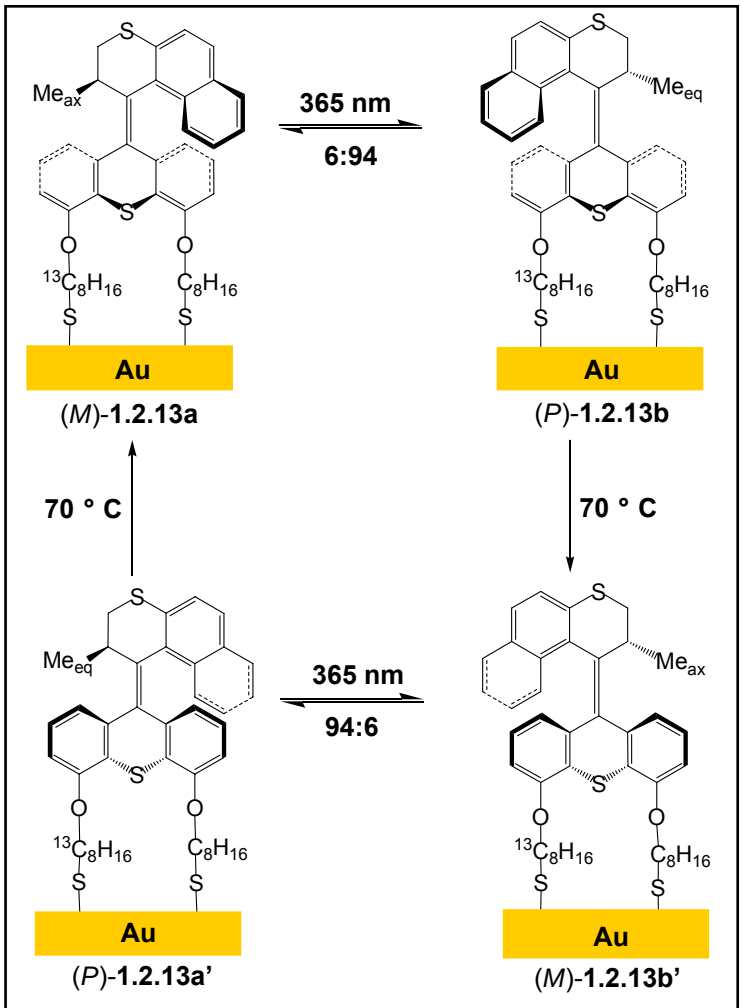

Figure 1.2.13. Surface anchored second-generation ratchet. Adapted from ref. 29.

The ultimate goal of attaching the rotor to a solid surface was realized recently

using a gold nano-sphere support and sulfur bearing tethers appended to the (thio)xanthene (Figure 1.2.13)[29] where one tether was isotopically labeled. Clockwise rotation of the rotor was directly observed by CD spectroscopy and indirectly by ^{1}H NMR spectroscopy. As with the previous ratchets presented by Feringa *et al*, photoisomerization of one isomer (*M*)-**1.2.13a** produced a high energy rotamer (*P*)-**1.2.13b**. This high-energy rotamer underwent a thermally-induced irreversible rotation to form (*M*)-**1.2.13b'**, which was again photochemically isomerized to high-energy conformer (*M*)-**1.2.13a'**. Another irreversible thermal relaxation produces the initial rotamer (*M*)-**1.2.13a**. The importance in appending the ratchet to a surface lies in the fact that a motor cannot do work without a stator, or some stationary surface against which to perform its function.

Another system used sequential photoisomerization of a [2]-catenane system that caused one ring to move around the other ring in a single direction.[26] Leigh's initial experiments were conducted using a [2]catenane system incorporating three binding sites into one ring of a catenane with each binding site having a lower binding affinity for a second, smaller ring than the one before it (Figure 1.2.14). Two strongly hydrogen bond donating amide fumaramides and a succinic amide ester were utilized as binding sites. The amide fumaramides are unique in that photoisomerization from the *E*- to the *Z*-isomer of maleamide greatly reduces their hydrogen bond donor characteristics. Furthermore, by functionalizing a fumaramide with benzophenone, the wavelength at which photoisomerization takes places could be tuned making it possible to isomerize one of the two selectively using wavelengths of 350 and 254 nm, respectively. Utilizing this fact, sites **A** and **B** were equipped with a benzophenone

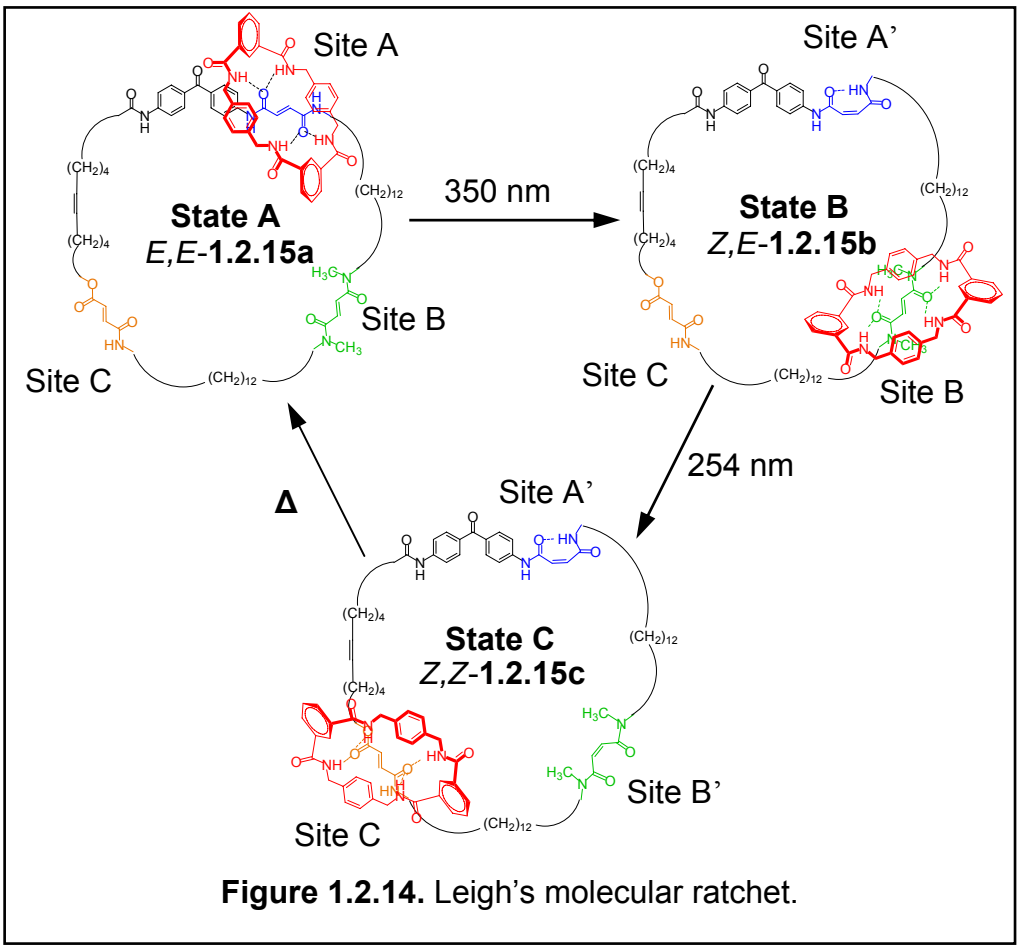

Figure 1.2.14. Leigh's molecular ratchet.

functionalized secondary and a non-functionalized tertiary amide fumaramide, respectively. The small ring possessed hydrogen bond donating benzylic amides capable of discriminating between the *E*- and *Z*- isomers.

Photoisomerization of the region with the highest binding affinity **A** for the smaller ring causes that region to become the region with the lowest binding affinity, or **A'**. The ring then travels to the second binding site (**B**) that now has the highest binding affinity of the three. After an additional photoisomerization, the region with the highest binding affinity (**B**) becomes the second lowest (**B'**) and the ring now travels to the region previously possessing the lowest affinity (**C**), but now possessing the highest affinity for the ring. Thus, the ring moves to the third binding site. A final thermal step

converts all the binding regions back to their initial configurations/energies (**A'** to **A** and **B'** to **B)** allowing the process to repeat. It is important to note this [2]catenane systems displays unidirectional motion only as a state function and ignores the actual translocation pathway. Photoisomerization does not direct movement of the smaller ring around the larger and thus translational isomerization can occur in either direction settling into the most thermodynamically stable conformation.

In an attempt to facilitate unidirectional motion another identical small ring was introduced producing a [3]catenane which could potentially block translation of the first ring in one direction in a sort of "follow-the-leader" isomerization process.[26] Photoisomerization of each binding group would occur as in the [2]catenane example with each small ring positioned over one of the two most strongly donating groups. However, it was found that while the barrier to reverse motion was increased substantially it was not eliminated, and again the rotation could only be described as unidirectional in state but not in process.

In conclusion, each of the previous molecular ratchets, or motors, possesses several common characteristics. They each had a function, which was to rotate in a single direction, either by process or by state function. Various techniques could be employed to observe this rotation. The rotation was cyclical and the rates at which they performed the rotations could be measured. Finally, each system required the selective input of energy, chemical or photochemical, to rectify the energy potential and cause forward rotation of the various components.

Let us turn our attention to the characteristic that allowed these ratchets to move in a cyclical manner. They all had at least two low energy states that an outside force

could modulate causing motion of the molecular components. There were two distinct low energy states present in work by Kelly and Feringa, while Leigh's design possessed three. In each case, modulating the energy potential raised the energy level of one conformation and/or lowered the other presenting a thermodynamic ultimatum of sorts preventing, or largely limiting, unproductive relocation.

As molecular motors all possess at least two stable conformations, certain catenanes and rotaxanes lend themselves well for use in molecular machines as their synthesis directly involves the desired multistable characteristics. This being the case Stoddart, one of, if not the most prolific contributor to the field of synthetic molecular machines this decade, entered into the study of these systems by developing an efficient means of catenane formation, a review of which will be presented in the following sections.

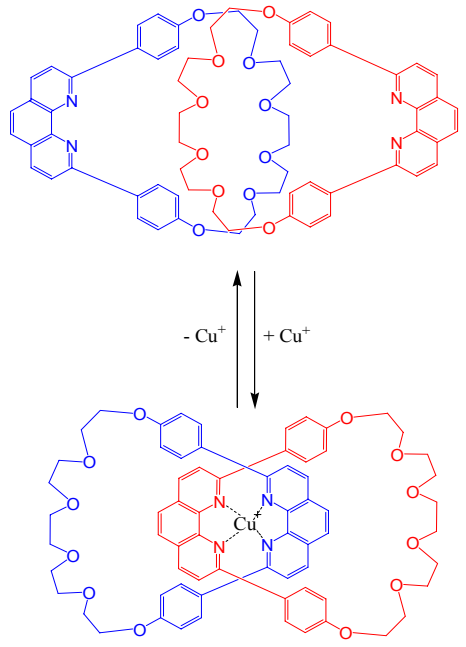

Figure 1.3.1. Sauvage transition metal [2]catenane switch.

Section 1.3 Template Directed Synthesis and Catenane Motion

The template directed synthesis of catenanes and rotaxanes has been a rich and productive vein of research.[7,31] Non-covalent bonding interactions between electron donors and acceptors provide an efficient means of catenane and rotaxane synthesis.[32] The synthesis of catenanes

bearing two or more binding sites using this methodology provides ready access to one key components of molecular machinery as described in the previous section.

Sauvage and Dietrich-Buchecker synthesized the first of these template-directed or self-assembling molecular machines, in this case a switch, utilizing the non-covalent bonding interactions copper cations with phenanthroline ligands as shown in Figure 1.3.1.[33,34] Demetallation of the Cu^{+} complex resulted in a change of conformation. More complex systems were developed involving the oxidation/reduction of the metal cation (Figure 1.3.2).[31,35,36,37] Oxidation of Cu^{+} in catenane **1.3.2a** to Cu^{2+} produced a high energy conformation which was immediately followed by rotation to intermediate catenane **1.3.2b**. Another rotation produced the lowest energy, most energetically favorable conformation catenane **1.3.2b'**. Reduction to catenane **1.3.2a'** was followed by two rotations reforming the starting complex. In this manner, the catenanes could be switched from one conformation to another via an external input much like Leigh's

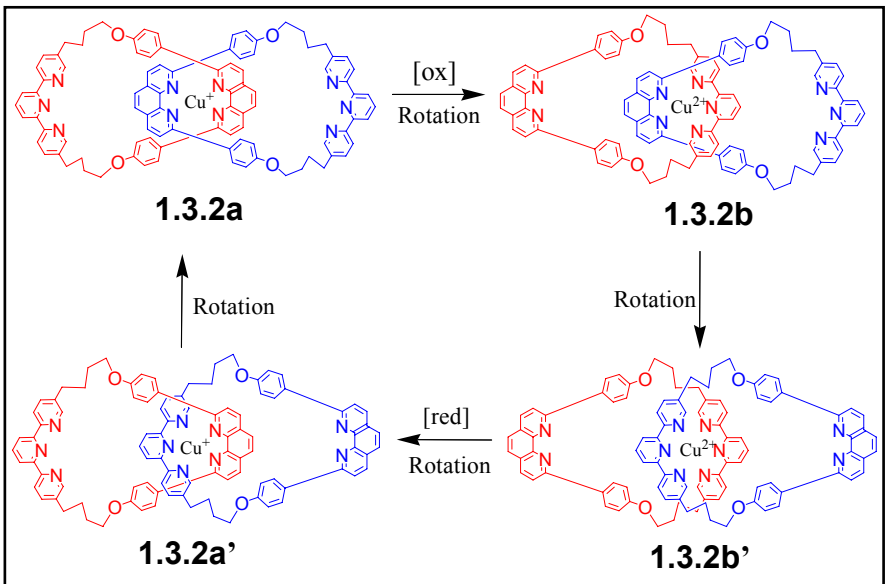

Figure 1.3.2. Oxidation-Reduction controlled switching of a catenane.

rotor. Unfortunately, it also had the characteristic that there was no discrimination in how the different conformations were achieved. Circumrotation was not restricted to a certain direction.

Rather than use metal-ligand interaction for catenane formation Stoddart chose another type of non-covalent bonding interaction involving electron-rich and electron-deficient recognition, or binding sites.[31,32] This method of catenane formation followed the seminal discovery that quaternary ammonium salts would form stable inclusion complexes with certain phenyl crown ethers.[32,38,39] More important, from our perspective and that of [2]catenane formation, was the inclusion complex formed in a solution of N,N'-dimethyldipyridinium and bisparaphenylene-34-crown-10, or more simply BPP34C10.[40] Stoddart *et al.* discovered that [2]catenanes could be formed in high yield using electron rich BPP34C10 and electron poor bis(dipyridinium) salts.[41] The high degree of order in solution was attributed to π-π stacking of the phenyl rings, hydrogen-bonding between the methylene hydrogen and oxygen of the hydroquinone, T-type hydrogen bonding, and electrostatic interactions.[42] As shown in Figure

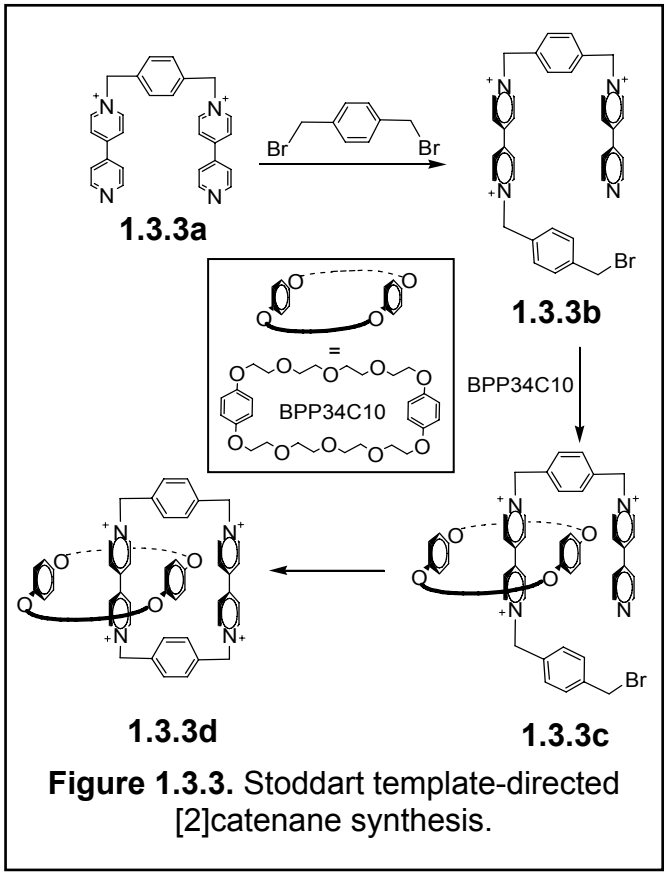

Figure 1.3.3. Stoddart template-directed [2]catenane synthesis.

1.3.3, addition of 1,4-bis(bromomethyl)benzene to dicationic bis(dipyridinium) **1.3.3a** produced tricationic species **1.3.3b**. In the presence of BPP34C10 the pseudorotaxane inclusion complex **1.3.3c** formed. A second substitution reaction closed the ring converting the pseudorotaxane into [2]catenane **1.3.3d** in 70 % yield. Numerous catenanes were produced using this technique with great success.[32]

By varying the strength of the bonding interactions it was found that one catenane conformation could be favored over another conformation. An example of this is shown in Figure 1.3.4.[42] Bonding interactions between the resorcinol containing crown ether and dipyridinium were significantly less favorable those with hydroquinone as seen by the relative concentrations, measured in the ^{1}H NMR spectrum, of 98 to 2 and 97 to 3 for catenanes **1.3.4a** and **1.3.4b**. The importance of this concept will become clear in the following chapters.

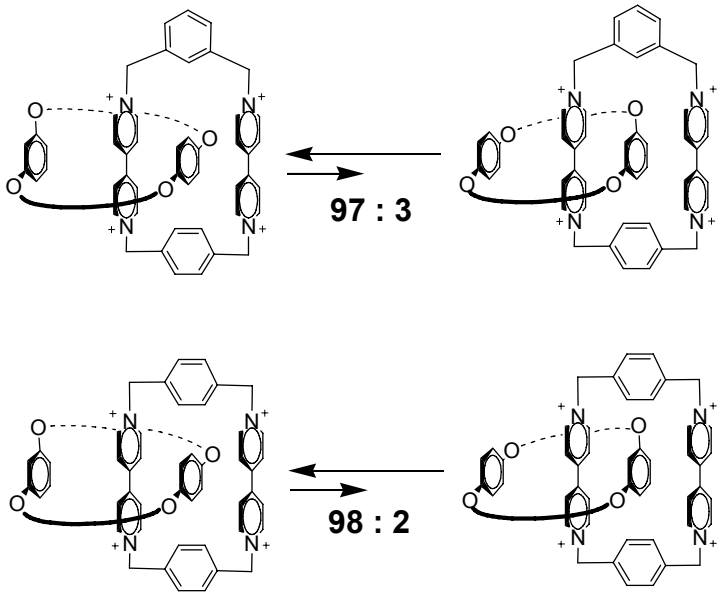

Figure 1.3.4. Equilibrium mixtures of [2]catenanes with different K_a.

Stoddart and company found that nuclear magnetic resonance (NMR) spectra for these catenanes were highly temperature dependent.[41] The spectrum of the catenanes would grow increasingly complex as temperatures were lowered. It was determined

that these [2]catenanes undergo four discernible types of motion, of which three were capable of being observed via variable temperature proton nuclear magnetic resonance (VT ^{1}H NMR). These three movements are shown in Figure 1.3.5. Type I motion, described as pirouetting, involves the electron-rich phenyl rings of BPP34C10 exchanging inside and alongside one of the electron poor-dipyridiniums. Type II

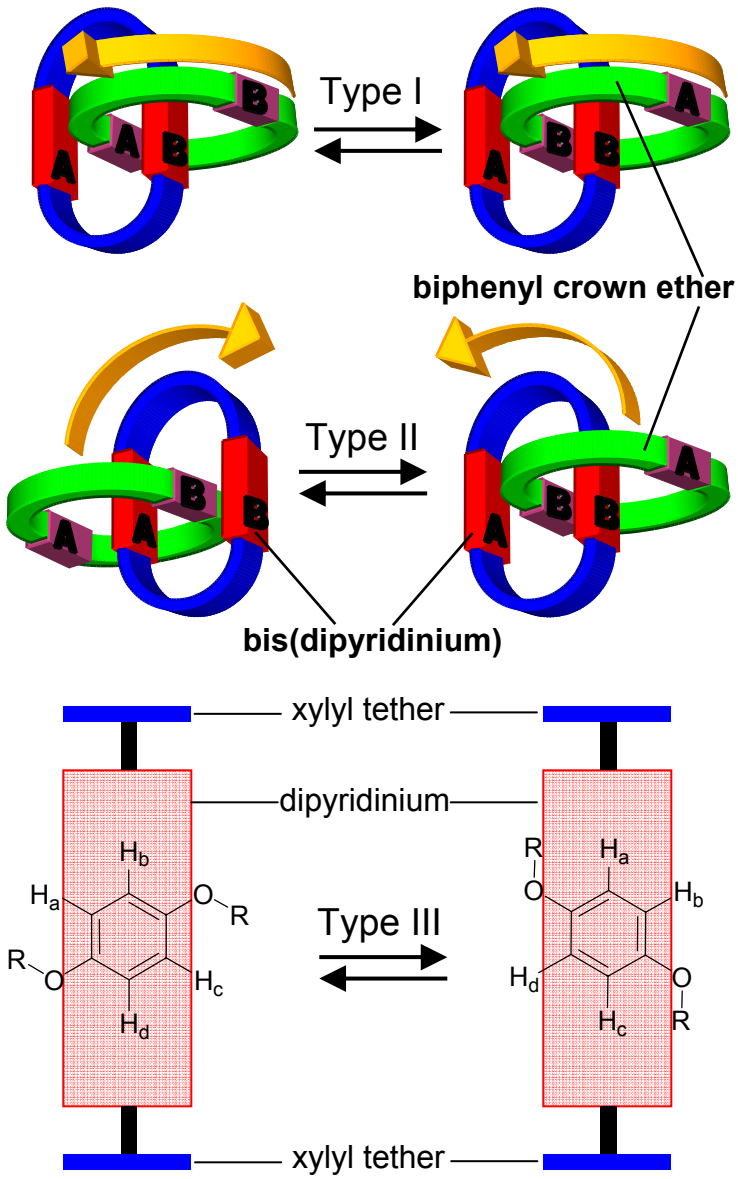

Figure 1.3.5. Types of movement associated with [2]catenanes.

motion, also described as circumrotation, involves BPP34C10 migrating from one dipyridinium to the other. While Figure 1.3.5 only shows pirouetting about dipyridinium **B**, the same movement around dipyridinium **A** is also possible. Similarly, circumrotation, or Type II motion, can occur over both top and bottom xylyl tethers. The third motion, Type III, involves one phenyl ring of BPP34C10 tilting, or rocking in the interior of the dipyridiniums. These three movements can be followed via VT ^{1}H NMR for which coalescence temperatures ($\mathbf{T_C}$) and chemical shift differences for the exchanging proton signals ($\mathbf{\Delta\upsilon}$) can be determined. A fourth type of movement involves displacement and reentry of bismetaphenylene-23-crown-10 (BMP32C10) into the bis(dipyridinium) interior but does not concern our study as this crown ether was not used.

Using values of $\mathbf{T_C}$ and $\mathbf{\Delta\upsilon}$ to calculate the free enthalpy of activation $\mathbf{\Delta G^{\ddagger}}$ is a well-established practice[43] and was employed to calculate the free enthalpy of activation $\mathbf{\Delta G^{\ddagger}}$ for the three types of movement.[42] From the Eyring equation we can obtain the following equation:

$$\mathbf{\Delta G^{\ddagger} = (4.58 \times 10^{-3})(T_C)[10.32 + \log(T_C/\mathit{k}_C)]}$$

which can be simplified to:

$$\mathbf{\Delta G^{\ddagger} = (4.58 \times 10^{-3})(T_C)[9.972 + \log(T_C/\Delta\upsilon)]}$$

and used to calculate $\Delta G_C^{\ddagger}$ in kilocalories per mole (kcal/mol) directly from the values obtained from the ^{1}H NMR spectra. For Stoddart's simple [2]catenanes, Type I movement was the most energy intensive having free energies of activation between 14 and 17 kcal/mol. This type of motion requires breaking all of the stabilizing bonding interactions. Movements of Type II and III were less energy intensive with values between 10 and 12 kcal/mol, due to breaking of only half of the stabilizing interactions. In addition to calculating the $\Delta G^{\ddagger}$ it is also to possible to calculate ΔG^{0} based on the relative abundance of conformers in solution measured by integration of the two exchanging peaks. In this manner Stoddart *et al*. were able to characterize the types of isomerization observed in their catenanes.

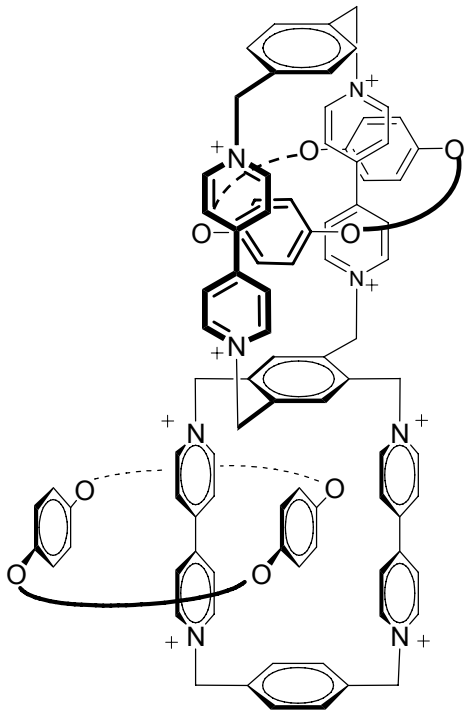

Figure 1.3.6 Stoddart's bis[2]catenane

One final note on Stoddart's work involves an interesting bis[2]catenane in which the *p*-xylyl tethers of two catenanes are fused as shown in Figure 1.3.6.[44] This catenane bears mentioning because it was the first in which one pathway of circumrotation was effectively blocked. In previous catenanes Type II circumrotation could occur by rotation over either the top or the bottom xylyl tether. Here only one pathway remains open. Unfortunately, the $\Delta G^{\ddagger}$ for translation of Type II was not reported so we do not have anyway to compare the activation enthalpy of

bis[2]catenane in Figure 1.2.6 with that of its mono[2]catenane analogue **1.3.3d**. As one pathway is removed there should be an associated increase in $\Delta G_C^{\ddagger}$ due to the decrease in entropy of activation caused by reaction pathway multiplicity.[45]

Section 1.4 Modulating the Potential Energy Surface

It is important to review the concept of modulating energy potentials as it drives all known molecular switches, rotors and motors.[8] As reviewed in the first section, Kelly's proposed thermodynamically driven ratchet possessed no means of modulating its energy potential. While the calculated energy potential was asymmetric, the free energy of activation in the forward and reverse directions were equal. In his chemically driven ratchet the free energy of activation for rotation was modulated via addition of a chemical reagent. After formation of the urethane linkage, the rotational activation energy was reduced by raising the free energy of the starting conformer and at the same time imposing a large barrier to reverse rotation. The system behaved as any other molecular ratchet and reaffirmed Feynman's thought experiment. Feringa and Harada's ratchets, as well as Leigh's to a certain extent, used photochemical isomerization to modulate an energy potential by converting low-energy conformations into high-energy conformations which could then relax to more favorable conformations only through forward motion.

In our research we sought to succeed where others failed through careful design and synthesis of a ratchet possessing a molecular gate and two isoenergetic binding sites that would preferentially select formation of one conformation over another without external energy input as depicted in Figure 1.4.1. An internal gate would provide the

means by which the energy potential could be modulated, essentially regulating movement of one group around another. Proof of the system's viability would come in the form of conformational population differences between two isoenergetic binding sites. While the ultimate goal has not yet been realized we have successfully demonstrated the ability to control movement between two binding sites by varying the

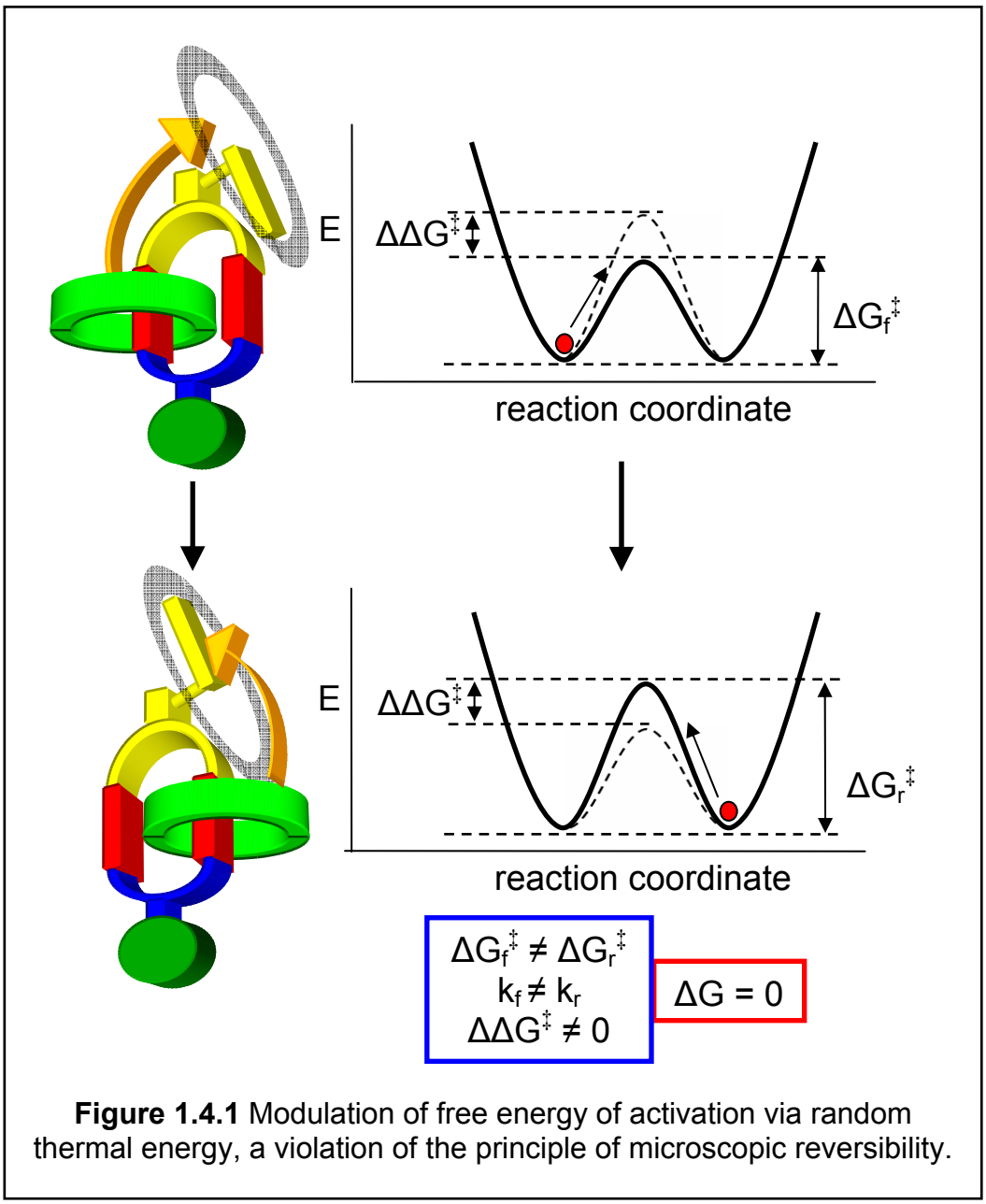

Figure 1.4.1 Modulation of free energy of activation via random thermal energy, a violation of the principle of microscopic reversibility.

gate size. This is the first step required to develop a molecular ratchet driven by random thermal energy. Now that we have laid the foundation for our studies and placed them in perspective by reviewing previous work we can begin the review of our work, the preparation and study of novel unbiased and biased [2]catenanes.

Chapter 2

Synthesis and Study of Symmetric [2]Catenanes

Section 2.1 Controlling Interconversion in [2]Catenanes

In order to control molecular motion in [2]catenane systems we must first demonstrate the ability to allow, or restrict, circumrotation of one ring around the other by selectively introducing an energy barrier. The example presented in Chapter 1 wherein circumrotation of BPP34C10 was limited to one pathway due to the presence of the second tetracationic macrocycle is an example.[44] However, no attempt was made to further restrict movement of the BPP34C10 or isolate one isomeric form. One could imagine a chain of such molecules, a tri[2]catenane for example, as seen in Figure 2.1,with a third tetracationic macrocycle inhibiting passage of the ring over the remaining pathway thereby trapping it. The BPP34C10 ring could no longer circumrotate, as doing so would require breaking a covalent bond and large amounts of energy. As we were interested in studying the

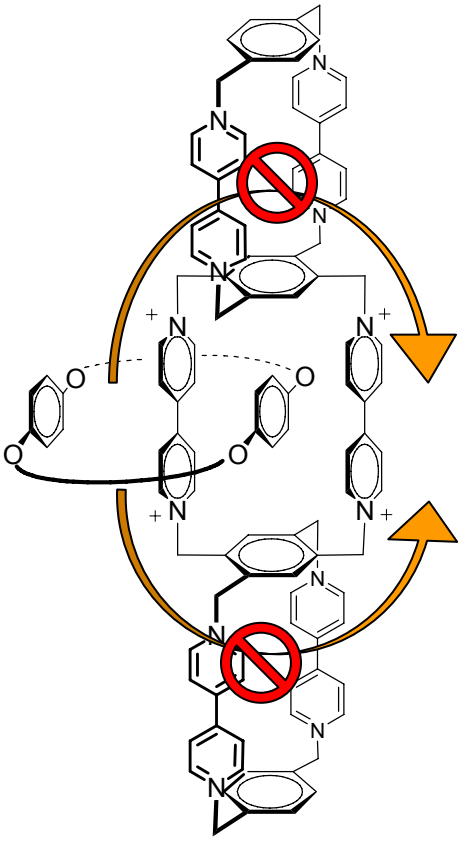

Figure 2.1.

dynamics of systems such as these it was necessary to eliminate some of the inherent problems in studying such complex systems (i.e. overly complex spectral data, signal overlap, cost of analysis).

To determine the extent translation could be restricted to a predetermined path, we designed a series of [2]catenanes wherein sterically bulky groups could be appended to either of two different phenyl ring spacers connecting two dipyridiniums.[46] With a blocking group attached to tether **B** as in Figure 2.2, translation occurs along Pathway **A** and over tether **A**. With Pathway **A** blocked via incorporation of a blocking group on tether **A**, interconversion occurs via Pathway **B**. With neither blocking group present on the tethers translocation would be allowed over Path **A** and **B**. Extending the work of Stoddart[32], we have prepared catenanes **2.1** thru **2.6** (Figure 2.3) possessing a resorcinol-based tether, containing either a large 'blocking' R-group, or a small 'open'

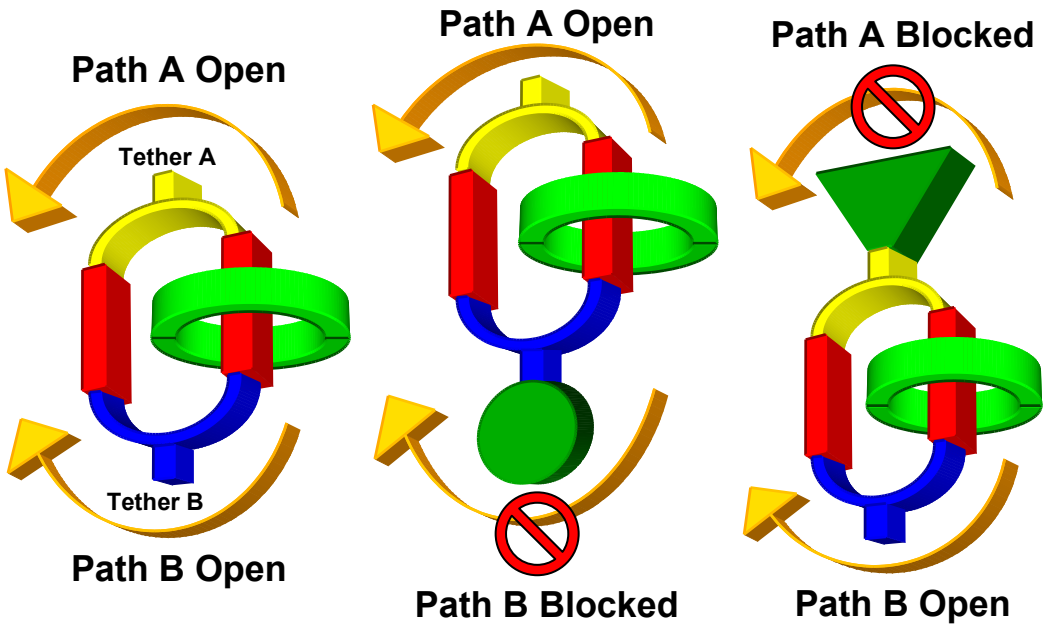

Figure 2.2. Cartoon Representation of Symmetric [2]Catenanes.

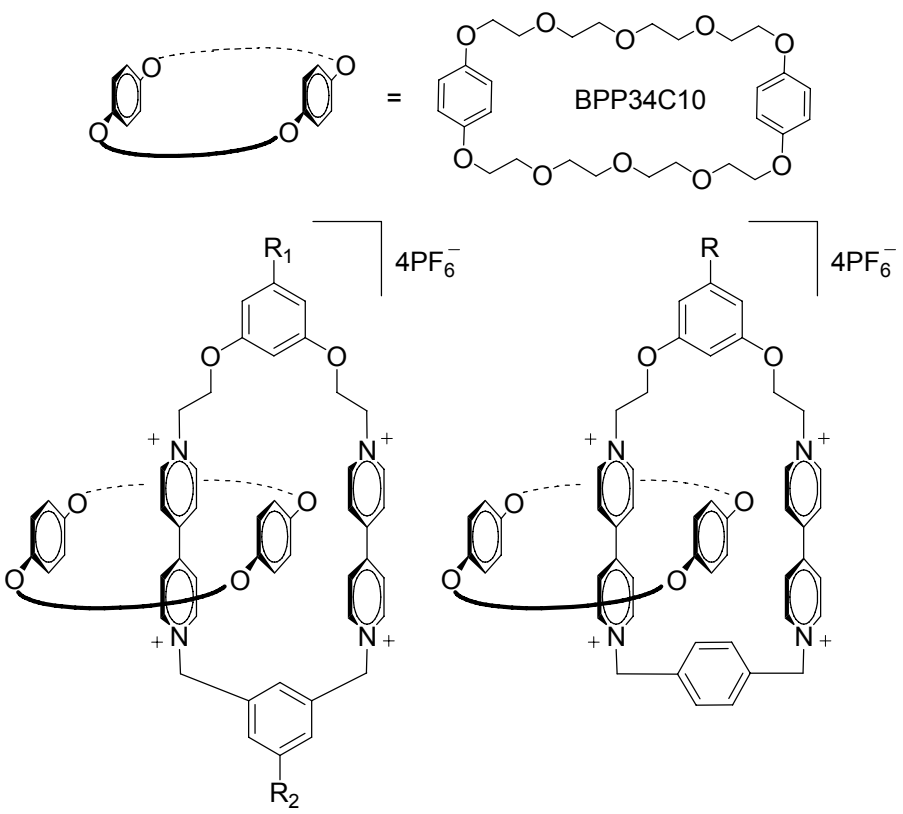

2.1 R_1 = H , R_2 = H
2.2 R_1 = H , R_2 = 4-tert-butylphenyl
2.3 R = H
2.4 R_1 = bis(4-methylphenyl)methyl , R_2 = H
2.5 R_1 = bis(4-methylphenyl)methyl , R_2 = 4-tert-butylphenyl
2.6 R = bis(4-methylphenyl)methyl

Figure 2.3. Catenanes 2.1-2.6.

hydrogen group, and a xylene-based tether also either blocked or open.

We desired to isolate the resorcinol moiety of our catenanes to minimize interaction between any groups appended to phenyl ring and dipyridinium binding sites, as this was the proposed attachment site of gates. By introducing ethyl spacers we hoped to diminish interaction between any substituents on the resorcinol ring and the two binding sites. Using these ethyl groups as spacers we synthesized and studied the conformational interconversion of [2]catenanes containing BPP34C10 catenated with

rings containing two electron-poor 4,4'-dipyridiniums tethered by different symmetric aryl tethers. Introduction of blocking groups on the tethers enabled the two pathways for circumrotation of the BPP34C10 to be open or blocked. As described below we were, indeed able to select the pathway for conformational interconversions in [2]catenanes through addition or removal of an energy barrier in the form of sterically imposing 'blocking' groups.

Section 2.2 Synthesis and Study of Symmetric [2]Catenane Components

Preparations of the two blocking groups were previously reported in the literature and are shown in Scheme 2.1.[46] We published the synthesis of the substituted resorcinol moiety **2.9**, which began with the Grignard addition of 4-methylphenylmagnesium bromide to ester **2.7**[47] and gave the tertiary alcohol **2.8**. This alcohol was reduced[48] and then deprotected[49] to give substituted resorcinol **2.9**.[46] Diester **2.10** was prepared by a Suzuki coupling, the

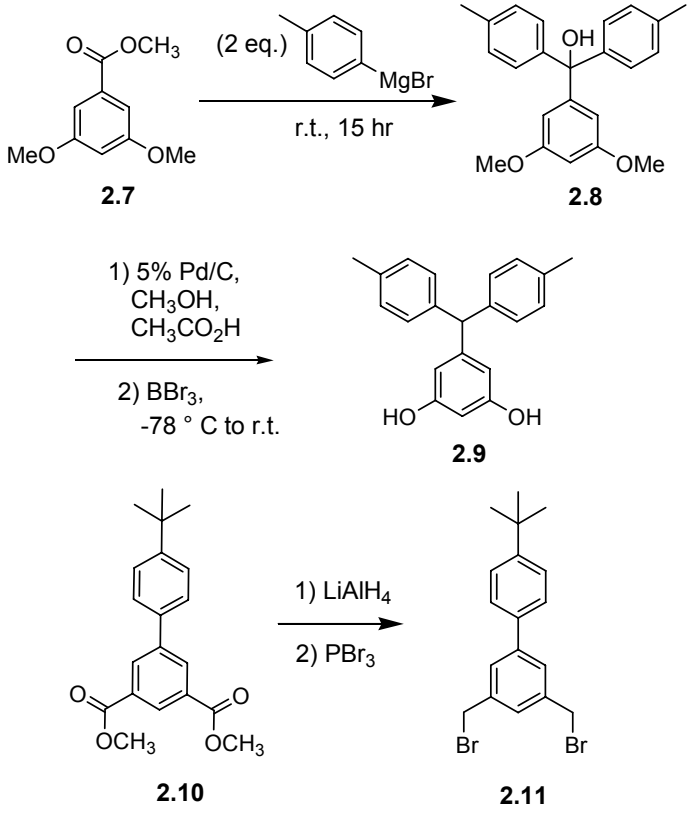

Scheme 2.1. Synthesis of Blocking Groups.

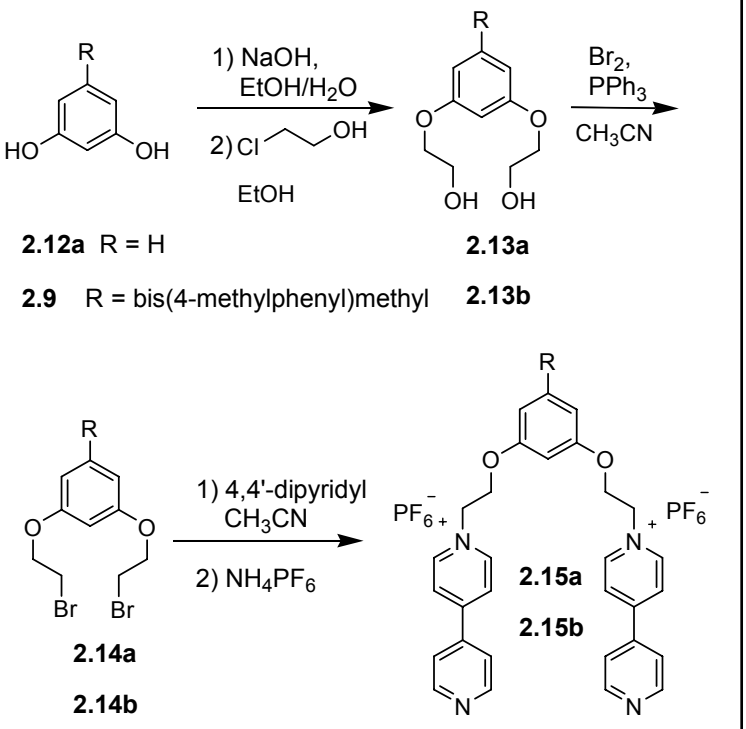

Scheme 2.2. Synthesis of Precursors.

product of which was then reduced and brominated to give substituted 1,3-bis(bromomethyl)-5-(4-*tert*-butylphenyl)benzene (**2.11**).[50] Spectral data obtained from the sample was identical to the available literature. Synthesis of the open, or unblocked 1,3-di(2-(4,4'-dipyridinium)ethoxy)benzene (**2.15a**) appears in Scheme 2.2.[46] Addition of the dipyridyl groups proceeded via introduction of the ethanol spacers followed by bromination and subsequent substitution with excess 4,4'-dipyridyl according to a related preparation by Stoddart.[42] Ethano spacer addition began with deprotonation of resorcinol using sodium hydroxide producing the dianion, which was then used in a substitution reaction with 2-chloroethanol. This product, compound **2.13a,** was obtained in 85 % yield. A ^{1}H NMR spectrum of the pure product showed two new multiplets and one broad singlet at 4.07 (4H), 3.96 (4H), and 2.01 (2H), respectively. In addition, the ^{13}C NMR spectrum revealed two new signals at 69.2 and 61.4 consistent with the methylene protons adjacent to oxygen and expected from addition of ethanol. This data, along with obtaining the anticipated low resolution mass of 198.1 (198.2

calculated) in the EI mass spectrum, indicated the desired diol product was obtained. Bromination of the ethano-bridged diol **2.12a** was accomplished using triphenylphosphine and bromine yielding 84 % of the pure product **2.14a**. Substitution of bromine on the α carbon further resolved the multiplets, shifting the α proton signal, now a defined triplet, downfield to 4.28 (J = 6.3 Hz, 4H) and the β proton triplet upfield to 3.63 (J = 6.3 Hz, 4H) with loss of the alcohol proton signal observed for the diol starting material. The ^{13}C NMR spectra revealed ethano-bridge carbon signals. Both display γ-type shifts upfield to 67.8 and 29.0 a result of introducing the bromine and its heavy atom effect with the lower signal corresponding to the carbon α to the bromide. Synthesis of the dipyridyl substituted **2.15a**, 1,3-bis(2-(4,4'-dipyridinium)ethoxy)benzene bis(hexafluorophosphate), was achieved in 99 % yield by treatment of the 1,3-di(2-bromoethoxy)benzene with four equivalents of 4,4'-dipyridyl followed by salt exchange from the bromide to hexafluorophosphate salt. Confirmation of the structure was obtained by mass, ^{13}C, and ^{1}H NMR spectra. The ^{1}H NMR spectrum showed four new multiplets at 9.33 (m, J = 7.0 Hz, 4H), 8.87 (m, J = 4.5 Hz, 4H), 8.68 (m, J = 7.0 Hz, 4H), and 7.98 (m, J = 4.5 Hz, 4H) ppm and a downfield shift in the ethanolic bridge protons to 5.31 (t, J = 4.8 Hz, 4 H) and 4.66 (t, J = 5.1, 4 Hz) ppm expected by formation of the cationic nitrogen and associated deshielding. These irreducibly complex symmetric multiplets are consistent with para-substituted aromatic rings in an AA'XX' type system.[51] New signals and shifts in the ^{13}C NMR spectrum also agreed with a dipyridyl substitution product. On the α bridging carbon the heavy atom effect introduced by the bromine has been removed and the signal moved back upfield to 62.6 ppm. Six new signals in the aromatic region, consistent with addition of

dipyridyl, were observed at 156.3, 153.1, 148.0, 143.0, 127.6, and 123.6 further supporting formation and isolation of the desired product. Mass spectral data of the dipyridyl salts provided readily identifiable signals which are typical of these compounds.[42] The loss of one hexafluorophosphate anion produced the monocationic species and appeared as a signal at 621.3 in the ESI mass spectrum. The loss of the remaining hexafluorophosphate anion produced a signal at 238.1 (M^{2+}). These spectroscopic studies, in addition to the correct mass spectrum, demonstrated formation of the desired product, 1,3-bis(2-(4,4'-dipyridinium)ethoxy)benzene bis(hexafluorophosphate). Synthesis of 2.15b was performed by Xingang Pan and will be full described by him. Preliminary supporting data has been published.[46]

Producing catenanes was simply a matter of adding 1.2 equivalents of the desired bottom tether, or stopper to the prepared solution (Scheme 2.3). For catenane **2.1**, possessing the 1,3-xylylene tether, 1.2 equivalents of α,α'-dibromo-*m*-xylene was added to the solution of dipyridinium and three equivalents of BPP34C10 (Scheme 2.3). Catenanes **2.2**, and **2.3** were formed via addition of 5-bis(bromomethyl)-4'-(1,1'-dimethylethyl)-1,1'-biphenyl and α,α'-dibromo-*p*-xylene, respectively, to solutions of

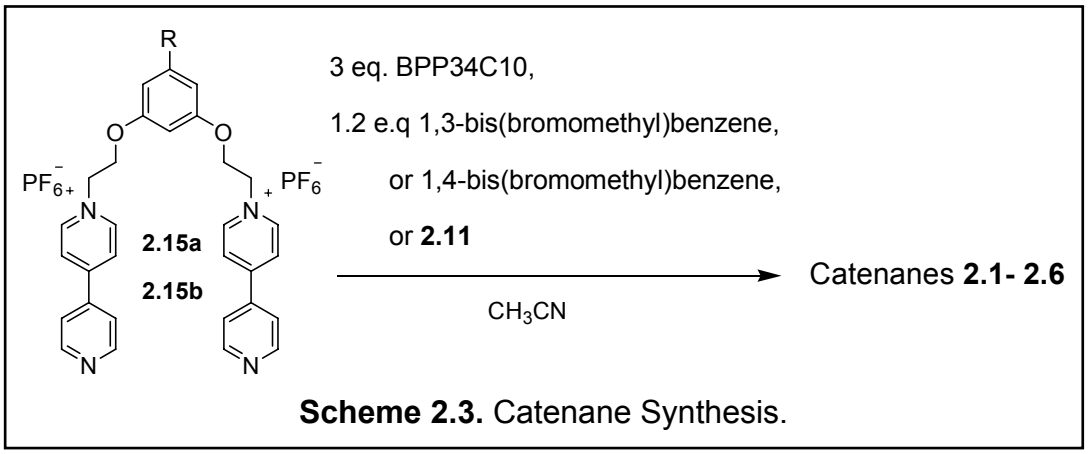

Scheme 2.3. Catenane Synthesis.

3-di(2-(4,4'-dipyridinium)ethoxy)benzene bis(hexafluorophosphate) and BPP34C10. After ten minutes, evidence for formation of the π-stacked complexes appeared in the form of the red color described in the literature (Stoddart 1995), indicating trication intermediate, pseudorotaxane, and product formation. Reactions were allowed to continue three d ensuring complete consumption of the starting materials during which time the solutions turned a deep red color and a yellow precipitate formed. After the synthesis the catenanes underwent a time consuming purification process.

Section 2.3 Purification of Catenanes

Purification of catenanes **2.1** thru **2.6** involved first removing acetonitrile under reduced pressure yielding a dark red solid. This solid was dissolved in a solution of methanol-ethyl acetate-acetone (1:1:1) and loaded onto a preparative thin-layer chromatography (PLC) plate. The products on the plates were eluted twice with methanol-ethyl acetate (1:1) at 35 ° C and finally with a solution of methanol-2M ammonium chloride-nitromethane (7:2:1) at room temperature. Eluting first with warm methanol-ethyl acetate removed BPP34C10 not bound by catenane to the top of the plate ($R_f = 1$) leaving the catenane and side products at the base. The major side products consisted of oligomeric pseudo-rotaxanes with dipyridinium serving as the axis and BPP34C10 as the ring. Any BPP34C10 bound to the pseudo-rotaxanes was dethreaded in the warm solvent leaving the bare polycationic oligomer and catenane near the base of the plate with an $R_f = 0$. Eluting with the 7:2:1 solution left the oligomer near $R_f = 0$ while the catenane, with its charged species shielded to a certain extent by the polarizable BPP34C10, was between $R_f = 0.3$ and 0.5. The product spot

was removed from the plate and washed from the silica gel using the final eluant. An excess of ammonium hexafluorophosphate was added to effect the salt exchange as the tetra-cation had been stripped of its hexafluorophosphate counter-ion in the purification process. Solvents methanol and nitromethane were removed via rotary evaporator leaving the product, a red solid, suspended in water. This red product was filtered, washed with distilled water, and allowed to dry. Impurities detected by ^{1}H NMR after the first separations were removed by an additional PLC purification. Mass, ^{13}C, and ^{1}H spectral analysis were utilized to identify the catenanes and confirmed formation of the desired products. In the ^{1}H NMR spectrum addition of the xylene and BPP34C10 were plainly visible, and will be discussed in detail in the next sections.

Section 2.4 Characterization of Catenane 2.1

For catenane **2.1** (Figure 2.4) addition of BPP34C10 shielded the α pyridinium protons shifting them upfield from 9.33 (m, *J* = 7.0 Hz, 4H) to 9.22 (m, *J* = 7.0 Hz, 4H). Formation of the new pyridinium species shifted the α' proton signals downfield from 8.68 (m, *J* = 7.0 Hz, 4H) to 9.15 (m, *J* = 7.0 Hz, 4H) ppm. Both β and β' dipyridinium protons were affected by addition of the BPP34C10 and formation of the second pyridinium being shifted to 8.24 (m, *J* = 7.0 Hz, 4H) and 8.14 (m, *J* = 7.0 Hz, 5H) ppm. These proton signals could not be distinguished from one another. The additional proton found in the integration at 8.14 ppm was attributed to overlap of the four β, or β', pyridinium protons and the single proton ortho to both xylene methylene groups ($H_{B'}$). The two protons ortho and para to the xylyl-methylenes ($H_{A'}$) appear as a doublet of doublets at 8.18 (m, *J* = 7.7, 1.64 Hz, 2H) while the proton meta to both

methylenes (H_C,) appeared as a triplet at 7.91 (t, J = 7.7 Hz, 1H). At 6.18 (s, 4H) we observed the xylyl methylene signals consistent with the anticipated product. The resorcinol proton (H_A-H_C) chemical shifts were not significantly altered from their previous positions by catenane formation and they will be discussed in detail when we present the variable temperature NMR experiments.

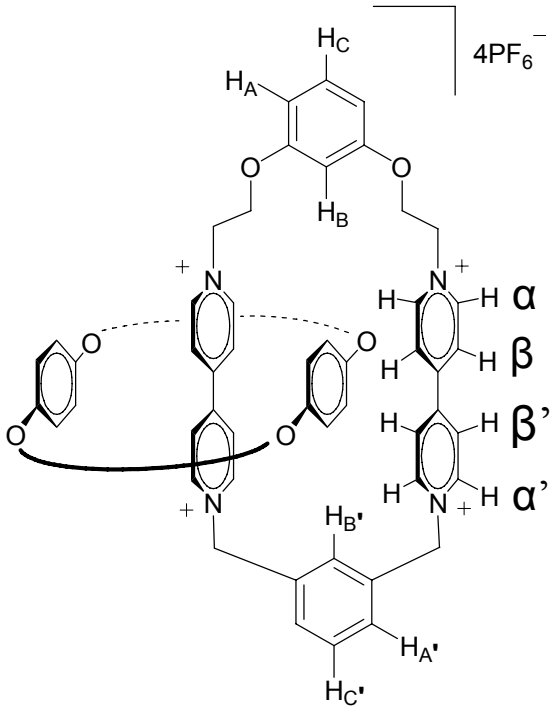

Figure 2.4. Catenane **2.1**.

As determined by Stoddart *et al*.[42] and described in Chapter 1, [2]catenanes of BPP34C10 and xylyl-tethered dipyridiniums undergo three types of motion observed on the NMR timescale. The movement we seek to control is Type II motion, or circumrotation whereby the BPP34C10 migrates from one dipyridinium to the other, as shown in Figure 2.5. Type I motion involves the electron-rich phenyl rings of BPP34C10 exchanging inside and alongside one of the electron poor-dipyridiniums. The third motion, Type III, involves one phenyl ring of BPP34C10 tilting, or rocking in the interior of the dipyridiniums.

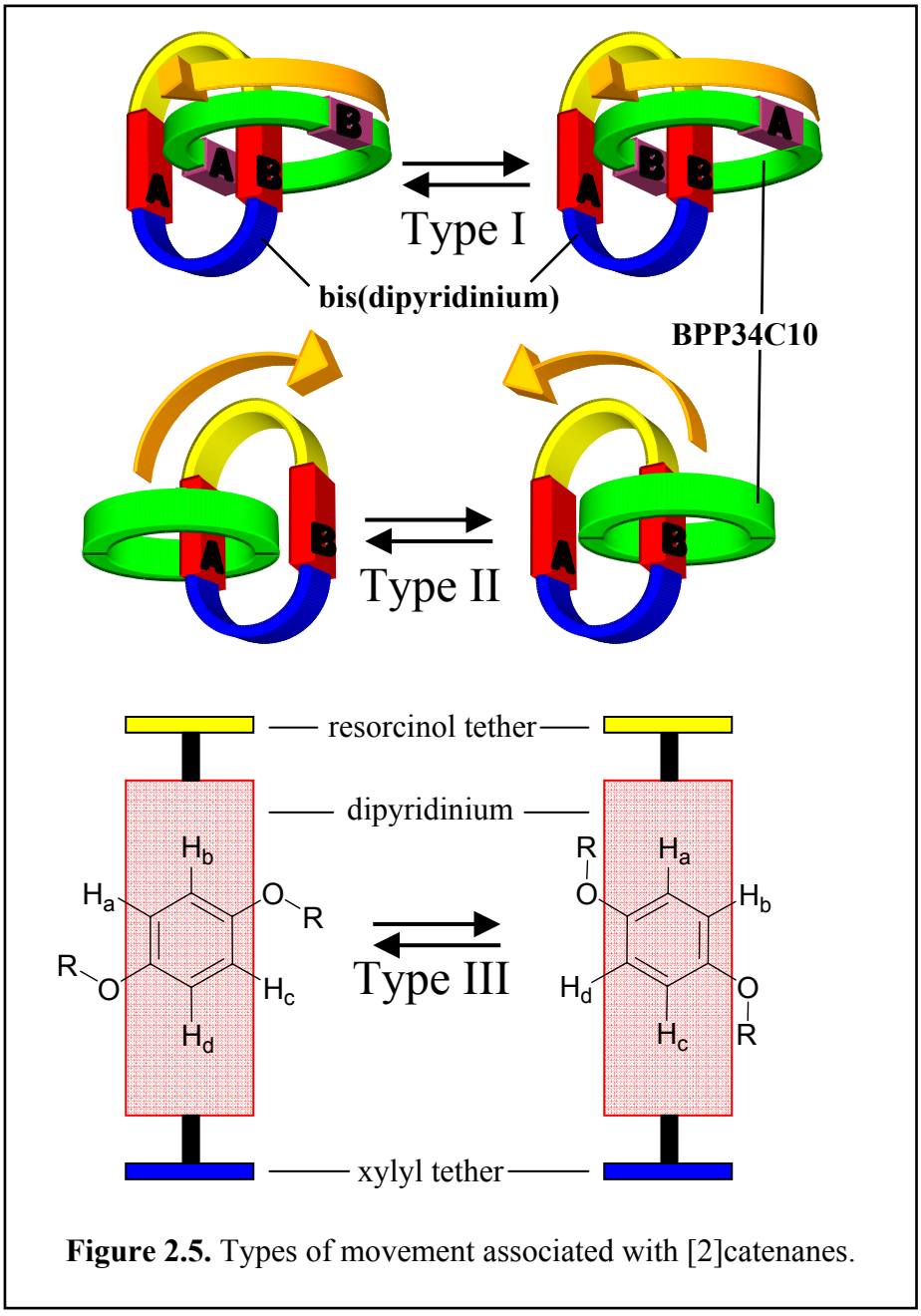

Figure 2.5. Types of movement associated with [2]catenanes.

Due to the relatively large energy of activation for Type I motion[42], signals for catenated BPP34C10 are broad and ill defined at room temperature: a result of it being in the slow exchange region. In its neat, uncomplexed form BPP34C10 gives rise to ^{1}H NMR signals at 6.75 (s, 8H), 3.98 (m, 8H), 3.83 (m, 8H), 3.70 (m, 16H) corresponding to the phenyl, α, β, and gamma protons on the ring, respectively, as described in the

literature.[41] Obtaining precise, discrete signals for catenated BPP34C10 with its phenyl and ether methylene protons at the same temperature was difficult as the processes of interconversion described by Stoddart, specifically processes I and III, meant one of the proton signals was undergoing coalescence at any given temperature. At higher temperatures, between 55 to 90 ° C, it was possible to observe the phenyl protons H_a, H_b, H_c, and H_d as a broad singlet between 5.84 and 5.69 when approaching this fast exchange region. Under slow exchange conditions, the phenyl signal at 6.75 ppm (s, 8H) was completely absent. Methylene protons appeared as a series of three broad multiplets between 3.85-3.66 ppm and typically integrated for 32 protons, in fast exchange, and 40 protons, in slow exchange. The increase in the integration intensity between 3.85 and 3.66 ppm at slow exchange temperatures corresponds to the lack of a downfield phenyl signal indicating the protons are shielded to the extent that they overlap with the methylene protons. The signals observed proved to be typical for all the catenanes in the study, and as their presence was only needed to confirm the structure of the catenane no attempts at further elucidating their character were made. In the mass spectra (ESI) we observed the loss of a single hexafluorophosphate anion with mass 1552.6 (M $3PF_6^+$). Also observed were various cationic states associated with loss of additional counter ions with masses of 703.4 (M PF_6^{2+}), 630.9 (M PF_6^{2+}), 420.6 (M PF_6^{4+}) 372.2, (M^{3+}), and 279.2 (M^{4+}) m/z. Together these spectra confirmed the structure of the catenane species.

Section 2.5 Characterization of Catenane 2.2

The synthesis of catenane **2.2** was similarly achieved. However, catenation of BPP34C10 did not shift the α pyridinium protons and they remained at 9.33 ppm (m, *J* = 6.7 Hz, 4H) with a slightly smaller coupling constant. Similar to the previous catenane, formation of the new pyridinium species shifted the α' proton signals downfield from 8.68 (m, *J* = 7.0 Hz, 4H) to 9.15 (m, *J* = 7.0 Hz, 4H) ppm. Both β and β' dipyridinium protons were affected by catenated BPP34C10 and formation of the second pyridinium causing a shift to 8.26 (m, *J* = 5.8 Hz, 4H) and 8.14 (m, *J* = 6.8 Hz, 4H) ppm nearly identical to their counterparts in catenane **2.1**. Absence of the proton ortho to the xylene methylene groups removed the overlap observed previously with the β-β' proton signal at 8.14 ppm (m, *J* = 6.8 Hz, 4H). The two protons ortho and meta to the xylyl-methylenes ($H_{A'}$) appeared as a doublet at 8.49 (d, *J* = 1.4 Hz, 2H) while the proton meta to both methylenes ($H_{B'}$) appeared as a triplet at 8.09 (t, *J* = 1.4 Hz, 1H). At 6.26 (s, 4H) we observed the xylyl methylene signals. Appropriate signals were observed for the protons on the blocking group with its four phenyl protons and nine methyl

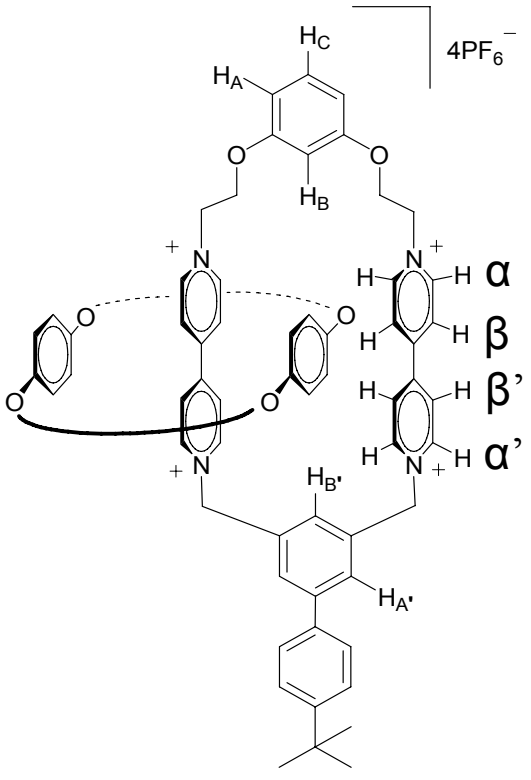

Figure 2.6. Catenane **2.2**.

protons being observed at 7.96 (m, J = 8.5 Hz, 2H), 7.67 (m, J = 8.5 Hz, 2H), and 1.42 (s, 9H), respectively. In the ESI mass spectrum we observed further evidence for catenane formation. Interestingly, after repeated submissions we did not obtain the monocationic species M $3PF_6^+$ typically observed, however we did observe a number of peaks corresponding to the di-, tri-, and tetracationic species either either with or without counter ions present; 769.4 (M PF_6^{2+}), 696.9 (M PF_6^{4+}), 464.6 (M PF_6^{3+}), 416.3 (M^{3+}), and 312.2 (M^{4+}) m/z. This evidence strengthened the conclusion that we had forced the desired catenane was produced.

Section 2.6 Characterization of Catenane 2.3 Synthesis and isolation of catenane **2.3** (Figure 2.7) was accomplished as in Scheme 2.3. Spectral data confirmed the structure. In many respects the characterization was very similar to spectra collected for catenanes **2.1** and **2.2** with some notable exceptions. Upon catenation of BPP34C10 the α pyridinium proton signals were shifted very slightly downfield to 9.37 (m, J = 7.0 Hz, 4H). Similar to the previous two catenanes, formation of the new pyridinium species shifted the α' proton signals downfield from 8.68 (m, J = 7.0 Hz, 4H) to 9.18 (m, J = 7.0 Hz, 4H) ppm. Unfortunately, we observed signal overlap on several protons in the region between 8.15-8.12 ppm (m, 12H).

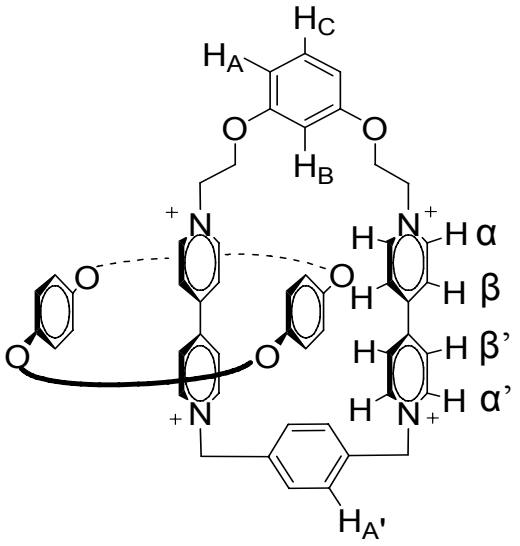

Figure 2.7. Catenane **2.3**.

Both the β and β' dipyridinium proton signals as well as the xylene phenyl proton signals overlapped forming a large complex multiplet, a phenomenon which was not observed in either of the two previous examples. At 6.11 (s, 4H) we observed the xylyl methylene signals. In the mass spectrum we observed the monocationic species (M $3PF_6^{3+}$) at 1552.6 as well as three other possible cations; 703.2 (M $2PF_6^{2+}$), 372.2 (M^{3+}), and 279.1 (M^{4+}) m/z, which further supporting the reported structure of the catenane.

Section 2.7 Variable Temperature ^{1}H NMR Experiments

After confirming the structure of the catenanes, variable temperature ^{1}H NMR experiments were conducted using a Varian 400 MHz instrument with samples dissolved in deutero-acetone. As described in Chapter 1, obtaining the spectra involved raising and lowering the temperature of the sample via temperature modulation of the gaseous atmosphere surrounding the sample. Determination of coalescence temperatures were subjective as is the case with all experiments of this type.[52] While the coalescence temperatures were measured with confidence to within two degrees, the numbers reported here were rounded to the nearest five degrees Celsius to reflect the level of precision capable with the technique. Friebolin notes the error associated with the technique as ± 2 K, which translates into an error of ± 0.2 kcal/mol in calculating the free enthalpy of activation. Rounding the temperature of coalescence to the nearest five degrees was well within this established margin of error. In addition, the free energy of activation reported was rounded to the nearest 0.5 kcal/mol in keeping with the error in temperature measurements.

It is important to note that each set of measurable decoalesced signals produced identical energy of activation values eliminating the possibility of error associated with choice of one signal set over another equally valid set. This observation confirmed the different protons were experiencing a shift due to the same process of rotational interconversion of conformers. Drift in chemical shift found in these catenane systems was also evident. The expansion regions shown in the individual spectra were scaled identically to highlight this phenomenon. This drift in shift was interesting but inconsequential, as it has no effect on the data gathered or on the final calculation of the activation energy.[41]

As described in Chapter 1, the equation:

$$\Delta G_C^{\ddagger} = (4.58 \times 10^{-3})(T_C)[9.972 + \log(T_C/\Delta\upsilon)]$$

where T_C is the temperature of coalescence and $\Delta\upsilon$ is the separation of exchanging resonances at the low temperature limit, was utilized to calculate the free energy of activation for circumrotation.[41,52]

Stacked plots of the various experiments show the coalescence processes and drift of the signals more clearly. For clarity, the stacked plots of the catenanes were limited to a single proton signal, the signal used in the free energy of activation calculations, when possible. All spectra included in the stack were referenced to the deutero-acetone quintuplet at 2.05 ppm to maintain an internal frame of reference. In all figures presented thus far only one of the two Type I process isomers has been shown. However, the other would be generated when the BPP34C10 migrated from

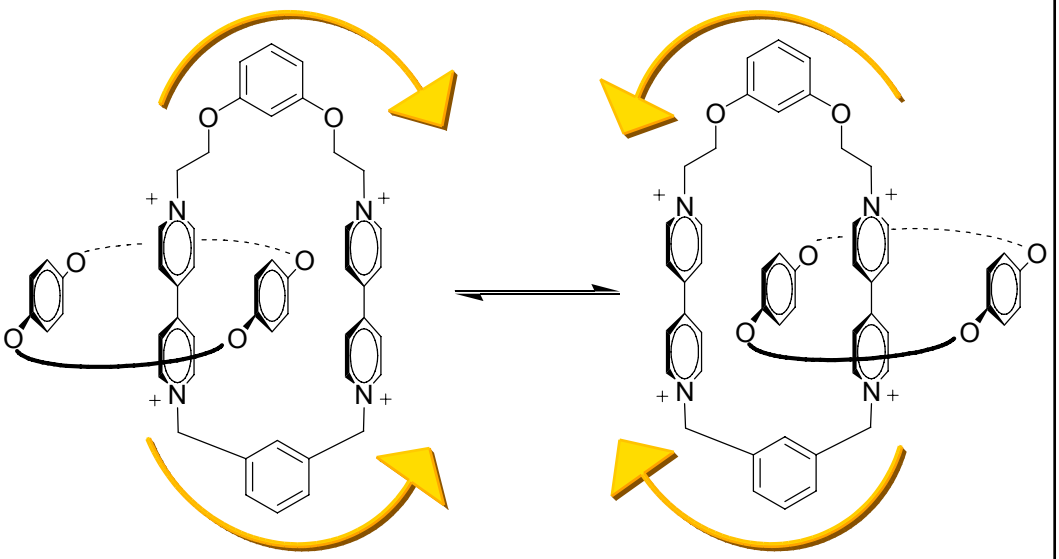

Figure 2.8. Unrestricted circumrotation and isomerization.

one dipyridinium group to the other as shown in Figure 2.8. The ratio of those two isomers should be one to one as they are energetically identical as indicated in the variable temperature ^{1}H NMR spectra.

Section 2.7.1 VT ^{1}H NMR Spectra of Catenane 2.1

For each of the catenanes, comparing the high temperature spectrum with the low temperature spectrum made obvious the signals from which we would measure the chemical shift differences, or **Δυ**, to perform the activation energy calculations. While the α and α-prime signals were distinct at 323 K in the fast-exchange region (Spectrum 2.1), in the slow exchange region (Spectrum 2.2) of 213 K produced an unacceptable overlap of signals in catenane **2.1**. However, the signal for proton H_A was clearly defined and its slow exchanging signals were resolved as the expected 1:1 ratio of

isomers. The resorcinol protons proved to be targets for use in determining the activation energy for nearly all the catenanes produced.

In Spectrum 2.1 and 2.2 we observe the fast exchange processes at 323 K and the slow exchange processes at 213 K. Each of the proton signals possessed its own coalescence temperature and chemical shift differential, which was measured if the signals were not convoluted. Identifying the signal set to be used was a matter of finding which set behaved most appropriately. In the case of Catenane **2.1**, this signal was for proton H_A.

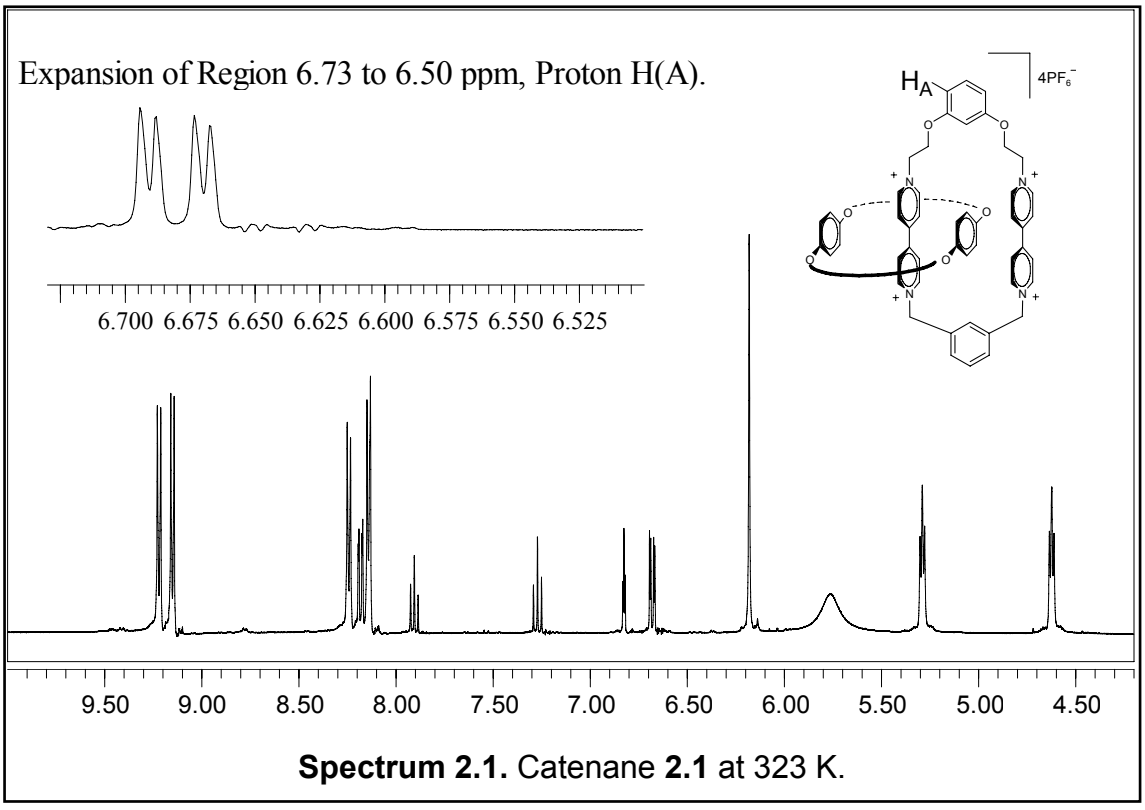

Spectrum 2.1. Catenane **2.1** at 323 K.

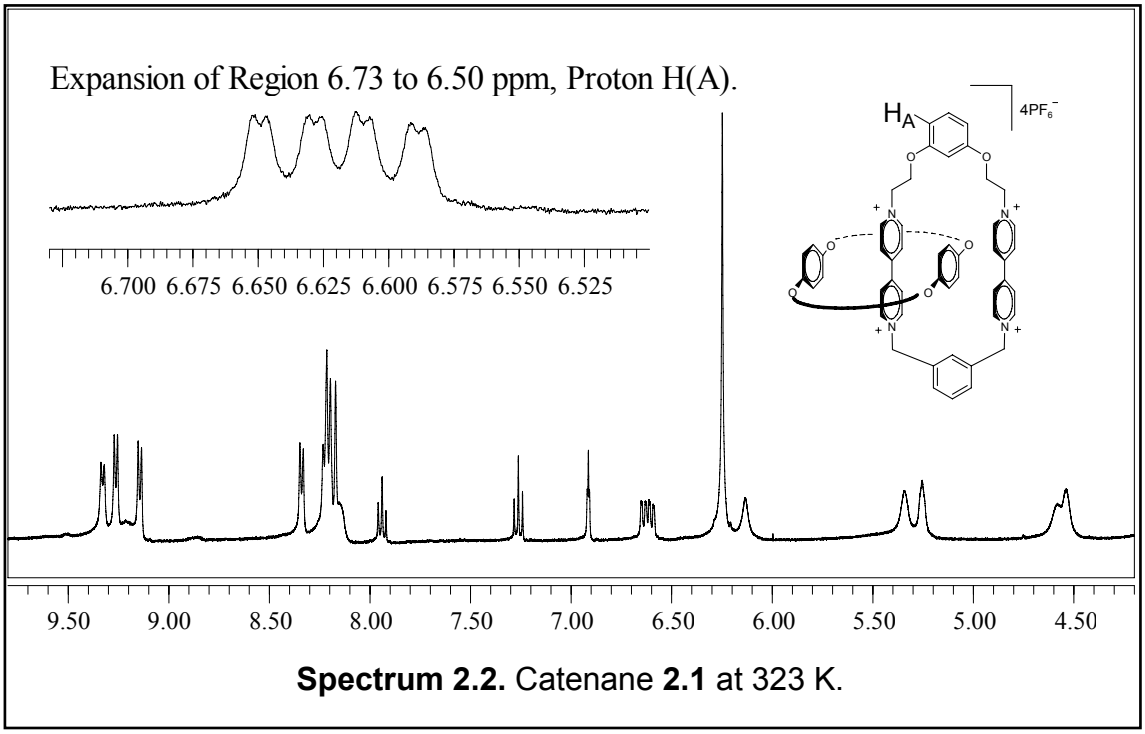

Spectrum 2.2. Catenane **2.1** at 323 K.

For catenane **2.1**, the separation of the exchanging resonances was measured at 15.5 Hz and the temperature of coalescence was 240 K. The activation energy required for circumrotation was calculated to be 12 kcal/mol. A stacked plot in Spectrum 2.3 shows the progression of spectrum as the temperature is lowered from the fast exchange region to coalescence and finally to the slow exchange region between 6.75 and 6.50 ppm. In the fast exchange region we observe the weighted average signal; a doublet of doublets. As the signals approached and finally reached coalescence, we observed them merge into one single broad peak. Coalescence gave way to reveal two distinct signals as we approach the slow exchange region. Finally, in the slow exchange region we observed two distinct signals, two doublet of doublets in this example, for the exchanging protons.

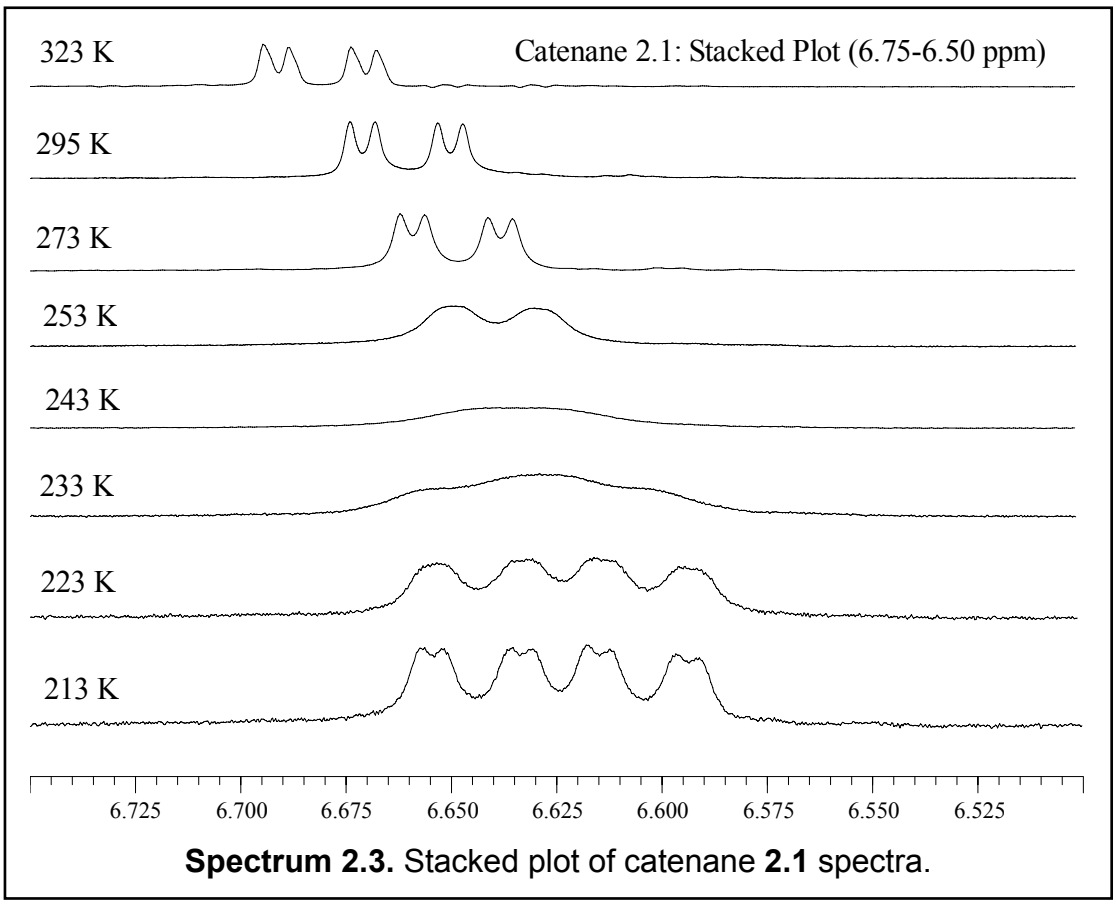

Spectrum 2.3. Stacked plot of catenane **2.1** spectra.

Section 2.7.2 VT ^{1}H NMR Spectra of Catenane 2.2

For catenane **2.2** the α and α' dipyridyl proton signals at 9.33 and 8.68 ppm nicely decoalesced to reveal the exchange partners at 233 K. While proton H_A decoalesced at 253 K the signals were overlapped in the slow exchange region and obtaining a value for **Δυ** proved to be impossible. At 9.33 and 8.68 ppm in the fast exchange region (Spectrum 2.4) we observed two complex multiplets. In the slow exchange region (Spectrum 2.5), we observed four complex multiplets with two very different **Δυ** values.

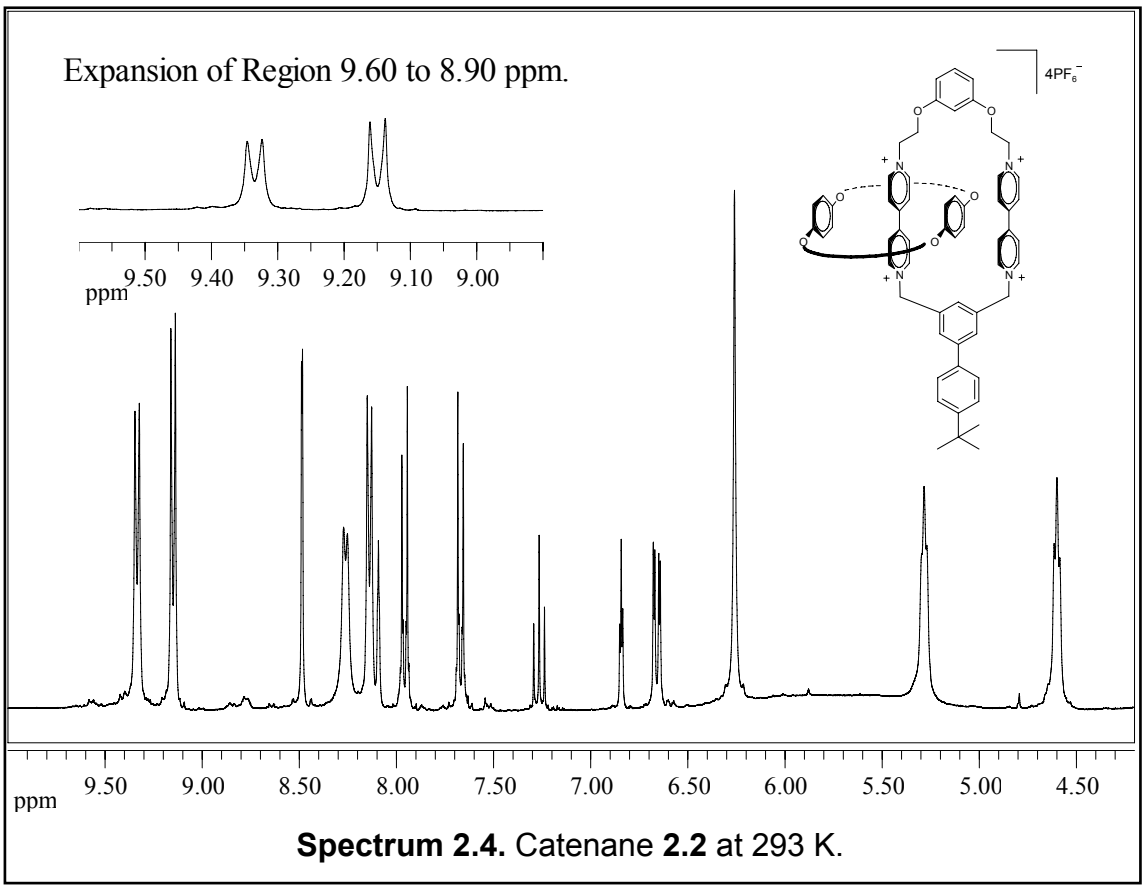

Spectrum 2.4. Catenane **2.2** at 293 K.

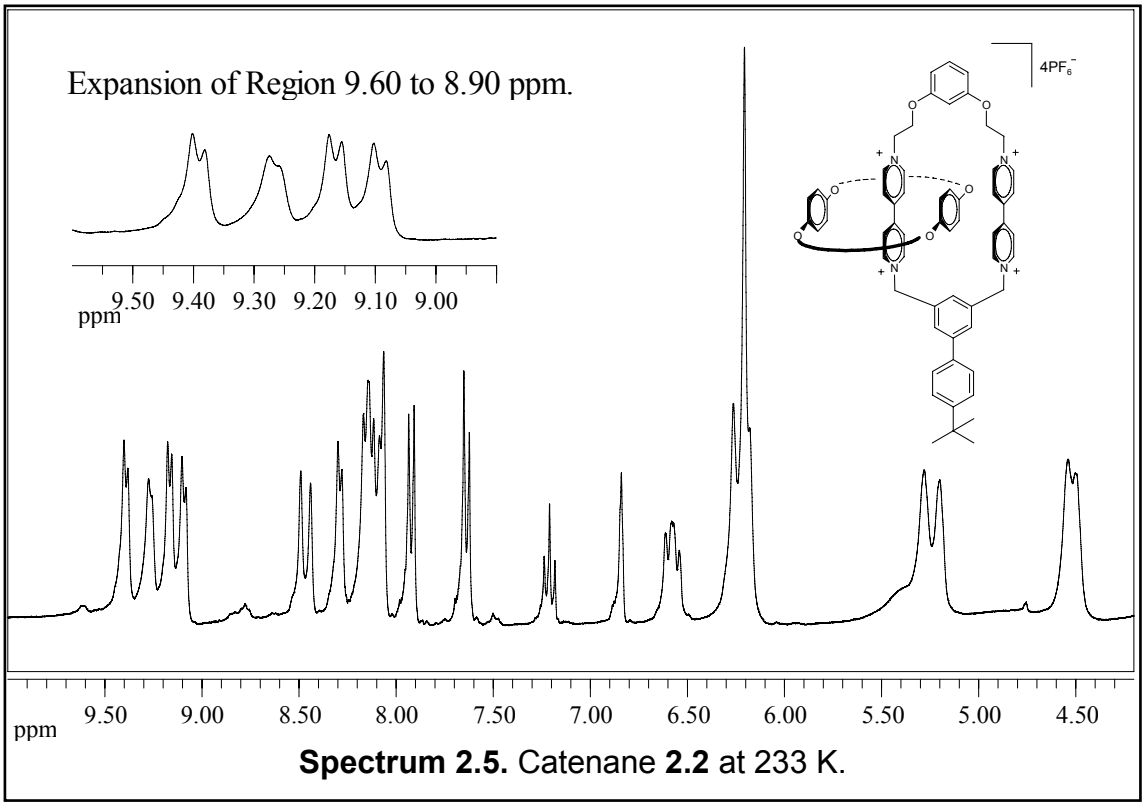

Spectrum 2.5. Catenane **2.2** at 233 K.

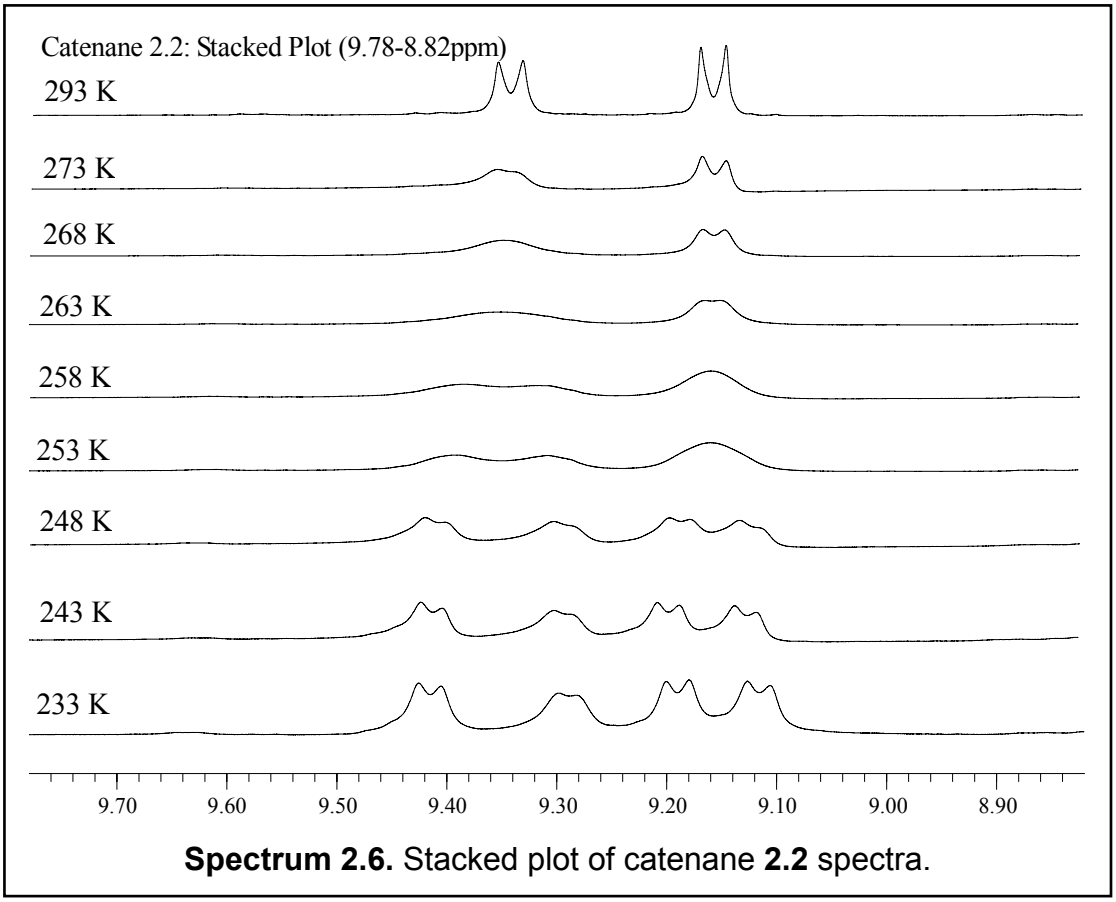

Spectrum 2.6. Stacked plot of catenane **2.2** spectra.

Moving to Spectrum 2.6, the stacked plot of spectra for catenane **2.2**, we observed the two α-α' multiplet signals as the averaged signal in fast exchange. Coalescence for these two protons occurred at two separate temperatures; 255 K for the signal at 8.68 ppm and 260 K for the downfield signal at 9.33 ppm. Without using sophisticated techniques, one can observe the 20 Hz difference in $\Delta\upsilon$ for the two different signals. For the 8.86 ppm signal the shift separation was measured at 22.3 Hz while the 9.33 ppm signal difference was measured at 38.1 Hz. Using either set of data the activation energy was calculated at 13 kcal/mol.

Section 2.7.3 VT ^{1}H NMR Spectra of Catenane 2.3

As was the case for catenane **2.1**, in catenane **2.3** we observed distinct α and α-prime dipyridinium signals in the fast-exchange region (Spectrum 2.7). However, in the slow exchange region overlap of signals was observed and **Δυ** could not be measured with confidence. Again the signal for the meta-proton H_A was clearly defined and its coalescence temperature easily determined (Spectrum 2.8).

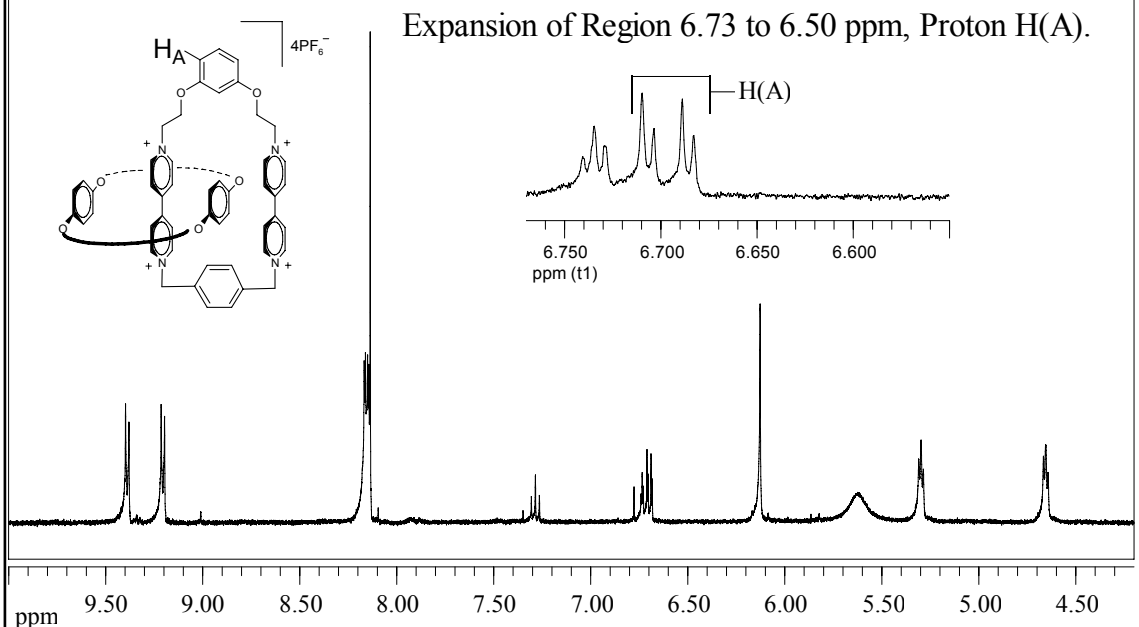

Spectrum 2.7. Catenane **2.3** at 328 K.

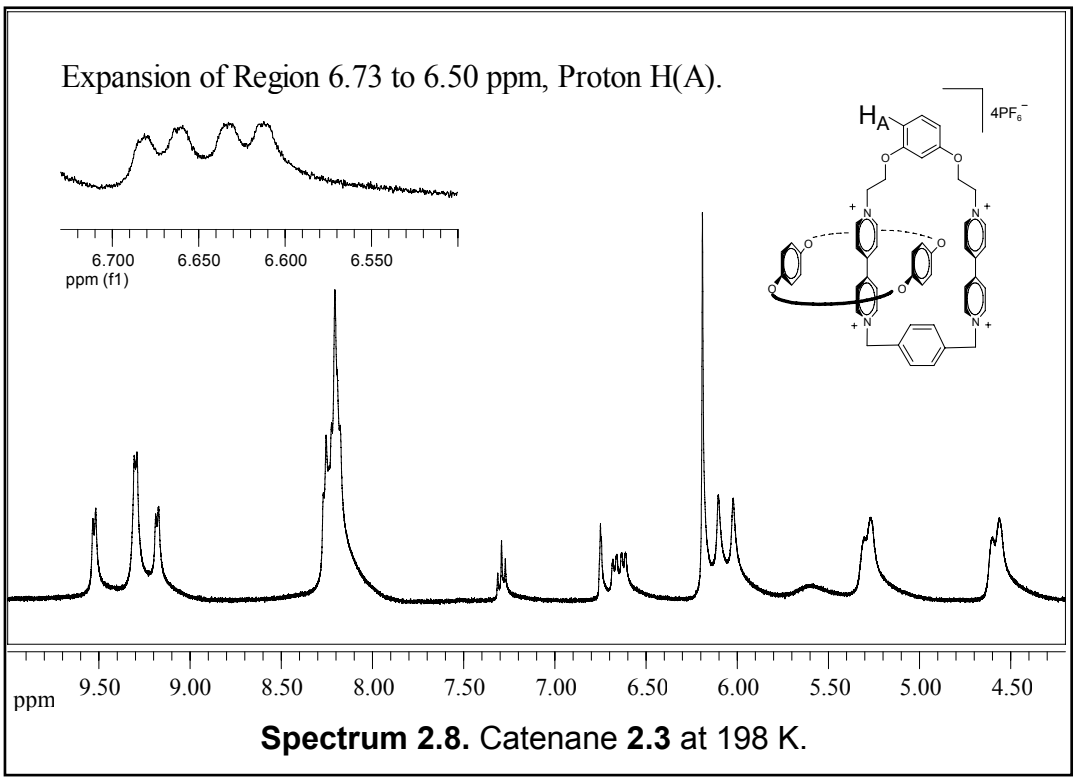

Spectrum 2.8. Catenane **2.3** at 198 K.

The stacked plot (Spectra 2.12) shows the progression of spectra as the temperature is lowered from the fast exchange region to coalescence and finally to the slow exchange region. In the fast exchange region we observe the weighted average signal; a doublet of doublets. Also observed in the stacked plot is the meta-meta proton signal on the resorcinol ring. This signal was not temperature dependent as the magnetic environment it experienced did not change in a manner capable of being measured on the NMR timescale. Thus, it remains a triplet at all temperature regimes. As the doublet of doublets approached and finally reached coalescence the signals merged into one single broad peak. Coalescence gave way to reveal two distinct signals as we approach the slow exchange region. Finally, in the slow exchange region we

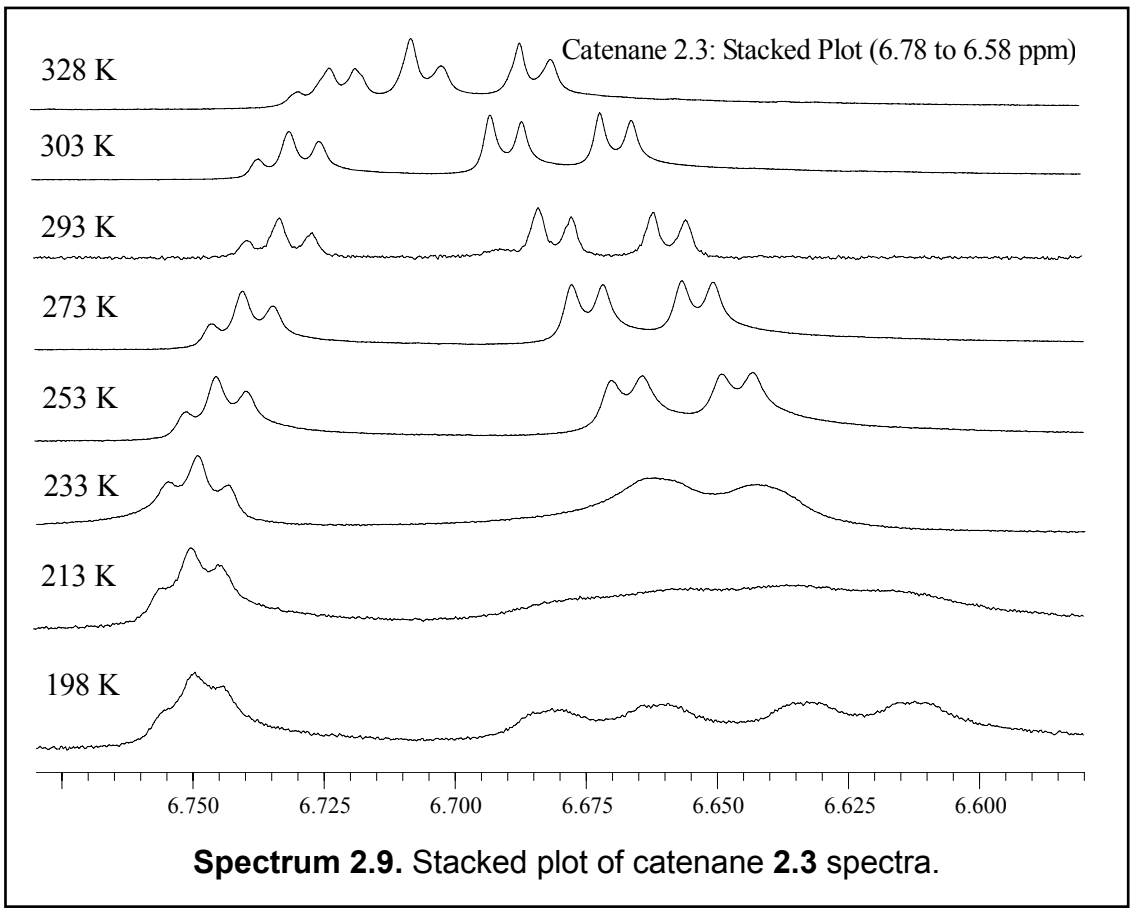

Spectrum 2.9. Stacked plot of catenane **2.3** spectra.

observed two doublet of doublets corresponding to each exchange partner. For catenane **2.3**, the separation of exchanging resonances was measured at 19.5 Hz and the temperature of coalescence was 220 K. The energy of activation was calculated to be 11 kcal/mol.

Section 2.8 Summary of Data and Conclusions

As mentioned at the beginning of this chapter, another three symmetric catenanes were synthesized in our laboratory by Xingang Pan and reported in the literature.[46] While catenane **2.2** had the bottom pathway blocked with a large bulky group, catenanes **2.4** thru **2.6** had the top pathway blocked. Synthesis and purification

of catenanes **2.4**, **2.5**, and **2.6** was nearly identical to the previous three catenanes and were prepared via three component reactions between 1,3-bis(2-(4,4'-dipyridinium)ethoxy)-5-di-*p*-tolylmethylbenzene bis(hexafluorophosphate) (X**)**, 1.2 equivalents of 1,3-xylenes, 1,4-xylenes, or 5-bis(bromomethyl)-4'-(1,1'-dimethylethyl)-1,1'-biphenyl and 3 equivalents of BPP34C10 in acetonitrile at room temperature for 3 d (Scheme 2.2). Data gathered from variable temperature ^{1}H NMR experiments as well as the calculated energies of activation of all six catenanes are summarized in Table 2.1.

catenane	substituents tether A[a] / tether B[b]	coalescence temperature (K)[c]	frequency difference (Hz)	energy of activation (kcal/mol)[d]
2.1	H / 1,3-xylyl	240	15.8	12
2.2	H / *t*-butylphenyl	255	22.3	13
2.3	H / 1,4-xylyl	220	19.5	11
2.4	Ditolylmethyl / 1,3-xylyl	255	39.3	12.5
2.5	ditolylmethyl / *t*-butylphenyl	>335	25.5	>18[e]
2.6	ditolylmethyl / 1,4-xylyl	240	64.8	12

a) Substituent on the 5-position of the resorcinol moeity of tether A where ditolylmethyl describes the di-*p*-tolylmethyl blocking group
b) Tether B can be either 1,3-xylyl , 1,4-xylyl, or t-butylphenyl where the later describes the 5-(4-*t*-butylphenyl)-1,3-xylyl blocking group
c) Approximated to the nearest 5 K
d) An error of 5 K in determining the coalescence temperature corresponds to an error of ± 0.2 kcal/mol in the activation energy
e) No exchange observed by 2D ^{1}H NMR exchange experiments

Table 2.1: Summary of Data and Calculated Energy of Activation

As mentioned in Chapter 1 a number of rotational temperature dependent isomerizations of related [2]catenanes were established by Stoddart, two of which are of

interest in this study (Figure 2.5).[41,42] Typically, rotation of BPP34C10 about a single dipyridyl group, or Type I movement, has an energy barrier of approximately 16 kcal/mol determined using established NMR techniques. The energy barrier for the translocation or circumrotation of the crown ether from one dipyridyl group to the other requires several kcal/mol less energy. As with these previous reports in the literature, catenanes **2.1-2.6** exhibited ^{1}H NMR spectra at room temperature that were in the fast exchange region for translocation of the crown ether around the second ring, but in an intermediate exchange region for the rotation of the crown ether about its center. At higher temperatures, both processes were in fast exchange and a single set of averaged signals was observed for the protons at the H_A, 2 and 2' dipyridyl positions. At temperatures ten degrees below coalescence, the 1:1 set of signals indicated that both exchange processes were in the slow exchange region.

The activation barrier for catenane **2.1**, possessing both the unsubstituted resorcinol and the 1,3-xylyl linker, was calculated to be 12 kcal/mol. When both the resorcinol and xylene groups were substituted with blocking groups in catenane **2.5**, both pathways were blocked. No evidence of coalescence was observed in the ^{1}H NMR spectra up to 60 ° C, nor was any evidence for exchange seen in 2D EXSY spectra. Therefore, the activation barrier for passing over either of these blocking groups must be significantly higher than 18 kcal/mol (Figure 2.9). When only the resorcinol ring was blocked as in catenane **2.4**, passage over the 1,3-xylyl ring required 12.5 kcal/mol (Figure 2.10). Passage over the 1,3-bis(ethyloxy)benzene tether in **2.2** required more energy (Figure 2.11). Passage along the 1,4-xylyl linker was less energetically demanding to traverse than the 1,3-xylyl group as indicated by the 11 kcal/mol

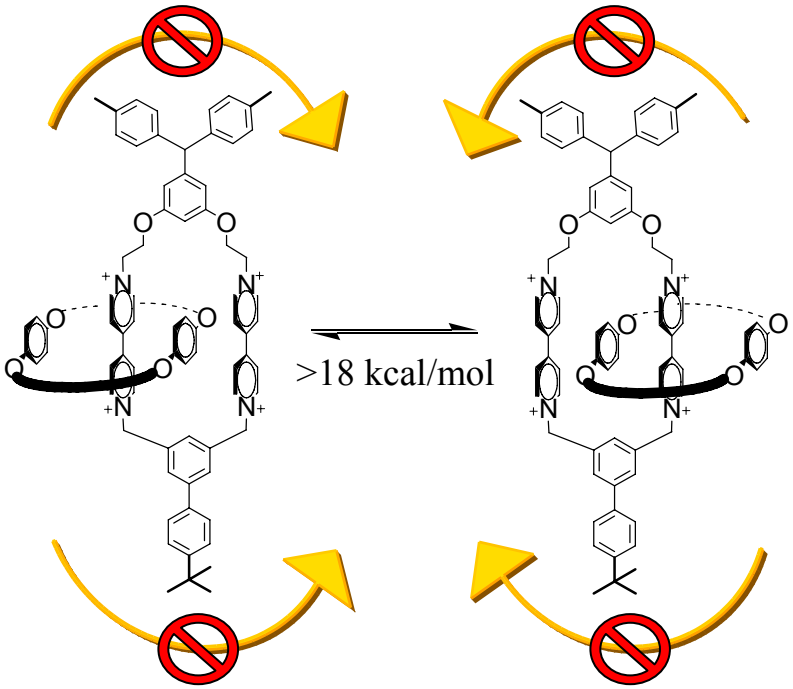

Figure 2.9. No circumrotation observed for catenane **2.5.**

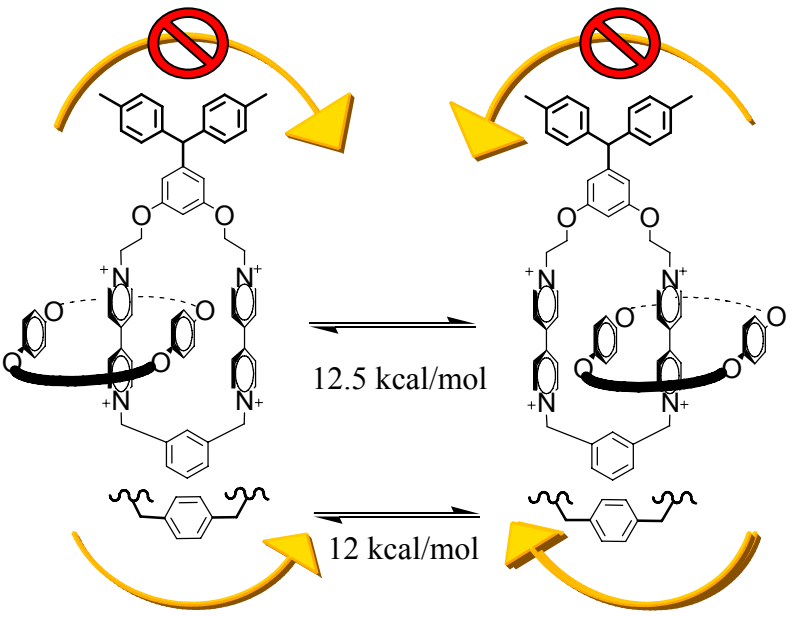

Figure 2.10. Circumrotation observed for catenanes **2.4** and **2.6.**

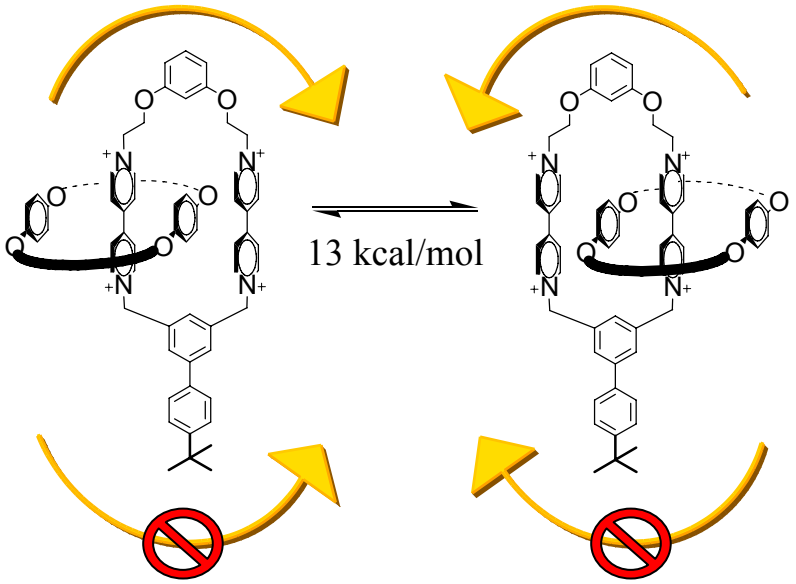

Figure 2.11. Circumrotation observed for catenane **2.2.**

barrier in **2.3**. Interestingly, catenanes **2.1** and **2.3** both display energies of activation 0.5 kcal/mol and 1 kcal/mol lower than their blocked analogues. We attribute this decrease in $\Delta G^{\ddagger}$ to the concomitant increase in entropy of activation caused by reaction pathway multiplicity.[45] With both tethers unblocked, there are two possible methods of circumrotation. Looking at it from another perspective the entropy of activation is decreased by limiting circumrotation to one pathway and manifests itself as an increase in the free energy of activation.

From these observations we concluded BPP34C10 requires more energy to rotate over the tighter, more constricted turn of the 1,3-xylyl tether in **2.4** than over the longer, narrower 1,4-xylyl tether in **2.6**. Passage over the longer 3-bis(ethyloxy)benzene in **2.2** demanded energy requirements somewhat greater than that

of the 1,3-xylyl tether, and both are significantly more energetically demanding than passage over the 1,4-xylyl tether.

Through appropriate incorporation of blocking groups on one or both of the phenyl tethers it was possible to block one or both of the two pathways for circumrotation in bistable catenanes **2.1** thru **2.6**. Energy barriers for displacement along a the different paths were: 12.5 kcal/mol for 1,3-bis(ethyloxy)benzene, 13 kcal/mol for 1,3-xylyl pathways, and 12 kcal/mol over the 1,4-xylyl pathway. Using these symmetric catenanes, we demonstrated the ability to dictate the pathway over which circumrotation occurred in a non-covalently bound system.

Chapter 3

Synthesis and Study of Asymmetric [2]Catenanes with Rotationally Free Symmetry Operators

Section 3.1 Thermodynamically Controlled Interconversion of Asymmetric Catenanes

Our symmetric resorcinol-based [2]catenanes demonstrated the ability to control certain types of molecular motion by alternately opening or blocking two different pathways.[46] Next, we sought to apply this knowledge to more complex systems. To study the use of random thermal energy to preferentially drive circumrotation in one direction over another we required a gate capable of being acted upon by the various components in the system. The question becomes to where does one attach the gate on the system to prevent interaction between the binding sites and the gate. For isomerizations in bistable catenanes, interaction between the gate and the binding site could cause perturbations in the bonding interactions of the electron rich BPP34C10 and electron poor dipyridinium causing one isomer to become more or less stable than the other isomer. This change in the thermodynamic stability of isomers would be observed as a change in the ratio of catenane isomers. Foreseeing problems associated with close proximity of gate to binding site we introduced ethoxy spacers in an attempt to isolate the gate and alleviate the potential interference. Our vision of the gated catenane involved appending a hinged group onto the resorcinol tether as shown in Figure 3.1.

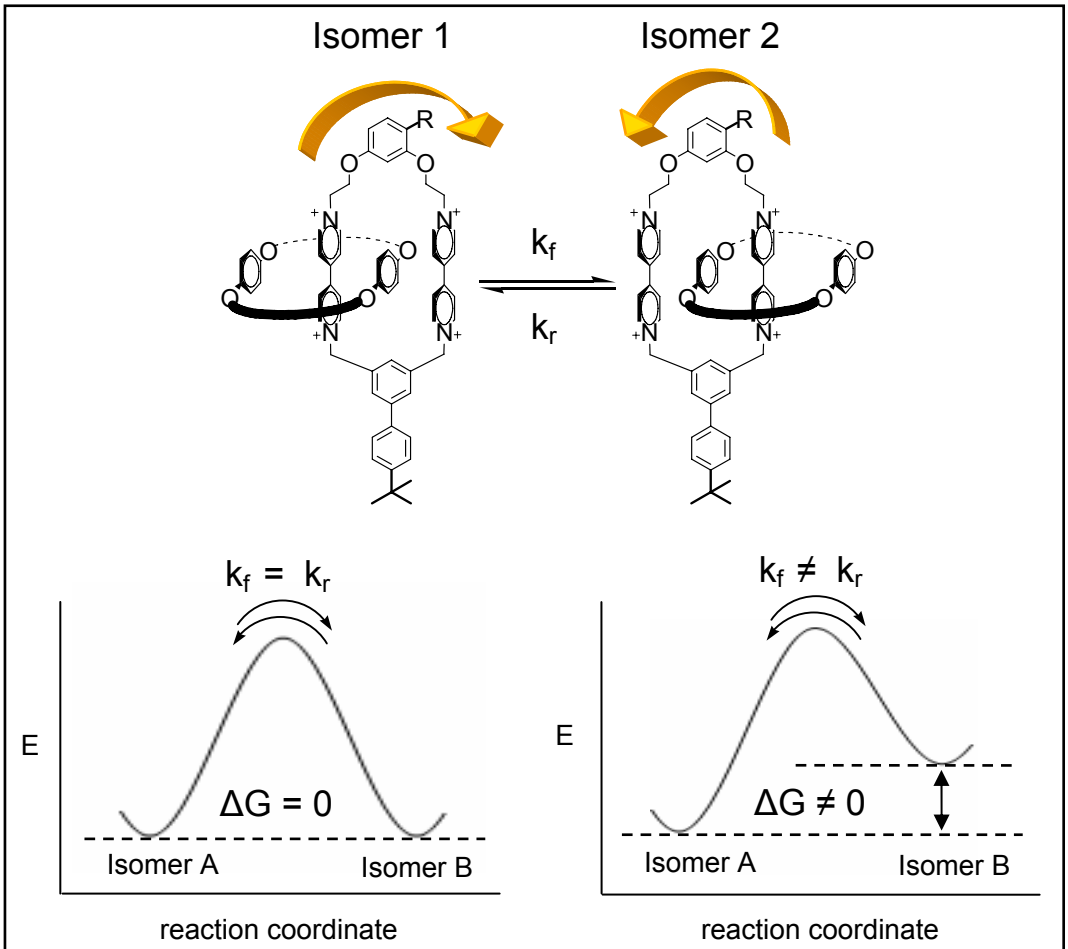

Figure 3.1. Possible thermodynamic outcomes of asymmetry introduction.

Specifically, this gate (R) would be appended to carbon four of the aryl ring. Unlike the previous [2]catenanes synthesized, these new catenanes possessed an additional degree of asymmetry. With this addition, it was important to determine whether or not the change would affect the thermodynamic balance of conformers, and if so, to what degree. Figure 3.1 also shows the two possible thermodynamic outcomes of the study and the relative rate constants for the arbitrarily designated "forward" (k_f) and "reverse" (k_r) directions. If the ratios of isomers are 1:1 we will know the rate constants are unity and the ground state energies are approximately zero. A shift away from unity will

indicate the rate constant in one direction is larger than the rate constant in the opposite and the ground state energies are not equal. Isomers in the reaction coordinate diagrams are given as isomers A and B rather than 1 and 2 because we can not yet assign one isomer or geometry to its corresponding ground state energy well.

Stoddart established how asymmetry could affect the ratio of conformers in catenanes as discussed in Chapter 1.[42] However, in each of those cases asymmetry was introduced via incorporation of asymmetric electron-rich biphenyl crown ethers. The associated difference in stabilizing π-bonding interactions of the two recognition sites altered the thermodynamic balance of conformers. Stoddart *et al.* very specifically altered the thermodynamic equilibrium to form one isomer preferentially. This bias in the stability of the two isomers is fundamentally opposed to our proposal. We isolated the binding sites to reduce or remove thermodynamic bias. Isolation of isoenergetic binding sites with respect to an asymmetric tether in a [2]catenane has not been

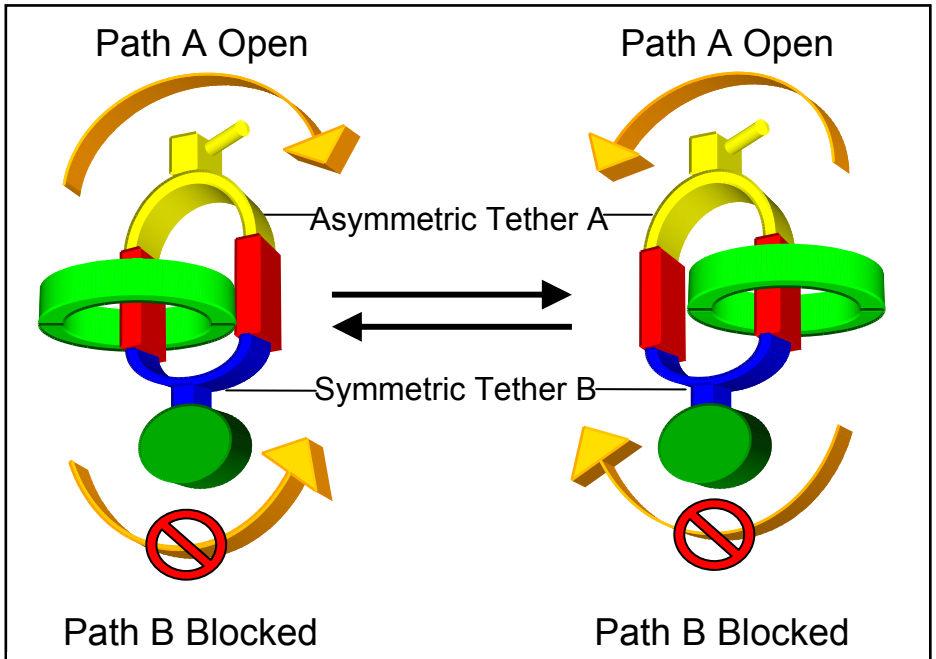

Figure 3.2. Introduction of asymmetric tether A.

previously demonstrated.

An interesting characteristic observed of our symmetric catenanes was their display of a thermodynamic equilibrium with 1:1 ratios of conformers. We recognized this ratio of conformers as a ready-made and powerful tool by which to observe any biased circumrotation displayed by our catenanes. Deviation from the thermodynamic equilibrium in a system possessing isoenergetic binding sites would be evidence of gating. Determining the extent to which asymmetry could affect the conformer ratios was very important and would serve as a control group to which we could compare circumrotation observed in the asymmetric gated catenanes. With this in mind we synthesized a series of asymmetric catenanes which did not possess large rotationally hindered gates, but rather smaller groups that we believed would offer less steric interference to circumrotation. As described in these sections, with the blocking group attached to tether **B**, translation occurs only along asymmetric Pathway **A** and over Tether **A** (Figure 3.2). Unlike the previous catenanes, Pathway **A** was not completely blocked because we desired to observe differences between the physical character of these asymmetric catenanes and their symmetric counterparts, concerning their ratios of conformers and the energies of activation for circumrotation. Extending our earlier work,[46] we prepared catenanes **3.1** thru **3.9** (Figure 3.3) possessing the asymmetric 1,3-bis(ethyloxy)benzene based tethers with the xylene-based tether either blocked or open.

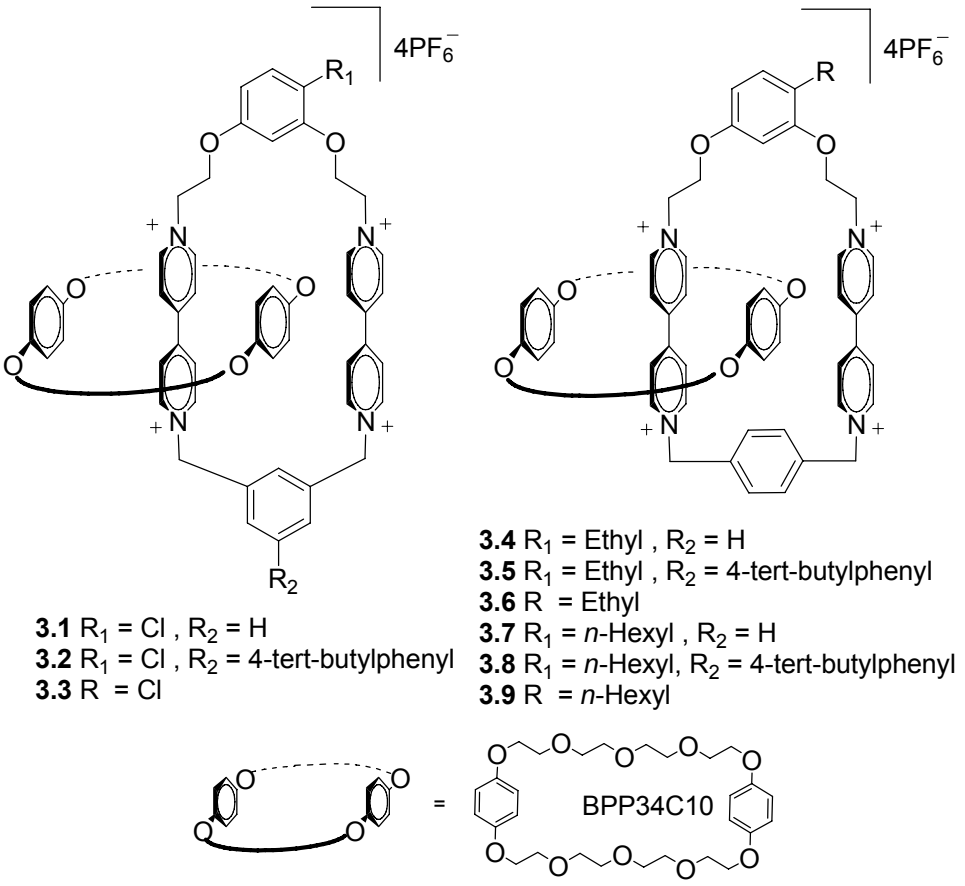

Figure 3.3. Catenane **3.1-3.9**.

We anticipated catenanes **3.1** thru **3.9,** with their unobtrusive and remote, chloro-, ethyl-, and *n*-hexyl moieties, would display ratios of conformers near 1:1 in the low temperature, slow exchange regime. As discussed below, however, we observed a bias in the system; an apparent function of the asymmetry introduction with ratios of conformers as great as 3.5 to 1. Measurable activation barriers for passage along the tethers were found to vary from 11 to 15 kcal/mol. Introduction of ethyl- and *n*-hexyl-substituents increased the energy of activation by at least 0.5 kcal/mol compared to their symmetric counterparts, while chloro-substitution did not increase the energy of

activation. This study demonstrated the ability of asymmetry operators to affect the thermodynamic equilibrium of two [2]catenane conformers away from 1 to 1.

Section 3.2 Synthesis and Study of Asymmetric [2]Catenane Components

Preparation of the lower blocking group **2.11** was identical to the method described in Chapter 2 and reported in the literature.[46] Syntheses of the 4-position substituted resorcinol derivatives of 1,3-bis(2-(4,4'-dipyridinium)ethoxy)benzene bis(hexafluorophosphate) are summarized in Scheme 3.1. All three resorcinol analogues, 4-chloro-benzene-1,3-diol (**3.10a**), 4-ethyl-benzene-1,3-diol (**3.10b**), and 4-*n*-hexyl-benzene-1,3-diol (**3.10c**) were commercially available and used without further purification. A summary of the reaction steps are given in Scheme 3.1 and below, with the details to come later in following sections.

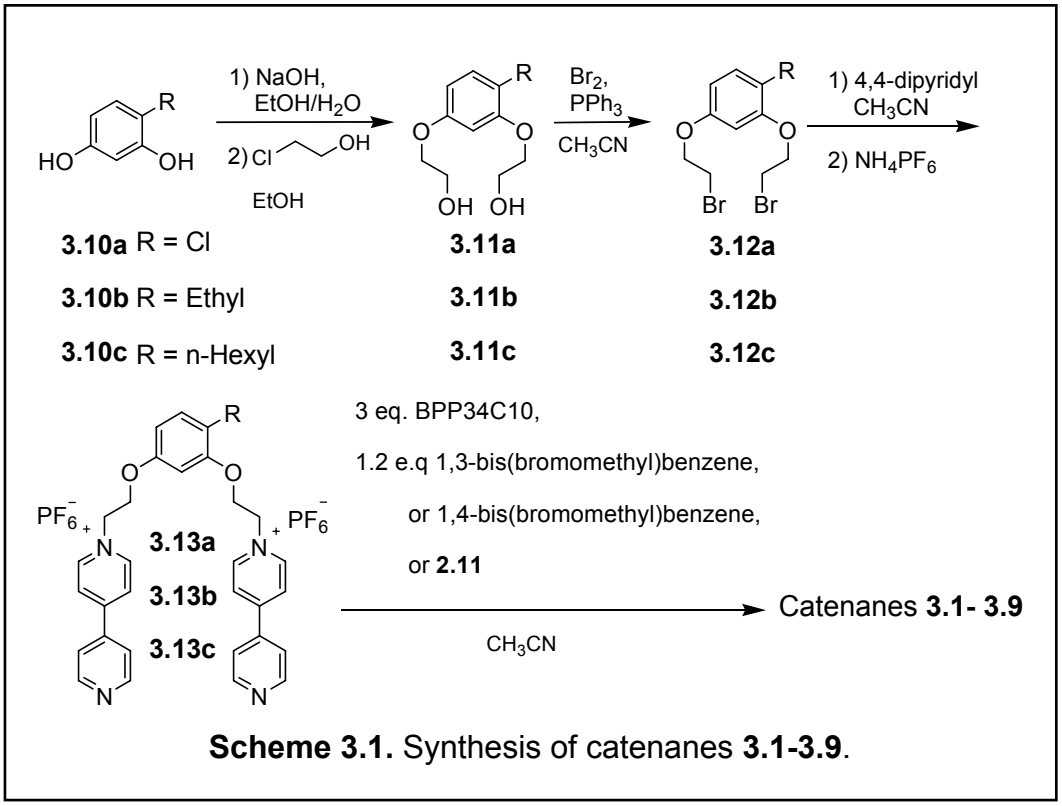

Scheme 3.1. Synthesis of catenanes **3.1-3.9**.

Deprotonation with sodium hydroxide followed by substitution using 2-chloroethanol converted these starting materials to 1,3-bis(2-hydroxyethoxy)-4-chlorobenzene (**3.11a**), bis(2-hydroxyethoxy)-4-ethylbenzene (**3.11b**), and bis(2-hydroxyethoxy)-4-*n*-hexylbenzene (**3.11c**), which were brominated to give bis(2-hydroxyethoxy)-4-chlorobenzene (**3.12a**), 1,3-bis(2-hydroxyethoxy)-4-ethylbenzene (**3.12b**), and 1,3-bis(2-hydroxyethoxy)-4-*n*-hexylbenzene (**3.12c**),whose treatment with excess 4,4'-dipyridyl gave 1,3-bis(2-(4,4'-dipyridinium)ethoxy)-4-chlorobenzene bis(hexafluorophosphate) (**3.13a**), 1,3-bis(2-(4,4'-dipyridinium)ethoxy)-4-ethylbenzene bis(hexafluorophosphate) (**3.13b**), and 1,3-bis(2-(4,4'-dipyridinium)ethoxy)-4-*n*-hexylbenzene bis(hexafluorophosphate) (**3.13c**), respectively. Catenanes **3.1-3.9** were formed through three component reactions between one equivalent of bis(pyridiniums) **3.13a**, **3.13b**, or **3.13c**, 1.2 equivalents of 1,3-xylenes, 1,4-xylenes or **2.11** and 3 equivalents of BPP34C10 in acetonitrile at room temperature for three d. After solvent removal, the catenanes were isolated by preparative thin-layer chromatography on silica as described in Chapter Two.

Section 3.2.1 Synthesis and Study of 3.13a

The first step in the synthesis of 1,3-bis(2-(4,4'-dipyridinium)ethoxy)-4-chlorobenzene bis(hexafluorophosphate) (**3.13a**) produced diol (**3.11a**) in 77 % yield (Scheme 3.2). A ^{1}H NMR spectrum of the pure product revealed

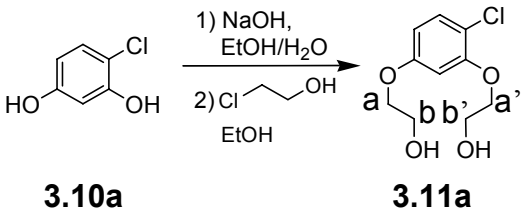

3.10a **3.11a**

Scheme 3.2.

the influence of the electron withdrawing substituent. Unlike previously discussed, ethoxy substitutions which displayed incredibly and irreducibly complex multiplets associated with the ethyl proton signals, the chloro-substituted resorcinol derivative produced deceptively simple signals for each of the protons on the chain, including the hydroxyl protons. At 4.14 (m, 2H) and 4.06 (m, 2H) we have two signals emanating from the protons on the carbon nearest the aryl ring (a and a') which both appear as triplets. However, upon closer examination the coupling constants between the peak signals are not internally consistent with 0.5 Hz difference between each indicating the systems are not first-order. This is due to long-range coupling to the hydroxyl proton. Further evidence for the complex nature of these multiplets comes from the protons on the second carbon (b and b') at 3.90 (m, J = 4.7, 2.8 Hz, 2H) and 3.85 (m, J = 4.7, 2.8 Hz, 2H) which appear as symmetric multiplets. Final conformation comes from the coupled hydroxyl protons themselves 4.00-3.96 (m, 2H). The ^{13}C NMR spectrum revealed four new signals at 72.6, 72.0, 62.24, and 62.17 ppm consistent with the altered magnetic environments and signal shifts observed in the ^{1}H NMR spectrum. These data, along with obtaining the anticipated low-resolution EI mass spectrum signals at m/z 255.7 (M Na^{+}), 232.0 (M^{+}), indicated the desired diol product was obtained. Bromination of the ethano-bridged diol (**3.11a**) was accomplished using triphenylphosphine and bromine yielding 45 % of the pure product (Figure 3.3). Substitution of bromine

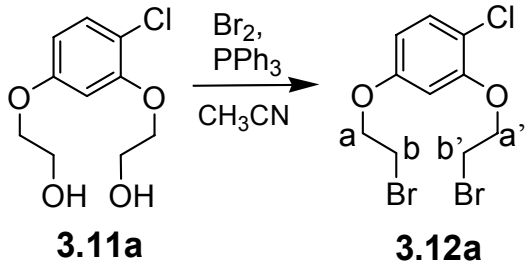

3.11a **3.12a**

Scheme 3.3.

on the b-b' carbons further resolved the multiplets. The a and a' proton signals shifted downfield to 3.66 (t, J = 6.4 Hz, 2H) and 3.64 (t, J = 6.4 Hz, 2H) while the b-b' proton signals shifted upfield to 4.31 (t, J = 6.4 Hz, 2H) and 4.26 (t, J = 6.4 Hz, 2H) with loss of the alcohol proton signal observed for the diol starting material. Analysis of the EI mass spectrum shows peaks at m/z 384.9 (M Na^+), 357.9 (M^+), and 277.1 (M^+ -Br) consistent with the calculated mass of 358.5 grams per mole.

Synthesis of the dipyridyl substituted 1,3-bis(2-(4,4'-dipyridinium)ethoxy)-4-chlorobenzene bis(hexafluorophosphate) (**3.13a**) was achieved via treatment of the dibromide (**3.12a**) with four equivalents of 4,4'-dipyridyl followed by salt exchange from the bromide to hexafluorophosphate salt (Scheme 3.4). Confirmation of the structure was made by mass, ^{13}C, and ^1H NMR

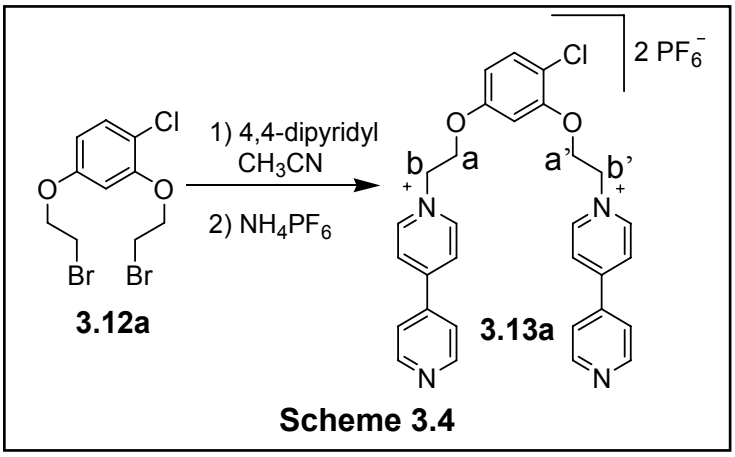

Scheme 3.4

spectra. As with the previously described catenanes the dipyridyl proton signals appeared in the form of irreducibly complex symmetric multiplets consistent with para-substituted aromatic rings in an AA'XX' type spectra.[51] The ^1H NMR spectrum showed five new multiplets at 9.35 (m, J = 6.0 Hz, 4H), 8.89 (m, 4H), 8.74 (m, J = 6.0 Hz, 2H), 8.69 (m, J = 6.0 Hz, 2H), and 8.05-7.97 (m, 4H) along with a downfield shift in the ethanolic bridge protons to 5.37 (m, J = 4.9 Hz, 2H), 5.33 (m, J = 4.9 Hz, 2H), and 4.73 (m, J = 4.9 Hz, 4H) ppm expected by formation of the cationic nitrogen and

associated deshielding. Mass spectral data of the dipyridyl salts provided readily identifiable signals which are typical of these compounds.[42] Loss of one hexafluorophosphate anion produced the monocationic species and appeared as a signal at 655.1 (M PF_6^+) in the ESI spectra. Loss of the remaining hexafluorophosphate anion produced a signal at 255.1 (M^{2+}). These spectroscopic studies, in addition to the correct mass spectrum, demonstrated formation of the desired product, 1,3-bis(2-(4,4'-dipyridinium)ethoxy)-4-chlorobenzene bis(hexafluorophosphate) (**3.13b**).

Section 3.2.2 Synthesis and Study of 3.13b

Synthesis of 1,3-bis(2-(4,4'-dipyridinium)ethoxy)-4-ethylbenzene bis(hexafluorophosphate) (**3.13b**) was typical and began as shown in Scheme 3.5.

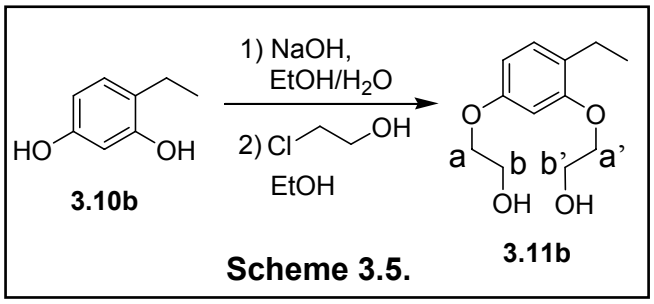

Scheme 3.5.

Bis(2-hydroxyethoxy)-4-ethylbenzene (**3.11b**) was synthesized from 4-ethylbenzene-1,3-diol (**3.10b**) in 81 % yield through deprotonation of **3.10b** followed by addition of 2-chloroethanol. The ^{1}H NMR spectrum of the pure **3.11b** displayed signals typical of the hydrogen or carbon substituted ethoxy-benzene diols. Between 4.07-4.00 (m, 6H) and 3.93-3.82 (m, 4H) ppm we have two complex multiplets from the ethoxy bridge protons with the hydroxyl proton signals superimposed on the downfield multiplet. At 2.56 (q, J = 7.5 Hz, 2H) and 1.12 (t, J = 7.5, 3H) ppm we observe the signals from the ethyl substitution on the aryl ring. These data, along with obtaining the anticipated molecular ion signal in the low-resolution EI mass spectrum at 226.2 (M^+ calculated 226.3),

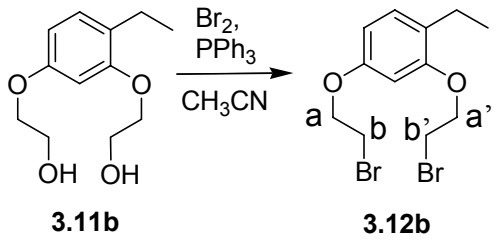

3.11b **3.12b**

Scheme 3.6.

indicated the desired diol product **3.11b** was obtained. Subsequent bromination was accomplished with a 95 % yield of 1,3-bis(2-hydroxyethoxy)-4-ethylbenzene (**3.12b**) (Scheme 3.6). Substitution of bromine on the b-b' carbons again resolved the multiplets, shifting the b-b' proton signals downfield to 4.27 ppm (m, J = 6.11 Hz, 4H) which were superimposed on the a-a' proton signals at 3.67 (m, J = 6.1 Hz, 2H) and 3.62 (m, J = 6.1 Hz, 2H) ppm. Loss of the hydroxyl proton signal was also observed. Analysis of the low-resolution EI mass spectrum gave the calculated molecular ion peak at 352.0 m/z.

Synthesis of the dipyridyl substituted **3.13b**, 1,3-bis(2-(4,4'-dipyridinium)ethoxy)-4-ethylbenzene bis(hexafluorophosphate), was achieved in 92 % yield by treatment of the dibromide **3.12b** with four equivalents of 4,4'-dipyridyl followed by salt exchange from the bromide to the hexafluorophosphate salt (Scheme 3.7). Confirmation of the structure was made by analysis of mass, ^{13}C, and ^{1}H NMR spectra. The ^{1}H NMR spectrum showed six new complex multiplets displaying the AA'XX' coupling patterns[51] at 9.39 (m, J = 6.6 Hz, 2H), 9.35 (m, J = 6.6 Hz, 2H),

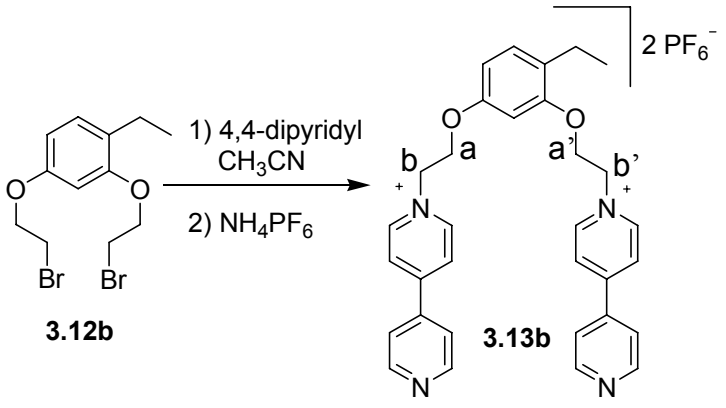

3.12b **3.13b**

Scheme 3.7.

8.89 (m, J = 6.2 Hz, 4H), 8.76 (m, J = 6.6 Hz, 2H), 8.70 (m, J = 6.6 Hz, 2H), and 8.03 (m, J = 6.2 Hz, 4H) consistent with addition of dipyridyl. Ethanolic spacer protons experienced the downfield shift to 5.37 (m, 2H), 5.32 (m, 2H), and 4.67 (m, 4H) ppm observed in previous examples. Mass spectral data confirmed the atomic weight of the compound. Loss of one hexafluorophosphate anion produced the monocationic species and appeared as a signal at m/z 649.2 (M PF_6^+) in the ESI spectra. Loss of the remaining hexafluorophosphate anion produced a signal at m/z 252.1 (M^{2+}). These spectroscopic studies, in addition to the correct mass spectrum, demonstrated successful formation of the desired product, 1,3-bis(2-(4,4'-dipyridinium)ethoxy)-4-ethylbenzene bis(hexafluorophosphate) (**3.13b**).

Section 3.2.3 Synthesis and Study of 3.13c

For the *n*-hexyl substituted resorcinol example, 4-*n*-hexylbenzene-1,3-diol (**3.11c**) was synthesized from 4-*n*-hexylbenzene-1,3-diol (**3.10c**) in 72 % yield (Scheme 3.8). In the ^{1}H NMR spectrum, the new ethyl substituents appeared as complex multiplets at 4.04 (m, J = 8 Hz, 4H) for the a-a' and 3.94 (m, J = 8 Hz, 4H) for the b-b' protons with the hydroxyl proton signals appearing at 2.31 ppm (bs, 2H). The *n*-hexyl substituent on the aryl ring appears as a series of ill-defined multiplets at 2.54 (m, 2H), 1.58-1.47 (m, 2H), 1.35-1.25 (m, 7H), and 0.88 (m, 3H) ppm. In addition, the ^{13}C NMR spectrum revealed four new

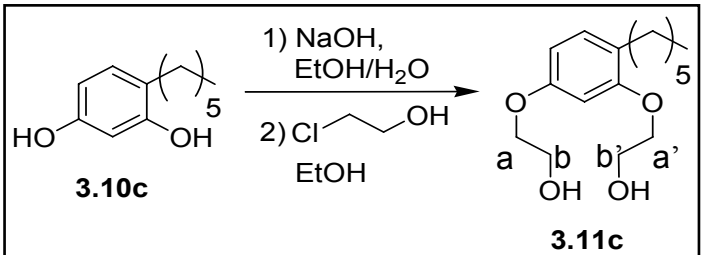

3.10c **3.11c**

Scheme 3.8.

signals at 71.5, 71.4, 62.4, and 62.4 ppm consistent with the methylene protons adjacent to oxygen and expected from addition of ethanol. These data, along with obtaining the anticipated molecular ion signal in the low-resolution EI mass spectrum at m/z 282.1 (M^+ calculated 282.4), indicated the formation of the desired product. As shown in Scheme 3.9, bromination using bromine and triphenylphosphine was accomplished in quantitative yield using diol 1,3-bis(2-hydroxyethoxy)-4-*n*-hexylbenzene (**3.11c**). Substitution of bromine on the b-b‘ carbons shifted the proton signals of the ethoxy-bridges downfield to 4.26 ppm (m, *J* = 6.0 Hz, 4H) with the signals overlapped. The a-a’ proton signals were observed at 3.66 (m, *J* = 6.0 2H) and 3.63 (m, *J* = 6.0 Hz, 2H) ppm. Loss of the alcohol proton signal at 2.31 ppm was also observed. Analysis of the low-resolution EI mass spectrum gave the calculated molecular ion peak at 407.9 m/z.

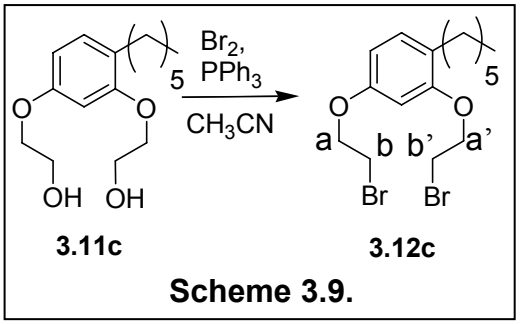

3.11c **3.12c**

Scheme 3.9.

Synthesis of the dipyridyl substituted **3.13c**, 1,3-bis(2-(4,4’-dipyridinium)ethoxy)-4-ethylbenzene bis(hexafluorophosphate), was achieved in 96 % yield by treatment of the dibromide **3.12c** with four equivalents of 4,4’-dipyridyl followed by salt exchange from the bromide salt to the hexafluorophosphate salt (Scheme 3.10). The structure was determined by mass, ^{13}C, and ^{1}H, NMR spectral analysis. Consistent with addition of dipyridyl, five new complex multiplets displaying the AA’XX’ coupling patterns[51] were observed at 9.47 (m, *J* = 7.1 Hz, 2H), 9.40 (m, *J* = 7.1 Hz, 2H), 8.87 (m, *J* = 6.0 Hz, 4H), 8.74 (m, *J* = 7.1 Hz, 4H), and 8.01 (m, *J* = 6.0 Hz, 4H) ppm. The ethanolic spacer proton signals appeared as multiplets and were

shifted downfield to 5.38 (m, 2H), 5.33 (m, 2H), and 4.71 (m, 4H) ppm which is nearly identical to the previous example. Analysis of the mass spectrum confirmed the proposed identity. Loss of one hexafluorophosphate anion produced the monocationic species and appeared as a signal at m/z 705.3 (M PF_6^+), while the dicationic species appeared at m/z 280.1 (M^{2+}) in the ESI spectra. These spectroscopic studies confirmed formation of the desired product, 1,3-bis(2-(4,4'-dipyridinium)ethoxy)-4-ethylbenzene bis(hexafluorophosphate) (**3.13c**).

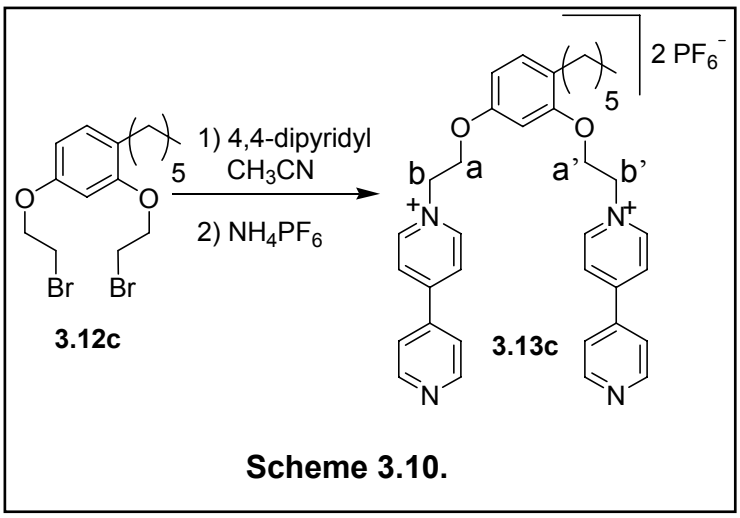

Scheme 3.10.

Section 3.3 Synthesis and Characterization of Catenanes 3.1-3.9

Synthesis of the catenanes began with dissolution of the dipyridyl substituted resorcinol derivatives and three equivalents of BPP34C10 in followed by addition of 1.2 equivalents of the desired stopper (Scheme 3.11). For catenanes **3.1**, **3.4**, and **3.7**

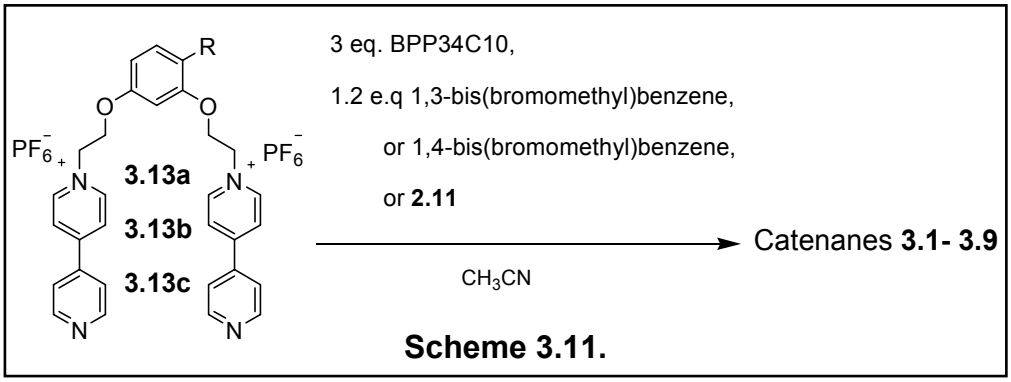

Scheme 3.11.

possessing the 1,3-xylylene tether, 1.2 equivalents of a,a'-dibromo-*m*-xylene was added to the solution of dipyridinium and three equivalents of BPP34C10. Catenanes **3.2**, **3.5**, and **3.8** were formed via addition of 5-bis(bromomethyl)-4'-(1,1'-dimethylethyl)-1,1'-biphenyl, while **3.3**, **3.6**, and **3.9** were formed through addition of a,a'-dibromo-*p*-xylene, to solutions of the substituted 3-di(2-(4,4'-dipyridinium)ethoxy)benzene bis(hexafluorophosphate) and BPP34C10 (Scheme 3.11). As observed before, evidence for formation of the π-stacked complexes appeared in less that twenty minutes as a red color, indicating pseudorotaxane and product formation. These reactions continued stirring three d to ensure complete consumption of the starting materials. The solutions turned a deep red color and a yellow precipitate formed during this time. These crude catenane products were purified by preparative TLC in the same manner described in Chapter 2.

Section 3.3.1 Characterization of Catenane 3.1

For catenane **3.1** (Figure 3.4), possessing a chlorine at the 4-position on the resorcinol ring and the 1,3-xylyl tether, addition of BPP34C10 yielded a conformationally mobile catenane exhibiting fast exchange at ambient

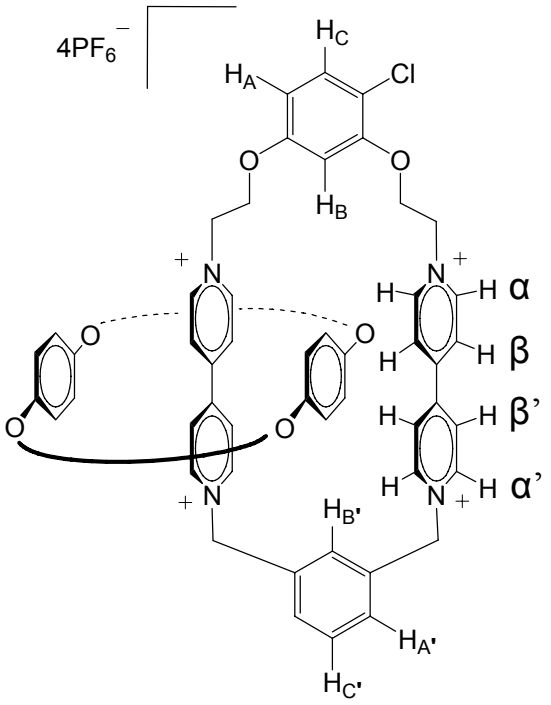

Figure 3.4 Catenane 3.1.

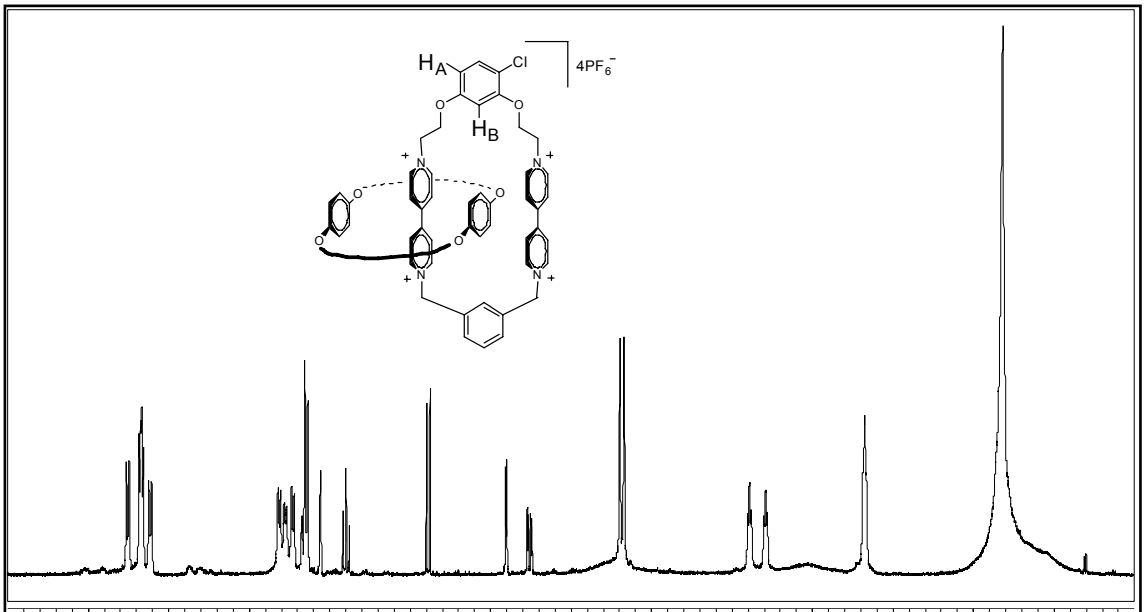

Spectrum 3.1. Catenane **3.1** at 293 K.

temperatures in the 1H NMR spectrum. The α pyridinium protons were shielded, shifting them upfield from 9.35 (m, *J* = 6.0 Hz, 4H) to 9.25 (m, *J* = 6.7 Hz, 2H) and 9.17 (m, *J* = 6.7 Hz, 4H) with the downfield signal overlapping the upfield α' signal (Spectrum 3.1). Formation of the new pyridinium species shifted the α' proton signals downfield from 8.89 (m, 4H) to 9.17 (m, *J* = 6.7 Hz, 4H), again with overlap of the α' signal, and 9.11 ppm (m, *J* = 6.7 Hz, 2H). Both β and β' dipyridinium protons were affected by addition of the BPP34C10 and formation of the second pyridinium being shifted to 8.31 (m, *J* = 6.7 Hz, 2H), 8.27 (m, *J* = 6.7 Hz, 2H), 8.23 (m, *J* = 6.7 Hz, 2H), and 8.15 (m, *J* = 6.7 Hz, 4H) ppm. Using 2D-NMR experiments such as COSY, HMBC, and HSQC these β proton signals remained indistinguishable from one another. The additional two protons found in the integration at 8.15 ppm (m, *J* = 6.7 Hz, 4H) were attributed to overlap of two β-β' pyridinium protons and the two protons ortho and para to both xylene methylene groups (H_A'). The proton meta to the xylyl-methylenes

($H_{C'}$) appeared as a triplet at 7.90 (t, J = 7.8 Hz, 1H) while the proton ortho to both methylenes ($H_{B'}$) appeared as a triplet at 8.06 (t, J = 1.6 Hz, 1H). At 6.20 (s, 2H) and 6.17 (s, 2H) we observed the xylyl methylene signals consistent with the anticipated product. Ethoxy bridge proton signals appeared relatively unaffected by the additions shifting only slightly from 5.37 (m, J = 4.9 Hz, 2H), 5.33 (m, J = 4.9 Hz, 2H), and 4.73 (m, J = 4.9 Hz, 4H), in the dicationic dipyridyl starting material, to 5.39 (s, 2H), 5.29 (s, 2H) and 4.68 (t, J = 3.8 Hz, 4H).

Compared to the symmetric catenanes these asymmetric catenanes containing substitution at the 4-position displayed much more complex spectra. In the tetracationic catenane chlorine significantly altered the magnetic environment of the two sides and we resolution of nearly all signals.

Following the trends established by our symmetric catenanes (Halterman 2006) and literature examples (Stoddart 1993, 1995, 1996) signals for catenated BPP34C10 were broad and ill defined appearing as a broad singlet at 5.03 (bs, 8H) and multiplet at 3.91-3.51 (m, 32H). In the mass spectrum (ESI) we observed various cationic states associated with loss of counter ions with masses of 648.3 (M PF_6^{2+}), 432.2 (M PF_6^{3+}), 383.5 (M^{3+}), and 288.2 (M^{4+}) m/z. Together these spectra confirmed the structure of the catenane species **3.1**.

Section 3.3.2 Characterization of Catenane 3.2

Synthesis of Catenane **3.2** (Figure 3.5), with 4-chloro and 5-(4-*t*-butylphenyl)-1,3 xylyl tethers, produced results similar to Catenane **3.1**. At and above room temperature we observed the fast exchange of signals in the ^{1}H NMR spectrum

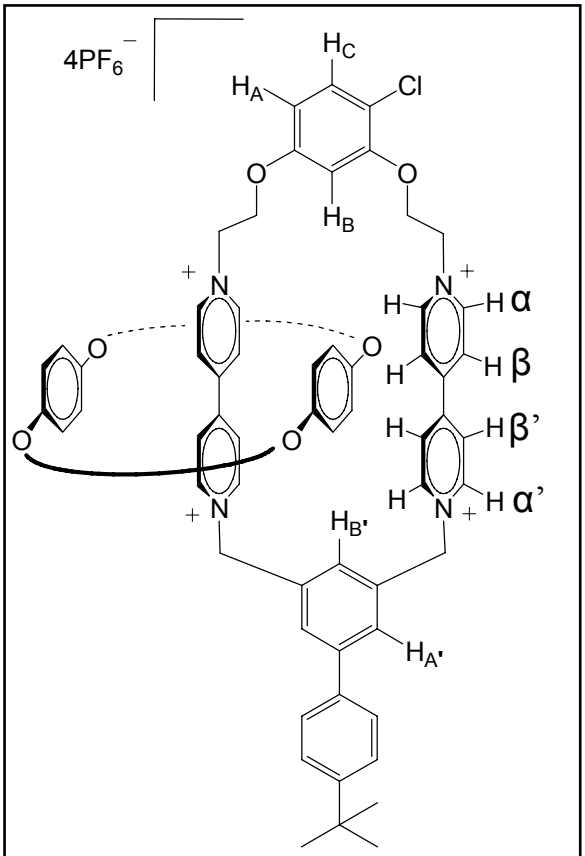

Figure 3.5. Catenane **3.2**.

indicating rapid movement of BPP34C10 between the two dipyridinium ground state binding sites. Addition of BPP34C10 caused a shift in the α pyridinium proton signals from 9.35 ppm (m, *J* = 6.0 Hz, 4H) to 9.34 (m, *J* = 7.0 Hz, 2H) and 9.27 (m, *J* = 7.0 Hz, 2H) ppm (Spectrum 3.2). Formation of the new pyridinium species shifted the α’ proton signals downfield from 8.89 (m, 4H) to 9.13 (d, *J* = 7.0 Hz, 1H) and 9.11 (d, *J* = 7.0 Hz, 1H) ppm. Both

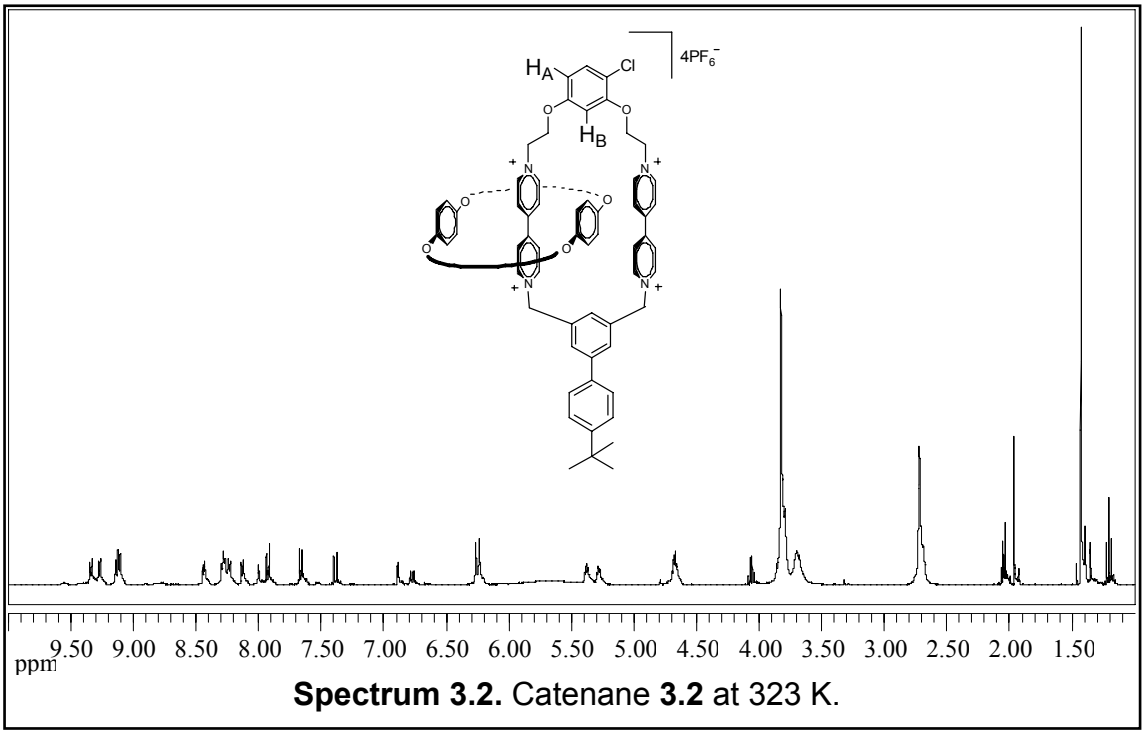

Spectrum 3.2. Catenane **3.2** at 323 K.

β and β' dipyridinium protons were affected by catenated BPP34C10 and formation of the second pyridinium causing a shift to 8.44 (m, *J* = 4.8 Hz, 2H), 8.29 (d, *J* = 4.8 Hz, 1H), 8.27 (d, *J* = 4.8 Hz, 1H), 8.23 (m, *J* = 7.0 Hz, 2H), and 8.13 (m, *J* = 7.0 Hz, 2H) ppm. The two protons ortho and meta to the xylyl-methylenes ($H_{A'}$) account for the integration of four protons at 8.28 ppm. The proton meta to both methylenes ($H_{B'}$) appeared as a triplet at 8.00 (t, *J* = 1.40 Hz, 1H). At 6.26 (s, 2H) and 6.24 (s, 2H) we observed the xylyl methylene signals. Appropriate signals were observed for the protons on the blocking group with its four phenyl protons and nine methyl protons being observed at 7.93 (m, *J* = 8.6 Hz, 2H), 7.66 (m, *J* = 8.6 Hz, 2H), and 1.43 (s, 9H), respectively, and nearly identical to the signals observed in the spectrum of catenane **2.2**. As observed previously, changes in the ethoxy-spacer proton signals were limited to shifts of only 0.02 ppm in the most extreme cases. In the ESI mass spectrum we observed signals for the di-, tri-, and tetracationic species with zero to two counter ions present; 786.3 (M $2PF_6^{2+}$), 476.2 (M PF_6^{3+}), 427.6 (M^{3+}),and 320.7 (M^{4+}) m/z. This evidence along with the other spectra confirmed we synthesized and isolated the desired catenane **3.2**.

Section 3.3.3 Characterization of Catenane 3.3

Synthesis and isolation of catenane **3.3** (Figure 3.6), with 4-chloro-resorcinol and 1,4-xylyl tethers, was supported by spectral data

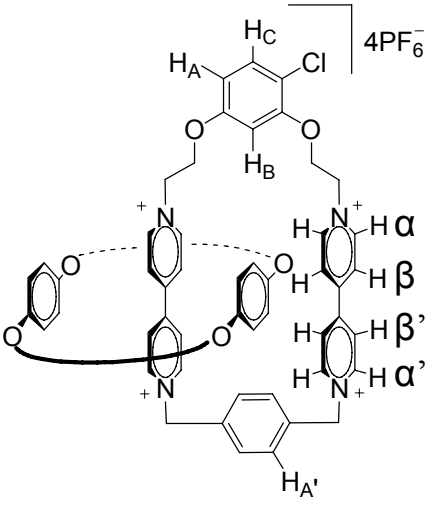

Figure 3.6. Catenane **3.3**.

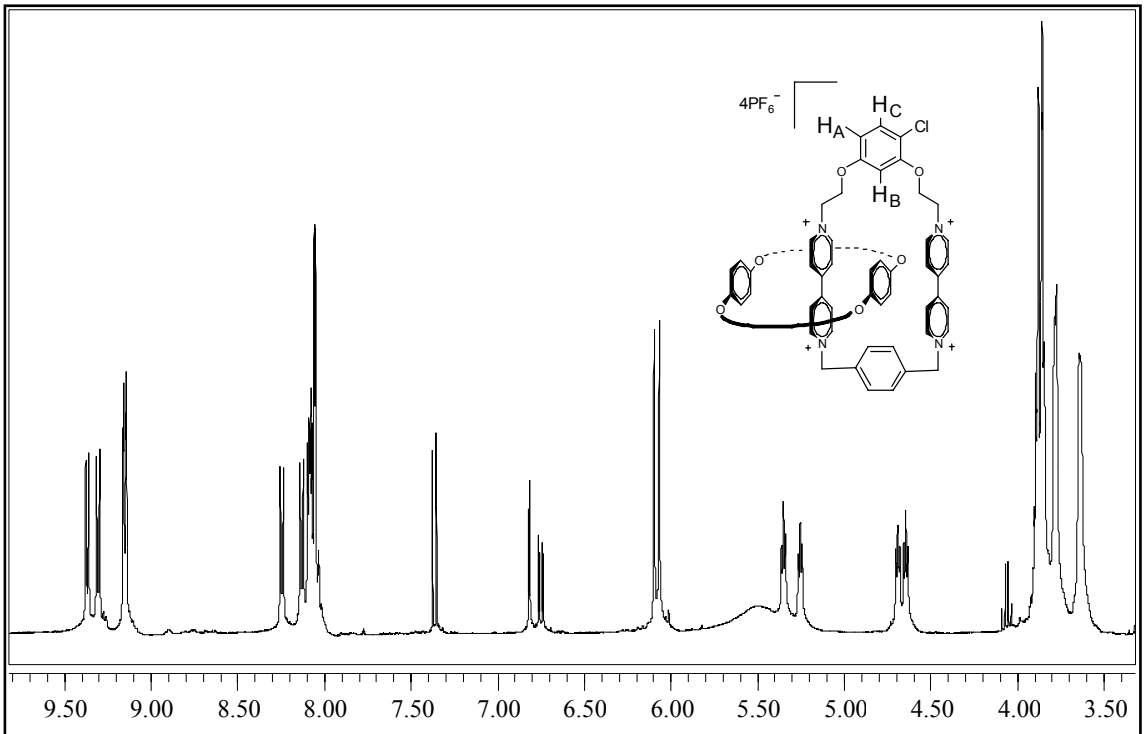

Spectrum 3.3. Catenane **3.3** at 323 K.

collected on the sample. At and above room temperature we observed the fast exchange of signals in the ^{1}H NMR spectrum indicating rapid movement of BPP34C10 between the two dipyridinium ground state binding sites. These spectra were very similar to spectra collected for the previous catenanes with some exceptions. Addition of BPP34C10 shifted the α pyridinium proton signals to 9.37 (m, *J* = 7.0 Hz, 2H) and 9.31 (m, *J* = 7.0 Hz, 2H) (Spectrum 3.3). Similar to the previous two catenanes, formation of the new pyridinium species shifted the α' proton signals downfield from 8.89 (m, 4H) to 9.15 ppm (m, *J* = 7.0 Hz, 4H). Unlike Catenane **2.3** we did not observed the degree of signal overlap for β-β' and xylene phenyl proton signals which is presumably due to chlorine substitution. The β-β' multiplets were fairly well resolved at 8.25 (m, *J* = 7.0 Hz, 2H), 8.13 (m, *J* = 7.0 Hz, 2H), 8.08 (m, *J* = 7.0 Hz, 4H). Signals for the xylene phenyl protons appeared at 8.06 (m, *J* = 2.5 Hz, 4H), while at 6.10 (s, 2H) and

6.07 (s, 2H) we observed the xylyl methylene proton signals. In the mass spectral data we observed the monocationic species (M^+, $3PF_6^-$) at 1586.5 m/z, as well as the other three possible cationic species, produced when the remaining counter ions are stripped, at 720.3 (M $2PF_6^{2+}$), 432.2 (M PF_6^{3+}), and 287.9 (M^{4+}) m/z, which further supported isolation of catenane **3.3**.

Section 3.3.4 Characterization of Catenane 3.4

For catenane **3.4** (Figure 3.7), possessing an ethyl group at the 4-position on the resorcinol ring and 1,3-xylyl tethers, we again observed that addition of BPP34C10 yielded a conformationally mobile catenane exhibiting fast exchange at ambient temperatures in the 1H NMR spectrum. The α pyridinium protons were shielded, shifting them upfield from 9.39 (m, *J* = 6.6 Hz, 2H) and 9.35 (m, *J* = 6.6 Hz, 2H) to 9.25 (m, *J* = 7.0 Hz, 2H) and 9.15 (m, *J* = 7.0 Hz, 4H) with the downfield signal overlapping the upfield α' signal (Spectrum 3.4). Formation of the new pyridinium species shifted the α' proton signals downfield from 8.89 (m, 4H) to 9.15 (m, *J* = 7.0 Hz, 4H), again with overlap of the α' signal, and 9.09 ppm (m, *J* = 7.0 Hz, 2H). The β and β' dipyridinium protons were shifted to 8.28 (m, *J* = 7.0 Hz, 2H), 8.27-8.22 (m, 4H),

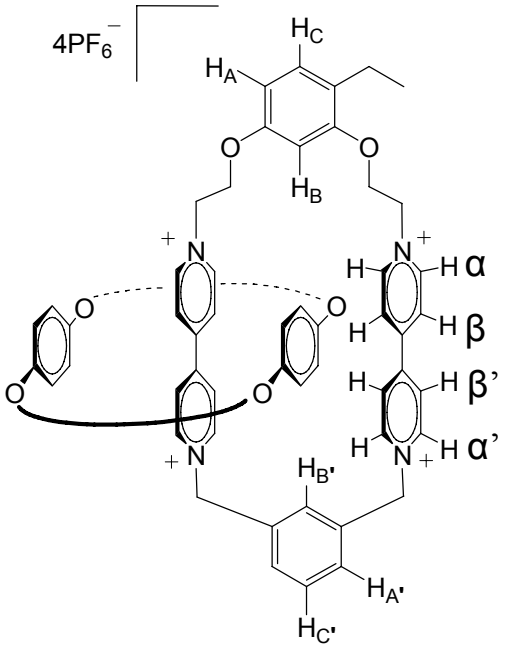

Figure 3.7. Catenane **3.4**.

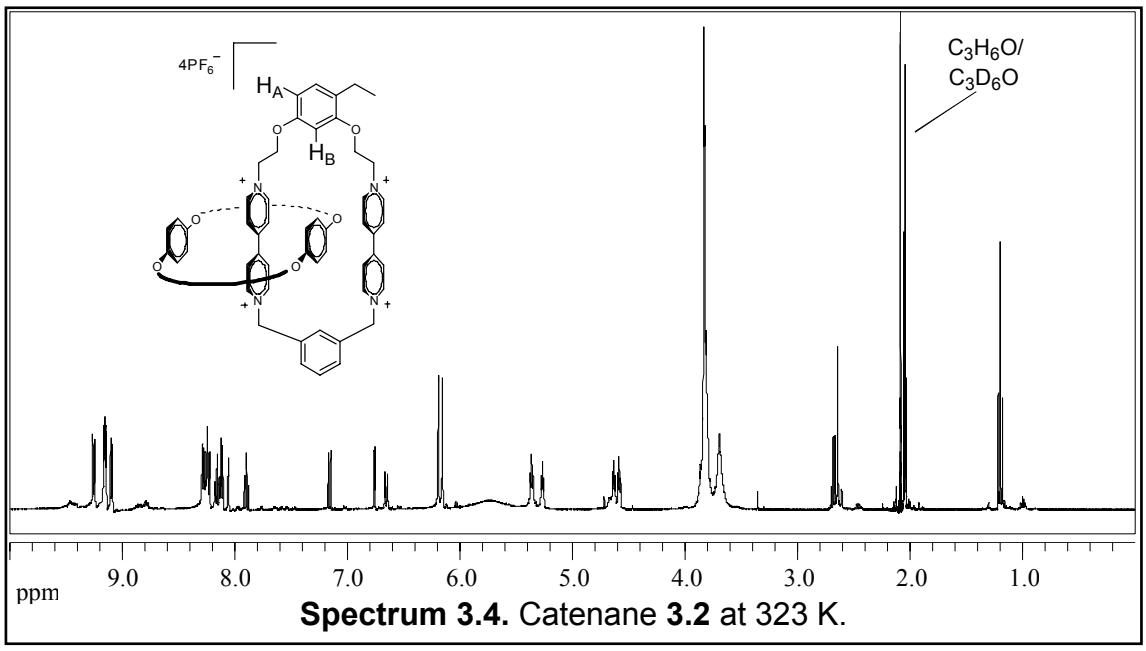

Spectrum 3.4. Catenane **3.2** at 323 K.

and 8.11 (m, *J* = 7.0 Hz, 2H), ppm. Signals for the protons ortho and meta to both xylene methylene groups (H_A,) appeared as a doublet of doublets at 8.16 (dd, *J* = 7.7, 1.2 Hz, 2H). The protons meta (H_B,) and ortho (H_C,) to the xylyl-methylenes appeared as triplets at 7.89 (t, *J* = 7.7 Hz, 1H) and 8.06 (t, *J* = 1.2, Hz, 1H), respectively; their shifts virtually identical to Catenane **3.1**. At 6.19 (s, 2H) and 6.16 (s, 2H) we observed the xylyl methylene signals consistent with all other catenanes. Ethoxy bridge proton signals shifted to 5.36 (m, *J* = 4.9 Hz, 2H), 5.27 (m, *J* = 4.8 Hz, 2H), 4.64 (m, *J* = 4.9 Hz, 2H) and 4.59 (m, *J* = 4.8 Hz, 2H). This enhanced resolution observed in the downfield multiplets was unusual for our catenanes. In the mass spectrum (ESI) we observed various cationic states associated with loss of counter ions with masses of 717.3 (M $2PF_6^{2+}$), 430.2 (M PF_6^{3+}), and 286.3 (M^{4+}) m/z. Together these spectra confirmed the structure of the catenane species **3.4**.

Section 3.3.5 Characterization of Catenane 3.5

Synthesis of catenane **3.5** (Figure 3.8), possessing the 4-ethyl-resorcinol and 5-(4-*t*-butylphenyl)-1,3-xylyl tethers, produced results similar to Catenane **3.2**.

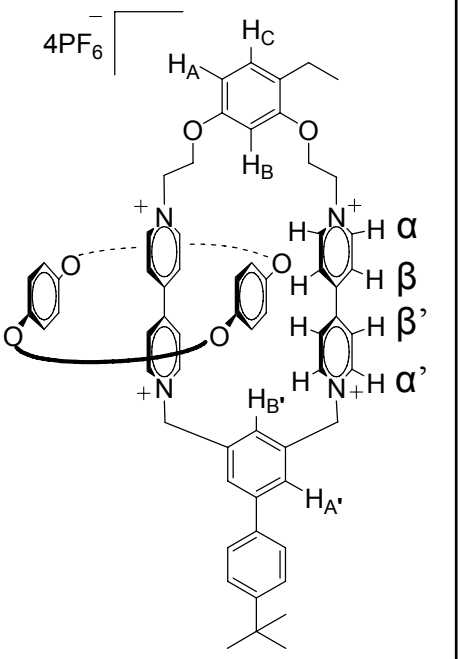

Figure 3.8 Catenane **3.5**.

Catenation caused a shift in the α pyridinium proton signals from 9.39 (m, *J* = 6.6 Hz, 2H) and 9.35 (m, *J* = 6.6 Hz, 2H) to 9.34 (m, *J* = 7.0 Hz, 2H) and 9.27 (m, *J* = 7.0 Hz, 2H) (Spectrum 3.5). Formation of the new pyridinium species shifted the α' proton signals downfield from 8.89 (m, 4H) to 9.15 (m, *J* = 7.0 Hz, 2H) and 9.10 (m, *J* = 7.0 Hz, 2H) ppm. β and β' dipyridinium protons were shifted to 8.44 (m, *J* = 6.6 Hz, 2H), 8.26 (m, *J* = 6.6, 7.0 Hz, 6H), and 8.11 (m, *J* = 7.0 Hz, 2H) ppm. Overlap with the two protons ortho

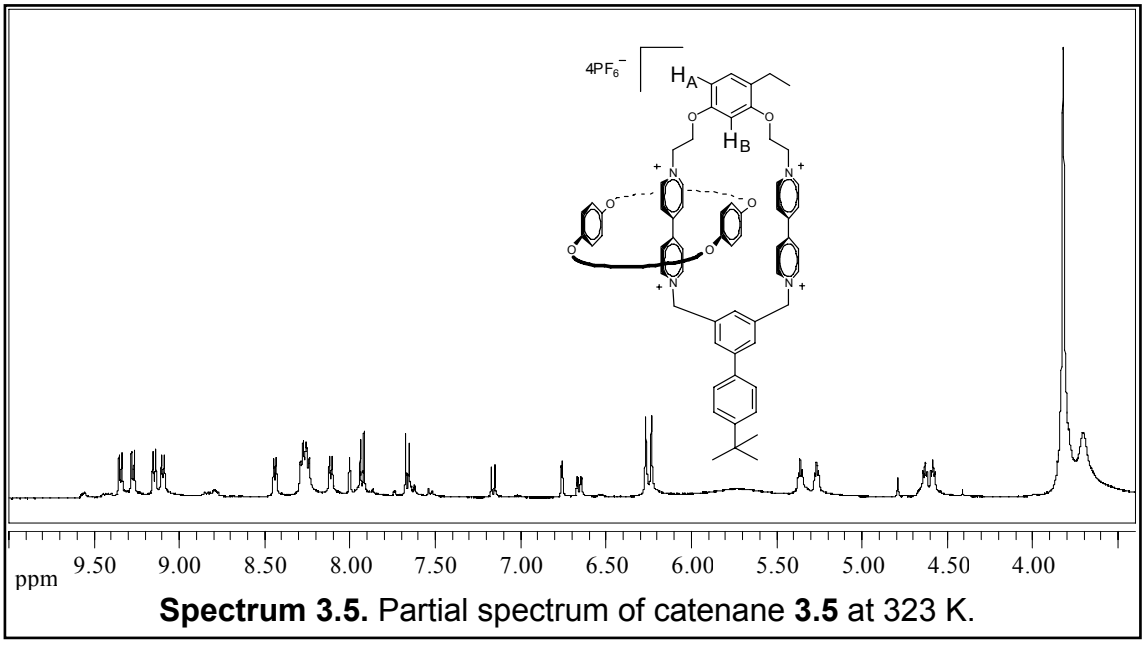

Spectrum 3.5. Partial spectrum of catenane **3.5** at 323 K.

and para to the xylyl-methylenes ($H_{A'}$) account for the integration of six protons at 8.26 ppm. The proton meta to both methylenes ($H_{B'}$) appeared as a triplet at 8.00 ppm (t, J = 1.5 Hz, 1H). At 6.27 (s, 2H) and 6.23 ppm (s, 2H) we observed the xylyl methylene signals. Appropriate signals were observed for the protons on the blocking group with its four phenyl protons and nine methyl protons being observed at 7.93 (m, J = 8.5 Hz, 2H), 7.66 (m, J = 8.5 Hz, 2H), and 1.43 (s, 9H), respectively, and nearly identical to the signals observed in the spectrum of Catenane **3.2**. The ethoxy-spacer proton signals were better resolved appearing at 5.36 (m, 2H), 5.27 (m, 2H), 4.63 (m, 2H) and 4.58 (m, 2H). In the ESI mass spectrum we observed further evidence for catenane formation. It showed the monocationic M $3PF_6^+$ species typically observed as well as peaks corresponding to the di-, tri-, and tetracationic species with differing numbers of counter ions present; 1718.6 (M $3PF_6^+$), 783.3 (M $2PF_6^{2+}$), 473.9 (M PF_6^{3+}), 427.6 (M^{3+}) and 319.4 (M^{4+}) m/z. This evidence along with the other spectra confirmed the structure of catenane **3.5**.

Section 3.3.6 Characterization of Catenane 3.6

Synthesis and isolation of catenane **3.6** (Figure 3.9), possessing the 4-ethyl-resorcinol and 1,4-xylyl tethers, was confirmed by spectral analysis. We observed that addition of BPP34C10 yielded a conformationally mobile catenane exhibiting fast exchange at ambient

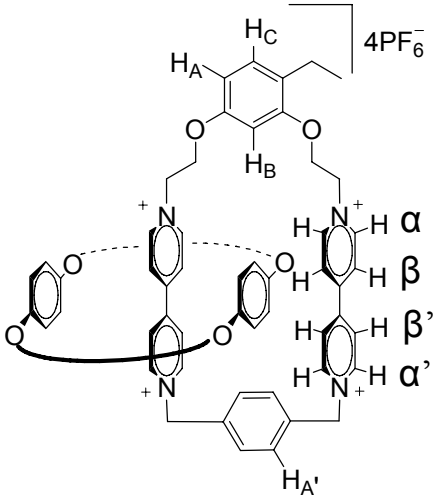

Figure 3.9. Catenane **3.6**.

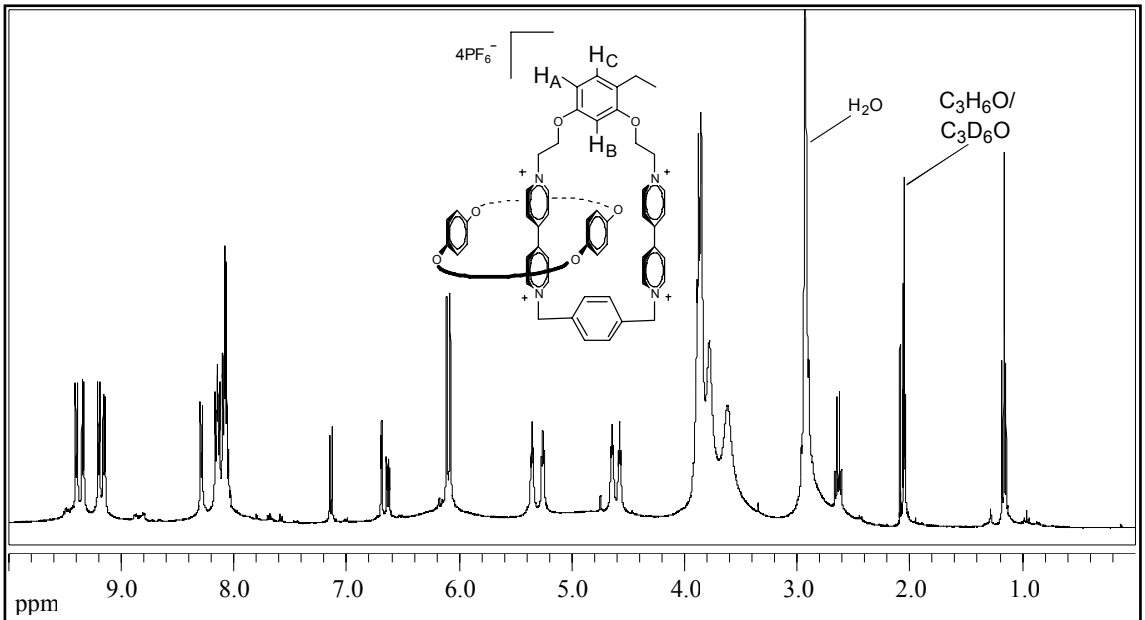

Spectrum 3.6. Catenane **3.6** at 293 K.

temperatures in the ^{1}H NMR spectrum. Catenating the crown ether shifted α pyridinium proton signals to 9.40 (m, *J* = 7.0 Hz, 2H) and 9.34 (m, *J* = 7.0 Hz, 2H) ppm (Spectrum 3.6). Formation of the new pyridinium species shifted the α' proton signals downfield to 9.20 (m, *J* = 7.0 Hz, 2H) and 9.15 (m, *J* = 7.0 Hz, 2H) ppm. Signals for the β and β' dipyridinium proton signals, as well as the xylyl-phenyl proton signals, overlapped forming a large complex multiplet. Six of the β-β' signals are outside the bulk of the multiplet at 8.29 (m, *J* = 7.0 Hz, 2H) and 8.15 (m, *J* = 7.0 Hz, 4H) ppm. However, the remaining signal, comprised of two signals and six protons, was lost under the xylyl-phenyl proton (H_A,) multiplet at 8.11-8.04 ppm (m, 6H). At 6.11 (s, 2H) and 6.08 (s, 2H) ppm we observed the xylyl methylene proton signals. The ethoxy-spacer signals were at 5.35 (m, 2H), 5.26 (m, 2H), 4.64 (m, 2H), and 4.58 (m, 2H) ppm. In the ESI mass spectrum we observed only bare cations at 572.3 (M^{2+}),

381.5 (M^{3+}), 286.1 (M^{4+}) m/z. These data along with the ^{1}H NMR spectrum confirmed the identity of catenane **3.6**.

Section 3.3.7 Characterization of Catenane 3.7

As with Catenane **3.1** and **3.4**, for catenane **3.7** (Figure 3.10), possessing the n-hexyl-resorcinol and 1,3-xylyl tethers, addition of BPP34C10 shielded the α pyridinium protons shifting them upfield from 9.47 (m, *J* = 7.1 Hz, 2H) and 9.40 (m, *J* = 7.1 Hz, 2H) to 9.26 (m, *J* = 7.0 Hz, 2H) and 9.17 (m, *J* = 7.0 Hz, 4H) with the downfield signal overlapping the upfield α' signal (Spectrum 3.7). Formation of the new pyridinium species shifted the α' proton signals downfield from 8.87 (m, *J* = 6.0 Hz, 4H) to 9.17 (m, *J* = 7.0 Hz, 4H), again with overlap of the α' signal, and 9.09 ppm (m, *J* = 7.0 Hz, 2H). β and β' dipyridinium protons were shifted to 8.31-8.23 (m, 6H) and 8.19-8.11 (m, 4H) with the latter overlapping the signal for protons ortho and para to both xylene methylene groups ($H_{A'}$). The protons meta ($H_{B'}$) and ortho ($H_{A'}$) to the xylyl-methylenes appeared at 8.07-8.05 (m, 1H) and 7.90 (t, *J* = 7.7 Hz, 1H) ppm, respectively. At 6.20 (s, 2H) and 6.17 (s, 2H) ppm we observed the xylyl methylene signals. Ethoxy bridge proton signals shifted to 5.36 (s, 2H), 5.28 (s, 2H), and 4.61 (m, *J* = 4.9 Hz, 4H). In the mass

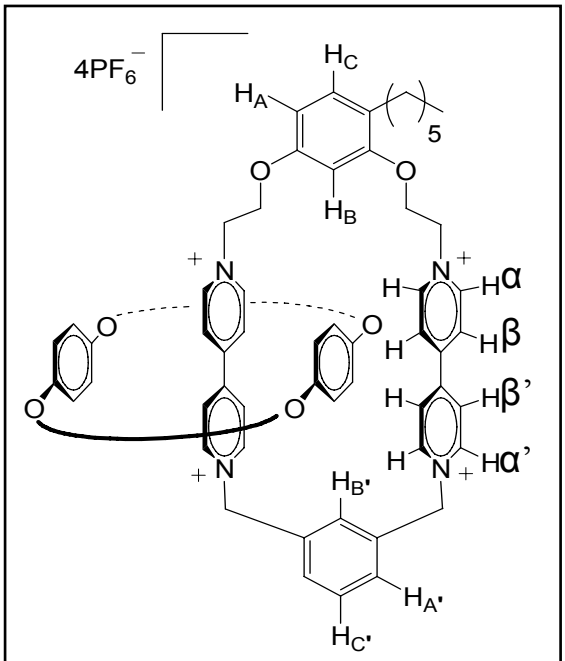

Figure 3.10. Catenane **3.7**.

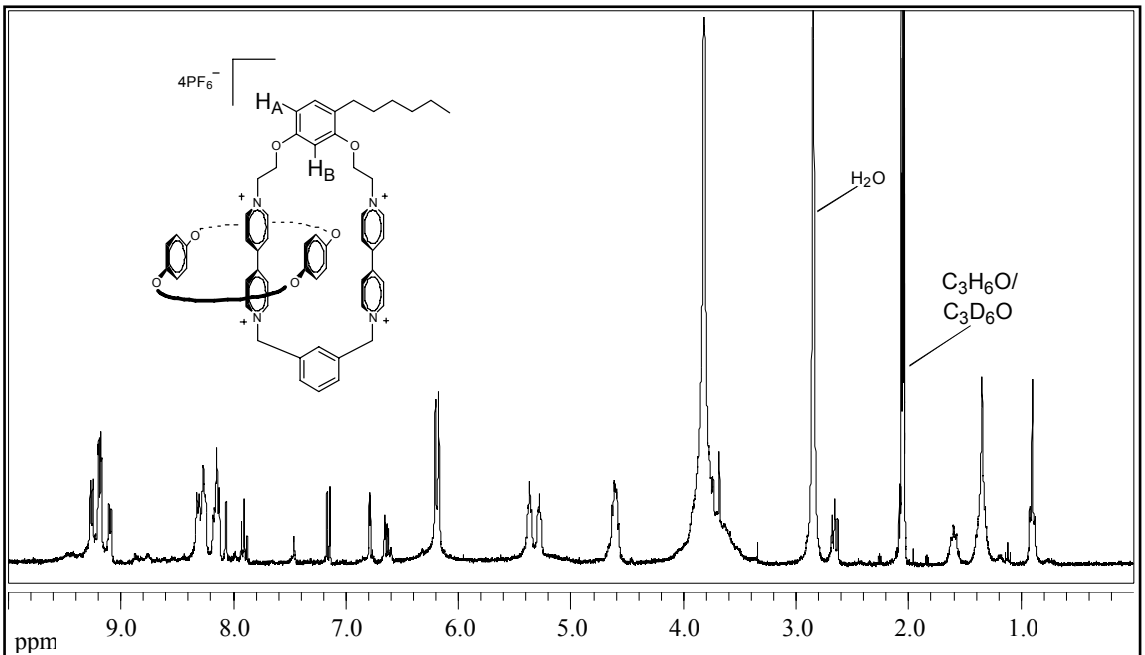

Spectrum 3.7. Catenane **3.7** at 293 K.

spectrum (ESI) we observed various cationic states arising from loss of counter ions with signals at 745.3 (M $2PF_6^{2+}$), 672.8 (M PF_6^{2+}), 600.5 (M^{2+}), 448.6 (M PF_6^{3+}), 400.2 (M^{3+}), and 300.2 (M^{4+}) m/z. Together these spectra confirmed the structure of catenane species **3.7**.

Section 3.3.8 Characterization of Catenane 3.8

Synthesis and analysis of catenane **3.8** (Figure 3.11), with *n*-hexyl-resorcinol and 5-(4-*t*-butylphenyl)-1,3-xylyl tethers, gave spectra similar to catenanes **3.2** and **3.5.** They showed addition of BPP34C10 and formation of a conformationally mobile catenane exhibiting

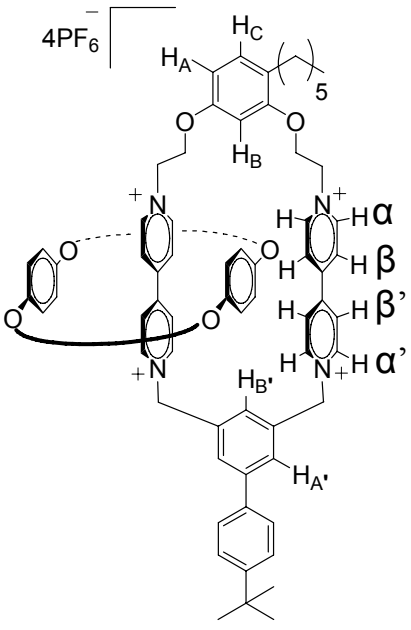

Figure 3.11. Catenane **3.8**.

fast exchange at ambient temperatures in the ^{1}H NMR spectrum. Catenation with BPP34C10 and the subsequent shielding caused a shift in the α pyridinium proton signals from 9.47 (m, *J* = 7.1 Hz, 2H) and 9.40 (m, *J* = 7.1 Hz, 2H) to 9.34 (m, *J* = 6.7 Hz, 2H), and 9.28 (m, *J* = 7.0 Hz, 2H) ppm (Spectrum 3.8). Formation of the new pyridinium species shifted the α' proton signals downfield from 8.87 (m, *J* = 6.0 Hz, 4H) to 9.14 (m, *J* = 6.7 Hz, 2H) and 9.07 (m, 2H). One set of β-β' dipyridinium protons signals appeared as a defined multiplet at 8.44 (m, *J* = 3.9 Hz, 2H). However, the remaining six appeared as a poorly resolved multiplet between 8.36-8.17 ppm (m, 6H). Then, between 8.17-8.06 ppm (m, 2H) we observed the signals for the protons both ortho and para to the xylyl methylenes (H_A'). The proton meta to both methylenes (H_B'), which typically appeared as a triplet, remained unresolved as a multiplet at 8.01

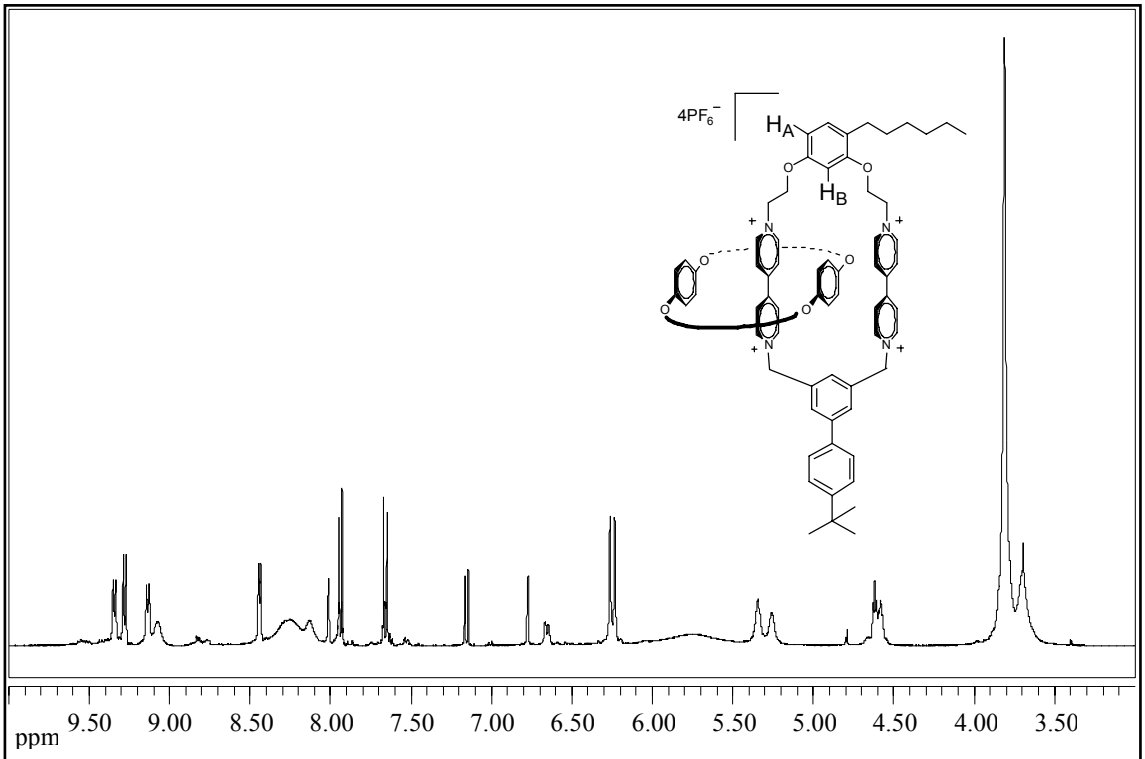

Spectrum 3.8. Partial spectrum of catenane **3.8** at 323 K.

ppm (m, 1H). At 6.26 (s, 2H) and 6.23 (s, 2H) ppm we observed the xylyl methylene signals. Signals for the blocking group with its four phenyl protons and nine methyl protons were observed at 7.94 (d, J = 8.5 Hz, 2H), 7.66 (d, J = 8.5 Hz, 2H), and 1.43 (s, 9H), respectively, which were nearly identical to the signals observed in the spectra of catenanes **3.2** and **3.5**. The ethoxy-spacer proton signals appeared as symmetric multiplets at 5.34 (m, 2H), 5.26 (m, 2H) and between 4.64-4.55 (m, 4H). In the ESI mass spectrum we observed further evidence for catenane formation with peaks appearing at 666.4 (M^{2+}), 492.9 (M PF_6^{3+}) and 333.2 (M^{4+}) m/z corresponding to di-, tri-, and tetracationic species. This evidence along with the other spectra served to confirm the structure of catenane **3.8**.

Section 3.3.9 Characterization of Catenane 3.9

Synthesis and isolation of catenane **3.9** (Figure 3.12), possessing the 4-*n*-hexyl-resorcinol and 1,4-xylyl tethers, was confirmed by analysis of spectra collected on the sample. We observed that catenation of BPP34C10 yielded a conformationally mobile catenane exhibiting fast exchange at ambient temperatures in the ^{1}H NMR spectrum. The pyridinium proton signals were shifted to 9.44 (m, J = 7.0 Hz, 2H) and 9.40 (m, J = 7.0 Hz, 2H) (Spectrum 3.9), a result of catenating Bpp34C10. As with previous catenanes, α' pyridinium proton signals were shifted downfield

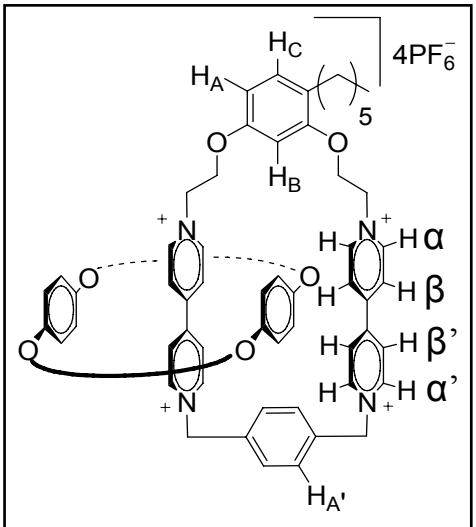

Figure 3.12. Catenane **3.9**.

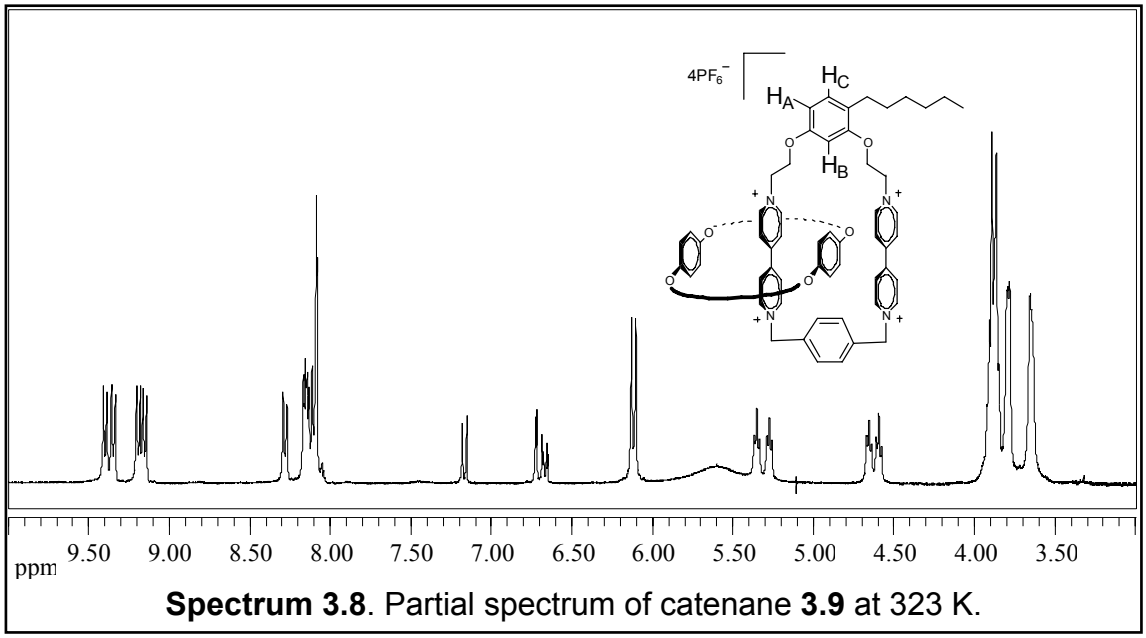

Spectrum 3.8. Partial spectrum of catenane **3.9** at 323 K.

to 9.25 (m, *J* = 7.0 Hz, 2H) and 9.20 (m, *J* = 7.0 Hz, 2H). The β-β' dipyridinium proton signals appeared at 8.34 (m, *J* = 7.0 Hz, 2H), 8.20 (m, *J* = 7.0 Hz, 4H) and 8.15 (m, *J* = 7.0 Hz, 2H). Multiplets at 8.12 (m, 2H) and 8.08 (m, 2H) emanated from the xylene protons. The xylyl methylene proton signals were observed at 6.16 (s, 2H) and 6.14 (s, 2H) ppm. Ethoxy-spacer signals were at 5.40 (m, 2H), 5.32 (m, 2H), 4.68 (m, 2H), and 4.63 (m, 2H) ppm. Finally, in the ESI mass spectrum we observed good evidence of catenane formation. It showed the monocationic M $3PF_6^+$ species and peaks corresponding to the sequential loss of counter ions forming di-, tri-, and tetracationic species; 1636.4 (M $3PF_6^+$), 745.3 (M $2PF_6^{2+}$), 448.8 (M PF_6^{3+}), and 300.4 (M^{4+}) m/z. These data along with the ^{1}H NMR spectrum confirmed the identity of catenane **3.9**.

Section 3.4 VT ^{1}H NMR Spectra of Catenanes

Section 3.4.1 VT ^{1}H NMR Spectra of Catenane 3.1

As with the symmetric catenanes each of the asymmetric catenanes possessed unique signal characteristics often allowing use of only select signal sets for measuring both chemical shift differences (**Δυ**) and determining temperature of coalescence in order to perform the activation energy calculations. While the α and α' signals of the dipyridinium protons were distinct in the fast-exchange region, in the slow exchange region an unacceptable overlap of signals for catenanes **3.1** to **3.9** was observed. Typically, the signals for the meta- and ortho-protons H_A and H_B were clearly defined and their coalescence temperatures easily determined. Catenane **3.1** was no exception.

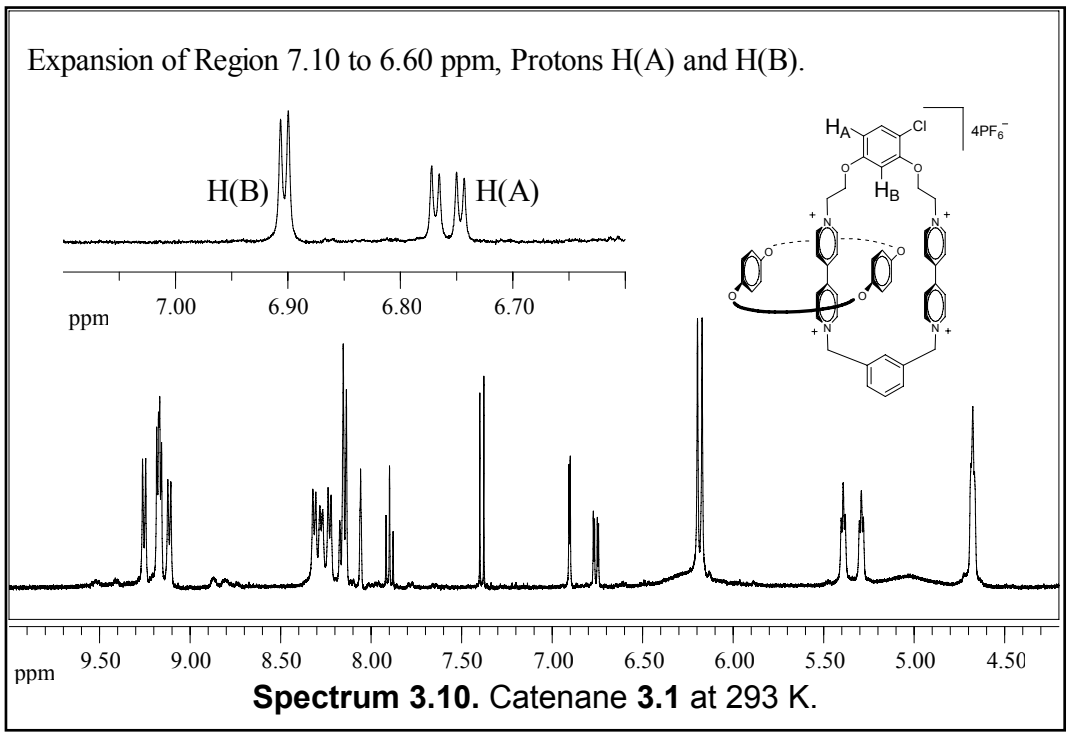

Spectrum 3.10. Catenane **3.1** at 293 K.

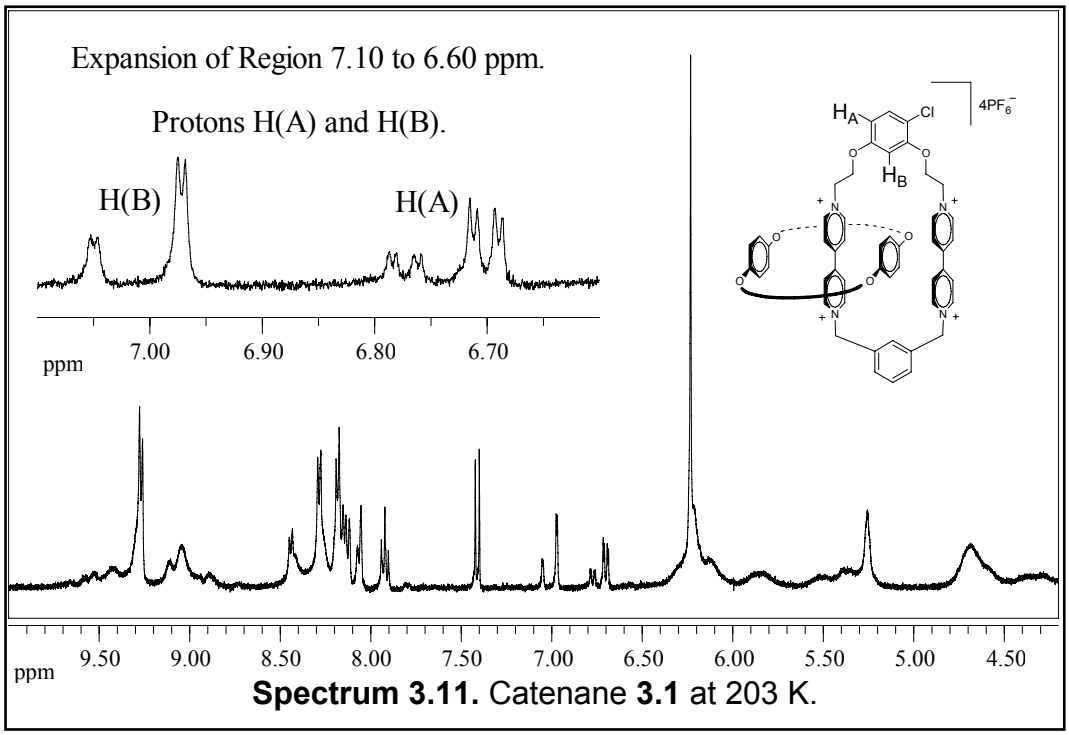

Spectrum 3.11. Catenane **3.1** at 203 K.

In Spectra 3.10 and 3.11 we observed fast exchange processes at 293 K and slow exchange processes at 203 K for catenane **3.1** possessing the 4-chloro-resorcinol and 1,3-xylyl tethers. For each proton signal the coalescence temperature and chemical shift differences were measured. For proton H_A of the resorcinol ring, the separation of the exchanging resonances was measured at 28.6 Hz and the temperature of coalescence was 245 K. The stacked plot (Spectrum 3.12) shows the progression of spectra as the temperature is lowered from the fast exchange region to coalescence and finally to the slow exchange region. In the fast exchange region we observe the weighted average signal; a doublet of doublets. In the slow exchange region we observed two distinct signals, two doublet of doublets with an integration ratio of 3 to 1. Proton H_B, the proton ortho to both heteroatom bonds on the resorcinol ring, appeared as a doublet at fast exchange and as two doublets in slow exchange with an integration ratio of 3 to 1.

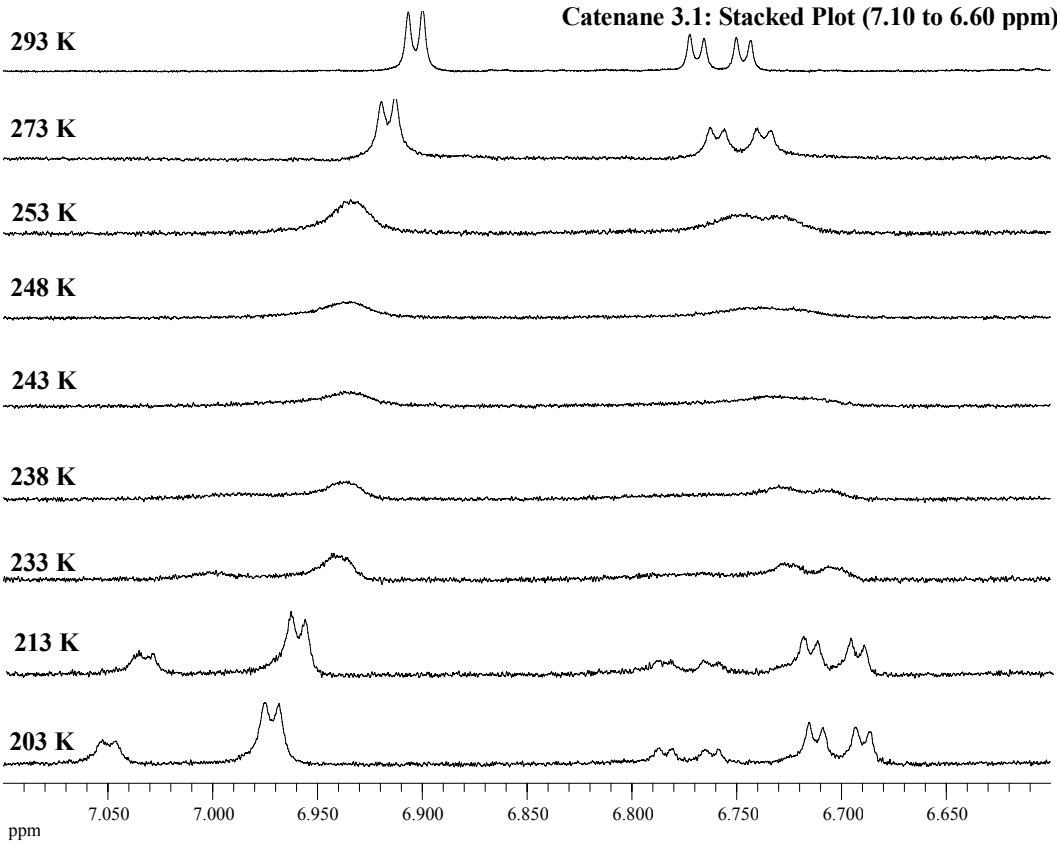

Spectrum 3.12. Stacked plot of catenane **3.1**.

We observed a separation of 31.0 Hz with a coalescence temperature of 245 K. Using either set of data we calculated an activation energy of 12 kcal/mol. These data will be discussed and compared with related catenanes in Section 3.4.

Section 3.4.2 VT 1H NMR Spectra of Catenane 3.2

Catenane **3.2**, having chloro- and 5-(4-*t*-butylphenyl)-1,3-xylyl groups, gave spectra displaying clean signals for the meta- and ortho-protons H_A and H_B whose coalescence temperatures and $\Delta\upsilon$ were easily determined by ^{1}H NMR spectroscopy. Fast and slow exchange regions are shown in Spectra 3.13 and 3.14.

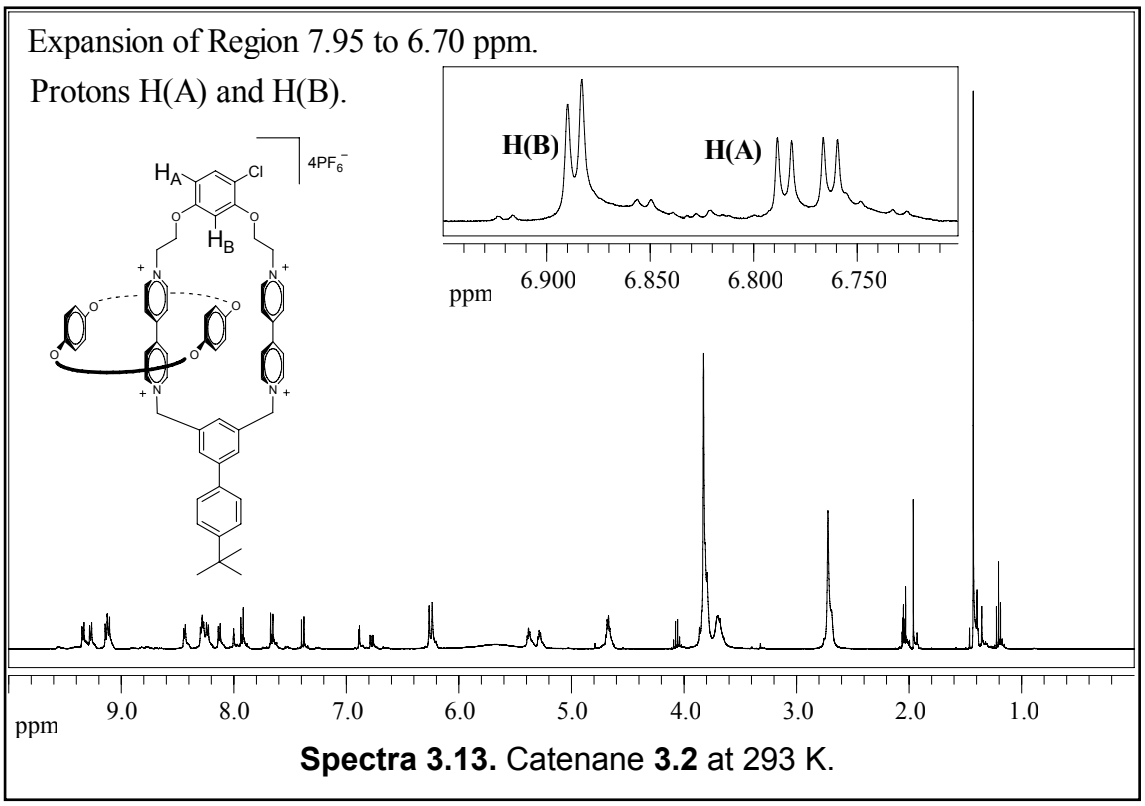

Spectra 3.13. Catenane **3.2** at 293 K.

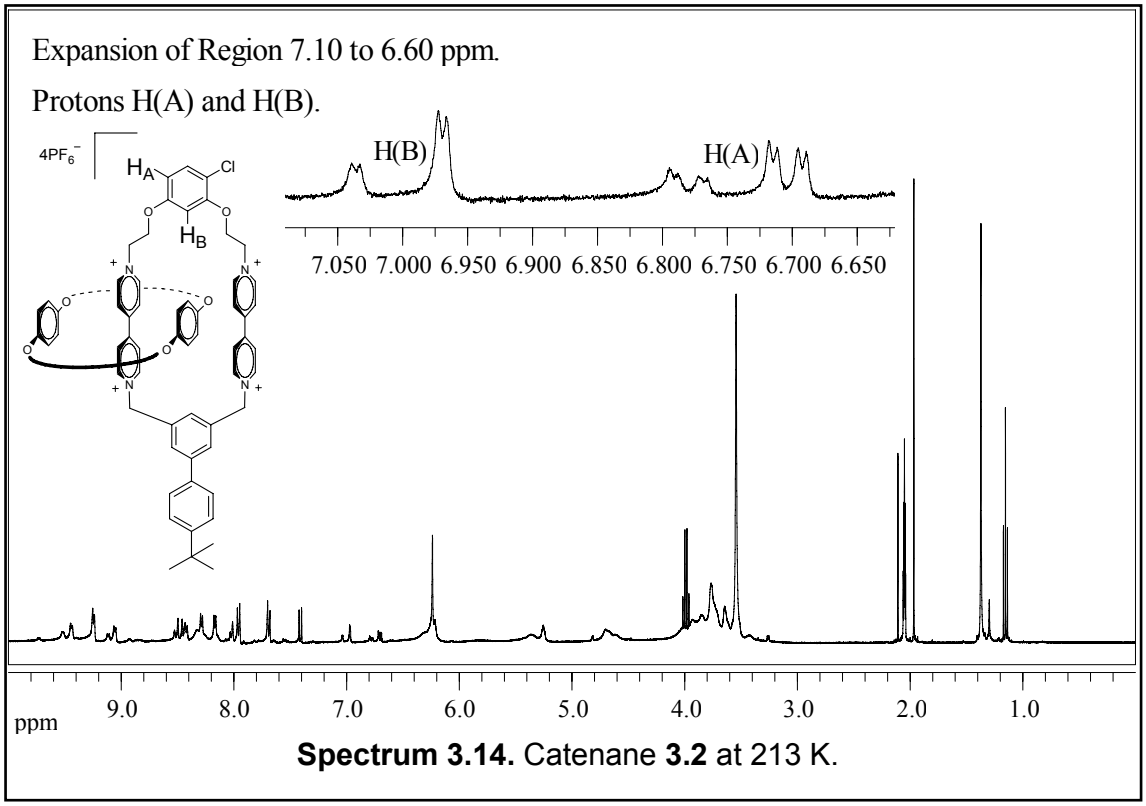

Spectrum 3.14. Catenane **3.2** at 213 K.

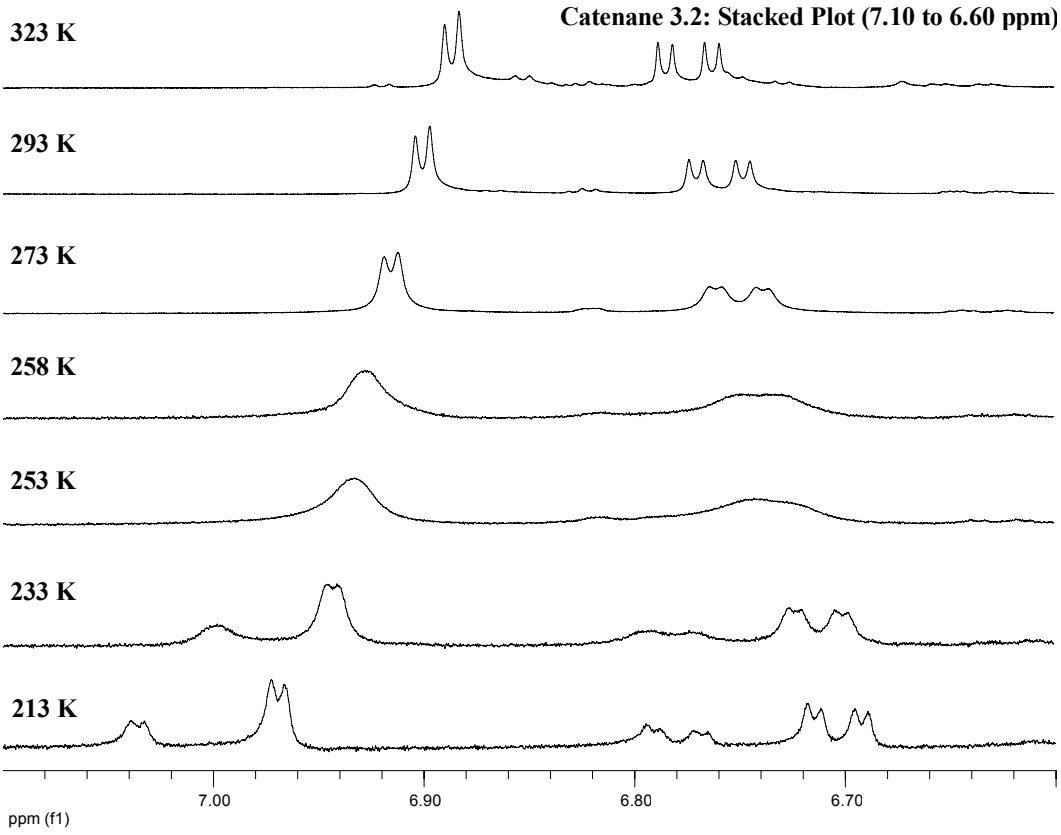

Spectrum 3.15. Stacked plot of catenane **3.2.**

The stacked plot in Spectrum 3.15 shows the progression of spectra as the temperature is lowered from the fast exchange region to coalescence and finally to the slow exchange region. As extracted from the data in spectrum3.6, coalescence for protons H_A and H_B occurred at 255 K with $\Delta\upsilon$ values of 30.4 and 26.7 Hz, respectively. The temperature of coalescence was higher when the bottom tether was blocked. Integration ratios were 2.5 to 1 and the energy of activation was calculated at 12.5 kcal/mol for both data sets.

Section 3.4.3 VT 1H NMR Spectra of Catenane 3.3

For catenane **3.3**, having 4-chloro-resorcinol and 1,4-xylyl tethers, we observed distinct α and α' dipyridinium signals in the fast-exchange region (Spectrum 3.16). While one well defined α proton signal was observed in the slow exchange region it proved impossible to follow through the coalescence process. The other dipyridinium signals in slow exchange were obscured due to signal overlap and **Δυ** could not be measured. Interestingly, proton H_A, which typically proved the most reliable signal did not decoalesce at the instruments lower temperature limits of -75 degrees Celsius (Spectrum 3.17). Signals for the ortho-proton H_B and meta proton H_C were clearly defined with deducible coalescence temperatures which were lower than either the 1,3-xylyl or blocked tethers in catenanes **3.1** and **3.2**.

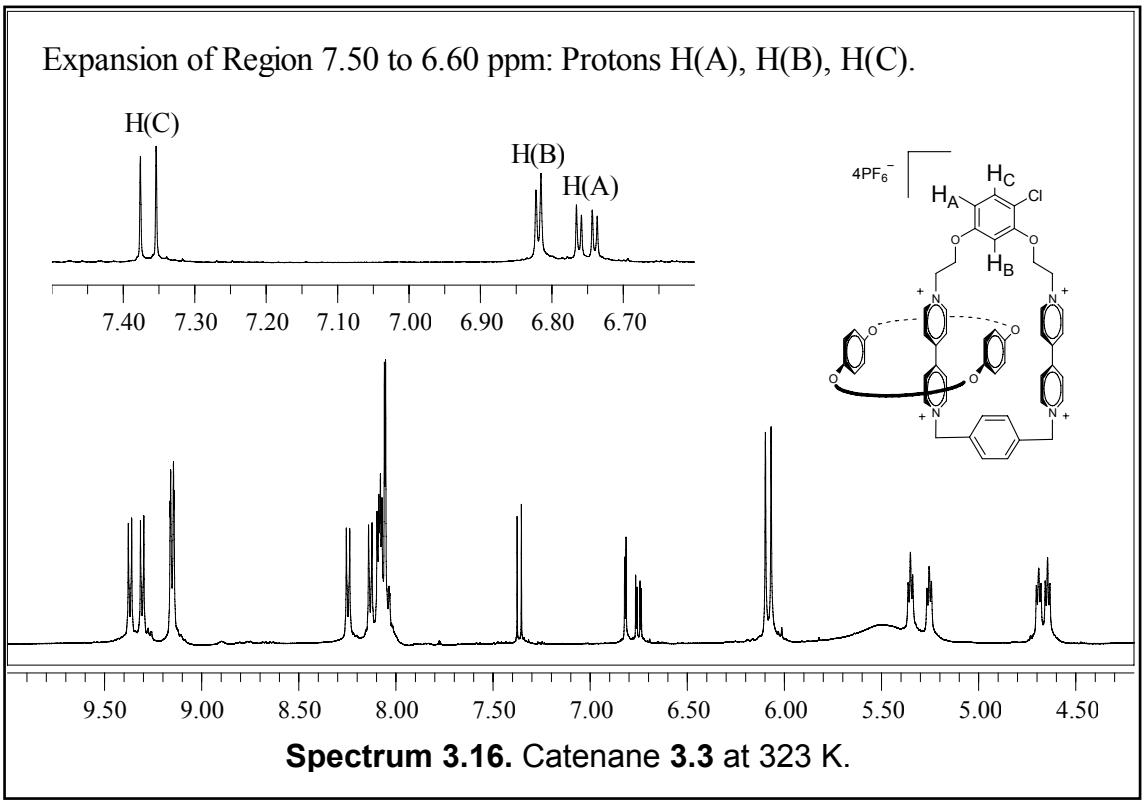

Spectrum 3.16. Catenane **3.3** at 323 K.

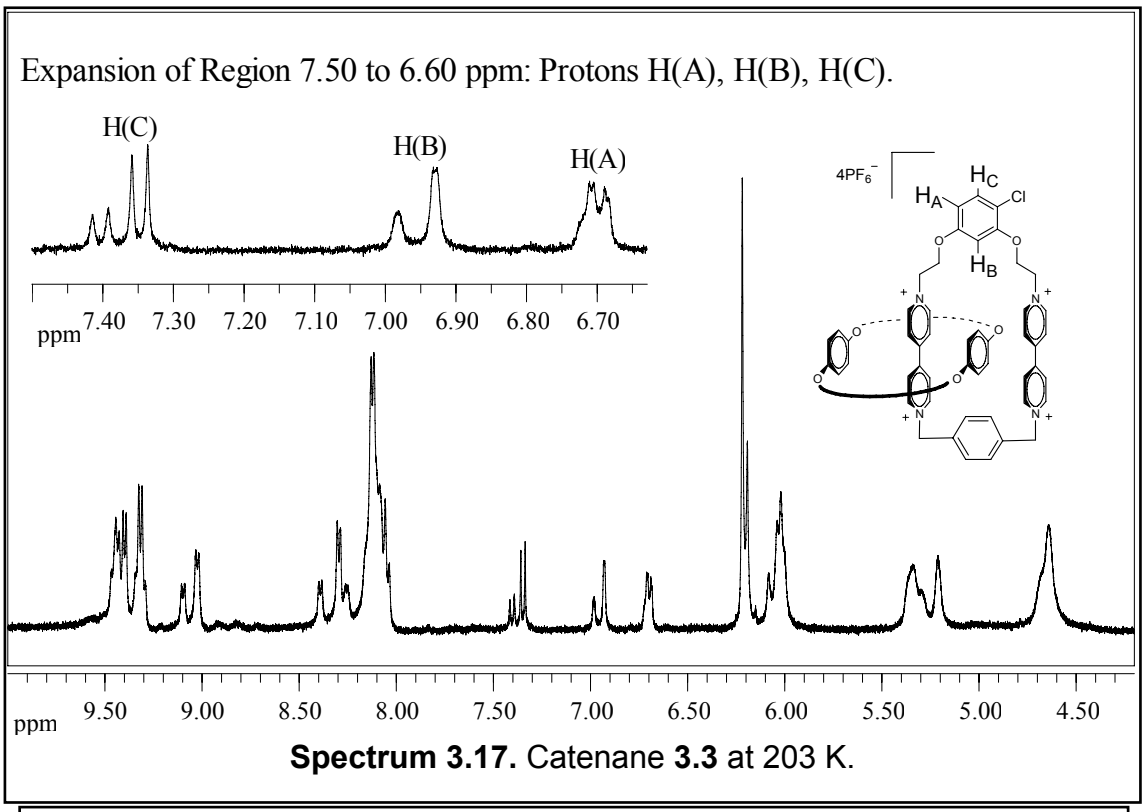

Spectrum 3.17. Catenane **3.3** at 203 K.

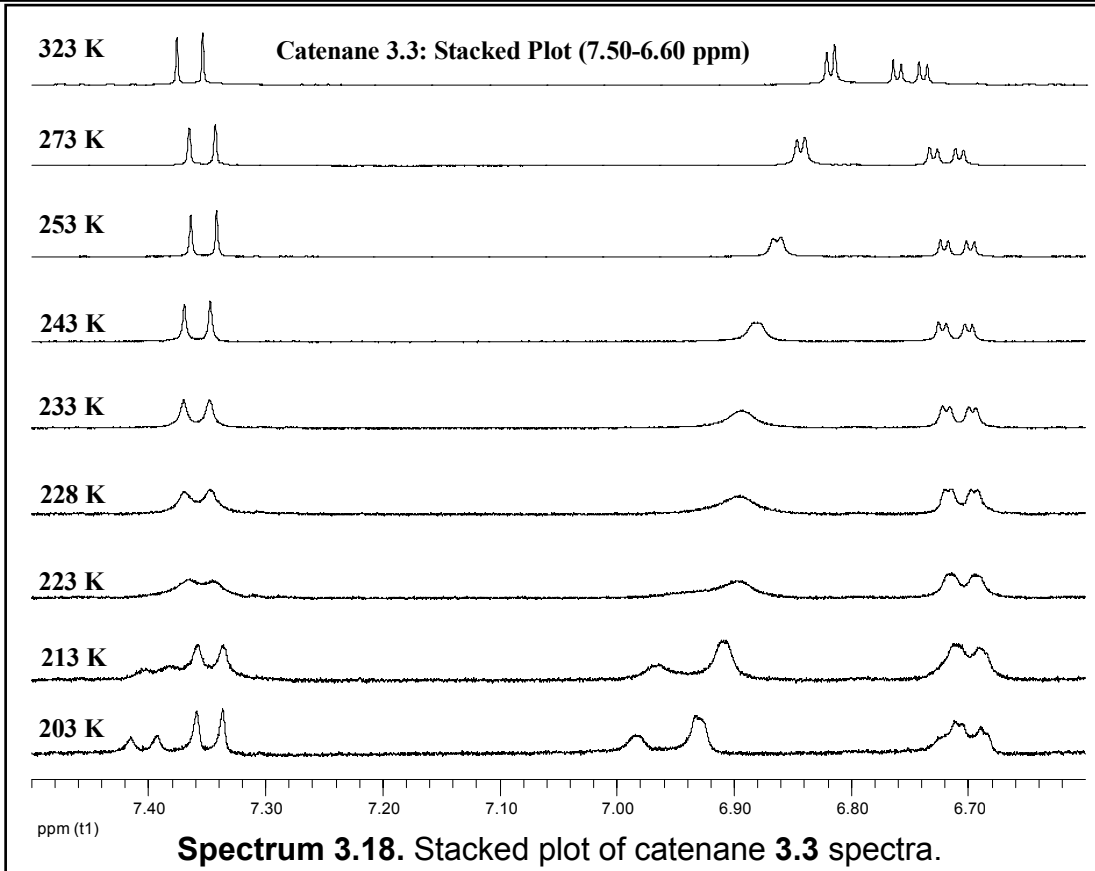

Spectrum 3.18. Stacked plot of catenane **3.3** spectra.

The stacked plot in Spectrum 3.18 shows the progression of spectra as the temperature was lowered from fast exchange to coalescence and finally to slow exchange. In the fast exchange region we observed the weighted average signals: a doublet of doublets for H_A, and doublets for H_B and H_C. As the multiplets approached and finally reached coalescence the signals merged into broad peaks. Coalescence gave way to reveal distinct multiplets as we approached the slow exchange region. Finally, for protons H_B and H_C, in the slow exchange region we observed two sets of multiplets emerge from each previous multiplet. Again, the signal for proton H_A failed to decoalesce at the instruments lower temperature limit. For proton H_B, the separation of exchanging resonances was measured at 22.1 Hz and the temperature of coalescence was 225 K. The multiplets for proton H_C had a separation of 22.3 Hz with a coalescence temperature of 220 K. The energy of activation was calculated to be 11 kcal/mol for each set of data. Integration ratios for each set of peaks were 2 to 1.

Section 3.4.4 VT ^{1}H NMR Spectra of Catenane 3.4

In spectra of Catenane **3.4**, possessing the 4-ethyl and 1,3-xylyl tethers, signals for the meta- and ortho-protons H_A and H_B were clearly defined and their coalescence temperatures determined.

In Spectrum 3.19 and 3.20 we observed fast exchange processes for catenane **3.4** at 323 K and slow exchange processes at 213 K. For each proton signal the coalescence temperatures and chemical shift differentials were measured. Proton H_A and H_B displayed separations of 27.8 and 37.4 Hz, respectively. The coalescence temperatures were 250 K for proton H_A and 255 K for proton H_B, which were higher than those observed in catenane **3.1** having the same 1,3-xylyl tether. In addition, the ratio of

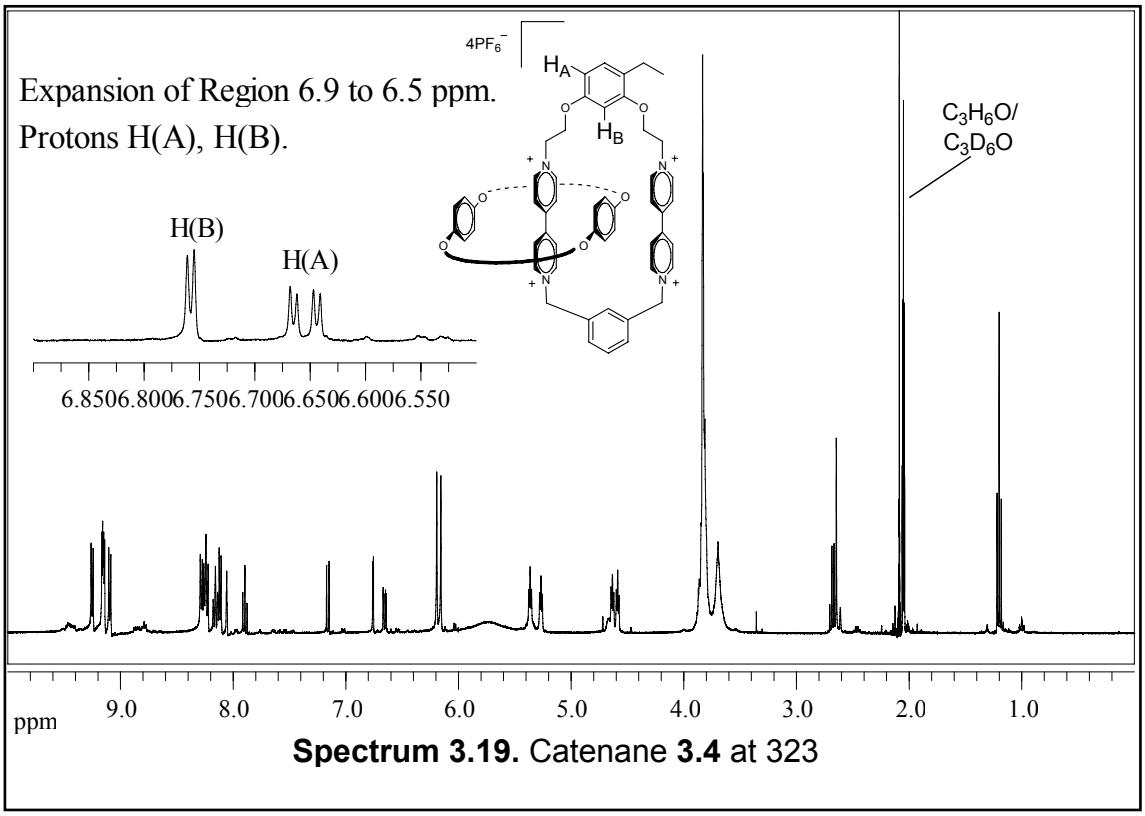

Spectrum 3.19. Catenane **3.4** at 323

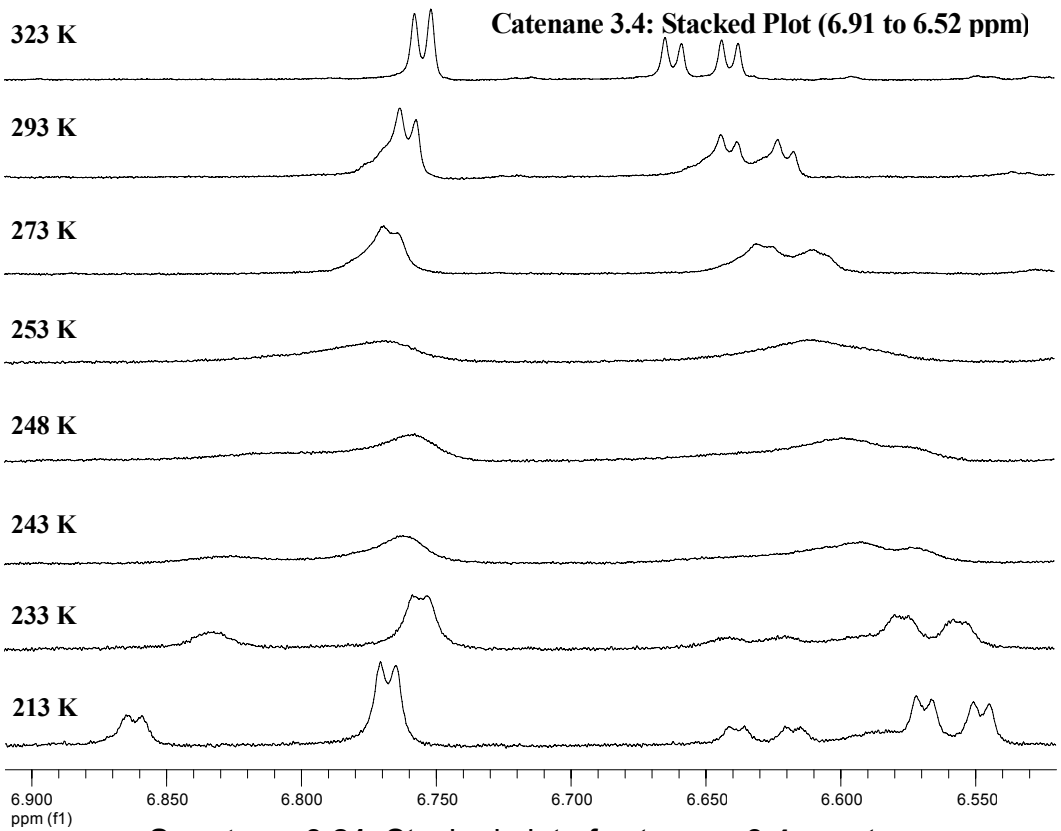

Spectrum 3.21. Stacked plot of catenane **3.4** spectra.

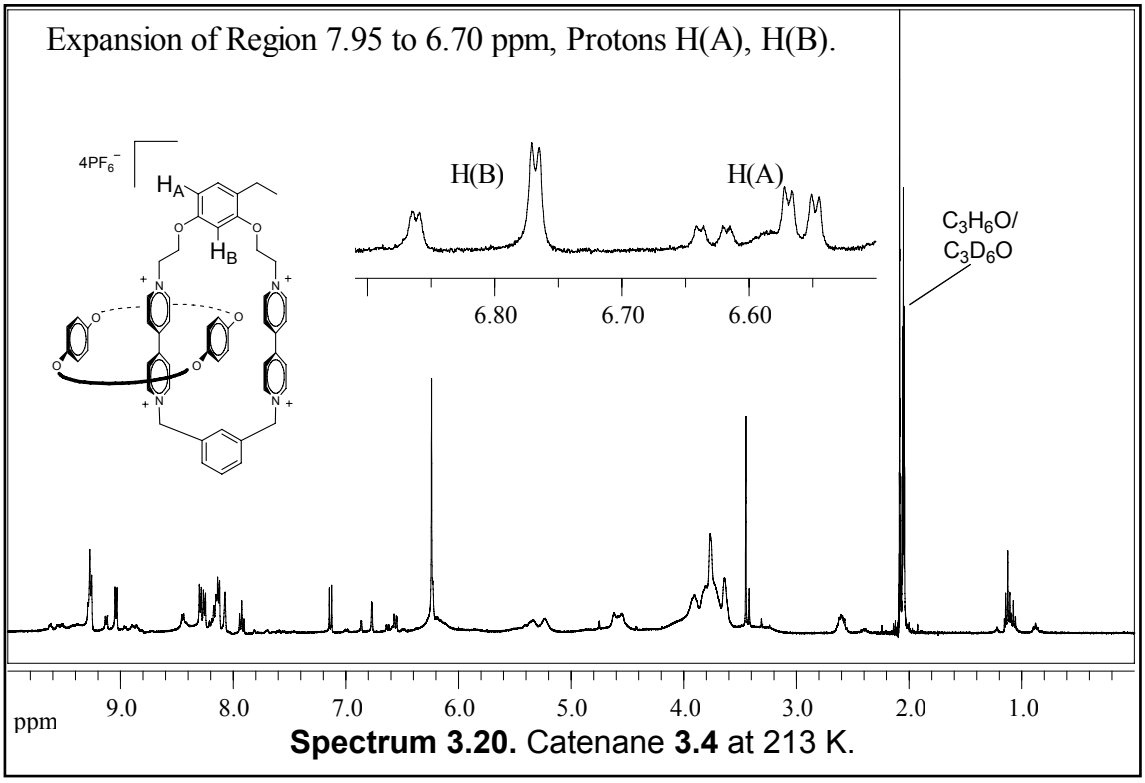

Spectrum 3.20. Catenane **3.4** at 213 K.

partners was 2.5 to 1 for each set. The stacked plot appears in Spectrum 3.21. In the slow exchange region we observed two distinct pairs of signals for both H_A and H_B. Using either set of data we calculated an activation energy of 12.5 kcal/mol.

Section 3.4.5 VT ^{1}H NMR Spectra of Catenane 3.5

Coalescence temperatures and **Δυ** were determined for protons H_A and H_B in Catenane **3.5**, possessing the 4-ethyl-resorcinol and 5-(4-*t*-butylphenyl)-1,3-xylyl tethers, as they were well behaved (Spectra 3.22 and 3.23). Coalescence for protons H_A and H_B occurred at 265 K with **Δυ** values of 29.0 and 31.9 Hz, respectively. This coalescence temperature was 10 K higher than its analogue 3.2 having the chloro, rather than ethyl substitution. Spectrum 3.24 shows the stacked plot of several spectra as the temperature was lowered to the slow exchange regime. The energy of activation was calculated at 13 kcal/mol for both data sets with a 2.5 to 1 ratio of isomers.

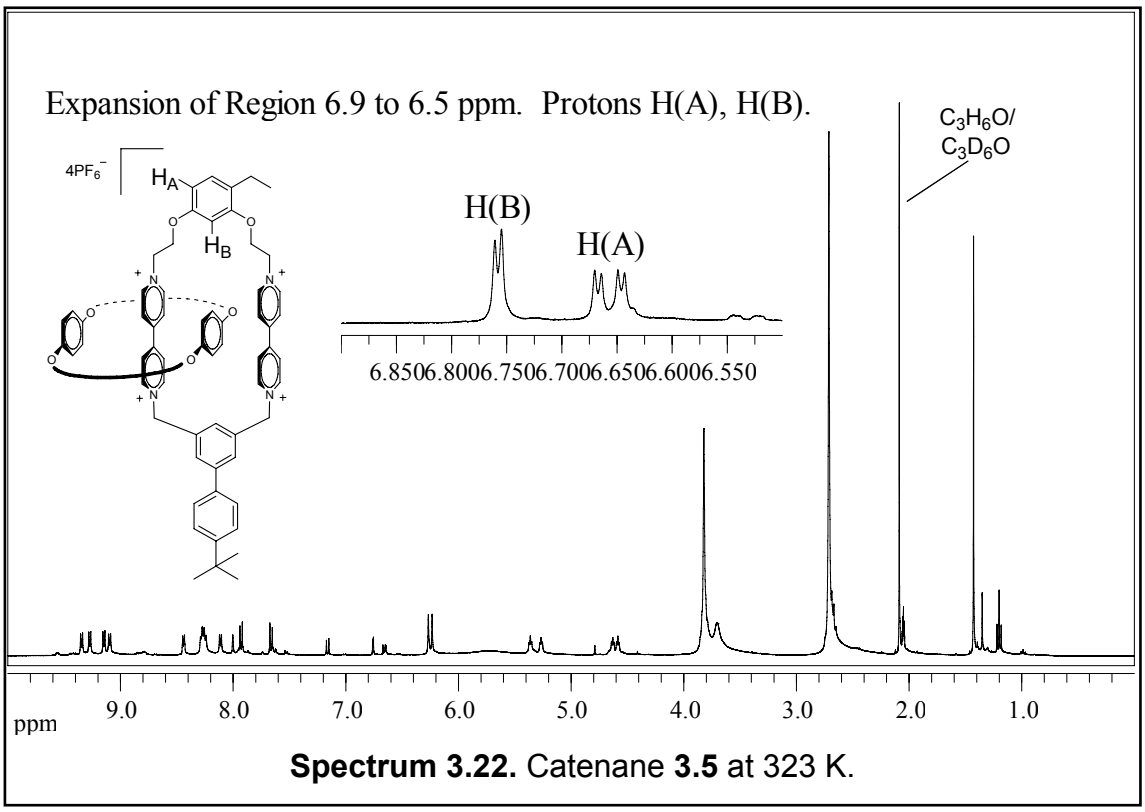

Spectrum 3.22. Catenane **3.5** at 323 K.

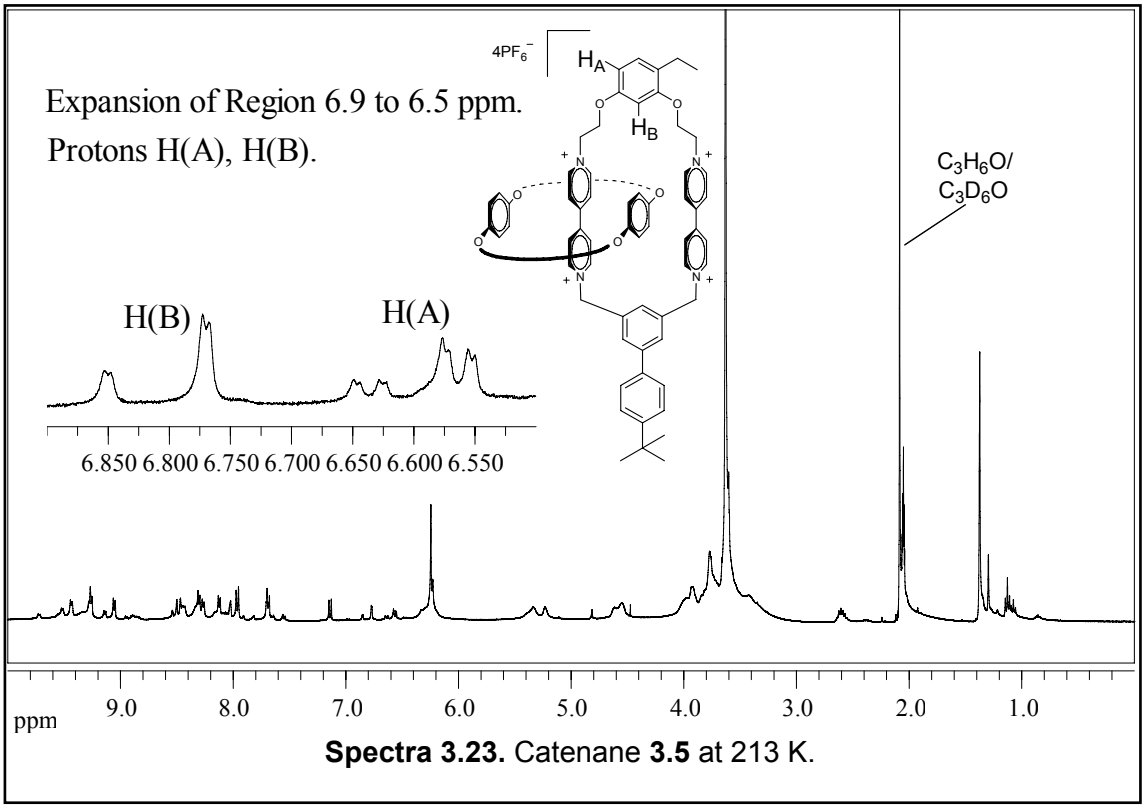

Spectra 3.23. Catenane **3.5** at 213 K.

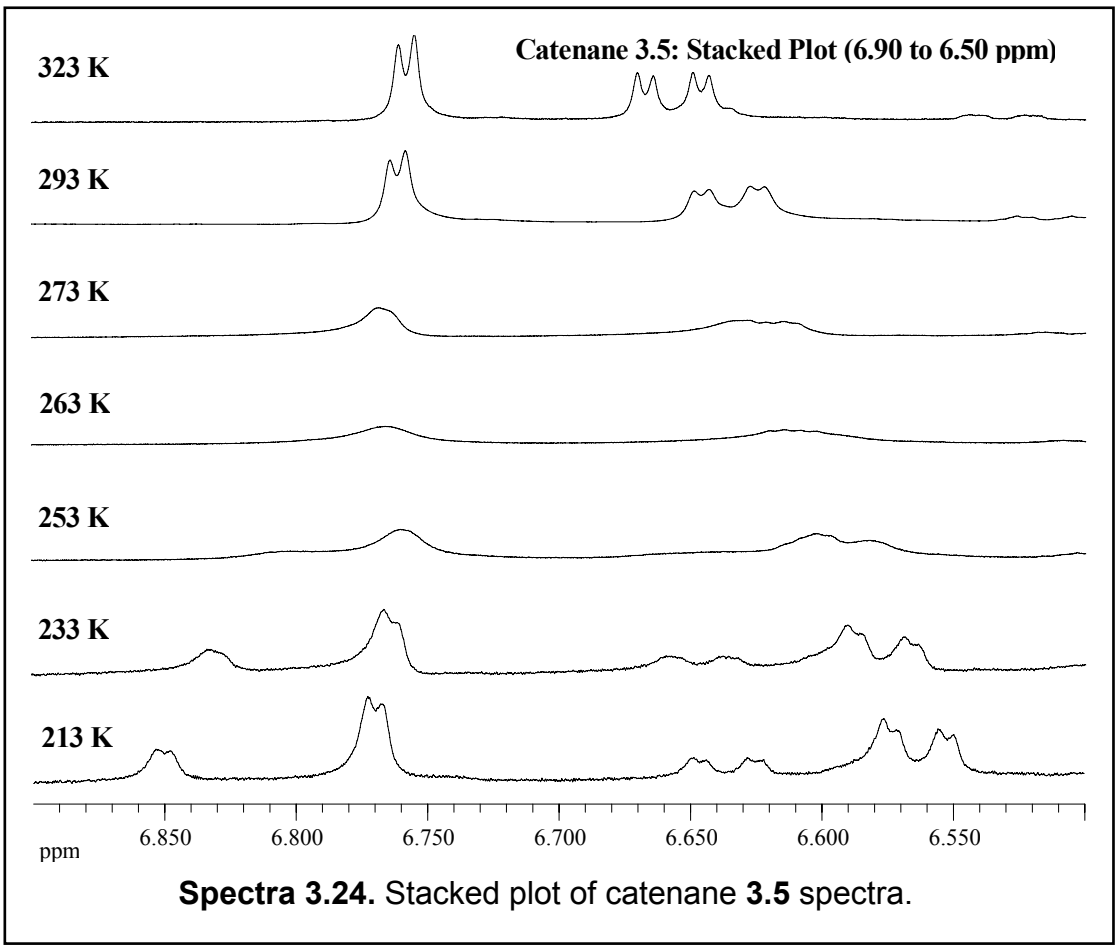

Spectra 3.24. Stacked plot of catenane **3.5** spectra.

Section 3.4.6 VT ^{1}H NMR Spectra of Catenane 3.6.

For catenane **3.6**, having the 4-ethyl and 1,4-xylyl groups, we observed three distinct signals for the three protons on the resorcinol ring in fast exchange (Spectrum 3.25). This was the first example in which all three signals were capable of being followed from fast exchange through coalescence to slow exchange (Spectra 3.27). While proton H_A was in the process of decoalescing at 198 K for Catenane **3.3** it had not yet fully split into its exchange partners. Signals for the ortho-proton H_B and meta proton H_C were clearly defined as well and their coalescence temperatures easily determined.

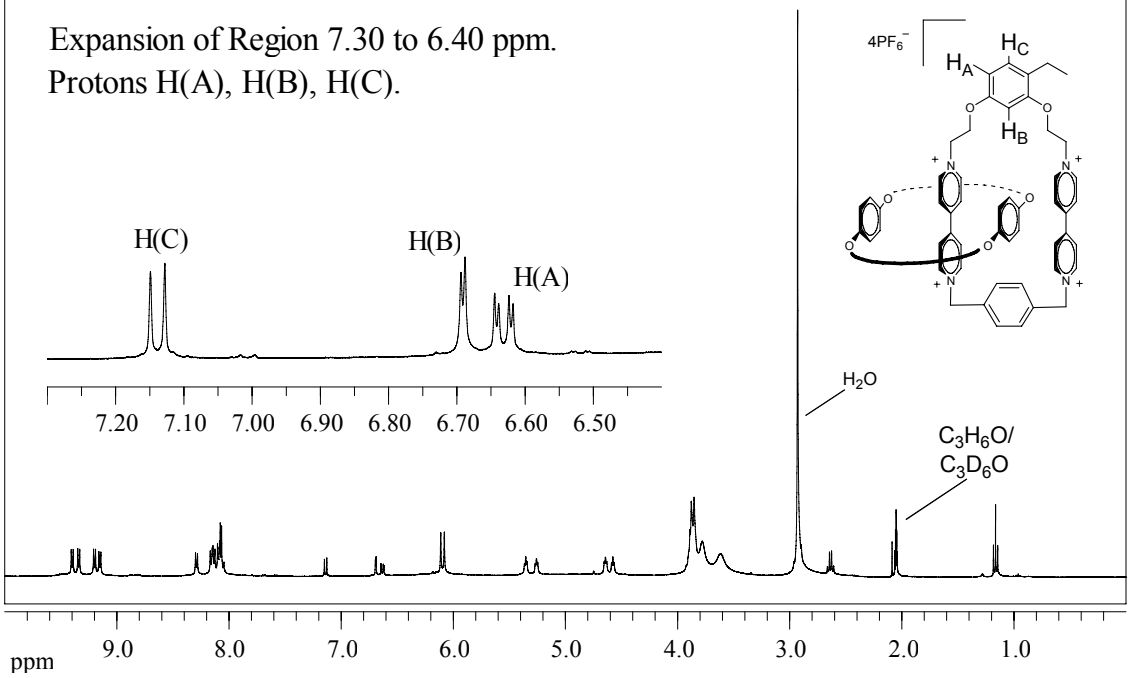

Spectra 3.25. Catenane **3.6** at 293 K.

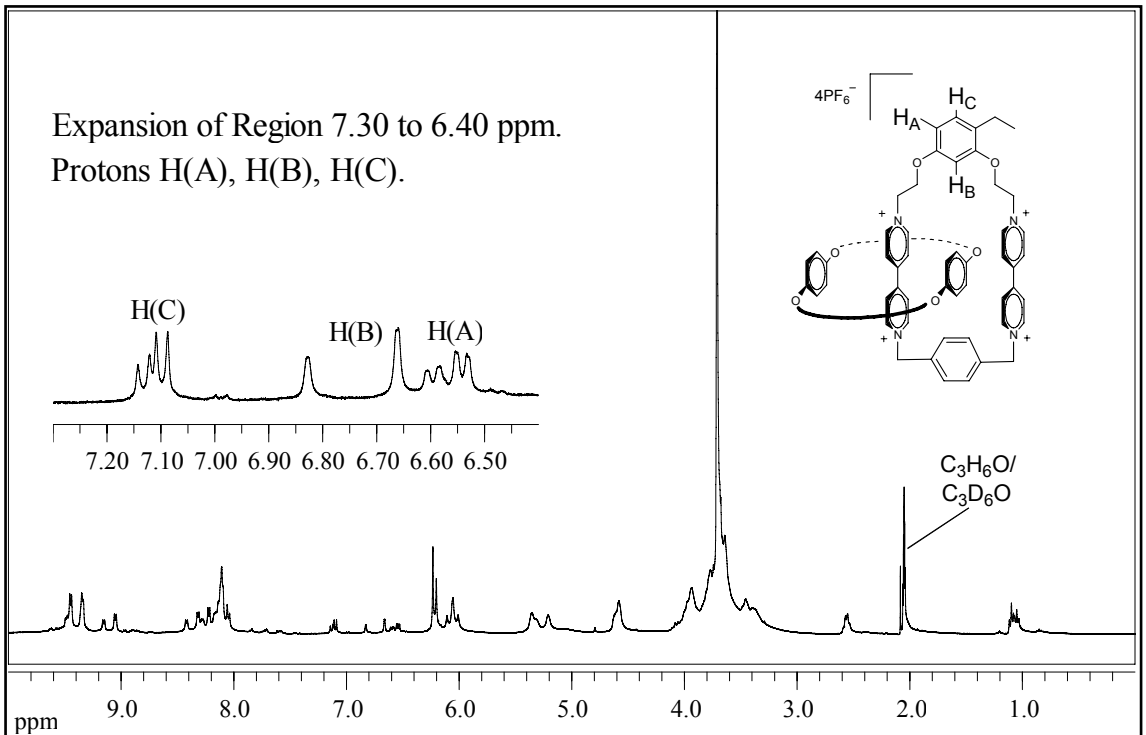

Spectra 3.26. Catenane **3.8** at 198 K.

The stacked plot (Spectra 3.27) shows the progression of spectra as the temperature was lowered from fast exchange to coalescence and finally to slow exchange. In the fast exchange region we observed the weighted average signals; a doublet of doublets for H_A, and doublets for H_B and H_C. As the multiplets approached and finally reached coalescence the signals merged into broad peaks. Coalescence gave way to reveal distinct multiplets as slow exchange occurred. Finally, in the slow exchange region we observed two sets of multiplets emerge from each of the previous multiplets. Proton HA displayed a $\Delta\upsilon$ of 21.5 Hz and a coalescence temperature of 225 K. For proton H_B, the separation of exchanging resonances was measured at 66.4 Hz with a 235 K temperature of coalescence. For proton H_C the separation was measured at 13.6 Hz with a coalescence temperature of 220 K. These coalescence temperatures were low and similar to catenane 3.3 which also had the 1,4-xylyl tether. The energy of activation was calculated to be 11 kcal/mol for each set of data with an isomer ration of 1.5 to 1 for each set.

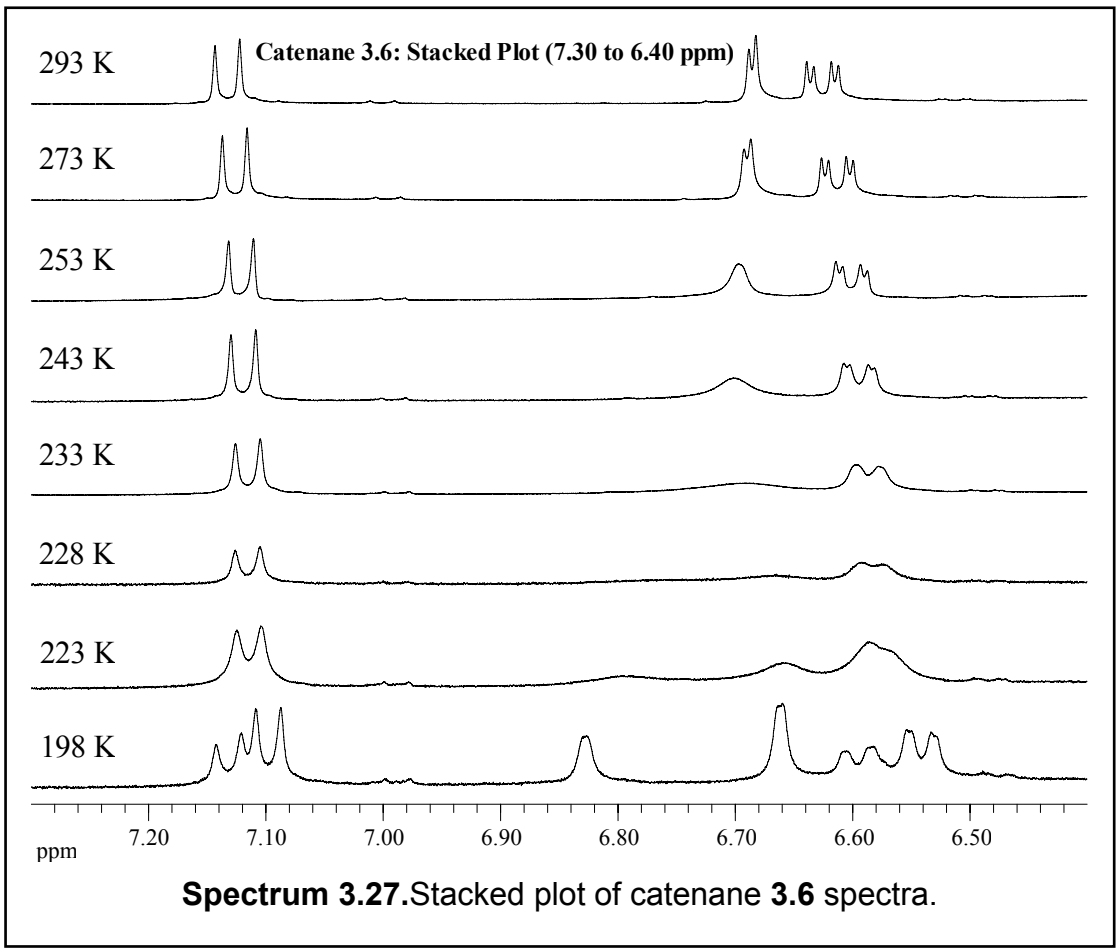

Spectrum 3.27. Stacked plot of catenane **3.6** spectra.

Section 3.4.7 VT 1H NMR Spectra of Catenane 3.7

Catenane **3.7**, possessing the 4-*n*-hexyl resorcinol and 1,3-xylyl tethers, displayed clean signals for the meta- and ortho-protons H_A and H_B in the ^{1}H NMR spectrum, for which coalescence temperatures and **Δυ** could be determined with confidence. Spectra 3.28 and 2.29 show the fast and slow exchange regimes, respectively.

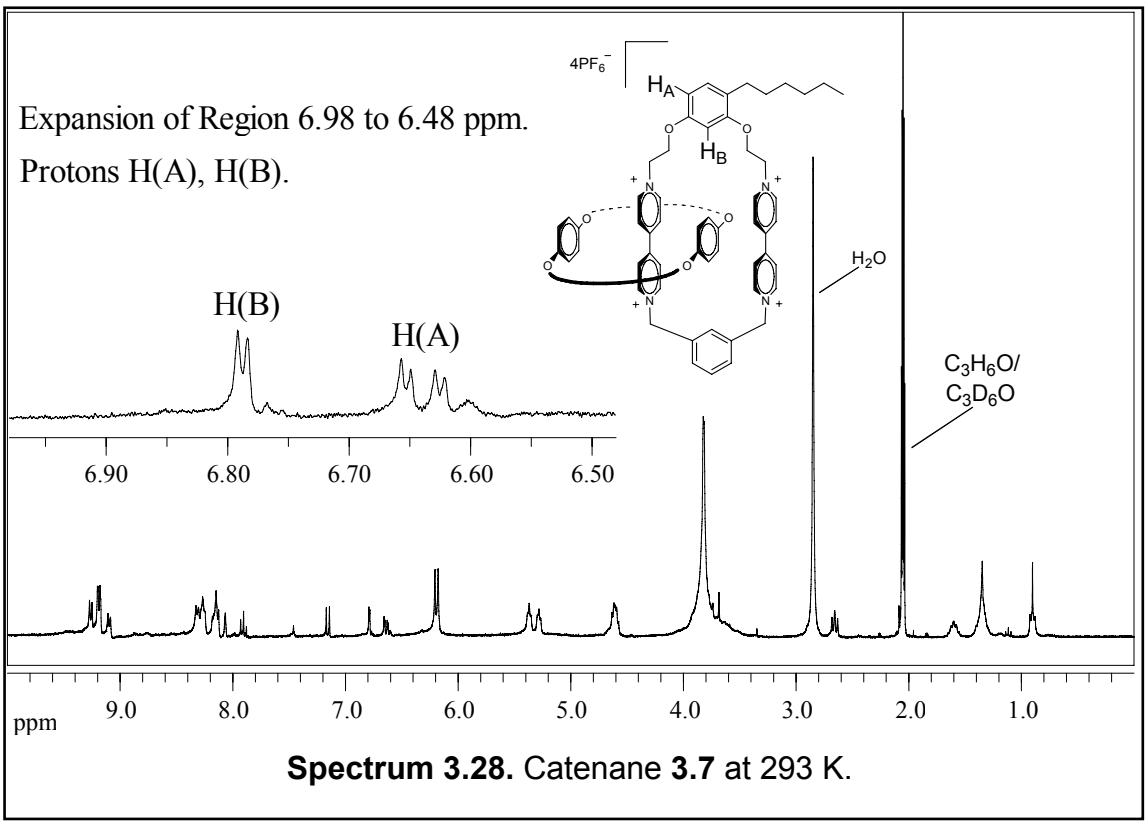

Spectrum 3.28. Catenane **3.7** at 293 K.

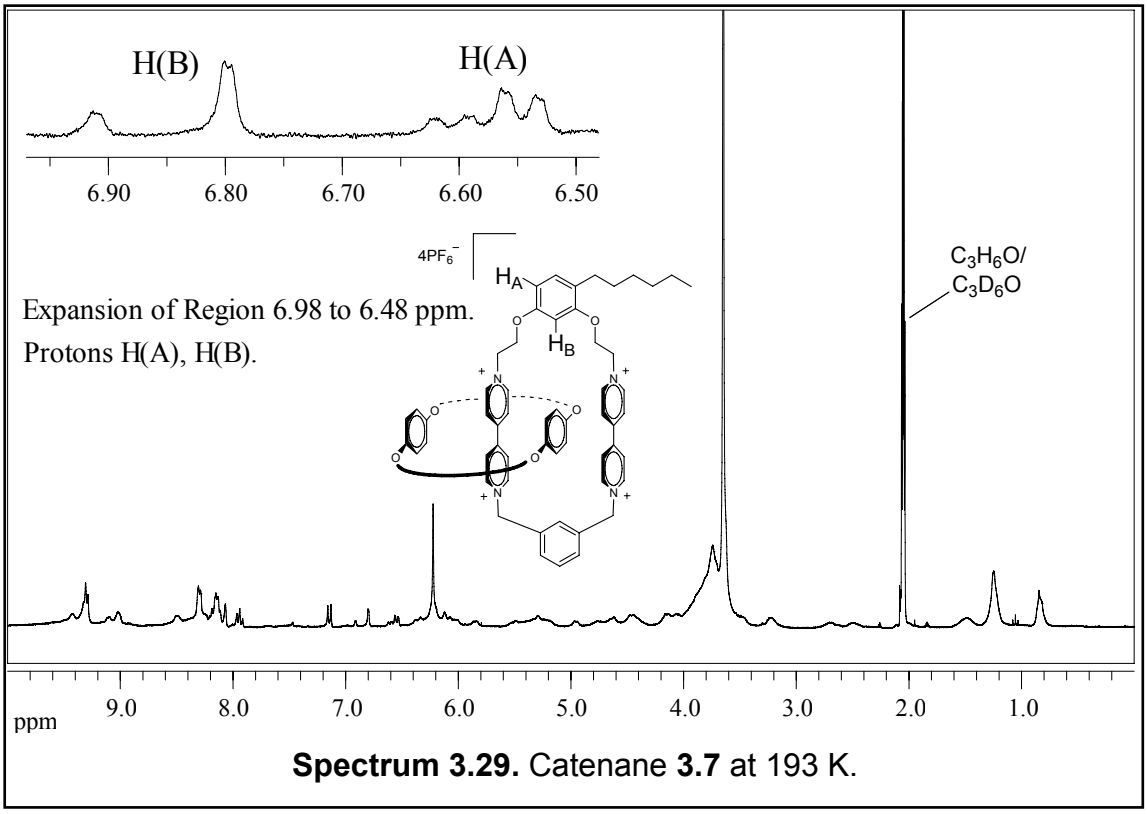

Spectrum 3.29. Catenane **3.7** at 193 K.

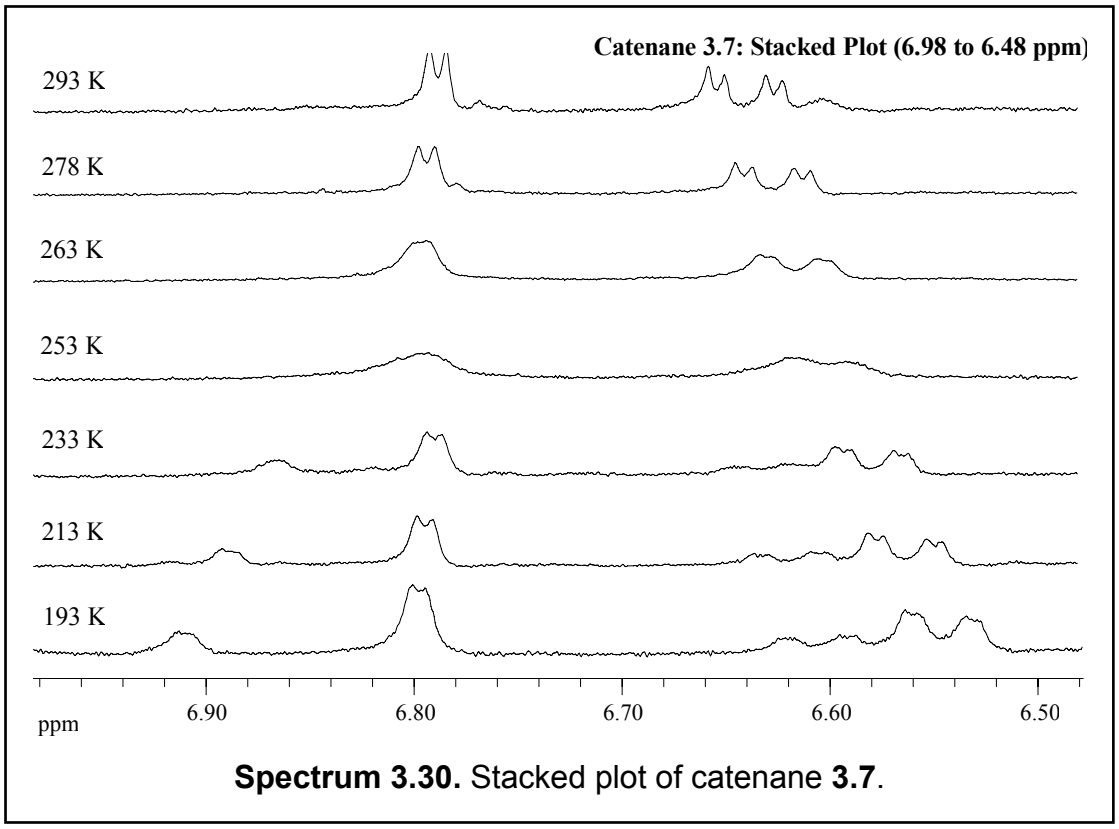

Spectrum 3.30. Stacked plot of catenane **3.7**.

Coalescence for protons H_A and H_B was be observed as the temperature was lowered (Spectrum 3.30) and occurred at 250 and 255 K with $\Delta\upsilon$ values of 17.3 and 33.8 Hz, respectively. These coalescence temperatures were similar to catenane **3.4** and 10 K higher than catenane **3.1**, all of which have the 1,3-xylyl tether. The energy of activation was calculated at 12.5 kcal/mol for both data sets with isomer ratios of 2.5 to 1.

Section 3.4.8 VT 1H NMR Spectra of Catenane 3.8

Ortho-proton H_A and meta proton H_B were well defined for Catenane **3.8**, possessing the 4-*n*-hexyl resorcinol and 5-(4-*t*-butylphenyl)-1,3-xylyl tethers, in both the fast (Spectrum 3.31) and slow exchange (Spectrum 3.32) regimes and data were gathered for both sets of signals

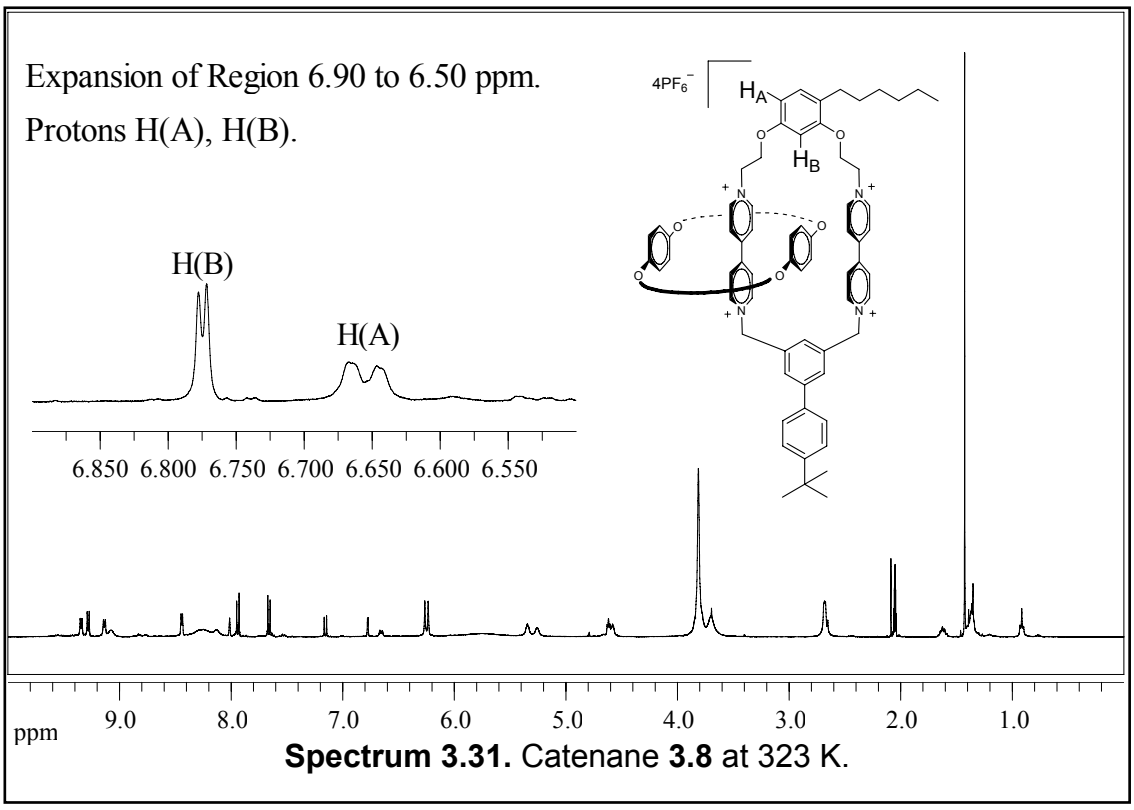

Spectrum 3.31. Catenane **3.8** at 323 K.

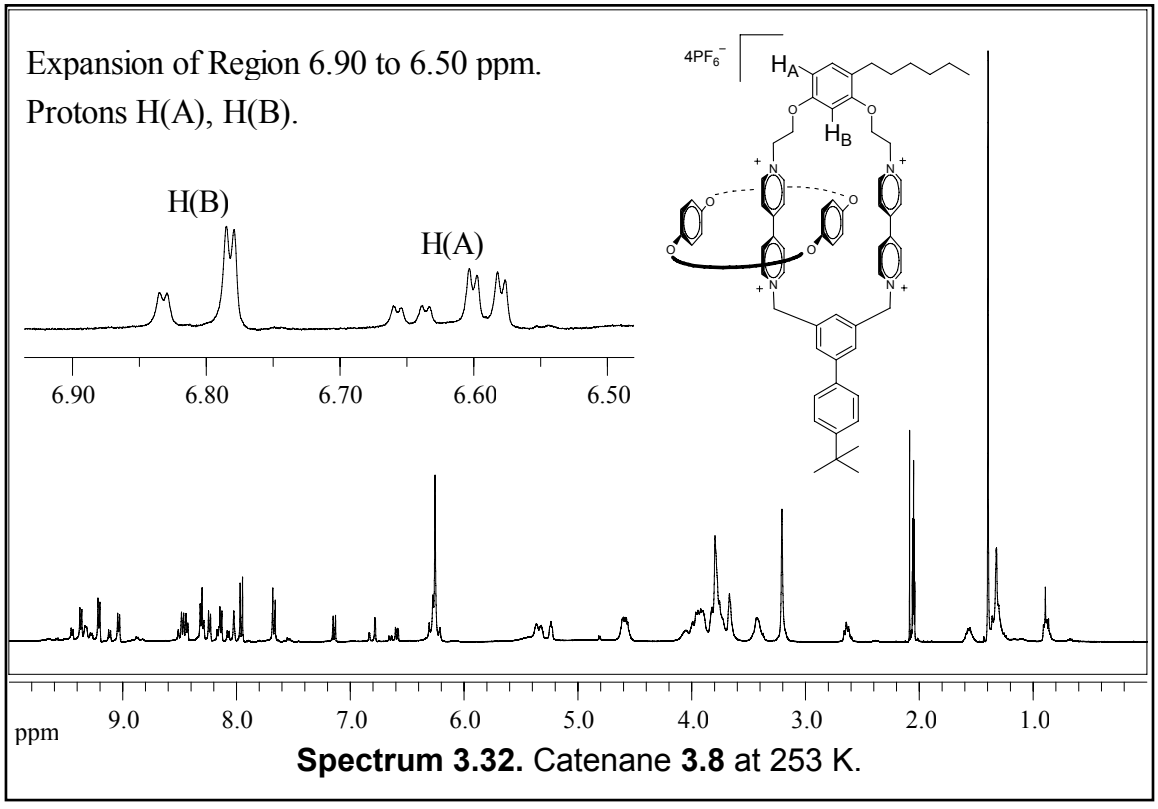

Spectrum 3.32. Catenane **3.8** at 253 K.

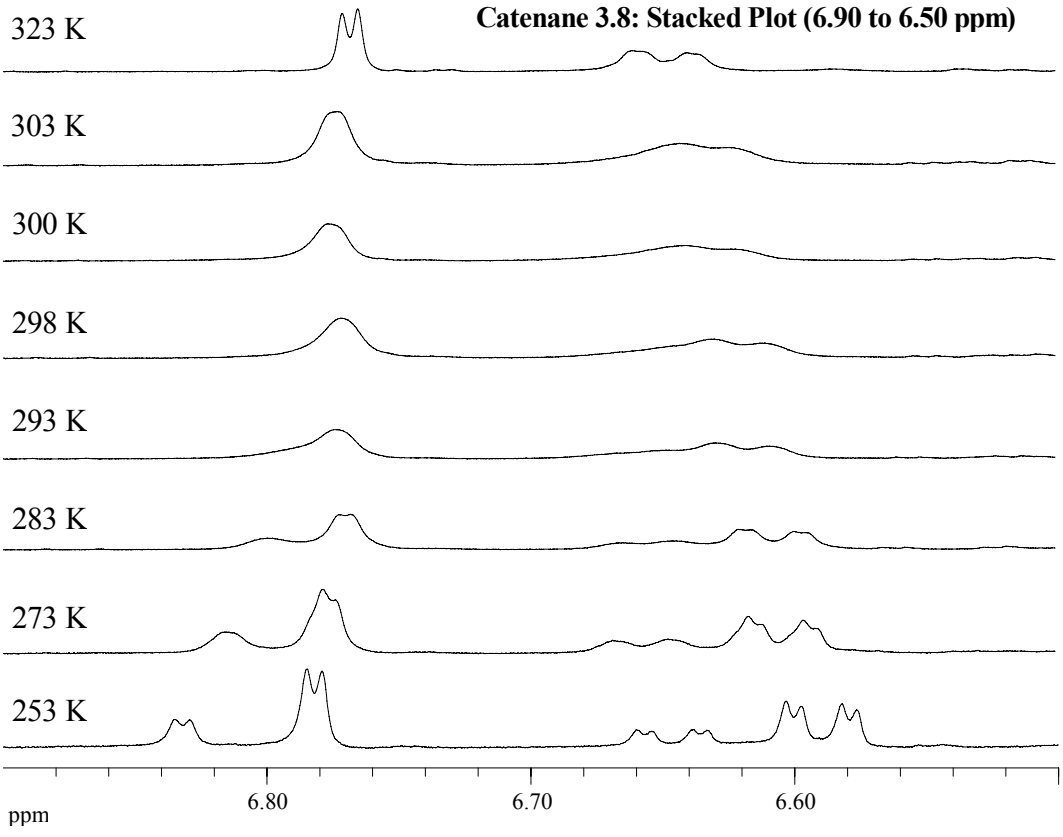

Spectrum 3.33. Stacked plot of catenane **3.8** spectra.

Coalescence for protons H_A and H_B occurred at 295 K with **Δυ** values of 22.7 and 20.0 Hz, respectively. This coalescence temperature was the highest of all the catenanes exceeding catenane **3.5** by 30 K. The energy of activation was calculated at 15 kcal/mol for both data sets with integration ratios of 3.5 to 1.

Section 3.4.9: VT ^{1}H NMR Spectra of Catenane 3.9

For catenane **3.9**, having the 4-*n*-hexyl resorcinol and 1,4-xylyl tethers, we observed distinct signals for ortho-proton H_A and meta proton H_B in both fast (Spectra 3.34) and slow exchange regions (Spectra 3.35).

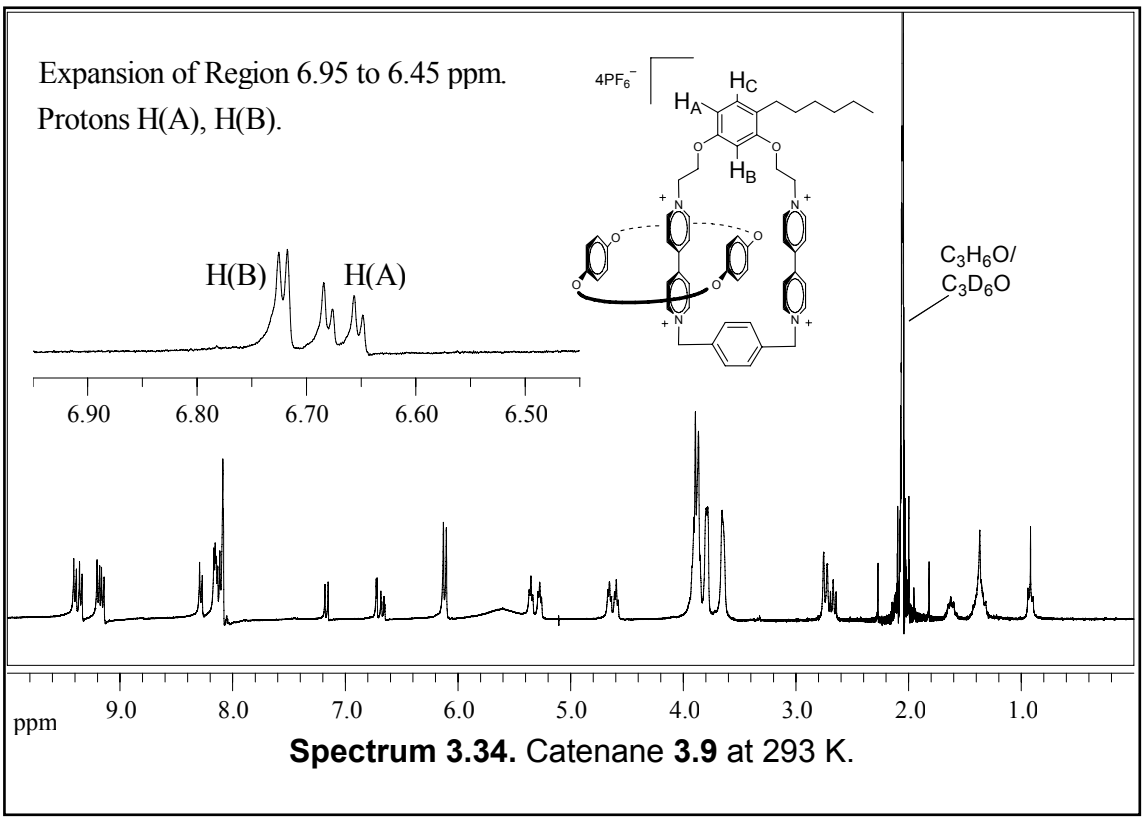

Spectrum 3.34. Catenane **3.9** at 293 K.

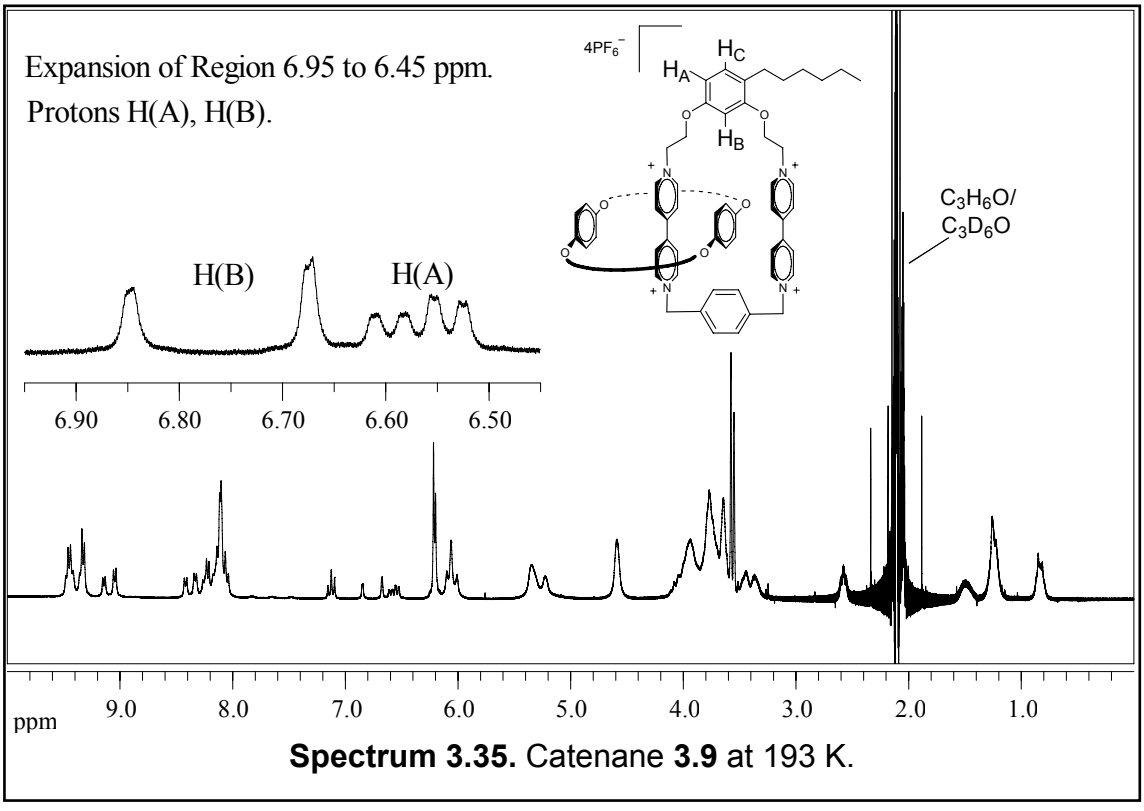

Spectrum 3.35. Catenane **3.9** at 193 K.

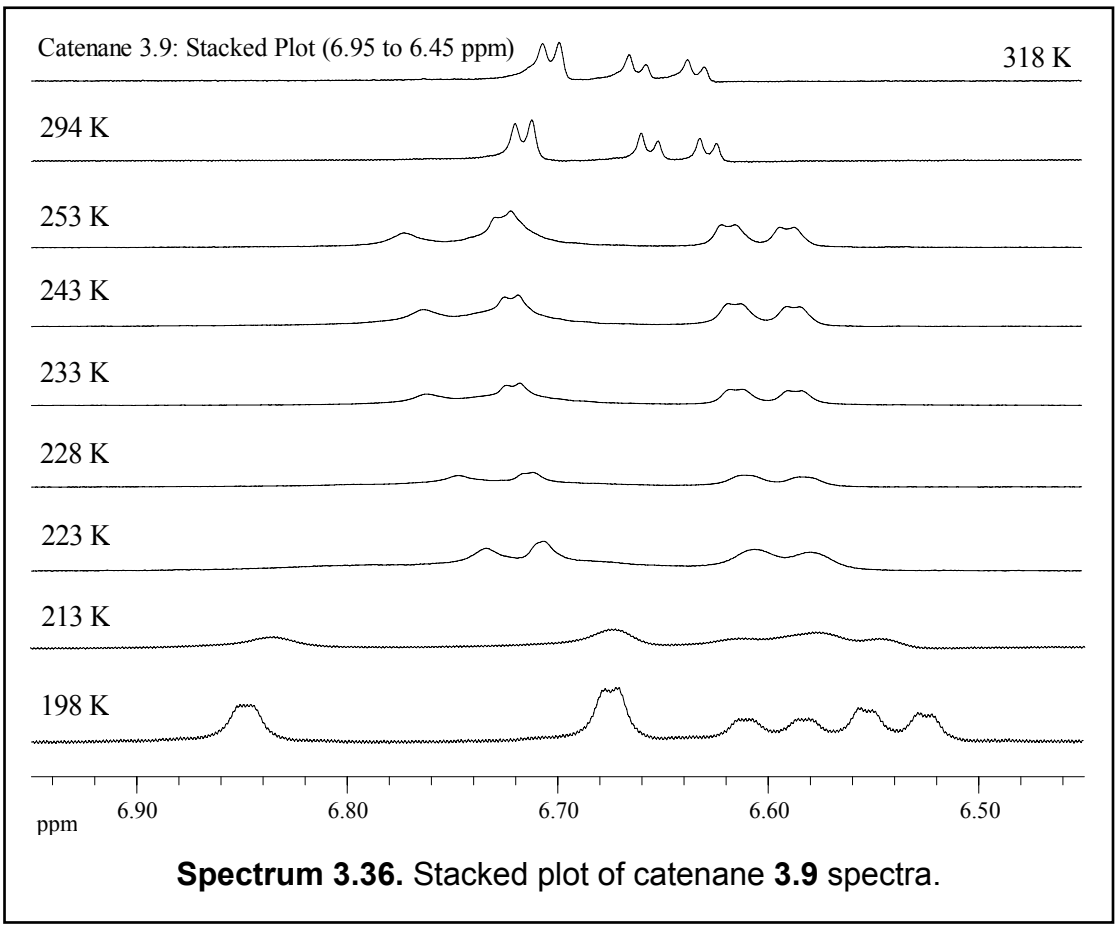

Spectrum 3.36. Stacked plot of catenane **3.9** spectra.

The stacked plot (Spectra 3.36) shows the progression of spectra as the temperature was lowered from fast exchange to coalescence and finally to slow exchange. For catenane H_B, the separation of exchanging resonances was measured at 52.0 Hz and the temperature of coalescence was 225 K. The two proton H_A doublet of doublets' separation was measured at 17.2 Hz with a coalescence temperature of 215 K. This coalescence temperature was consistent with the two previous catenanes having the 1,4-xylyl tethers. The energy of activation was calculated to be 11 kcal/mol for each set of data, and the ratio of isomers was determined to be 1.5 to 1.

Section 3.5 Summary of Data and Conclusions

Data gathered from variable temperature ^{1}H NMR experiments as well as the calculated energies of activation of all six catenanes are summarized in Table 3.1. Only one proton's **Δυ** and coalescence temperature was included in the table for each catenane as the energy of activation was identical for each set. Several trends emerged from data.

catenane	substituents tether A[a] / tether B[b]	coalescence temperature (K)[c]	frequency difference (Hz)	energy of activation (kcal/mol)[d]
3.1	chloro / 1,3-xylyl	245	28.6	12
3.2	chloro / *t*-butylphenyl	255	30.4	12.5
3.3	chloro / 1,4-xylyl	225	22.1	11
3.4	ethyl / 1,3-xylyl	250	27.8	12.5
3.5	ethyl / *t*-butylphenyl	265	29.0	13
3.6	ethyl / 1,4-xylyl	225	21.5	11
3.7	*n*-hexyl / 1,3-xylyl	250	17.3	12.5
3.8	*n*-hexyl / *t*-butylphenyl	295	22.7	15
3.9	*n*-hexyl / 1,4-xylyl	215	17.2	11

a) Substituent on the 4-position of the resorcinol moeity of tether A
b) Tether B can be either 1,3-xylyl , 1,4-xylyl, or t-butylphenyl where the later describes the 5-(4-*t*-butylphenyl)-1,3-xylyl blocking group
c) Approximated to the nearest 5 K
d) An error of 5 K in determining the coalescence temperature corresponds to an error of ± 0.2 kcal/mol in the activation energy

Table 3.1: Summary of data and calculated Energies of activation

Rotational temperature dependent isomerizations of [2]catenanes with top to bottom asymmetry has been established.[46] We are interested in studying the circumrotational isomerization of the crown ether over the two possible pathways. In Chapter 2 we established the relationship between circumrotation and placement of large blocking groups on the two tethers. Large blocking groups prohibited movement over the blocked pathway. When both tethers were substituted with blocking groups no circumrotation was observed. In studying catenanes **3.1** thru **3.9** we desired to determine the effects left to right asymmetry, in the form of asymmetric substitution on the resorcinol tether, would have on circumrotation. To accomplish this we synthesized three different resorcinol tethers and produced their associated asymmetric catenanes.

We examined two specific characteristics of the catenanes; the activation energy for circumrotation and the ratio of conformers as displayed in the slow exchange regime of the ^{1}H NMR spectra. If asymmetry had no effect on circumrotational isomerization we would expect to see no change in the isomer ratios or energy of activation. However, appending groups of different size and bond length, all effectively making tether A larger, should have an effect on isomerization. An increase in the energy of activation might be anticipated for catenanes **3.2**, **3.5**, and **3.8** where translocation is forced over tether A as established previously. Monitoring ratios of isomers in the slow exchange region provides an excellent means of measuring the relative thermodynamic stability of the two isomers.[42,53] We sought to use this qualitative measure in our gating catenanes to determine their effectiveness. For the ratios to provide meaning, it was important to establish how the introduction of asymmetry would affect the ratios of conformers. Simple, relatively inflexible substituents, such as the chlorine or ethyl

substituents on catenanes **1.3-3.6** without significant freedom of movement could be expected to display a 1:1 ratio of isomers if they had no influence on the binding energy of the BPP34C10 and dipyridiniums. Catenanes **3.7-3.9** substituted with the long, flexible *n*-hexyl chain had the potential to interfere with binding on one dipyridinium thus altering the equilibrium ratio of conformers. While some of our observations were not expected, the data provided the desired benchmarks from which we could measure the effectiveness of our potentially gating catenanes.

Figures 3.13, 3.14 and 3.15 that follow show catenanes **3.1** thru **3.9** grouped according to the type of B tether they possess. The activation barrier for catenane **3.1,** possessing the chloro-substituted resorcinol and the 1,3-xylyl linker, was calculated to be 12 kcal/mol (Figure 3.13). When tether B was blocked, as in Catenane **3.2** (Figure

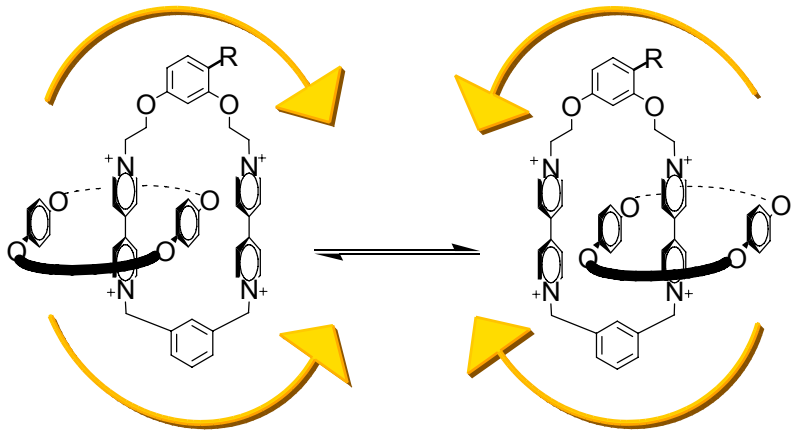

Catenane 3.1 $\Delta G^{\ddagger}$ = 12 kcal/mol (R = chloro)

Catenane 3.4 $\Delta G^{\ddagger}$ = 12.5 kcal/mol (R = ethyl)

Catenane 3.7 $\Delta G^{\ddagger}$ = 12.5 kcal/mol (R = *n*-hexyl)

Figure 3.13. Circumrotation observed for catenanes **3.1**, **3.4**, and **3.7**.

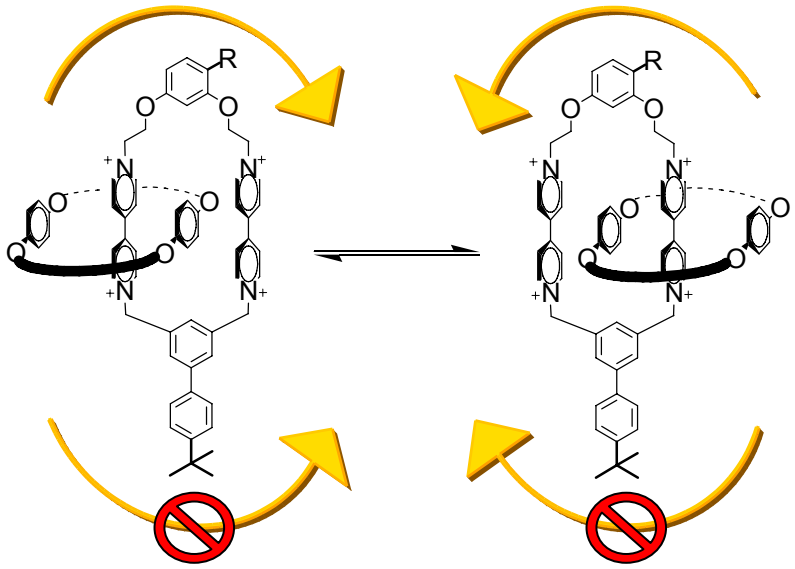

Catenane 3.2 $\Delta G^{\ddagger}$ = 12.5 kcal/mol (R = chloro)

Catenane 3.5 $\Delta G^{\ddagger}$ = 13 kcal/mol (R = ethyl)

Catenane 3.8 $\Delta G^{\ddagger}$ = 15 kcal/mol (R = *n*-hexyl)

Figure 3.14. Circumrotation observed for catenanes **3.2**, **3.5**, and **3.8**.

3.14), 12.5 kcal/mol were required for isomerization. Using the 1,4-xylyl tether decreased the energy of activation to 11 kcal/mol (Figure 3.15). These values were identical to $\Delta G^{\ddagger}$ values calculated for catenanes **2.1** and **2.3** having unsubstituted resorcinol and 1,3-xylyl tethers or 1,4-xylyl tethers. Compared to catenane **2.2**, having the unsubstituted resorcinol top pathway and blocked bottom pathway, the free energy of activation for catenane **3.2** decreased by 0.5 kcal/mol. As we increased the size and bulk of the resorcinol substituent, and subsequently the tether itself, we observed an increase in activation energy. Catenane **3.4** with its ethyl substituent and 1,3-xylyl tether showed a 12.5 kcal/mol energy of activation, which is a 0.5 kcal/mol increase over the chloro-substituted analogue as seen in Figure 3.13. Blocking pathway B

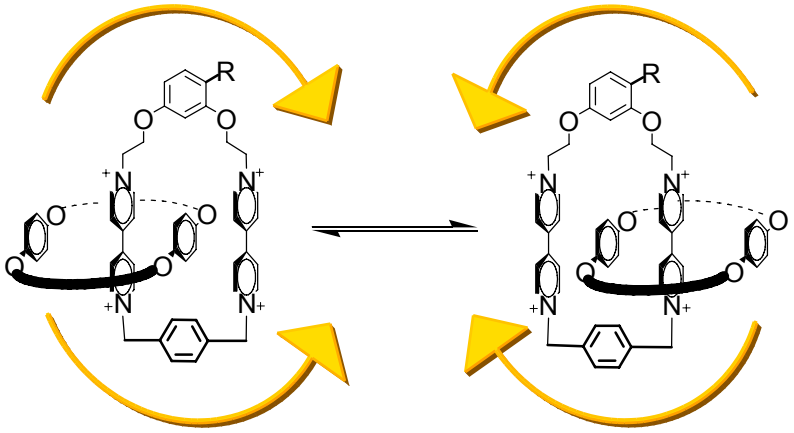

Catenane 3.3 $\Delta G^{\ddagger}$ = 11 kcal/mol (R = chloro)

Catenane 3.6 $\Delta G^{\ddagger}$ = 11 kcal/mol (R = ethyl)

Catenane 3.9 $\Delta G^{\ddagger}$ = 11 kcal/mol (R = *n*-hexyl)

Figure 3.15. Circumrotation observed for catenanes **3.3**, **3.6**, and **3.9**.

thereby restricting translocation to the ethyl-resorcinol pathway, as in Catenane **3.5**, increased $\mathbf{\Delta G^{\ddagger}}$ back up to 13 kcal/mol, while the value for the 1,4-xylyl pathway remained 11 kcal/mol for Catenane **3.6**. Increasing the length and bulk of the substituent once again with *n*-hexyl brought about a two kcal/mol increase in the activation energy for catenane **3.8**, compared to its ethyl counterpart, to 15 kcal/mol. For catenanes **3.7** and **3.9**, the values of $\mathbf{\Delta G^{\ddagger}}$ remained identical to ethyl-substituted analogue at 12.5 and 11 kcal/mol, respectively, and shown in Figure 3.15.

As observed for the symmetric catenanes, passage along the 1,4-xylyl linker was less energetically demanding than the 1,3-xylyl group indicated by the 11 kilocalorie barriers in catenanes **3.3**, **3.6**, and **3.9** shown in Figure 3.15, supporting our previous conclusions. In addition, when presented with two pathways, one of which is

energetically more demanding, but not completely blocked, as with catenanes possessing the 1,3- and 1,4-xylyl tethers, circumrotation occurred over the lower energy pathway. The chlorine substituent on the resorcinol did not cause an increase in $\Delta G^{\ddagger}$ compared to the unsubstituted form as the energies were the same indicating circumrotation over the chloro-substituted resorcinol was not hindered to any appreciable degree. In fact, we observed a slight decrease in activation energy when circumrotation was restricted to tether A. It appears the chloro-substituent remains small enough for BPP34C10 to pass over without experiencing steric strain substantially different from that posed by unsubstituted resorcinol.

When the ethyl and hexyl substituents were introduced we observed an increase in energy requirements for translation in catenanes **3.4**, **3.5**, **3.7**, and **3.8**, over that observed for the chloro-substituted catenanes as seen in Figures 3.14 and 3.15. With these alkyl substitutions we observed the 12.5 kcal/mol energy of activation found in catenane **2.4** indicating circumrotation was occurring over the open 1,3-xylyl tether in catenanes **3.4** and **3.7**. For catenane **3.5** where pathway B was blocked we observed the same energy of activation requirement as symmetric catenane 2.2 (13 kcal/mol) where, similarly, pathway B was blocked, yet no resorcinol substituent was present. Like the chloro-, ethyl-substitution did not increase the activation energy to an appreciable degree. For catenane **3.8**, possessing blocked tether B we observed a significant increase consistent with blocking the bottom and forcing circumrotation over a now bulkier resorcinol tether. From these differences we can conclude that BPP34C10 requires more energy to travel over longer, larger *n*-hexyl substituent than the smaller ethyl group. In turn the ethyl group required less energy to pass than the chlorine which

was no more energetically demanding than hydrogen. Traversing the larger, alkyl substituted 3-bis(ethyloxy)benzene tethers required more energy than the 1,3-xylyl tether, both of which were significantly more energetically demanding than passage over the 1,4-xylyl tether.

In Chapter 2 we presented our bistable symmetric catenanes as existing in equilibrium with equal amounts of each isomer present. However, as seen in Table 3.2 introduction of asymmetry altered the equilibrium in such a way as to favor formation of one isomer of the bistable catenanes. Thus, the isomer ratios for these six catenanes are symmetry dependent as shown in Figure 3.16. Isomer ratios for each catenane were measured approximately 40 degrees below the coalescence temperature, when possible, to reduce error introduced by changes in the equilibrium. However, we found the ratios did not vary to a significant degree below the coalescence temperature.

Substituents		Tether A		
		Chloro	Ethyl	*n*-Hexyl
Tether B	1,4-xylyl	2:1	1.5:1	1.5:1
	1,3-xylyl	3:1	2.5:1	2.5:1
	t-butyl-1.3-xylyl	2.5:1	2.5:1	3.5:1

Ratios rounded to the nearest 0.5.

Table 3.2 Summary of isomer ratios

Substituting ethyl or chloro for n-hexyl, we observed a 2.5:1 ratio, or 0.5 decrease in the ratio magnitude for catenanes **3.2** and **3.5**. Ethyl- and *n*-hexyl-substitution have identical ratios of conformers for catenanes with 1,3-xylyl tethers (2.5:1) and 1,4-xylyl tethers (1.5:1) when translocation is not restricted to the top pathway. Observation of these identical and lower conformer ratios is an indication of

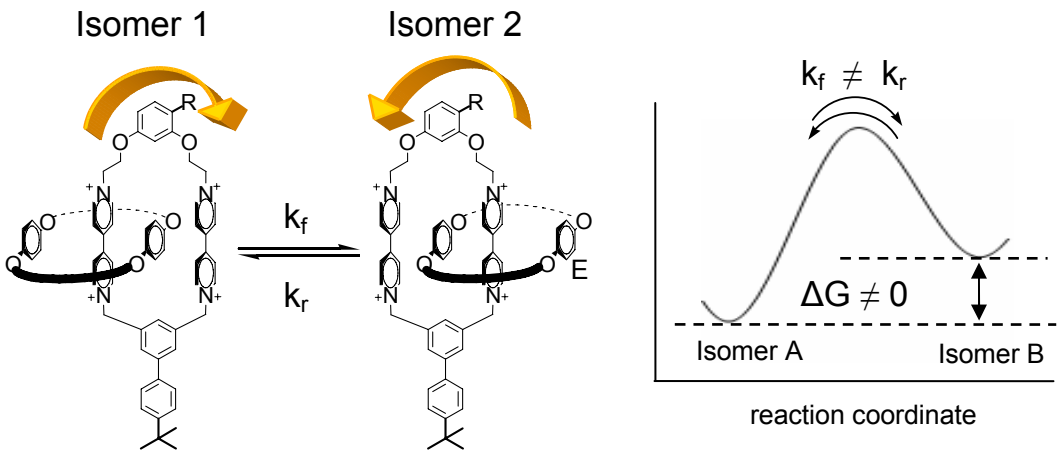

Figure 3.16. Thermodynamic stability a function of asymmetry.

BPP34C10 undergoing translocation over pathway B effectively bypassing tether A. Chloro-substituted catenanes did not follow the pattern established by the alkyl substituents. Catenane **3.2** with tether B blocked showed a lower ratio of isomers (2.5:1) than did catenane **3.1** (3:1) with its open 1,3-xylyl tether. While chloro-substitution did not increase the activation energy compared to unsubstituted resorcinol, it altered the ratio of conformers in an unexpected manner.

For these catenanes containing conformationally non-mobile groups, such as the chloro-substituent, and conformationally limited or ill-defined groups, such as the ethyl- and *n*-hexyl- substituents, thermodynamic differences will drive isomerization and the ratios provide the relative concentrations of isomers. Using these integration ratios as a measure of the relative concentration[53] we were able to calculate the values of ΔG° for each catenane as shown in Table 3.3. Here we see the relatively small differences in free energy between the isomers of these bistable catenanes.

Substituents		Tether A		
		Chloro	Ethyl	*n*-Hexyl
Tether B	1,4-xylyl	0.3	0.2	0.2
	1,3-xylyl	0.4	0.4	0.4
	t-butyl-1.3-xylyl	0.4	0.4	0.6

Values include an associated error of ± 10 %

Table 3.3 Calculated values of ΔG° (kcal/mol)

Incorporation of asymmetric 1,3-bis(ethyloxy)benzene tethers with chloro-, ethyl-, and *n*-hexyl substituents affected the isomerization equilibrium of our [2]catenanes. We observed an equilibrium in which one ground state of the bistable molecule was thermodynamically more stable. This ground state difference appears to be a function of asymmetry. While this was unexpected, it did provide a benchmark from which to compare our gating catenanes. Energy barriers for displacement along the different paths were: 12.5 kcal/mol for 1,3-bis(ethyloxy)-4-chlorobenzene, 13 kcal/mol for 1,3-bis(ethyloxy)-4-ethylbenzene, and 15 kcal/mol over the 1,3-bis(ethyloxy)-4-*n*-hexylbenzene pathway. Increasing the steric bulk of the substituent increased the energy required for circumrotation. Using asymmetric catenanes, we demonstrated the ability to control both the path of and energy required for circumrotation.

We, unfortunately, do not know on which side the BPP34C10 prefers to bind. All attempts at correlating the structures through NMR spectroscopy proved inconclusive. This lack of data limits our ability to interpret why we have unequal mixtures of isomers. We do not know which one is actually favored. We anticipate that

the 4-position substituent of the resorcinol ring does not necessarily directly interact with the BPP34C10. However, it may induce conformational changes of the ethano-spacers with respect to the dipyridinium rings that could lead to more favorable complexation on one side. Evidence for this twisting is seen in the chemical shift non-equivalence of the proton on carbon two of the resorcinol ring, designated H_B. This position should be symmetric with respect to BPP34C10 binding with either dipyridinium, yet it displays the largest chemical shift change in the two slowly exchanging conformations.

Chapter 4

Synthesis and Study of 'Gating' Benzyl Substituted Asymmetric [2]Catenanes

Section 4.1 Design of a 'Gating' Catenane

As reviewed in the introduction, the principle of microscopic reversibility requires the energy barrier for a reaction be equal in both forward and reverse directions given two ground states of equal energy.[14,21] It also requires equal forward and reverse rate constants between these isoenergetic states. We sought to examine this view using the novel bistable catenane design shown in Figure 4.1. Incorporated into the system is a gate capable of existing in several different conformations. There are low energy, wide conformations (**4.1a** and **4.1b**) and a high energy, narrow conformation with the

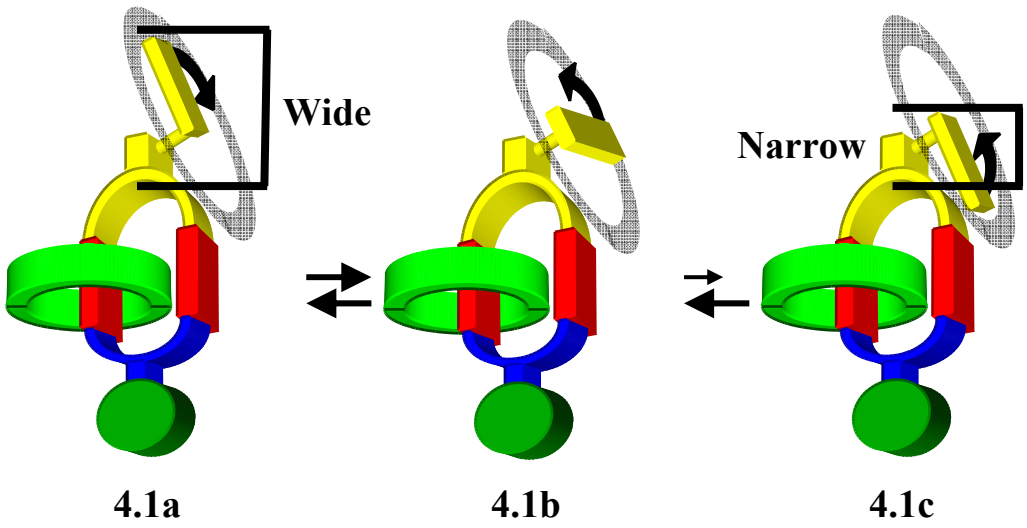

Figure 4.1. Isomer 1 and gate conformers.

latter being available but sterically disfavored (**4.1c**). Normal thermal fluctuations would keep the narrow gate (**4.1c**) from forming in high concentration. It is important to note that any force, such as movement of the ring as shown in Figure 4.2, capable of isomerizing the gate into the narrow conformation could aid passage over the gate and

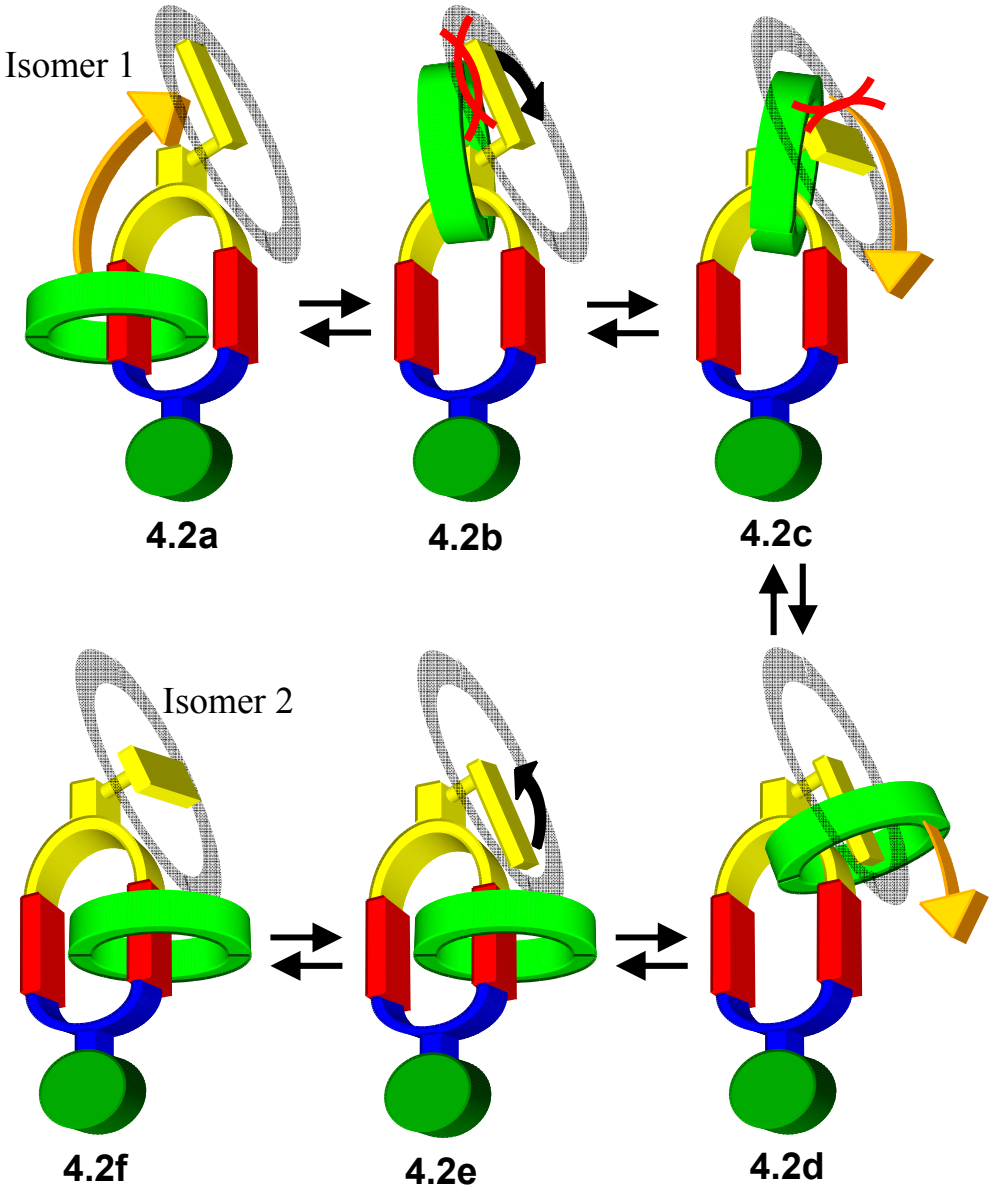

Figure 4.2. Formation of isomer 2 via circumrotation.

tether A from the left binding site.

As the ring moves towards the gate (**4.2a**) and the two begin interacting (**4.2b**), the gate should push away from the ring into the more reactive, yet energetically higher conformation (**4.2b-4.2d**) allowing passage over the gate thus forming isomer 2 (**4.2e**) with the gate moving back to its wider, lower energy conformation (**4.2f**). Going in the reverse direction, the ring moves over tether A from right to left reforming isomer 1. However, this movement requires a confluence of disfavorable events. It requires formation of the thermally disfavored gate position shown in **4.2e**. This microscopic reverse pathway would require the gate to move on its own into a higher energy form in order to allow passage of the catenane over the tether, a statistically disfavored event. If the ring should encounter the gate in its normal wide configurations (**4.3b** and **4.3c**), the interaction could prevent the gate from swinging back down into the more reactive

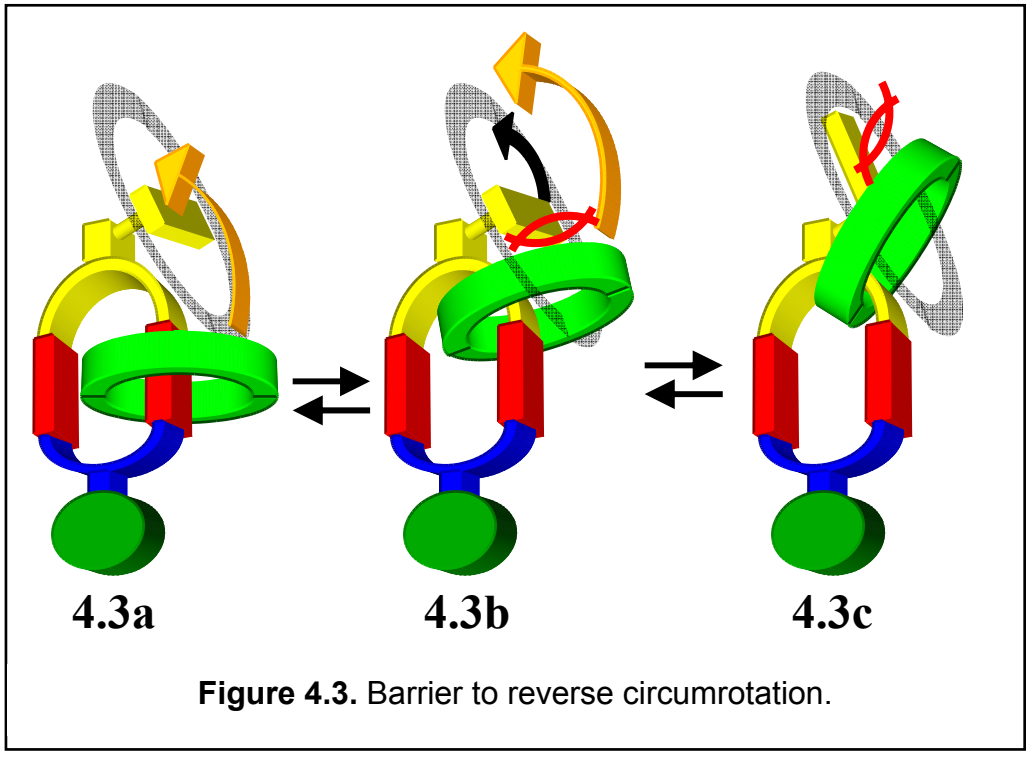

Figure 4.3. Barrier to reverse circumrotation.

conformation, increasing the amount of energy required to form isomer 1. From either direction, there will be interaction between the gate and the BPP34C10 ring. In one direction, such as formation of isomer 2 from isomer 1, it is a positive interaction allowing circumrotation and in the opposite direction, as with formation of isomer 1 from isomer 2, it is negative working against circumrotation. In these ways, we hoped to modulate the potential energy surface using random thermal fluctuations thereby forming two energetically different pathways to circumrotation as shown in Figure 4.4. Previous attempts at making a thermally driven molecular ratchet failed because there

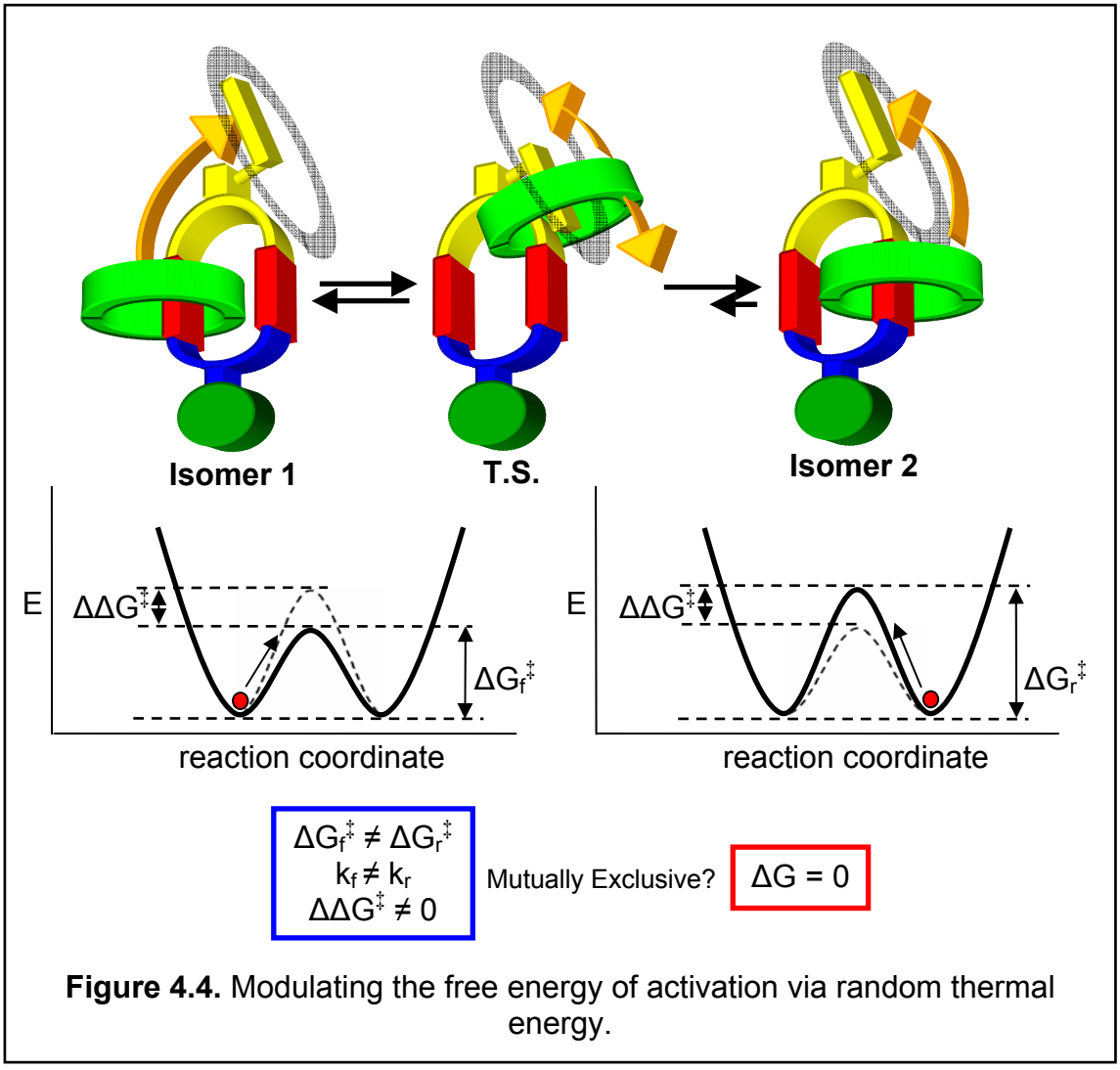

Figure 4.4. Modulating the free energy of activation via random thermal energy.

was no modulation of the activation energy. Kelly's design[21] possessed an asymmetric energy potential, but as was presented in Feynman's lectures[14,21], it is not the shape of the potential energy barrier that dictates the direction of reaction, but its magnitude. Microscopic reversibility cannot be overcome if the energy potential does not change between the two ground states. Here we have a *Gedankenmaschine* where the activation energy has the potential to be raised and lowered by random thermal fluctuations. This raises very important questions about the nature of microscopic reversibility. While it is possible and quite common to have the following three conditions observed in a single system: unequal forward and reverse rate constants, unequal free energies of activation, and $\Delta\Delta G^{\ddagger}$ greater than zero, these conditions have not been true when ΔG^{0} equals zero. Indeed, the laws of thermodynamics dictate the condition cannot exist.

The modular nature of [2]catenane synthesis should enable us to prepare bistable catenanes possessing tethers that would give energetically different pathways for circumrotation. We could very easily synthesize a [2]catenane with an open pathway B (Figure 4.5) as opposed to blocked pathway B. This is a very important and necessary feature because we require confirmation that kinetics and not thermodynamic ground state differences direct formation of the isomers. Thus, a series of controls were envisioned. These controls possessed the same two low-energy binding sites but allowed BPP34C10 to bypass the gate on tether A. Passage over open tether B would eliminate passage over the more energy intensive gating tether allowing free isomerization and equilibration to occur. This would allow us to characterize the

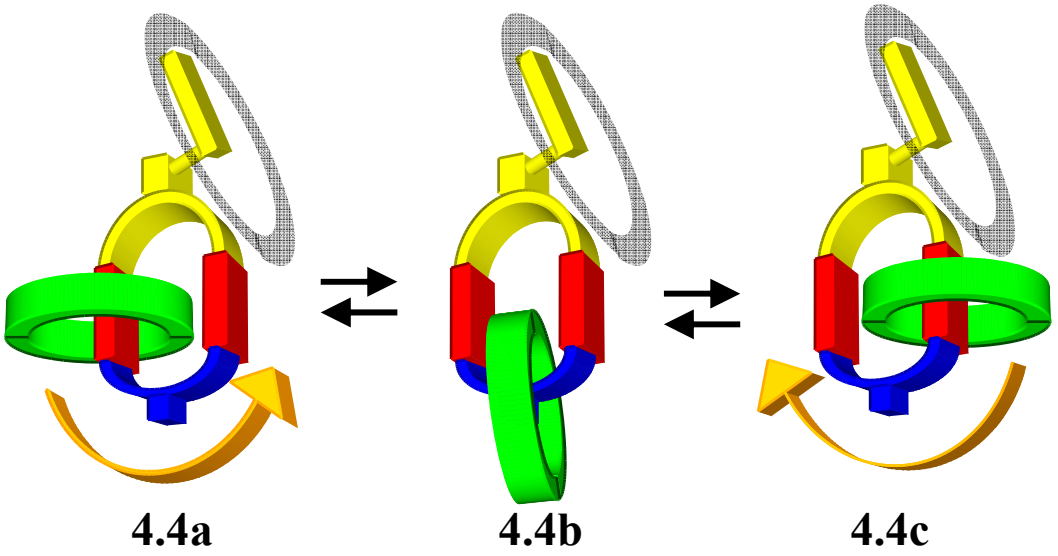

Figure 4.5. Circumventing the gate.

ground state energy of the isomers as being thermodynamically isoenergetic or as having unique ground states.

Using these concepts, we synthesized a series of [2]catenanes possessing the requisite functions we hoped would demonstrate isomerization consistent with a gate driven by random thermal fluctuations (Figure 4.6). Each possesses a different gate: beginning with the short benzyl gate and ending with the longer *p*-phenylbenzyl gate. Our rationale for the different lengths was that we hoped to tune the activity of the gate by making it progressively longer, thereby enhancing any gating effect. While these catenanes did not produce the definitive results we desired, they did provide insight on the direction future designs should take and illustrated that we could modulate the energy potential for isomerization by increasing the size of the mobile gates.

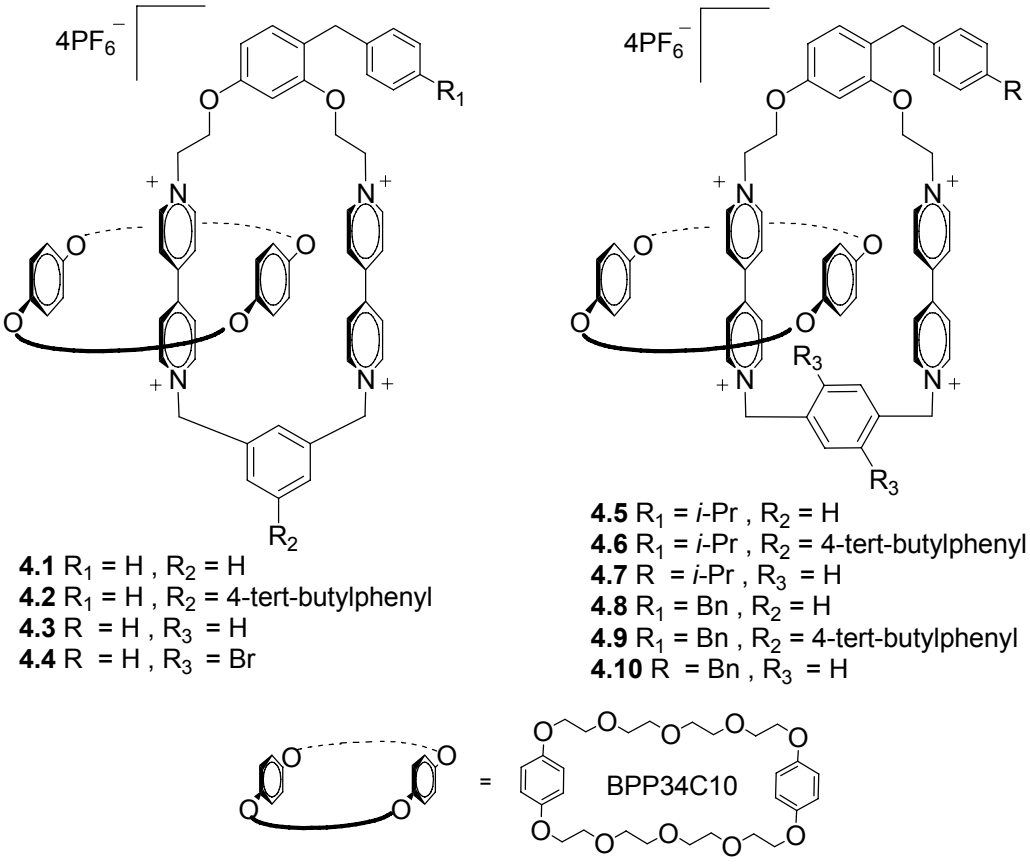

4.1 R_1 = H , R_2 = H
4.2 R_1 = H , R_2 = 4-tert-butylphenyl
4.3 R = H , R_3 = H
4.4 R = H , R_3 = Br

4.5 R_1 = *i*-Pr , R_2 = H
4.6 R_1 = *i*-Pr , R_2 = 4-tert-butylphenyl
4.7 R = *i*-Pr , R_3 = H
4.8 R_1 = Bn , R_2 = H
4.9 R_1 = Bn , R_2 = 4-tert-butylphenyl
4.10 R = Bn , R_3 = H

Figure 4.6. Gating catenanes **4.1-4.10**.

Section 4.2 Synthesis and Study of Benzyl Substituted [2]Catenane Components

Synthesis of the three substituted resorcinol gating groups was accomplished through analogous methods as described via the three key resorcinol derivatives depicted in Figure 4.7. Reduction of 2,4-dihydroxybenzophenone **4.11** using sodium cyanoborohydride[54] produced 4-benzylbenzene-1,3-diol **4.12** in 90 % yield (Scheme 4.1). Analysis by ^{1}H NMR revealed a new signal at 3.91 ppm (s, 2H) indicating addition of two protons to the methylene bridge proton and the mass spectrum (EI) gave the correct M^+ peak of 200.0 m/z both confirming the identity of the compound. The resorcinol aryl protons appeared as a multiplet at 7.30-7.15 ppm (m, 5H).

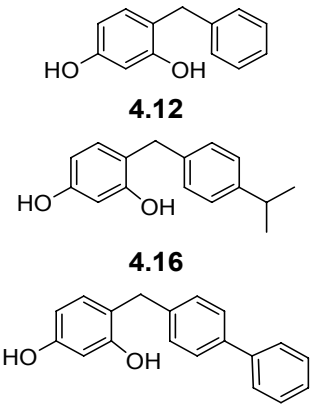

4.12

4.16

4.19

Figure 4.7.

Grignard addition of 2,4-dimethoxybenzene magnesium bromide to the commercially available aldehyde **4.13** gave the secondary alcohol **4.14** which was reduced[48,54] to **4.15** and then deprotected[49] to give isopropyl substituted resorcinol **4.16** as shown in Scheme 4.2. The addition was carried out in 78 % yield. Analysis of the pure product via ^{1}H NMR showed the four protons on the benzyl gate at 7.19 (s, 4H) with the three resorcinol protons at 7.03 (d, J = 8.2 Hz, 1H), 6.53 (d, J = 2.4 Hz, 1H), and 6.47 (dd, J = 8.2, 2.4 Hz, 1H) ppm. At 3.94 ppm (s, 1H) we observed the lone methylene proton

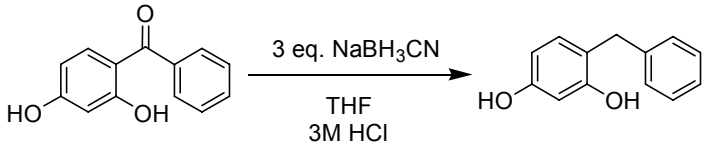

4.11 **4.12**

Scheme 4.1.

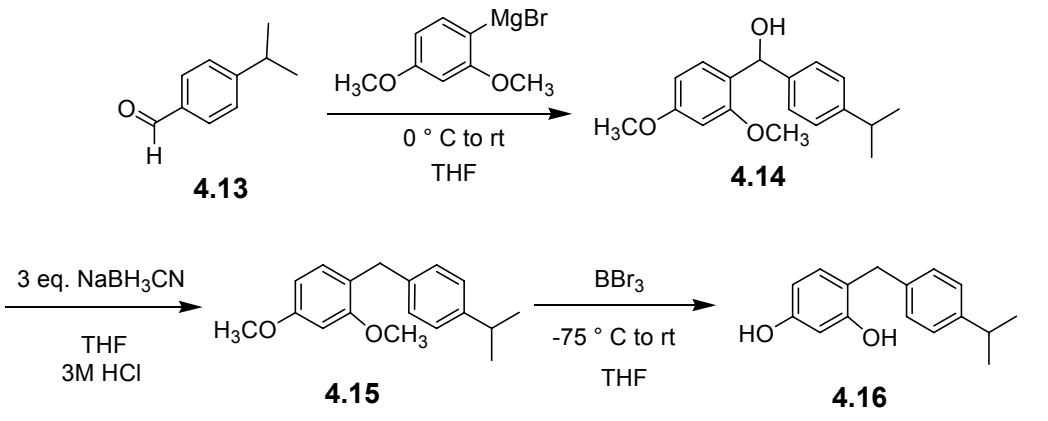

Scheme 4.2.

while the methoxy signals appeared at 3.85 (s, 3H) and 3.83 (s, 3H) ppm. Signals for the isopropyl group appeared at 2.93 (sept., *J* = 6.9 Hz, 1H) and 1.29 (d, J = 6.9 Hz, 6H) ppm. The hydroxyl proton appeared at 2.23 (bs, 1H) ppm as a broad singlet. A mass spectrum (EI) gave peaks for the sodium adduct at 309.1 m/z (M Na^+) and the molecular ion 286.1 m/z (M^+).

Reduction of alcohol **4.14** using sodium cyanoborohydride was signaled by the absence of the hydroxyl proton peak with a concurrent increase in the integration of the methylene peak. The mass spectrum gave the molecular ion peak of 270.2 (M^+). Deprotection was indicated in the ^{1}H NMR spectrum by the loss of methoxy protons signals at 3.85 (s, 3H) and 3.83 (s, 3H) and addition of two new hydroxyl proton signals at 5.65 (s, 1H) and 5.25 (s, 1H) ppm. In addition, a decrease in the molecular ion peak to 242.2 m/z consistent with loss of two methyl groups was observed in the EI mass spectrum.

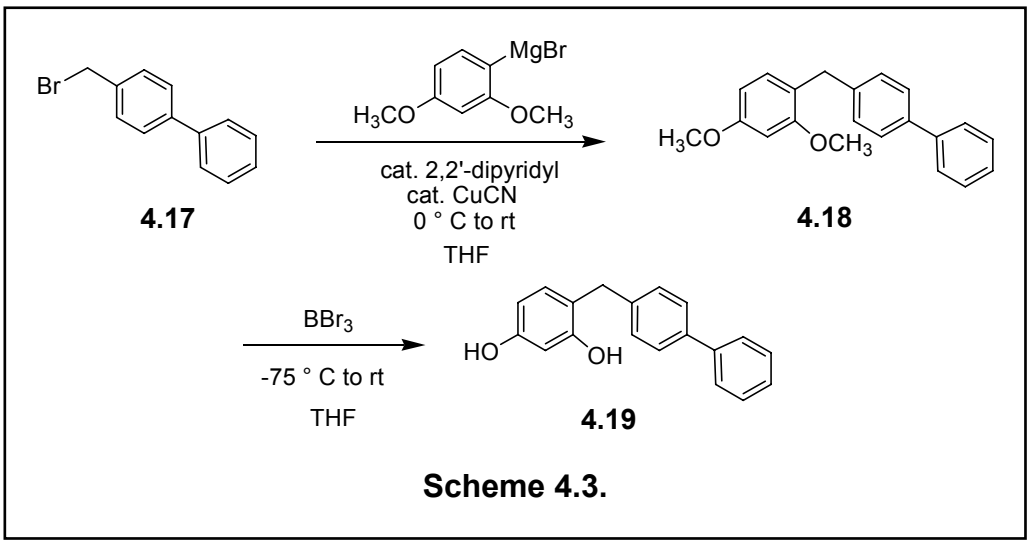

Scheme 4.3.

The cross coupling reaction of 2,4-dimethoxybenzene magnesium bromide to *p*-phenylbenzyl bromide **4.17** gave the secondary alcohol **4.18**[59] which was reduced[48,54] and then deprotected[49] to give substituted resorcinol **4.19** as shown in Scheme 4.3. The biphenyl protons appeared as a series of multiplets at 7.67-7.61 (m, 2H), 7.59-7.53 (m, 2H), 7.52-7.45 (m, 2H), 7.42-7.37 (m, 1H), and 7.37-7.31 (m, 2H) ppm. Resorcinol protons signals were located at 7.08 (d, J = 8.2 Hz, 1H), 6.55 (d, J = 2.1 Hz, 1H), and 6.50 (dd, J = 8.2, 2.1 Hz, 1H) with the two bridging methylene protons at 4.01 ppm (s, 2H). Methoxy signals for the coupling product **4.18** were at 3.88 (s, 3H) and 3.87 (s, 3H). The ESI mass spectrum provided the sodium adduct of the molecular ion with a peak at 327.2 (M Na^+) while EI produced the molecular ion at 304.1 m/z (M^+). Upon deprotection of **4.18** to form resorcinol derivative **4.19** the ^{1}H NMR revealed loss of the methoxy protons and addition of two hydroxyl protons at 4.70 (s, 1H) and 4.66 (s, 1H) ppm consistent with the structure of **4.19**. The ^{13}C NMR spectrum, with 15 distinct signals present, was consistent with the number of magnetically different carbons.

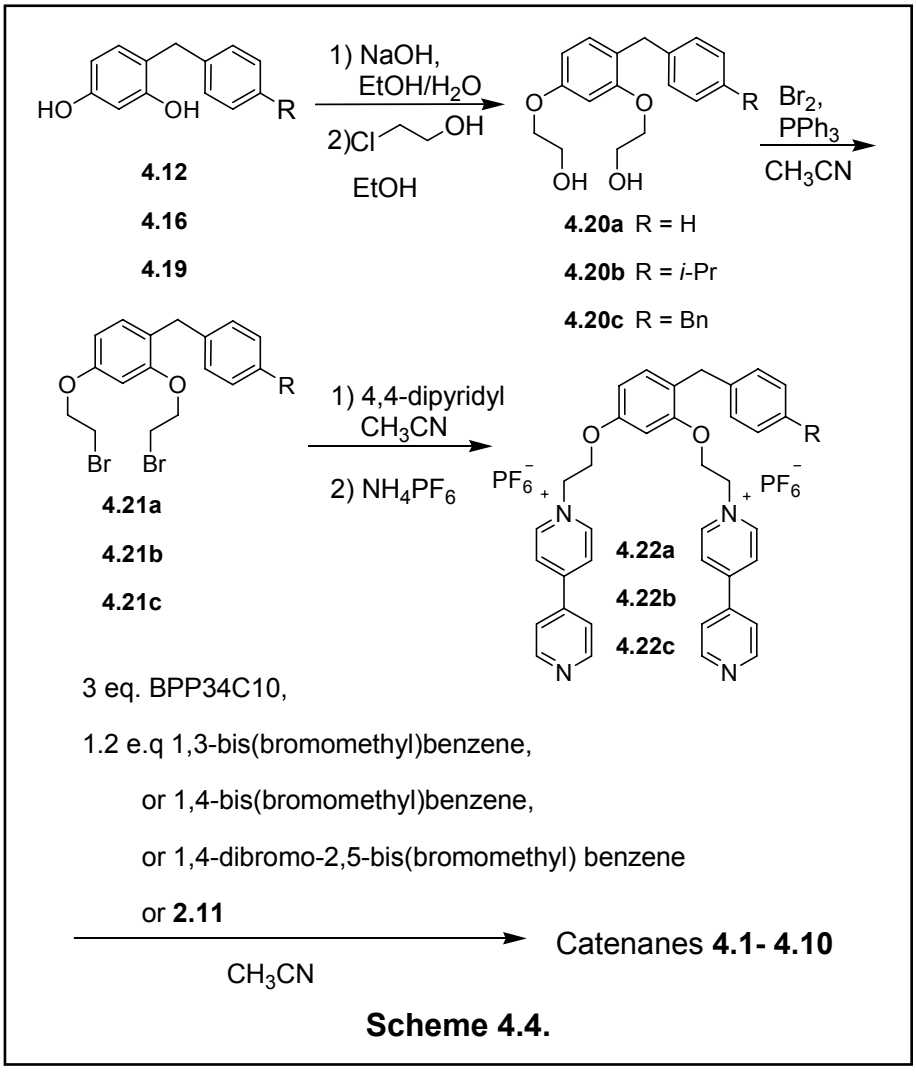

Scheme 4.4.

Analysis of the EI mass spectrum showed the anticipated molecular ion peak of 276.2 m/z (M^+).

Syntheses of the 4-substituted resorcinol derivatives of 1,3-bis(2-(4,4'-dipyridinium)ethoxy)benzene bis(hexafluorophosphate) are summarized in Scheme 4.4. A summary of the reaction steps immediately follows with the details to come in later sections. The three resorcinol analogues, 4-benzylbenzene-1,3-diol (**4.12**), 4-(4-isopropylbenzyl)benzene-1,3-diol (**4.16**), and 4-(4-phenylbenzyl)benzene-1,3-diol (**4.19**) were deprotonated with sodium hydroxide and reacted with 2-chloroethanol to

form the substitution products: 1,3-bis(2-hydroxyethoxy)-4-benzylbenzene (**4.20a**), bis(2-hydroxyethoxy)-4-(4-isopropylbenzyl)benzene (**4.20b**), and bis(2-hydroxyethoxy)-4-(4-phenylbenzyl)benzene (**4.20c**), which were brominated to give bis(2-hydroxyethoxy)-4-benzylbenzene (**4.21a**), 1,3-bis(2-hydroxyethoxy)-4-(4-isopropyl)benzene (**4.21b**), and 1,3-bis(2-hydroxyethoxy)-4-(4-phenylbenzyl)benzene (**4.21c**). Treatment with excess 4,4'-dipyridyl followed by salt exchange with ammonium hexafluorophosphate gave 1,3-bis(2-(4,4'-dipyridinium)ethoxy)-4-benzylbenzene bis(hexafluorophosphate) (**4.22a**), 1,3-bis(2-(4,4'-dipyridinium)ethoxy)-4-(4-isopropyl)benzene bis(hexafluorophosphate) (**4.22b**), and 1,3-bis(2-(4,4'-dipyridinium)ethoxy)-4-(4-phenylbenzyl)benzene bis(hexafluorophosphate) (**4.22c**), respectively. Catenanes **4.1-4.10** were formed through three component reactions between one equivalent of bis(pyridiniums) **4.22a**, **4.22b**, or **4.22c**, 1.2 equivalents of 1,3-xylenes, 1,4-xylenes or **2.11** and 3 equivalents of BPP34C10 in acetonitrile at room temperature for three days as described in previous chapters. After solvent removal, the catenanes were isolated by preparative thin-layer chromatography on silica as described in Chapter Two.

Section 4.2.1 Synthesis and Study of 4.22a

The first step in the synthesis of 1,3-bis(2-(4,4'-dipyridinium)ethoxy)-4-benzylbenzene bis(hexafluorophosphate) (**4.22a**) produced diol (**4.20a**) in 68 % yield (Scheme 4.5). The ^{1}H NMR spectrum of the pure product displayed signals typical of the hydrogen or carbon substituted ethoxy-benzene diols. At 4.06 (m, J = 8.5 Hz, 2H), 3.94 (m, J = 8.5 Hz, 6H) and 3.77 (m, 2H) ppm we observed three complex multiplets

from the ethoxy bridge protons with the methylene bridge proton signals superimposed on the middle multiplet. The signal for the hydroxyl protons was observed at 1.88 (bs, 2H) as a broad singlet. These data, along with obtaining the anticipated molecular ion signal in the low-resolution EI mass spectrum at 288.1 (M^+) and the sodium adduct peak in the ESI spectrum at 311.1 (M Na^+) m/z, indicated the desired diol was obtained.

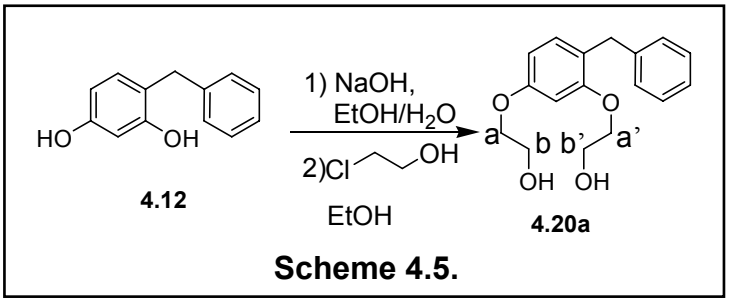

4.12 **4.20a**

Scheme 4.5.

Bromination was accomplished with a 93 % yield giving dibromide **4.21a**. Substitution of bromine on carbons b-b'resolved the multiplets, shifting the H_b-H_b, proton signals downfield to 4.26 (t, *J* = 6.1 Hz, 2H) and 4.23 (t, *J* = 6.1 Hz, 2H) while the H_a-H_a, protons were shifted to 3.63 (t, *J* = 6.1 Hz, 2H) and 3.57 (t, *J* = 6.1 Hz, 2H) leaving the methylene signal at 3.94 ppm (s, 2H). The resolution observed for the ethoxy bridge protons was remarkable compared to previous dipyridiniums. Each signal appeared as a well-defined symmetric triplet with a high degree of correlation between the coupling constants. Loss of the alcohol proton signal was also observed. Analysis of the low-resolution EI mass spectrum gave the calculated molecular ion peak at 413.9 (M^+).

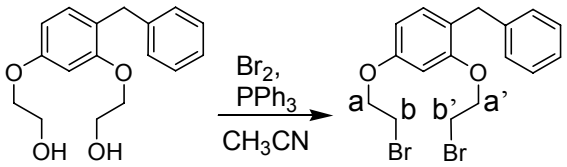

4.20a **4.21a**

Scheme 4.6.

Synthesis of the dipyridyl substituted **4.22a** was achieved in 36 % yield by treatment of dibromide **4.21a** with four equivalents of 4,4'-dipyridyl followed by salt exchange from the bromide to the hexafluorophosphate salt. Confirmation of the structure was made by analysis of mass, ^{13}C, and ^{1}H NMR spectra. The ^{1}H NMR spectrum showed seven new complex multiplets displaying the AA'XX' coupling patterns[51] at 9.31 (m, J = 7.0 Hz, 2H), 9.12 (m, J = 7.0 Hz, 2H), 8.88 (m, J = 6.1 Hz, 4H), 8.67 (m, J = 7.0 Hz, 2H), 8.42 (m, J = 7.0 Hz, 2H), 7.98 (m, J = 4.5 Hz, 2H), and 7.91 (m, J = 4.5 Hz, 2H) consistent with addition of dipyridyl. Ethanolic spacer protons experienced a downfield shift to 5.31 (m, 2H), 5.26 (m, 2H), and 4.68 (m, J = 4.8 Hz, 4H) ppm as observed in the previous asymmetric catenane examples. In the mass spectrum, loss of one hexafluorophosphate anion produced the monocationic species which appeared as a signal at 711.2 m/z (M PF_6^+) in the ESI spectra. Loss of the remaining hexafluorophosphate anion produced a signal at 283.1 m/z (M^{2+}). These spectroscopic studies, in addition to the correct mass spectrum, demonstrated successful formation of the desired product **4.22a**.

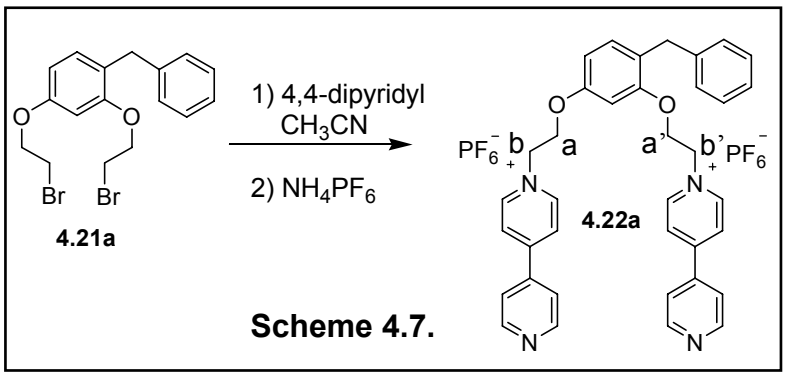

Scheme 4.7.

Section 4.2.2 Synthesis and Study of 4.22b

Synthesis of dipyridyl and isopropylbenzyl substituted **4.22b** was typical and began as shown in Scheme 4.8. Bis(2-hydroxyethoxy)-4-(4-isopropylbenzyl)benzene

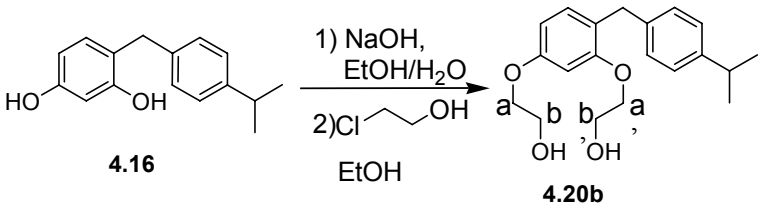

Scheme 4.8.

(**4.20b**) was synthesized from 4-(4-isopropyl)benzene-1,3-diol (**3.10b**) in 69 % yield (Scheme 4.8). The ^{1}H NMR spectrum of pure **4.20b** displayed signals typical of the hydrogen and carbon substituted ethoxy-benzene diols seen in previous examples. Between 4.05-4.01 (m, 2H), 3.95-3.89 (m, 4H), and 3.79-3.74 (m, 2H) we have three complex multiplets from the ethoxy bridge protons. The methylene protons signal and alcohol protons appeared at 3.87 (s, 2H) and 2.40-2.11 (bs, 2H) respectively. Using ESI mass spectrometry we observed the sodium adduct of the molecular ion at 353.2 (M Na^{+}) while the EI spectrum gave the bare molecular ion at 330.2 (M^{+}) m/z indicating the desired diol product was obtained. Bromination was accomplished in 99 % yield through treatment with bromine and triphenylphosphine as shown in Scheme 4.9. Substitution of bromine on the α carbon resolved the multiplets, shifting the α-α' proton signals downfield between 4.30-4.20 ppm (m, 4H). Again, resolution of the β-β' proton signals in **4.21b** was excellent appearing as well-shaped triplets at 3.62 (t, J = 6.2 2H) and 3.57 (t, J = 6.2 Hz, 2H) ppm with excellent correlation between coupling

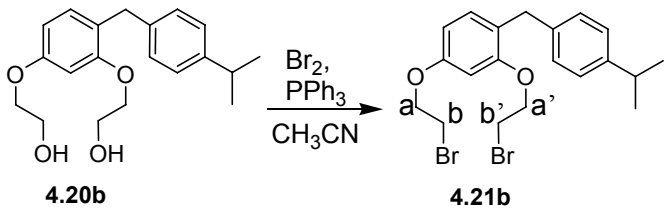

Scheme 4.9.

constants. Loss of the alcohol proton signal was observed. Analysis of the low-resolution EI mass spectrum gave the calculated molecular ion peak at 456.1 (M^+) m/z.

Synthesis of the dipyridyl substituted **4.22b** was achieved in 81 % yield by treatment of dibromide **4.21b** with four equivalents of 4,4'-dipyridyl followed by salt exchange from the bromide to the hexafluorophosphate salt (Scheme 4.10). Confirmation of the structure was made by analysis of mass, ^{13}C, and ^1H NMR spectra. The ^1H NMR spectrum showed six new complex multiplets displaying the AA'XX' coupling patterns[51] at 9.40-9.37 (m, 2H), 9.33-9.28 (m, 2H), 8.94-8.88 (m, 4H), 8.75-8.71 (m, 2H), 8.60-8.55 (m, 2H), and 8.07-8.01 (m, 2H) consistent with addition of dipyridyl.

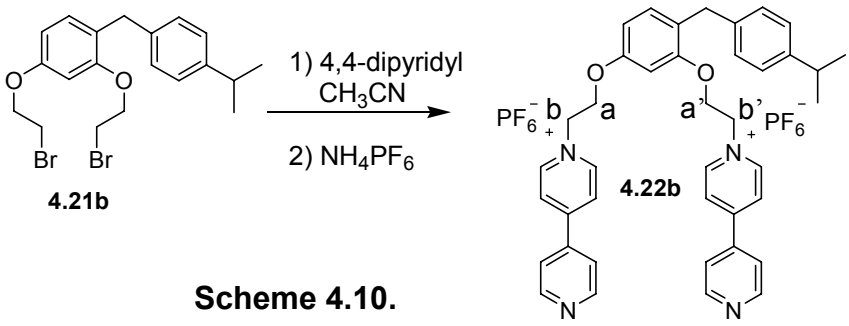

Scheme 4.10.

Ethanolic spacer protons experienced the downfield shift to 5.40-5.30 (m, 4H) and 4.77-4.69 (m, 4H) ppm observed in previous examples. The methylene proton signal remained very close to its original chemical shift throughout the reaction series at or near 3.85 ppm (s, 2H). Mass spectral data confirmed the atomic weight of the compound. Loss of a single hexafluorophosphate anion produced the monocationic species which appeared as a peak at 753.3 (M PF_6^+) in the ESI spectra. Loss of the remaining hexafluorophosphate anion produced a signal at 304 (M^{2+}) m/z. These spectroscopic studies, in addition to the correct mass spectrum, demonstrated successful

formation of the desired product, 1,3-bis(2-(4,4'-dipyridinium)ethoxy)-4-(4-isopropylbenzyl)-benzene bis(hexafluorophosphate) (**4.22b**).

Section 4.2.3 Synthesis and Study of 4.22c

For the *p*-phenylbenzyl substituted resorcinol example **4.22c**, 4-(4-phenylbenzyl)-benzene-1,3-diol (**4.20c**) was synthesized from 4-(4-phenylbenzyl)-benzene-1,3-diol (**4.19**) in 72 % yield (Scheme 4.11). In the ^{1}H NMR spectrum, the new ethyl substituents appeared as complex multiplets at 4.10-4.06 (m, 2H), 4.01-3.94 (m, 4H), and 3.96 (s, 2H) with the hydroxyl proton signals appearing at 1.75 ppm (s, 2H). The signal for the methylene bridging carbon appeared at 3.96 ppm (s, 2H). The *p*-phenylbenzyl substituent on the aryl ring appears as a series of ill-defined multiplets at 7.58-7.54 (m, 2H), 7.52-7.48 (m, 2H), 7.44-7.38 (m, 2H), 7.34-7.28 (m, 1H), and 7.26-7.23 (m, 2H) ppm. These data, along with obtaining the anticipated molecular ion peak in the low-resolution ESI mass spectrum at 364.2 (M+) m/z, indicated the formation of the desired product. Bromination of **4.20c** was accomplished in 99 % yield again using bromine and triphenylphosphine (Scheme 4.12). Substitution of bromine on the b-b' carbons shifted the b-b' proton signals of the ethoxy-bridges downfield to 4.29-4.24 ppm (m, 4H) which appeared as a complex multiplet. The a-a' proton signals were observed at 3.65-3.57 ppm (m, 4H) while the methylene proton

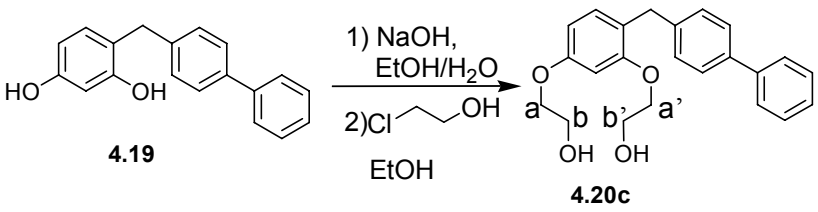

Scheme 4.11.

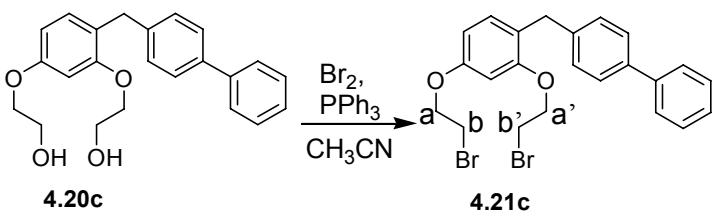

4.20c **4.21c**

Scheme 4.12.

signal remained relatively unchanged at 3.98 ppm (s, 2H). Loss of the alcohol proton signal at 1.75 ppm was also observed. Analysis of the low-resolution EI mass spectrum gave the calculated molecular ion peak at 490.2 m/z (M^+ calculated 490.23 m/z).

Synthesis of the 1,3-bis(2-(4,4'-dipyridinium)ethoxy)-4-(4-phenylbenzyl)-benzene bis(hexafluorophosphate) **4.22c**, was achieved in 87 % yield by treatment of the dibromide **4.21c** with four equivalents of 4,4'-dipyridyl followed by salt exchange from the bromide salt to the hexafluorophosphate salt (Scheme 4.13). The structure was confirmed by mass, ^{13}C, and ^{1}H, NMR spectral analysis. Consistent with addition of dipyridyl, eight new complex multiplets displaying the AA'XX' coupling patterns[51] were observed at 9.36 (m, J = 7.0 Hz, 2H), 9.15 (m, J = 7.0 Hz, 2H), 8.87 (m, J = 4.5 Hz, 2H), 8.70 (m, J = 7.0 Hz, 2H), 8.64 (m, J = 4.5, 1.68 Hz, 2H), 8.39 (m, J = 7.0 Hz, 2H), 7.99 (m, J = 4.5 Hz, 2H), and 7.70 (m, J = 4.5 Hz, 2H) ppm. The ethanolic spacer proton signals appeared as multiplets and were shifted downfield to 5.36-5.27 (m, 4H)

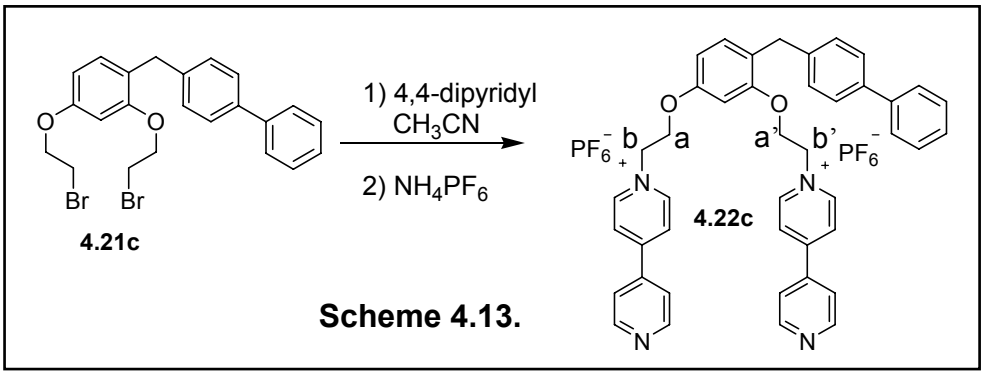

Scheme 4.13.

and 4.71 (m, J = 4.1 Hz, 4H) ppm similar to the previous dipyridinium. Analysis of the mass spectrum confirmed the proposed identity. Loss of one hexafluorophosphate anion produced the monocationic species and appeared as a signal at 787.3 (M PF_6^+), while the dicationic species appeared at 321.7 m/z (M^{2+}) in the ESI mass spectrum. These spectroscopic studies confirmed formation of the desired product **4.22c**.

Section 4.3 Synthesis and Characterization of Catenanes 4.1-4.10

A short summary of the catenane syntheses follows with details to follow. Synthesis of the catenanes began with dissolution of the dipyridyl substituted resorcinol derivatives and three equivalents of BPP34C10 in acetonitrile (Scheme 4.14) followed by addition of 1.2 equivalents of the desired stopper. For catenanes **4.1**, **4.5**, and **4.8** possessing the 1,3-xylylene tether with various 4-substitutions on the resorcinol ring, 1.2 equivalents of α,α'-dibromo-*m*-xylene was added to the solution of dipyridinium and three equivalents of BPP34C10. Catenanes possessing the blocked lower tether B **4.2**, **4.6**, and **3.9** were formed via addition of 5-bis(bromomethyl)-4'-(1,1'-dimethylethyl)-1,1'-biphenyl, while **4.3**, **4.7**, and **4.10** possessing the 1,4-xylyl tether were formed through addition of α,α'-dibromo-*p*-xylene, to solutions of the substituted

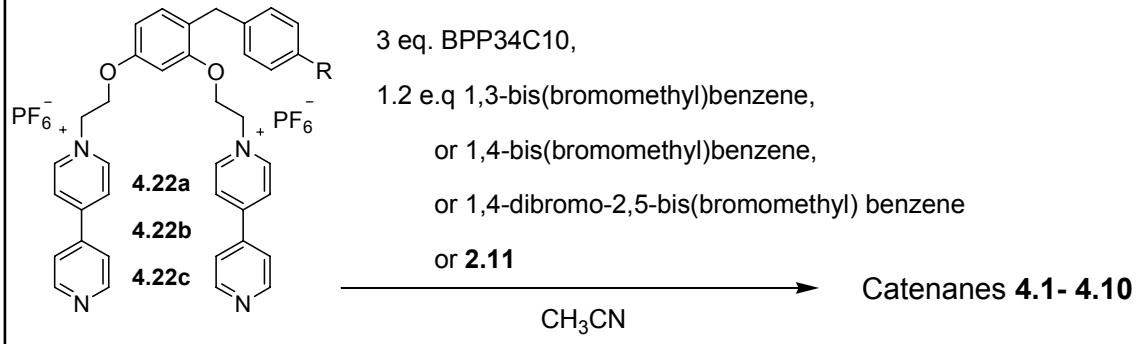

Scheme 4.14. Catenane formation.

3-di(2-(4,4'-dipyridinium)ethoxy)benzene bis(hexafluorophosphate) and BPP34C10. Synthesis of catenane **4.4** was accomplished via addition of 1,4-dibromo-2,5-bis(bromomethyl)benzene to a dipyridinium **4.22a** and BPP34C10 solution. As observed previously, evidence for formation of the π-stacked complexes appeared in less than twenty minutes as a red color, indicating pseudorotaxane and product formation. These reactions continued stirring three days to ensure complete consumption of the starting materials. The solutions turned a deep red color and a yellow precipitate formed during this time. Crude catenanes were purified by preparative TLC in the same manner described in Chapter 2.

Section 4.3.1 Characterization of Catenane 4.1

For catenane **4.1**, having the 4-benzyl group and 1,3-xylyl bottom tether (Figure 4.7), the ^{1}H NMR spectrum at room temperature exhibited a fast exchange average. Addition of BPP34C10 shielded the α pyridinium protons shifting them from 9.31 (m, *J* = 7.0 Hz, 2H) and 9.12 (m, *J* = 7.0 Hz, 2H) to 9.25 (m, *J* = 6.3 Hz, 2H) and 9.18 (m, *J* = 6.7 Hz, 4H) with the downfield signal overlapping the upfield α' signal. Formation of the new pyridinium species shifted the α' proton signals from 8.88 (m, *J* = 6.1 Hz, 4H) to 9.18 (m, *J* = 6.7 Hz, 4H) ppm, again with overlap of the α' signal, and 8.82 ppm (m, *J* = 6.1 Hz, 2H). Both

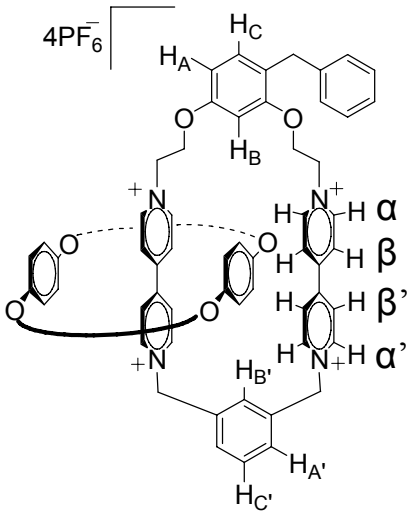

Figure 4.7. Catenane **4.1.**

β and β' dipyridinium protons were affected by addition of the BPP34C10 and formation of the second pyridinium being shifted to 8.27-8.21 (m, 4H) and 8.13 (m, 7H) ppm. The additional three protons found in the integration at 8.13 ppm (m, 7H) was attributed to overlap of two β-β' pyridinium protons and the two protons ortho and para to both xylene methylene groups ($H_{A'}$) as well as the proton ortho to both methylenes ($H_{B'}$). The proton meta to the xylyl-methylenes ($H_{C'}$) appeared as a triplet at 7.91 ppm (t, J = 7.7 Hz, 1H). Signals for the aryl benzyl gate protons appeared at 7.42-7.34 (m, 2H) and 7.32-7.26 (m, 3H), while at 6.21 (s, 2H) and 6.17 (s, 2H) ppm we observed the xylyl methylene signals consistent with the anticipated product. The ethoxy bridge proton signals appeared relatively unaffected by the catenation shifting only slightly, from 5.31 (m, 2H), 5.26 (m, 2H), and 4.68 (m, J = 4.8 Hz, 4H) ppm in the dicationic dipyridyl starting material, to 5.27 (m, J = 4.6 Hz, 4H), 4.6 (m, 2H), and 4.50 (m, 2H) ppm. The tolyl methylene bridge proton peak shifted slightly to 4.04 ppm (s, 2H).

Following the trends established in Chapters Two and Three signals for catenated BPP34C10 were broad and ill defined at room temperature appearing as a broad singlet at 5.74 (bs, 8H) and multiplet between 3.90-3.64 (m, 32H). In the mass spectrum (ESI) we observed various cationic states associated with loss of counter ions with peaks at 748.3 (M $2PF_6^{2+}$), 603.3 (M^{2+}), 450.5 (M PF_6^{3+}), 402.2 (M^{3+}), 301.7 (M^{4+}) m/z. Together these spectra confirmed the structure of the catenane species.

Section 4.3.2 Characterization of Catenane 4.2

Catenane **4.2**, having the 4-benzyl group and bulky bottom tether (Figure 4.8), displayed an ^1H NMR spectrum at 323 K exhibiting a fast exchange average. The

spectrum showed results similar to the other asymmetric catenanes substituted with blocking tether B. Addition of BPP34C10 caused a shift in the α pyridinium proton signals from 9.31 (m, *J* = 7.0 Hz, 2H) and 9.12 (m, *J* = 7.0 Hz, 2H) ppm to 9.35 (m, *J* = 7.0 Hz, 2H) and 9.31 (m, *J* = 7.0 Hz, 2H) ppm. Formation of the new pyridinium species shifted the α' proton signals downfield from 8.88 (m, *J* = 6.1 Hz, 4H) to 9.15 (m, *J* = 7.0 Hz, 2H) and 8.82 (m, *J* = 7.0 Hz, 2H) ppm. Both β and β' dipyridinium protons shifted to 8.44 (m, *J* = 3.1 Hz, 2H), 8.25 (m, 4H), and 8.13 (m, 4H) ppm. The two protons ortho and meta to the xylyl-methylenes ($H_{A'}$) account for the integration of four protons at 8.13 ppm. The proton meta to both methylenes ($H_{B'}$) appeared as a triplet at 8.03 (t, *J* = 1.4 Hz, 1H). At 6.28 (s, 2H) and 6.24 (s, 2H) we observed the xylyl methylene signals. Appropriate signals were observed for the protons on the blocking group with its four phenyl protons and nine methyl protons being observed at 7.93 (m, *J* = 8.5 Hz, 2H), 7.66 (m, *J* = 8.5 Hz, 2H), and 1.43 (s, 9H), respectively, and are identical to the signals observed in the spectrum of Catenane **3.2**. The ethoxy-spacer protons shifted and resolved somewhat appearing at 5.28 (m, 2H), 5.24 (m, 2H), 4.64 (m, 2H), and 4.49 (m, 2H) ppm. In the ESI mass spectrum we observed signals for the di-, tri-, and tetracationic species with zero to two counter ions present; 814.4 (M $2PF_6^{2+}$), 669.9 (M^{2+}), 494.6 (M PF_6^{3+}), 446.9 (M^{3+}) and 334.9 (M^{4+})

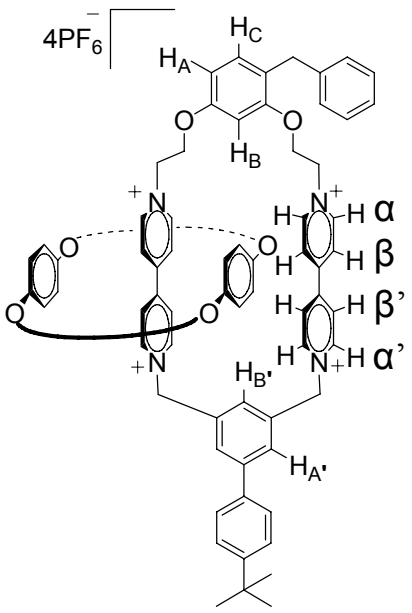

Figure 4.8. Catenane **4.2**.

m/z. This evidence along with the ^{1}H NMR spectrum confirmed we synthesized and isolated the desired catenane.

Section 4.3.3 Characterization of Catenane 4.3

Synthesis and isolation of catenane **4.3** (Figure 4.9), having the 4-benzyl group and 1,4-xylyl bottom tether, was supported by spectral data collected on the sample. Spectra collected were very similar to previous catenanes having the 1,4-xylyl tether with obvious differences due benzyl substitution. The ^{1}H NMR spectrum at room temperature exhibited a fast exchange average. Addition of BPP34C10 shifted the α pyridinium proton signals to 9.36 ppm (m, J = 6.2 Hz, 4H). Similar to the previous two catenanes, formation of the new pyridinium species shifted the α' proton signals downfield from 8.88 (m, J = 6.2 Hz, 4H) to and 9.18 (m, J = 6.2 Hz, 2H) and 8.88 (m, J = 6.2 Hz, 2H). We observed a great deal of signal overlap at 8.15-8.06 ppm (m, 12H). β and β' dipyridinium proton as well as the xylene aryl proton signals overlapped forming a large complex multiplet. At 6.13 (s, 2H) and 6.10 (s, 2H) we observed the xylyl methylene proton signals. Peaks for the resorcinol, benzyl gate, and methylene bridge protons remained largely unchanged. In the mass spectral data we observed the tri- and tetra-cationic species at 450.5 (M PF_6^{3+}) and 301.9 (M^{4+}), respectively, further supporting the identity of the catenane.

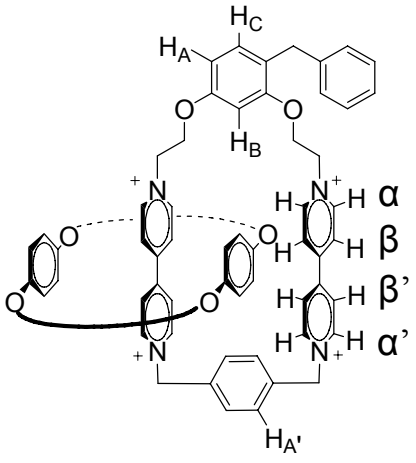

Figure 4.9 Catenane **4.3**.

Section 4.3.4 Characterization of Catenane 4.4

Spectra collected on catenane **4.4** were very similar to the previous catenane **4.3** (Figure 4.10) having the 1,4-xylyl tether with differences due to bromine substitution on the 1,4-xylyl tether B. Catenation of BPP34C10 shifted the α pyridinium proton signals to 9.42 (m, *J* = 6.8 Hz, 2H) and 9.39 (m, *J* = 6.8 Hz, 2H) ppm. Similar to the previous two catenanes, formation of the new pyridinium species shifted the α' proton signals downfield from 8.88 (m, *J* = 6.1 Hz, 4H) to and 9.20 (m, *J* = 6.8 Hz, 2H) and 8.90 (m, *J* = 6.8 Hz, 2H). The chemical shift of the 1,4-xylyl protons ($H_{A'}$), now diastereomers, moved downfield to 8.58 (s, 1H) and 8.52 (s, 1H) ppm. β and β' dipyridinium protons appeared as complex multiplets at 8.18 (m, *J* = 6.8 Hz, 2H) and 8.16-8.10 (m, 6H) ppm. At 6.45-6.34 (m, 2H) and 6.29-6.22 (m, 2H) we observed the xylyl methylene proton signals as complex multiplets. This added complexity was a product of the protons' proximity to the aryl halogens. Peaks for the resorcinol, benzyl gate, and methylene bridge protons remained largely unchanged. In the mass spectral data we observed the tri- and tetra-cationic species at 503.1 (M PF_6^{3+}) and 341.3 (M^{4+}), respectively, further supporting the identity of the catenane.

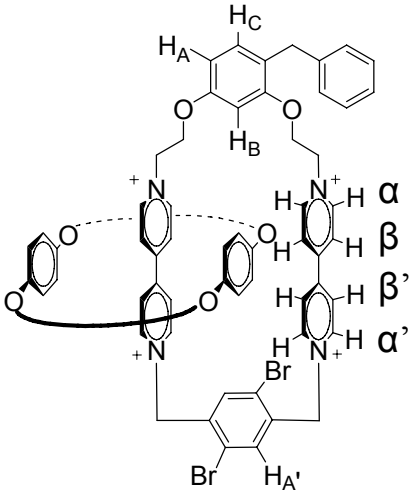

Figure 4.10. Catenane **4.4**.

Section 4.3.5 Characterization of Catenane 4.5

In catenane **4.5** (Figure 4.11), having the 4-isopropylbenzyl group and 1,3-xylyl bottom tether, the ^{1}H NMR spectrum at room temperature exhibited a fast exchange average. Catenation of BPP34C10 shielded the α pyridinium protons shifting them upfield to 9.26 (m, *J* = 6.8 Hz, 2H) and 9.18 (m, *J* = 6.8 Hz, 4H) ppm with the downfield signal overlapping the upfield α' signal. Formation of the new pyridinium species shifted the α' proton signals downfield from to 9.18 (m, *J* = 6.8 Hz, 4H), again with overlap of the α' signal, and 9.01 ppm (m, *J* = 6.8 Hz, 2H). The β and β' dipyridinium protons were shifted to 8.27-8.20 (m, 6H) and 8.19-8.11 (m, 4H) ppm. Signals for the protons both ortho and meta to the xylene methylene groups ($H_{A'}$) overlap the β' signal and account for the increase in signal integration. The protons meta ($H_{C'}$) and ortho ($H_{A'}$) to the xylyl-methylenes appeared as signals at 7.90 (t, *J* = 7.7 Hz, 1H) and 8.07 (m, 1H), respectively. The aryl proton signals for the gate were at 7.25-7.20 ppm (m, 4H) with the isopropyl septet and doublet chemical shifts at 2.91 (sept, *J* = 6.9, 1H) and 1.24 (d, *J* = 6.9 Hz, 6H). At 6.20 (s, 2H) and 6.17 (s, 2H) we observed the xylyl methylene signals consistent with the other catenanes. Ethoxy bridge proton signals shifted to 5.28 (m, 4H), 4.62 (m, 2H), and 4.45 (m, 2H) ppm. In the mass spectrum (ESI) we observed various cationic states associated with loss of counter ions with masses of 769.3 (M $2PF_6^{2+}$),

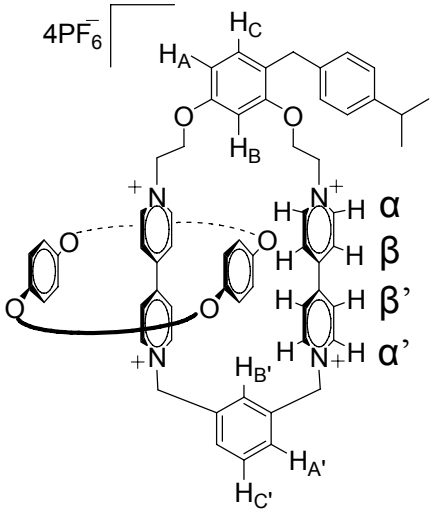

Figure 4.11. Catenane **4.5**.

464.6 (M PF_6^{3+}), and 312.4 (M^{4+}) m/z. Together these spectra confirmed the structure of the catenane species.

Section 4.3.6 Characterization of Catenane 4.6

Synthesis and spectrometric identification of catenane **4.6** (Figure 4.12), possessing the 4-isopropylbenzyl group and blocking tether B, produced results similar to Catenanes **3.2** and **4.2**. At 323 K the ^{1}H NMR spectrum exhibited a fast exchange average. Catenation caused only a very slight shift in the α pyridinium proton peaks from 9.40-9.37 (m, 2H) and 9.33-9.28 (m, 2H) to 9.36 (m, *J* = 5.7 Hz, 2H) and 9.28 (m, *J* = 5.7 Hz, 2H) ppm and at the same time resolving the signals significantly. Formation of the new pyridinium species shifted the α' proton signals downfield to 9.13 (m, *J* = 6.2 Hz, 2H), 9.02-8.94 (m, 2H). B and β' dipyridinium protons were shifted to 8.42 (m, *J* = 4.4 Hz, 2H), 8.34 (m, *J* = 6.2 Hz, 2H), and 8.20-8.05 (m, 6H). Overlap with the two protons ortho and para to the xylyl-methylenes account for the integration of six protons at 8.20-8.05 ppm. The proton meta to both methylenes appeared as an unresolved multiplet at 8.02 ppm(m, 1H). At 6.26 (s, 2H) and 6.23 (s, 2H) we observed the xylyl methylene signals. The blocking group signals consisting of four phenyl protons and nine methyl protons were observed at 7.93 (m, *J* =

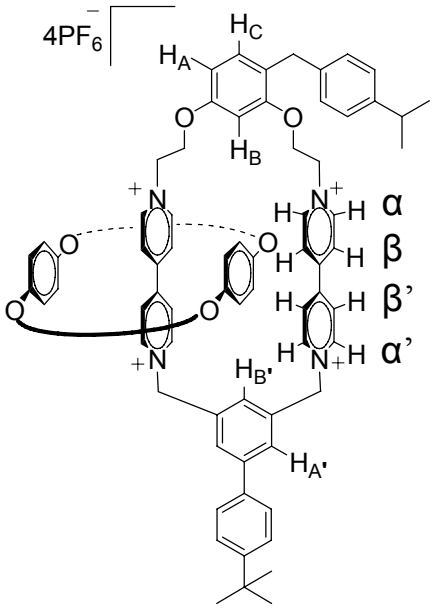

Figure 4.12. Catenane **4.6**.

8.3 Hz, 2H), 7.67 (d, *J* = 8.3 Hz, 2H), and 1.45 (s, 9H), respectively, identical to the signals observed in the spectrum of Catenane **4.2**. The ethoxy-spacer proton signals were at 5.25 (s, 4H), 4.65 (s, 2H), and 4.47 (s, 2H) ppm. Peaks for the resorcinol protons remained virtually unchanged. In the ESI mass spectrum we observed further evidence for catenane formation. The spectrum indicated presence of the di-, tri-, and tetracationic species with differing numbers of counter ions present; .8 (M $2PF_6^{2+}$), 508.6 (M PF_6^{3+}), 460.3 (M^{3+}), and 345.2 (M^{4+}) m/z. This evidence along with the other spectra confirmed the structure of the compound.

Section 4.3.7 Characterization of Catenane 4.7

Synthesis and isolation of catenane **4.7** (Figure 4.13), possessing the 4-isopropylbenzyl group and 1,4-xylyl tether B, was confirmed by spectral analysis. The ^{1}H NMR spectrum at room temperature exhibited a fast exchange average. Catenating the crown ether shifted α pyridinium proton signals to 9.40 (m, *J* = 7.0 Hz, 2H) and 9.35 (m, *J* = 7.0 Hz, 2H) ppm. Formation of the new pyridinium species shifted the α' proton signals downfield to 9.18 (m, *J* = 7.0 Hz, 2H) and 9.05 (m, *J* = 7.0 Hz, 2H) ppm. Two of the β-β' signals appeared at 8.18 (m, *J* = 7.0 Hz, 2H) and 8.14 (m, *J* = 7.0 Hz, 2H) ppm. At 8.12-8.06 (m, 8H) we observed overlap of the remaining two dipyridyl signals with the xylyl-aryl protons signal. At 6.13 (s,

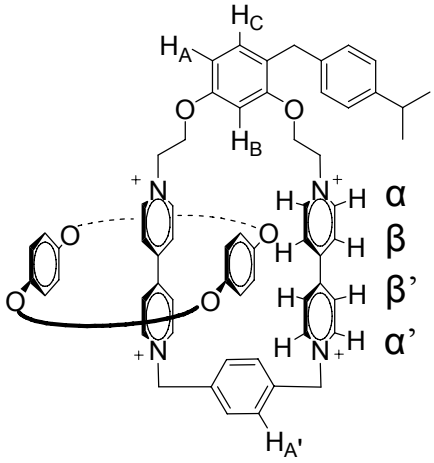

Figure 4.13. Catenane **4.7**.

2H) and 6.10 (s, 2H) ppm we observed the xylyl-methylene proton signals. The ethoxy-spacer signals were observed at 5.27 (m, J = 4.9 Hz, 4H), 4.65 (m, 2H), 4.47 (m, 2H), and 3.98 (s, 2H) ppm. Peaks for the resorcinol, isopropylbenzyl gate, and methylene bridge protons remain largely unchanged from the dipyridinium starting material. The ESI mass spectrum showed the monocationic M $3PF_6^+$ species typically observed as well as peaks corresponding to the di-, tri-, and tetracationic species: 1684.2 (M $3PF_6^+$), 769.3 (M $2PF_6^{2+}$), 464.83 (M PF_6^{3+}), and 312.4 (M^{4+}) m/z. These data along with the ^{1}H NMR spectrum confirmed the identity of the catenane.

Section 4.3.8 Characterization of Catenane 4.8

Catenane **4.8** (Figure 4.14), having the 4-phenylbenzyl gate and 1,3-xylyl tether B, displayed ^{1}H NMR spectrum at 323 K exhibiting a fast exchange average. Addition of BPP34C10 shielded the α pyridinium protons shifting them from 9.36 (m, J = 7.1 Hz, 2H) and 9.15 (m, J = 7.1 Hz, 2H) to 9.17 (m, J = 6.3 Hz, 6H) ppm with signal overlap of the upfield α' signal. The remaining α' pyridinium signal appeared at 8.78 (d, J = 7.0 Hz, 2H) ppm. β and β' dipyridinium protons were shifted to 8.24 (m, J = 6.3 Hz, 2H), 8.10 (m, J = 7.0 Hz, 2H), and 7.96 (m, J = 7.0 Hz, 4H). The signal from the two xylene protons both ortho and para to the methylenes (H_A,) appeared at 8.15

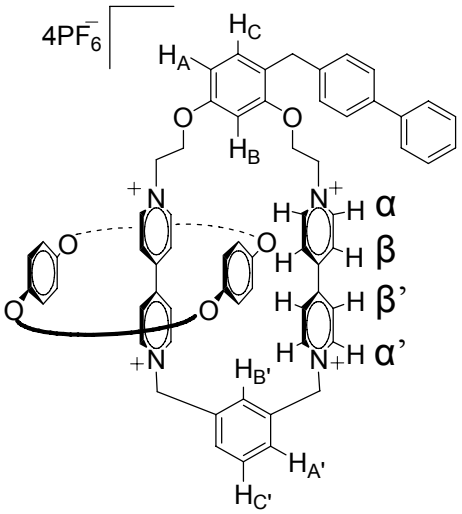

Figure 4.14. Catenane **4.8**.

(m, J = 7.0 Hz, 2H). The protons meta ($H_{C'}$) and ortho ($H_{B'}$) to the xylyl-methylenes gave signals at 8.04-8.00 (m, 1H) and 7.88 (m, J = 7.7 Hz, 1H) ppm, respectively. Signals for the *p*-phenylbenzyl gate appeared at 7.76 (m, J = 7.5 Hz, 2H), 7.71 (m, J = 8.2 Hz, 2H), 7.57 (m, J = 7.5 Hz, 2H), 7.46 (m, J = 7.5 Hz, 1H), and 7.38 (m, J = 8.2 Hz, 2H) ppm. At 6.19 (s, 2H) and 6.17 (s, 2H) ppm we observed the xylyl methylene peaks. The ethoxy bridge proton signals shifted to 5.29 (m, J = 4.0 Hz, 4H), 4.65 (m, 2H), 4.52 (m, 2H) ppm. Chemical shifts for the resorcinol and methylene bridge protons remained unchanged from the dipyridinium spectrum. In the mass spectrum (ESI) we observed the di-, tri-, and tetracations at 786.3 (M $2PF_6^{2+}$), 476.2 (M PF_6^{3+}), and 320.7 (M^{4+}) m/z. Together these spectra confirmed the structure of the catenane species.

Section 4.3.9 Characterization of Catenane 4.9

Synthesis and analysis of catenane **4.9** (Figure 4.15), possessing the 4-phenylbenzyl group and blocking tether B, revealed spectra similar to other asymmetric catenanes with Pathway B blocked. Unlike the previous catenanes, the ^{1}H NMR spectrum of catenane **4.9** at room temperature was not in the fast exchange region. At 323 K, the ^{1}H NMR spectrum did

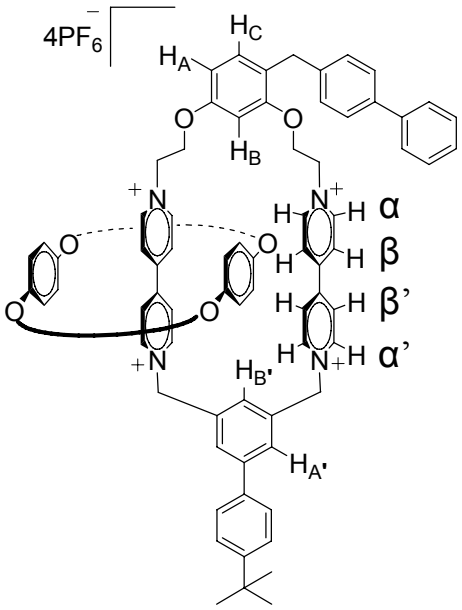

Figure 4.15. Catenane **4.9**.

exhibit a fast exchange average. Catenation caused a shift in the α pyridinium proton signals from 9.36 (m, *J* = 7.1 Hz, 2H) and 9.15 (m, *J* = 7.0 Hz, 2H) to 9.28 (m, *J* = 6.9 Hz, 2H) and 9.25 (m, *J* = 6.8 Hz, 2H) ppm. Formation of the new pyridinium species shifted the α' proton signals downfield from 8.87 (m, *J* = 4.5 Hz, 2H) and 8.70 (m, *J* = 7.0 Hz, 2H) to 9.12 (m, *J* = 6.9 Hz, 2H) and 8.80 (m, 2H). The β -β' dipyridinium protons signals appeared at 8.41 (m, *J* = 5.5 Hz, 2H) and 8.32-8.04 (m, 6H) ppm. The aryl proton ortho to both xylyl-methylenes, which typically appeared as a triplet, remained unresolved as a multiplet at 7.97 ppm (m, 1H) while the meta proton was superimposed on the phenyl protons of the blocking group at 7.92 ppm. At 6.25 (s, 2H) and 6.22 (s, 2H) ppm we observed the xylyl methylene signals. Signals for the blocking group with its four phenyl protons and nine methyl protons were observed at 7.92 (m, *J* = 8.5 Hz, 3H), 7.66 (m, *J* = 8.5 Hz, 2H), and 1.44 (s, 9H), respectively, which were nearly identical to the signals observed in the ^{1}H NMR spectra of catenanes **4.2** and **4.6**. Neither the ethoxy-spacers, resorcinol tether, nor the methylene bridge protons experienced a significant chemical shift change. In the ESI mass spectrum we observed further evidence for catenane formation with peaks appearing at 852.3 (M $2PF_6^{2+}$), 520.3 (M PF_6^{3+}), and 353.9 (M^{4+}) m/z corresponding to di-, tri-, and tetracationic species. This evidence along with the other spectra served to confirm the structure of the catenane.

Section 4.3.10 Characterization of Catenane 4.10

Catenane **4.10** (Figure 4.16), having the 4-phenylbenzyl group and 1,4-xylyl tether B, displayed a ^{1}H NMR spectrum at room temperature exhibiting a fast exchange

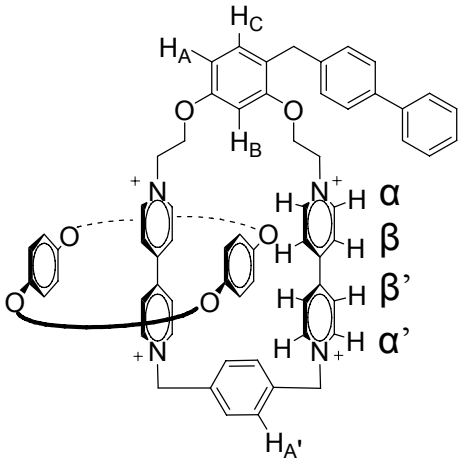

Figure 4.16. Catenane **4.10**.

average. The structure was confirmed by analysis of spectra collected on the sample. The α pyridinium proton signals were shifted to 9.31 ppm (m, *J* = 7.0 Hz, 4H) while the α' pyridinium proton signals were shifted downfield to 9.17 (m, *J* = 7.0 Hz, 2H), 8.84 (m, *J* = 7.0 Hz, 2H). The β-β' dipyridinium proton signals appeared at 8.12 (m, *J* = 7.0 Hz, 2H), 8.07 (m, *J* = 7.0 Hz, 2H), 7.97 (d, *J* = 7.0 Hz, 2H), and 7.89 (d, *J* = 7.0 Hz, 2H) ppm. At 8.06-8.01 ppm (m, 4H) we observed a complex multiplet for the xylyl tether aryl protons. The protons of the *p*-phenylbenzyl gate appeared at 7.72-7.68 (m, 2H), 7.66 (m, *J* = 8.3 Hz, 2H), 7.52 (m, *J* = 7.7 Hz, 2H), 7.41 (m, *J* = 7.7 Hz, 1H), and 7.36 (d, *J* = 8.3 Hz, 2H) ppm. The xylyl methylene proton signals were observed at 6.09 (s, 2H) and 6.07 (s, 2H) ppm, while the ethoxy-spacer protons were at .25 (m, 4H), 4.66 (m, 2H), and 4.51 (m, 2H) ppm. Peaks for the resorcinol and methylene bridge protons remained unchanged. Finally, in the ESI mass spectrum we observed more evidence of catenane formation. It showed the di-, tri-, and tetracationic species: 786.3 (M $2PF_6^{2+}$), 475.9 (M PF_6^{3+}), 320.7 (M^{4+}) m/z. These data along with the ^{1}H NMR spectrum confirmed the identity of the catenane.

Section 4.4 VT ^{1}H NMR Spectra of Catenanes

As with the asymmetric catenanes in chapter two each of these gated catenanes **4.1-4.10** possessed unique signal characteristics often allowing use of only select signal

sets for measuring both chemical shift differences (**Δυ**) and determining temperature of coalescence in order to perform the activation energy calculations. Resorcinol protons H_A and H_B were most often utilized as the phenyl protons of the gate were often overlapping H_C. While the α and α' signals were distinct in the fast-exchange region, in the slow exchange region an unacceptable overlap of signals for catenanes **4.1** to **4.10** was observed making them impossible to utilize. As will be described below, the protons of the resorcinol ring proved the most reliable probes of coalescence temperatures and chemical shift differences.

Section 4.4.1 VT ^{1}H NMR Spectra of Catenane 4.1

In Spectrum 4.1 and 4.2 we observed fast exchange processes at 293 K and slow exchange processes at 198 K, respectively, for catenane 4.1, having the benzyl gate and 1,3-xylyl tether. For each proton signal the coalescence temperature and chemical shift differences were measured. For proton H_B, the separation of the exchanging resonances was measured at 46.2 Hz and the temperature of coalescence was 255 K. The stacked plot, shown in Spectrum 4.3, reveals the progression of spectra as the temperature is lowered from the fast exchange region to coalescence and finally to the slow exchange region. In the fast exchange region we observe the weighted average signal, a doublet. In the slow exchange region, we observed two distinct doublets with an integration ratio of 3.5 to 1 identical to that for catenane **3.8**. Using these data, we calculated an activation energy of 12.5 kcal/mol. This value is consistent with other catenanes having the 1,3-xylyl tether, such as **3.4** and **3.7**.

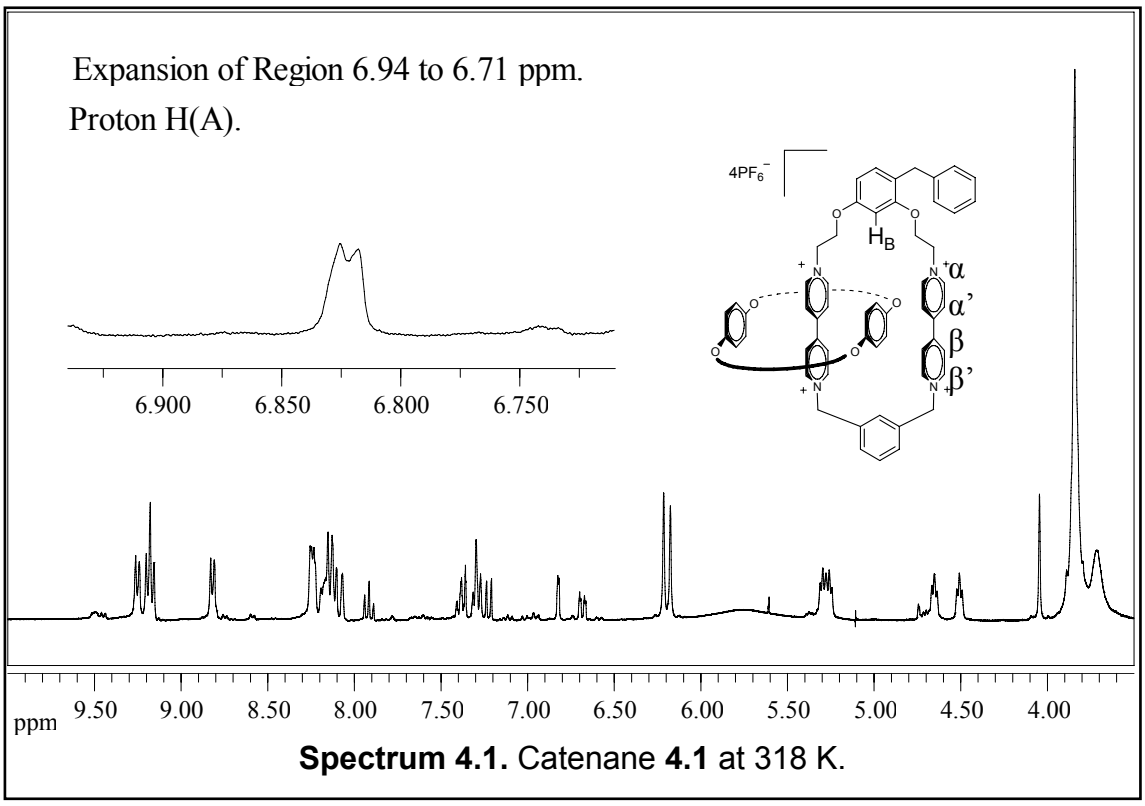

Spectrum 4.1. Catenane **4.1** at 318 K.

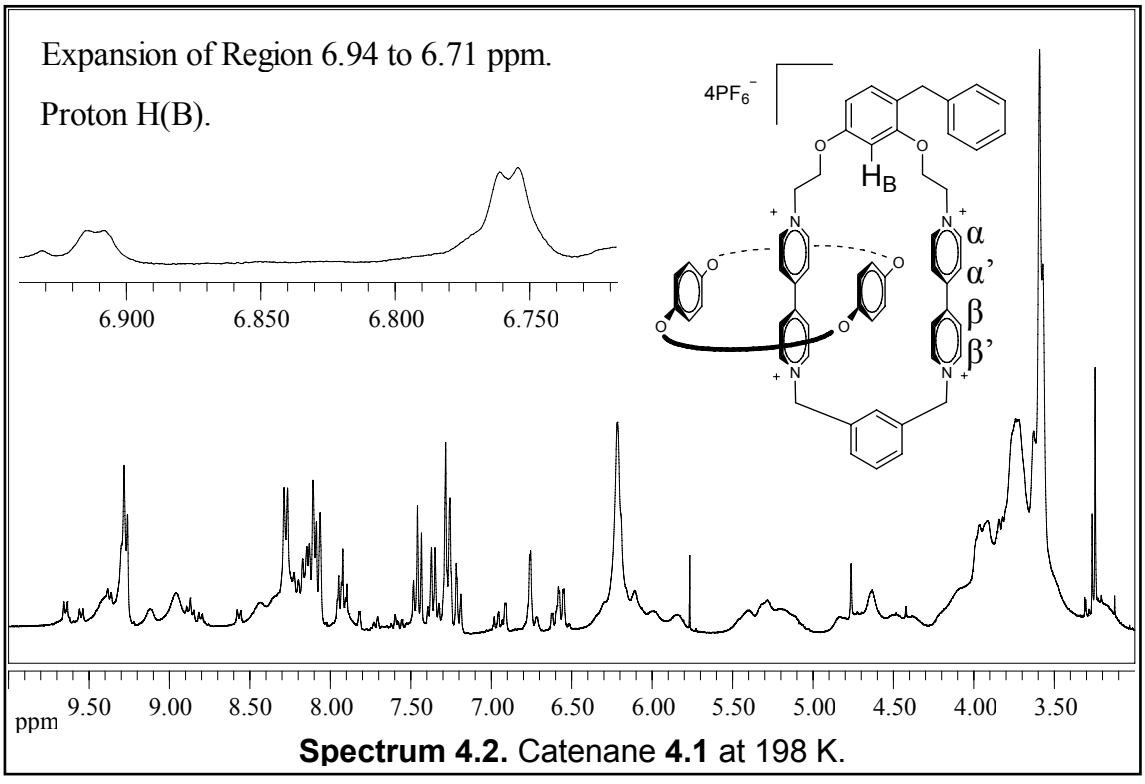

Spectrum 4.2. Catenane **4.1** at 198 K.

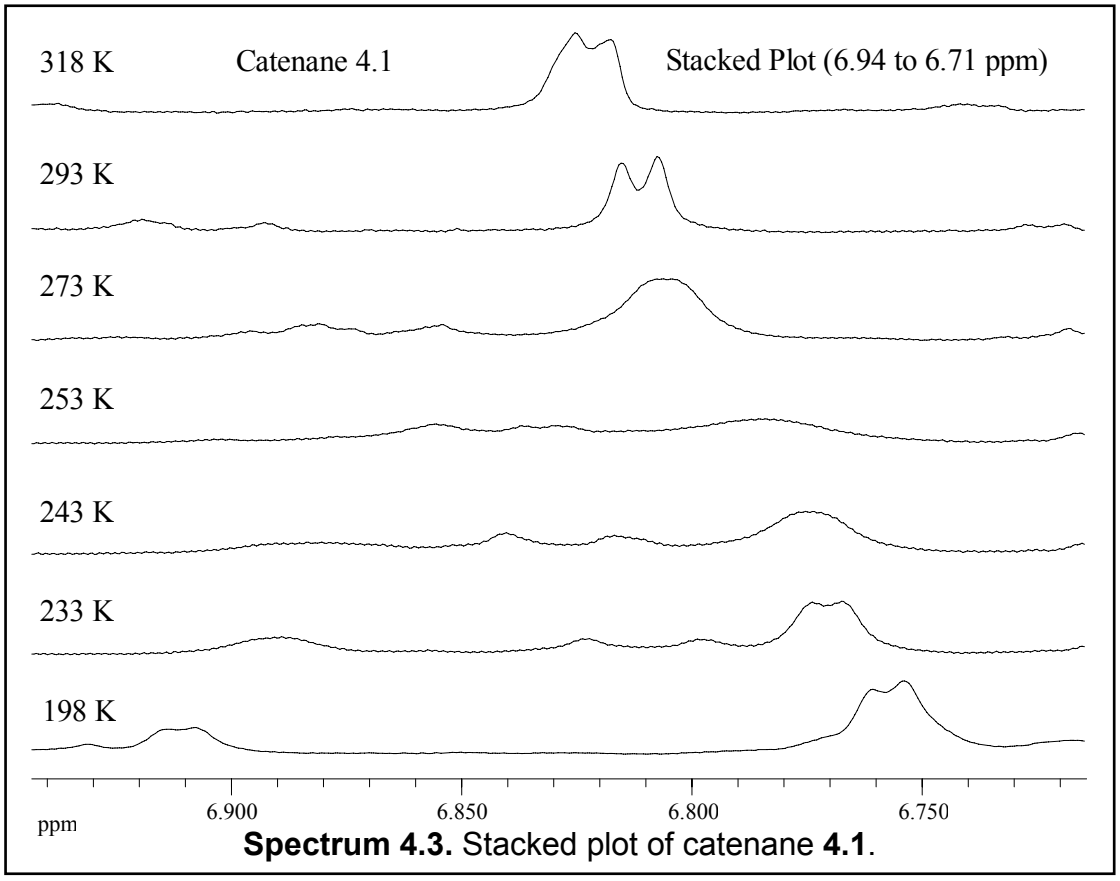

Spectrum 4.3. Stacked plot of catenane **4.1**.

Section 4.4.2 VT ^{1}H NMR Spectra of Catenane 4.2

Unlike catenane **4.1**, having the 1,3-tether, spectra for catenane **4.2** with the blocked lower tether (Spectrum 4.4 and 4.5) displayed clean signals for both meta- and ortho-protons H_A and H_B whose coalescence temperatures and **Δυ** were easily determined in the ^{1}H NMR spectra. The stacked plot, shown in Spectrum 4.6, reveals the progression of spectra as the temperature is lowered from the fast exchange region to coalescence and finally to the slow exchange region. Coalescence for protons H_A and H_B on catenane **4.2** occurred at 265 and 280 K with **Δυ** values of 17.6 and 56.0 Hz, respectively. Integration ratios were 4 to 1 and the energy of activation was calculated at 13.5 kcal/mol for both data sets.

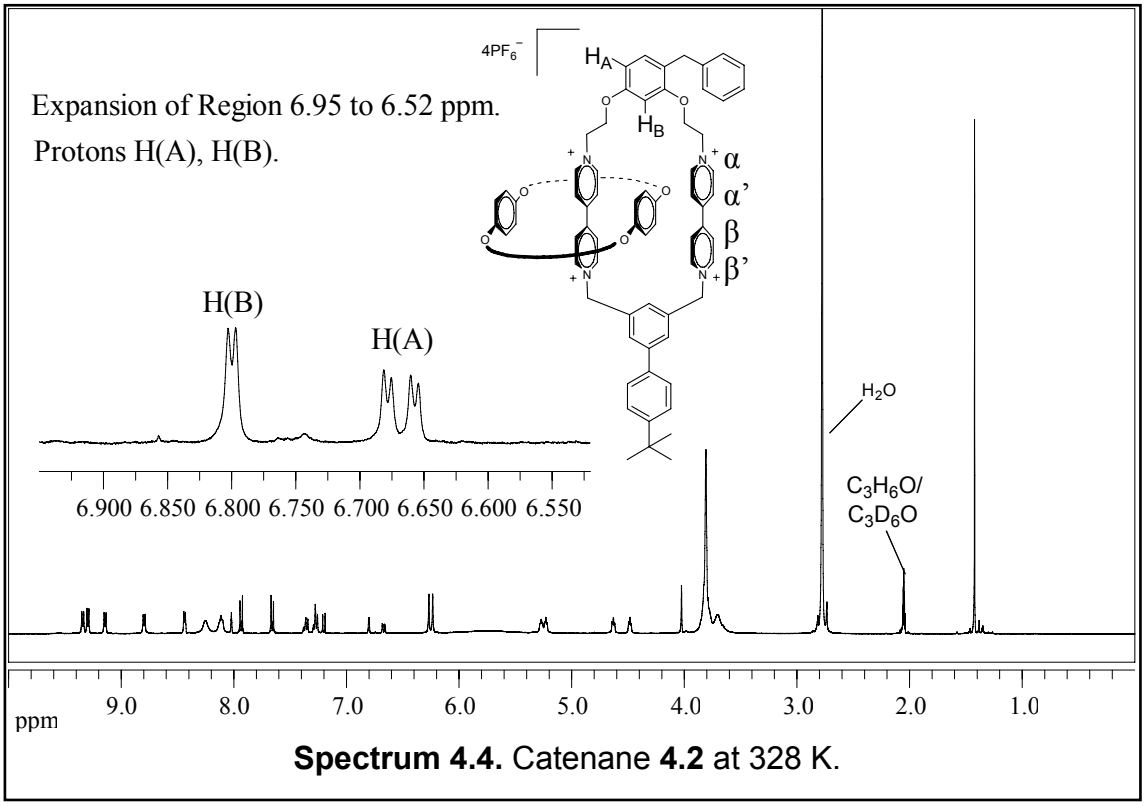

Spectrum 4.4. Catenane **4.2** at 328 K.

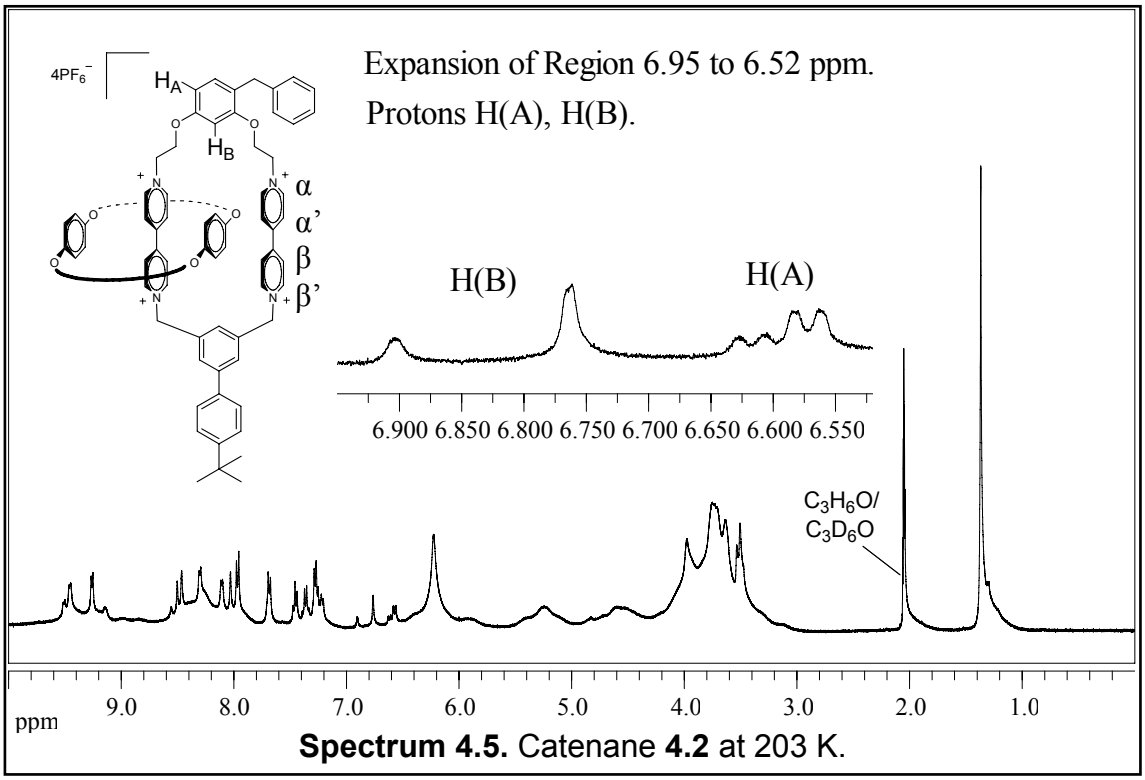

Spectrum 4.5. Catenane **4.2** at 203 K.

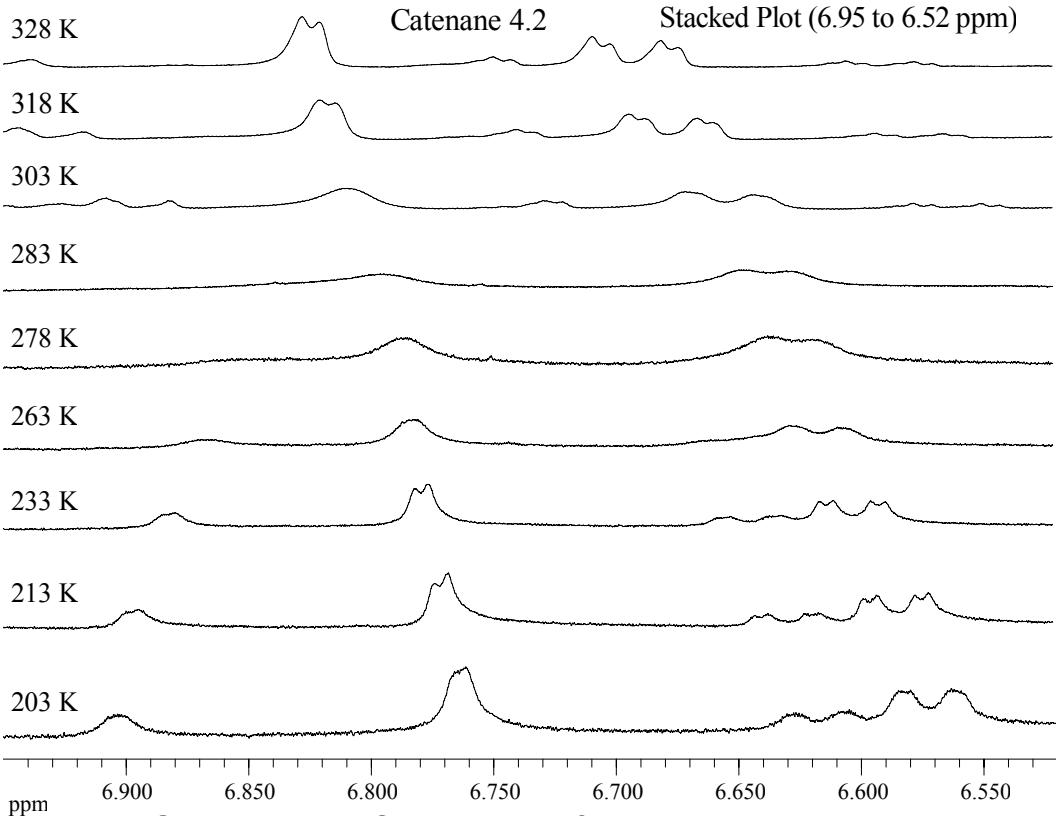

Spectrum 4.6. Stacked plot of catenane **4.2** spectra.

Section 4.4.3 VT ^{1}H NMR Spectra of Catenane 4.3

For catenane **4.3**, possessing the 4-benzyl and 1.4-xylyl substituents, we observed distinct signals for protons H_A and H_B and which were clearly defined with deducible coalescence temperatures (Figures 4.7 and 4.8). The stacked plot in Spectrum 4.8 shows the progression of catenane **4.3** spectra as the temperature was lowered from fast exchange to coalescence and finally to slow exchange. In the fast exchange region we observed the weighted average signals: a doublet of doublets for H_A and a doublet for H_B. As the multiplets approached and finally reached coalescence the signals merged into broad peaks. Coalescence gave way to distinct multiplets as we

approached the slow exchange region. Finally, for protons H_A and H_B, in the slow exchange region we observed two sets of multiplets emerge from each previous multiplet. For proton H_A, the separation of exchanging resonances was measured at 27.0 Hz and the temperature of coalescence was 220 K. The multiplets for proton H_B had a separation of 76.1 Hz with a coalescence temperature of 230 K. The energy of activation was calculated to be 11 kcal/mol for each set of data. This lower free energy of activation is similar to the previous 1,4-xylyl tethered catenanes **3.3**, **3.6**, and **3.9**. Integration ratios for each set of peaks were 1 to 1.

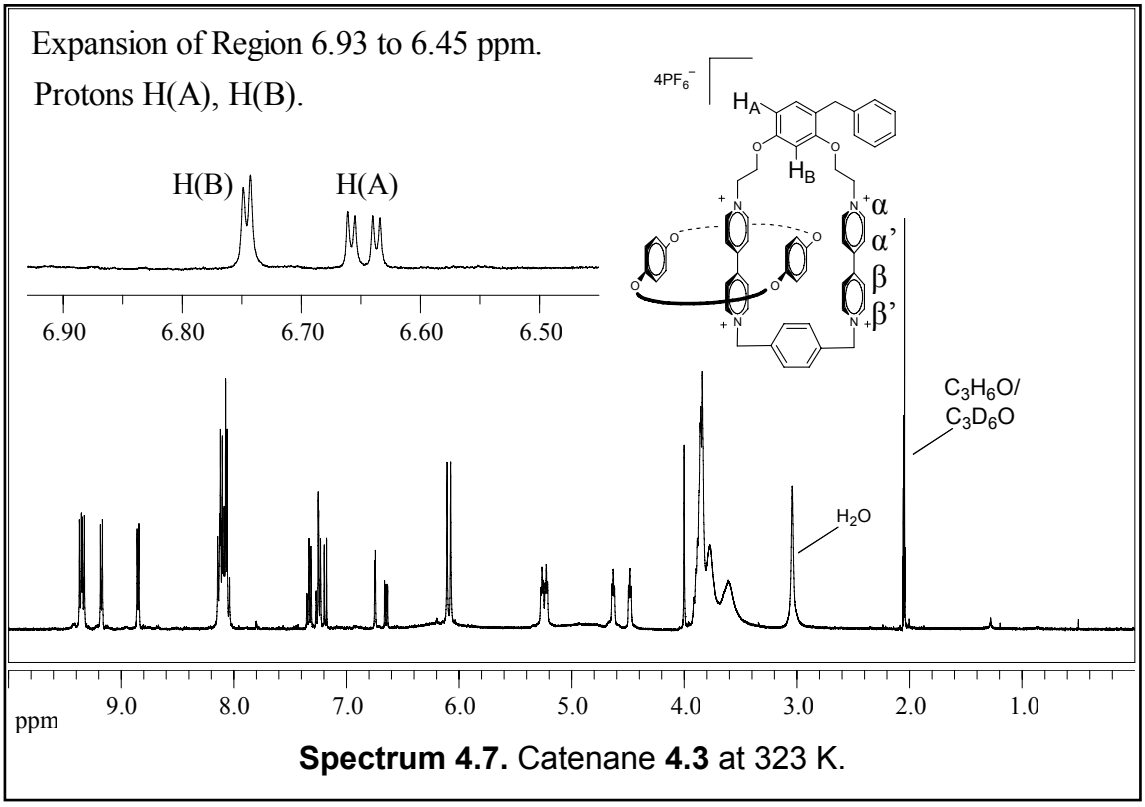

Spectrum 4.7. Catenane **4.3** at 323 K.

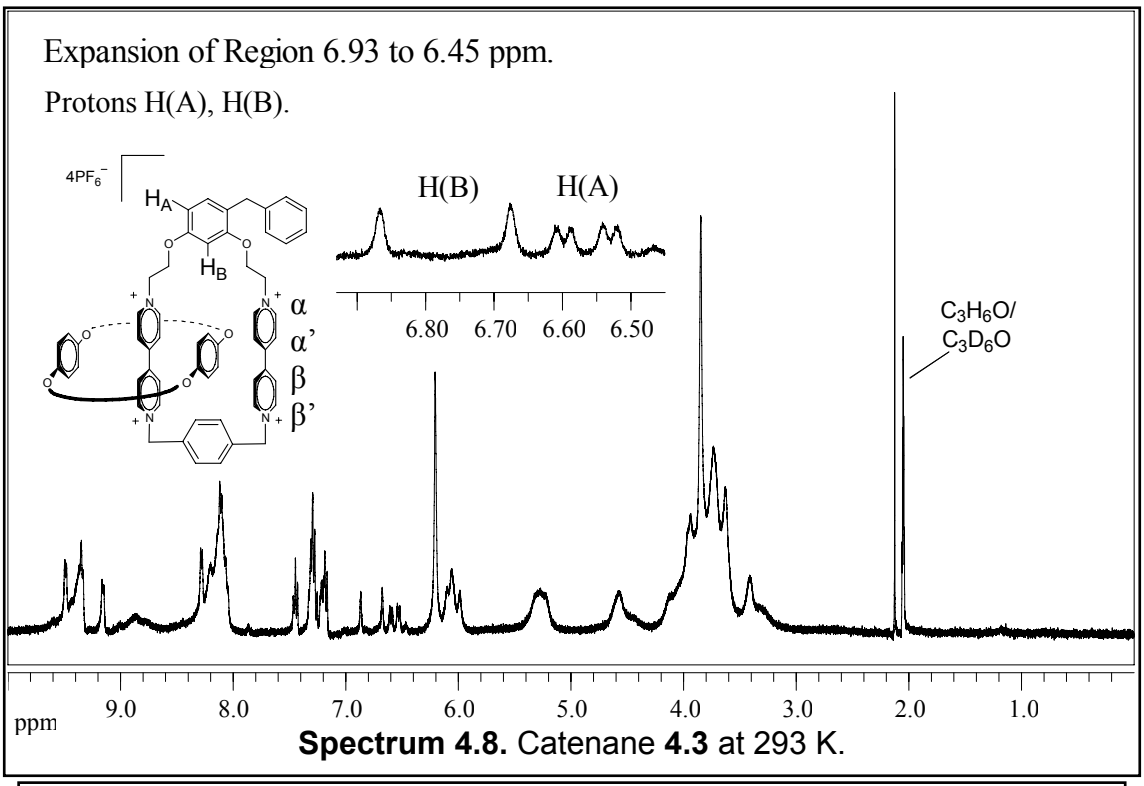

Spectrum 4.8. Catenane **4.3** at 293 K.

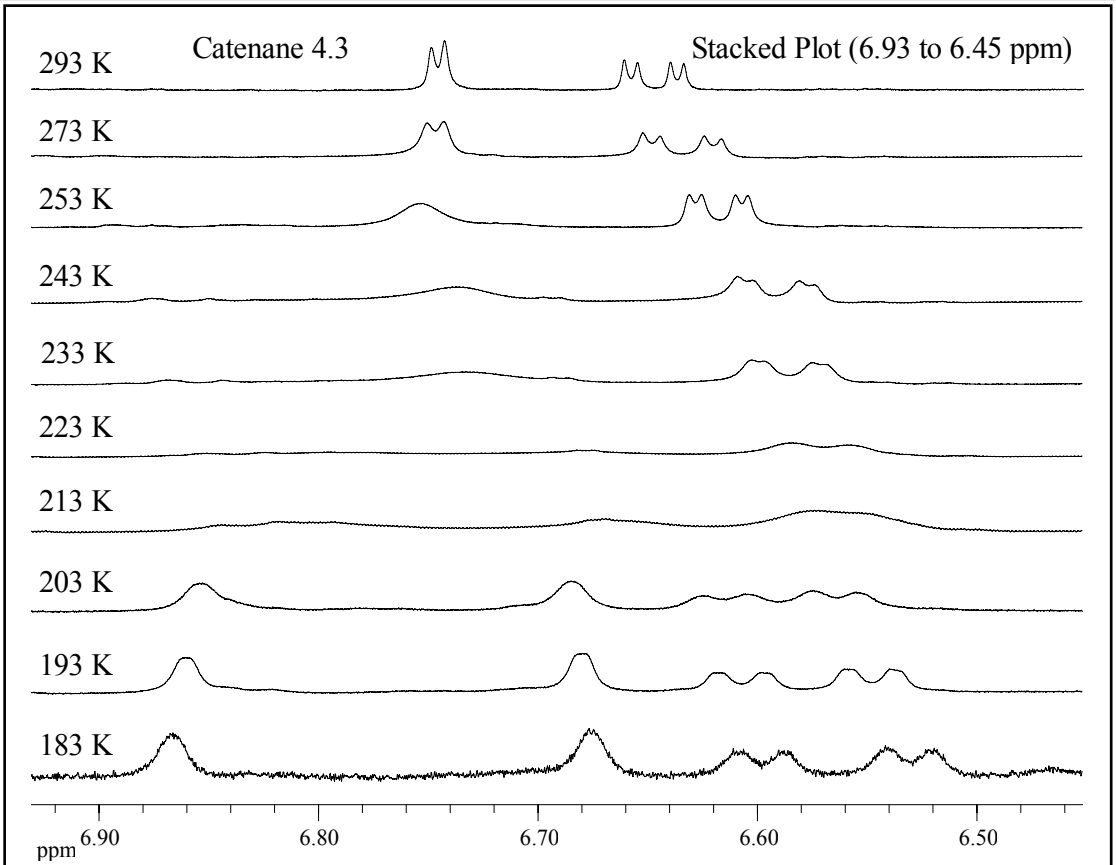

Spectrum 4.9. Stacked plot of catenane **4.3** spectra.

Section 4.4.4 VT ^{1}H NMR Spectra of Catenane 4.4

For Catenane **4.4**, having the 4-benzyl gate and 1,4-dibromo-2,5-xylyl tether, signals for the meta- and ortho-protons H_A and H_B were clearly defined at the low temperature limit and their coalescence temperatures determined from following spectra. In Spectrum 4.10 and 4.11 we observed the fast exchange regime for Catenane **4.4** at 328 K and slow exchange regime at 193 K. For proton H_B the coalescence temperature and chemical shift differential were measured at 230 K and 26.5 Hz. In addition, the ratio of exchanging partners was 3 to 1. The stacked plot appears in Spectrum 4.12. In the slow exchange region, we observed two distinct signals. The activation energy was calculated to be 11.5 kcal/mol using either set of data. The presence of the bromines on the 1,4-xylyl tether raised the free energy of activation 0.5 kcal/mol from its unsubstituted analogue catenane **4.3**.

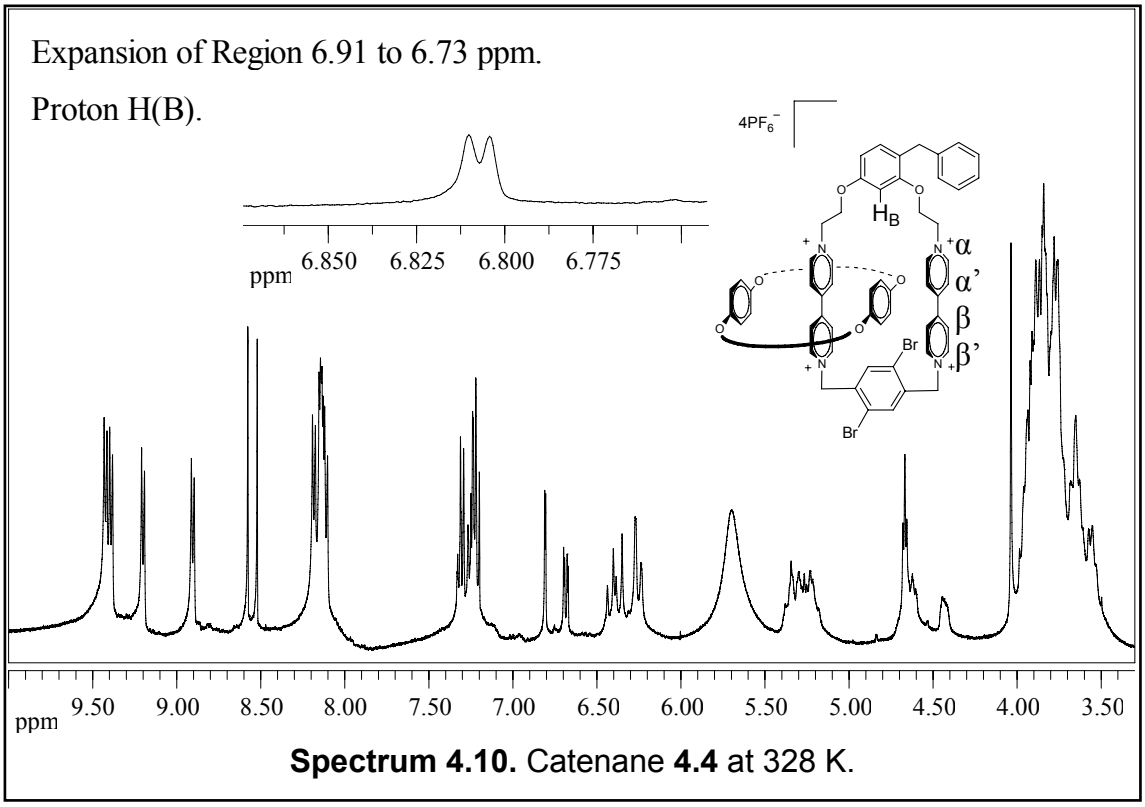

Spectrum 4.10. Catenane **4.4** at 328 K.

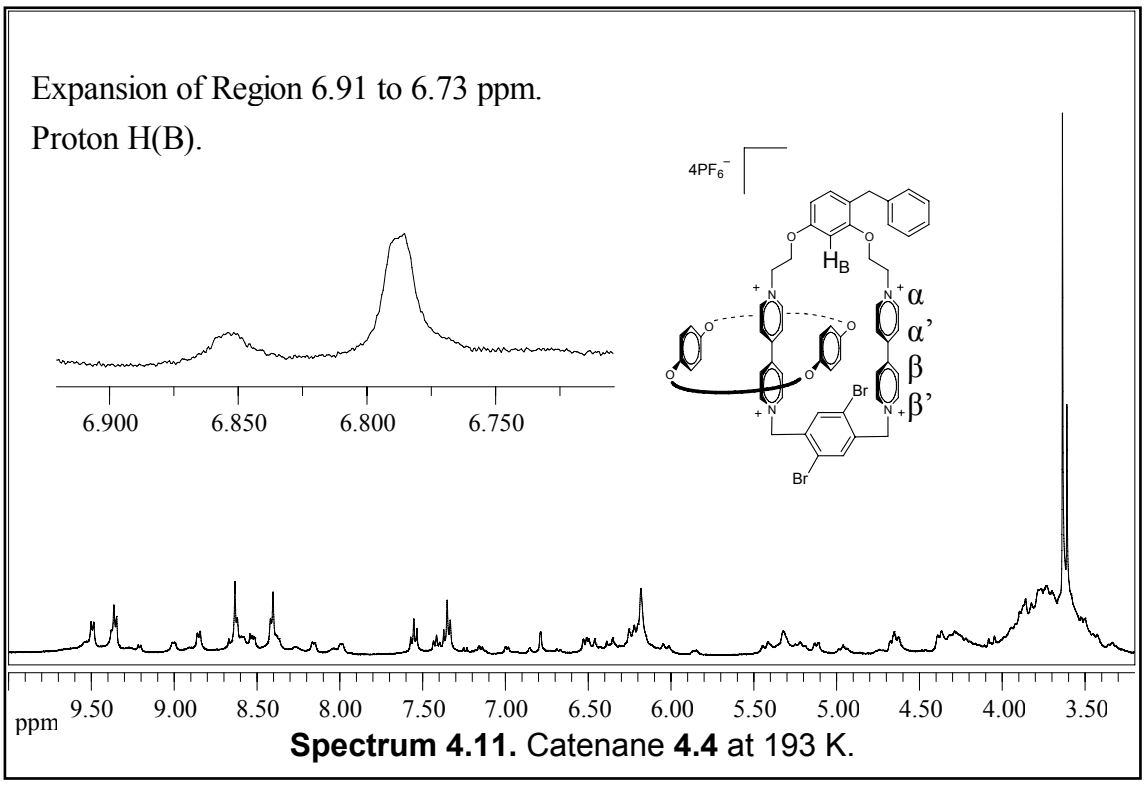

Spectrum 4.11. Catenane **4.4** at 193 K.

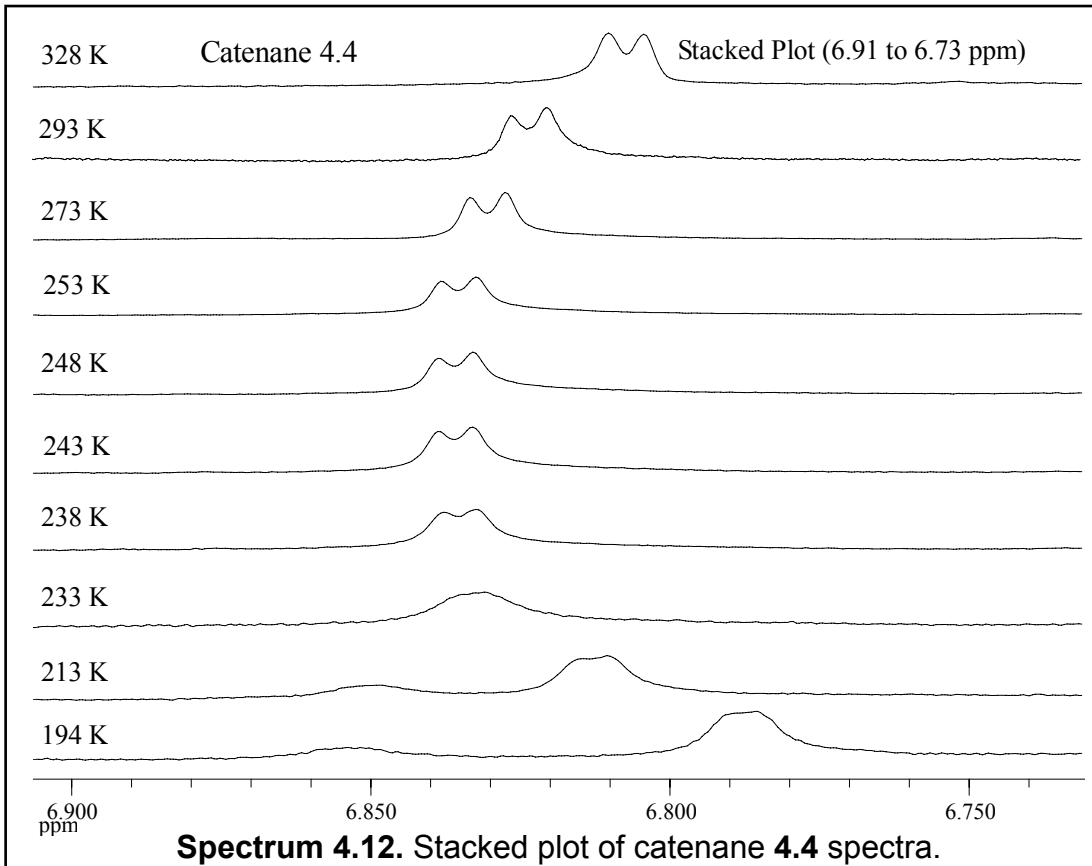

Spectrum 4.12. Stacked plot of catenane **4.4** spectra.

Section 4.4.5 VT ^{1}H NMR Spectra of Catenane 4.5

Coalescence temperatures and **Δυ** were determined for protons H_A and H_B in Catenane **4.5**, having the 4-isopropylbenzyl and 1,3-xylyl moieties. A small amount of signal overlap was observed in the low-temperature spectrum (Spectrum 4.14) that was not observed in the high temperature spectrum (Spectrum 4.13). However, the overlap did not interfere with obtaining the desired data. Coalescence for protons H_A and H_B occurred at 240 and 250 K with **Δυ** values of 18.2 and 42.3 Hz, respectively. Spectrum 4.15 shows a stacked plot of spectra as the temperature was lowered to the slow exchange regime. The free energy of activation was calculated at 12.5 kcal/mol for both data sets with a 2 to 1 ratio of isomers. This $\Delta G^{\ddagger}$ was identical to that of 1,3-xylyl tether bearing catenanes **3.4**, **3.7**, and **4.1**.

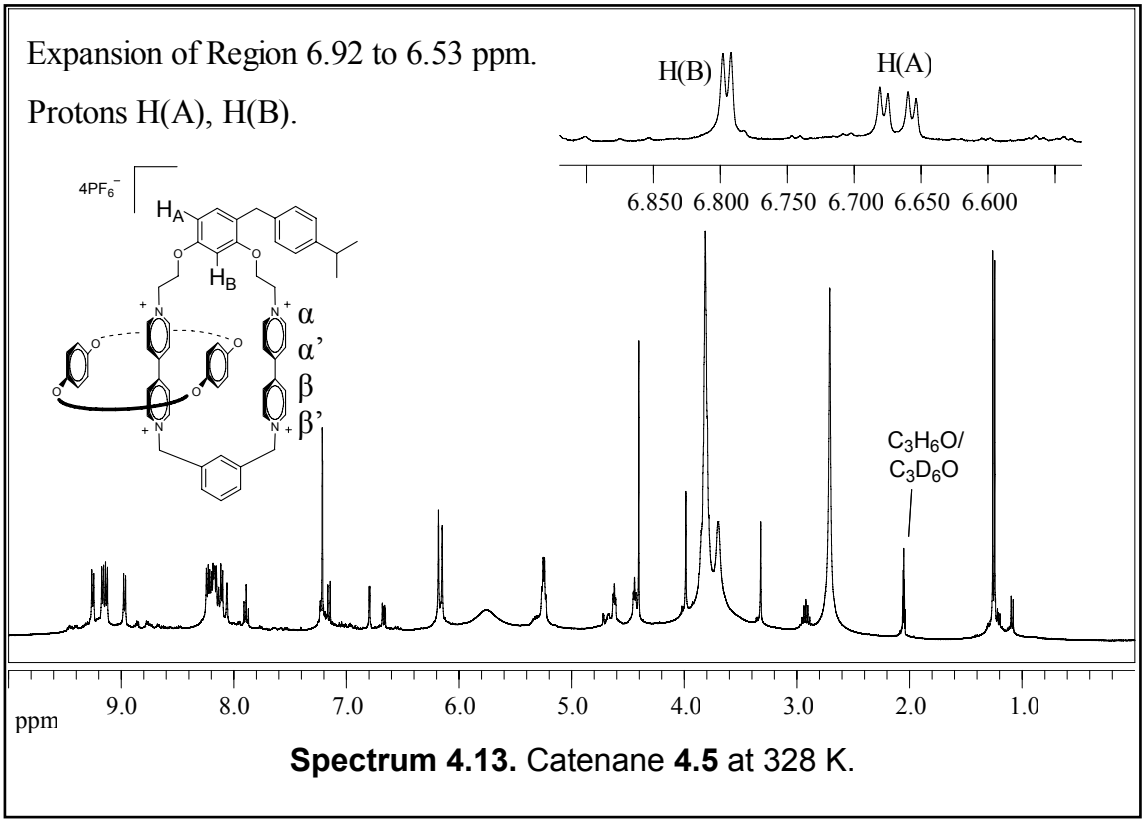

Spectrum 4.13. Catenane **4.5** at 328 K.

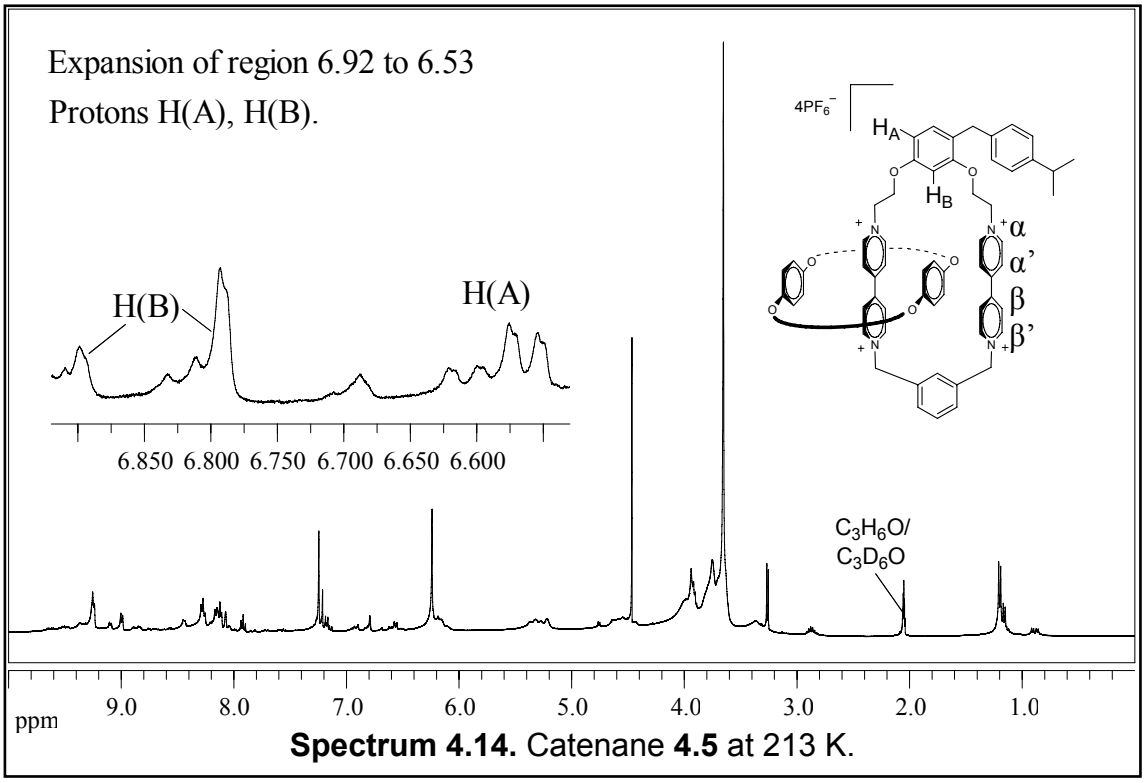

Spectrum 4.14. Catenane **4.5** at 213 K.

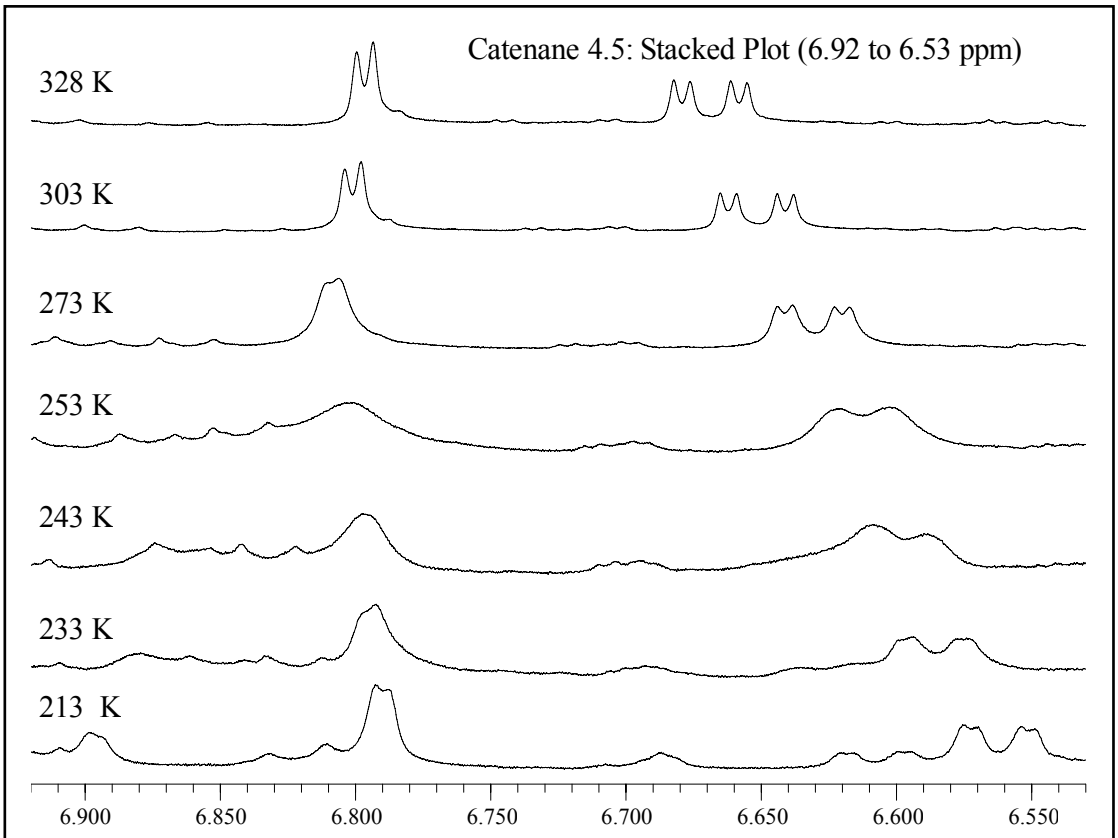

Spectrum 4.15. Stacked lot of catenane **4.5** spectra.

Section 4.4.6: VT ^{1}H NMR Spectra of Catenane 4.6

For catenane **4.6**, bearing the 4-isopropylbenzyl gate and blocking tether, we observed two distinct signals for the protons on the 2- and 6-positions of the resorcinol ring. Coalescence temperatures for both were significantly higher compared to the previous catenanes. The ^{1}H NMR spectrum at room temperature was in the slow exchange region and displayed the associated complex spectrum. We did not observe the fast exchange region due to solvent constraints. However, we were able to obtain the coalescence temperatures for both. These data along with measurements for **Δυ** allowed us to calculate the energy of activation using both sets of signals. In Spectrum 4.7 we observe both sets of signals near coalescence, while Spectrum 4.8 shows the slow exchange region. The stacked plot (Spectrum 4.18) shows the progression of spectra as the temperature was lowered from coalescence to slow exchange. Coalescence gave way to reveal distinct multiplets as slow exchange occurred. In the slow exchange region, for catenane **4.6**, we observed two sets of multiplets emerge from each of the previous multiplets. Proton H_A displayed a **Δυ** of 17.9 Hz and a coalescence temperature of 365 K. For proton H_B, the separation of exchanging resonances was measured at 31.4 Hz with a 375 K temperature of coalescence. The energy of activation was calculated to be 19 kcal/mol for each set of data with an isomer ration of 3 to 1 for each set. This represents a 3.5 kcal/mol increase in the energy requirements over the benzyl gate and is the highest $\Delta G^{\ddagger}$ of any exchanging catenane we synthesized.

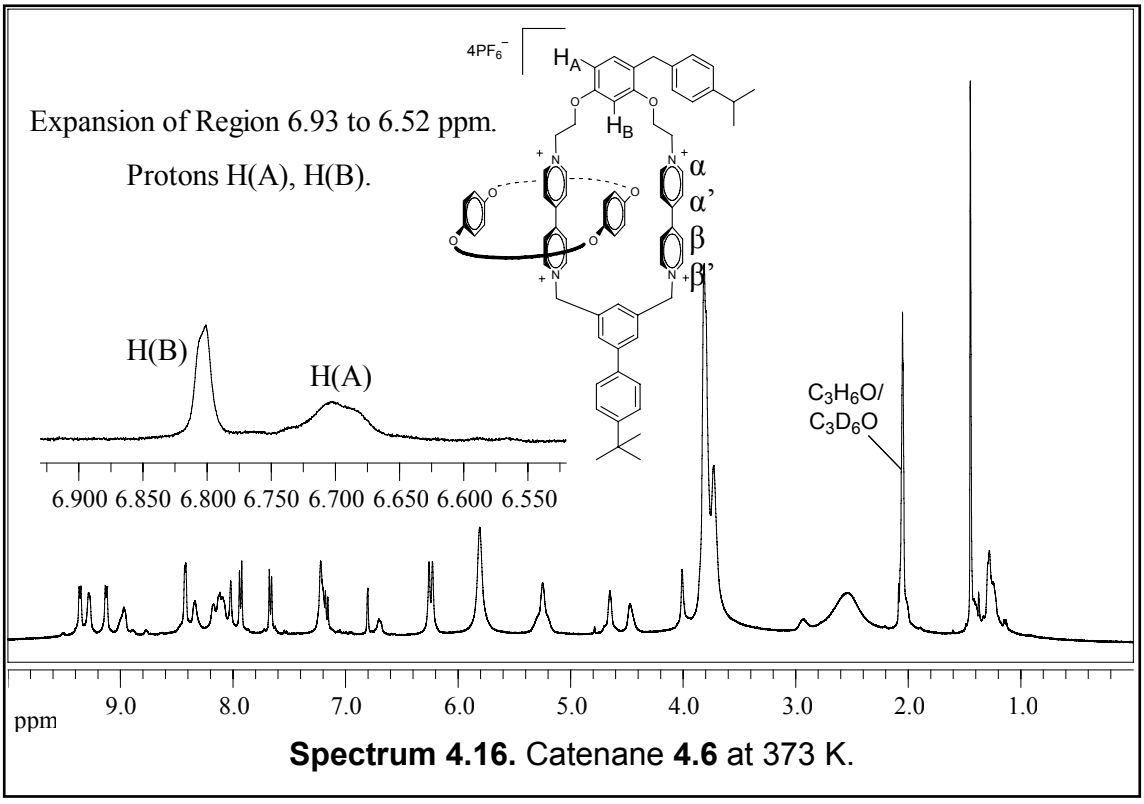

Spectrum 4.16. Catenane **4.6** at 373 K.

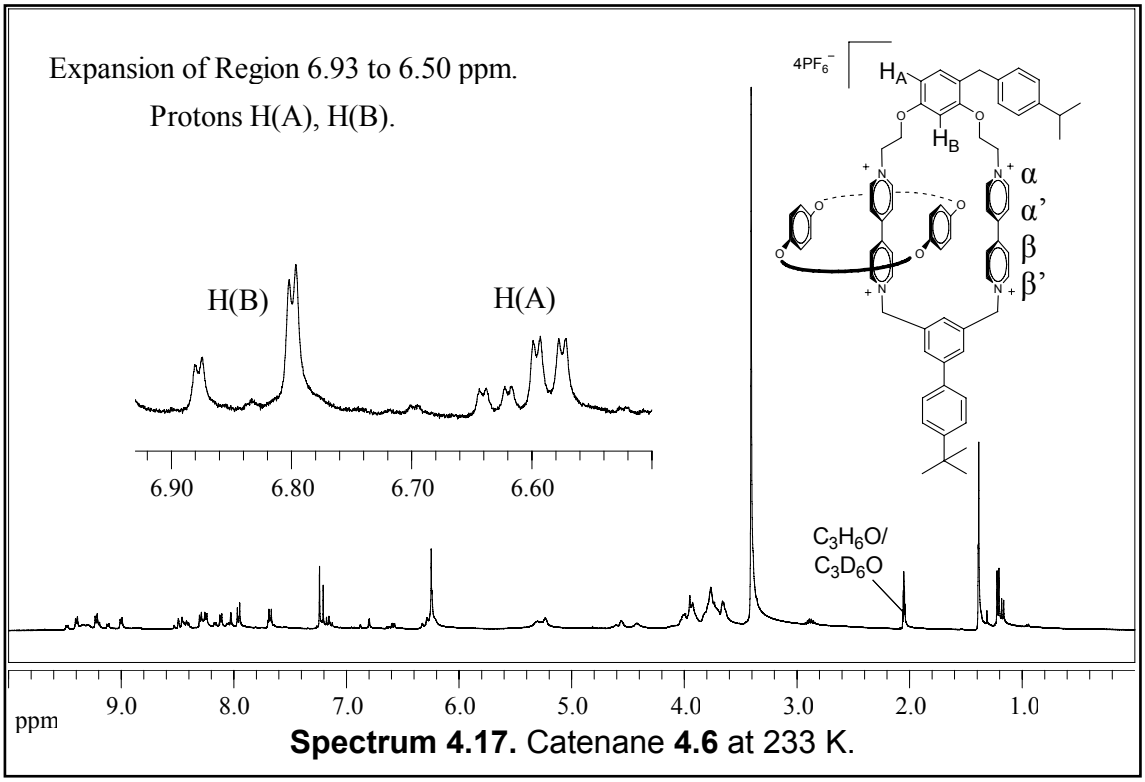

Spectrum 4.17. Catenane **4.6** at 233 K.

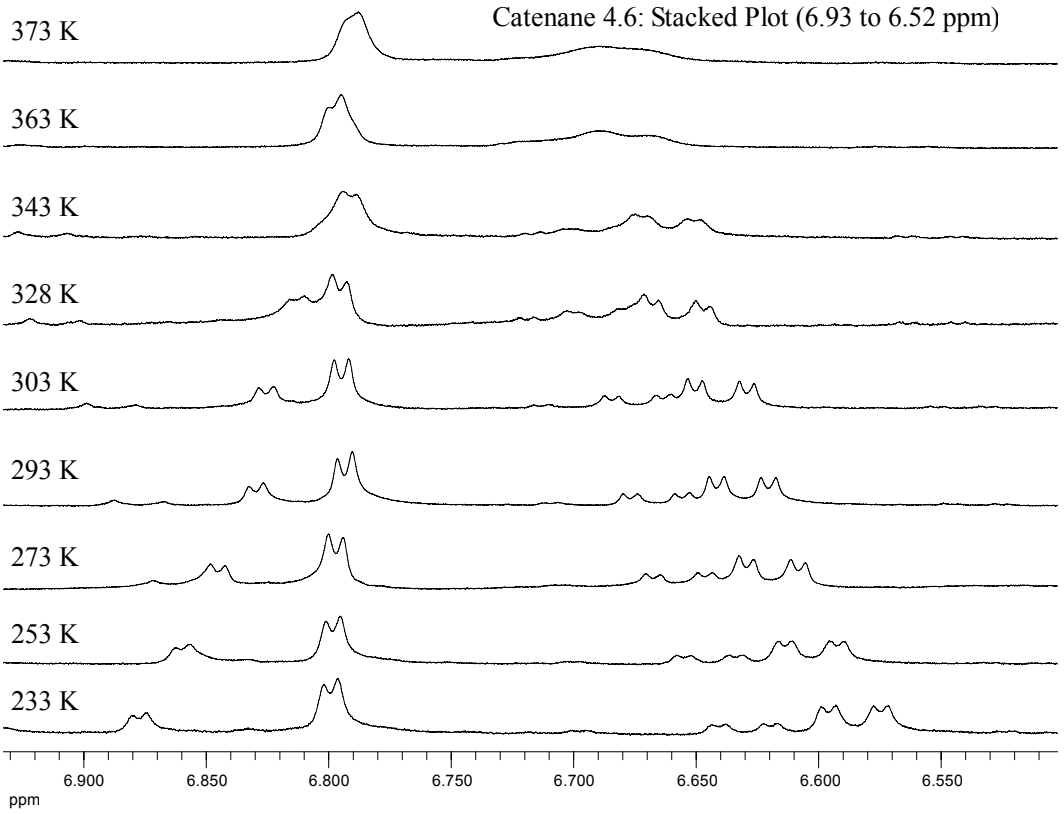

Spectrum 4.18. Stacked plot of catenane **4.6**.

Section 4.4.7 VT ^{1}H NMR Spectra of Catenane 4.7

Catenane **4.7**, having the 4-isopropylbenzyl gate and 1,4-xylyl tether, displayed clean signals for the meta- and ortho-protons H_A and H_B for which coalescence temperatures and $\Delta\upsilon$ could be determined from the following spectra. Spectrum 4.19 shows fast exchange and Spectrum 4.20 shows the slow exchange region. The stacked plot (Spectrum 4.21) shows the progression of spectra as the temperature was lowered from coalescence to slow exchange. Coalescence gave way to reveal distinct multiplets as slow exchange occurred. Coalescence for protons H_A and H_B occurred at 220 and 230 K with $\Delta\upsilon$ values of 17.6 and 56.9 Hz, respectively. The free energy of activation

was calculated at 11 kcal/mol for both data sets and was the same $\Delta G^{\ddagger}$ calculated for catenanes **3.3**, **3.6**, **3.9**, and **4.3** possessing the 1,4-xylyl tether B. Like catenane **4.1**, the an isomer ratio of 1 to 1 was found.

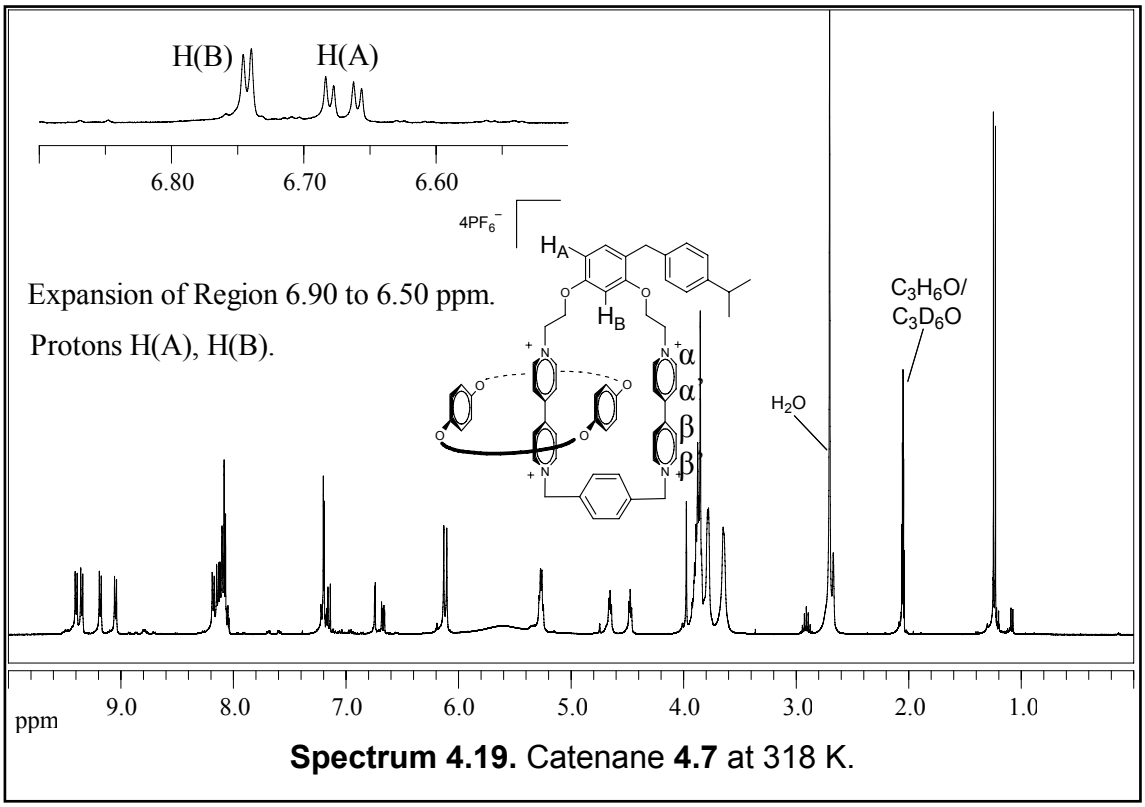

Spectrum 4.19. Catenane **4.7** at 318 K.

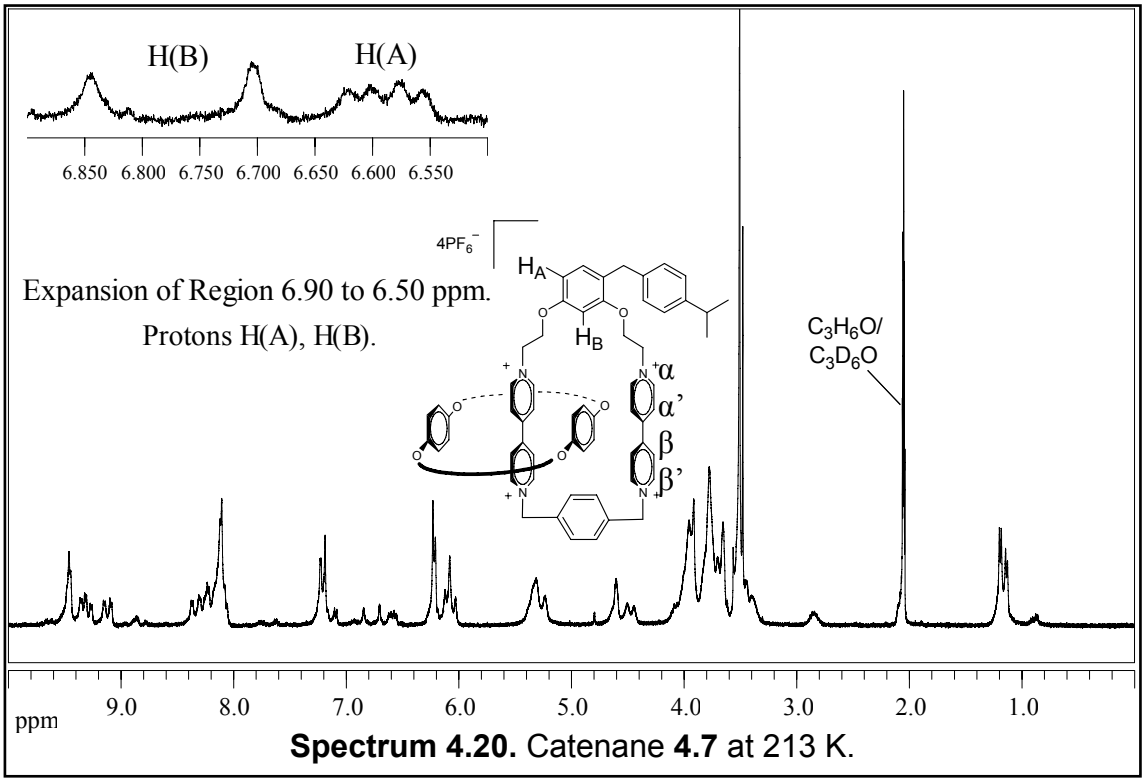

Spectrum 4.20. Catenane **4.7** at 213 K.

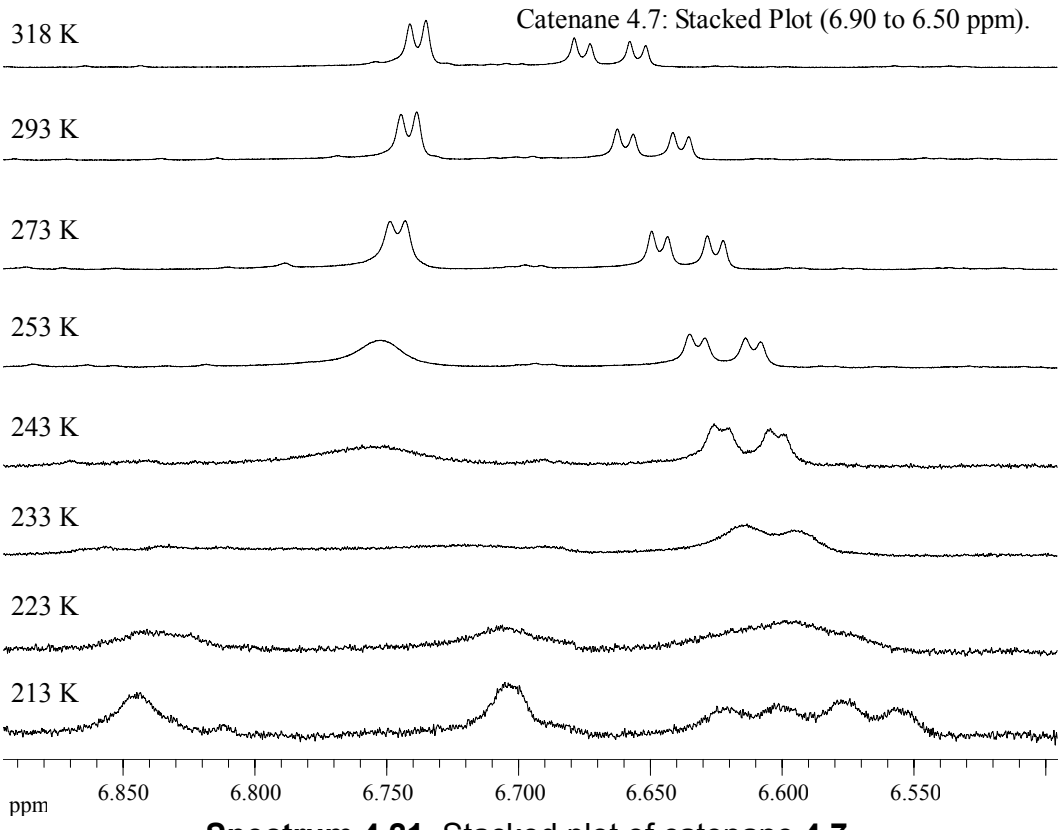

Spectrum 4.21. Stacked plot of catenane **4.7**.

Section 4.4.8 VT ^{1}H NMR Spectra of Catenane 4.8

Proton H_A and meta proton H_B were well defined for catenane **4.8**, containing the 4-phenylbenzyl gate and 1,3-xylyl tether B, in both the fast (Spectrum 4.22) and slow exchange (Spectrum 4.23) regimes and data were gathered for both sets of signals. The stacked plot (Spectrum 4.24) shows the progression of spectra as the temperature was lowered from coalescence to slow exchange. Coalescence gave way to reveal distinct multiplets as slow exchange occurred. Coalescence for protons H_A and H_B occurred at 250 and 260 K with **Δυ** values of 17.9 and 65.4 Hz, respectively. The energy of activation was calculated at 12.5 kcal/mol for both data sets with integration ratios of 6.5 to 1, for catenane **4.8**

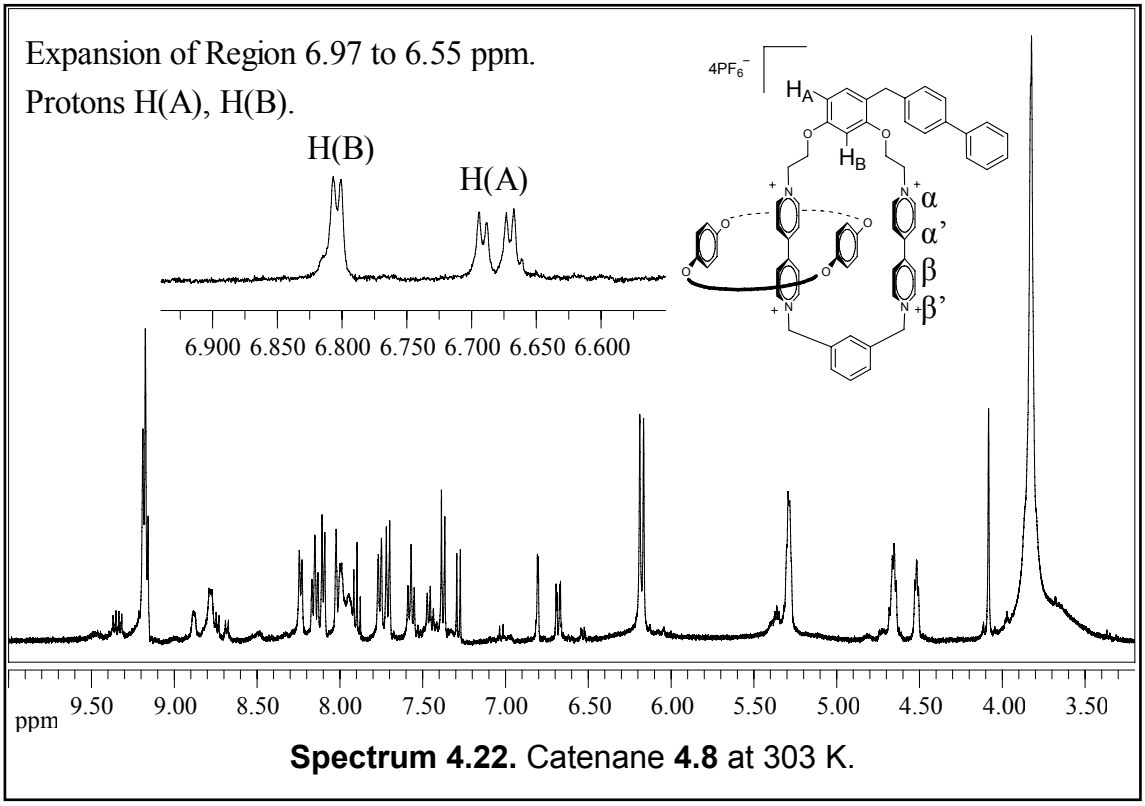

Spectrum 4.22. Catenane **4.8** at 303 K.

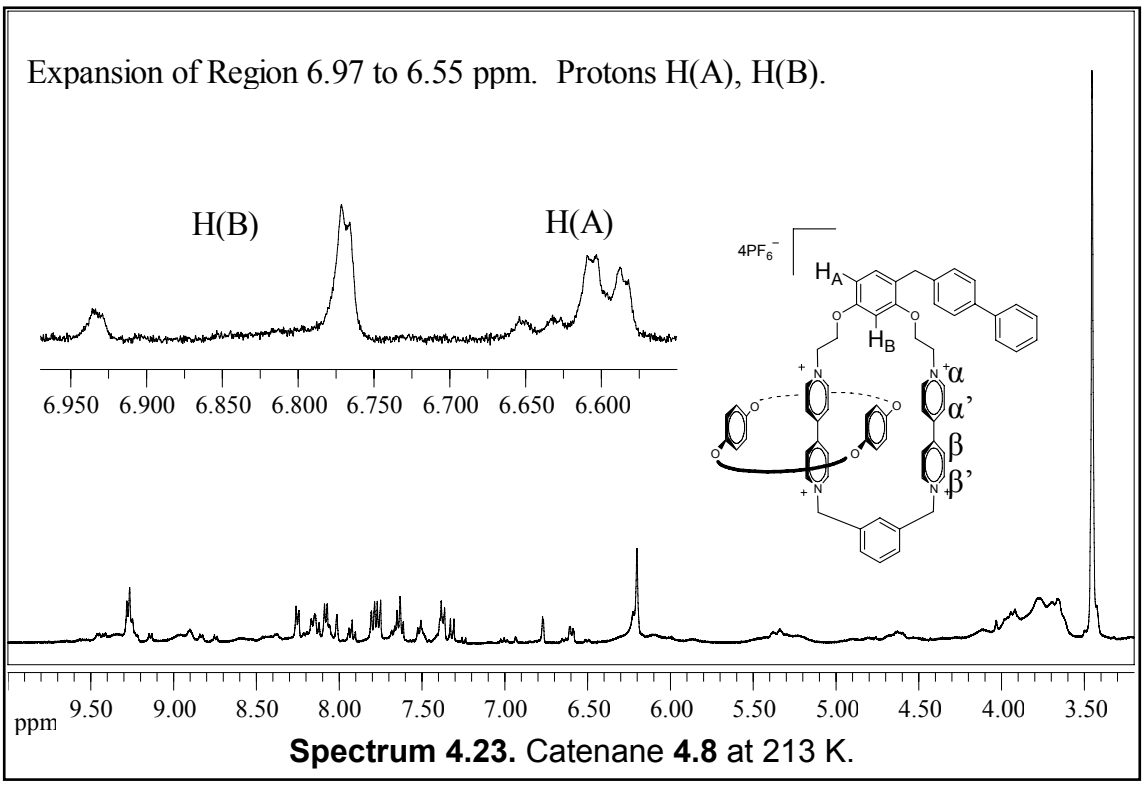

Spectrum 4.23. Catenane **4.8** at 213 K.

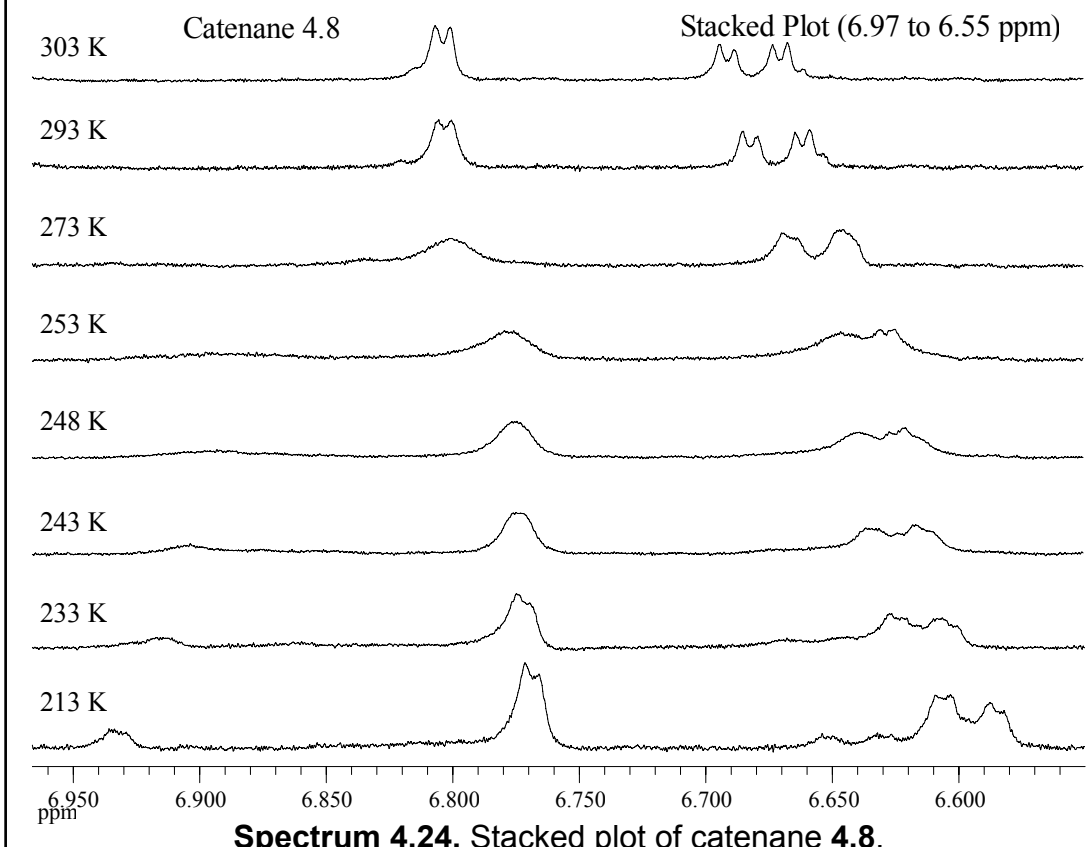

Spectrum 4.24. Stacked plot of catenane **4.8**.

Section 4.4.9 VT ^{1}H NMR Spectra of Catenane 4.9

For catenane **4.9**, having the 4-phenylbenzyl group and blocking tether, we observed distinct signals for ortho-para-proton H_A and meta proton H_B in both fast (Spectrum 4.25) and slow exchange regions (Spectrum 4.26). The stacked plot (Spectrum 4.27) shows the progression of spectra as the temperature was lowered from fast exchange to coalescence and finally to slow exchange. For proton H_A, the separation of exchanging resonances was measured at 19.2 Hz and the temperature of coalescence was 315 K. Separation between the two H_B doublets was measured at 53.4 Hz with a coalescence temperature of 325 K. The energy of activation was calculated to be 16 kcal/mol for each set of data, and the ratio of isomers was determined to be 5.5 to 1 at 233K, for **4.9**.

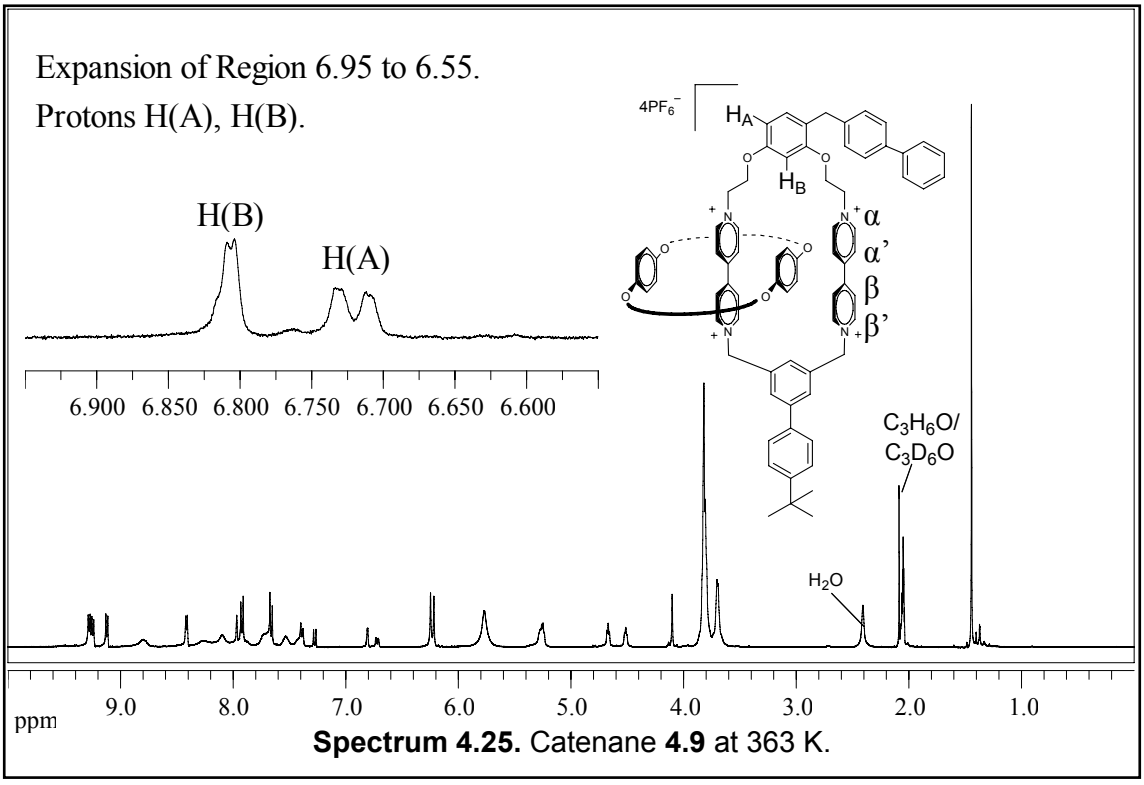

Spectrum 4.25. Catenane **4.9** at 363 K.

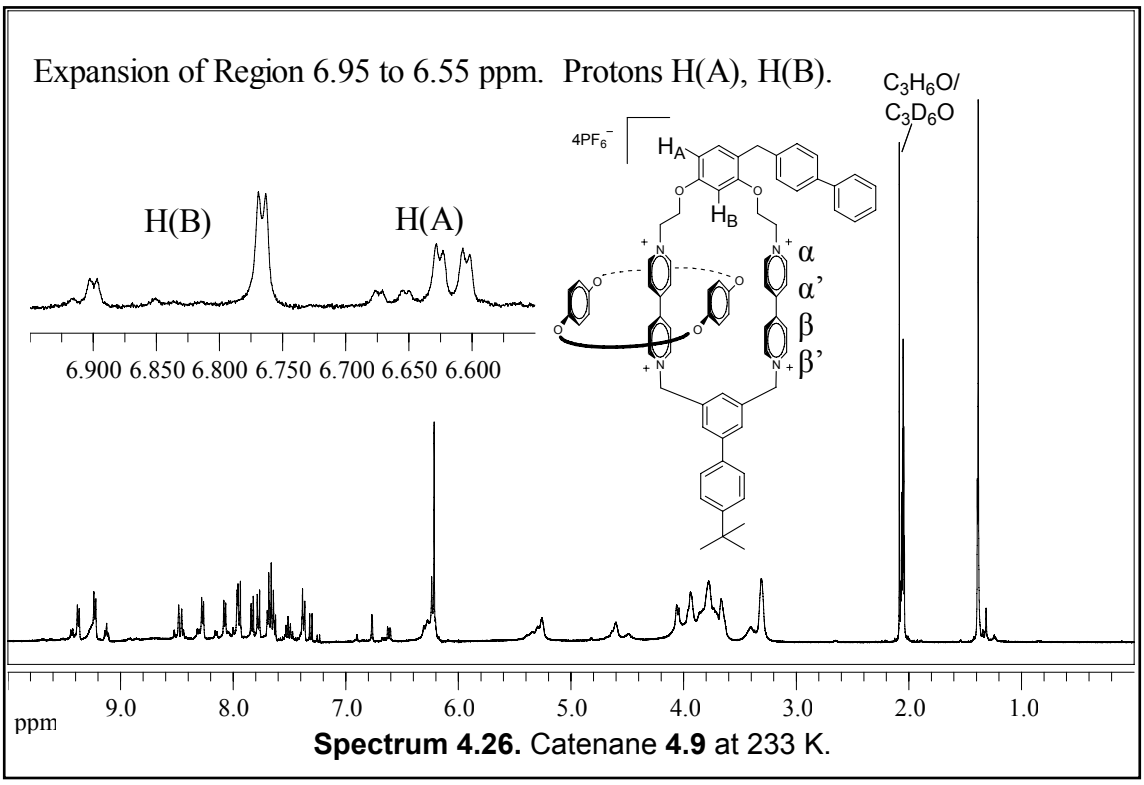

Spectrum 4.26. Catenane **4.9** at 233 K.

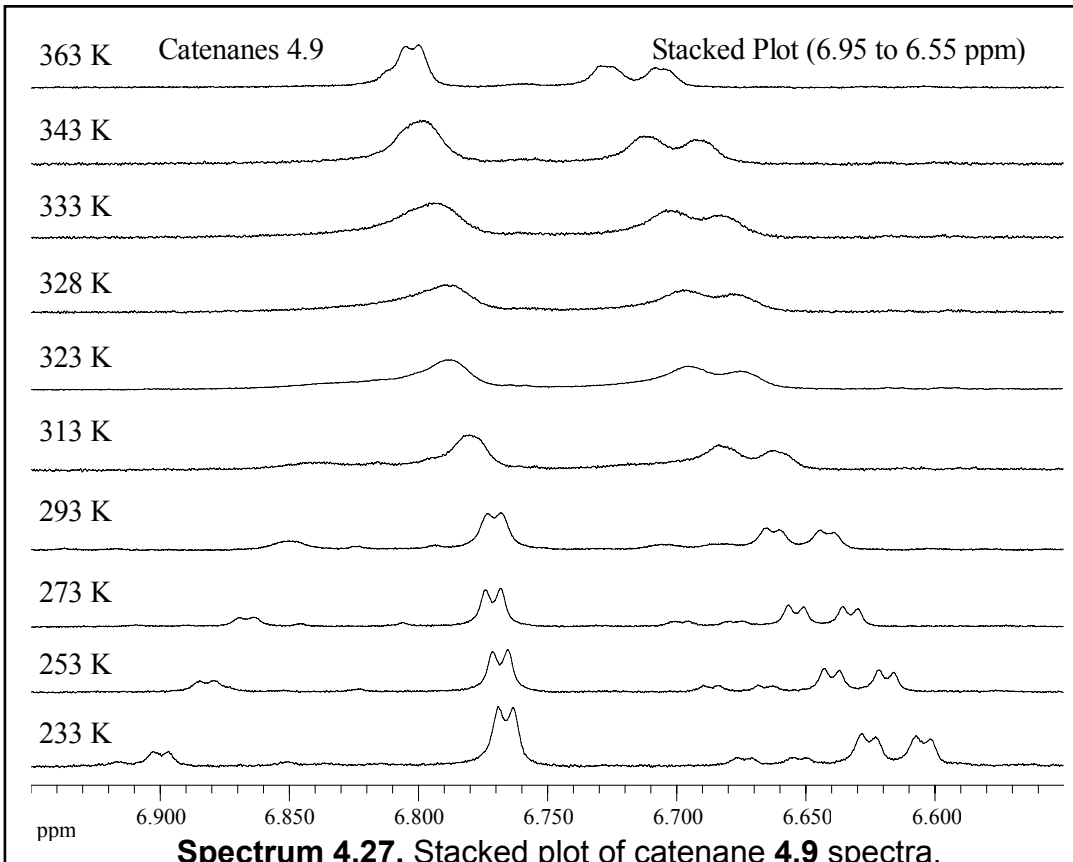

Spectrum 4.27. Stacked plot of catenane **4.9** spectra.

Section 4.4.10 VT ^{1}H NMR Spectra of Catenane 4.10

For catenane **4.10**, having the 4-phenylbenzyl and 1,4-xylyl substitutions, we observed distinct signals for proton H_A and meta proton H_B in both fast (Spectra 4.28) and slow exchange regions (Spectra 4.29). The stacked plot (Spectra 4.30) shows the progression of spectra as the temperature was lowered from fast exchange to coalescence and finally to slow exchange. For catenane H_B, the separation of exchanging resonances was measured at 78.5 Hz and the temperature of coalescence was 235 K. The two proton H_A doublet of doublets' separation was measured at 25.3 Hz with a coalescence temperature of 225 K. The energy of activation was calculated to be 11 kcal/mol for each set of data, and the ratio of isomers was determined to be 2.5 to 1 at 193 K.

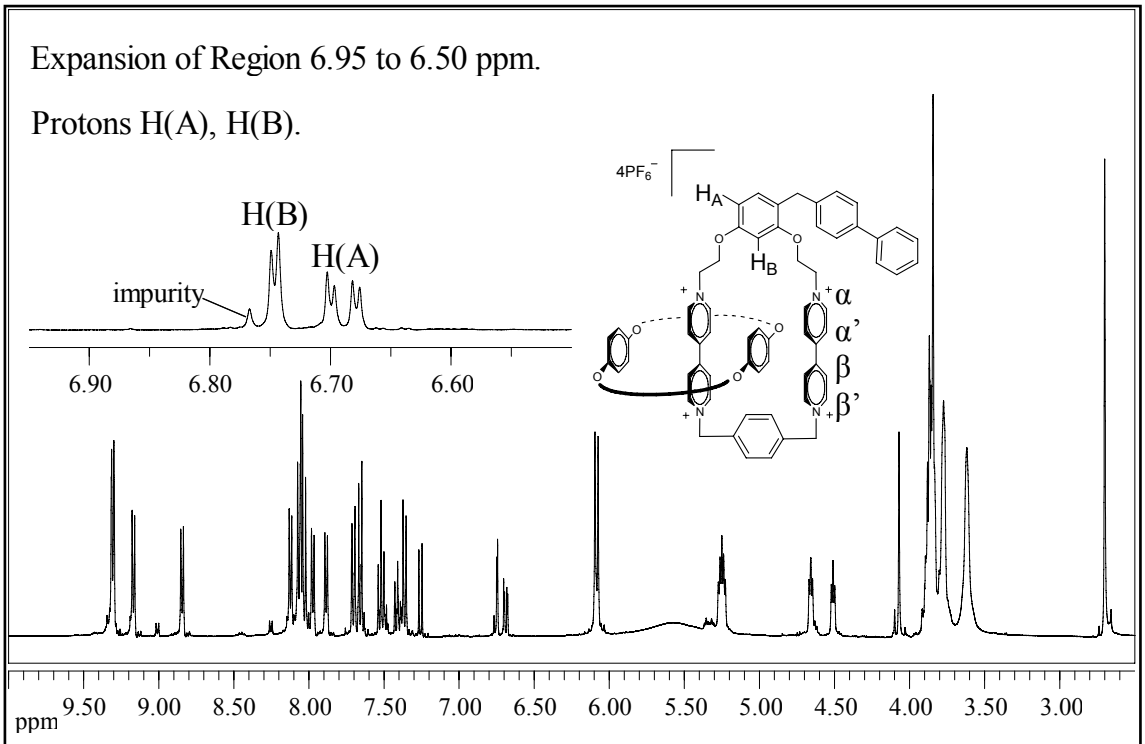

Spectrum 4.28. Catenane **4.10** at 293 K.

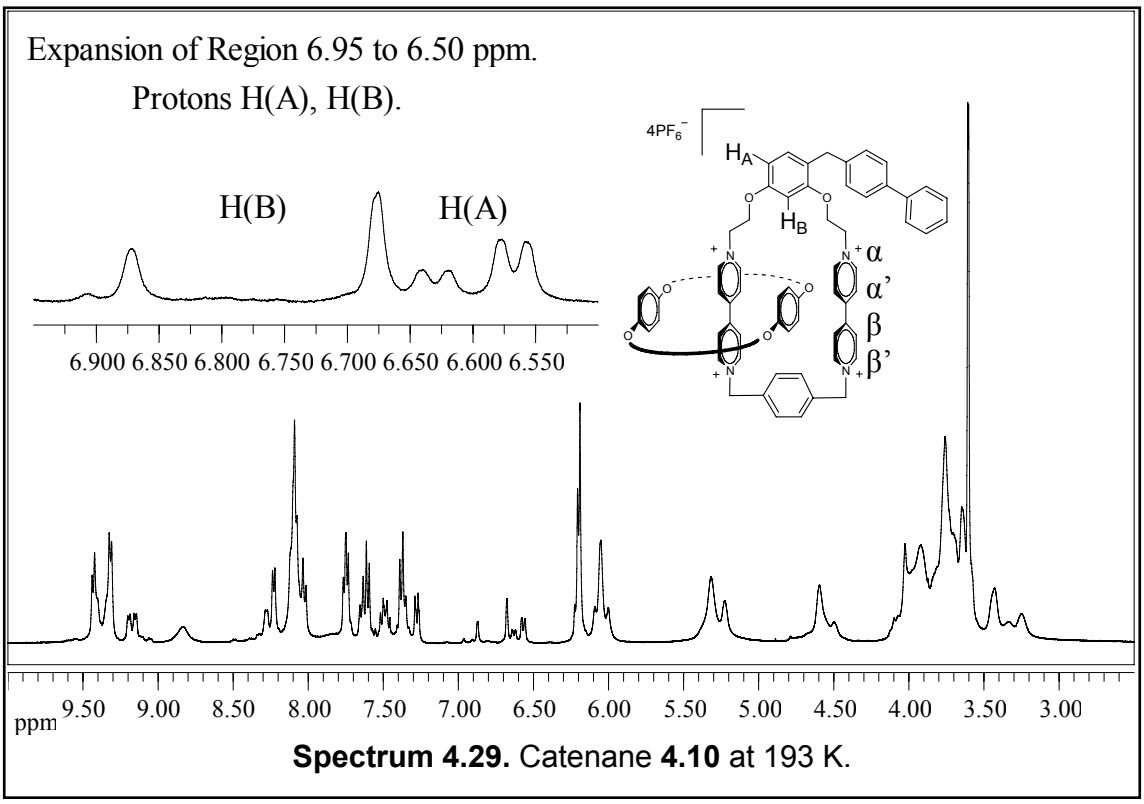

Spectrum 4.29. Catenane **4.10** at 193 K.

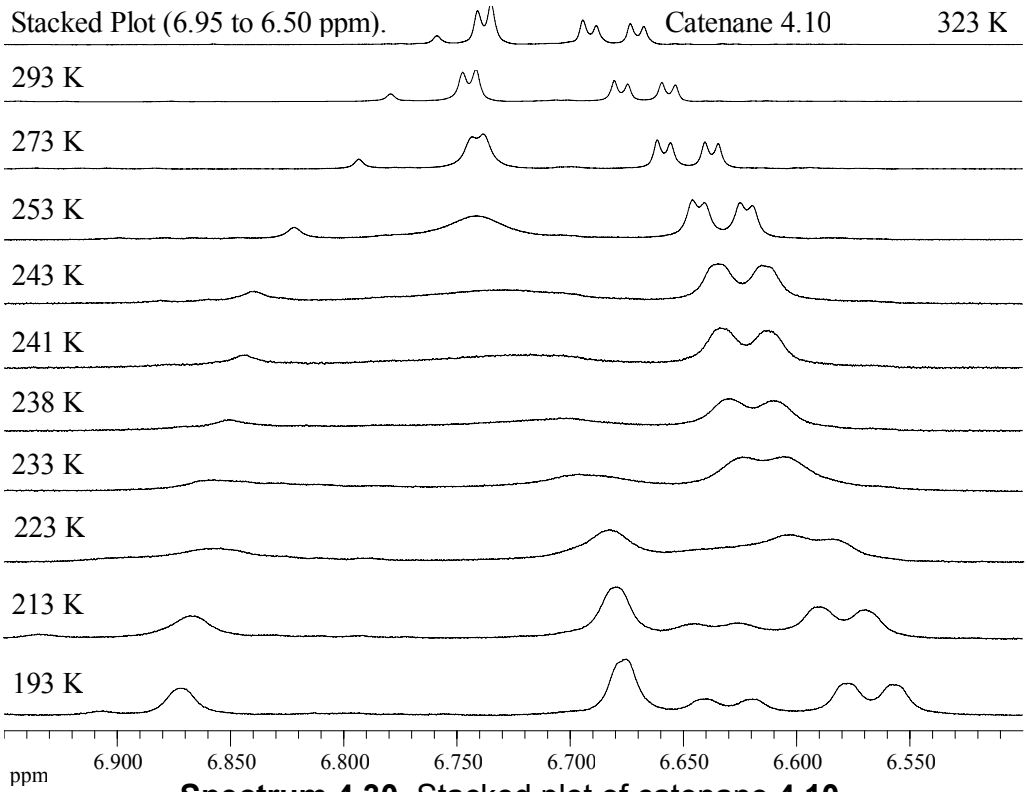

Spectrum 4.30. Stacked plot of catenane **4.10**.

Section 4.5 Summary of Data and Conclusions

Data gathered from variable temperature ^{1}H NMR experiments as well as the calculated energies of activation of all six catenanes are summarized in Table 4.1. As the calculated values for activation energy for each data set were identical only the data for Proton B was included in the table.

catenane	substituents tether A[a] / tether B[b]	coalescence temperature (K)[c]	frequency difference (Hz)	energy of activation (kcal/mol)[d]
4.1	benzyl / 1,3-xylyl	255	46.2	12.5
4.2	benzyl / *t*-butylphenyl	280	56	13.5
4.3	benzyl / 1,4-xylyl	230	76.1	11
4.4	benzyl / dibromoxylyl	230	26.5	11.5
4.5	4-isopropylbenzyl / 1,3-xylyl	255	42.3	12.5
4.6	4-isopropylbenzyl / *t*-butylphenyl	375	31.4	19
4.7	4-isopropylbenzyl / 1,4-xylyl	230	56.9	11
4.8	4-phenylbenzyl / 1,3-xylyl	260	65.4	12.5
4.9	4-phenylbenzyl / *t*-butylphenyl	325	53.4	16
4.10	4-phenylbenzyl / 1,4-xylyl	235	78.5	11

a) Substituent on the 4-position of the resorcinol moeity of tether A
b) Tether B can be either 1,3-xylyl , 1,4-xylyl, 1,4-dibromo-2,5-xylyl, or *t*-butylphenyl where 'dibromoxylyl' describes the 1,4-dibromo-2,4-xylyl tether and t-butylphenyl describes the 5-(4-*t*-butylphenyl)-1,3-xylyl blocking tether
c) Approximated to the nearest 5 K
d) An error of 5 K in determining the coalescence temperature corresponds to an error of ± 0.2 kcal/mol in the activation energy

Table 4.1. Summary of data and calculated free energy of activation.

In Chapter 2 we established a relationship between circumrotation of the BPP34C10 ring around a bis(dipyridinium) ring and the placing large blocking groups on a tether. These blocking groups prevented movement over the blocked pathway. When both tethers were substituted to contain blocking groups no circumrotation was observed. Chapter 3 described how we were able to increase the amount of energy required for, yet still allow circumrotation over tether A based on the size of the group on the resorcinol ring. While studying catenanes **4.1** thru **4.10** we observed the same phenomenon; increasing the steric bulk of the substituent on the resorcinol ring increased the amount of energy required for circumrotation. In addition to increasing the steric bulk of the substituents, benzyl substitution made it rigid thus removing much of its rotation freedom. While the *n*-hexyl substituent in catenane **3.8** possessed steric bulk, it also has many degrees of rotational freedom in its chain. The resorcinol substituents on catenanes **4.1** thru **4.10** have only one point of rotational freedom located on the two bonds of the benzyl methylene of the resorcinol ring. The phenyl gates can move in a circular motion about the methylene-resorcinol sigma bond as the axes of rotation, the path of which was denoted by the grey track in Figures 4.1 thru 4.4. We successfully synthesized and studied ten novel [2]catenanes incorporating various benzyl groups as gating groups.

As we did previously, we examined two specific characteristics displayed by these catenanes: the activation energy for circumrotation and the conformer ratios displayed in the slow exchange regime of the ^{1}H NMR spectra. The activation barriers for catenanes **4.1**, **4.5**, and **4.8**, all possessing the 1,3-xylyl tether, were calculated to be approximately 12.5 kcal/mol (Figure 4.17). We established in Chapter 2 the energy

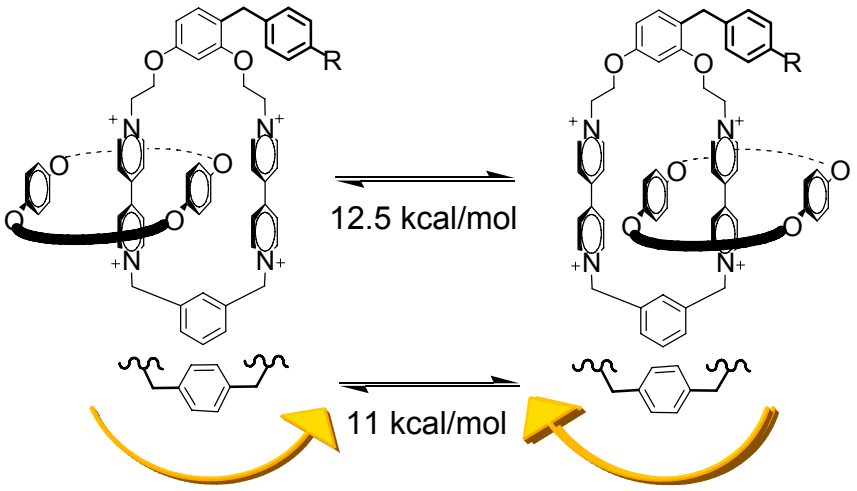

Figure 4.17. Circumrotation observed for gate bearing 1,3- and 1,4-xylyl tethered catenanes.

barrier for circumrotation over this tether required 12.5 kcal/mol, which was the same value calculated for catenanes **3.4** and **3.7** as well. As shown in Figure 4.17, substituting the 1,4-xylyl tether decreased the energy of activation to 11 kcal/mol for catenanes **4.3**, **4.5**, and **4.9**. Again, this is in keeping with previous observations from chloro, ethyl, and *n*-hexyl gated catenanes. Catenane **4.4** with its 1,4-dibromo-xylyl tether experiences a small measurable increase in activation energy to 11.5 kcal/mol as might have been expected from the increase in steric bulk of tether B. When tether B was blocked in catenanes **4.2**, **4.6**, and **4.8**, and circumrotation was limited to tether A, we observed an increase in the energy required for translocation (Figure 4.18). The benzyl gate of catenane **4.2**, with a blocking group on the lower xylyl tether to force BPP34C10 circumrotation over the benzyl gate, required 13.5 kcal/mol, which was 1.5 kcal/mol less than the *n*-hexyl analogue catenane **3.8**. For the isopropylbenzyl-gated catenane **4.6** having the same blocking group, the activation energy was calculated at 19 kcal/mol, an increase of over 5.5 kcal/mol over the benzyl-gated catenane. Lastly, for

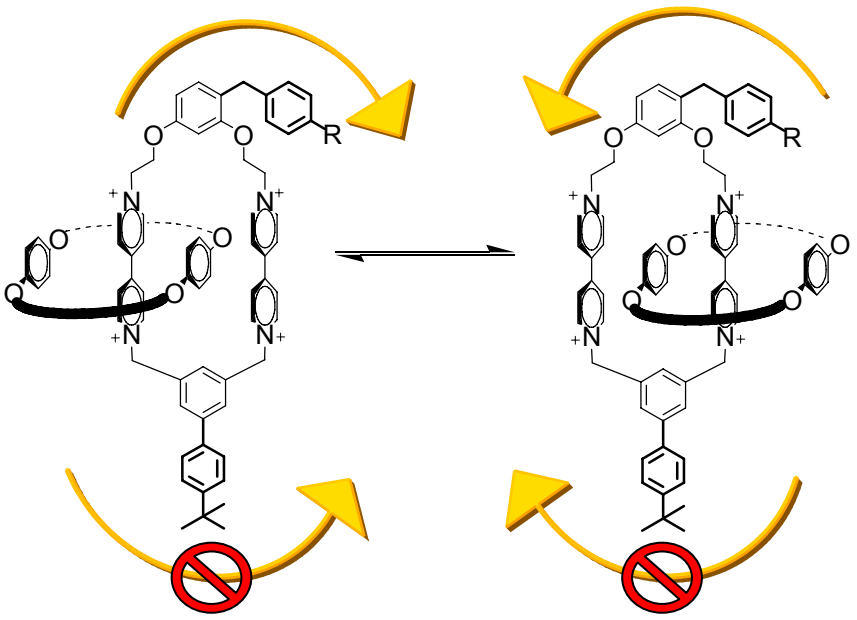

Catenane 4.2 $\Delta G^{\ddagger}$ = 13.5 kcal/mol (R = H)

Catenane 4.6 $\Delta G^{\ddagger}$ = 19 kcal/mol (R = isopropyl)

Catenane 4.9 $\Delta G^{\ddagger}$ = 16 kcal/mol (R = phenyl)

Figure 4.18. Circumrotation observed for catenanes **4.2**, **4.6**, and **4.9**.

the *p*-phenylbenzyl-substituted catenane **4.8** we calculated an activation energy of 16 kcal/mol for translocation over tether A.

Passage along the 1,4-xylyl linker was less energetically demanding than the 1,3-xylyl group as indicated by the 11 kcal/mol barriers in catenanes **4.3**, **4.7**, and **4.10**. This supported our previous conclusion of it being the more open pathway allowing easier circumrotation. In addition, when presented with two pathways, one of which is energetically more demanding, but not completely blocked, as with catenanes possessing the 1,3- and 1,4-xylyl tethers, circumrotation occurred over the lower energy

pathway. The bromine substituent on tether B caused an increase of 0.5 kcal/mol in $\mathbf{\Delta G^{\neq}}$ compared to the unsubstituted form indicating hindered circumrotation.

From these differences, we can conclude that BPP34C10 requires more energy to rotate over benzyl substituents as they become larger and more sterically imposing. In regards to energy requirements for circumrotation, we have established that traversing the larger, phenyl substituted 3-bis(ethyloxy)benzene tethers required more energy than the 1,3-xylyl tether, both of which were significantly more energetically demanding than passage over the 1,4-xylyl tethers. Passage over the benzyl gate requires less energy than the *n*-hexyl substituent discussed in chapter three, while the isopropyl benzyl gate requires the most energy of all the asymmetric catenanes studied with the *p*-phenylbenzyl gate being the second most energy intensive. This decrease in the energy of circumrotation for the *p*-phenylbenzyl gate compared to the isopropylbenzyl gate indicates another unanticipated process may be occurring in our system. The ethoxy tethers introduced to isolate the gate may allow the gate to fold down, a possibility which will be discussed later.

In Chapter 2 we presented our bistable symmetric catenanes which exist in equilibrium. Integration of the decoalesced peaks in the ^{1}H NMR indicated equal concentration of each isomer. This ratio indicated the isoenergetic nature of the conformers. However, in Chapter 3 we observed that introduction of asymmetry affected the thermodynamic stability of one binding site causing a shift from equal concentration to as much as a three-fold excess concentration of one isomer. Indeed, the chloro-substituted catenane with no rotational freedom for the substituent caused a shift of two to one in the isomer concentration in even the 1,4-xylyl tether where

translocation along the low energy, unbiased pathway was allowed. The other two 1,4-xylyl tethered catenanes displayed ratios of 1.5 to 1 again indicating ground state energy differences between the two isomers. *p*-Phenylbenzyl substitution of the catenane displayed the same ground state difference. In addition, we observed large differences in isomer ratios for several of phenyl-substituted catenanes and an interesting phenomenon not observed in previous asymmetric catenanes. As we observed for the catenanes presented in Chapter 3, we found the isomer ratios did not vary to a significant degree below the coalescence temperature. Table 4.2 summarizes the relative isomeric ratios for each catenane.

Substituents		Tether A		
		benzyl	isopropylbenzyl	phenylbenzyl
Tether B	1,4 xylyl	1:1	1:1	2.5:1
	1,4-dibromo-2,5-xylyl	3:1	-	-
	1,3-xylyl	3.5:1	2:1	6.5:1
	t-butylbenzyl-1,3-xylyl	4:1	3:1	5.5.1

Ratios rounded to the nearest 0.5.

Table 4.2. Summary of isomer ratios.

Two notable exceptions, the benzyl- and *p*-isopropylbenzyl-substituted catenanes, become apparent when analyzing the data. Contrary to the trend established by the other asymmetric catenanes the 1,4-xylyl substitution for these two yielded 1:1 ratios of conformers. Like the symmetric catenanes, this ratio indicates the two energy minima are isoenergetic. The catenanes bearing these two gates seemed to display one of the systems anticipated characteristics and provide evidence supporting thermal ratcheting.

For Catenane **4.2**, having the blocking group on the bottom tether, migration of the crown ether is only possible over tether A, and we observed a 4:1 ratio of isomers. Our control possessing the 1,3-xylyl tether present in **4.1**, sees a decrease in activation energy by approximately 1 kcal/mol with an isomer ratio of 3.5 to 1. There are two possible conclusions that can be made at this point. There is the possibility that we are in fact observing gating. It could be that, for the benzyl gated catenanes, one ground state is thermodynamically more stable producing a 3.5 to 1 ratio of isomers, and the increase to 4 shows gating is occurring in catenane **4.1**. However, this small increase is unsatisfying and well within the realm of experimental error. Another conclusion is that the unsubstituted 1,3-xylyl tether, which was originally designed to provide a low energy, non-ratcheting pathway, was not functioning as such (Figure 4.19). Its energy of activation is not substantially lower than that of **4.2** lending credibility to the view that perhaps the tether itself hinders movement

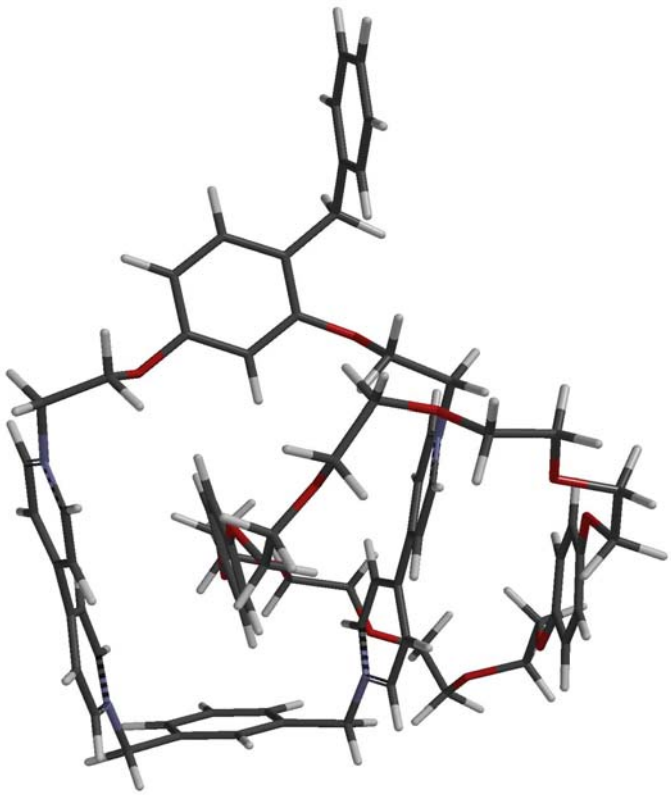

Figure 4.19. AM1 minimized structure of catenane **4.1**.

over the 1,3-xylyl group. Molecular modeling programs supported this conclusion. Figure 4.19 presents the AM1 minimized structure[56] of catenane **4.1** and shows how the 1,3-xylyl tether could behave more as a blocking group than a free path of circumrotation.

Regardless of the possible explanations, we require another control to which we can compare our gating catenane. Catenane **4.3** with its energetically less demanding 1,4-xylyl tether was found to be a suitable control. Using molecular modeling once again we observed how this bottom tether could provide the low energy unhindered route we desired. Unlike the 1,3-xylyl tether, this tether offers a wider, less 'V-shaped' and restricted path for circumrotation as shown by the AM1 calculated conformation shown in Figure 4.20. We observed the energy for circumrotation decrease an additional 1.5 kcal/mol compared to **4.1**, or a 2.5 kcal/mol lower than the catenane with blocked tether B in Catenane **4.2**. Here we observed the 1 to 1 ratio of conformers indicating isoenergetic ground states. However, we cannot directly

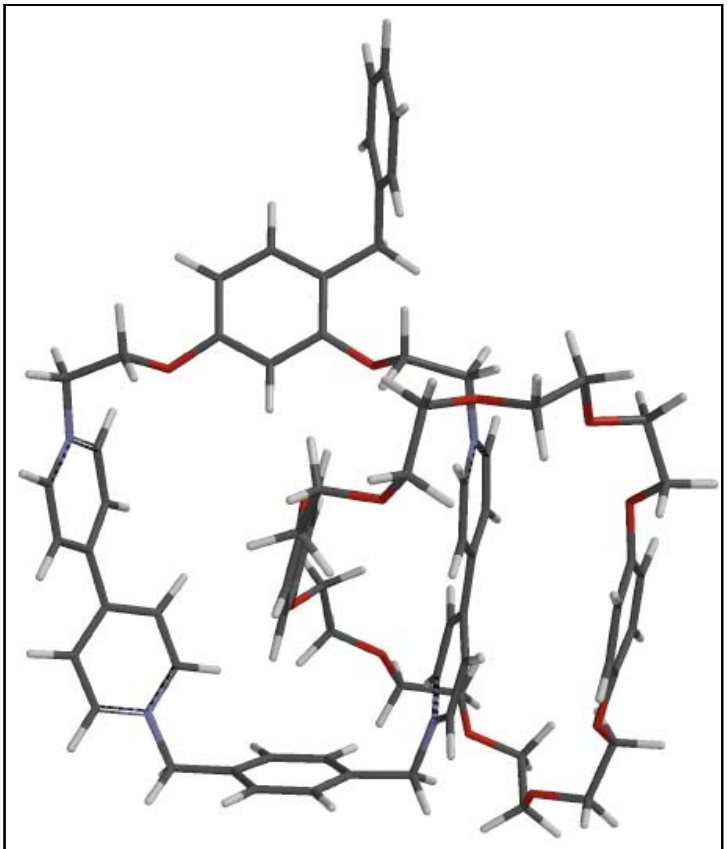

Figure 4.20. AM1 minimized structure of catenane **4.3**.

compare the ground state energies of the 1,4- and 1,3-xylyl tethers, because it is possible that changing the tether also changed the conformational energy differences. Thus, we require a control of our control in the form of catenane **4.4**.

We have established that increasing the steric bulk on the tethers increases the amount of energy required for circumrotation. By increasing the steric bulk of the lower tether B we sought to drive circumrotation over the gate. Catenane **4.4**, possessing the same length 1,4-xylyl spacer as **4.3**, but also having bromo-substituents at the 2,5-positions, was prepared and displayed a 2:1 ratio of isomers. This substitution also increased the free energy of activation to 11.5 kcal/mol. The increase in activation energy along with the 2 to 1 ratio of isomers indicates interconversion through both the ratcheting and non-ratcheting pathways. Addition of the bromines did not completely block pathway B but rather increased its free energy of activation to the point that circumrotation occurred over gated path A. This result supports the conclusion that ratcheting can occur with this longer bottom tether as well as the narrower 1,3-xylyl tether. It is important to note that catenane **4.4** is chiral and likely exists as enantiomers; however, chirality would not affect the thermodynamic stability of one isomer over another. We observed the same phenomenon in catenanes **4.5** thru **4.7** and while an isopropylbenzyl gated catenane analogue to **4.4** was not synthesized, it would be reasonable to assume it would follow the trend.

While hinting at the desired device the results remain unsatisfying and unconvincing in that they provide no definitive evidence for a thermally driven molecular ratchet. It could be argued that the bromo-substituted 1,4-xylyl tether causes a subtle conformational shift in the catenane thereby causing one isomer to become

more or less stable, as we observed with addition of chlorine to tether A on catenane **3.1**. Worse than being unsatisfying, catenanes **4.8**, **4.9**, and **4.10** give apparently contradictory evidence. Catenane **4.10** follows the trend established in the Chapter 3 with a substantial thermodynamic ground state preference for one isomer. For catenane **4.8**, with its 1,3-xylyl tether, we observe a strong preference for one isomer with a 6.5 to 1 ratio. If previous indicators were to be trusted, we would expect a greater disparity in the isomer ratios for its blocked tether analogue, catenane **4.9**. However, it shows a lower isomer ratio of 5.5 to 1. Clearly, the *p*-phenylbenzyl gate does not follow the trend established by the two other gating catenanes. The most important question remains unanswered. We do not yet have structural evidence as to which BPP34C10 orientation constitutes the major isomer. While attempts at synthesizing labeled catenanes were made, they failed and without knowing the configuration of the major isomer, we can only guess at how our gate is behaving in the system. These contradictory results also point to another problem which has been mentioned but not yet discussed; there is the possibility that the rotational freedom of the flexible ethoxy spacers allows formation of unanticipated low energy pathways. This possibility will be discussed in the next chapter.

If we assume the isomer ratios of these catenanes are thermally-directed, rather than kinetically directed, the ratios provide the relative concentrations of isomers. Using these integration ratios as a measure of the relative concentration[53] we calculated the values of ΔG° for each catenane as shown in Table 4.3.[53] Here we see the relatively small differences in free energy between isomers of these bistable catenanes.

Substituents		Tether A		
		benzyl	isopropylbenzyl	phenylbenzyl
Tether B	1,4-xylyl	0	0	0.4
	1,4-dibromo-2,5-xylyl	0.4	-	-
	1,3-xylyl	0.5	0.4	0.8
	t-butyl-1.3-xylyl	0.6	0.5	0.8

Values include an associated error of ± 10 %

Table 4.3. Calculated values of **ΔG°** (kcal/mol)

Catenanes having the benzyl and isopropylbenzyl gates with the 1,4-xylyl tether did not show a thermodynamic ground state preference for either isomer. This finding is contrary to the symmetry dependence observed for 1,4-xylyl tethered catenanes in Chapters Two and Three. For the 1,4-xylyl tethered and *p*-phenylbenzyl gated catenane **4.10**, we again observe a thermodynamic ground state preference for one isomer. Given the lack of symmetry dependence displayed by the benzyl and isopropyl gated catenanes **4.3** and **4.7**, we conclude that the long *p*-phenylbenzyl gate must be interacting with the BPP34C10 and proximal binding site causing a perturbation in their binding ability, thus destabilizing the isomer.

We were able to establish the following characteristics for these 'gating' catenanes. Energy barriers for displacement along tether A were: 13.5 kcal/mol for 1,3-bis(ethyloxy)-4-benzylbenzene, 19 kcal/mol for 1,3-bis(ethyloxy)-4-(4-isopropylbenzyl)benzene, and 16 kcal/mol over the 1,3-bis(ethyloxy)-4-(4-isopropylbenzyl)benzene pathway. While increasing the bulk of the substituent caused an increase in the energy required for circumrotation, increasing the length of the substituent did not. The thermodynamic stability of benzyl and isopropylbenzyl

substituted asymmetric catenanes with 1,4-xylyl tethers does not appear to be symmetry dependent. The longer *p*-phenylbenzyl gate appears to allow direct interaction between the gate and the binding site shifting the equilibrium away from 1 to 1. Using asymmetric catenanes with rigid phenyl groups attached, we demonstrated the ability to control both the path of and energy required for circumrotation.

Chapter 5

Conclusions and Future Directions

To demonstrate a thermally driven molecular ratchet we desired to create a system incorporating several basic characteristics; it must possess a method of modulating an energy barrier between at least two isoenergetic, or nearly isoenergetic, states without requiring the directed input of additional energy. As discussed in the introduction, the ability to modulate the energy barrier was an important concept found to be lacking in previous attempts at making such a device. We noted from reading the literature that certain catenanes presented themselves as ideal molecular candidates for these experiments. Self-assembling [2]catenanes possessing an electron rich crown ether, BPP-34-crown-10 (BPP34C10), and electron poor dipyridiniums, coordinate via π-stacking and hydrogen bonding interactions. These coordination sites provide two relatively stable ground state conformers of equal energy. Furthermore, it is possible to measure the free energy of activation for conformational interconversion between these two symmetric and isoenergetic states as well as determine their relative concentrations via variable temperature ^{1}H NMR spectroscopy, a well-established method of quantitative and qualitative analysis. Incorporating the fundamental tenets of our '*Gedankenmaschine*' into a molecule, we produced a series of [2]catenanes possessing the desired traits (Figure 5.1).

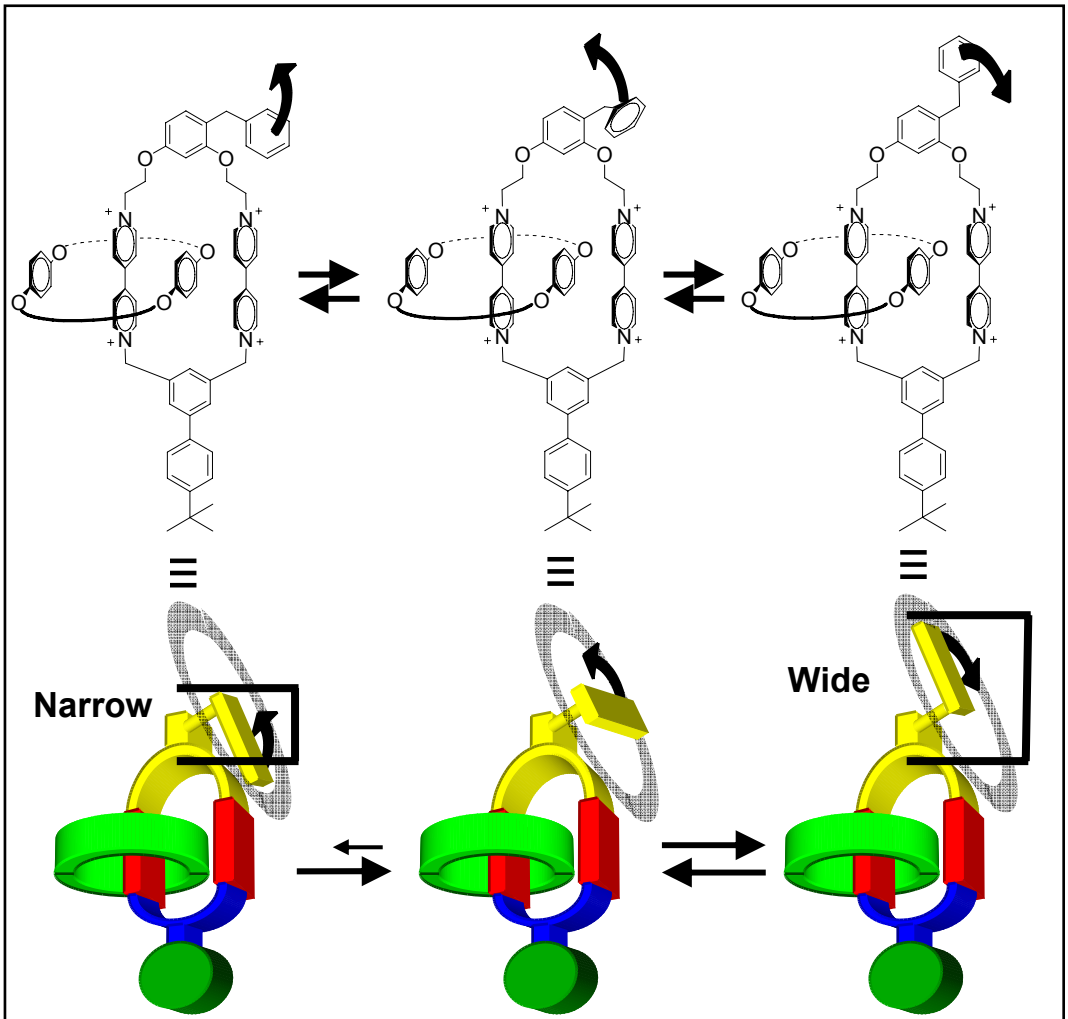

Figure 5.1 From '*Gedankenmaschine*' to molecule.

In this ratchet system there are two possible pathways for circumrotation, one of which is biased or gated (Pathway A), and another that is unbiased (Pathway B), either allowing or disallowing free movement of BPP34C10 over the bottom pathway B. Unrestricted movement along the bottom, unblocked and lower energy pathway would provide information concerning the energetic differences, if any, between the two ground states. This would provide a control group from which to measure the ratcheting ability of a particular catenane. Blocking this low energy pathway with a large bulky group would restrict movement of the crown-ether ring to the biased, gated

top pathway. Any gating effect would be expressed as a change to a non-equilibrium steady-state ratio of conformers that is different from the equilibrium control. Realization of the second characteristic would have allowed unambiguous interpretation of the isomer ratios provided in the ^{1}H NMR data. However, even if the ratios were not isoenergetic, by synthesizing blocked and unblocked versions of the catenanes we could compare the ratios of conformers. Again, any change from the unblocked control could be attributed to a gating effect.

For systems using the benzyl and isopropyl benzyl gates we observed what appeared to be ratcheting. When the narrow 1,4-xylyl tether was present as in **5.2a-c**, passage over this non-biased linker is favored as indicated by the low energy of activation. We observed a 1:1 ratio of left (**5.2c**) and right isomers (**5.2a**) indicating that these two conformations are isoenergetic. Upon blocking the lower tether with a sterically imposing group as in **5.2d-k**, the crown ether ring cannot migrate over tether B forcing it over the higher energy, gated pathway A. The resulting 3.5 or 2 to 1 ratio between the isoenergetic ground state conformers indicates that the ratcheting group is indeed favoring circumrotation two to three times faster in one direction than in the reverse direction.

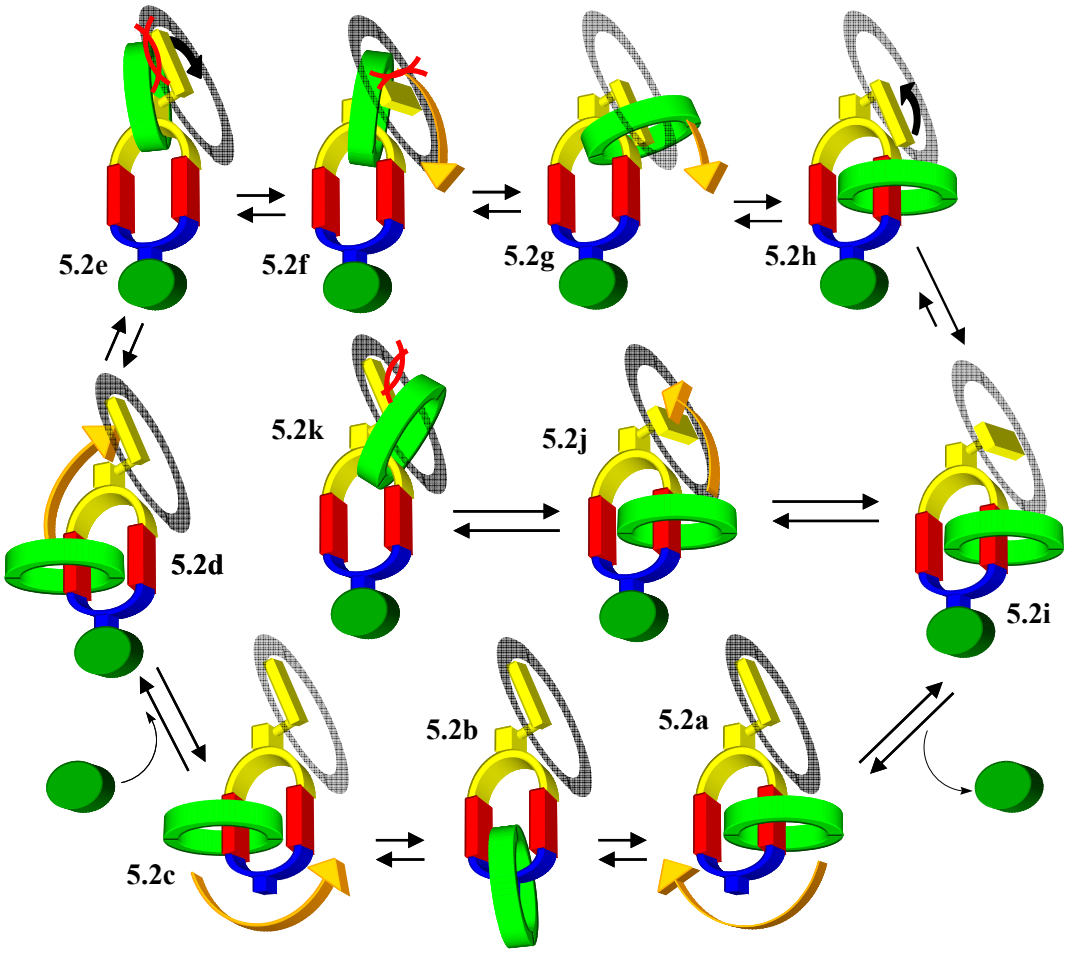

Figure 5.2 Proposed molecular motions of a gating catenane.

The benzyl groups prefer the ground state conformation wherein it is approximately perpendicular to the resorcinol ring as shown in **5.2d**, a characteristic supported by molecular modeling calculations. As the crown ether moves up the left with it comes into Van der Waals contact with the benzyl gate (**5.2e-f**). These interactions force the benzyl gate into the thermodynamically less stable, but more reactive conformation shown in **5.2g** allowing passage of BPP34C10 over the gate and formation of isomer 2 (**5.2h**). Once isomer 2 forms and the crown ether occupies the right binding site, normal thermodynamic fluctuations return the benzyl group to it low

energy ground state (**5.2i**). Even though the microscopic reverse conformation (**5.2h**) continues to be available it becomes more difficult to achieve due to the same interactions which formed it initially (**5.2 j-k**). Movement of the crown ether towards the gate group and the resulting interaction limits the rotational mobility of the gate group, forcing it into the less reactive, wider conformation (**5.2j-k**). As the crown ether tries to pass over the wider gate group, several possible scenarios emerge. If it possesses enough energy to overcome the barrier, it can translate over the more energy intensive energy gate conformation. However, if it does not then it returns to the low energy ground state and repeats the process until it either has enough energy to overcome the gate or the microscopic reverse becomes available as in **5.2h**. Energetically speaking we were trying to establish a system in which the equilibrium constant was based not on ground state energy differences between the isomers, but rather the ability of rapidly fluctuating system components to discriminate between an energetically enhanced, and thus more reactive pathway in one direction and an energetically crippled, less reactive pathway in the reverse direction effectively limiting the microscopic reverse. In this way we sought to modulate the energy potential and succeed where others had failed.

While the differences in isomer ratios are an interesting observation, and consistent with what we expected for ratcheting, the exact structure of the favored conformation could not be determined. Thus, we have no way of determining the true nature of the gates' behavior. Important questions remain to be answered the most important being which isomer is dominant. This question could be addressed by

synthesizing isotope labeled catenanes, such as the series of proposed catenanes in Figure 5.3, and remains a possibility for exploration by future researchers.

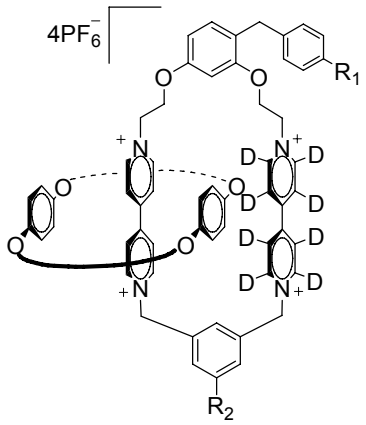

Figure 5.3. Isotopically labeled benzyl gated catenane.

One issue, perhaps the most damaging, with the physical design pertains to the ethoxy spacers incorporated into tether A. While originally intended to isolate the resorcinol-based gate from the two ground state binding sites, their relatively high degree of rotational flexibility have the potential to produce unintended consequences. We observed in Chapter 5 the AM1 molecular model calculated for the benzyl catenane with 1,3-xylyl tether. The lower tether was not parallel to the dipyridinium groups as depicted in the other figures, but perpendicular, which affected the translocation movement of the crown ether. Given the increased number of bonds with rotational freedom in the ethoxy spacers it is easy to imagine the entire resorcinol moiety, gate and all, folding down perpendicular to the dipyridiniums just as we observed for tether B. The AM1 calculated molecular model of catenane **4.8** in Figure 5.4 shows this very phenomenon. For the *p*-phenylbenzyl-gated catenane **4.8**, this narrow, or 'down' oriented conformation was calculated to be 4 kcal/mol lower in energy than the corresponding wide, or 'up' orientation. Benzyl-gated catenane **4.1** displayed a 4 kcal/mol preference for the wide gate, or 'up' conformation. This helps explain the comparatively lower energy of activation for the longer *p*-phenylbenzyl gate. While the benzyl and isopropyl-gated catenanes favored the wider gate

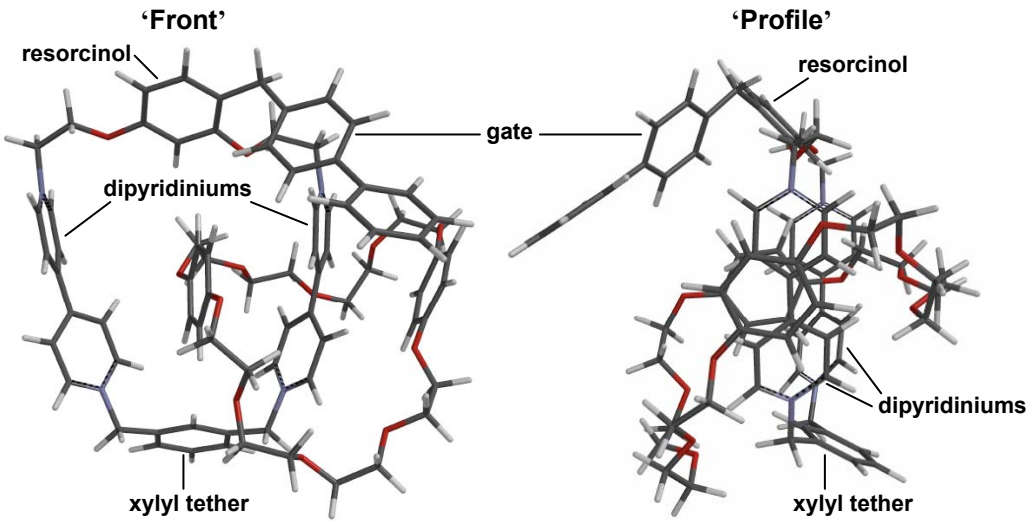

Figure 5.4. AM1 minimized structure of catenane **4.9** having the *p*-phenylbenzyl gate and 1,3-xylyl tether.

conformation the *p*-phenylbenzyl-gated catenane favored the narrow conformation. The effects of this orientation are two fold. Van der Waals interaction between the gate and binding site could affect the bonding interactions between BPP34C10 and the dipyridinium causing one ground state to be less stable. Indeed, the 1,4-xylyl tethered catenane in Chapter 4 having the longest gate displayed a 2.5 to 1 preference for one isomer over another a clear function of the thermodynamic ground state. This ratio was greater than in any of the previous asymmetric catenanes. Differences in ground state energy would appear as a lowered energy of activation. The second effect of the perpendicular resorcinol orientation would be to present a lowered energy of activation for circumrotation in the reverse direction, or perhaps even the elimination of gate bias. In this scenario, BPP34C10 would very easily find the microscopic reverse. The combined influence of gate length and resorcinol ring orientation could serve to mask

or eliminate any gating effects. This would help explain why we did not observe this same effect in the benzyl or isopropyl benzyl gates.

A proposed remedy for this 'floppy' tether component was identified and new catenanes will be synthesized in an attempt to increase the rigidity of the dipyridinium ring (Figure 5.5). We have eliminated the ethoxy spacer and replaced it with the more rigid phenyl spacer. Use of this spacer also requires use of a different tether B, as product yields using the previous set of xylyl tethers were negligible.

However, even with labeling and increased rigidity, the possibility of asymmetry affecting the isomers' relative thermodynamic stability remains difficult to eliminate as an explanation for the differences in isomer concentration. Given this difficulty the best way to determine the effectiveness of the gates would be to eliminate the opportunity for asymmetry to introduce thermodynamic preferences between

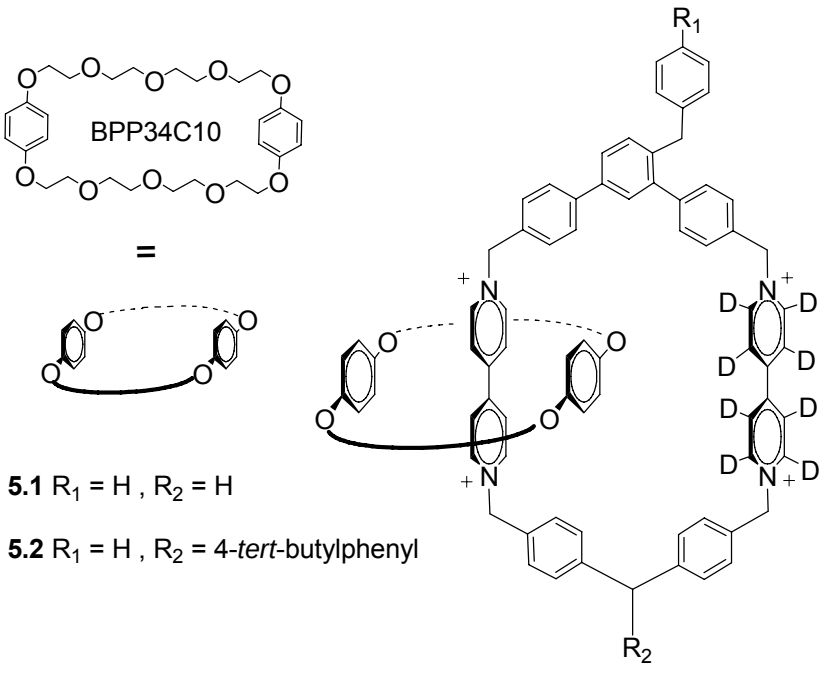

Figure 5.5. Proposed catenanes with increased rigidity.

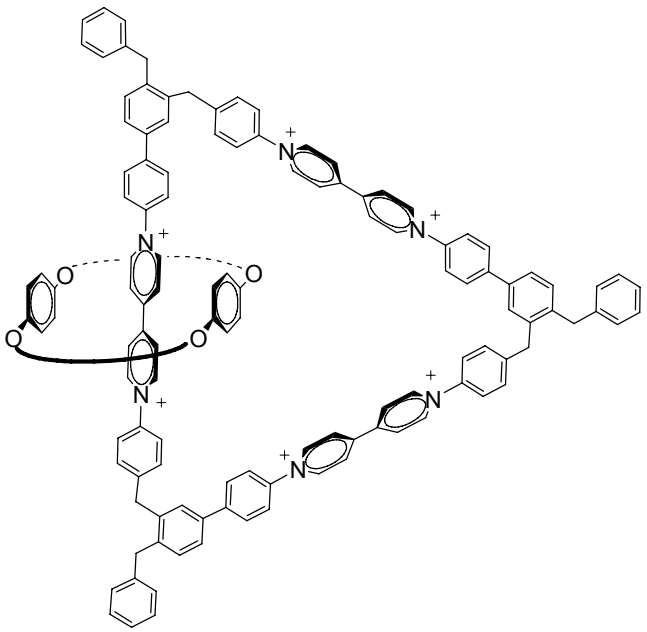

Figure 5.6. Proposed tristable catenane.

isomers. A tristable catenane possessing three gates and three binding sites, of the type shown in Figure 5.6, has been proposed and a similar design is under development in our laboratory. In this catenane there would be no differences in the relative thermodynamic stabilities of the conformations as the positions are symmetric relative to one another. Gating would be measured using the same spin-polarization transfer NMR techniques introduced in Chapter 1 and used by Kelly.

On our quest to synthesize a molecular machine capable of eluding the tenet of microscopic reversibility, we made a number of important discoveries concerning the characteristics of our novel symmetric and asymmetric [2]catenanes. We established the ability to regulate the energy of activation for circumrotation by increasing or decreasing the steric bulk of the tether substituents, and by making the steric bulk on the tethers large enough we were able to dictate the path over which circumrotation would occur. In addition, we showed that introduction of asymmetry into our catenanes, as a rule, perturbed the isoenergetic nature of the binding sites. Two exceptions to this rule were observed, which could be explained by thermal gating. However, at this time we cannot provide conclusive evidence of this result. Lastly, we

established the ability of a gate to fold down into a low energy pathway, albeit one followed in both directions, as evidenced by the long *p*-phenylbenzyl gate having a lower energy barrier to migration than did the shorter isopropylbenzyl gate.

While perhaps not as satisfying as showing an exception to the principle of microscopic reversibility, we were able to draw several conclusions about these gating catenanes that provide insight into the design's strengths, weaknesses, as well as allowing us to make predictions about the behavior of *Gedankenmaschinen* yet to be given material form.

Experimental

General Procedures

Chemicals and solvents were purchased from Fisher-Acros or Aldrich and used without further purification unless otherwise noted. Reagents 3,5-dimethoxybenzoic acid methyl ester (**2.7**), 3,5-bis(bromomethyl)-4'-(1,1'-dimethylethyl)-1,1'-biphenyl (**2.11**), and BPP34C10 were prepared according to published procedures.[50,57,58] Experimental details for preparation of catenanes **2.4**-**2.6** were published by our laboratory and further details will be provided by Xingang Pan in his dissertation. Preparative thin-layer chromatography (PLC) was performed using either 2mm or 1mm glass-backed sheets pre-coated with silica gel 60 F_{254} purchased from Fisher Scientific. Column chromatography was carried out using silica gel 60 F (0.040 to 0.063 mm particle size). ^{1}H and ^{13}C NMR spectra were recorded on either a Varian 400 or 300 MHz machine using residual solvent as internal standards. Chemical shifts are denoted in ppm and coupling constants in Hz. Abbreviations for NMR spectra are as follows: s = singlet, bs = broad singlet, d = doublet, t = triplet, q = quartet, m = multiplet. NMR samples were dissolved in CD_3COCD_3 or $CDCl_3$ purchased from Cambridge Isotope Laboratories.

Purification of Catenanes.

After stirring for 3 to 4 d the catenane solutions were purified and isolated according to the following method. The dark red solid was dissolved in approximately 10 mL of CH_3OH-EtOAc-CH_3COCH_3 (1:1:1) and loaded onto a 2 mm PLC plate.

After drying, the plate was eluted twice with CH_3OH-EtOAc (1:1) at 35 ° C and finally with CH_3OH-2M NH_4Cl-CH_3NO_2 (7:2:1) at room temperature. The product was washed from the silica gel using the final eluant and NH_4PF_6 (0.300 g) was added to the red solution. Solvents CH_3OH and CH_3NO_2 were removed via rotary evaporator leaving a red solid suspended in water. This red product was filtered, washed with distilled water, and allowed to dry. Impurities detected after the first separation were removed by an additional purification using a 0.5 mm PLC plate and identical procedures.

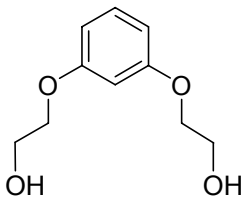

1,3-bis(2-hydroxyethoxy)benzene (2.13a). Sodium hydroxide (12.00 g, 300.0 mmol) was dissolved in a solution of ethanol (150 mL) and water (50 mL). To this solution was added 1,3-dihydroxybenzene (11.01 g, 100.0 mmol) previously dissolved in ethanol (150 mL) creating a dark red solution that was allowed to stir for 10 min. 2-Chloroethanol (24.15 g, 300.0 mmol) was added to the stirring solution after which the entirety was refluxed 4 d. Precipitate formed in the reaction vessel and the solution became ruby red in color. After cooling to room temperature, the solvent was removed *in vacuo* leaving a red solid that was dissolved in EtOAc (100 mL) and washed with water (200 mL). The water was extracted twice more with EtOAc (100 mL). After combining, the organic fractions were washed with brine (100 mL) and dried over $MgSO_4$. Removal of solvent yielded 16.9 g (85 % yield) of product **2.13a** that was utilized without further purification.

^{1}H NMR ($CDCl_3$, 300MHz): δ 7.19 (t, J = 7.9, 1H), 6.56 (d, J = 2.4 Hz, 1H), 6.51 (m, 2H), 4.07 (m, 4H), 3.96 (m, 4H), 2.01 (s, 2H).

^{13}C NMR ($CDCl_3$, 75MHz): δ 159.8, 130.0, 107.1, 101.7, 69.2, 61.4

MS (ESI): m/z 198.1 (M^+) ($C_{10}H_{14}O_4$ requires 198.22).

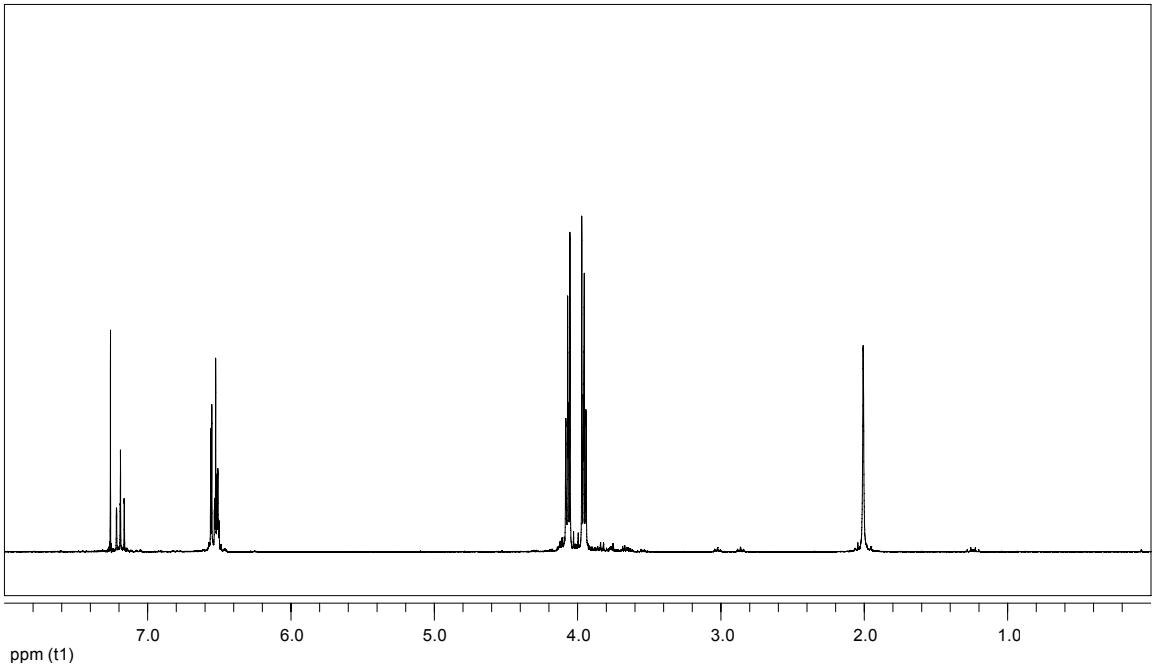
7.0
6.0
5.0
4.0
3.0
2.0
1.0
ppm (t1)

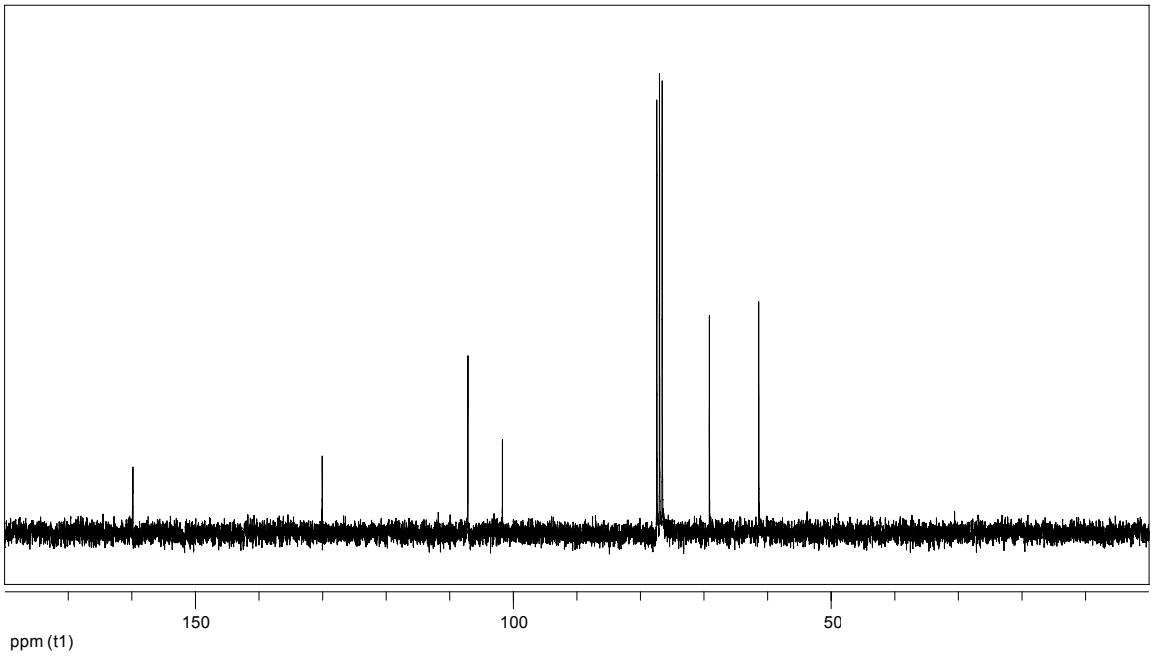
150
100
50
ppm (t1)

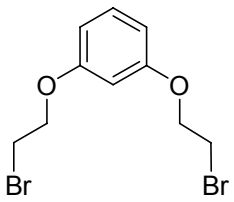

1,3-Bis(2-bromoethoxy)benzene (2.14a). PPh_3 (30.0 g, 114.3 mmol) was added to CH_3CN (100 mL) and cooled to -10 ° C. Br_2 (18.27 g, 159.8 mmol) dissolved in CH_3CN (20 mL) was slowly added to the stirring PPh_3 mixture so as not to exceed 0 ° C. The mixture was allowed to warm to room temperature after the addition was complete. 1,3-Di(2-hydroxyethoxy)benzene (**2.13a**) (9.90 g, 50.0 mmol) dissolved in CH_3CN was added to the mixture and allowed to stir overnight. Solvent was removed *in vacuo* and the crude product purified via column chromatography using CH_2Cl_2 to elute. The product **2.14a** was obtained in 83.7 % yield (22.4 g) and analysis by NMR showed it to be pure.

^{1}H NMR ($CDCl_3$, 300MHz): δ 7.20 (t, *J* = 8.2 Hz, 1H), 6.56 (d, *J* = 2.4 Hz, 1H), 6.54-6.48 (m, 2H), 4.28 (t, *J* = 6.3 Hz, 4H), 3.63 (t, *J* = 6.3 Hz, 4H).

^{13}C NMR ($CDCl_3$, 75MHz): δ 159.3, 130.2, 107.5, 102.1, 67.8, 29.0.

MS (EI): m/z 324.0 (M^+), 243.1, 216.1, 137.2, 109.2 ($C_{10}H_{12}O_2Br_2$ requires 324.01).

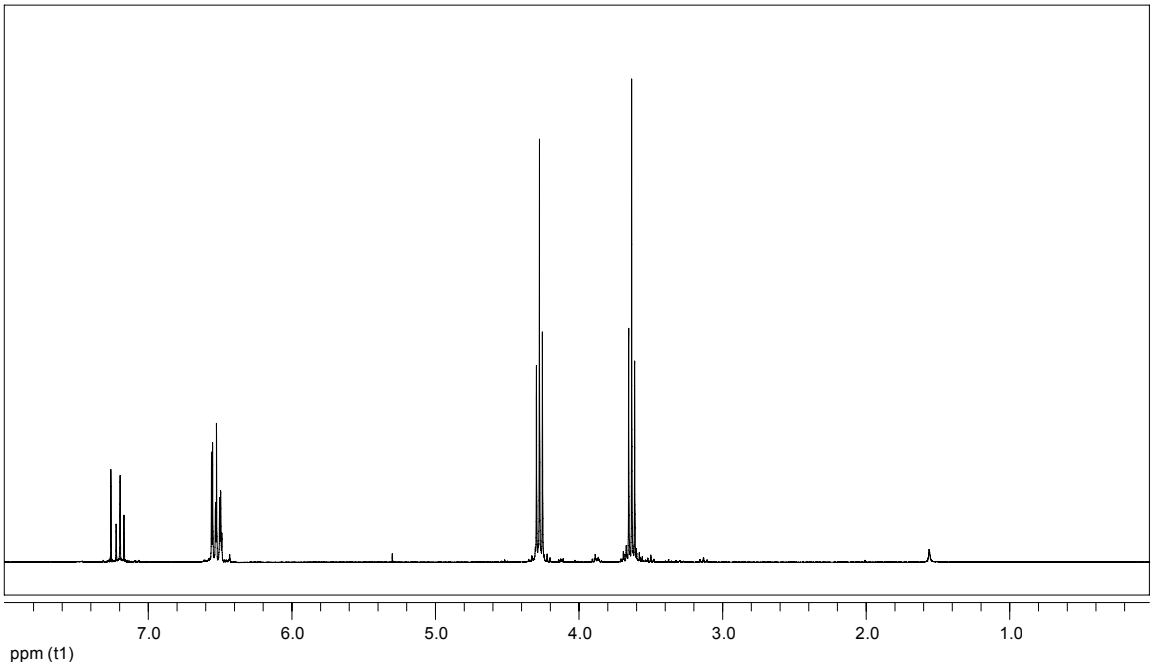
7.0
6.0
5.0
4.0
3.0
2.0
1.0
ppm (t1)

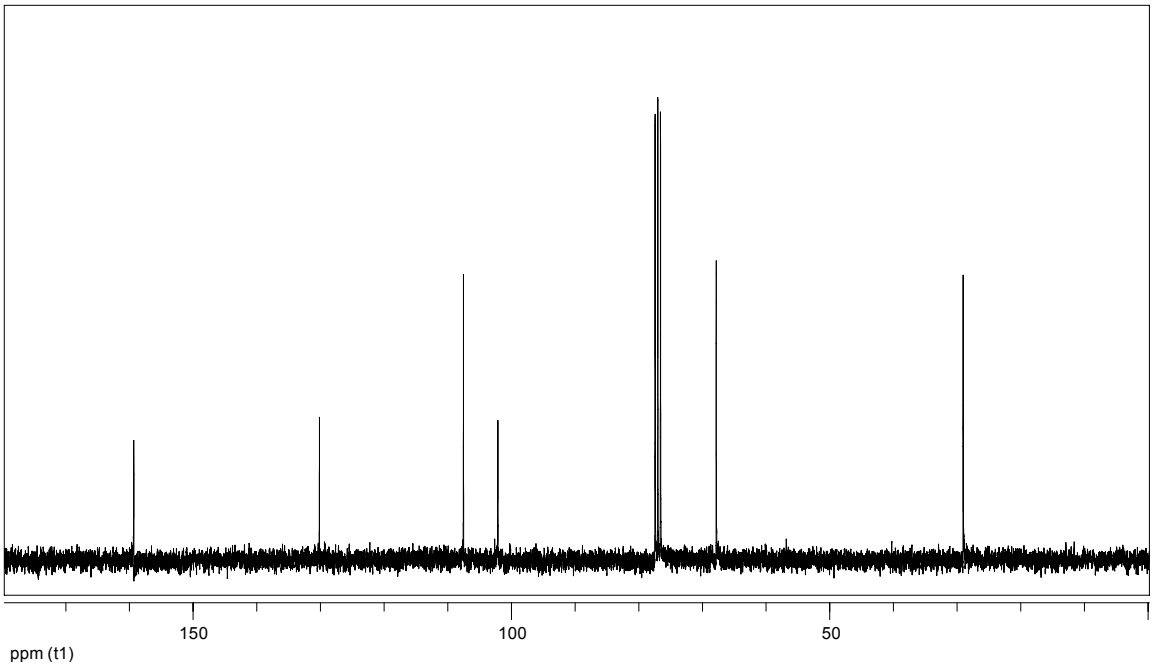
150
100
50
ppm (t1)

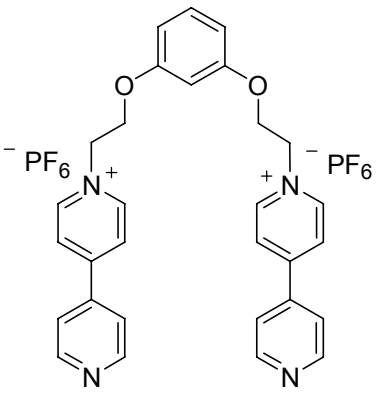

1,3-Bis(2-(4,4'-dipyridinium)ethoxy)benzene bis(hexafluorophosphate) (2.15a). 1,3-Di(2-bromoethoxy)benzene (**2.14a**) (11.30 g, 27.70 mmol) and 4,4-dipyridyl (17.30 g, 110.80 mmol) were added to 200 mL of CH_3CN. This solution was stirred at 70 ° C for two d. After cooling to room temperature the solvent was removed *in vacuo* leaving a brown solid. Water was added and upon heating the solid dissolved producing a brown solution. Addition of NH_4PF_6 (11 g) produced a brown oil which was isolated and washed with $CHCl_3$ (3x20 mL) leaving a yellow oil which was then dissolved in CH_3CN and dried with $MgSO_4$. Removal of the solvent *in vacuo* left 23.5 g, or 98.7 % yield of product **2.14a** in the form of yellow crystals.

^{1}H NMR ($CDCl_3$, 300MHz): δ ppm 9.33 (m, *J* = 7.0 Hz, 4H), 8.87 (m, *J* = 4.5, 1.70 Hz, 4H), 8.68 (m, *J* = 7.0 Hz, 4H), 7.98 (m, *J* = 4.5 Hz, 4H), 7.18 (t, *J* = 8.2 Hz, 1H), 6.66 (t, *J* = 2.3 Hz, 1H), 6.60 (dd, *J* = 8.2, 2.3 Hz, 2H), 5.31 (t, *J* = 5.0 Hz, 4 H), 4.66 (t, *J* = 5.0 Hz, 4 H)

^{13}C NMR ($CDCl_3$, 75MHz): δ 160.9, 156.3, 153.1, 148.0, 143.0, 132.1, 127.6, 123.6, 109.5, 103.8, 68.1, 62.6.

MS (ESI): m/z 621.3 (M PF_6^+), 238.1 (M^{2+}) ($C_{30}H_{28}O_2N_4^{2+}$ requires 476.6)

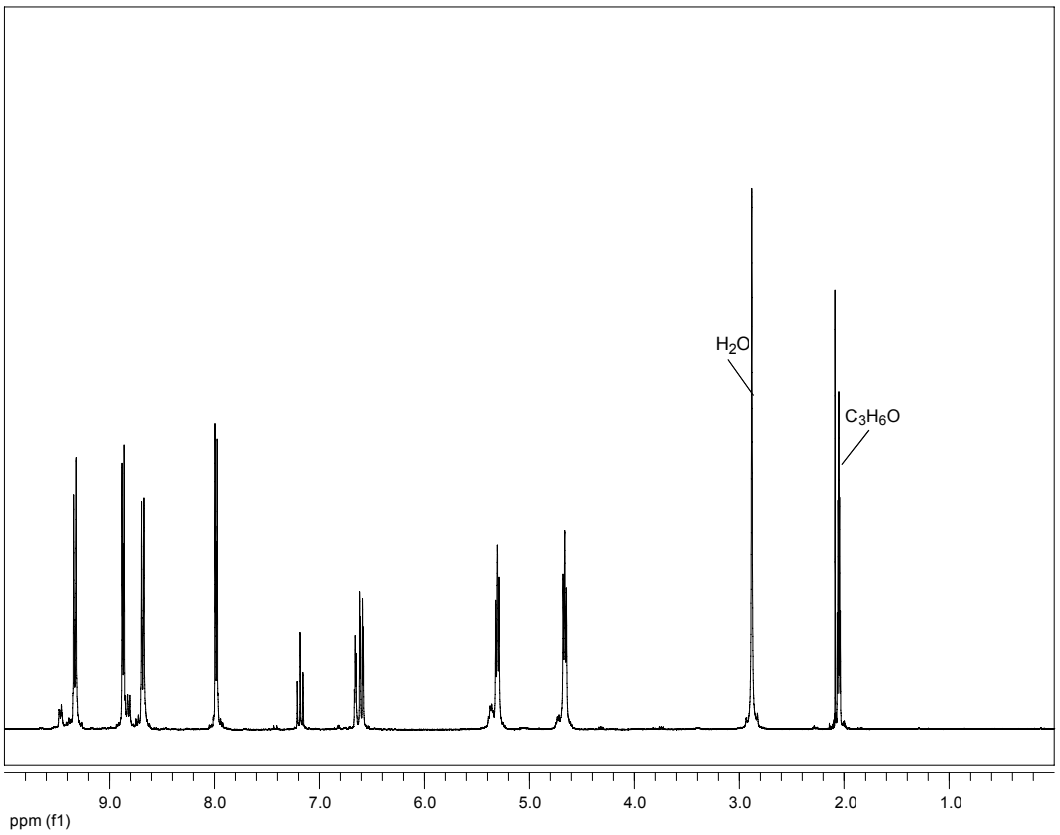
H2O
C3H6O
9.0
8.0
7.0
6.0
5.0
4.0
3.0
2.0
1.0
ppm (f1)

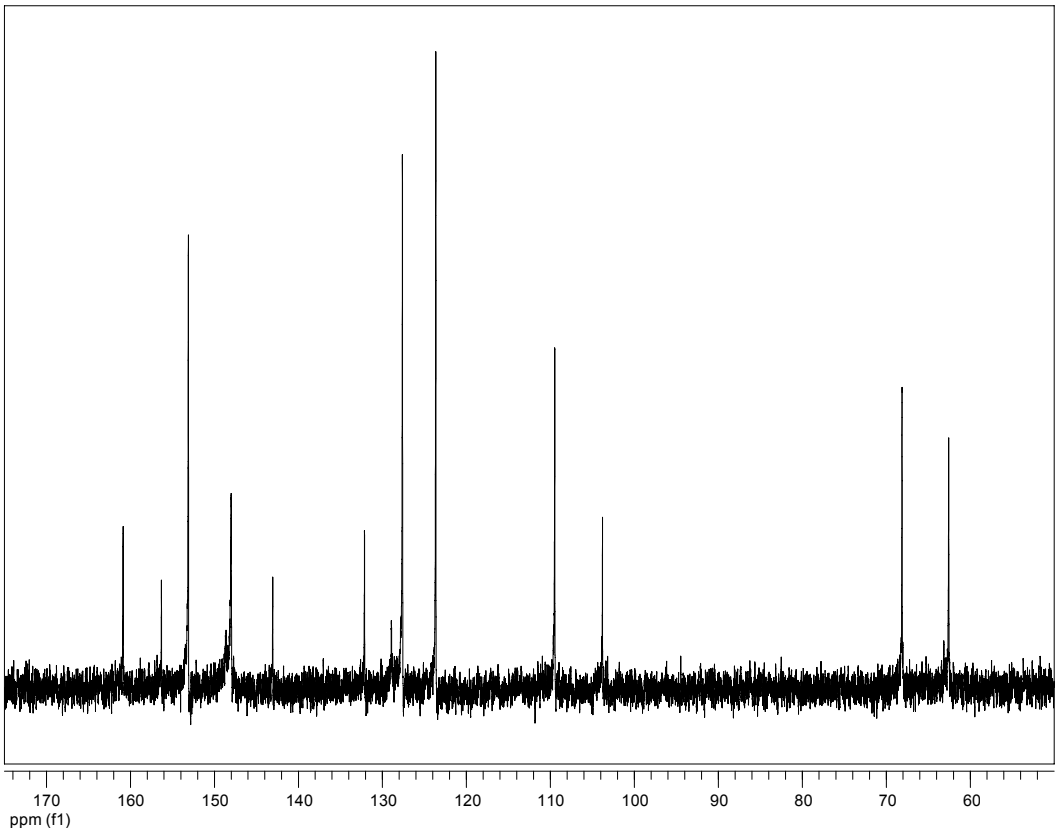
170
160
150
140
130
120
110
100
90
80
70
60
ppm (f1)

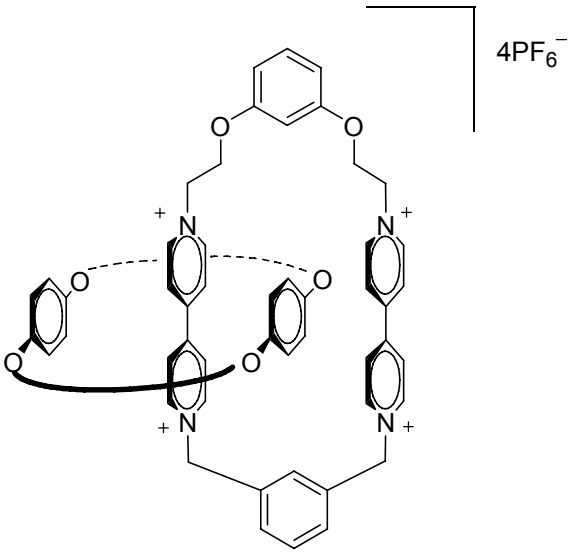

Catenane 2.1. 1,3-Di(2-(4,4'-dipyridinium)ethoxy)benzene (**2.15a**) (0.123 g, 0.160 mmol) and BPP34C10 (0.223 g, 0.416 mmol) were combined and dissolved in CH_3CN (15 mL). This solution was allowed to stir for 10 min. at which point α,α'-dibromo-*m*-xylene (0.051 g, 0.19 mmol) was added and the reaction vessel sealed with a septum. This red solution stirred 4 d under ambient conditions after which time the solvent was removed *in vacuo*. The catenane was purified and after drying 74 mg (27 %) of pure catenane **2.1** was recovered.

^{1}H NMR ($CDCl_3$, 400 MHz): δ ppm 9.22 (m, *J* = 7.0 Hz, 4H), 9.15 (m, *J* = 7.0 Hz, 4H), 8.24 (m, *J* = 7.0 Hz, 4H), 8.18 (m, *J* = 7.8 Hz, 2H), 8.14 (m, *J* = 7.0 Hz, 5H), 7.91 (t, *J* = 7.7 Hz, 1H), 7.27 (t, *J* = 8.4 Hz, 1H), 6.83 (t, *J* = 2.4 Hz, 1H), 6.68 (dd, *J* = 8.4, 2.4 Hz, 2H), 6.18 (s, 4H), 5.84-5.69 (m, 6H), 5.29 (s, 4H), 4.62 (s, 4H), 3.85-3.66 (m, 34H).

^{13}C NMR ($CDCl_3$, 75MHz): δ 160.7, 153.6, 148.2, 147.9, 147.5, 147.2, 136.1, 135.7, 133.9, 132.9, 132.2, 127.7, 127.3, 116.4, 108.0, 106.8, 72.1, 72.0, 71.6, 69.2, 68.0, 66.2, 62.7

MS (ESI): 1552.6 (M $3PF_6^+$), 703.4 (M PF_6^{2+}), 630.9 (M PF_6^{2+}), 420.6 (M PF_6^{4+}) 372.2, (M^{3+}), 279.2 (M^{4+}) ($C_{66}H_{76}N_4O_{12}^{4+}$ requires 1117.33).

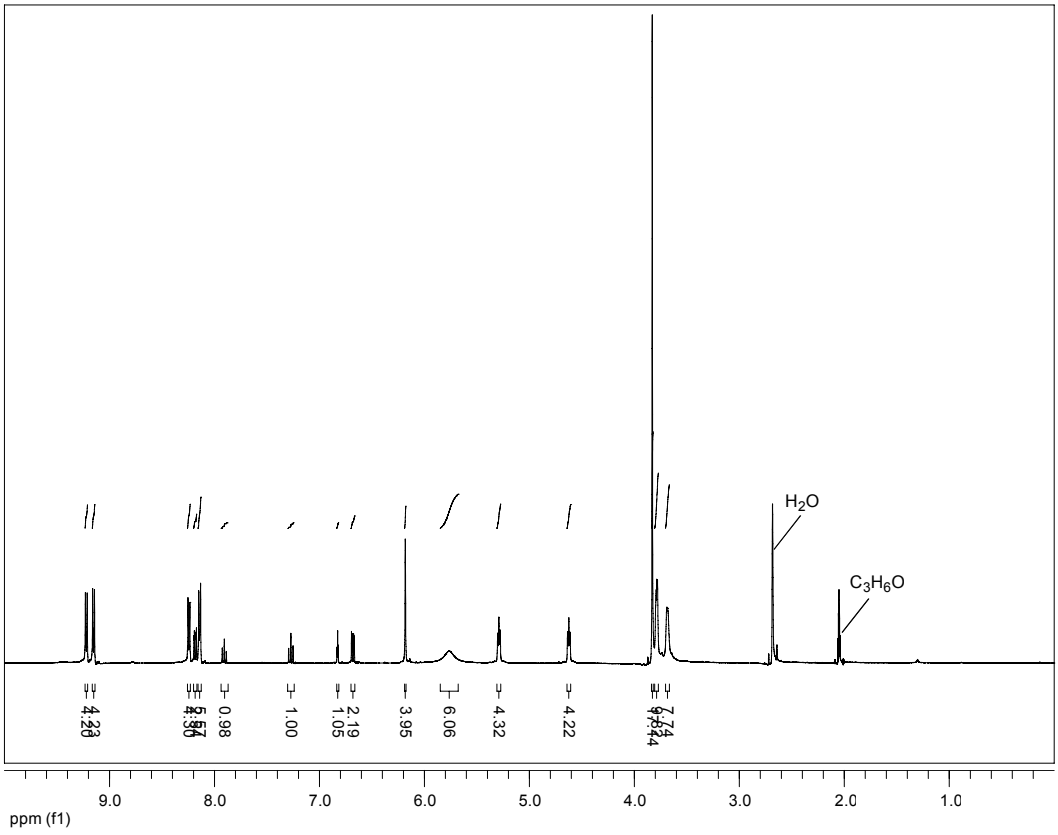

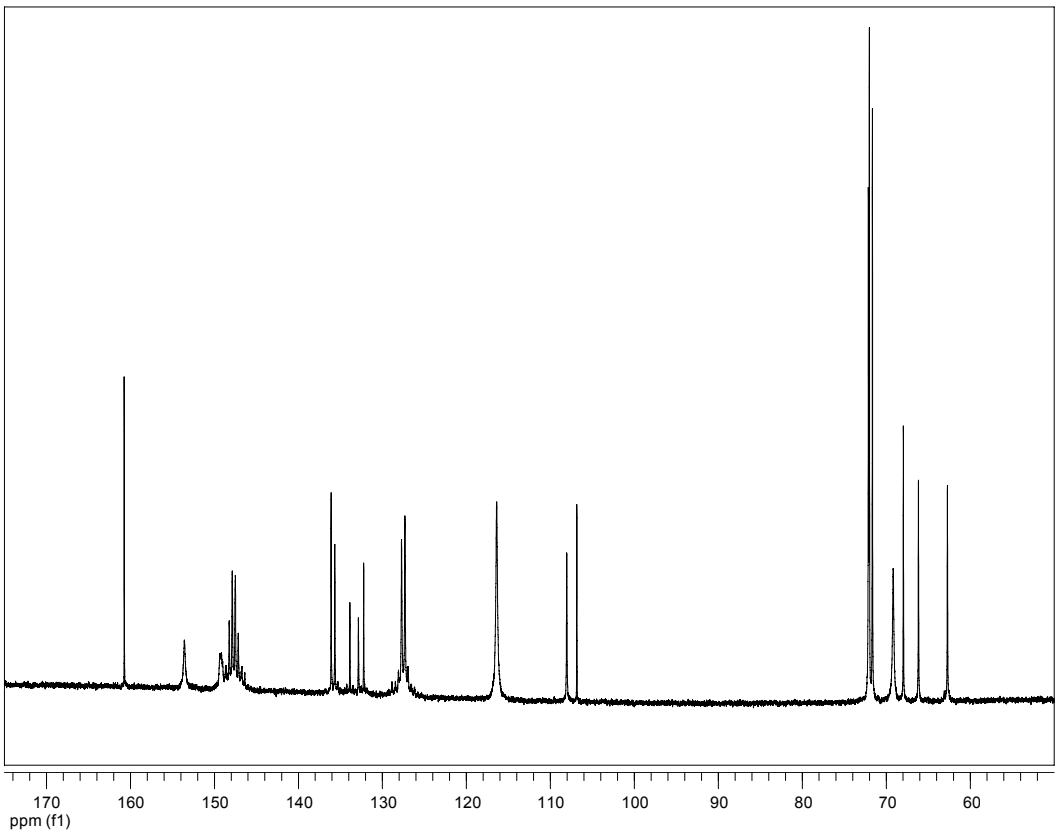
170
160
150
140
130
120
110
100
90
80
70
60
ppm (f1)

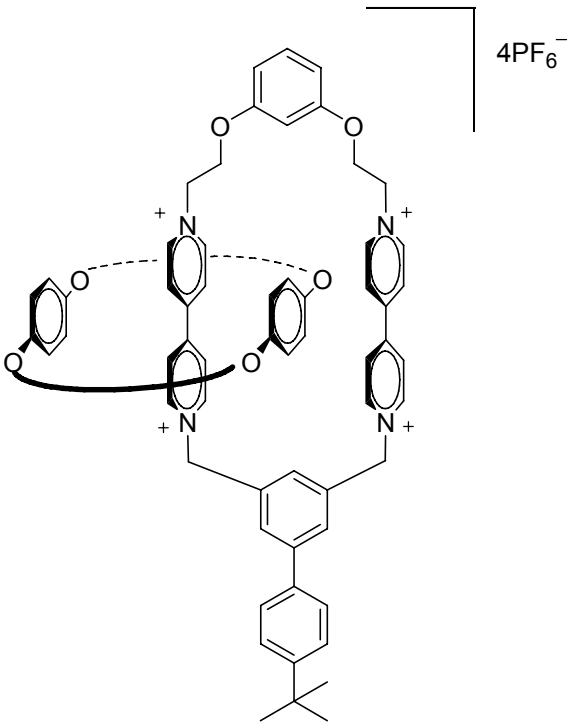

Catenane 2.2. 1,3-Di(2-(4,4'-dipyridinium)ethoxy)benzene (**2.15a**) (0.123 g, 0.160 mmol) and BPP34C10 (0.223 g, 0.416 mmol) were combined and dissolved in CH_3CN (15 mL). This solution was allowed to stir for 10 min. at which point 5-bis(bromomethyl)-4'-(1,1'-dimethylethyl)-1,1'-biphenyl (0.076 g, 0.19 mmol) was added and the reaction vessel sealed with a septum. This red solution stirred 4 d under ambient conditions after which time the solvent was removed *in vacuo*. The catenane was purified and after drying, 72 mg (23 %) of pure product catenane **2.2** was recovered.

^{1}H NMR ($CDCl_3$, 400 MHz): δ ppm 9.33 (m, *J* = 6.9 Hz, 4H), 9.15 (m, *J* = 6.9 Hz, 4H), 8.49 (m, *J* = 1.4 Hz, 2H), 8.26 (m, *J* = 5.8 Hz, 4H), 8.14 (m, *J* = 6.8 Hz, 4H), 8.09 (t, *J* = 1.4 Hz, 1H), 7.96 (m, *J* = 8.5 Hz, 2H), 7.67 (m, *J* = 8.5 Hz, 2H), 7.27 (t, *J* = 8.3 Hz, 1H), 6.84 (t, *J* = 2.3 Hz, 1H), 6.66 (dd, *J* = 8.3, 2.3 Hz, 1H), 6.26 (s, 4H), 5.28 (m, 4H), 4.60 (m, 4H), 3.96-3.58 (m, 34H), 1.42 (s, 9H).

^{13}C NMR ($CDCl_3$, 75MHz): δ 160.7, 153.5, 147.8, 147.6, 145.1, 137.6, 136.7, 133.5, 132.2, 132.0, 128.9, 127.9, 127.7, 127.3, 116.3, 108.0, 106.7, 72.0, 71.9, 71.6, 69.1, 67.9, 66.2, 62.6, 36.2, 32.5, 2.0.

MS (ESI): 769.4 (M^{2+}, $+PF_6^-$), 696.9 (M^{4+}, $+PF_6^-$), 464.6 (M^{3+}, $+PF_6^-$), 416.3 (M^{3+}), 312.2 (M^{4+}) ($C_{76}H_{88}N_4O_{12}^{4+}$ requires 1249.53)

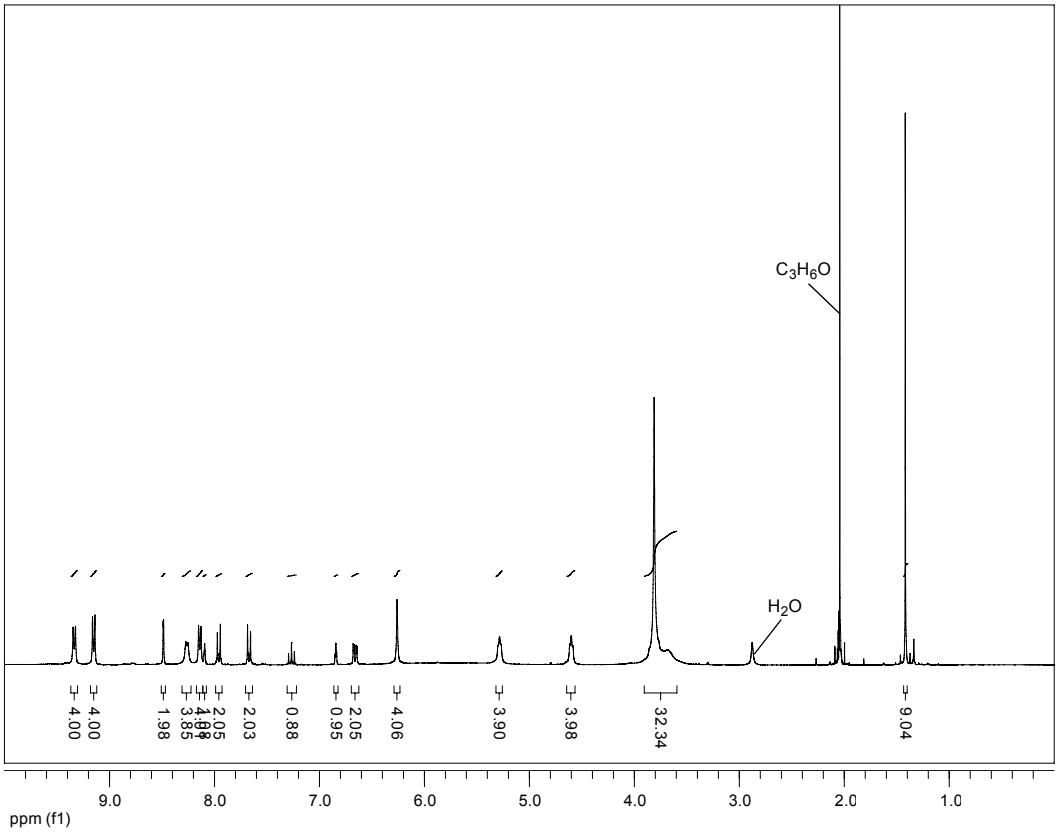

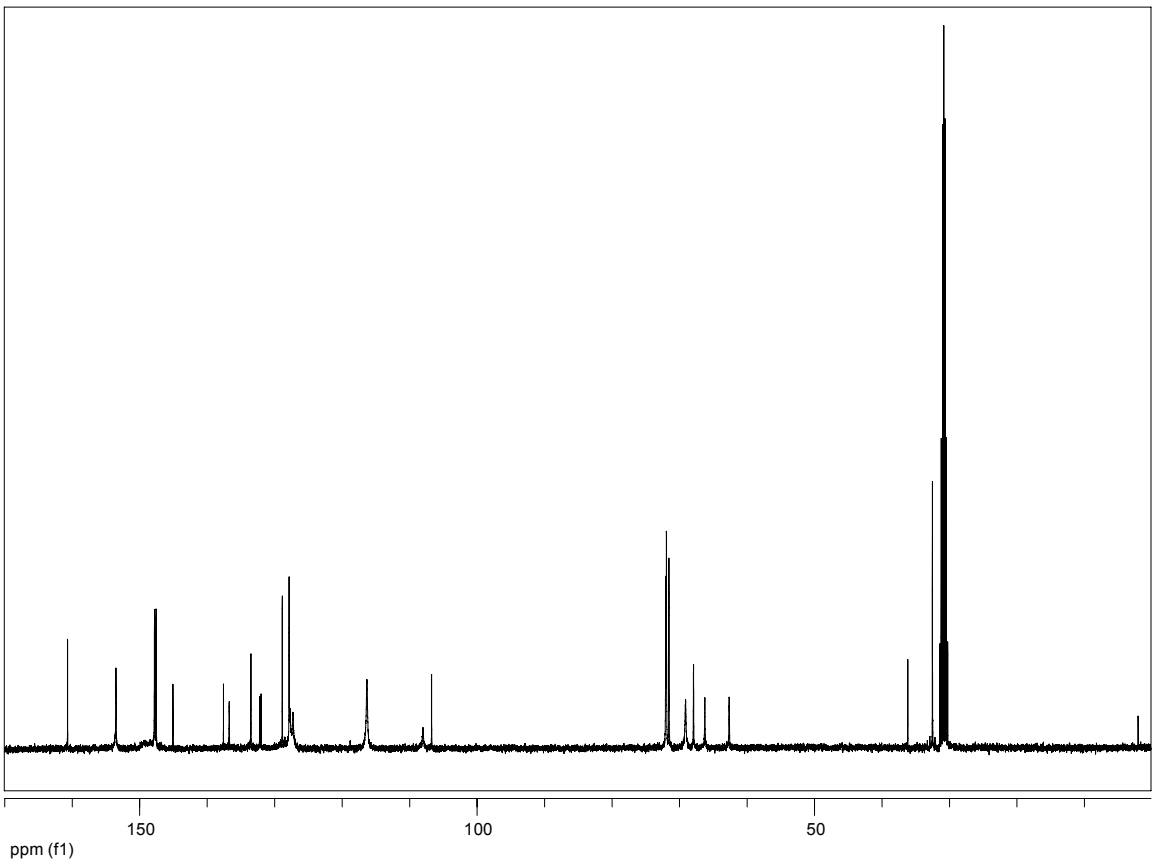
150
100
50
ppm (f1)

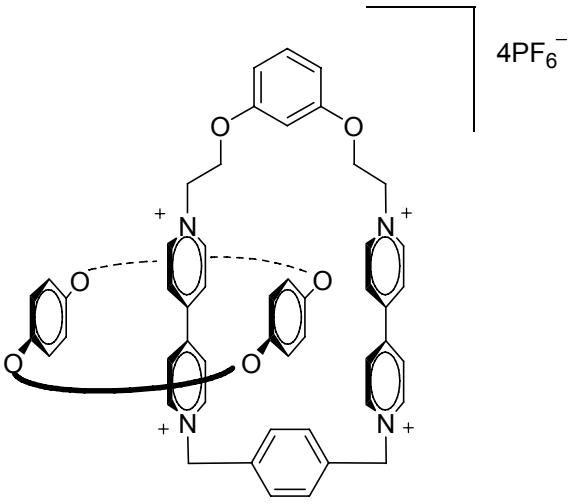

Catenane 2.3. 1,3-Di(2-(4,4'-dipyridinium)ethoxy)benzene (0.123 g, 0.160 mmol) and BPP34C10 (0.223 g, 0.416 mmol) were dissolved in CH_3CN (15 mL). This solution was allowed to stir for 10 min. at which point α,α'-dibromo-*p*-xylene (0.051 g, 0.19 mmol) was added and the reaction vessel sealed with a septum. This red solution stirred 4 d under ambient conditions after which time the solvent was removed *in vacuo*. The catenane was purified and after drying 91 mg (32 %) of pure catenane **2.3** was recovered.

^{1}H NMR ($CDCl_3$, 400 MHz): δ ppm 9.37 (m, *J* = 7.0 Hz, 4H), 9.18 (m, *J* = 7.0 Hz, 4H), 8.15-8.12 (m, 12H), 7.28 (t, *J* = 8.2 Hz, 1H), 6.72 (s, 1H), 6.69 (dd, *J* = 8.3, 2.3 Hz, 1H), 6.11 (s, 4H), 5.62 (s, 8H), 5.28 (s, 4H), 4.64 (s, 4H), 3.91-3.58 (m, 32H).

^{13}C NMR ($CDCl_3$, 75MHz): δ 146.0, 144.9, 130.9, 130.3, 125.8, 105.8, 104.5, 70.1, 70.0, 69.7, 67.2, 65.7, 64.7, 60.6.

MS (ESI): 1552.6 (M^+, $+3PF_6^-$), 703.2 (M^{2+}, $+2PF_6^-$), 372.2 (M^{3+}), 279.1 (M^{4+}) ($C_{66}H_{76}N_4O_{12}^{4+}$ requires 1117.33).

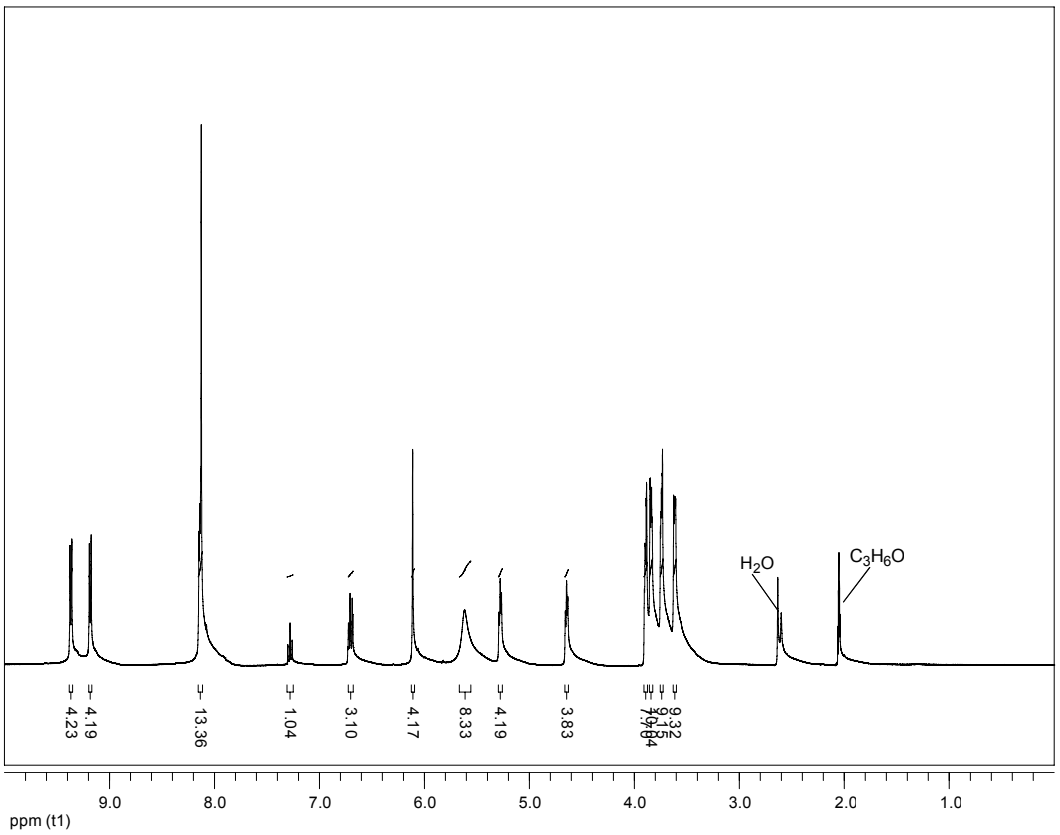
H2O
C3H6O
4.23
4.19
13.36
1.04
3.10
4.17
8.33
4.19
3.83
9.32
ppm (t1)
9.0
8.0
7.0
6.0
5.0
4.0
3.0
2.0
1.0

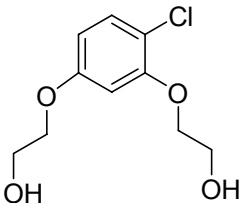

1,3-Bis(2-hydroxyethoxy)-4-chlorobenzene (3.11a). Sodium hydroxide (8.30 g, 207 mmol) was dissolved in a solution of ethanol (150 mL) and water (20 mL). To this solution was added 4-chloro-benzene-1,3-diol (10.00 g, 69.18 mmol) previously dissolved in ethanol (25 mL) creating a dark red solution that was allowed to stir for 10 min. 2-Chloroethanol (16.71 g, 207.5 mmol) was added to the stirring solution after which the entirety was refluxed 3 d. Precipitate formed in the reaction vessel and the solution became ruby red in color. After cooling to room temperature, the solvent was removed *in vacuo* leaving a red solid that was dissolved in EtOAc (100 mL) and washed with water (100 mL). The water was extracted twice more with EtOAc (30 mL). After combining, the organic fractions were washed with brine (50 mL) and dried over $MgSO_4$. Flash chromatography using diethyl ether provided 12.7 g, a 79 % yield, of pure **3.11a**.

^{1}H NMR ($CDCl_3$, 300MHz): δ ppm 7.24 (d, *J* = 8.7 Hz, 1H), 6.71 (d, *J* = 2.7 Hz, 1H), 6.53 (dd, *J* = 8.7, 2.7 Hz, 1H), 4.14 (s, 2H), 4.06 (s, 2H), 4.00-3.96 (m, 2H), 3.90 (m, *J* = 4.7, 2.8 Hz, 2H), 3.85 (m, *J* = 4.7, 2.8 Hz, 1H),

^{13}C NMR ($CDCl_3$, 75MHz): δ 161.1, 157.1, 131.8, 115.6, 108.5, 103.4, 72.6, 72.0, 62.24, 62.17.

MS (EI): m/z 255.7 (M Na^+), 232.0 (M^+) ($C_{10}H_{13}ClO_4$ requires 232.7).

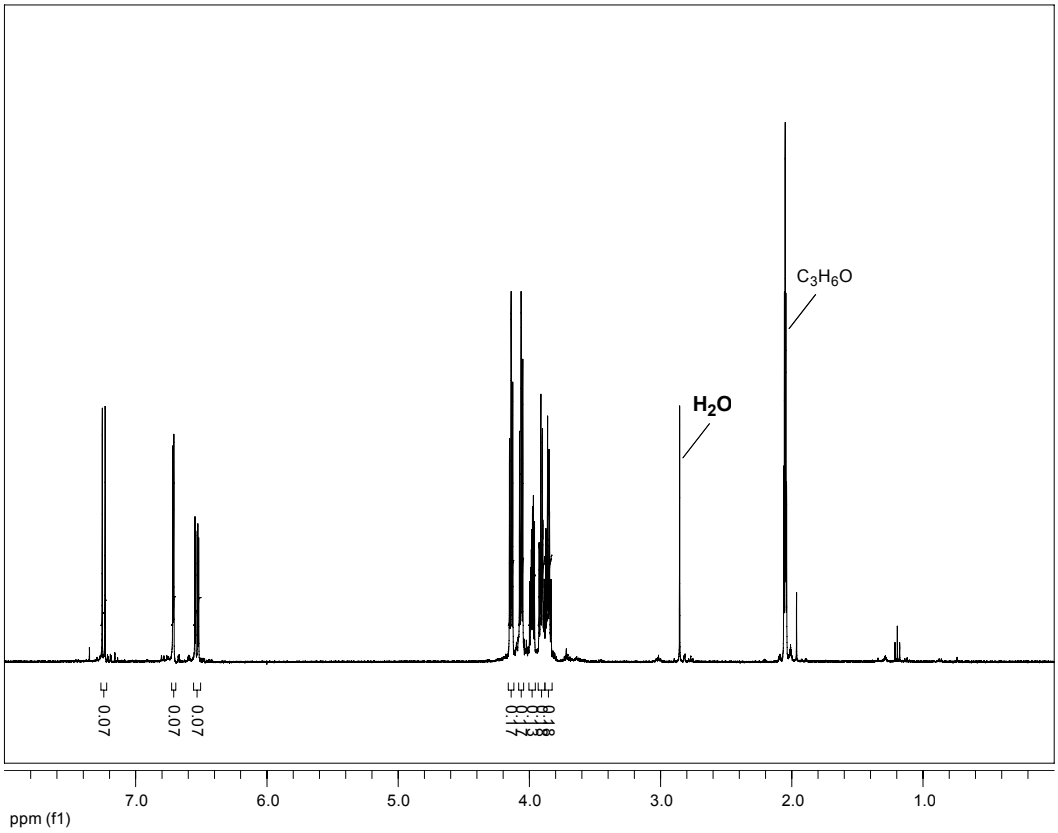
C_3H_6O
H_2O
0.07
0.07
0.07
7.0
6.0
5.0
4.0
3.0
2.0
1.0
ppm (f1)

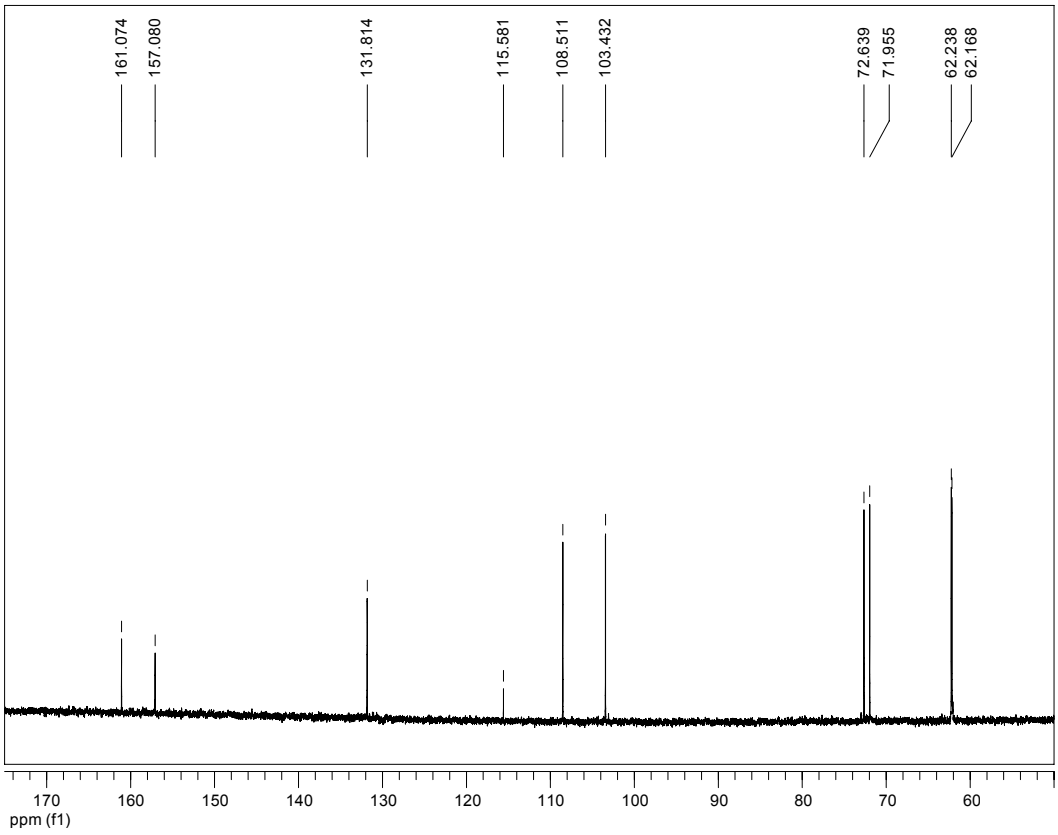
161.074
157.080
131.814
115.581
108.511
103.432
72.639
71.955
62.238
62.168
170
160
150
140
130
120
110
100
90
80
70
60
ppm (f1)

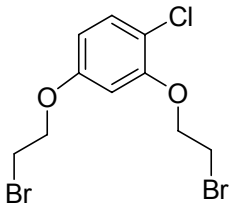

1,3-Bis(2-bromoethoxy)-4-chlorobenzene (3.12a). PPh_3 (41.64 g, 158.7 mmol) was added to CH_3CN (200 mL) and cooled to -10 ° C. Br_2 (25.36 g, 158.7 mmol) dissolved in CH_3CN (30 mL) was slowly added to the stirring PPh_3 mixture so as not to exceed 0 ° C. The mixture was allowed to warm to room temperature after the addition was complete. 1,3-Bis(2-hydroxyethoxy)-4-chloro-benzene (15.77 g, 69.00 mmol) dissolved in CH_3CN (30 mL) was added to the mixture and allowed to stir for 2 hours. Solvent was removed *in vacuo* and the crude product purified via column chromatography using CH_2Cl_2 to elute. The product **3.12a** was obtained in 45 % yield (25.6 g) and analysis by NMR showed it to be pure.

^{1}H NMR ($CDCl_3$, 300MHz): δ ppm 7.26 (d, *J* = 8.7 Hz, 1H), 6.54 (d, *J* = 2.7 Hz, 1H), 6.47 (dd, *J* = 8.7, 2.7 Hz, 1H), 4.31 (t, *J* = 6.5 Hz, 2H), 4.26 (t, *J* = 6.1 Hz, 2H), 3.66 (dd, *J* = 6.5 Hz, 2H), 3.64 (dd, *J* = 6.5 Hz, 2H)

MS (EI): m/z 384.9 ($M\ Na^+$), 357.9 (M^+), 277.1 (M^+ -Br) ($C_{10}H_{11}Br_2ClO_2$ requires 358.5).

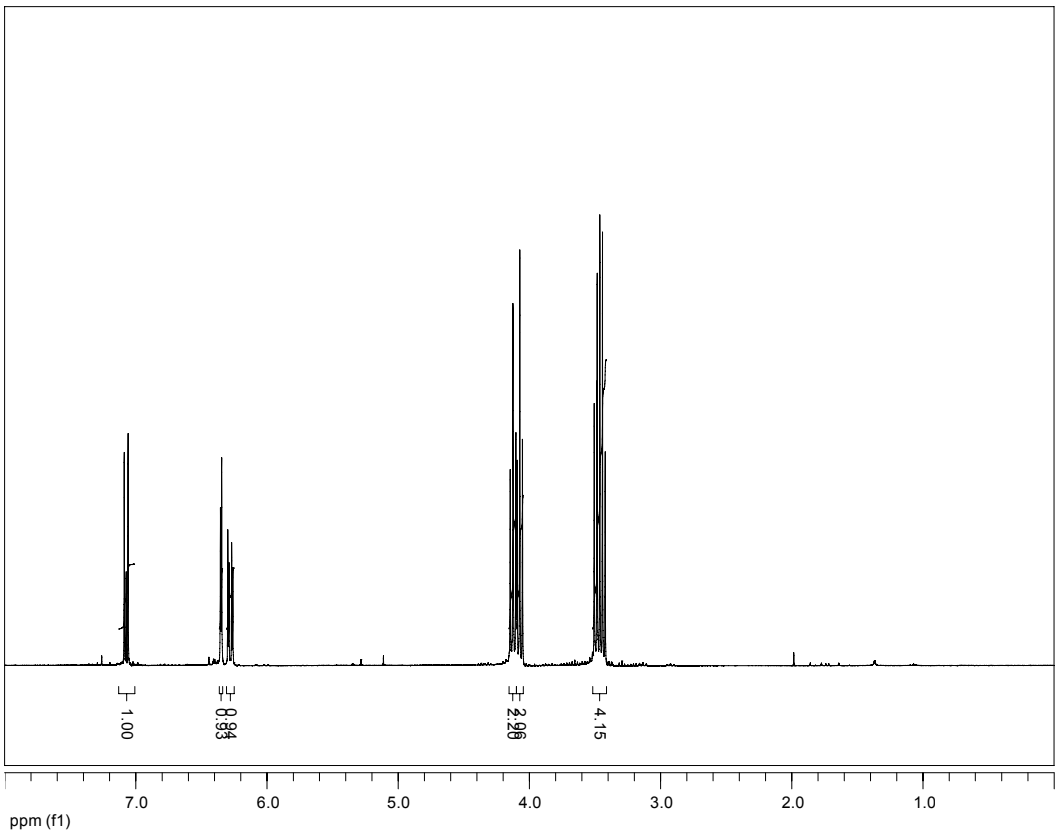
1.00
0.94
0.93
2.26
2.06
4.15
7.0
6.0
5.0
4.0
3.0
2.0
1.0
ppm (f1)

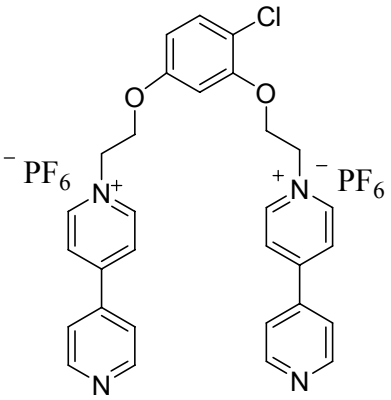

1,3-Bis(2-(4,4'-dipyridinium)ethoxy)-4-chlorobenzene bis(hexafluorophosphate) (3.13a). 1,3-Bis(2-bromoethoxy)-4-chloro-benzene (3.99 g, 11.2 mmol) and 4,4-dipyridyl (7.00 g, 44.8 mmol) were added to 40 mL of CH_3CN. This solution was stirred at 70 ° C for two d during which a yellow solid precipitated onto the sides of the flask. After cooling to room temperature the solvent was decanted with residual solvent being removed *in vacuo* leaving a dark yellow solid. Water was added and upon heating the solid dissolved producing a yellow solution. Addition of NH_4PF_6 (6.0 g, 34 mmol) produced a yellow oil which was isolated and washed with $CHCl_3$ (3x20 mL) to remove impurities leaving the same yellow oil which was then dissolved in CH_3CN and dried with $MgSO_4$. Removal of the solvent *in vacuo* left 6.9 g (77 %) of solid, yellow **3.13a**.

^{1}H NMR ($CDCl_3$, 300MHz): δ ppm 9.35 (m, *J* = 6.0 Hz, 4H), 8.89 (m, 4H), 8.74 (m, *J* = 6.0 Hz, 2H), 8.69 (m, *J* = 6.4 Hz, 2H), 8.05-7.97 (m, 4H), 7.28 (d, *J* = 8.8 Hz, 1H), 6.84 (d, *J* = 2.7 Hz, 1H), 6.65 (dd, *J* = 8.8, 2.7 Hz, 1H), 5.37 (m, *J* = 4.9 Hz, 2H), 5.33 (m, *J* = 4.9 Hz, 2H), 4.73 (m, *J* = 4.9 Hz, 4H)

MS (ESI): m/z 655.1 (M PF_6^+), 255.1 (M^{2+}) ($C_{30}H_{27}ClO_2N_4^{2+}$ requires 511.0)

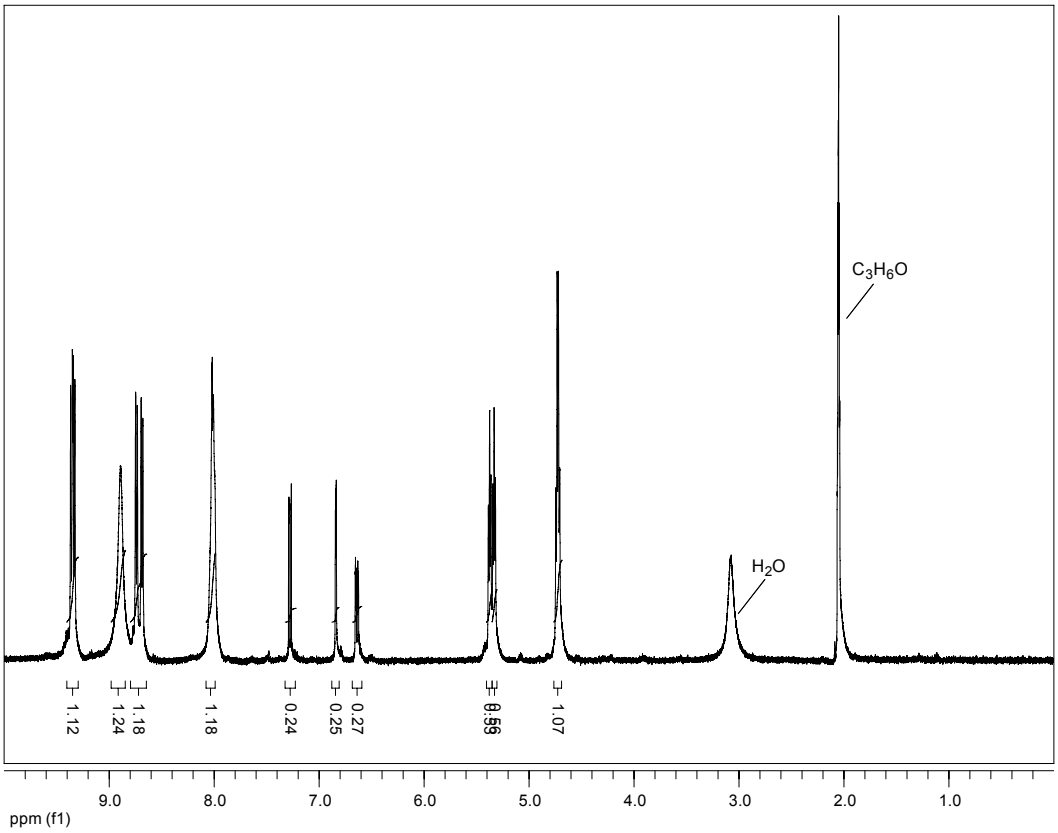
C3H6O
H2O
1.12
1.24
1.18
1.18
0.24
0.25
0.27
0.55
1.07
9.0
8.0
7.0
6.0
5.0
4.0
3.0
2.0
1.0
ppm (f1)

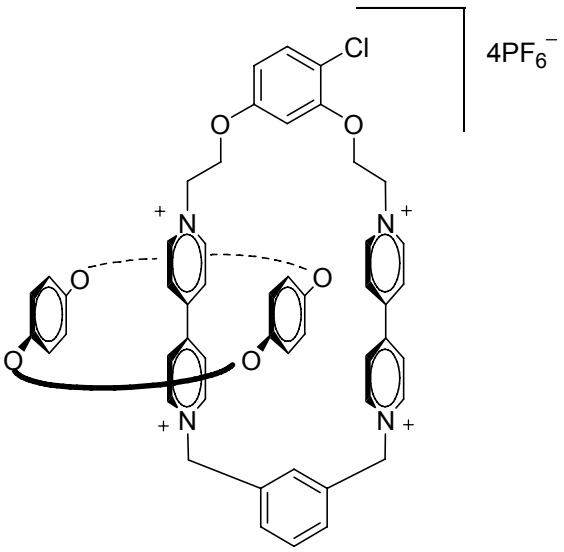

Catenane 3.1. 1,3-Bis(2-(4,4'-dipyridinium)ethoxy)-4-chlorobenzene bis(hexafluorophosphate) (0.128 g, 0.160 mmol) and BPP34C10 (0.172 g, 0.320 mmol) were combined and dissolved in CH_3CN (15 mL). This solution was allowed to stir for 10 min. at which point α,α'-dibromo-*m*-xylene (0.051 g, 0.19 mmol) was added and the reaction vessel sealed with a septum. This red solution stirred 4 d under ambient conditions after which time the solvent was removed *in vacuo*. The catenane was purified and after drying 55 mg (20 %) of catenane **3.1** was recovered.

^{1}H NMR ($CDCl_3$, 400 MHz): δ ppm 9.25 (m, *J* = 7.0 Hz, 2H), 9.17 (m, *J* = 7.0, 4.05 Hz, 4H), 9.11 (m, *J* = 6.7 Hz, 2H), 8.31 (m, *J* = 6.6 Hz, 2H), 8.27 (m, *J* = 6.5 Hz, 2H), 8.23 (m, *J* = 6.7 Hz, 2H), 8.15 (m, *J* = 7.7, 6.9 Hz, 4H), 8.06 (t, *J* = 1.6, Hz, 1H), 7.90 (t, *J* = 7.8 Hz, 1H), 7.39 (d, *J* = 8.9 Hz, 1H), 6.90 (d, *J* = 2.7 Hz, 1H), 6.76 (dd, *J* = 8.9, 2.7 Hz, 1H), 6.20 (s, 2H), 6.17 (s, 2H), 5.39 (s, 2H), 5.29 (s, 2H), 5.03 (bs, 8H), 4.68 (t, *J* = 3.8 Hz, 4H), 3.91-3.51 (m, 32H).

MS (ESI): 648.3 (M $1PF_6^{2+}$), 432.2 (M PF_6^{3+}), 383.5 (M^{3+}), 288.2 (M^{4+}) ($C_{66}H_{75}ClN_4O_{12}^{4+}$ requires 1151.77).

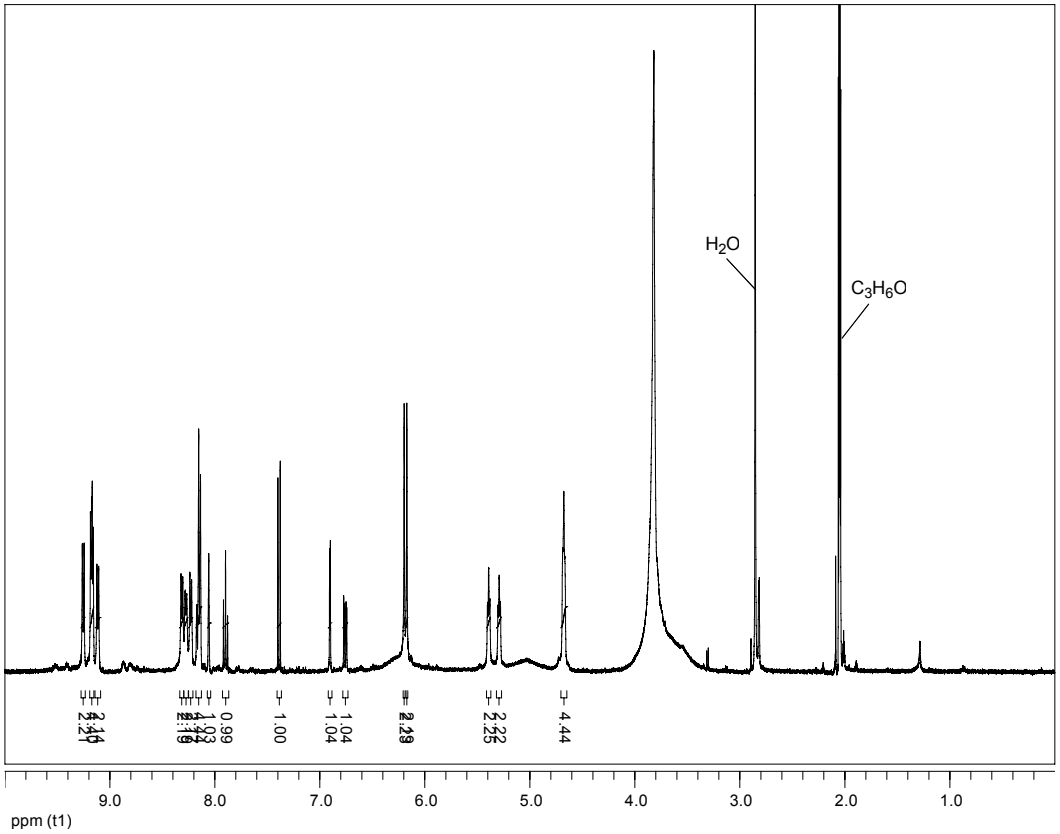
H2O
C3H6O
0.99
1.00
1.04
4.44
9.0
8.0
7.0
6.0
5.0
4.0
3.0
2.0
1.0
ppm (t1)

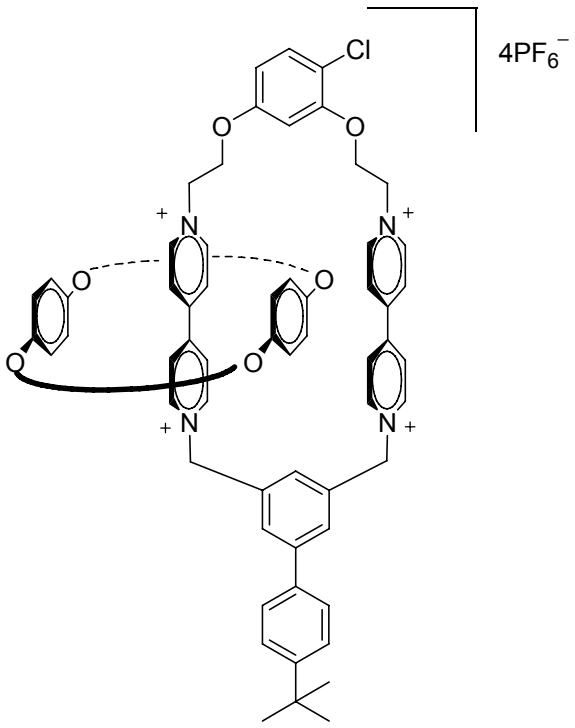

Catenane 3.2. 1,3-Bis(2-(4,4'-dipyridinium)ethoxy)-4-chlorobenzene bis(hexafluorophosphate) (0.128 g, 0.160 mmol) and BPP34C10 (0.223 g, 0.416 mmol) were combined and dissolved in CH_3CN (15 mL). This solution was allowed to stir for 10 min. at which point 5-bis(bromomethyl)-4'-(1,1'-dimethylethyl)-1,1'-biphenyl (0.0765 g, 0.192 mmol) was added and the reaction vessel sealed with a septum. This red solution stirred 4 d under ambient conditions after which time the solvent was removed *in vacuo*. The catenane was purified and after drying 51 mg, or a 17 % yield of pure product catenane **3.2** was recovered.

^{1}H NMR ($CDCl_3$, 400 MHz): δ ppm 9.34 (m, *J* = 7.0 Hz, 2H), 9.27 (m, *J* = 7.0 Hz, 2H), 9.13 (d, *J* = 7.1 Hz, 1H), 9.11 (d, *J* = 7.1 Hz, 1H), 8.44 (m, *J* = 4.1, 1.6 Hz, 2H), 8.29 (d, *J* = 4.8 Hz, 1H), 8.27 (d, *J* = 4.8 Hz, 1H), 8.23 (m, *J* = 7.0 Hz, 2H), 8.13 (m, *J* = 7.0 Hz, 2H), 8.00 (t, *J* = 1.4 Hz, 1H), 7.93 (m, *J* = 8.6 Hz, 2H), 7.66 (m, *J* = 8.6 Hz, 2H), 7.39 (d, *J* = 8.9 Hz, 1H), 6.89 (d, *J* = 2.7 Hz, 1H), 6.77 (dd, *J* = 8.9, 2.7 Hz, 1H),

6.26 (s, 2H), 6.24 (s, 2H), 5.66 (bs, 8H), 5.38 (m, 2H), 5.29 (m, 2H), 4.68 (m, *J* = 9.5, 5.0 Hz, 4H), 3.88-3.62 (m, 32H), 1.43 (s, 9H).

MS (ESI): 786.3 (M $2PF_6^{2+}$), 476.2 (M PF_6^{3+}), 427.6 (M^{3+}), 320.7 (M^{4+}) ($C_{76}H_{87}ClN_4O_{12}^{4+}$ requires 1283.97).

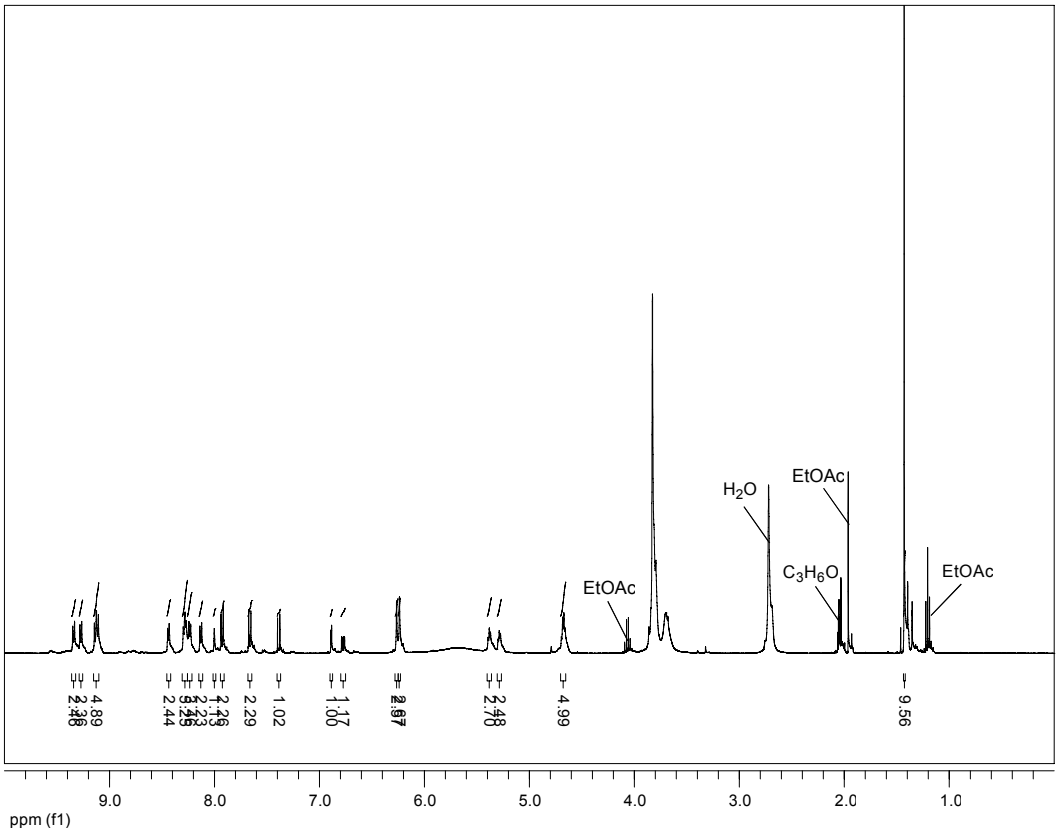

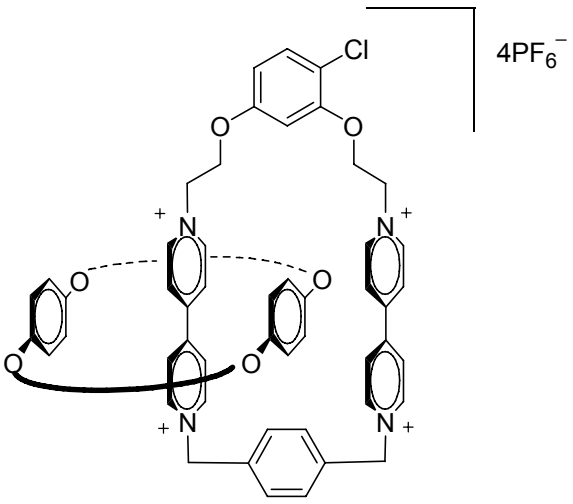

Catenane 3.3. 1,3-Bis(2-(4,4'-dipyridinium)ethoxy)-4-chlorobenzene bis(hexafluorophosphate) (0.128 g, 0.160 mmol) and BPP34C10 (0.223 g, 0.416 mmol) were combined and dissolved in CH_3CN (15 mL). This solution was allowed to stir for 10 min. at which point α,α'-dibromo-*p*-xylene (0.051 g, 0.19 mmol) was added and the reaction vessel sealed with a septum. This red solution stirred 4 d under ambient conditions after which time the solvent was removed *in vacuo*. The mixture was purified and after drying 70 mg (25 %) of pure product catenane **3.3** was recovered.

^{1}H NMR ($CDCl_3$, 400 MHz): δ ppm 9.37 (m, *J* = 7.1 Hz, 2H), 9.31 (m, *J* = 7.1 Hz, 2H), 9.15 (m, *J* = 7.1, 1.3 Hz, 4H), 8.25 (m, *J* = 7.1 Hz, 2H), 8.13 (m, *J* = 7.1 Hz, 2H), 8.08 (m, *J* = 7.0, 3.4 Hz, 4H), 8.06 (m, *J* = 2.5 Hz, 4H), 7.37 (d, *J* = 8.8 Hz, 1H), 6.82 (d, *J* = 2.7 Hz, 1H), 6.75 (dd, *J* = 8.8, 2.7 Hz, 1H), 6.10 (s, 2H), 6.07 (s, 2H), 5.64-5.39 (m, 8H), 5.35 (m, 2H), 5.25 (m, 2H), 4.69 (m, 2H), 4.64 (m, 2H), 3.91-3.82 (m, 20H), 3.80-3.76 (m, 6H), 3.66-3.62 (m, 6H).

MS (ESI): 1586.5 (M $3PF_6^+$), 720.3 (M $2PF_6^{2+}$), 432.2 (M PF_6^{3+}), 287.9 (M^{4+}) ($C_{66}H_{75}ClN_4O_{12}^{4+}$ requires 1151.77).

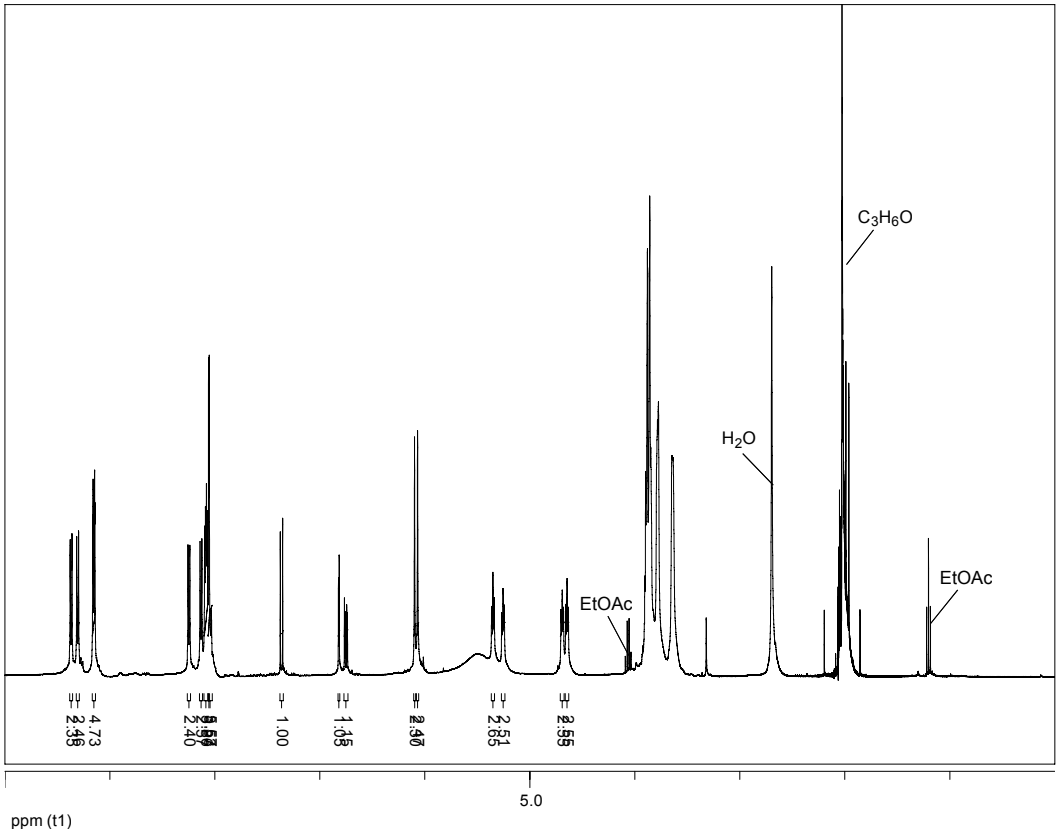
C3H6O
H2O
EtOAc
EtOAc
4.73
2.40
1.00
1.15
2.51
5.0
ppm (t1)

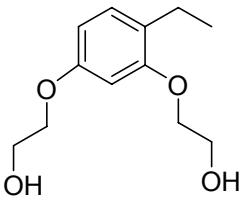

1,3-Bis(2-hydroxyethoxy)-4-ethylbenzene (3.11b). Sodium hydroxide (4.34 g, 108 mmol) was dissolved in a solution of ethanol (30 mL) and water (5 mL). To this solution was added 4-ethyl-benzene-1,3-diol (5.00 g, 36.2 mmol) previously dissolved in ethanol (15 mL) creating a dark red solution that was allowed to stir for 10 min. 2-Chloroethanol (8.74 g, 108 mmol) was added to the stirring solution after which the entirety was refluxed 3 d. Precipitate formed in the reaction vessel and the solution became ruby red in color. After cooling to room temperature, the solvent was removed *in vacuo* leaving a red solid that was dissolved in EtOAc (50 mL) and washed with water (100 mL). The water was extracted twice more with EtOAc (30 mL). After combining, the organic fractions were washed with brine (50 mL) and dried over $MgSO_4$. Flash chromatography using diethyl ether provided 6.6 g (81 % yield) of pure **3.11b**.

^{1}H NMR ($CDCl_3$, 300MHz): δ ppm 7.00 (d, *J* = 8.2 Hz, 1H), 6.53 (d, *J* = 2.4 Hz, 1H), 6.44 (dd, *J* = 8.2, 2.4 Hz, 1H), 4.07-4.00 (m, 6H), 3.93-3.82 (m, 4H), 2.56 (q, *J* = 7.5 Hz, 2H), 1.12 (t, *J* = 7.5, 3H)

^{13}C NMR ($CDCl_3$, 75MHz): δ ppm 160.3, 159.3, 130.8, 126.5, 106.9, 101.5, 71.5, 71.4, 62.40, 62.37, 24.2, 16.0.

MS (EI): m/z 226.2 (M^+), 211.2, 183.2, 149.1, 139.1, 123.1; (EI): m/z 249.1 (M Na^+) ($C_{12}H_{18}O_4$ requires 226.3).

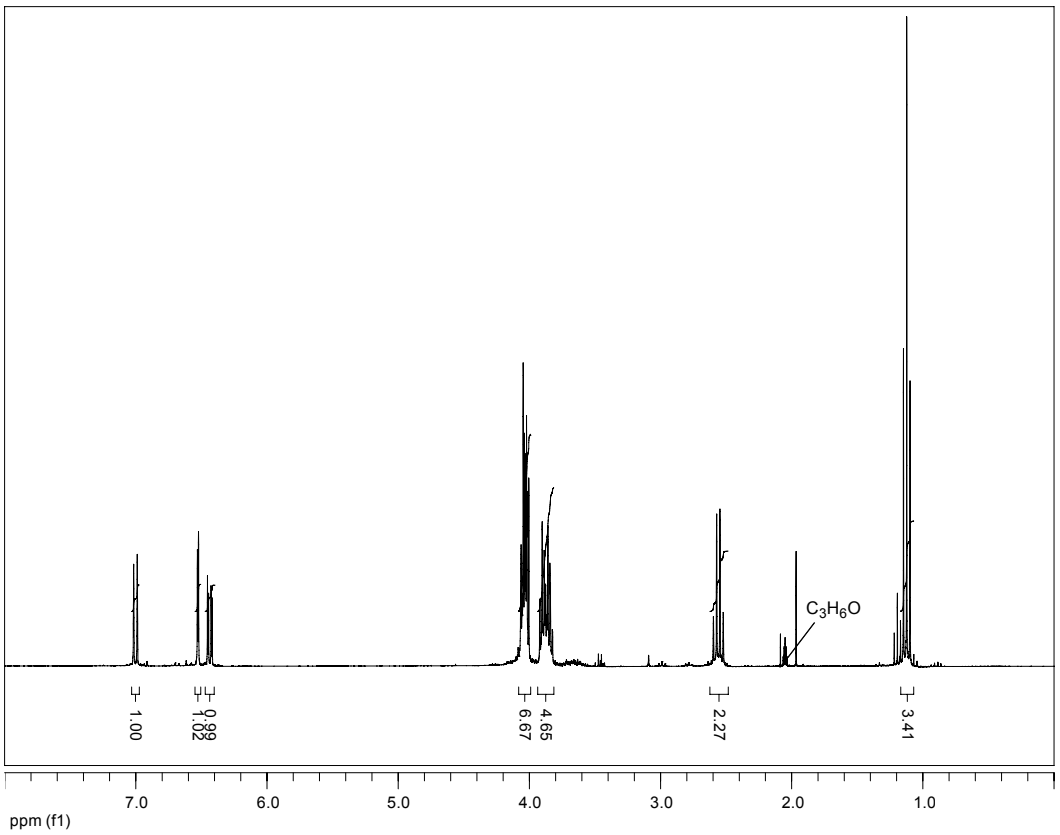
C3H6O
1.00
1.09
1.02
9.87
4.95
2.27
3.41
7.0
6.0
5.0
4.0
3.0
2.0
1.0
ppm (f1)

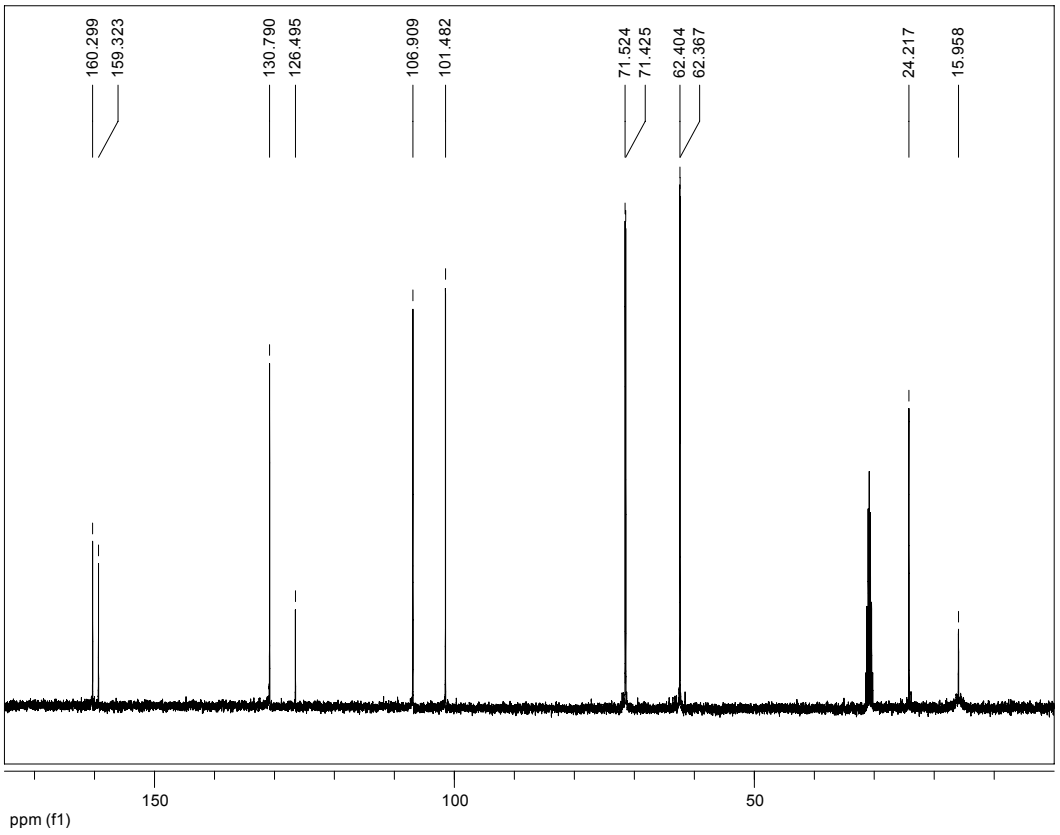
160.299
159.323
130.790
126.495
106.909
101.482
71.524
71.425
62.404
62.367
24.217
15.958
150
100
50
ppm (f1)

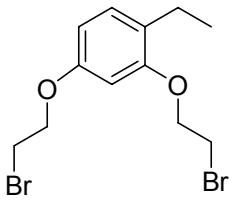

1,3-Bis(2-bromoethoxy)-4-ethylbenzene (3.12b). PPh_3 (21.84 g, 83.24 mmol) was added to CH_3CN (100 mL) and cooled to -10 ° C. Br_2 (13.30 g, 83.24 mmol) dissolved in CH_3CN (20 mL) was slowly added to the stirring PPh_3 mixture so as not to exceed 0 ° C. The mixture was allowed to warm to room temperature after the addition was complete. 1,3-Bis(2-hydroxyethoxy)-4-ethyl-benzene (8.04 g, 36.1 mmol) dissolved in CH_3CN (20 mL) was added to the mixture and allowed to stir for 5 hours. Solvent was removed *in vacuo* and the crude product purified via column chromatography using CH_2Cl_2 to elute. The product was obtained in 95 % yield (12.1 g) and analysis by NMR showed it to be pure **3.12b**.

^{1}H NMR ($CDCl_3$, 300MHz): δ ppm 7.06 (d, *J* = 8.5 Hz, 1H), 6.45 (dd, *J* = 8.4, 2.2 Hz, 1H), 6.42 (s, 1H), 4.27 (m, *J* = 6.1 Hz, 4H), 3.67 (m, *J* = 6.1 Hz, 2H), 3.62 (m, *J* = 6.1 Hz, 2H), 2.61 (q, *J* = 7.5 Hz, 2H), 1.18 (t, *J* = 7.5 Hz, 3H).

MS (EI): m/z 352.0 (M^+) ($C_{12}H_{16}O_2Br_2$ requires 352.1).

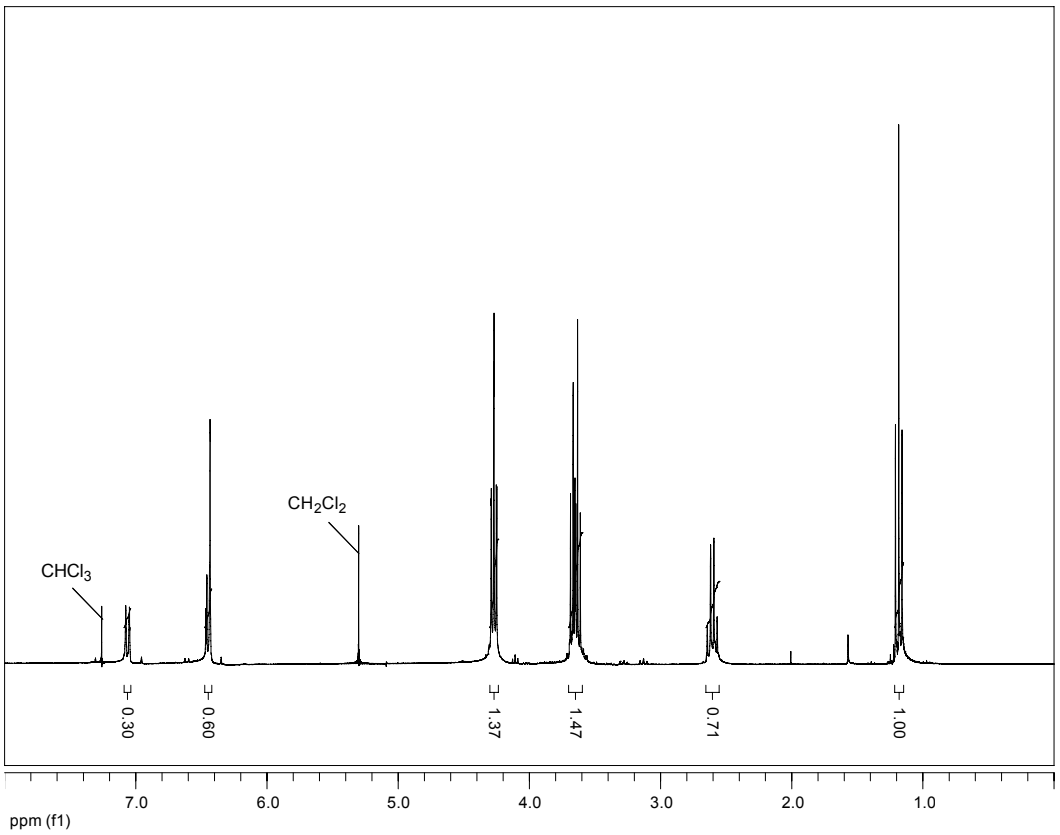
CHCl3
CH2Cl2
0.30
0.60
1.37
1.47
0.71
1.00
7.0
6.0
5.0
4.0
3.0
2.0
1.0
ppm (f1)

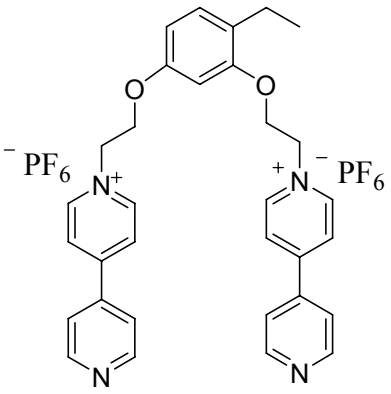

1,3-Bis(2-(4,4'-dipyridinium)ethoxy)-4-ethylbenzene bis(hexafluorophosphate) (3.13b). 1,3-Bis(2-bromoethoxy)-4-ethyl-benzene (8.7 g, 25 mmol) and 4,4-dipyridyl (15.6 g, 100 mmol) were added to 100 mL of CH_3CN. This solution was stirred at 70 ° C for two d during which time a yellow brown solid was deposited on the sides of the flask. After cooling to room temperature the solvent was decanted and the solid washed with additional CH_3CN (2x30 mL). Residual solvent was then removed *in vacuo* leaving a brown solid. Water was added and upon heating the solid dissolved producing a yellow solution. Addition of NH_4PF_6 (12.0 g, 0.750 mmol) produced a yellow oil which was isolated and washed with $CHCl_3$ (3x30 mL) to extract impurities leaving a yellow oil which was then dissolved in CH_3CN and dried with $MgSO_4$. Removal of the solvent *in vacuo* left 18.3 g of solid yellow **3.13b** for a yield of 92 %.

^{1}H NMR ($CDCl_3$, 300MHz): δ ppm 9.39 (m, *J* = 6.6 Hz, 2H), 9.35 (m, *J* = 6.6 Hz, 2H), 8.89 (m, *J* = 6.2, 2.7 Hz, 4H), 8.76 (m, *J* = 7.0 Hz, 2H), 8.70 (m, *J* = 6.9 Hz, 2H), 8.03 (m, 4H), 7.02 (d, *J* = 8.3 Hz, 1H), 6.66 (d, *J* = 2.4 Hz, 1H), 6.53 (dd, *J* = 8.3, 2.4 Hz, 1H), 5.37 (m, 2H), 5.32 (m, 2H), 4.67 (m, 4H), 2.45 (q, *J* = 7.5 Hz, 2H), 0.97 (t, *J* = 7.5 Hz, 3H).

MS (ESI): m/z 649.2 (M PF_6^+), 252.1 (M^{2+}) ($C_{32}H_{32}O_2N_4^{2+}$ requires 504.6).

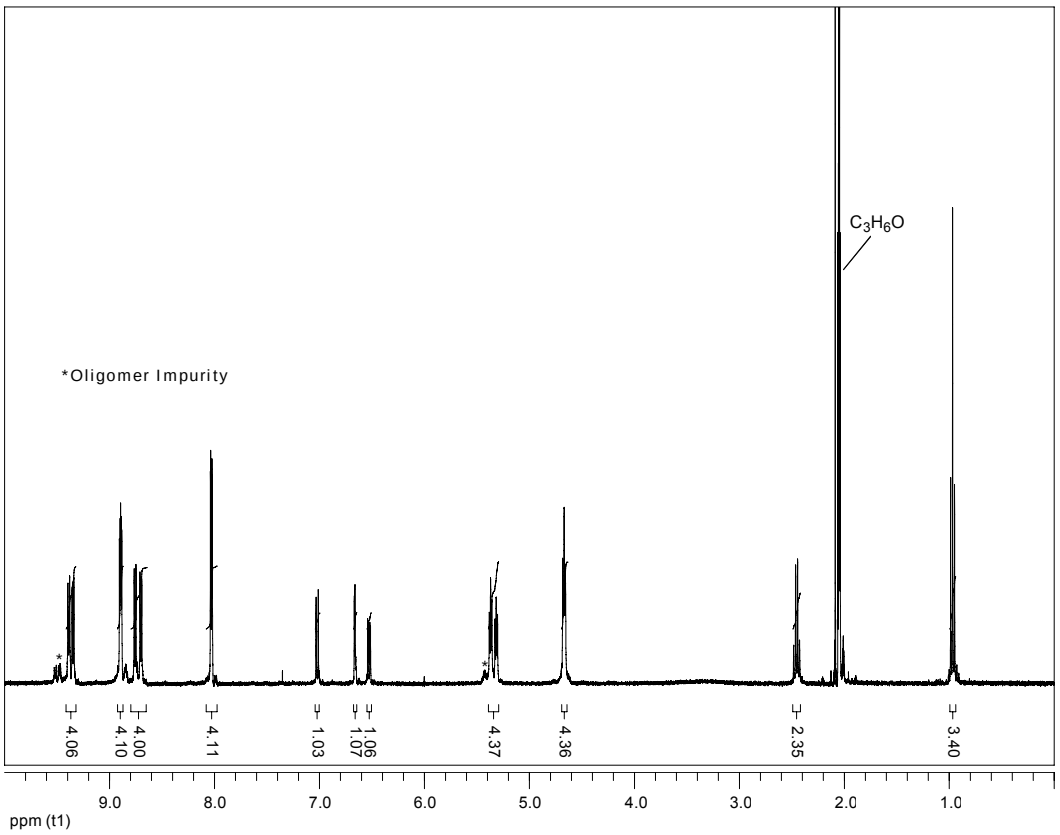
C_3H_6O
*Oligomer Impurity
4.06
4.10
4.00
4.11
1.03
1.06
1.07
4.37
4.36
2.35
3.40
9.0
8.0
7.0
6.0
5.0
4.0
3.0
2.0
1.0
ppm (t1)

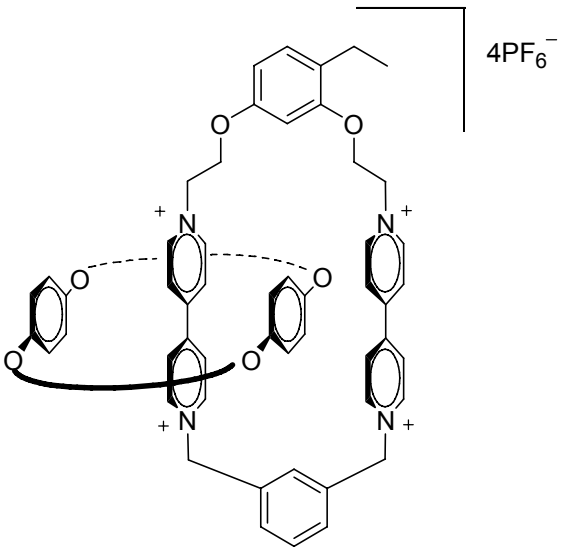

Catenane 3.4. 1,3-Bis(2-(4,4'-dipyridinium)ethoxy)-4-ethylbenzene bis(hexafluorophosphate) (0.123 g, 0.160 mmol) and BPP34C10 (0.172 g, 0.320 mmol) were combined and dissolved in CH_3CN (15 mL). This solution was allowed to stir for 10 min. at which point α,α'-dibromo-*m*-xylene (0.051 g, 0.19 mmol) was added and the reaction vessel sealed with a septum. This red solution stirred 4 d under ambient conditions after which time the solvent was removed *in vacuo*. The catenane was purified and after drying 29 mg (11 %) of pure product catenane **3.4** was recovered. **^{1}H NMR** ($CDCl_3$, 400 MHz): δ ppm 9.25 (m, *J* = 7.0 Hz, 2H), 9.15 (m, *J* = 7.0 Hz, 4H), 9.09 (m, *J* = 7.0 Hz, 2H), 8.28 (m, *J* = 7.0 Hz, 2H), 8.27-8.22 (m, 4H), 8.16 (dd, *J* = 7.7, 1.2 Hz, 2H), 8.11 (m, *J* = 7.0 Hz, 2H), 8.06 (t, *J* = 1.2, Hz, 1H), 7.89 (t, *J* = 7.7 Hz, 1H), 7.16 (d, *J* = 8.4 Hz, 1H), 6.76 (d, *J* = 2.4 Hz, 1H), 6.65 (dd, *J* = 8.4, 2.4 Hz, 1H), 6.19 (s, 2H), 6.16 (s, 2H), 5.72 (bs, 8H), 5.36 (m, *J* = 4.9 Hz, 2H), 5.27 (m, *J* = 4.8 Hz, 2H), 4.64 (m, *J* = 4.9 Hz, 2H), 4.59 (m, *J* = 4.8 Hz, 2H), 3.89-3.63 (m, 32H), 2.68 (q, *J* = 7.7 Hz, 2H), 1.20 (t, *J* = 7.7 Hz, 3H)

MS (ESI): 717.3 (M $2PF_6^{2+}$), 430.2 (M PF_6^{3+}), 286.3 (M^{4+}) ($C_{68}H_{80}N_4O_{12}^{4+}$ requires 1145.38).

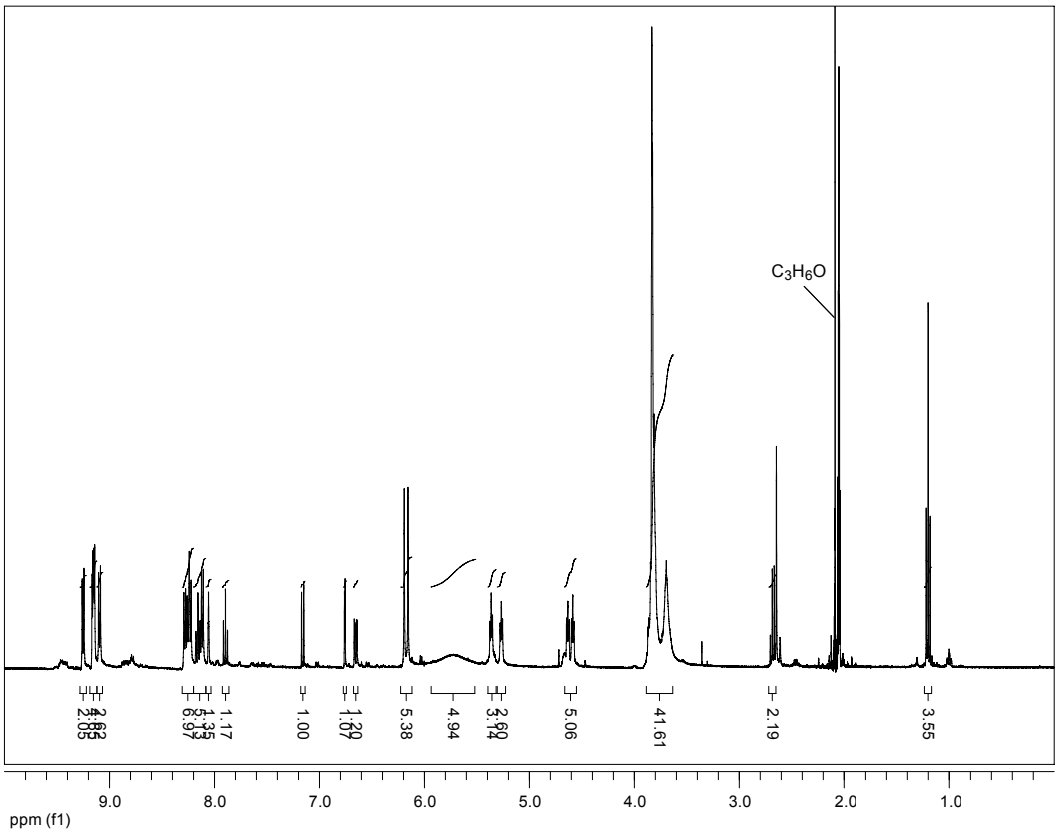

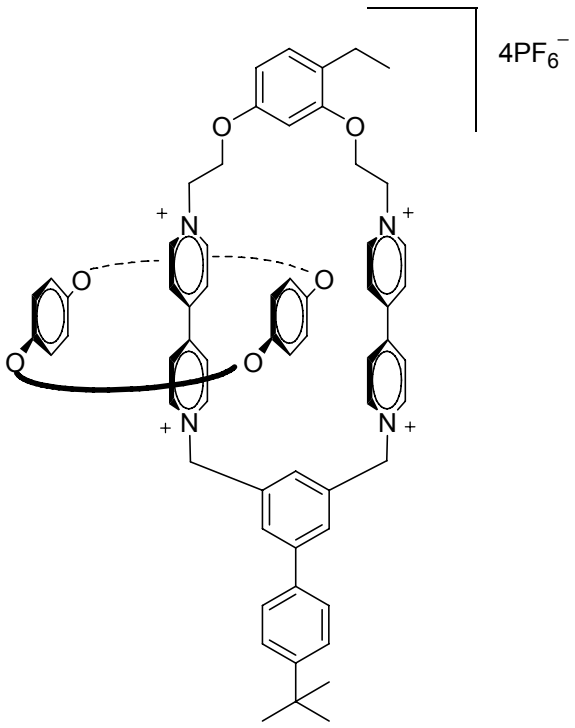

Catenane 3.5. 1,3-Bis(2-(4,4'-dipyridinium)ethoxy)-4-ethylbenzene bis(hexafluorophosphate) (0.123 g, 0.160 mmol) and BPP34C10 (0.223 g, 0.416 mmol) were combined and dissolved in CH_3CN (15 mL). This solution was allowed to stir for 10 min. at which point 5-bis(bromomethyl)-4'-(1,1'-dimethylethyl)-1,1'-biphenyl (0.0765 g, 0.192 mmol) was added and the reaction vessel sealed with a septum. This red solution stirred 4 d under ambient conditions after which time the solvent was removed *in vacuo*. The catenane was purified and after drying 48 mg (16 %) of pure product catenane **3.5** was recovered.

^{1}H NMR ($CDCl_3$, 400 MHz): δ ppm 9.34 (m, *J* = 6.6 Hz, 2H), 9.27 (m, *J* = 6.6 Hz, 2H), 9.15 (m, *J* = 7.0 Hz, 2H), 9.10 (m, *J* = 7.0 Hz, 2H), 8.44 (m, *J* = 6.6 Hz, 2H), 8.26 (m, *J* = 6.6, 7.0 Hz, 6H), 8.11 (m, *J* = 7.0 Hz, 2H), 8.00 (t, *J* = 1.5 Hz, 1H), 7.93 (m, *J* = 8.5 Hz, 2H), 7.66 (m, *J* = 8.5 Hz, 2H), 7.16 (d, *J* = 8.4 Hz, 1H), 6.76 (d, *J* = 2.4 Hz, 1H), 6.66 (dd, *J* = 8.4, 2.4 Hz, 1H), 6.27 (s, 2H), 6.23 (s, 2H), 6.03-5.46 (m, 8H), 5.36

(m, 2H), 5.27 (m, 2H), 4.63 (m, 2H), 4.58 (m, 2H), 3.87-3.64 (m, 32H), 2.68 (q, J = 7.5 Hz, 2H), 1.43 (s, 9H), 1.20 (t, J = 7.5 Hz, 3H)

MS (ESI): m/z 1718.6 (M $3PF_6^+$), 783.3 (M $2PF_6^{2+}$), 473.9 (M PF_6^{3+}), 427.6 (M^{3+}), 319.4 (M^{4+}) ($C_{78}H_{92}N_4O_{12}^{4+}$ requires 1277.58).

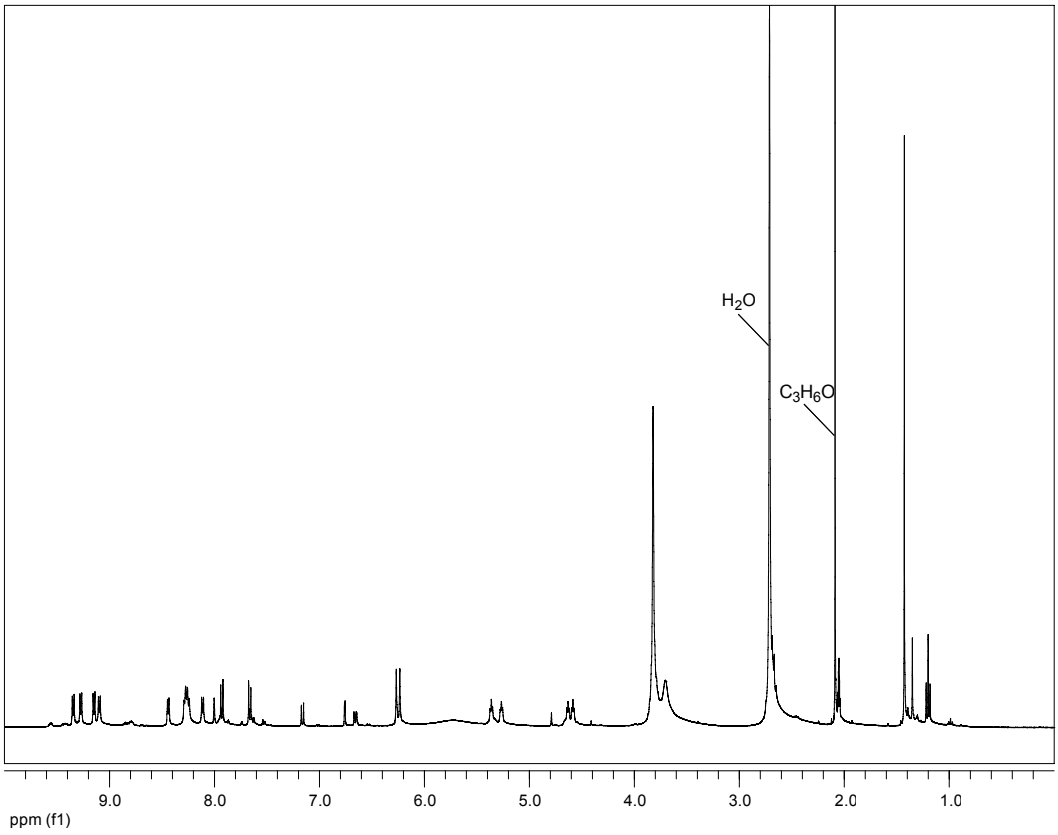

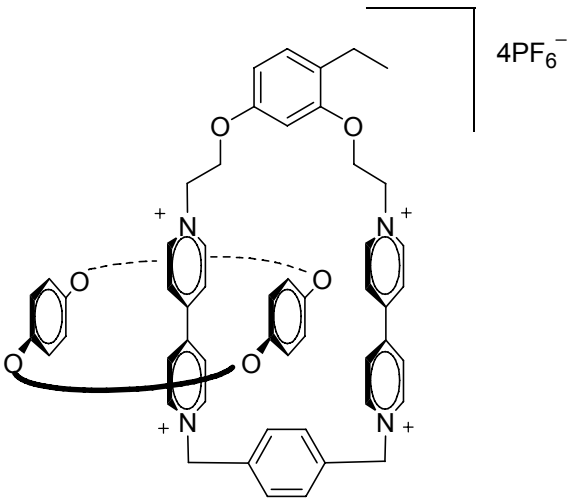

Catenane 3.6. 1,3-Bis(2-(4,4'-dipyridinium)ethoxy)-4-ethylbenzene bis(hexafluorophosphate) (0.123 g, 0.160 mmol) and BPP34C10 (0.223 g, 0.416 mmol) were combined and dissolved in CH_3CN (15 mL). This solution was allowed to stir for 10 min. at which point α,α'-dibromo-*p*-xylene (0.051 g, 0.19 mmol) was added and the reaction vessel sealed with a septum. This red solution stirred 3 d under ambient conditions after which time the solvent was removed *in vacuo*. The catenane was purified and after drying 67 mg (24 %) of pure product **3.6** was recovered.

^{1}H NMR ($CDCl_3$, 400 MHz): δ ppm 9.40 (m, *J* = 7.0 Hz, 2H), 9.34 (m, *J* = 7.0 Hz, 2H), 9.20 (m, *J* = 7.0 Hz, 2H), 9.15 (m, *J* = 7.0 Hz, 2H), 8.29 (m, *J* = 7.0 Hz, 2H), 8.15 (m, *J* = 7.0 Hz, 4H), 8.11-8.04 (m, 6H), 7.14 (d, *J* = 8.4 Hz, 1H), 6.69 (d, *J* = 2.4 Hz, 1H), 6.63 (dd, *J* = 8.4, 2.4 Hz, 1H), 6.11 (s, 2H), 6.08 (s, 2H), 5.35 (m, 2H), 5.26 (m, 2H), 4.64 (m, 2H), 4.58 (m, 2H), 3.95-3.48 (m, 32H), 2.63 (dd, *J* =7.5 Hz, 2H), 1.16 (t, *J* = 7.5 Hz, 3H).

MS (ESI): 572.3 (M^{2+}), 381.5 (M^{3+}), 286.1 (M^{4+}) ($C_{68}H_{80}N_4O_{12}{}^{4+}$ requires 1145.38).

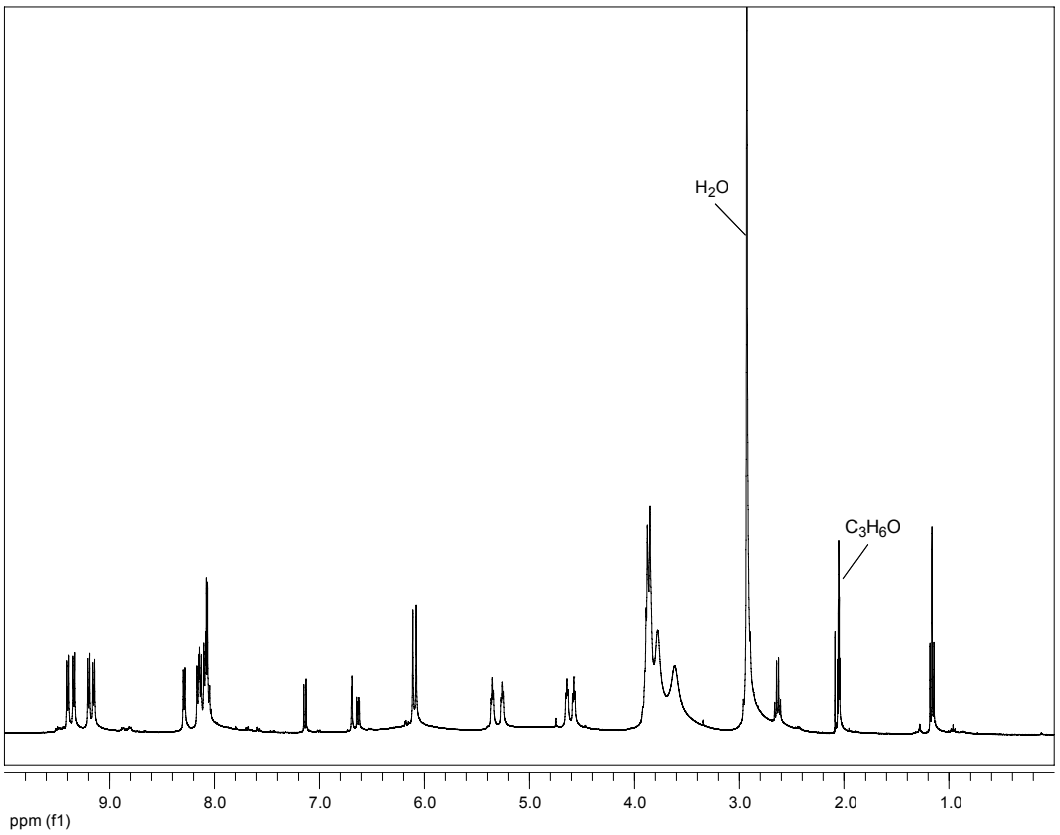
H2O
C3H6O
9.0
8.0
7.0
6.0
5.0
4.0
3.0
2.0
1.0
ppm (f1)

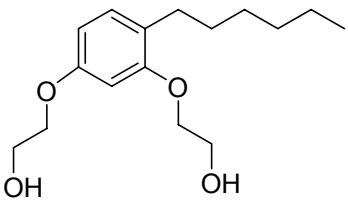

1,3-Bis(2-hydroxyethoxy)-4-*n*-hexylbenzene (3.11c). Sodium hydroxide (4.73 g, 118 mmol) was dissolved in a solution of ethanol (50 mL) and water (15 mL). To this solution was added 4-*n*-hexyl-benzene-1,3-diol (7.66 g, 39.0 mmol) previously dissolved in ethanol (15 mL) creating a dark red solution that was allowed to stir for 10 min. 2-Chloroethanol (9.52 g, 7.93 mL, 118 mmol) was added to the stirring solution after which the entirety was refluxed 4 d. Precipitate formed in the reaction vessel and the solution became ruby red in color. After cooling to room temperature, the solvent was removed *in vacuo* leaving a red solid that was dissolved in EtOAc (50 mL) and washed with water (100 mL). The water was extracted twice more with EtOAc (30 mL). After combining, the organic fractions were washed with brine (50 mL) and dried over $MgSO_4$. Flash chromatography using diethyl ether provided 10.0 g (72 % yield) of pure **3.11c**.

^{1}H NMR ($CDCl_3$, 300MHz): δ 7.02 (d, *J* = 8.3 Hz, 1H), 6.48-6.42 (m, 2H), 4.04 (m, *J* = 8.3 Hz, 4H), 3.94 (m, *J* = 8.3 Hz, 4H), 2.54 (m, 2H), 2.31 (bs, 2H), 1.58-1.47 (m, 2H), 1.35-1.25 (m, 7H), 0.88 (m, 3H).

^{13}C NMR (C_3D_6O, 75MHz): δ 160.3, 159.4, 131.6, 125.1, 106.9, 101.5, 71.5, 71.4, 62.4, 62.4, 33.5, 31.9, 31.1, 24.3, 15.4.

MS (EI): m/z 282.1 (M^+), 211.1, 149.1, 121.2 ($C_{16}H_{26}O_4$ requires 282.4).

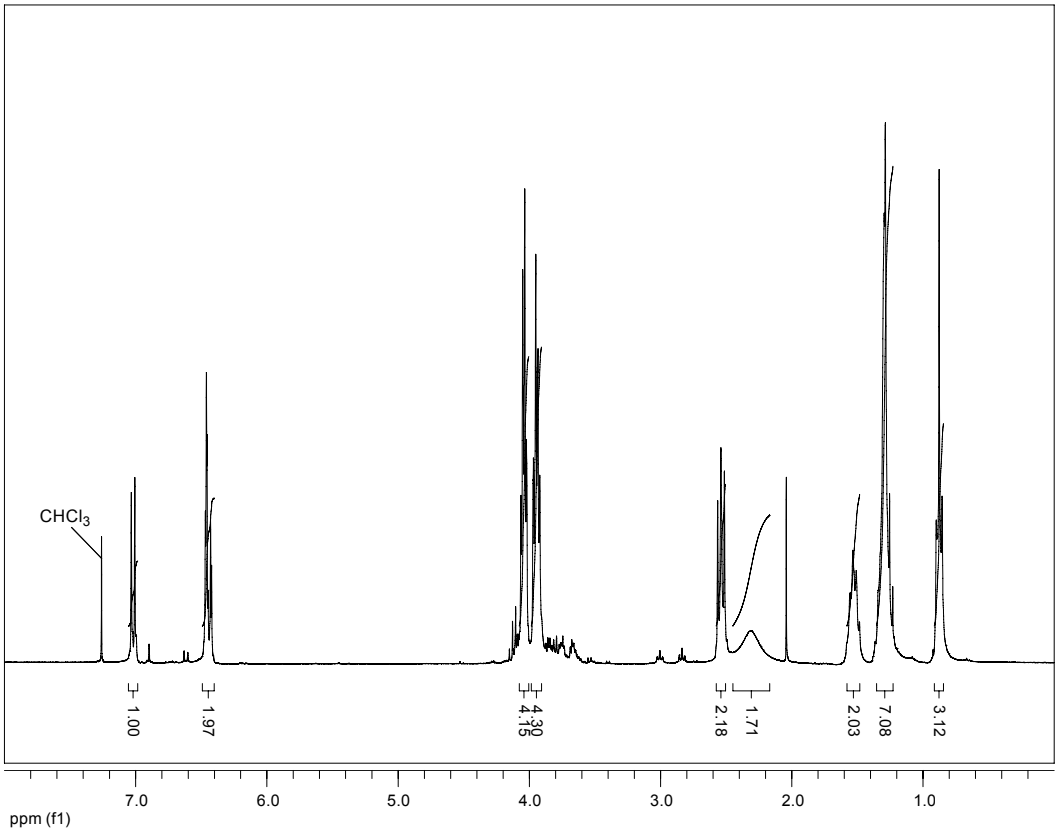
CHCl3
1.00
1.97
4.30
4.15
2.18
1.71
2.03
7.08
3.12
7.0
6.0
5.0
4.0
3.0
2.0
1.0
ppm (f1)

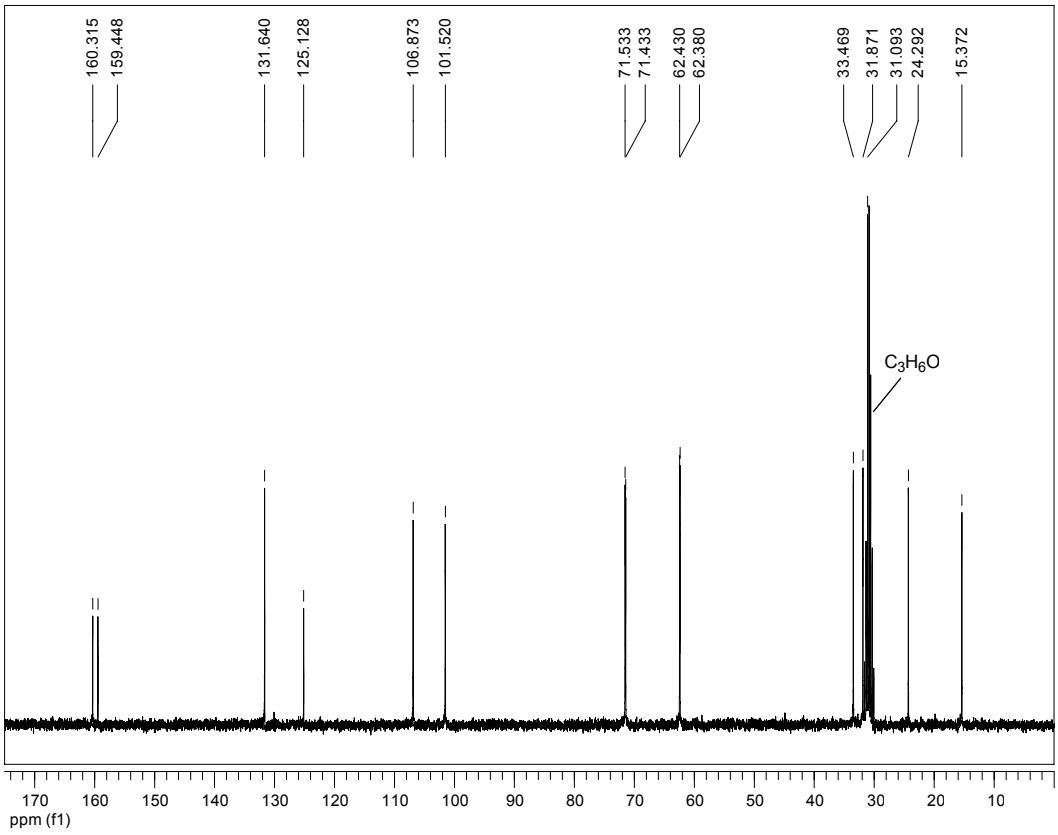
160.315
159.448
131.640
125.128
106.873
101.520
71.533
71.433
62.430
62.380
33.469
31.871
31.093
24.292
15.372
C3H6O
170
160
150
140
130
120
110
100
90
80
70
60
50
40
30
20
10
ppm (f1)

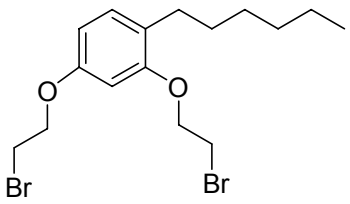

1,3-Bis(2-bromoethoxy)-4-*n*-hexylbenzene (3.12c). PPh_3 (12.63 g, 48.10 mmol) was added to CH_3CN (100 mL) and cooled to -10 ° C. Br_2 (7.69 g, 5.50 mmol) dissolved in CH_3CN (10 mL) was slowly added to the stirring PPh_3 mixture so as not to exceed 0 ° C. The mixture was allowed to warm to room temperature after the addition was complete. 1,3-Bis(2-hydroxyethoxy)-4-*n*-hexyl-benzene (5.24 g, 48.1 mmol) dissolved in CH_3CN (10 mL) was added to the mixture and allowed to stir overnight. Solvent was removed *in vacuo* and the crude product purified via column chromatography using CH_2Cl_2 to elute. The product was obtained in 100 % yield (7.9 g) and analysis by NMR showed it to be pure **3.12c**.

^{1}H NMR ($CDCl_3$, 300MHz): δ ppm 7.04 (d, *J* = 6.1 Hz, 1H), 6.46-6.41 (m, 2H), 4.26 (m, *J* = 6.1 Hz, 4H), 3.66 (m, *J* = 6.1 Hz, 2H), 3.63 (m, *J* = 6.2 Hz, 2H), 2.56 (m, 2H), 1.62-1.50 (m, 2H), 1.37-1.29 (m, 6H), 0.93-0.86 (m, 3H)

MS (EI): m/z 407.9 (M^+), 346.0 ($C_{16}H_{24}O_2Br_2$ requires 408.2).

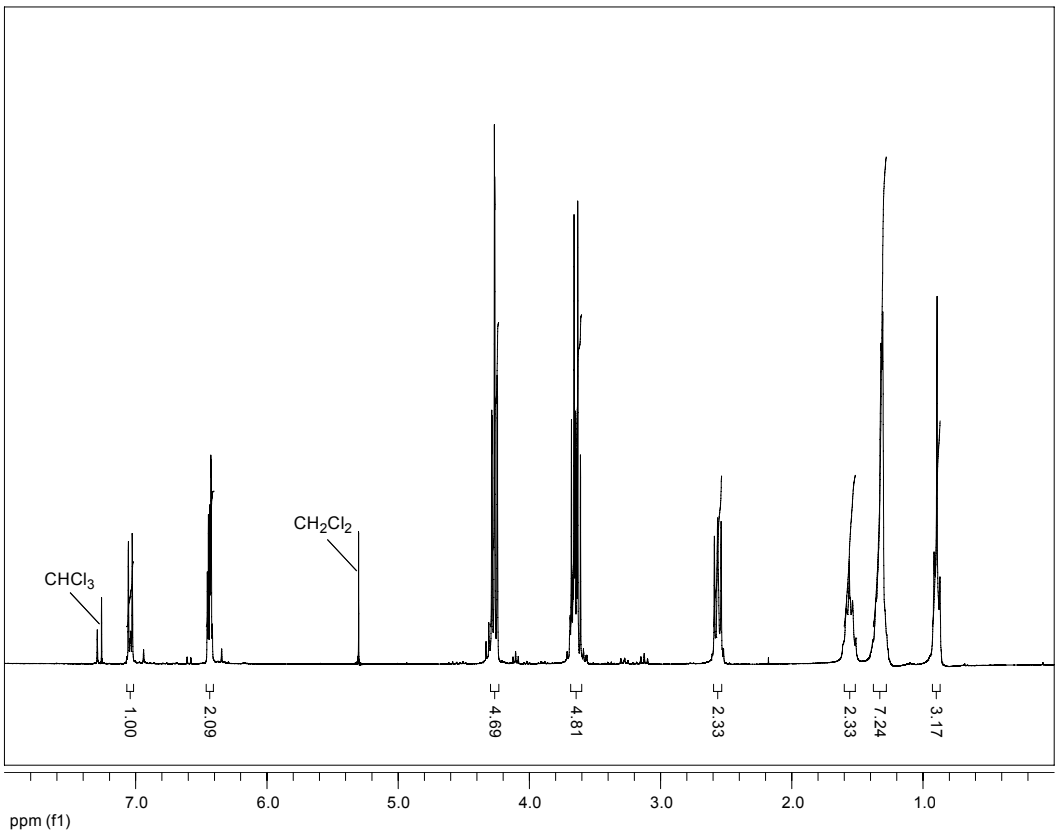
CHCl3
CH2Cl2
1.00
2.09
4.69
4.81
2.33
2.33
7.24
3.17
7.0
6.0
5.0
4.0
3.0
2.0
1.0
ppm (f1)

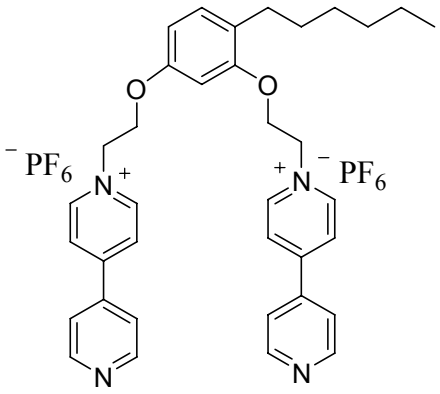

1,3-Bis(2-(4,4'-dipyridinium)ethoxy)-4-*n*-hexylbenzene bis(hexafluorophosphate) (3.13c). 1,3-Bis(2-bromoethoxy)-4-*n*-hexyl-benzene (1.00 g, 2.45 mmol) and 4,4-dipyridyl (1.66 g, 10.6 mmol) were added to 15mL of CH_3CN. This solution was stirred at 70 ° C for two d during which a dark yellow solid was produced. After cooling to room temperature the solvent was decanted with residual solvent being removed *in vacuo* leaving a brown solid. Water was added and upon heating the solid dissolved producing a brown solution. Addition of NH_4PF_6 (11 g) produced a brown oil which was isolated and washed with $CHCl_3$ (3x20 mL) to remove impurities leaving a yellow oil which was then dissolved in CH_3CN and dried with $MgSO_4$. Removal of the solvent *in vacuo* left 1.7 g (96 %) of solid, yellow **3.13c**.

^{1}H NMR ($CDCl_3$, 300MHz): δ ppm 9.47 (m, *J* = 7.1 Hz, 2H), 9.40 (m, *J* = 7.1 Hz, 2H), 8.87 (m, 4H), 8.74 (m, *J* = 7.1 Hz, 4H), 8.01 (m, *J* = 6.1 Hz, 4H), 7.00 (d, *J* = 8.3 Hz, 1H), 6.73 (d, *J* = 2.4 Hz, 1H), 6.51 (dd, *J* = 8.3, 2.4 Hz, 1H), 5.38 (m, 2H), 5.33 (m, 2H), 4.71 (m, *J* = 5.0 Hz, 4H), 2.41 (m, 2H), 1.33-1.23 (m, 2H), 1.21-1.09 (m, 6H), 0.73 (m, 3H).

MS (ESI): m/z 705.3 (M PF_6^+), 280.1 (M^{2+}) ($C_{36}H_{40}O_2N_4^{2+}$ requires 560.7).

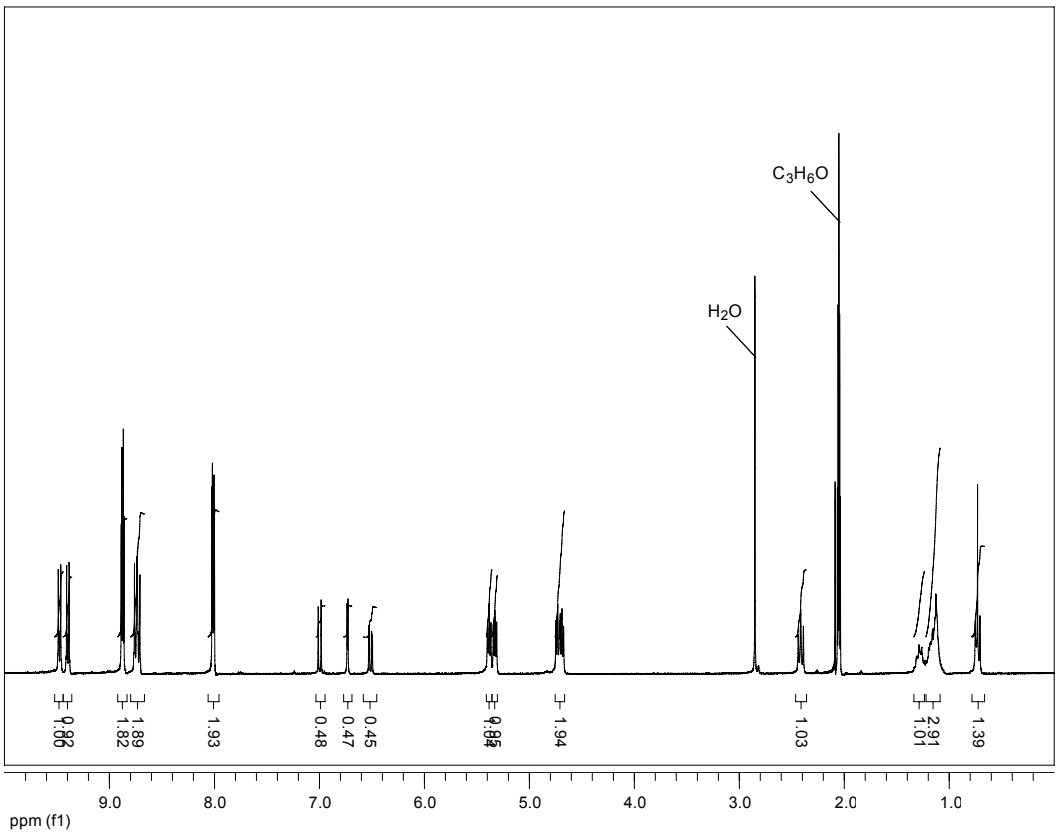
C3H6O
H2O
1.82
1.89
1.93
0.48
0.47
0.45
1.94
1.03
1.01
2.91
1.39
9.0
8.0
7.0
6.0
5.0
4.0
3.0
2.0
1.0
ppm (f1)

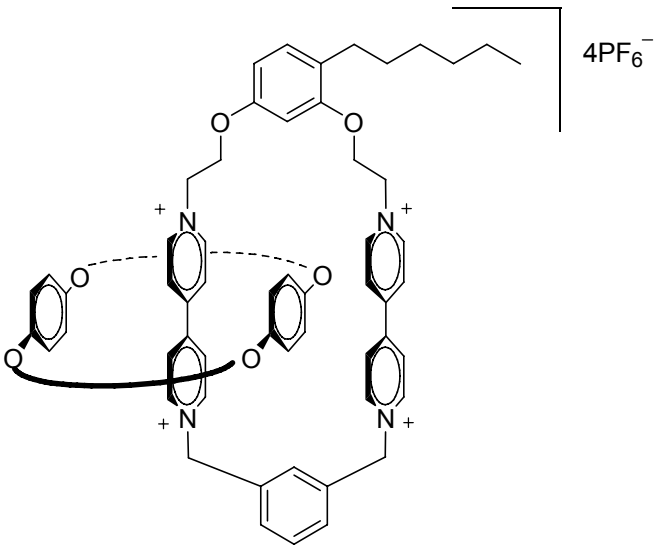

Catenane 3.7. 1,3-Bis(2-(4,4'-dipyridinium)ethoxy)-4-*n*-hexylbenzene bis(hexafluorophosphate) (**3.13c**) (0.123 g, 0.160 mmol) and BPP34C10 (0.223 g, 0.416 mmol) were combined and dissolved in CH_3CN (15 mL). This solution was allowed to stir for 10 min. at which point α,α'-dibromo-*m*-xylene (0.051 g, 0.192 mmol) was added and the reaction vessel sealed with a septum. This red solution stirred 4 d under ambient conditions after which time the solvent was removed *in vacuo*. The catenane was purified and after drying 43 mg (15 %) of pure product **3.7** was recovered.

^{1}H NMR ($CDCl_3$, 400 MHz): δ 9.26 (m, *J* = 6.9 Hz, 2H), 9.17 (m, *J* = 6.9 Hz, 4H), 9.09 (m, *J* = 6.9 Hz, 2H), 8.31-8.23 (m, 6H), 8.19-8.11 (m, 4H), 8.07-8.05 (m, 1H), 7.90 (t, *J* = 7.7 Hz, 1H), 7.16 (d, *J* = 8.4 Hz, 1H), 6.78 (d, *J* = 2.4 Hz, 1H), 6.66 (dd, *J* = 8.4, 2.4 Hz, 1H), 6.20 (s, 2H), 6.17 (s, 2H), 5.77 (bs, 8H), 5.36 (s, 2H), 5.28 (s, 2H), 4.61 (m, *J* = 4.9 Hz, 4H), 3.90-3.62 (m, 32H), 2.08 (m, *J* = 3.1 Hz, 2H), 1.68-1.56 (m, 2H), 1.43-1.29 (m, 6H), 0.91 (t, *J* = 6.9 Hz, 3H).

MS (ESI): 745.3 (M $2PF_6^{2+}$), 672.8 (M PF_6^{2+}), 600.5 (M^{2+}), 448.6 (M PF_6^{3+}), 400.2 (M^{3+}), 300.2 (M^{4+}) ($C_{72}H_{88}N_4O_{12}^{4+}$ requires 1201.49).

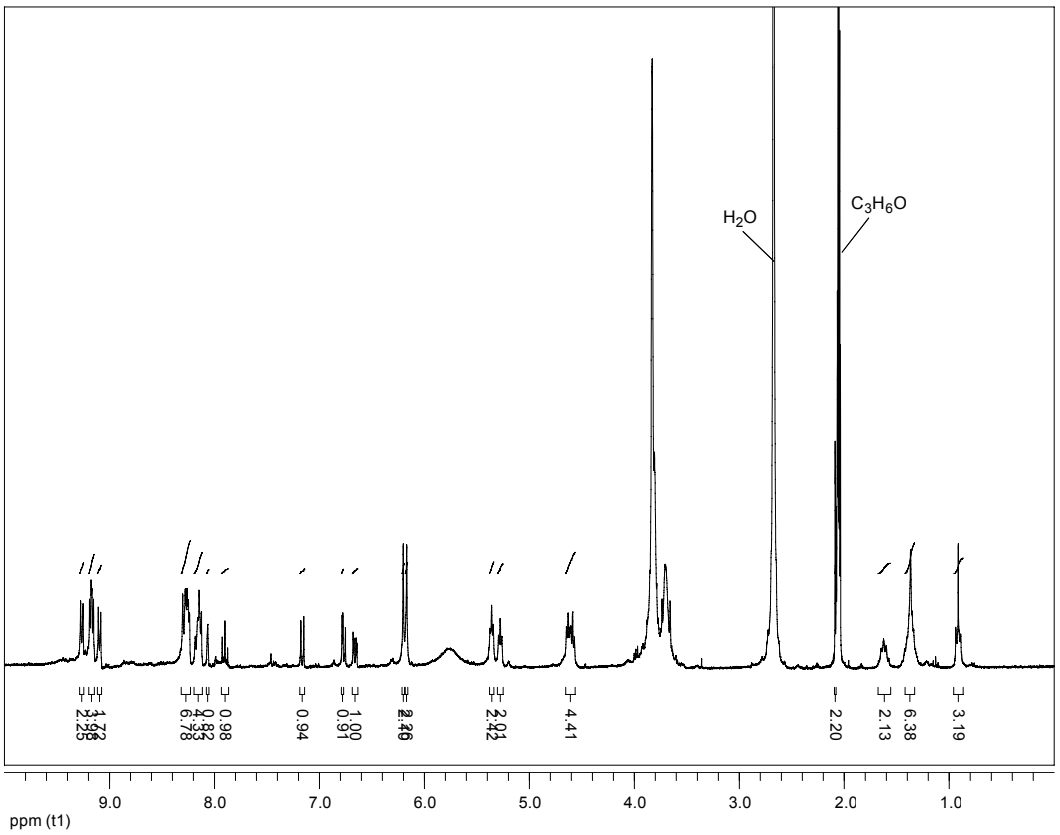
H2O
C3H6O
9.0
8.0
7.0
6.0
5.0
4.0
3.0
2.0
1.0
ppm (t1)

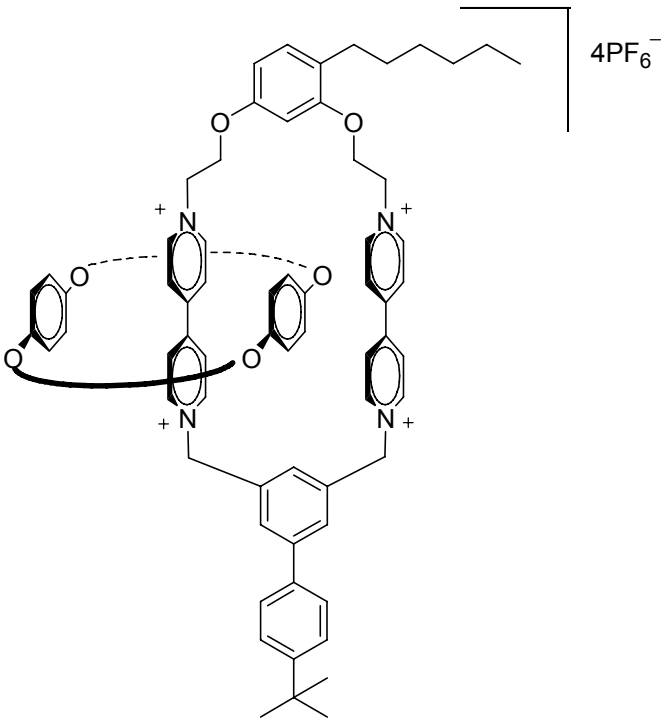

Catenane 3.8. 1,3-Bis(2-(4,4'-dipyridinium)ethoxy)-4-*n*-hexylbenzene bis(hexafluorophosphate) (0.123 g, 0.160 mmol) and BPP34C10 (0.223 g, 0.416 mmol) were combined and dissolved in CH_3CN (15 mL). This solution was allowed to stir for 10 min. at which point α,α'-dibromo-*p*-xylene (0.051 g, 0.192 mmol) was added and the reaction vessel sealed with a septum. This red solution stirred 4 d under ambient conditions after which time the solvent was removed *in vacuo*. The catenane was purified and after drying 17 mg (6 %) of pure product **3.8** was recovered.

^{1}H NMR ($CDCl_3$, 400 MHz): δ ppm 9.34 (m, *J* = 6.7 Hz, 2H), 9.28 (m, *J* = 6.7 Hz, 2H), 9.14 (m, *J* = 6.6 Hz, 2H), 9.07 (m, 2H), 8.44 (m, *J* = 3.8 Hz, 2H), 8.36-8.06 (m, 2H), 8.01 (m, 1H), 7.94 (d, *J* = 8.5 Hz, 2H), 7.66 (d, *J* = 8.5 Hz, 2H), 7.15 (d, *J* = 8.5 Hz, 1H), 6.77 (d, *J* = 2.0 Hz, 1H), 6.65 (dd, *J* = 8.4, 2.0 Hz, 1H), 6.26 (s, 2H), 6.23 (s, 2H), 5.74 (bs, 8H), 5.34 (m, 2H), 5.26 (m, 2H), 4.64-4.55 (m, 4H), 3.88-3.63 (m, 32H),

2.68-2.65 (m, 2H), 1.62 (m, 2H), 1.43 (s, 9H), 1.40-1.33 (m, 7H), 0.91 (m, *J* = 6.9 Hz, 3H)

MS (ESI): 666.4 (M^{2+}), 492.9 (M PF_6^{3+}), 333.2 (M^{4+}) ($C_{82}H_{100}N_4O_{12}^{4+}$ requires 1333.69).

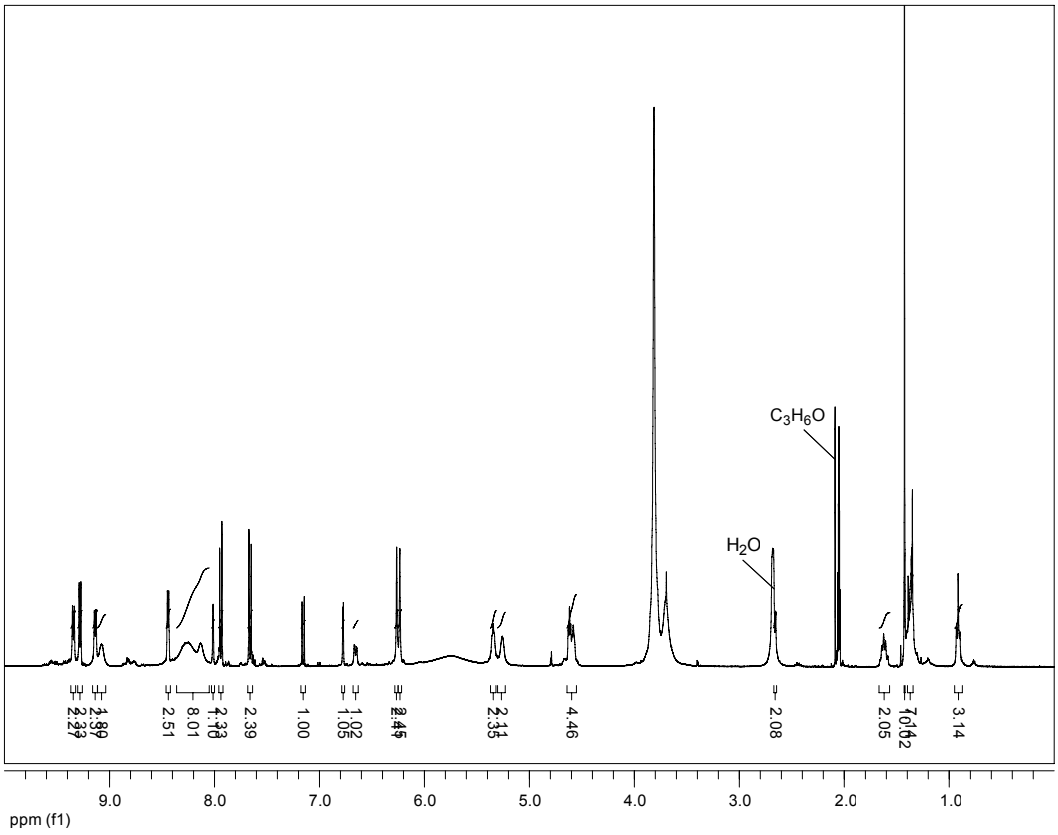

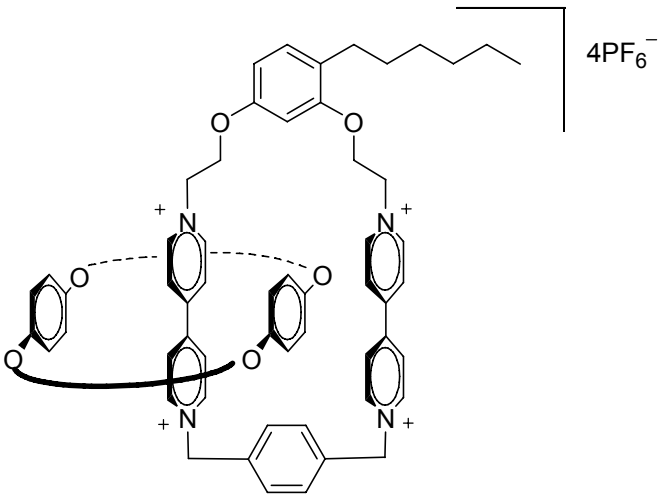

Catenane 3.9. 1,3-Bis(2-(4,4'-dipyridinium)ethoxy)-4-*n*-hexylbenzene bis(hexafluorophosphate) (15a) (0.123 g, 0.160 mmol) and BPP34C10 (0.223 g, 0.416 mmol) were combined and dissolved in CH_3CN (15 mL). This solution was allowed to stir for 10 min. at which point α,α'-dibromo-*p*-xylene (0.051 g, 0.19 mmol) was added and the reaction vessel sealed with a septum. This red solution stirred 4 d under ambient conditions after which time the solvent was removed *in vacuo*. The catenane was purified and after drying 75 mg (26 %) of pure **3.9** was recovered.

^{1}H NMR ($CDCl_3$, 400 MHz): δ ppm 9.44 (m, *J* = 7.0 Hz, 2H), 9.40 (m, *J* = 7.0 Hz, 2H), 9.25 (m, *J* = 7.0 Hz, 2H), 9.20 (m, *J* = 7.0 Hz, 2H), 8.34 (m, *J* = 7.0 Hz, 2H), 8.20 (m, *J* = 7.0 Hz, 4H), 8.15 (m, *J* = 70 Hz, 2H), 8.12 (m, 2H), 8.08 (m, 2H), 7.19 (d, *J* = 8.4 Hz, 1H), 6.76 (d, *J* = 2.4 Hz, 1H), 6.68 (dd, *J* = 8.4, 2.4 Hz, 1H), 6.16 (s, 2H), 6.14 (s, 2H), 5.40 (m, 2H), 5.32 (m, 2H), 4.68 (m, 2H), 4.63 (m, 2H), 4.02-3.54 (m, 40H), 2.68 (t, *J* = 7.4 Hz, 2H), 1.63 (m, 2H), 1.37 (m, 6H), 0.93 (m, *J* = 6.7 Hz, 3H).

MS (ESI): 1636.4 (M $3PF_6^+$), 745.3 (M $2PF_6^{2+}$), 448.8 (M PF_6^{3+}), 300.4 (M^{4+}) ($C_{72}H_{88}N_4O_{12}^{4+}$ requires 1201.49).

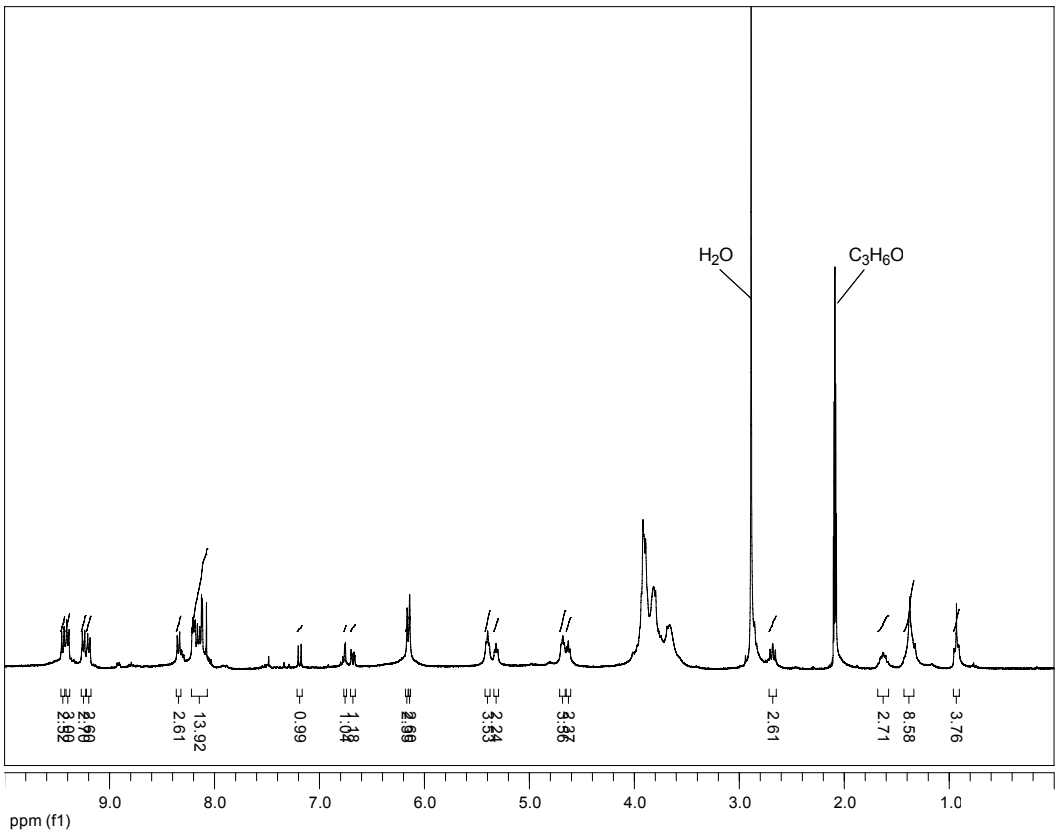
H2O
C3H6O
2.61
13.92
0.99
2.61
2.71
8.58
3.76
9.0
8.0
7.0
6.0
5.0
4.0
3.0
2.0
1.0
ppm (f1)

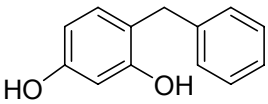

4-benzylbenzene-1,3-diol (4.12). Dihydroxybenzophenone (10.0 g, 46.7 mmol) was dissolved in 100mL of THF. To this stirring solution was added Methyl Orange (2.0 mg) and sodium cyanoborohydride (8.80 g, 140 mmol). Using a dropping funnel equipped with a stopcock, 3M HCl was added in a drop wise fashion at a rate fast enough to maintain a red/pink color throughout the solution. The endpoint of the reaction was determined by the persistence of the red color without addition of HCl. After completion, the organic phase was isolated and washed with water (3x50 mL) and brine (2x50 mL), dried with $MgSO_4$. Purification by flash chromatography using EtOAc gave 8.4 g of white solid for a 90 % yield of **4.12**.

^{1}H NMR ($CDCl_3$, 300MHz): δ ppm 7.30-7.15 (m, 5H), 6.90 (d, *J* = 8.1 Hz, 1H), 6.39-6.34 (m, 2H), 3.91 (s, 2H), 2.09 (s, 2H)

MS (ESI): m/z 223.0 ($M\ Na^+$); (EI): 200.0 (M^+) ($C_{13}H_{12}O_2$ requires 200.23).

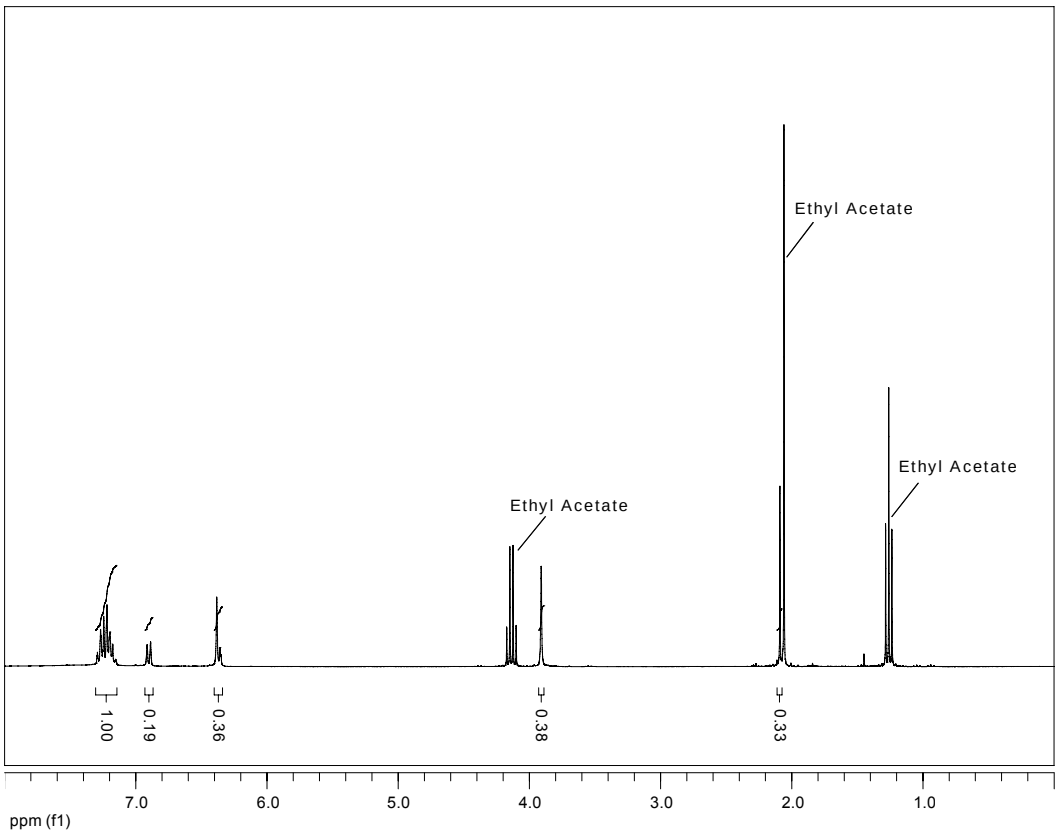
Ethyl Acetate
Ethyl Acetate
Ethyl Acetate
1.00
0.19
0.36
0.38
0.33
7.0
6.0
5.0
4.0
3.0
2.0
1.0
ppm (f1)

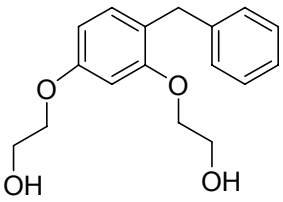

1,3-Bis(2-hydroxyethoxy)-4-benzylbenzene (4.20a). Sodium hydroxide (10.90 g, 273.0 mmol) was dissolved in a solution of ethanol (200 mL) and water (30 mL). To this solution was added 4-benzylbenzene-1,3-diol (18.23 g, 91.10 mmol) previously dissolved in ethanol (15 mL) creating a dark red solution that was allowed to stir for 10 min. 2-Chloroethanol (21.99 g, 273.1 mmol) was added to the stirring solution after which the entirety was refluxed 3 d. Precipitate formed in the reaction vessel and the solution became ruby red in color. After cooling to room temperature, the solvent was removed *in vacuo* leaving a red solid that was dissolved in EtOAc (100 mL) and washed with water (100 mL). The water was extracted twice more with EtOAc (30 mL). After combining, the organic fractions were washed with brine (50 mL) and dried over $MgSO_4$. Flash chromatography using diethyl ether provided 17.8 g (68 % yield) of pure **4.20a**.

^{1}H NMR ($CDCl_3$, 300MHz): δ ppm 7.31-7.24 (m, 2H), 7.21-7.14 (m, 3H), 7.08 (d, J = 7.8 Hz, 1H), 6.49-6.45 (m, 2H), 4.06 (m, J = 8.6, 3.9 Hz, 2H), 3.94 (m, J = 8.6, 3.9 Hz, 6H), 3.77 (m, 2H), 1.88 (bs, 2H)

MS (ESI): m/z 311.1 (M Na^+); (EI): m/z 288.1 (M^+), 243.1, 199.1 ($C_{17}H_{20}O_4$ requires 288.3).

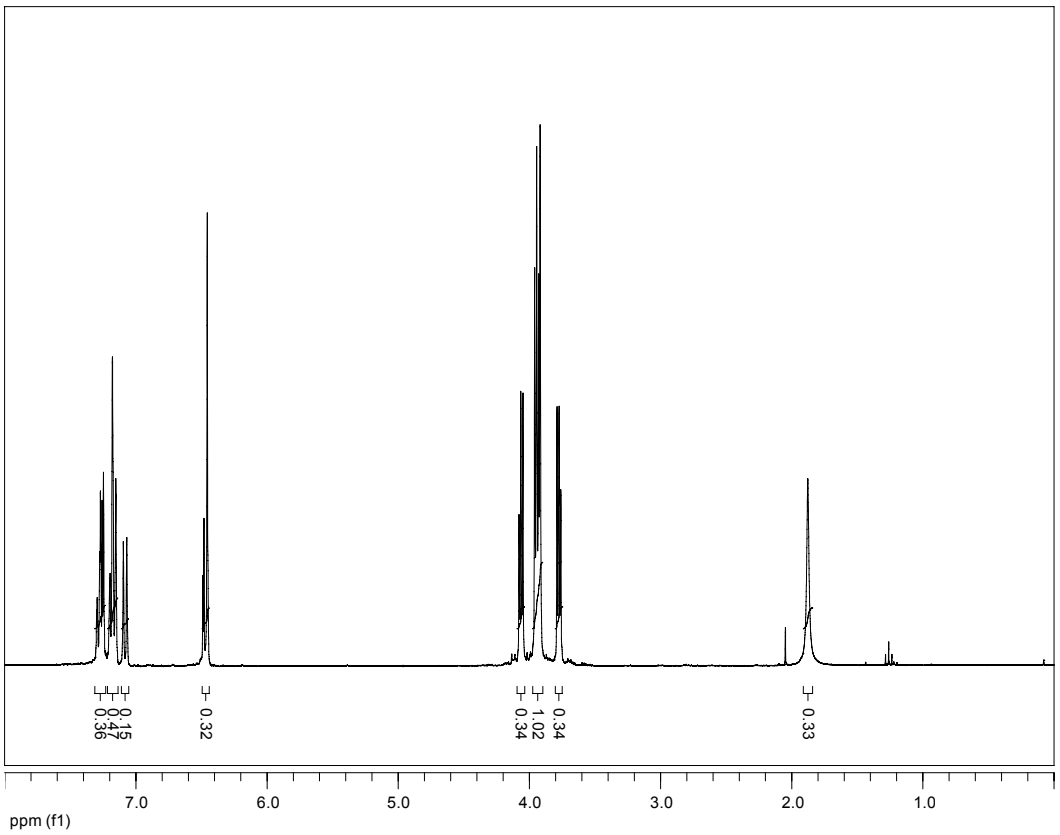
0.36
0.47
0.15
0.32
0.34
1.02
0.34
0.33
7.0
6.0
5.0
4.0
3.0
2.0
1.0
ppm (f1)

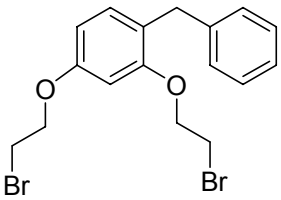

1,3-Bis(2-bromoethoxy)-4-benzylbenzene (4.21a). PPh_3 (16.40 g, 62.40 mmol) was added to CH_3CN (200 mL) and cooled to -10 ° C. Br_2 (9.97 g, 62.4 mmol) dissolved in CH_3CN (20 mL) was slowly added to the stirring PPh_3 mixture so as not to exceed 0 ° C. The mixture was allowed to warm to room temperature after the addition was complete. 1,3-Bis(2-hydroxyethoxy)-4-benzylbenzene (7.60 g, 27.1 mmol) dissolved in CH_3CN (10 mL) was added to the mixture and allowed to stir for 2 hours. Solvent was removed *in vacuo* and the crude product purified via column chromatography using CH_2Cl_2 to elute. The product was obtained in 93 % yield (10.4 g) and analysis by NMR showed it to be pure **4.21a**.

^{1}H NMR ($CDCl_3$, 300MHz): δ ppm 7.32-7.14 (m, 5H), 7.04 (d, *J* = 9.0 Hz, 1H), 6.45 (m, 2H), 4.26 (t, *J* = 6.2 Hz, 2H), 4.23 (t, *J* = 6.2 Hz, 2H), 3.94 (s, 2H), 3.63 (t, *J* = 6.1 Hz, 2H), 3.57 (t, *J* = 6.1 Hz, 2H)

MS (EI): m/z 413.9 (M+), 336.9 (M^+, -Br) ($C_{17}H_{18}Br_2O_2$ requires 414.1).

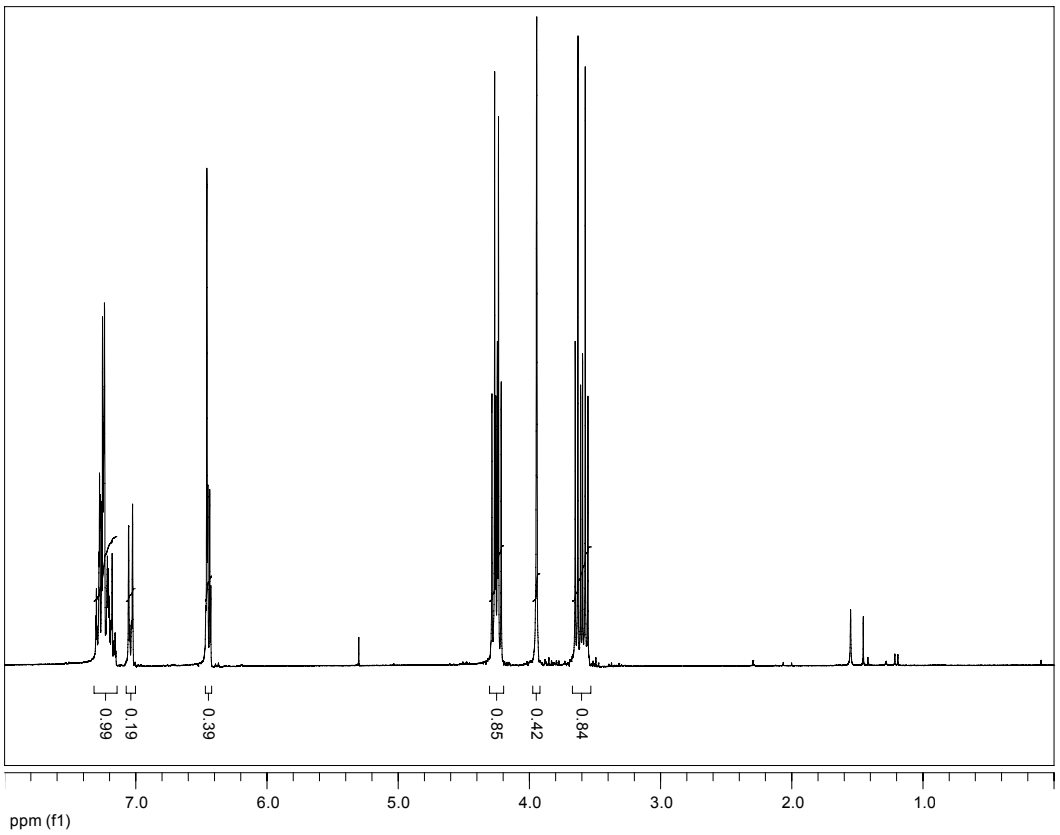
0.99
0.19
0.39
0.85
0.42
0.84
7.0
6.0
5.0
4.0
3.0
2.0
1.0
ppm (f1)

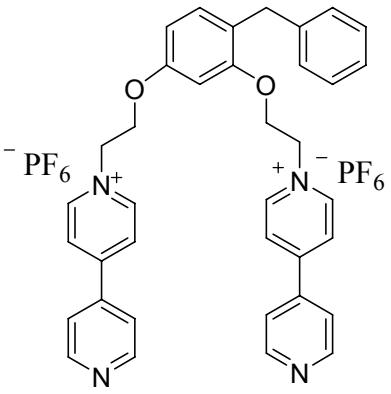

1,3-Bis(2-(4,4'-dipyridinium)ethoxy)-4-benzylbenzene bis(hexafluorophosphate) (4.22a). 1,3-Bis(2-bromoethoxy)-4-benzylbenzene (13.75 g, 33.69 mmol) and 4,4-dipyridyl (21.05 g, 134.77 mmol) were added to 200 mL of CH_3CN. This solution was stirred at 70 ° C for two d producing a green viscous oil and a yellow precipitate. After cooling the solvent was decanted and the solid material dried *in vacuo* leaving yellow and green solids. Water was added and upon heating the solid dissolved producing a green solution. Addition of NH_4PF_6 (13.73 g, 84.22 mmol) produced a dark yellow oil which was isolated and washed with warm $CHCl_3$ (3x20 mL) to extract impurities leaving a light-yellow oil which was then dissolved in CH_3CN and dried with $MgSO_4$. Removal of the solvent *in vacuo* left 10.4 g (36 %) of yellow foam-like solid of pure **4.22a**.

^{1}H NMR ($CDCl_3$, 300MHz): δ ppm 9.31 (m, *J* = 7.07 Hz, 2H), 9.12 (m, *J* = 7.07 Hz, 2H), 8.88 (m, *J* = 6.11, 1.03 Hz, 4H), 8.67 (m, *J* = 7.04 Hz, 2H), 8.42 (m, *J* = 7.03 Hz, 2H), 7.98 (m, *J* = 4.46, 1.72 Hz, 2H), 7.91 (m, *J* = 4.48, 1.72 Hz, 2H), 7.10 (m, *J* = 7.34, 7.34 Hz, 2H), 7.02 (d, *J* = 8.32 Hz, 1H), 7.00-6.92 (m, 3H), 6.75 (d, *J* = 2.36 Hz, 1H), 6.57 (dd, *J* = 8.31, 2.38 Hz, 1H), 5.31 (m, 2H), 5.26 (m, 2H), 4.68 (m, *J* = 9.62, 4.79 Hz, 4H), 3.88 (s, 2H).

MS (ESI): m/z 711.2 (M PF_6^+), 283.1 (M^{2+}) ($C_{37}H_{34}N_4O_2^{2+}$ requires 566.7).

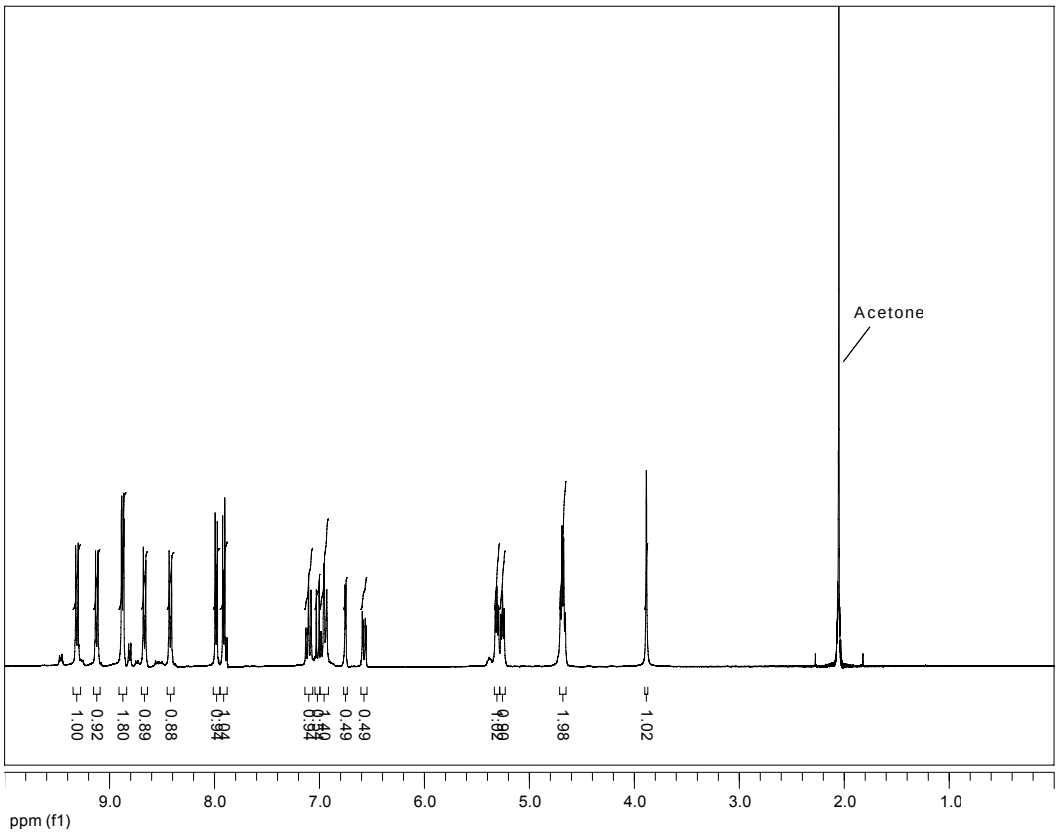

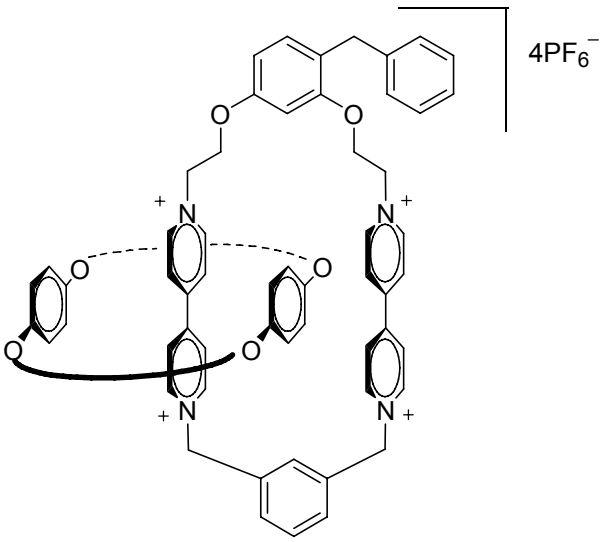

Catenane 4.1. 1,3-Bis(2-(4,4'-dipyridinium)ethoxy)-4-*n*-hexylbenzene bis(hexafluorophosphate) (0.123 g, 0.160 mmol) and BPP34C10 (0.223 g, 0.416 mmol) were combined and dissolved in CH_3CN (15 mL). This solution was allowed to stir for 10 min. at which point α,α'-dibromo-*m*-xylene (0.051 g, 0.19 mmol) was added and the reaction vessel sealed with a septum. This red solution stirred 4 d under ambient conditions after which time the solvent was removed *in vacuo*. The catenane was purified and after drying 35 mg (12 %) of pure product **4.1** was recovered.

^{1}H NMR ($CDCl_3$, 400 MHz): δ ppm 9.25 (m, *J* = 6.3 Hz, 2H), 9.18 (m, *J* = 6.7 Hz, 4H), 8.82 (m, *J* = 6.1 Hz, 2H), 8.27-8.21 (m, 4H), 8.13 (m, 7H), 7.91 (t, *J* = 7.7 Hz, 1H), 7.42-7.34 (m, 2H), 7.32-7.26 (m, 3H), 7.22 (d, *J* = 8.4 Hz, 1H), 6.82 (d, *J* = 2.3 Hz, 1H), 6.68 (dd, *J* = 8.4, 2.3 Hz, 1H), 6.21 (s, 2H), 6.17 (s, 2H), 5.74 (bs, 8H), 5.27 (m, *J* = 4.6 Hz, 4H), 4.65 (m, 2H), 4.50 (m, 2H), 4.04 (s, 2H), 3.90-3.64 (m, 32H).

MS (ESI): 748.3 (M $2PF_6^{2+}$), 603.3 (M^{2+}), 450.5 (M PF_6^{3+}), 402.2 (M^{3+}), 301.7 (M^{4+}) ($C_{73}H_{82}N_4O_{12}^{4+}$ requires 1207.45).

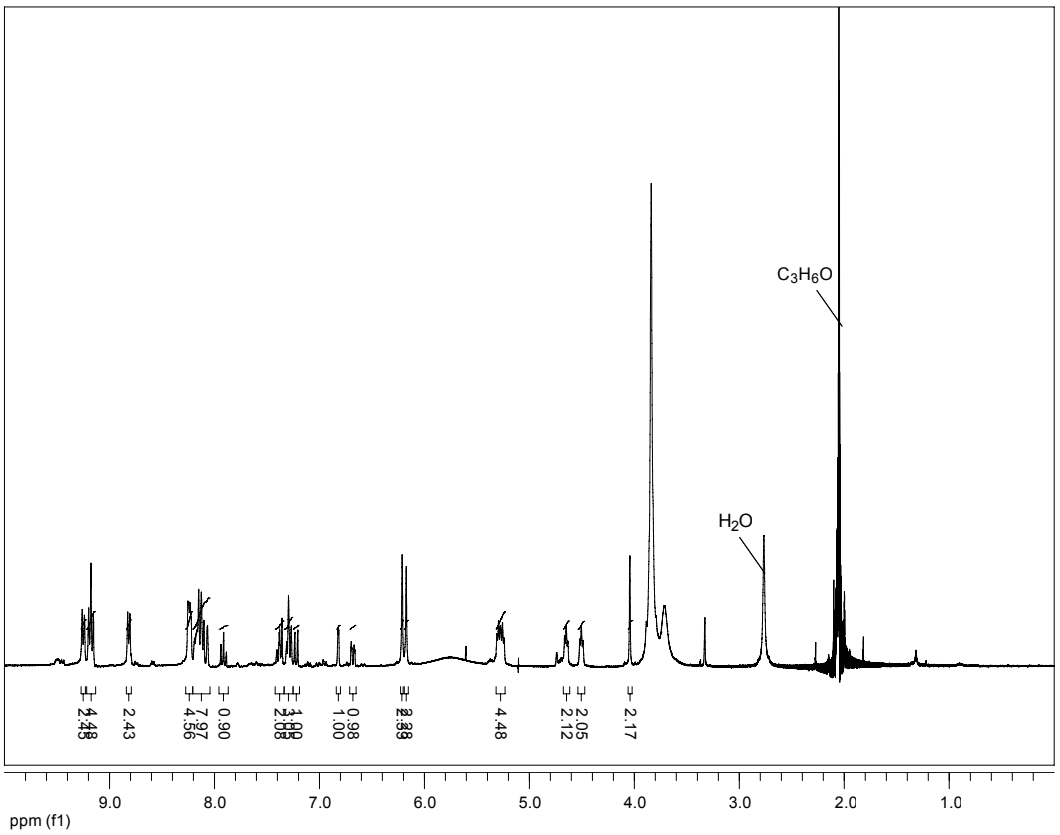
C3H6O
H2O
2.43
0.90
0.98
1.00
4.48
2.05
2.12
2.17
9.0
8.0
7.0
6.0
5.0
4.0
3.0
2.0
1.0
ppm (f1)

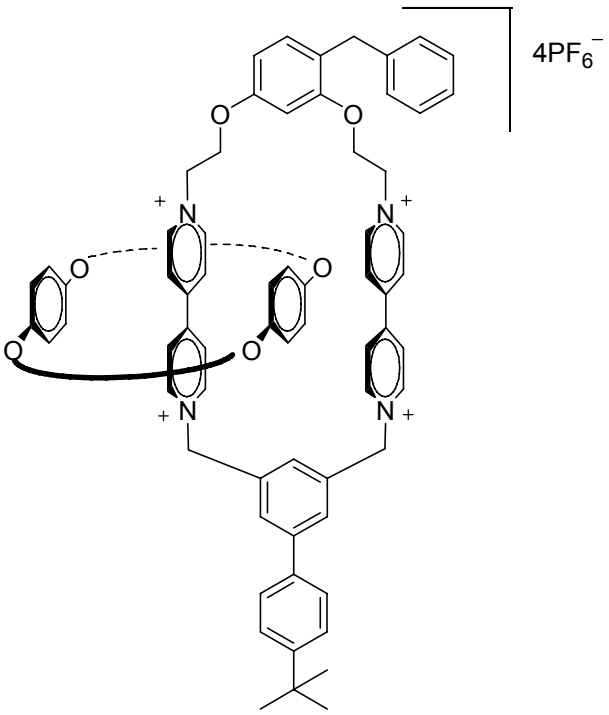

Catenane 4.2. 1,3-Bis(2-(4,4'-dipyridinium)ethoxy)-4-benzylbenzene bis(hexafluorophosphate) (0.123 g, 0.160 mmol) and BPP34C10 (0.223 g, 0.416 mmol) were combined and dissolved in CH_3CN (15 mL).. This solution was allowed to stir for 10 min. at which point 5-bis(bromomethyl)-4'-(1,1'-dimethylethyl)-1,1'-biphenyl (0.0765 g, 0.192 mmol) was added and the reaction vessel sealed with a septum. This red solution stirred 4 d under ambient conditions after which time the solvent was removed *in vacuo*. The catenane was purified and after drying 44 mg (14 %) of pure product **4.2** was recovered.

^{1}H NMR ($CDCl_3$, 400 MHz): δ ppm 9.35 (m, *J* = 7.0 Hz, 2H), 9.31 (m, *J* = 7.0 Hz, 2H), 9.15 (m, *J* = 7.0 Hz, 2H), 8.82 (m, *J* = 7.0 Hz, 2H), 8.44 (m, *J* = 3.1 Hz, 2H), 8.25 (m, 4H), 8.13 (m, 4H), 8.03 (t, *J* = 1.4 Hz, 1H), 7.93 (m, *J* = 8.5 Hz, 2H), 7.66 (m, *J* = 8.5 Hz, 2H), 7.39-7.33 (m, 2H), 7.30-7.25 (m, 3H), 7.20 (d, *J* = 8.4 Hz, 1H), 6.81 (d, *J* = 2.3 Hz, 1H), 6.67 (dd, *J* = 8.4, 2.3 Hz, 1H), 6.28 (s, 2H), 6.24 (s, 2H), 5.74 (s, 8H),

5.28 (m, 2H), 5.24 (m, 2H), 4.64 (m, 2H), 4.49 (m, 2H), 4.03 (s, 2H), 3.94-3.48 (m, 32H), 1.43 (s, 9H)

MS (ESI): 814.4 (M $2PF_6^{2+}$), 669.9 (M^{2+}), 494.6 (M PF_6^{3+}), 446.9 (M^{3+}), 334.9 (M^{4+}) ($C_{83}H_{94}N_4O_{12}^{4+}$ requires 1339.65).

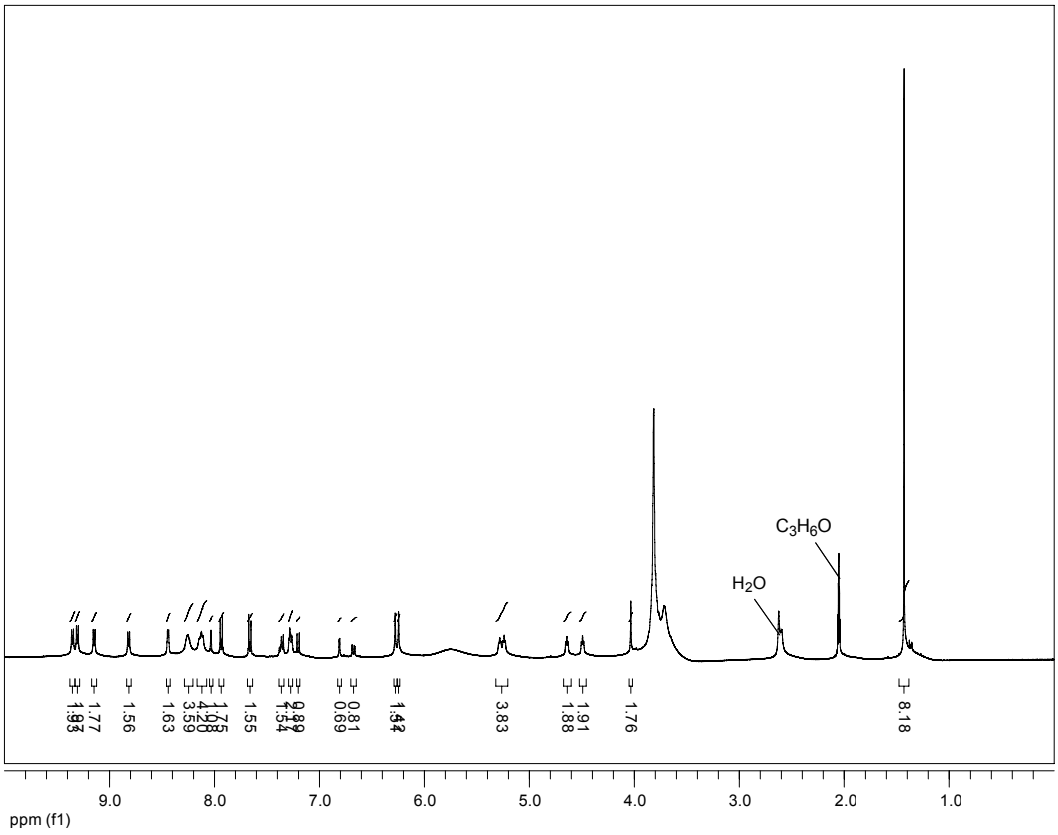

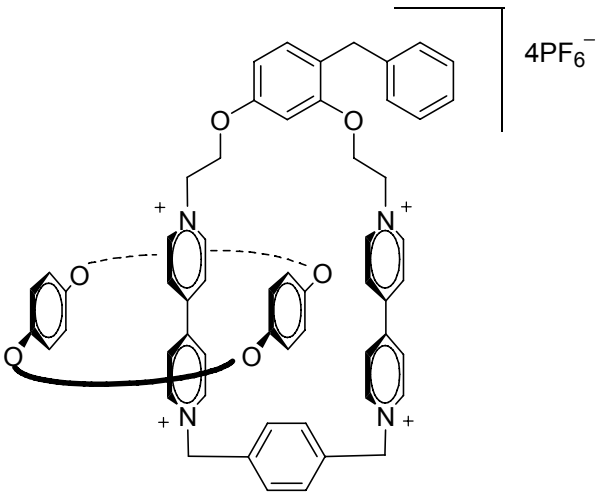

Catenane 4.3. 1,3-Bis(2-(4,4'-dipyridinium)ethoxy)-4-*n*-hexylbenzene bis(hexafluorophosphate) (0.123 g, 0.160 mmol) and BPP34C10 (0.223 g, 0.416 mmol) were combined and dissolved in CH_3CN (15 mL). This solution was allowed to stir for 10 min. at which point α,α'-dibromo-*p*-xylene (0.051 g, 0.19 mmol) was added and the reaction vessel sealed with a septum. This red solution stirred 4 d under ambient conditions after which time the solvent was removed *in vacuo*. The catenane was purified and after drying 79 mg (28 %) of pure product **4.3** was recovered.

^{1}H NMR ($CDCl_3$, 400 MHz): δ ppm 9.36 (m, *J* = 6.2 Hz, 4H), 9.18 (m, *J* = 6.2 Hz, 2H), 8.88 (m, *J* = 6.2 Hz, 2H), 8.15-8.06 (m, 12H), 7.39-7.32 (m, 2H), 7.31-7.24 (m, 3H), 7.21 (d, *J* = 8.3 Hz, 1H), 6.76 (d, *J* = 2.1 Hz, 1H), 6.69 (dd, *J* = 8.3, 2.1 Hz, 1H), 6.13 (s, 2H), 6.10 (s, 2H), 5.60 (s, 8H), 5.26 (m, *J* = 4.4 Hz, 4H), 4.66 (m, 2H), 4.51 (m, 2H), 4.04 (s, 2H), 3.96-3.59 (m, 32H).

MS (ESI): 450.5 (M PF_6^{3+}), 301.9 (M^{4+}) ($C_{73}H_{82}N_4O_{12}^{4+}$ requires 1207.45).

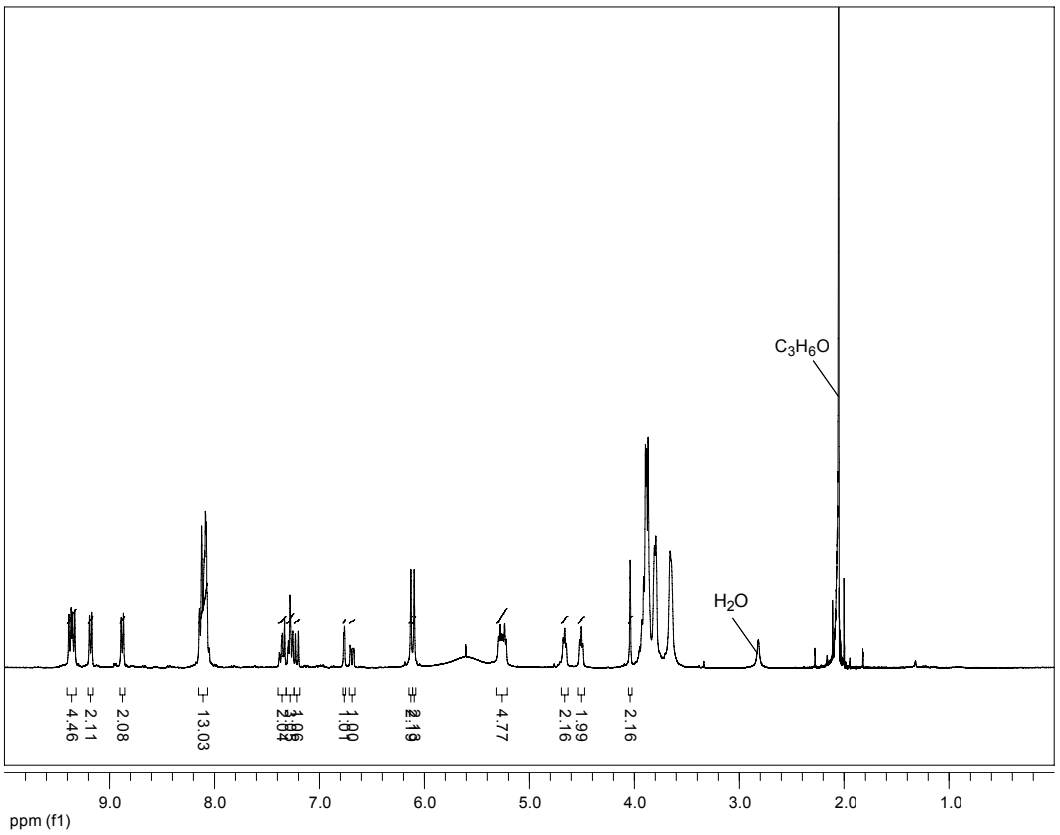
C3H6O
H2O
4.46
2.11
2.08
13.03
1.99
2.16
4.77
2.16
9.0
8.0
7.0
6.0
5.0
4.0
3.0
2.0
1.0
ppm (f1)

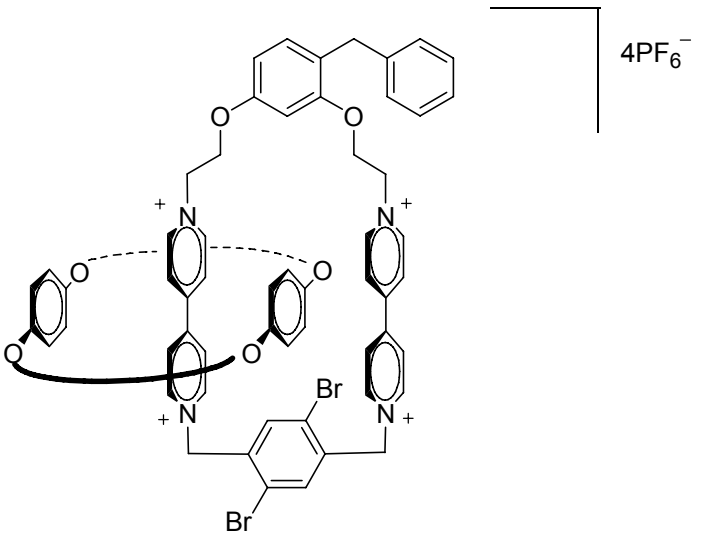

Catenane 4.4. 1,3-Bis(2-(4,4'-dipyridinium)ethoxy)-4-benzylbenzene bis(hexafluorophosphate) (0.123 g, 0.160 mmol) and BPP34C10 (0.223 g, 0.416 mmol) were combined and dissolved in CH_3CN (15 mL). This solution was allowed to stir for 10 min. at which point 1,4-dibromo-2,5-bis(bromomethyl) benzene (0.0810 g, 0.192 mmol) was added and the reaction vessel sealed with a septum. This red solution stirred 4 d under ambient conditions after which time the solvent was removed *in vacuo*. The catenane was purified and after drying 64 mg (21 %) of pure product **4.4** was recovered. **^{1}H NMR** ($CDCl_3$, 400 MHz): δ ppm 9.42 (m, *J* = 6.8 Hz, 2H), 9.39 (m, *J* = 6.8 Hz, 2H), 9.20 (m, *J* = 6.8 Hz, 2H), 8.90 (m, *J* = 6.7 Hz, 2H), 8.58 (s, 1H), 8.52 (s, 1H), 8.18 (m, *J* = 6.8 Hz, 2H), 8.16-8.10 (m, 6H), 7.34-7.19 (m, 6H), 6.81 (d, *J* = 2.3 Hz, 1H), 6.68 (dd, *J* = 8.3, 2.3 Hz, 1H), 6.45-6.34 (m, 2H), 6.29-6.22 (m, 2H), 5.70 (s, 8H), 5.38-5.18 (m, 4H), 4.69-4.59 (m, 3H), 4.47-4.40 (m, 1H), 4.04 (s, 2H), 3.99-3.49 (m, 32H). **MS** (ESI): 503.1 (M PF_6^{3+}), 341.3 (M^{4+}) ($C_{73}H_{80}Br_2N_4O_{12}^{4+}$ requires 1365.24).

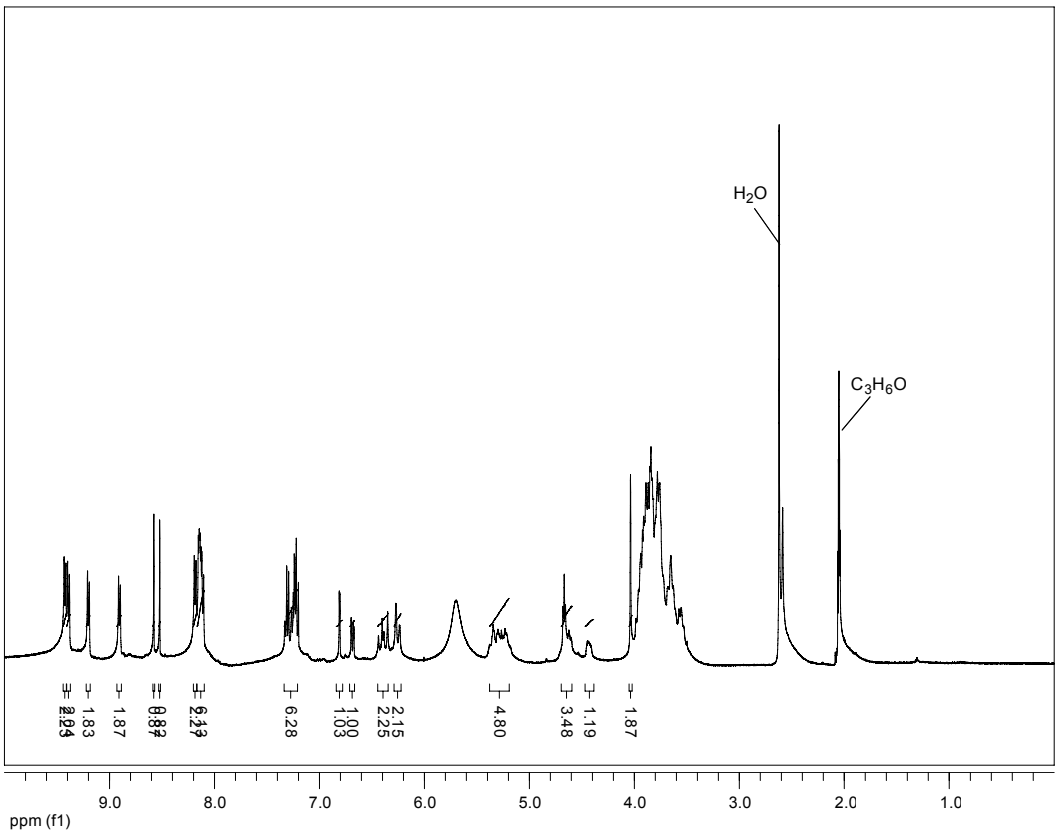
H2O
C3H6O
1.87
6.28
1.00
1.03
2.15
2.25
4.80
3.48
1.19
1.87
9.0
8.0
7.0
6.0
5.0
4.0
3.0
2.0
1.0
ppm (f1)

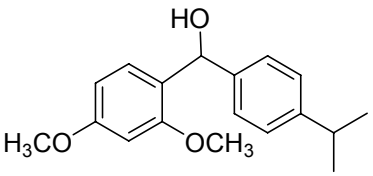

(2,4-Dimethoxyphenyl)-*p*-isopropylbenzylmethanol (4.14). A 100 mL round bottom flask, equipped with a stir bar, and condenser, containing magnesium (2.84 g, 117 mmol) was flushed with nitrogen after which dry THF (50 mL) was added followed by 2 drops of 1,2-dibromoethane and one very small crystal of iodine. 4-Bromo-1,3-dimethoxybenzene (12.7 g, 8.40 mL, 58.3 mmol) was added to the mixture slowly and a vigorous exothermic reaction was observed. The reaction was allowed to stir at room temperature overnight. This reagent was transferred to a flask containing 4-isopropylbenzaldehyde (8.64 g, 8.83 mL, 36.4 mmol) in dry THF (100 mL) at 0 ° C. The mixture was allowed to warm to room temperature and stirred overnight. The reaction was quenched with saturated NH_4Cl (20 mL) and extracted with diethyl ether (3×50 mL). The ether layer was washed with water (3×50 mL) and dried with $MgSO_4$. The filtrate was evaporated providing a white solid which was found to be a mixture of the desired product and excess 4-isopropylbenzaldehyde. Pure product **4.14** (13.0 g, 78 %) was obtained after flash chromatography (CH_2Cl_2).

^{1}H NMR ($CDCl_3$, 300MHz): δ ppm 7.19 (s, 4H), 7.03 (d, J = 8.2 Hz, 1H), 6.53 (d, J = 2.4 Hz, 1H), 6.47 (dd, J = 8.2, 2.4 Hz, 1H), 3.94 (s, 1H), 3.85 (s, 3H), 3.83 (s, 3H), 2.93 (sept., J = 6.9 Hz, 1H), 2.23 (bs, 1H), 1.29 (d, J = 6.9 Hz, 6H).

MS (ESI): m/z 309.1 (M Na^+), 286.1 (M^+) ($C_{18}H_{22}O_3$ requires 286.37).

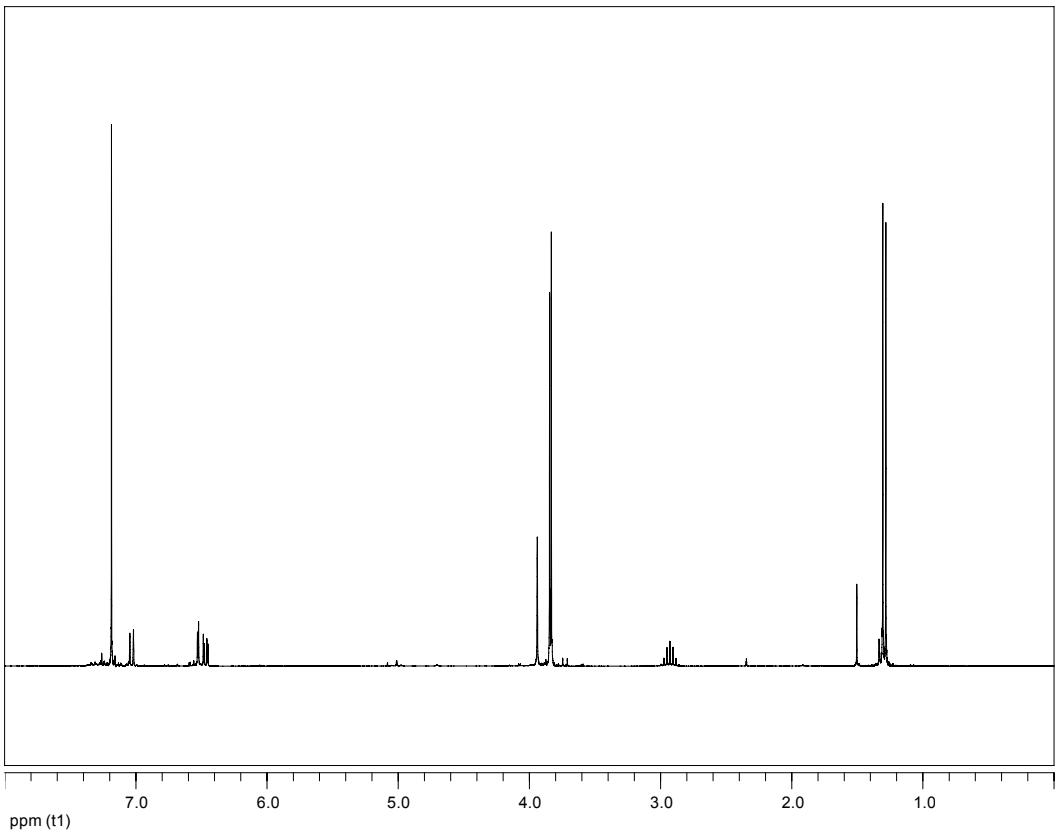
7.0
6.0
5.0
4.0
3.0
2.0
1.0
ppm (t1)

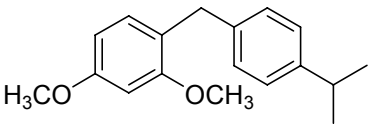

4-(4-Isopropylbenzyl)-1,3-dimethoxybenzene (4.15). (2,4-Dimethoxyphenyl)-p-isopropylbenzylmethanol (6.10 g, 21.3 mmol) was dissolved in 100 mL of THF. To this stirring solution was added Methyl Orange (3.0 mg) and sodium cyanoborohydride (6.69 g, 106 mmol). Using a dropping funnel equipped with a stopcock, 3M HCl was added in a drop wise fashion at a rate fast enough to maintain a red/pink color throughout the solution. The endpoint of the reaction was determined by the persistence of the red color without addition of HCl. After completion, the organic phase was isolated and washed with water (3x50 mL), brine (2x50 mL), and then dried with $MgSO_4$. Purification by flash chromatography using CH_2Cl_2 gave 5.7 g of white solid for a 99 % yield of **4.15**.

^{1}H NMR ($CDCl_3$, 300MHz): δ ppm 7.19 (s, 4H), 7.03 (d, *J* = 8.2 Hz, 1H), 6.53 (d, *J* = 2.4 Hz, 1H), 6.47 (dd, *J* = 8.2, 2.4 Hz, 1H), 3.94 (s, 2H), 3.85 (s, 3H), 3.83 (s, 3H), 2.93 (sept., *J* = 6.9 Hz, 1H), 1.29 (d, *J* = 6.9 Hz, 6H).

MS (EI): m/z 270.2 (M^+), 227.2, 151.2, 91.1 ($C_{18}H_{22}O_2$ requires 270.37)

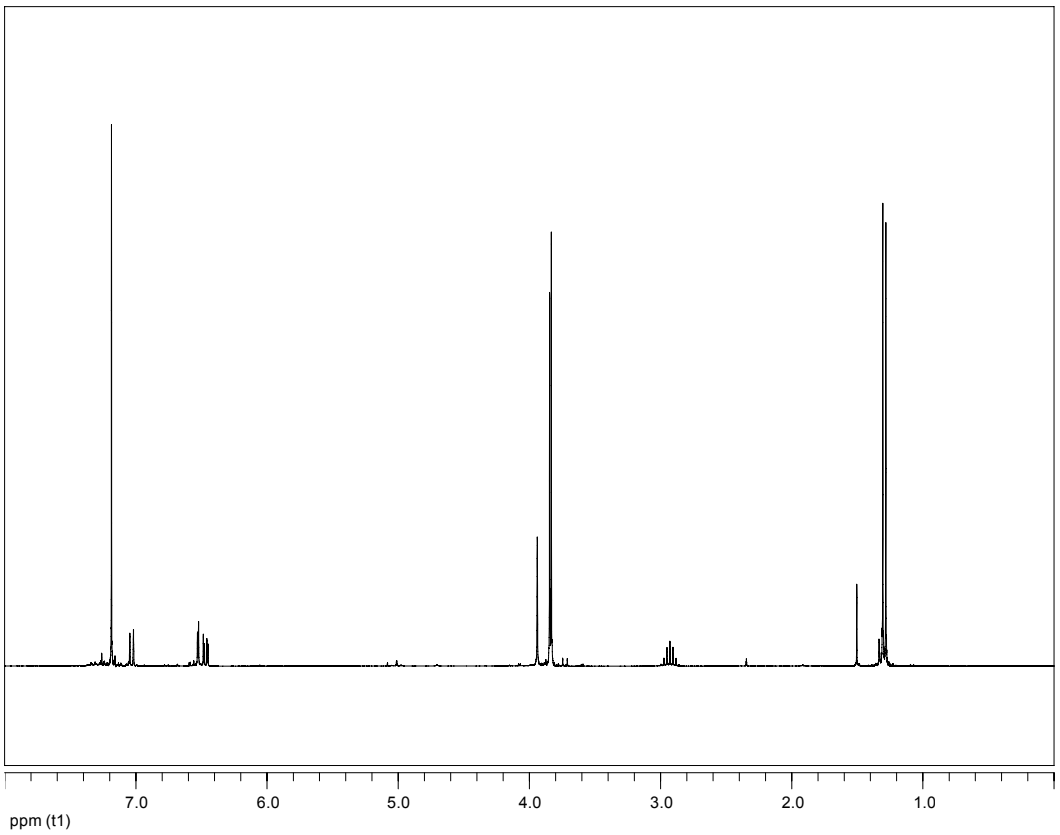
7.0
6.0
5.0
4.0
3.0
2.0
1.0
ppm (t1)

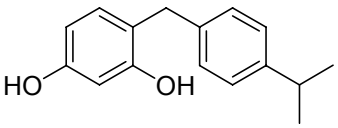

4-(4-isopropylbenzyl)benzene-1,3-diol (4.16). To a solution of 4-(4-isopropylbenzyl)-1,3-dimethoxybenzene (7.80, 28.8 mmol) in dry methylene chloride (100 mL), boron tribromide (16.6 g, 6.30 mL, 66.4 mmol) were added at 0 ° C. The mixture was allowed to warm to room temperature overnight and quenched with distilled water (100 mL). The organic layer was then removed and the aqueous layer extracted with methylene chloride (3×30 mL). The organic portions were combined, washed with brine (2x50 mL), and dried with $MgSO_4$. The solvent was removed *in vacuo* producing a solid that was then purified by flash chromatography. Side products were eluted using methylene chloride and the product with a solution of Et_2O:Hexane (70:30) giving 6.2 g of product **4.16** for a yield of 88 %.

^{1}H NMR ($CDCl_3$, 300MHz): δ ppm 7.16 (s, 4H), 6.96 (d, *J* = 8.1 Hz, 1H), 6.38 (dd, *J* = 8.1, 2.5 Hz, 1H), 6.33 (d, *J* = 2.5 Hz, 1H), 5.65 (s, 1H), 5.25 (s, 1H), 3.89 (s, 2H), 2.89 (sept., *J* = 6.9, Hz, 1H), 1.24 (d, *J* = 6.9 Hz, 6H).

MS (EI): m/z 242.2 (M^+), 199.2 ($C_{16}H_{18}O_2$ requires 242.31).

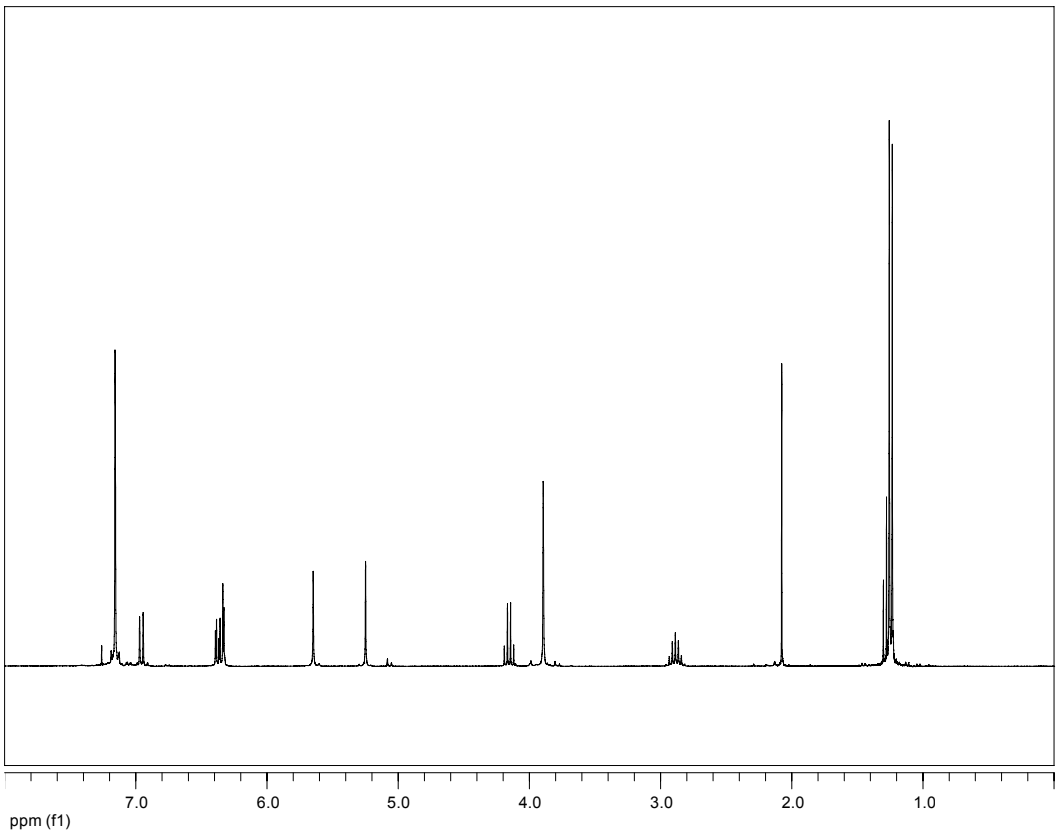
7.0
6.0
5.0
4.0
3.0
2.0
1.0
ppm (f1)

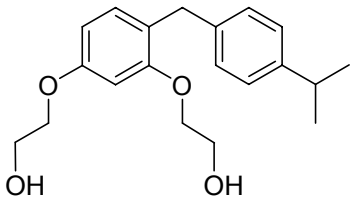

1,3-Bis(2-hydroxyethoxy)-4-(4-isopropylbenzyl)benzene (4.20b). Sodium hydroxide (2.33 g, 58.2 mmol) was dissolved in a solution of ethanol (100 mL) and water (15 mL). To this solution was added 4-(4-isopropylbenzyl)-benzene-1,3-diol (4.70 g, 19.4 mmol) previously dissolved in ethanol (10 mL) creating a dark red solution that was allowed to stir for 10 min. 2-Chloroethanol (4.68 g, 3.90 mL, 58.2 mmol) was added to the stirring solution after which the entirety was refluxed 3 d. Precipitate formed in the reaction vessel and the solution became ruby red in color. After cooling to room temperature, the solvent was removed *in vacuo* leaving a red solid that was dissolved in EtOAc (100 mL) and washed with water (50 mL). The water was extracted twice more with EtOAc (30 mL). After combining, the organic fractions were washed with brine (50 mL) and dried over $MgSO_4$. Flash chromatography using diethyl ether provided 4.4 g (69 % yield) of pure **4.20b**.

^{1}H NMR ($CDCl_3$, 300MHz): δ 7.14-7.08 (m, 4H), 7.05 (d, *J* = 8.7 Hz, 1H), 6.45 (dd, *J* = 8.7, 2.6 Hz, 1H), 6.44 (d, *J* = 2.6 Hz, 1H), 4.05-4.01 (m, 2H), 3.95-3.89 (m, 4H), 3.87 (s, 2H), 3.79-3.74 (m, 2H), 2.85 (sept., *J* = 6.9, 1H), 2.40-2.11 (bs, 2H), 1.21 (d, *J* = 6.9 Hz, 6H).

MS (ESI): m/z 353.2 (M Na^+); (EI): m/z 330.2 (M^+), 287.2, 241.2, 199.2, 133.2 ($C_{20}H_{26}O_4$ requires 330.42).

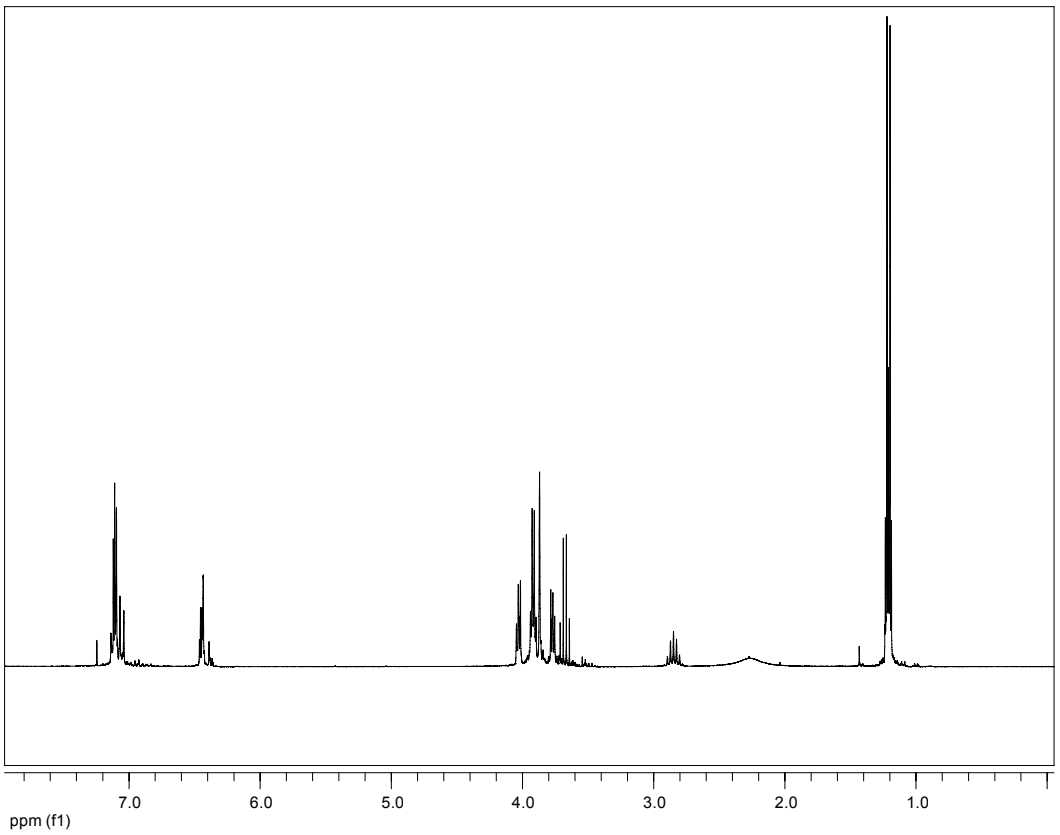
7.0
6.0
5.0
4.0
3.0
2.0
1.0
ppm (f1)

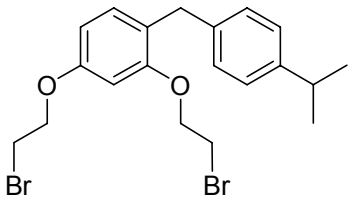

1,3-Bis(2-bromoethoxy)-4-(4-isopropylbenzyl)benzene (4.21b). PPh_3 (11.71 g, 44.62 mmol) was added to CH_3CN (100 mL) and cooled to -10 ° C. Br_2 (7.13 g, 44.6 mmol) dissolved in CH_3CN (10 mL) was slowly added to the stirring PPh_3 mixture so as not to exceed 0 ° C. The mixture was allowed to warm to room temperature after the addition was complete. 1,3-Bis(2-hydroxyethoxy)-4-(4-isopropylbenzyl)benzene (6.25 g, 19.4 mmol) dissolved in CH_3CN (5 mL) was added to the mixture and allowed to stir for 2 hours. Solvent was removed *in vacuo* and the crude product purified via column chromatography using CH_2Cl_2 to elute. The product was obtained in 99 % yield (8.77 g) and analysis by NMR showed it to be pure **4.21b**.

^{1}H NMR ($CDCl_3$, 300MHz): δ 7.15-7.12 (m, 4H), 7.04 (d, *J* = 8.7 Hz, 1H), 6.44 (m, 2H), 4.30-4.20 (m, 4H), 3.90 (s, 2H), 3.62 (t, *J* = 6.2 Hz, 2H), 3.57 (t, *J* = 6.2 Hz, 2H), 2.87 (sept., *J* = 6.9 Hz, 1H), 1.23 (d, *J* = 6.9 Hz, 1H).

MS (EI): m/z 456.1 (M^+), 413.1, 349.2 ($C_{20}H_{24}Br_2O_2$ requires 456.21).

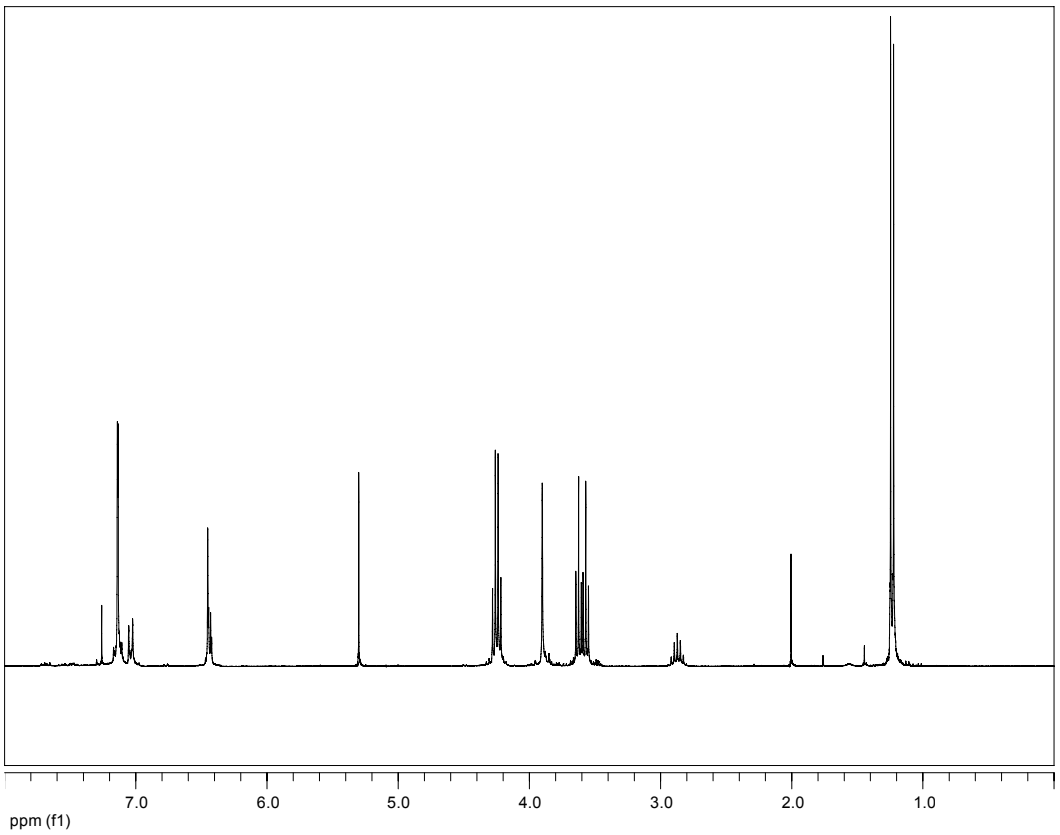
7.0
6.0
5.0
4.0
3.0
2.0
1.0
ppm (f1)

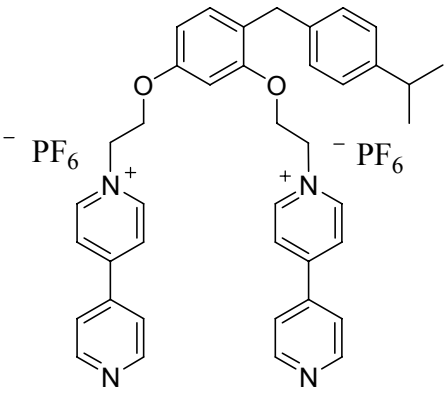

1,3-Bis(2-(4,4'-dipyridinium)ethoxy)-4-(4-isopropylbenzyl)benzene bis(hexafluorophosphate) (4.22b). 1,3-Bis(2-bromoethoxy)-4-(4-isopropylbenzyl)benzene (4.60 g, 10.1 mmol) and 4,4-dipyridyl (6.44 g, 41.1 mmol) were added to 100 mL of CH_3CN. This solution was stirred at 70 ° C for two d producing a brown viscous oil. The solvent was removed *in vacuo* leaving a brown solid. Water was added and upon heating the solid dissolved producing a dark yellow solution. Addition of NH_4PF_6 (4.11 g, 25.3 mmol) produced a yellow oil which was isolated and washed with warm $CHCl_3$ (3x20 mL) to extract impurities leaving a yellow oil which was then dissolved in CH_3CN and dried with $MgSO_4$. Removal of the solvent *in vacuo* left 7.8 g (81 % yield) of yellow foam-like solid of product **4.22b**.

^{1}H NMR ($C_3D_6O_2$, 300MHz): δ 9.40-9.37 (m, 2H), 9.33-9.28 (m, 2H), 8.94-8.88 (m, 4H), 8.75-8.71 (m, 2H), 8.60-8.55 (m, 2H), 8.07-8.01 (m, 2H), 8.00-7.95 (m, 2H), 7.07-6.98 (m, 4H), 6.93 (d, *J* = 8.3 Hz, 1H), 6.79 (d, *J* = 2.4 Hz, 1H), 6.58 (dd, *J* = 8.3, 2.4 Hz, 1H), 5.40-5.30 (m, 4H), 4.77-4.69 (m, 4H), 3.85 (s, 2H), 2.73 (sept., *J* = 6.9 Hz, 1H), 1.09 (d, *J* = 6.9 Hz, 6H).

MS (ESI): m/z 753.3 (M PF_6^+), 304 (M^{2+}) ($C_{40}H_{40}N_4O_2^{2+}$ requires 608.77)

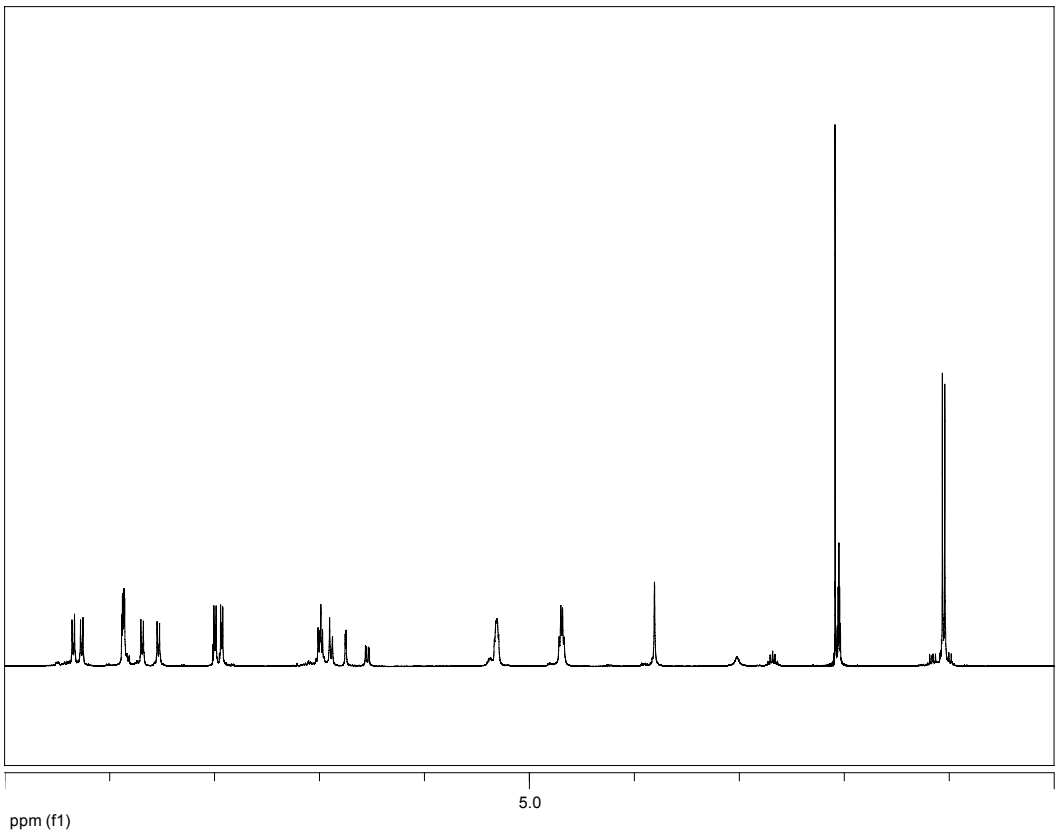
5.0
ppm (f1)

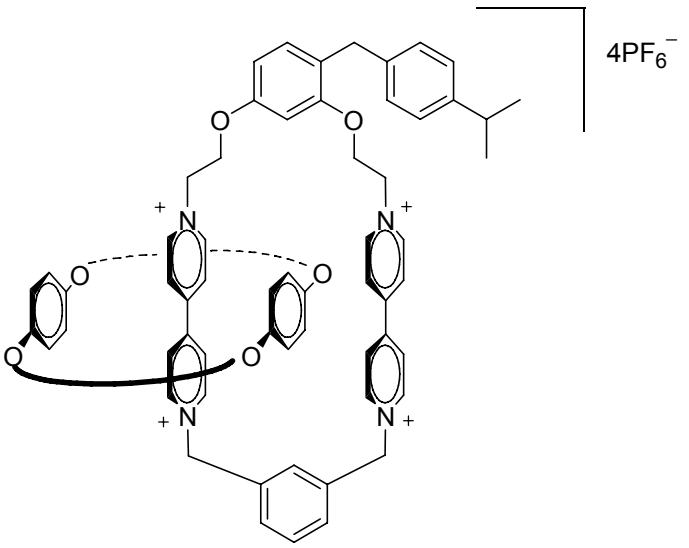

Catenane 4.5. 1,3-Bis(2-(4,4'-dipyridinium)ethoxy)-4-(4-isopropyl)benzylbenzene bis(hexafluorophosphate) (0.144 g, 0.160 mmol) and BPP34C10 (0.223 g, 0.416 mmol) were combined and dissolved in CH_3CN (15 mL). This solution was allowed to stir for 10 min. at which point α,α'-dibromo-*m*-xylene (0.051 g, 0.19 mmol) was added and the reaction vessel sealed with a septum. This red solution stirred 4 d under ambient conditions after which time the solvent was removed *in vacuo*. The catenane was purified and after drying 58 mg (20 %) of pure product **4.5** was recovered.

^{1}H NMR ($CDCl_3$, 400 MHz): δ ppm 9.26 (m, *J* = 6.9 Hz, 2H), 9.18 (m, *J* = 6.9, 5.10 Hz, 4H), 9.01 (m, *J* = 6.9 Hz, 2H), 8.27-8.20 (m, 6H), 8.19-8.11 (m, 4H), 8.07 (m, 1H), 7.90 (t, *J* = 7.7 Hz, 1H), 7.25-7.20 (m, 4H), 7.15 (d, *J* = 8.4 Hz, 1H), 6.81 (d, *J* = 2.4 Hz, 1H), 6.65 (dd, *J* = 8.4, 2.4 Hz, 1H), 6.20 (s, 2H), 6.17 (s, 2H), 5.28 (m, 4H), 4.62 (m, 2H), 4.45 (m, 2H), 3.97 (s, 2H), 3.90-3.71 (m, 40H), 2.91 (sept, *J* = 6.9 Hz, 1H), 1.24 (d, *J* = 6.9 Hz, 6H).

MS (ESI): 769.3 (M $2PF_6^{2+}$), 464.6 (M PF_6^{3+}), 312.4 (M^{4+}) ($C_{76}H_{88}N_4O_{12}^{4+}$ requires 1249.53).

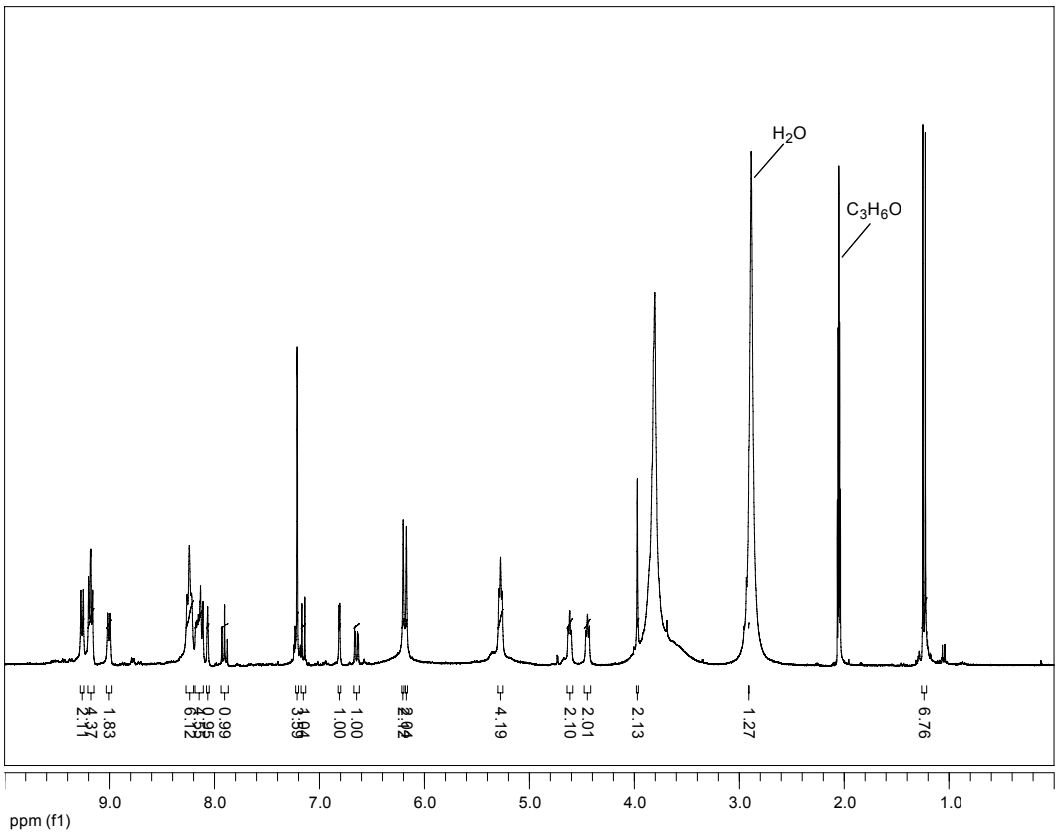
H2O
C3H6O
9.0
8.0
7.0
6.0
5.0
4.0
3.0
2.0
1.0
ppm (f1)

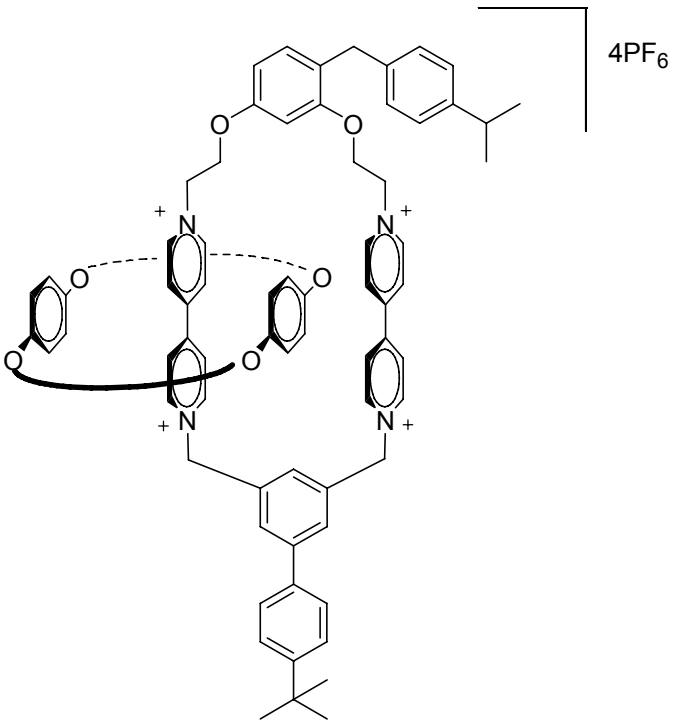

Catenane 4.6. 1,3-Bis(2-(4,4'-dipyridinium)ethoxy)-4-(4-isopropyl)benzylbenzene bis(hexafluorophosphate) (0.144 g, 0.160 mmol) and BPP34C10 (0.223 g, 0.416 mmol) were combined and dissolved in CH_3CN (15 mL). This solution was allowed to stir for 10 min. at which point 5-bis(bromomethyl)-4'-(1,1'-dimethylethyl)-1,1'-biphenyl (0.0765 g, 0.192 mmol) was added and the reaction vessel sealed with a septum. This red solution stirred 4 d under ambient conditions after which time the solvent was removed *in vacuo*. The catenane was purified and after drying 41 mg (13 %) of pure product **4.6** was recovered.

^{1}H NMR ($CDCl_3$, 400 MHz): δ ppm 9.36 (m, *J* = 5.7 Hz, 2H), 9.28 (m, *J* = 5.7 Hz, 2H), 9.13 (m, *J* = 6.2 Hz, 2H), 9.02-8.94 (m, 2H), 8.42 (m, *J* = 4.4 Hz, 2H), 8.34 (m, *J* = 6.1 Hz, 2H), 8.20-8.05 (m, 6H), 8.02 (m, 1H), 7.93 (m, *J* = 8.3 Hz, 2H), 7.67 (d, *J* = 8.3 Hz, 2H), 7.22 (s, 4H), 7.17 (d, *J* = 6.3 Hz, 1H), 6.80 (d, *J* = 2.3 Hz, 1H), 6.69 (dd, *J* = 6.3, 2.3 Hz, 1H), 6.26 (s, 2H), 6.23 (s, 2H), 5.81 (s, 8H), 5.25 (s, 4H), 4.65 (s, 2H),

4.47 (s, 2H), 4.01 (s, 2H), 3.86-3.67 (m, 32H), 2.93 (s, 2H), 1.45 (s, 9H), 1.30-1.22 (m, 7H).

MS (ESI): m/z 835.8 (M $2PF_6^{2+}$), 508.6 (M PF_6^{3+}), 460.3 (M^{3+}), 345.2 (M^{4+}) ($C_{86}H_{100}N_4O_{12}^{4+}$ requires 1381.73).

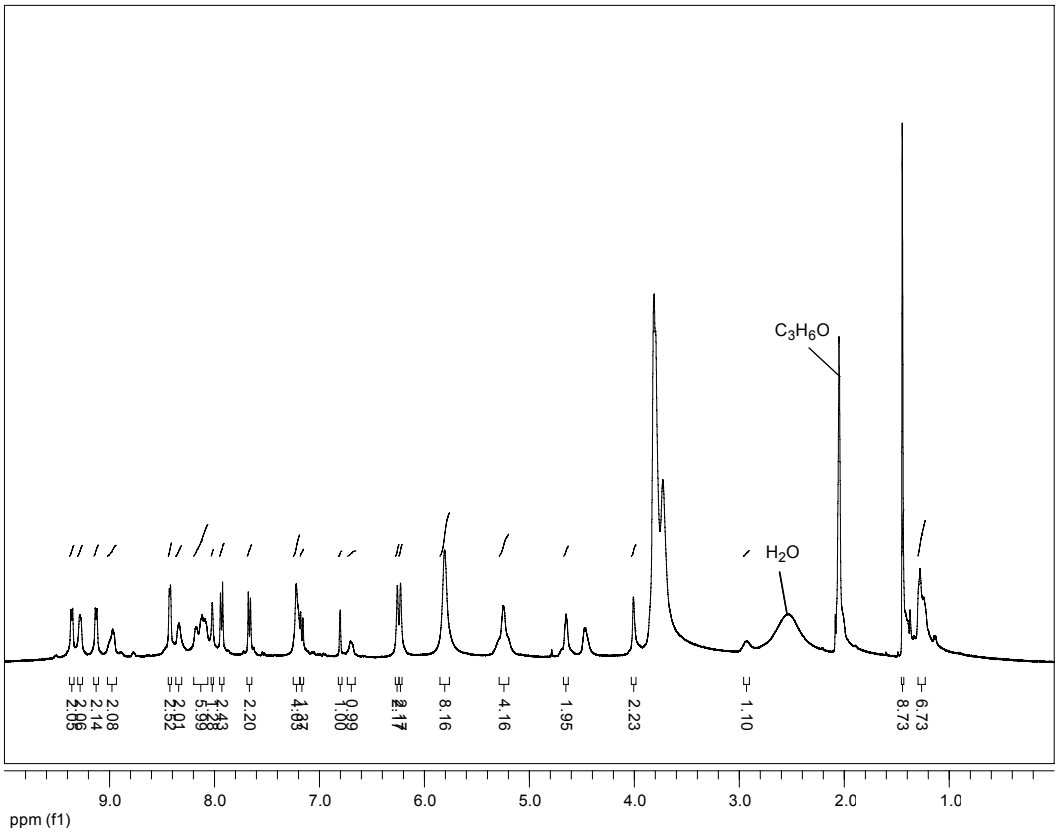

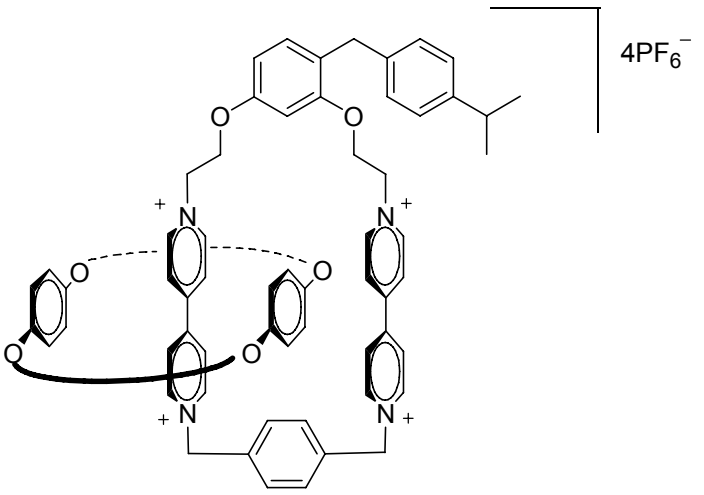

Catenane 4.7. 1,3-Bis(2-(4,4'-dipyridinium)ethoxy)-4-(4-isopropyl)benzylbenzene bis(hexafluorophosphate) (0.144 g, 0.160 mmol) and BPP34C10 (0.223 g, 0.416 mmol) were combined and dissolved in CH_3CN (15 mL). This solution was allowed to stir for 10 min. at which point α,α'-dibromo-*p*-xylene (0.051 g, 0.19 mmol) was added and the reaction vessel sealed with a septum. This red solution stirred 4 d under ambient conditions after which time the solvent was removed *in vacuo*. The catenane was purified and after drying 61 mg (21 %) of pure product **4.7** was recovered.

^{1}H NMR ($CDCl_3$, 400 MHz): δ ppm 9.40 (m, *J* = 7.0 Hz, 2H), 9.35 (m, *J* = 7.0 Hz, 2H), 9.18 (m, *J* = 7.0 Hz, 2H), 9.05 (m, *J* = 7.0 Hz, 2H), 8.18 (m, *J* = 7.0\ Hz, 2H), 8.14 (m, *J* = 7.0 Hz, 2H), 8.12-8.06 (m, 8H), 7.22-7.17 (m, 4H), 7.15 (d, *J* = 8.4 Hz, 1H), 6.74 (d, *J* = 2.4 Hz, 1H), 6.67 (dd, *J* = 8.4, 2.4 Hz, 1H), 6.13 (s, 2H), 6.10 (s, 2H), 5.61 (bs, 8H), 5.27 (m, *J* = 4.91 Hz, 4H), 4.65 (m, 2H), 4.47 (m, 2H), 3.98 (s, 2H), 3.91-3.60 (m, 32H), 2.91 (sept, *J* = 6.9 Hz, 1H), 1.24 (d, *J* = 6.9 Hz, 6H).

^{13}C NMR ($CDCl_3$, 75MHz): δ 159.3, 158.2, 155.3, 153.4, 149.8, 149.6, 148.9, 148.3, 148.0, 147.1, 147.0, 140.9, 138.7, 138.0, 133.2, 132.9, 132.7, 131.7, 131.5, 130.6, 130.2, 129.5, 128.9, 128.2, 128.2, 127.8, 127.5, 126.9, 126.6, 116.2, 108.4, 105.2, 72.2, 72.0, 71.7, 70.4, 69.3, 68.1, 66.6, 63.0, 62.9, 36.5, 35.4, 25.5.

MS (ESI): 1684.2 (M $3PF_6^+$), 769.3 (M $2PF_6^{2+}$), 464.83 (M PF_6^{3+}), 312.4 (M^{4+}) ($C_{76}H_{88}N_4O_{12}^{4+}$ requires 1249.53).

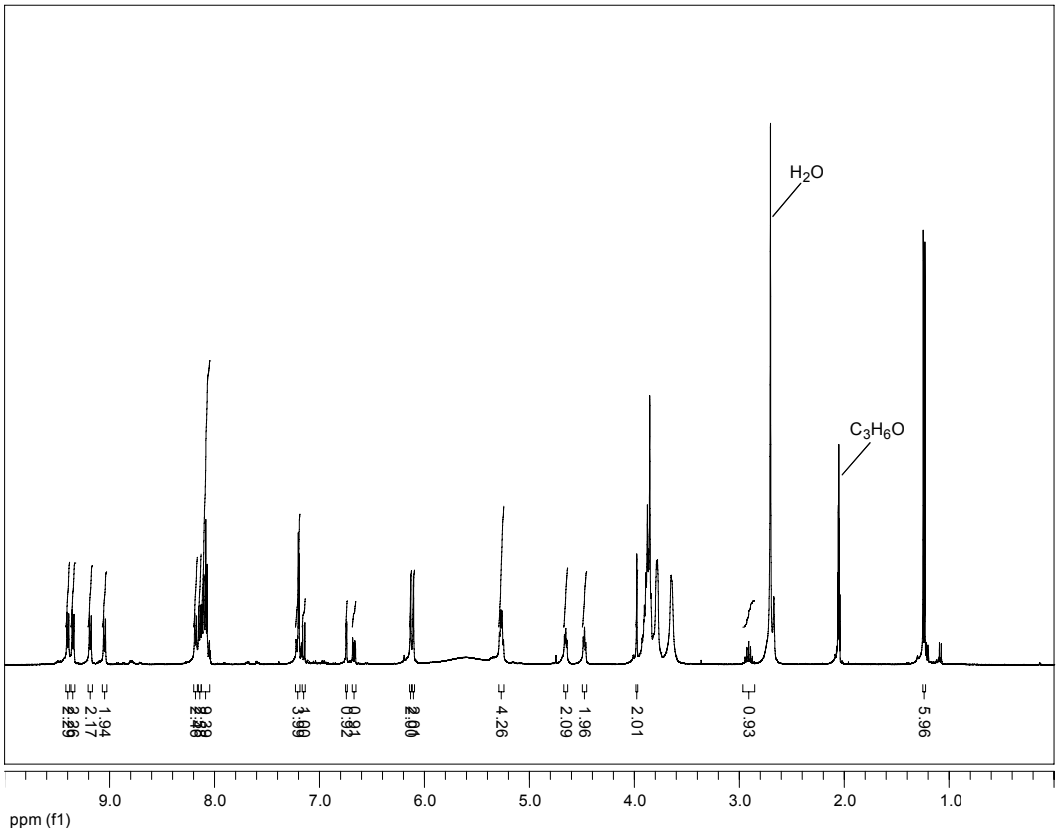

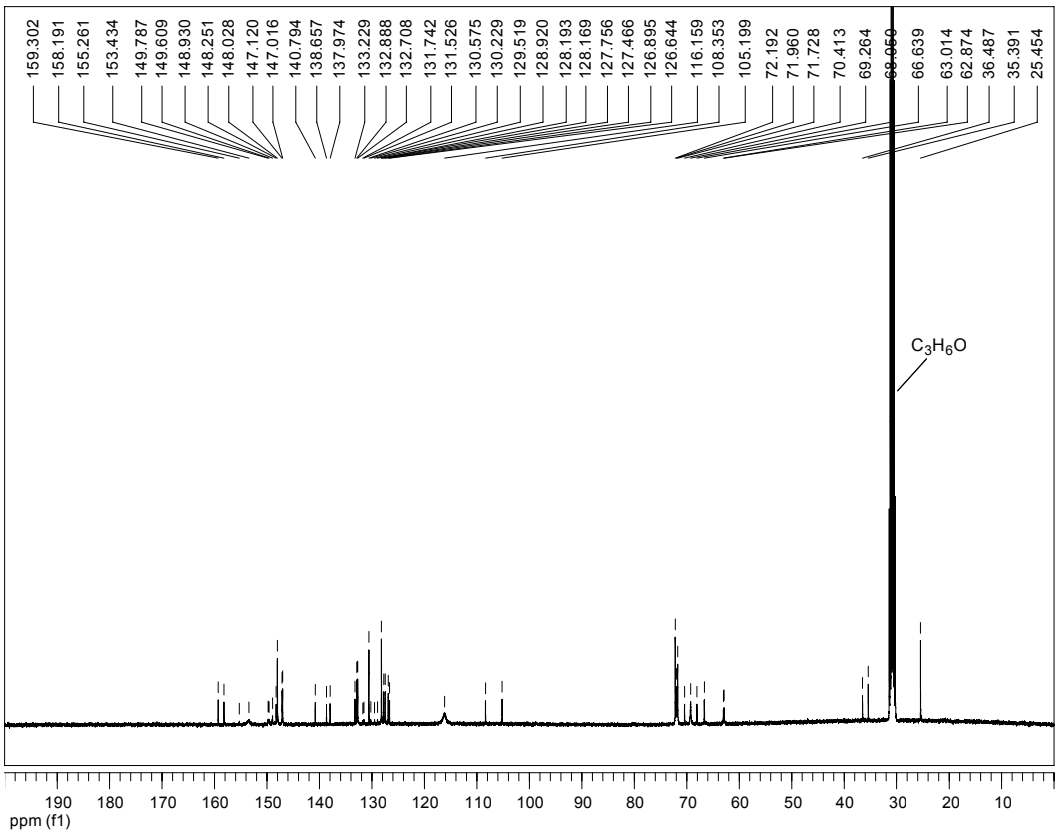
159.302
158.191
155.261
153.434
149.787
149.609
148.930
148.251
148.028
147.120
147.016
140.794
138.657
137.974
133.229
132.888
132.708
131.742
131.526
130.575
130.229
129.519
128.920
128.193
128.169
127.756
127.466
126.895
126.644
116.159
108.353
105.199
72.192
71.960
71.728
70.413
69.264
68.050
66.639
63.014
62.874
36.487
35.391
25.454
C3H6O
190 180 170 160 150 140 130 120 110 100 90 80 70 60 50 40 30 20 10
ppm (f1)

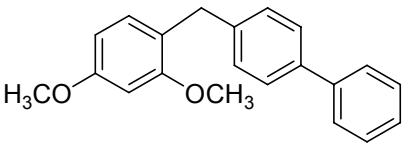

4-(4-phenylbenzyl)-1,3-dimethoxybenzene (4.18). A 200 mL round bottom flask, equipped with a stir bar, and condenser, containing magnesium (1.48 g, 60.7 mmol) was flushed with nitrogen after which THF (80 mL) was added followed by 2 drops of 1,2-dibromoethane and one very small crystal of iodine. 4-Bromo-1,3-dimethoxybenzene (6.59 g, 4.37 mL, 30.3 mmol) was added to the mixture slowly and a vigorous exothermic reaction was observed. The reaction was allowed to stir at room temperature overnight. This reagent was transferred to a flask containing a solution of 4-phenylbenzyl bromide (9.00 g, 36.4 mmol), 2,2'-dipyridyl (0.473 g, 3.02) and CuCN (.270 g, 3.02 mmol) in THF (100 mL) at 0 ° C. The mixture was allowed to warm to room temperature and stirred overnight. The reaction was quenched with saturated NH_4Cl (20 mL) and extracted with diethyl ether (3×50 mL). The ether layer was washed with water (3×50 mL) and dried with $MgSO_4$. The filtrate was evaporated providing a white solid which was found to be a mixture of the desired product and excess 4-phenylbenzyl bromide. Pure product **4.18** (7.87g, 85 %) was obtained after flash chromatography (CH_2Cl_2).

^{1}H NMR ($CDCl_3$, 300MHz): δ 7.67-7.61 (m, 2H), 7.59-7.53 (m, 2H), 7.52-7.45 (m, 2H), 7.42-7.37 (m, 1H), 7.37-7.31 (m, 2H), 7.08 (d, *J* = 8.2 Hz, 1H), 6.55 (d, *J* = 2.1 Hz, 1H), 6.50 (dd, *J* = 8.2, 2.1 Hz, 1H), 4.01 (s, 2H), 3.88 (s, 3H), 3.87 (s, 3H).

MS (ESI): m/z 327.2 (M Na^+); (EI): m/z 304.1 (M^+), 289.1, 273.1, 200.0, 167.1, 152.0 ($C_{21}H_{20}O_2$ requires 304.38).

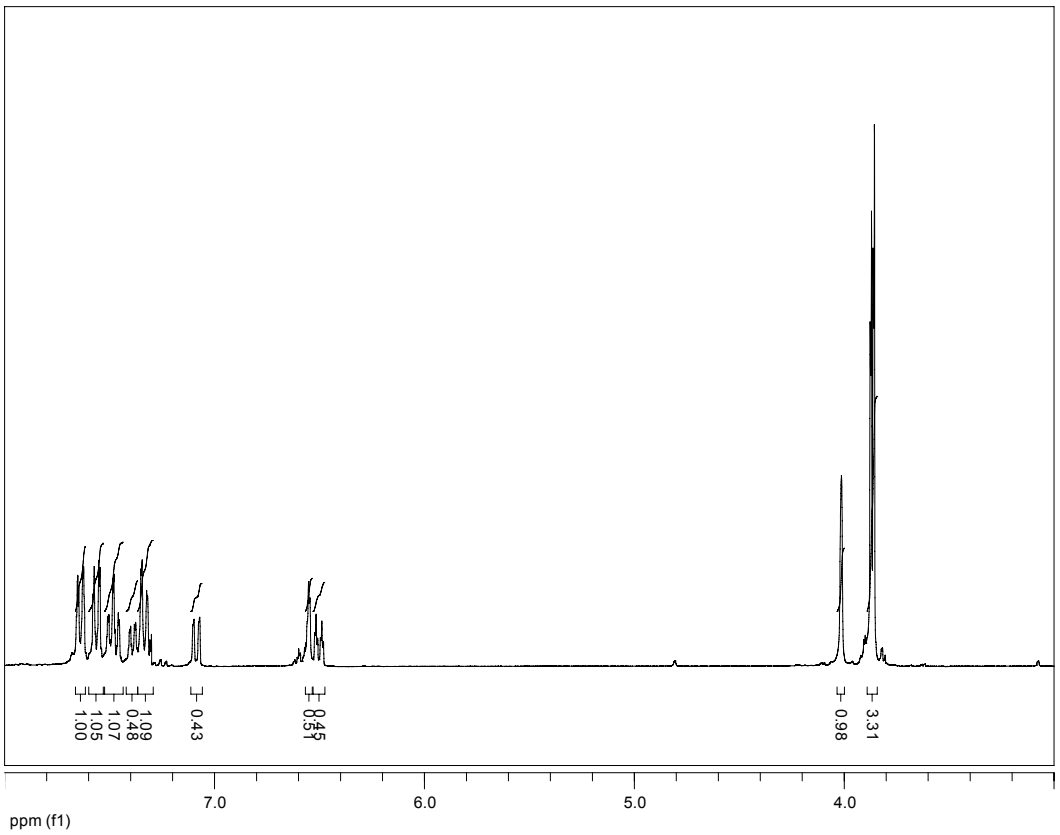
1.00
1.05
1.07
0.48
1.09
0.43
0.45
0.51
0.98
3.31
7.0
6.0
5.0
4.0
ppm (f1)

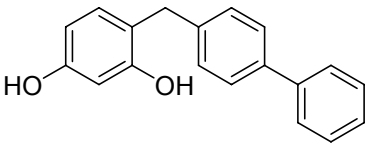

4-(4-phenylbenzyl)benzene-1,3-diol (4.19). To a solution of 4-(4-phenylbenzyl)-1,3-dimethoxybenzene (8.80 g, 28.9 mmol) in dry methylene chloride (100 mL), boron tribromide (16.66 g, 6.290 mL, 66.49 mmol) were added at 0 °C. The mixture was allowed to warm to room temperature overnight and quenched with distilled water (100 mL). The organic layer was then removed and the aqueous layer extracted with methylene chloride (3×30 mL). The organic portions were combined, washed with brine (2x50 mL), and dried with $MgSO_4$. The solvent was removed *in vacuo* producing a solid which was then purified by flash chromatography. Side products were eluted using methylene chloride and the product with a solution of Et_2O:Hexanes (60:40) giving 7.4 g of product **4.19** for a yield of 98 %.

^{1}H NMR ($CDCl_3$, 300MHz): δ 7.58-7.55 (m, 2H), 7.53-7.51 (m, 2H), 7.46-7.39 (m, 2H), 7.36-7.31 (m, 1H), 7.30-7.26 (m, 2H), 7.01 (d, *J* = 8.1 Hz, 1H), 6.40 (dd, *J* = 8.1, 2.5 Hz, 1H), 6.35 (d, *J* = 2.5 Hz, 1H), 4.70 (s, 1H), 4.66 (s, 1H), 3.96 (s, 2H).

^{13}C NMR ($CDCl_3$, 75MHz): δ 155.4, 154.7, 140.9, 139.3, 139.2, 131.6, 128.9, 128.7, 127.4, 127.1, 127.0, 119.2, 107.8, 103.3, 35.3.

MS (EI): m/z 276.2 (M+), 167, 154.1 ($C_{19}H_{16}O_2$ requires 276.33).

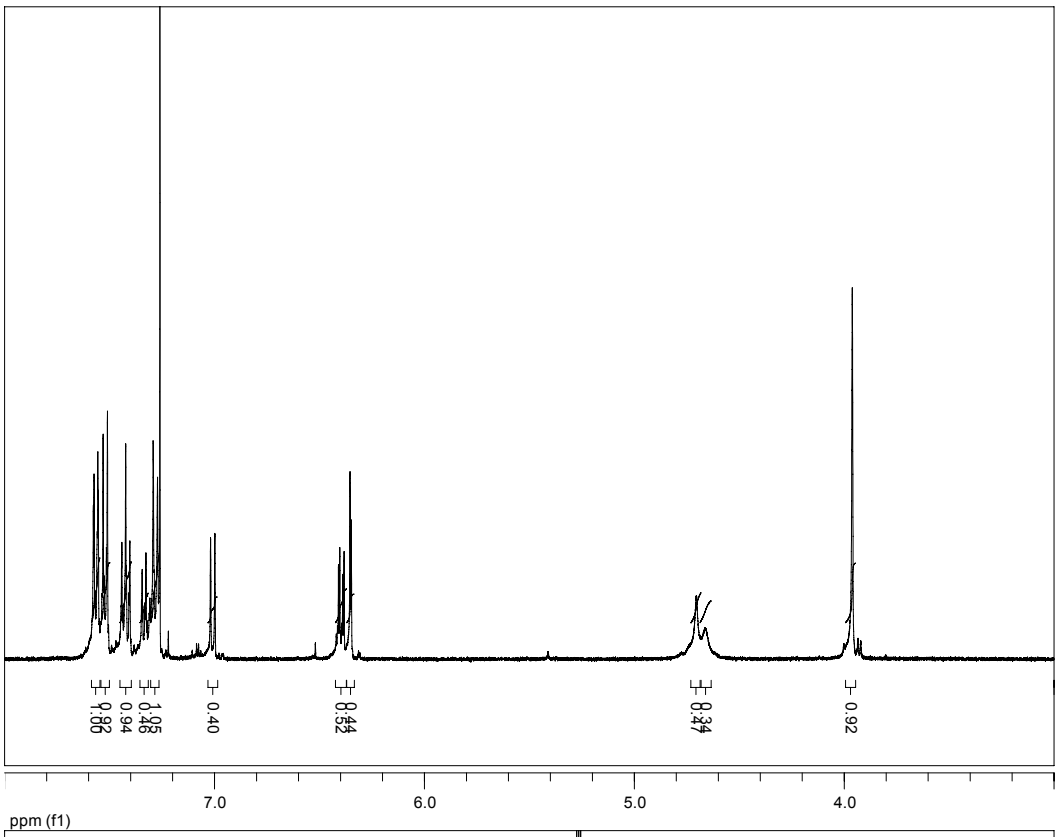
1.00
0.96
1.05
0.40
0.44
0.34
0.92
7.0
6.0
5.0
4.0
ppm (f1)

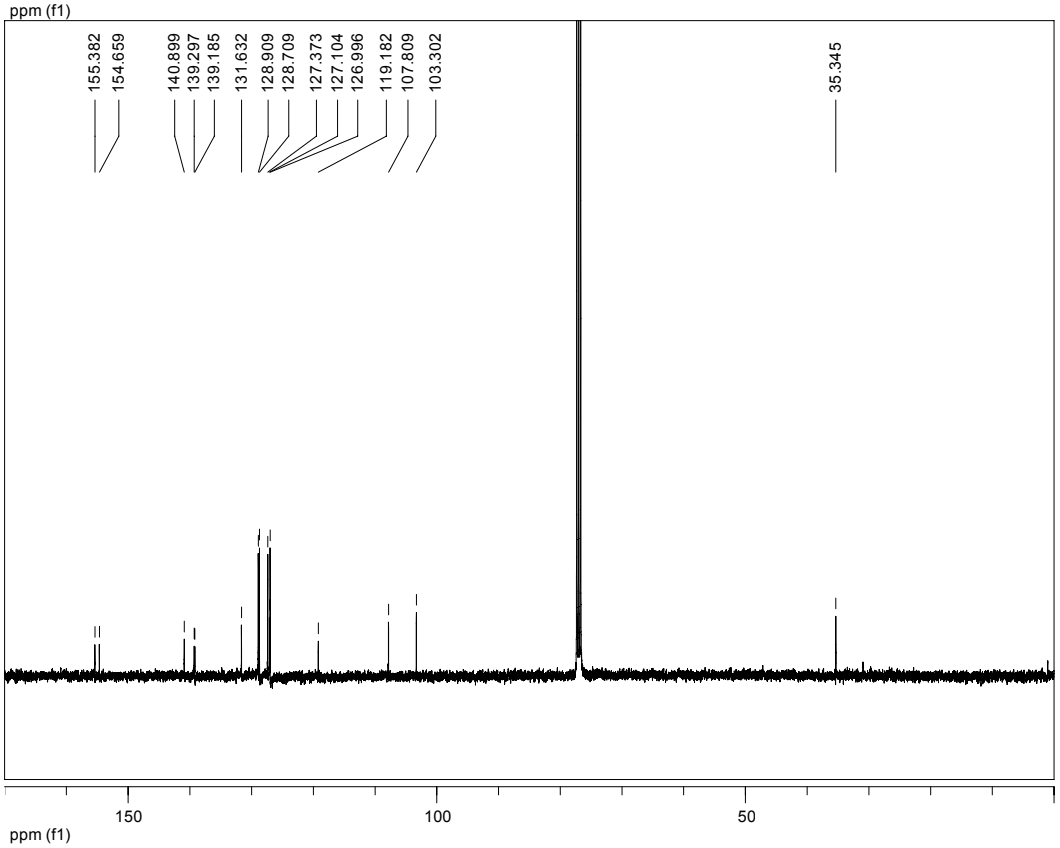
155.382
154.659
140.899
139.297
139.185
131.632
128.909
128.709
127.373
127.104
126.996
119.182
107.809
103.302
35.345
150
100
50
ppm (f1)

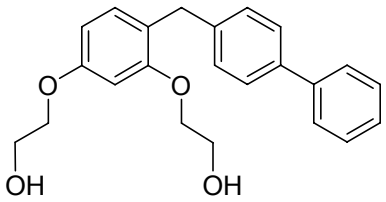

1,3-Bis(2-hydroxyethoxy)-4-(4-phenylbenzyl)benzene (4.20c). Sodium hydroxide (2.94 g, 73.50 mmol) was dissolved in a solution of ethanol (50 mL) and water (8 mL). To this solution was added 4-(4-phenylbenzyl)benzene-1,3-diol (6.77 g, 24.5 mmol) previously dissolved in ethanol (10 mL) creating a dark red solution that was allowed to stir for 10 min. 2-Chloroethanol (5.92 g, 73.5 mmol) was added to the stirring solution after which the entirety was refluxed 2 d. Precipitate formed in the reaction vessel and the solution became ruby red in color. After cooling to room temperature, the solvent was removed *in vacuo* leaving a red solid that was dissolved in EtOAc (100 mL) and washed with water (50 mL). The water was extracted twice more with EtOAc (30 mL). After combining, the organic fractions were washed with brine (50 mL) and dried over $MgSO_4$. Flash chromatography using diethyl ether provided 3.8 g (42 % yield) of pure **4.20c**.

^{1}H NMR ($CDCl_3$, 300MHz): δ 7.58-7.54 (m, 2H), 7.52-7.48 (m, 2H), 7.44-7.38 (m, 2H), 7.34-7.28 (m, 1H), 7.26-7.23 (m, 2H), 7.12 (d, *J* = 8.1 Hz, 1H), 6.51-6.47 (m, 2H), 4.10-4.06 (m, 2H), 4.01-3.94 (m, 4H), 3.96 (s, 2H), 3.85-3.81 (m, 2H), 1.75 (s, 2H).

MS (ESI): m/z 364.2 (M+), 320.2, 304.3, 167.2, 154.2 ($C_{23}H_{24}O_4$ requires 364.43).

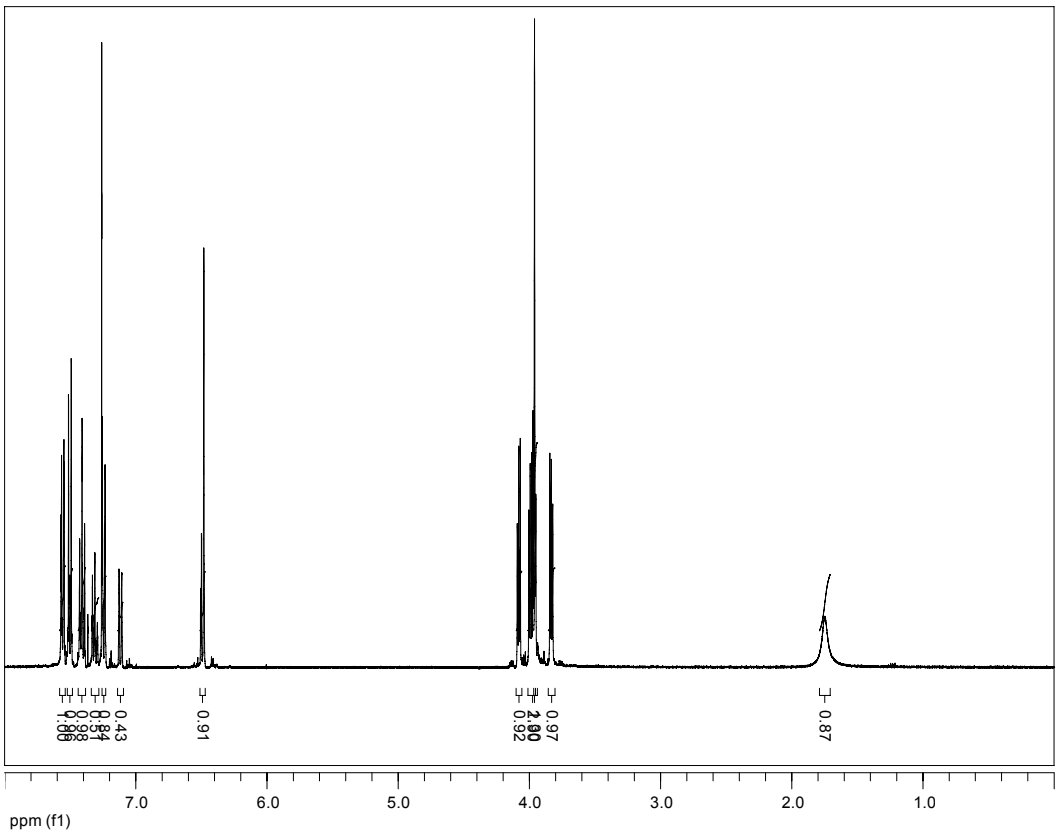
0.43
0.91
0.97
0.87
7.0
6.0
5.0
4.0
3.0
2.0
1.0
ppm (f1)

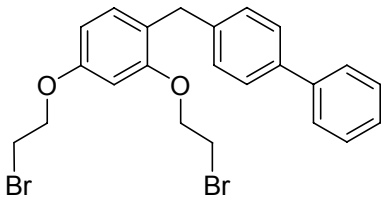

1,3-Bis(2-bromoethoxy)-4-(4-phenylbenzyl)benzene (4.21c). PPh_3 (3.64 g, 13.89 mmol) was added to CH_3CN (30 mL) and cooled to -10 ° C. Br_2 (2.22 g, 13.8 mmol) dissolved in CH_3CN (5 mL) was slowly added to the stirring PPh_3 mixture so as not to exceed 0 ° C. The mixture was allowed to warm to room temperature after the addition was complete. 1,3-Bis(2-hydroxyethoxy)-4-(4-phenylbenzyl)-benzene (2.20 g, 6.04 mmol) dissolved in CH_3CN (5 mL) was added to the mixture and allowed to stir for 2 hours. Solvent was removed *in vacuo* and the crude product purified via column chromatography using CH_2Cl_2 to elute. The product was obtained in 99 % yield (2.94 g) and analysis by NMR showed it to be pure **4.21b**.

^{1}H NMR ($CDCl_3$, 300MHz): δ 7.60-7.55 (m, 2H), 7.53-7.48 (m, 2H), 7.45-7.40 (m, 2H), 7.35-7.32 (m, 1H), 7.31-7.28 (m, 2H), 7.08 (d, *J* = 8.8 Hz, 1H), 6.48-6.45 (m, 2H), 4.29-4.24 (m, 4H), 3.98 (s, 2H), 3.65-3.57 (m, 4H).

^{13}C NMR ($CDCl_3$, 75MHz): δ 155.4, 154.7, 140.9, 139.3, 139.2, 131.6, 128.9, 128.7, 127.5, 127.4, 127.1, 127.0, 119.2, 107.8, 103.3, 35.4.

MS (EI): m/z 490.2 (M^+), 381.2, 274.2 ($C_{23}H_{22}Br_2O_2$ requires 490.23).

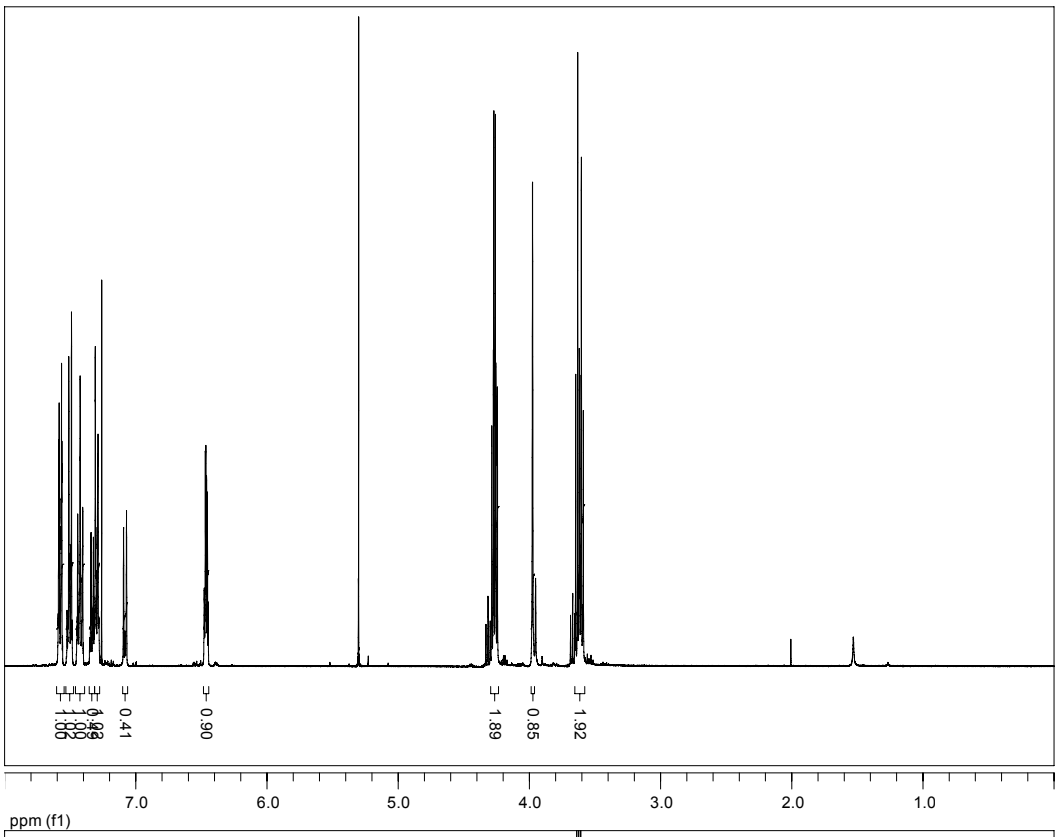
0.41
0.90
1.89
0.85
1.92
7.0
6.0
5.0
4.0
3.0
2.0
1.0
ppm (f1)

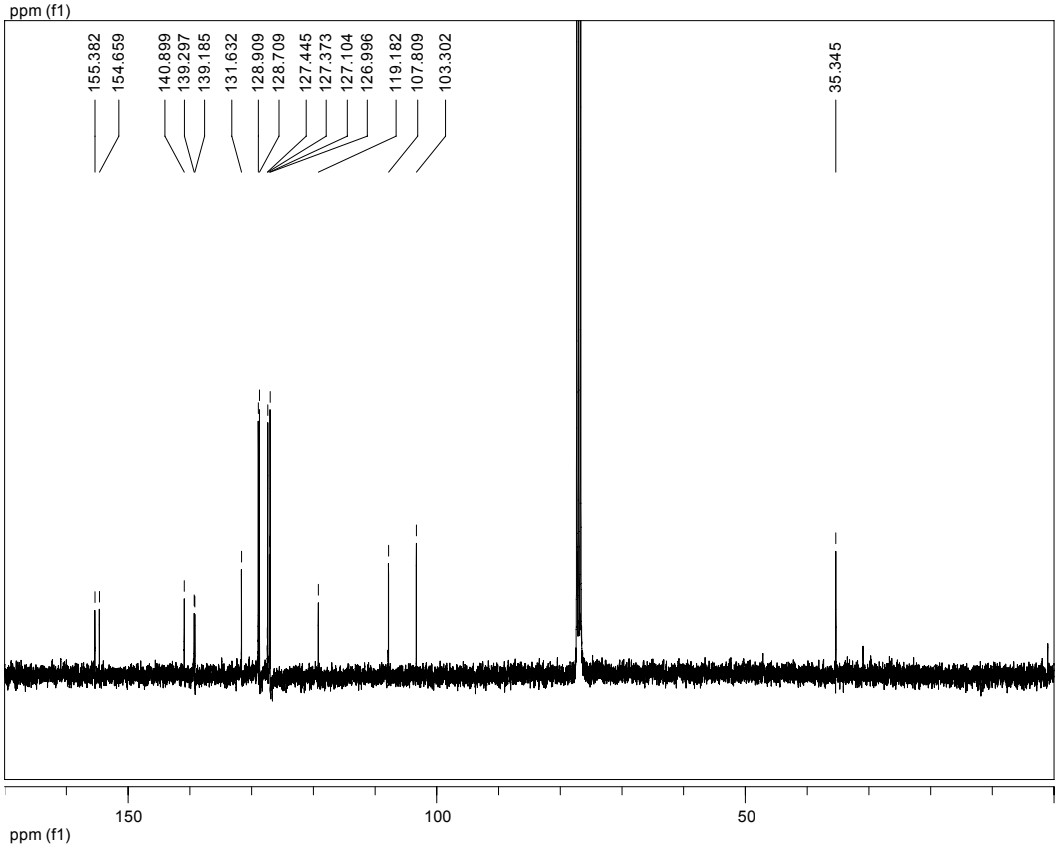
155.382
154.659
140.899
139.297
139.185
131.632
128.909
128.709
127.445
127.373
127.104
126.996
119.182
107.809
103.302
35.345
150
100
50
ppm (f1)

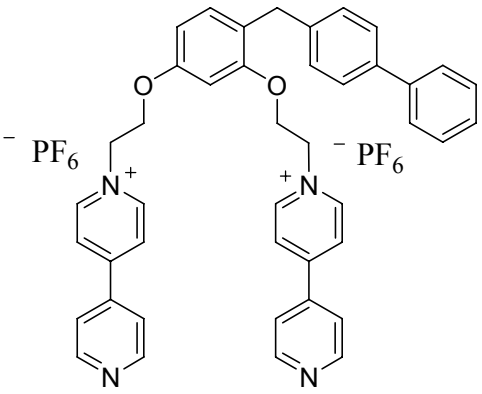

1,3-Bis(2-(4,4'-dipyridinium)ethoxy)-4-(4-phenylbenzyl)benzene bis(hexafluorophosphate) (4.22c). 1,3-Bis(2-bromoethoxy)-4-(4-phenylbenzyl)benzene (3.00 g, 6.12 mmol) and 4,4-dipyridyl (3.82 g, 24.5 mmol) were added to 50 mL of CH_3CN. This solution was stirred at 70 ° C for two d producing a dark yellow viscous oil. The solvent was removed *in vacuo* leaving a brown solid. Water was added and upon heating the solid dissolved producing a yellow solution. Addition of NH_4PF_6 (2.50 g, 15.3 mmol) produced a yellow oil which was isolated and washed with warm $CHCl_3$ (3x20 mL) to extract impurities leaving a yellow oil which was then dissolved in CH_3CN and dried with $MgSO_4$. Removal of the solvent *in vacuo* left 5.3 g (87 % yield) of yellow foam-like solid of product **4.22c**.

^{1}H NMR ($CDCl_3$, 300MHz): δ ppm 9.36 (m, *J* = 7.1 Hz, 2H), 9.15 (m, *J* = 7.1 Hz, 2H), 8.87 (m, *J* = 4.5, 1.7 Hz, 2H), 8.70 (m, *J* = 7.1 Hz, 2H), 8.64 (m, *J* = 4.5, 1.7 Hz, 2H), 8.39 (m, *J* = 7.03 Hz, 2H), 7.99 (m, *J* = 4.5, 1.7 Hz, 2H), 7.70 (m, *J* = 4.5, 1.7 Hz, 2H), 7.49-7.31 (m, 9H), 7.10 (d, *J* = 8.3 Hz, 1H), 6.78 (d, *J* = 2.4 Hz, 1H), 6.60 (dd, *J* = 8.3, 2.4 Hz, 1H), 5.36-5.27 (m, 4H), 4.71 (m, *J* = 9.0, 4.16 Hz, 4H).

^{13}C NMR ($CDCl_3$, 75MHz): δ 160.1, 158.7, 156.7, 156.4, 153.5, 153.3, 147.937, 143.4, 142.9, 142.7, 142.4, 140.4, 133.9, 131.1, 130.9, 130.8, 129.5, 128.9, 128.8, 128.6,

128.6, 128.0, 127.7, 124.2, 124.1, 124.0, 123.8, 123.6, 108.6, 102.4, 68.7, 68.6, 63.0, 62.9, 36.6.

MS (ESI): m/z 787.3 (MPF_6^+), 321.7 (M^{2+}) ($C_{43}H_{38}N_4O_2^{2+}$ requires 642.79).

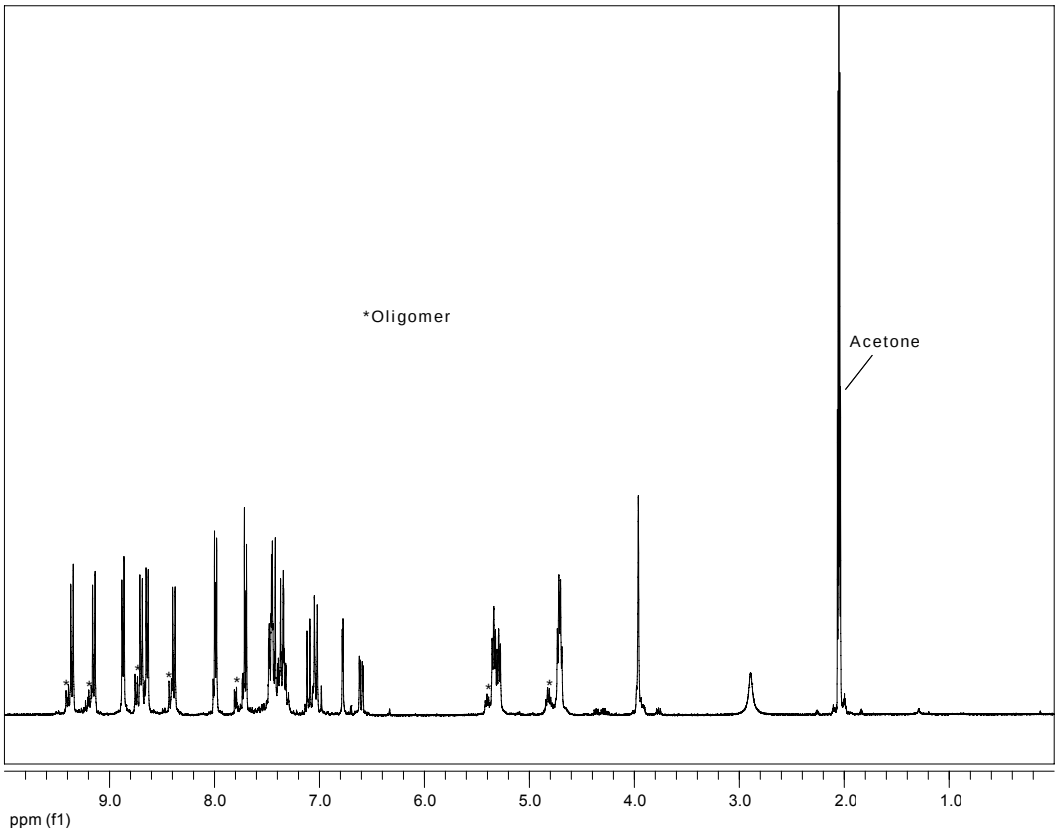

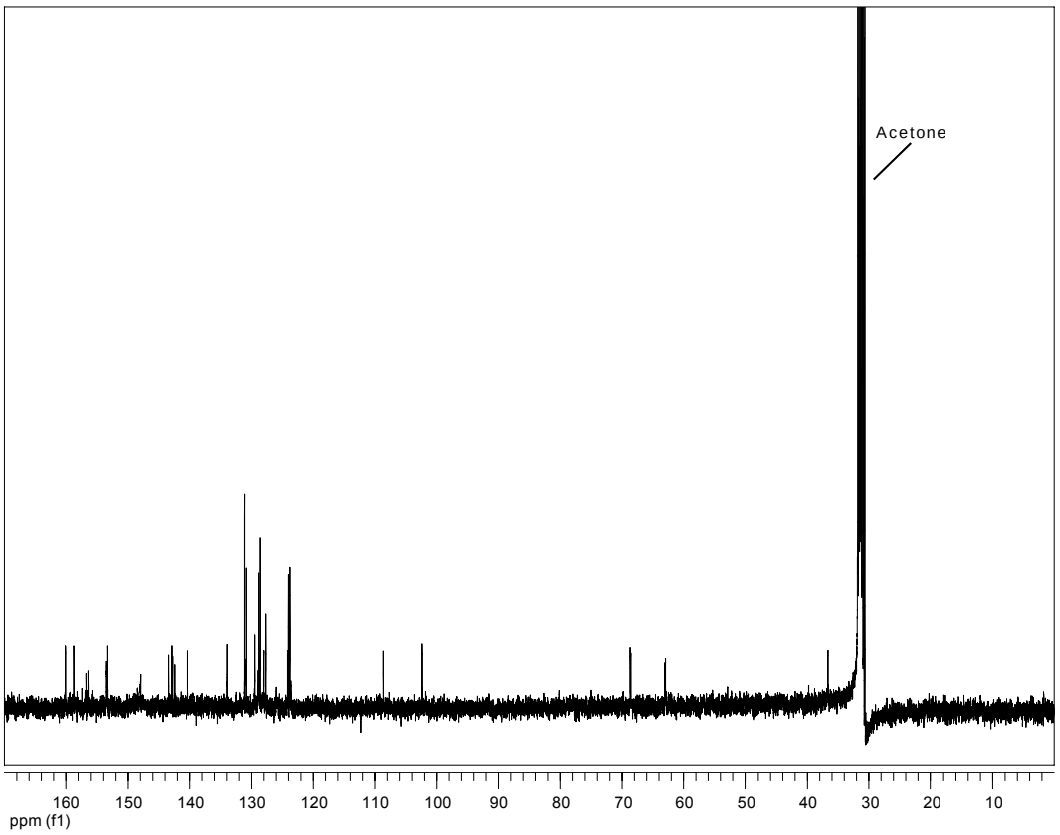
Acetone
160
150
140
130
120
110
100
90
80
70
60
50
40
30
20
10
ppm (f1)

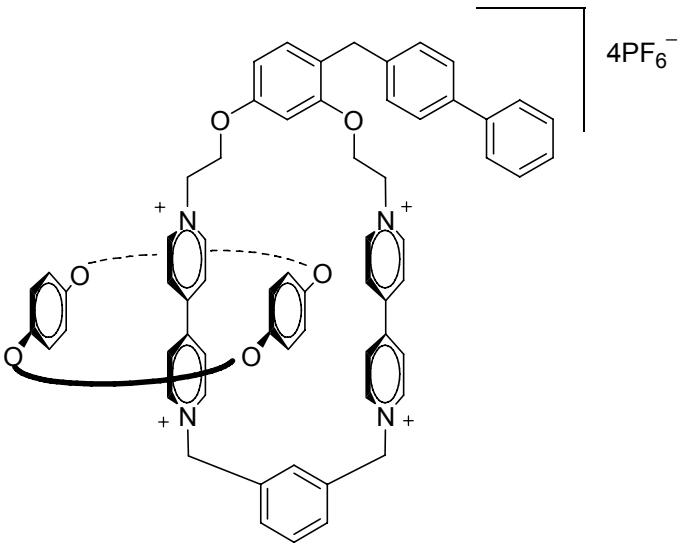

Catenane 4.8. 1,3-Bis(2-(4,4'-dipyridinium)ethoxy)-4-(4-phenyl)benzylbenzene bis(hexafluorophosphate) (0.149 g, 0.160 mmol) and BPP34C10 (0.172 g, 0.32 mmol) were combined and dissolved in CH_3CN (15 mL). This solution was allowed to stir for 10 min. at which point α,α'-dibromo-*m*-xylene (0.051 g, 0.19 mmol) was added and the reaction vessel sealed with a septum. This red solution stirred 4 d under ambient conditions after which time the solvent was removed *in vacuo*. The catenane was purified and after drying 30 mg (10 %) of pure product catenane **4.8** was recovered. **^{1}H NMR** ($CDCl_3$, 400 MHz): δ ppm 9.17 (m, *J* = 6.5 Hz, 6H), 8.78 (d, *J* = 7.0 Hz, 2H), 8.24 (m, *J* = 6.5 Hz, 2H), 8.15 (m, *J* = 7.0 Hz, 2H), 8.10 (m, *J* = 7.0 Hz, 2H), 8.04-8.00 (m, 1H), 7.96 (m, *J* = 7.0 Hz, 4H), 7.88 (m, *J* = 7.7 Hz, 1H),7.76 (m, *J* = 7.5 Hz, 2H), 7.71 (m, *J* = 8.1 Hz, 2H), 7.57 (m, *J* = 7.7, 7.7 Hz, 2H), 7.46 (m, *J* = 7.3 Hz, 1H), 7.38 (m, *J* = 8.1 Hz, 2H), 7.28 (d, *J* = 8.4 Hz, 1H), 6.80 (d, *J* = 2.4 Hz, 1H), 6.68 (dd, *J* = 8.4, 2.4 Hz, 1H), 6.19 (s, 2H), 6.17 (s, 2H), 5.29 (m, *J* = 4.0 Hz, 4H), 4.65 (m, 2H), 4.52 (m, 2H), 4.08 (s, 2H), 3.93-3.47 (m, 32H).

MS (ESI): 786.3 (M $2PF_6^{2+}$), 476.2 (M PF_6^{3+}), 320.7 (M^{4+}) ($C_{79}H_{86}N_4O_{12}^{4+}$ requires 1283.55).

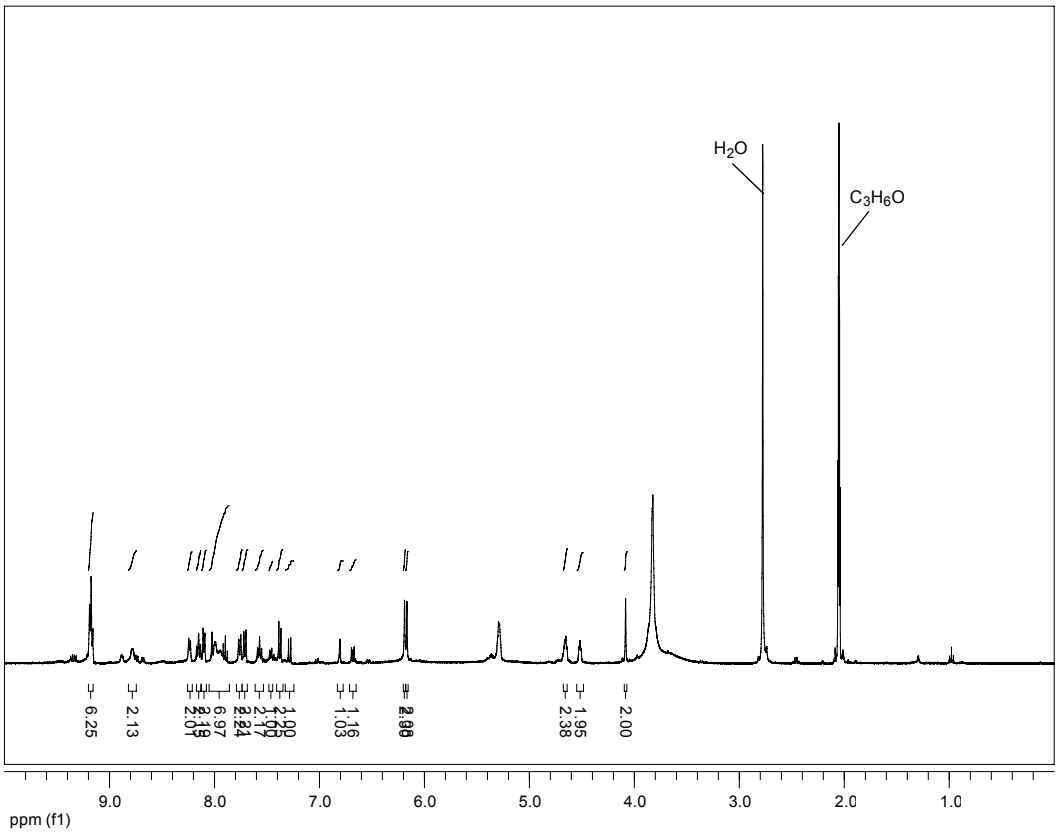

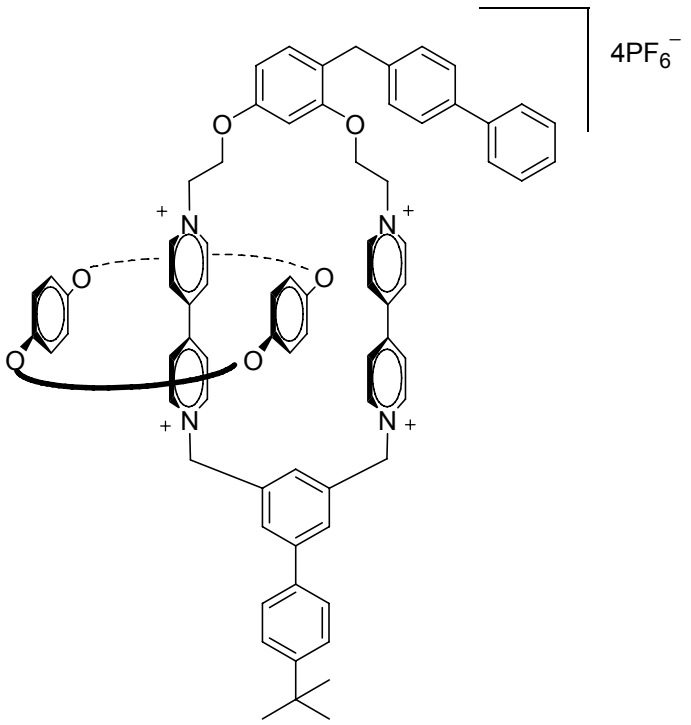

Catenane 4.9. 1,3-Bis(2-(4,4'-dipyridinium)ethoxy)-4-(4-phenyl)benzylbenzene bis(hexafluorophosphate) (0.149 g, 0.160 mmol) and BPP34C10 (0.172 g, 0.32 mmol) were combined and dissolved in CH_3CN (15 mL). This solution was allowed to stir for 10 min. at which point 5-bis(bromomethyl)-4'-(1,1'-dimethylethyl)-1,1'-biphenyl (0.0765 g, 0.192 mmol) was added and the reaction vessel sealed with a septum. This red solution stirred 4 d under ambient conditions after which time the solvent was removed *in vacuo*. The catenane was purified and after drying 71 mg (22 %) of pure product catenane **4.9** was recovered.

^{1}H NMR ($CDCl_3$, 400 MHz): δ ppm 9.28 (m, *J* = 6.8 Hz, 2H), 9.25 (m, *J* = 6.8 Hz, 2H), 9.12 (m, *J* = 6.8 Hz, 2H), 8.80 (m, 2H), 8.41 (m, *J* = 5.5 Hz, 2H), 8.32-8.04 (m, 6H), 7.97 (m, 1H), 7.92 (m, *J* = 8.4 Hz, 3H), 7.75-7.64 (m, 7H), 7.53 (m, 2H), 7.45-7.37 (m, 3H), 7.27 (d, *J* = 8.2 Hz, 1H), 6.81 (d, *J* = 2.0 Hz, 1H), 6.72 (dd, *J* = 8.2, 2.0

Hz, 1H), 6.25 (s, 2H), 6.22 (s, 2H), 5.77 (s, 8H), 5.25 (m, J = 4.7 Hz, 4H), 4.67 (m, 2H), 4.51 (m, 2H), 4.10 (s, 2H), 3.87-3.64 (m, 32H), 1.44 (s, 9H).

MS (ESI): 852.3 (M $2PF_6^{2+}$), 520.3 (M PF_6^{3+}), 353.9 (M^{4+}) ($C_{89}H_{98}N_4O_{12}^{4+}$ requires 1415.75).

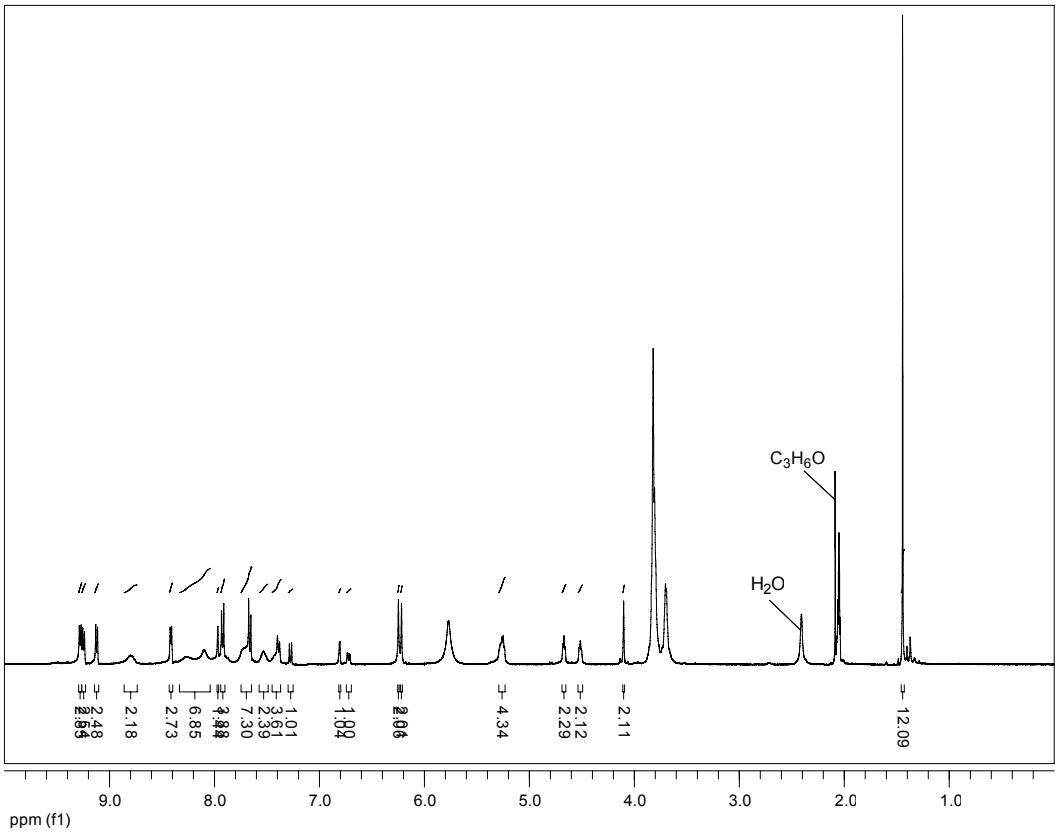

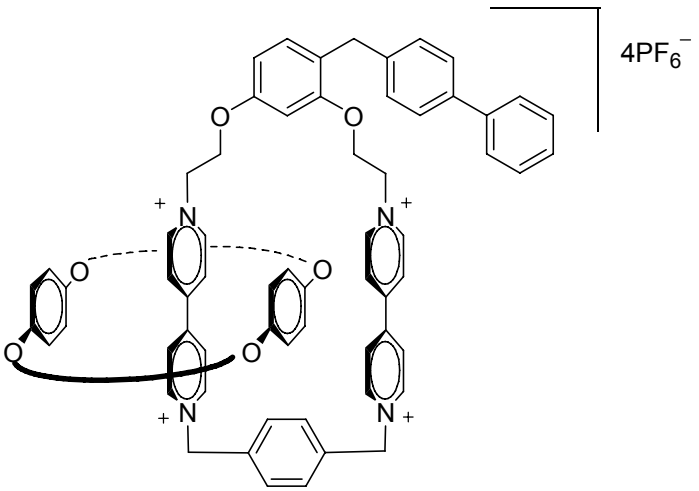

Catenane 4.10. 1,3-Bis(2-(4,4'-dipyridinium)ethoxy)-4-(4-phenyl)benzylbenzene bis(hexafluorophosphate) (0.123 g, 0.160 mmol) and BPP34C10 (0.223 g, 0.416 mmol) were combined and dissolved in CH_3CN (15 mL). This solution was allowed to stir for 10 min. at which point α,α'-dibromo-*p*-xylene (0.051 g, 0.19 mmol) was added and the reaction vessel sealed with a septum. This red solution stirred 4 d under ambient conditions after which time the solvent was removed *in vacuo*. The catenane was purified and after drying 102 mg (34 %) of pure product **4.10** was recovered.

^{1}H NMR ($CDCl_3$, 400 MHz): δ ppm 9.31 (m, *J* = 6.0 Hz, 4H), 9.17 (m, *J* = 7.0 Hz, 2H), 8.84 (m, *J* = 7.0 Hz, 2H), 8.12 (m, *J* = 6.9 Hz, 2H), 8.07 (m, *J* = 7.0 Hz, 2H), 8.06-8.01 (m, 4H), 7.97 (d, *J* = 7.0 Hz, 2H), 7.89 (d, *J* = 7.0 Hz, 2H) 7.72-7.68 (m, 2H), 7.66 (m, *J* = 8.3 Hz, 2H), 7.52 (m, *J* = 7.7 Hz, 2H), 7.41 (m, *J* = 7.4 Hz, 1H), 7.36 (d, *J* = 8.3 Hz, 2H), 7.26 (d, *J* = 8.3 Hz, 1H), 6.75 (d, *J* = 2.4 Hz, 1H), 6.69 (dd, *J* = 8.3, 2.4 Hz, 1H), 6.09 (s, 2H), 6.07 (s, 2H), 5.59 (s, 8H), 5.25 (m, 4H), 4.66 (m, 2H), 4.51 (m, 2H), 4.07 (m, 2H), 3.90-3.57 (m, 32H).

MS (ESI): 786.3 (M $2PF_6^{2+}$), 475.9 (M PF_6^{3+}), 320.7 (M^{4+}) ($C_{79}H_{86}N_4O_{12}^{4+}$ requires 1283.55).

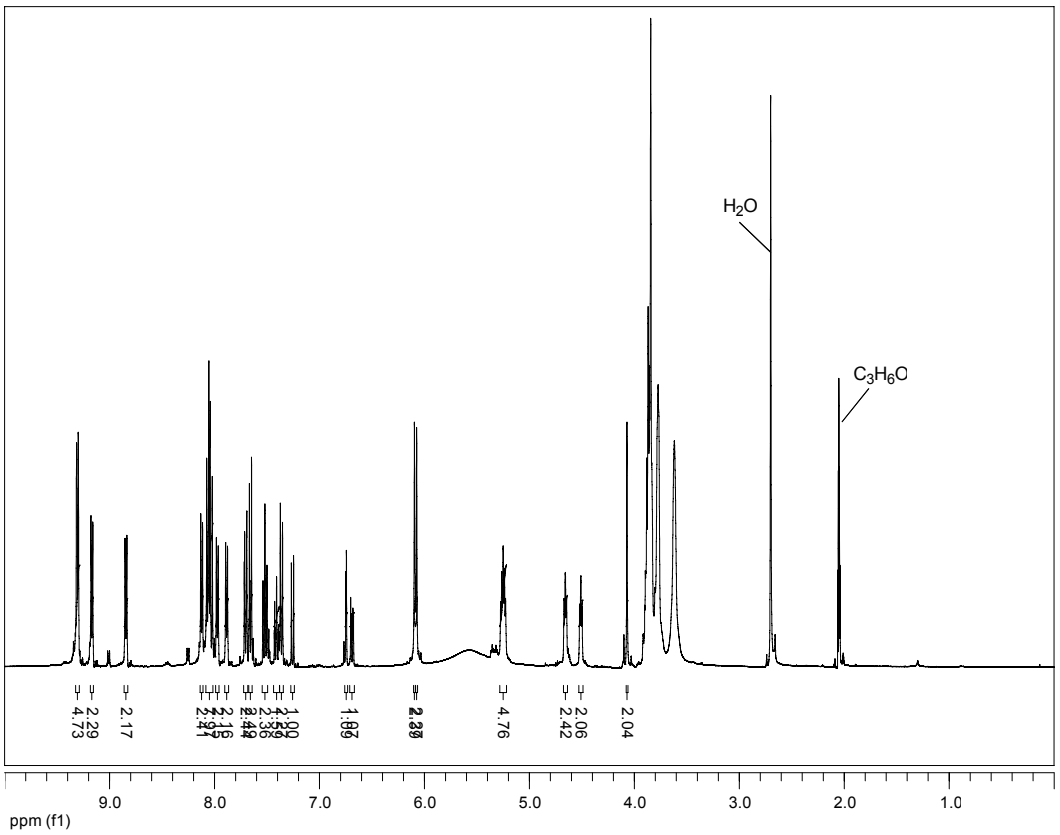
H2O
C3H6O
4.73
2.29
2.17
4.76
2.42
2.06
2.04
9.0
8.0
7.0
6.0
5.0
4.0
3.0
2.0
1.0
ppm (f1)

References

1. Balzani, V.; Credi, A.; Venturi, M. Molecular Level Devices and Machines. In *Stimulating Concepts in Chemistry*; Vogtle, F., Stoddart, J.F., Shibasaki, M., Eds.; Wiley-VCH Publishers: Weinheim, 2000; pp. 255-266.
2. Regan, B. C.; Aloni, S.; Jensen, K.; Zettl, A. *Appl. Phys. Lett.* **2005**, *86,* 123119.
3. Lehn, J.-M. *Supramolecular Chemistry*; VCH Publishers: Weinheim, 1995.
4. Balzani, V.; Scandola, F. *Supramolecular Photochemistry*; Horwood: Chichester, 1991.
5. Balzani, V.; Credi, A.; Venturi, M. Molecular Level Devices. In *Supramolecular Science: Where It Is and Where It Is Going*; Unargo, R., Dalcanale, E., Eds.; Kulwer Academic Publishers: Dordrecht, 1999; pp 1-22.
6. Balazini, V.; Scandola, F. Photochemical and Photophysical Devices. In *Comprehensive Supramolecular Chemistry*; Lehn, J. M., Atwood, J.L.; Davies, J.E.D. ; MacNicol, D.D.; Vögtle, F. Reinhoudt, D. N. Eds.; Elsevier Science: New York, 1996; 10, pp 687-746.
7. Collin, J.-P.; Kern, J.-M.; Raehm, L.; Sauvage, J.-P. Metallo-Rotaxanes and Catenanes as Redox Switches: Toward Molecular Machines. In *Molecular Switches* Ed. Feringa, B.L.,Wiley-VCH Publishers; Weinherim, 2001; pp 249-280.
8. van Delden, R. A.; ter Wiel, M. K. J.; Koumura, N.; Feringa, B. L. Synthetic Molecular Motors. In *Molecular Motors*; Schliwa, M., Ed; Wiley-VCH Publishers: Weinheim, 2003; pp 559-577.

9. Balzani, V.; Credi, A.; Raymo, F. M.; Stoddart, J. F. *Angew. Chem. Int. Ed. Engl*. **2000**, *39*, 3348–3391.

10. Feynman, R.; Leighton, R.; Sands, M. *The Feynman Lectures on Physics* Addison-Wesley: Reading, MA, 1963; Volume 1, Chapter 44.

11. Stoddart, J.F. *Acc. Chem. Res*. **2001**, *34*, 410-411.

12. Bustamante, C.; Keller, D.; Oster, G. *Acc. Chem. Res*. **2001**, *34*, 412-420.

13. Astumian, R.D.; Hänggi, P. *Physics Today* **2002**. 33-39.

14. Feynman, R.; Leighton, R.; Sands, M. *The Feynman Lectures on Physics* Addison-Wesley: Reading, MA, 1963; Volume 1, Chapter 46.

15. von Smoluchowski, M. *Vortgage über die Kinetische Theorie der Materie und der Elektrizita*; Planck, M. Ed.; Teubner und Leipzig: Berlin, 1914; pp 89-121.

16. von Smoluchowski, M. *Phys. Z.* **1912**, *13*, 1069-1080.

17. Chatterjee, M. N.; Euan, D. A.; Leigh, R. K. *J. Am. Chem. Soc*. **2006**, *128*, 4058-4073.

18. Howard, J. *Nature* **1997**, *389*, 561-567.

19. Oster, G.; Wang, H. How Protein Motors Convert Chemical Energy into Mechanical Work. In *Molecular Motors*; Schliwa, M. Ed.; Wiley-VCH Publishers: Weinheim, 2003; pp 207-227.

20. Kelly, T. R.; Tellitu, I.; Sestelo, J. P. *Angew. Chem. Int. Ed. Engl*. **1997**, *36*, 1866-1868.

21. Kelly, T. R. *Acc. Chem. Res*. **2001**, *34*, 514-522.

22. Davis, A. P. *Angew. Chem. Int. Ed*. **1998**, *37*, 909-910.

23. Kelly, T. R.; Bowyer, M. C.; Bhaskar, K. V.; Bebbington, D.; Garcia, A.; Lang, F.; Kim, M. H.; Jette, M. P. *J. Am. Chem.* Soc. **1994**,*116*, 3657-3658.

24. Sestelo, J. P.; Tellitu, I.; Kelly, T. R. *J. Org. Chem.* **1998,** *63,* 3655-3665.

25. Kelly, T. R.; De Silva, H. A.; Silva, R. A. *Nature* **1999**, *401*, 150-152.

26. Leigh, D. A.; Wong, J. K. Y.; Dehez, F.; Zerbetto, F. *Nature* **2003**, *424*, 174-179.

27. Koumura, N.; Zijlstra, R. W. J.; van Delden, R. A.; Harada, R; Feringa, B. L. *Nature* **1999**, *401*, 152-155.

28. Koumura, N.; Geertsema, E. M.; Meetsma, A.; Feringa, B. L. *J. Am. Chem. Soc.* **2000**, *122,* 12005-12006.

29. van Delden, R. A.; ter Wiel, M. J. K.; Pollard, M. M.; Vicario, J.; Koumura, N.; Feringa, B. L. *Nature* **2005**, *437*, 1337-1340.

30. Koumura, N.; Geertsema, E. M.; van Gelder, M. B.; Meetsma, A.; Feringa, B. L. *J. Am. Chem. Soc.* **2002,** *124,* 5037-5051.

31. Raymo, F. M.; Stoddart, J. F. Switchable Catenanes and Molecular Shuttles. In *Molecular Switches*; Feringa, B.L. Ed.; Wiley-VCH Publishers: Weinherim, 2001; pp 219-248.

32. Raymo, F. M.; Stoddart, J. F. Organic Template-Directed Syntheses of Catenanes, Rotaxanes, and Knots. In *Catenane, Rotaxanes, and Knots*; Sauvage, J.-P.; Dietrich-Buchecker, C. Eds.; Wiley-VCH Publishers: Weinheim, 1999; pp 143-176.

33. Dietrich-Buchecker, C.; Sauvage, J.-P. *Chem. Rev.* **1987**, *87*, 795-810.

34. Sauvage, J.-P. *Acc. Chem. Res.* **1990**, *23,* 319-327.

35. Livoreil, A.; Dietrich-Buchecker, C.; Sauvage, J.-P. *J. Am. Chem. Soc.* **1994**, *116,* 9399-9400.

36. Livoreil, A.; Sauvage, J.-P.; Armaroli, N.; Balzani, V.; Flamingni, L.; Ventura, B. *J. Am. Chem. Soc.* **1997**, *119,* 12114-12124.

37. Baumann, F.; Livoreil, A.; Kaim, W.; Sauvage, J.-P. *Chem. Commun.*, **1997**, 35-36.

38. Allwood, B. L.; Shahriari-Zavareh, H.; Stoddart, J. F.; Williams, D. *Chem. Comm.*, **1987**, 1058-1061.

39. Allwood, B. L.; Shahriari-Zavareh, H.; Spencer, N.; Stoddart, J. F.; Williams, D. *Chem. Comm.*, **1987**, 1061-1064.

40. Allwood, B. L.; Spencer, N.; Shahriari-Zavareh, H.; Stoddart, J. F.; Williams, D. *Chem. Comm.*, **1987**, 1064-1066.

41. Anelli, P. L.; Ashton, P. R.; Ballardini, R.; Balzani, V.; Delgado, M.; Gandolfi, M. T.; Goodnow, T. T.; Kaifer, A. E.; Philp, D.; Pietraszkiewicz, M. P.; Prodi, L.; Reddington, M. V.; Slawin,, A. M. V.; Spencer, N.; Stoddart, J. F.; Vicent, C.; Williams, D. J. *J. Am. Chem. Soc*. **1992**, *114*, 193-218.

42. Amabilino, D. B.; Anelli, P. L.; Ashton, P. R.; Brown, G. R.; Cordova, E.; Godinez, L. A.; Hayes, W.; Kaifer, A. E.; Philp, D.; Slawin,, A. M. V.; Spencer, N.; Stoddart, J. F.; Tolley, M. S.; Williams, D. J. *J. Am. Chem. Soc.* **1995**, *117*, 11142-11170.

43. Friebolin, H. Dynamic NMR Spectroscopy. In *Basic One- and Two-Dimensional NMR Spectroscopy*; VCH-Verlag Publishers: Weinheim, 1991; pp 263-291.

44. Ashton, P. R.; Reder, A. S.; Spencer, N.; Stoddart, J. F. *J. Am. Chem. Soc*. **1993**, *115*, 5286-5287.

45. Oth, J. F. M.; Gilles, J. M. *J. Phys. Chem. A* **2000,** *104,* 7980-7994.

46. Halterman, R. L.; Martyn, D. E.; Pan, X.; Ha, D. B.; Frow, M.; Haessig, K. *Org. Lett.* **2006**, *8*, 2119-2121.

47. Yang, Y.; Escobedo, J. O.; Wong, A.; Schowalter, C. M.; Touchy, M. C.; Jiao, L.; Crowe, W. E.; Fronczek, F. R.; Strongin, R. M. *J. Org Chem.* **2005**, *70*, 6907-6912.

48. Gribble, G. W.; Leese, R. M.; Evans, B. E. *Synthesis* **1977**, *61*, 172-176.

49. Punna, S.; Meunier, S.; Finn, M. G. *Org. Lett.* **2004**, *6*, 2777-2779.

50. Müller, W.; Lowe, D. A.; Neijt, H.; Urwyler, S.; Herrling, P. L.;Blaser, D.; Seebach, D. *Helv. Chim. Acta* **1992**, *75,* 855-864.

51. Silverstein, R. M.; Webster, F. X. Proton Magnetic Resonance Spectroscopy. In *Spectrometric Identification of Organic Compounds*; John Wiley and Sons: New York, 1998; pp. 174-178.

52. Friebolin, H. P. Dynamic NMR Spectroscopy. *Basic 1D and 2D NMR Spectroscopy*; VCH Publishers: New York, 1991; Chapter 11, pp 271-272.

53. Brown, D.A.; Cuffe, L.P.; Fitzpatrich, G.M.; Fitzpatrick, N.J.; Glass, W.K.; Herlihy, K.M. *Coll Czech. Chem. Commun*. **2001**, *66*, 99-108.

54. Elliger, C.A. *Syn. Comm*. **1985**, *15*, 1315-1324.

55. Rakesh, S. *Tet. Lett*. **1991**, 5571-5573.

56. AM1 calculation by Spartan 1.0.

57. Brockmann, H.; Kluge, F.; Muxfeldt, H. *Chem. Ber*. **1957**, *90*, 2302-2318.

58. Helgeson, R.C; Tarnowski, T.L.; Timko, J.M.; Cram, D.J. *J. Am. Chem. Soc.* **1977**, *99*, 6411-6418.